

VOLUME 77

JUNE 7, 1973

NUMBER 12

JPCA X

---

THE JOURNAL OF

PHYSICAL  
CHEMISTRY

---

PUBLISHED BIWEEKLY BY THE AMERICAN CHEMICAL SOCIETY

# THE JOURNAL OF PHYSICAL CHEMISTRY

---

**BRYCE CRAWFORD, Jr.**, *Editor*

STEPHEN PRAGER, *Associate Editor*

ROBERT W. CARR, Jr., FREDERIC A. VAN-CATLEDGE, *Assistant Editors*

**EDITORIAL BOARD:** A. O. ALLEN (1970-1974), C. A. ANGELL (1973-1977), J. R. BOLTON (1971-1975), F. S. DANTON (1972-1976), M. FIXMAN (1970-1974), H. S. FRANK (1970-1974), R. R. HENTZ (1972-1976), J. R. HUIZENGA (1969-1973), W. J. KAUFMANN (1969-1973), R. L. KAY (1972-1976), W. R. KRIGBAUM (1969-1973), W. J. MOORE (1969-1973), R. M. NOYES (1973-1977), J. A. POPLE (1971-1975), B. S. RABINOVITCH (1971-1975), H. REISS (1970-1974), S. A. RICE (1969-1975), F. S. ROWLAND (1973-1977), R. L. SCOTT (1973-1977), W. A. ZISMAN (1972-1976)

AMERICAN CHEMICAL SOCIETY, 1155 Sixteenth St., N.W., Washington, D. C. 20036

## Books and Journals Division

JOHN K CRUM *Director*

RUTH REYNARD *Assistant to the Director*

CHARLES R. BERTSCH *Head, Editorial Processing Department*

D. H. MICHAEL BOWEN *Head, Journals Department*

BACIL GUILLEY *Head, Graphics and Production Department*

SELDON W. TERRANT *Head, Research and Development Department*

©Copyright, 1973, by the American Chemical Society. Published biweekly by the American Chemical Society at 20th and Northampton Sts., Easton, Pa. 18042. Second-class postage paid at Washington, D. C., and at additional mailing offices.

All manuscripts should be sent to *The Journal of Physical Chemistry*, Department of Chemistry, University of Minnesota, Minneapolis, Minn. 55455.

*Additions and Corrections* are published once yearly in the final issue. See Volume 76, Number 26 for the proper form.

*Extensive or unusual alterations in an article after it has been set in type are made at the author's expense*, and it is understood that by requesting such alterations the author agrees to defray the cost thereof.

The American Chemical Society and the Editor of *The Journal of Physical Chemistry* assume no responsibility for the statements and opinions advanced by contributors.

Correspondence regarding accepted copy, proofs, and reprints should be directed to Editorial Processing Department, American Chemical Society, 20th and Northampton Sts., Easton, Pa. 18042. Head: CHARLES R. BERTSCH. Assistant Editor: EDWARD A. BORGER. Editorial Assistant: JOSEPH E. YURVATI.

Advertising Office: Centcom, Ltd., 142 East Avenue, Norwalk, Conn. 06851.

## Business and Subscription Information

Send all new and renewal subscriptions *with payment* to: Office of the Controller, 1155 16th Street, N.W., Washington, D. C. 20036. Subscriptions should be renewed promptly to avoid a break in your series. All correspondence and telephone calls regarding changes of

address, claims for missing issues, subscription service, the status of records, and accounts should be directed to Manager, Membership and Subscription Services, American Chemical Society, P.O. Box 3337, Columbus, Ohio 43210. Telephone (614) 421-7230.

On changes of address, include both old and new addresses with ZIP code numbers, accompanied by mailing label from a recent issue. Allow four weeks for change to become effective.

Claims for missing numbers will not be allowed (1) if loss was due to failure of notice of change in address to be received before the date specified, (2) if received more than sixty days from date of issue plus time normally required for postal delivery of journal and claim, or (3) if the reason for the claim is "issue missing from files."

Subscription rates (1973): members of the American Chemical Society, \$20.00 for 1 year; to nonmembers, \$60.00 for 1 year. Those interested in becoming members should write to the Admissions Department, American Chemical Society, 1155 Sixteenth St., N.W., Washington, D. C. 20036. Postage to Canada and countries in the Pan-American Union, \$5.00; all other countries, \$6.00. Single copies for current year: \$3.00. Rates for back issues from Volume 56 to date are available from the Special Issues Sales Department, 1155 Sixteenth St., N.W., Washington, D. C. 20036.

Subscriptions to this and the other ACS periodical publications are available on microfilm. Supplementary material not printed in this journal is now available in microfiche form on a current subscription basis. For information on microfilm or microfiche subscriptions, write Special Issues Sales Department at the address above.

Spectrophotometric Determination of the Rate of Dissociation of Nitrogen Trifluoride behind Shock Waves . . . . .	<b>K. O. MacFadden and E. Tschuikow-Roux*</b>	1475
Flash Photolysis of Aromatic Sulfur Molecules . . . . .	<b>F. C. Thyron</b>	1478
Photo-Induced Decarboxylation of Aliphatic Acids and Esters in Solution. Dependence upon State of Protonation of the Carboxyl Group . . . . .	<b>Lalitha J. Mittal, J. P. Mittal, and E. Hayon</b>	1482
Photochemistry of 4-Nitropyridine in Acid Solutions . . . . .	<b>A. Cu and A. C. Testa*</b>	1487
Analysis of the Temperature Dependence of the Electron Spin Resonance Spectrum of $-OOCF_2CF_2COO-$ Using Density Matrix Techniques . . . . .	<b>Carolyn M. Bogan and Lowell D. Kispert*</b>	1491
Indium-115 Nuclear Magnetic Resonance Study of Indium Complexes in Solvent Extraction System . . . . .	<b>Hiroki Haraguchi,* Keiichiro Fuwa, and Shizuo Fujiwara</b>	1497
Rotational Isomerism of the Phenylalanine Anion in Mixed Aqueous Solvents by Nuclear Magnetic Resonance . . . . .	<b>J. M. Purcell, J. E. Ramirez, and J. R. Cavanaugh*</b>	1501
Vibrational Spectra, Structure, and Nature of the Phosphorus-Nitrogen Bond in <i>N,P,P,P</i> -Tetramethylphosphine Imide and <i>N</i> -Methyl- <i>d</i> <sub>3</sub> - <i>P,P,P</i> -trimethylphosphine Imide . . . . .	<b>J. Bragin,* S. Chan, E. Mazzola, and H. Goldwhite</b>	1506
Matrix Isolation Infrared Study of the Reaction between Tin Vapor and Molecular Oxygen. The Characterization of Molecular Tin Dioxide . . . . .	<b>A. Bos and J. S. Ogden*</b>	1513
An Additivity Equation for Calculating Second Moments of the Electronic Charge Distribution . . . . .	<b>Z. B. Maksić and J. E. Bloor*</b>	1520
Electron-Transfer and <i>f-d</i> Absorption Bands of Some Lanthanide and Actinide Complexes and the Standard (II-III) Oxidation Potential for Each Member of the Lanthanide and Actinide Series . . . . .	<b>L. J. Nugent,* R. D. Baybarz, J. L. Burnett, and J. L. Ryan</b>	1528
Liquid Junction Potentials by Computer Simulation. II. The Lewis and Sargent Cell. A Harned's Rule for Single Ions . . . . .	<b>Chang-Hwei Chen and Henry S. Frank*</b>	1540
Kinetic Study of Permanganate Oxidation Reactions. IV. Reaction with Bromide Ion . . . . .	<b>Samuel A. Lawani and John R. Sutter*</b>	1547
Kinetics of Twelve-Step Competitive-Consecutive Second-Order Reactions. The Alkaline Hydrolysis of Triethyl Citrate . . . . .	<b>F. A. Kundell, D. J. Robinson, and W. J. Svirbely*</b>	1552
Solvent Isotope Effects on <i>pK</i> <sub>a</sub> of Anilinium Ions in Aqueous Sulfuric Acid . . . . .	<b>J. L. Jensen* and M. P. Gardner</b>	1557
Protolysis and Nitrogen Inversion of Anilines in Sulfuric Acid . . . . .	<b>Donald E. Leyden* and Ronald E. Channell</b>	1562
Determination of Ion-Pairing Dissociation Constants Using Electron Spin Resonance Spectroscopy . . . . .	<b>Philip Graceffa and T. R. Tuttle, Jr.*</b>	1566
Noise Generated during Sodium and Hydrogen Ion Transport across a Cation Exchange Membrane . . . . .	<b>Stephen H. Stern and Michael E. Green*</b>	1567 ■
The Shape of the Coexistence Curve of Ternary Liquid Mixtures near the Plait Point . . . . .	<b>L. E. Wold, Jr., G. L. Pruitt, and G. Morrison*</b>	1572 ■

Mass Spectrometric Studies of Gaseous Oxides of Rhenium	Harry B. Skinner and Alan W. Searcy*	1578
Reactions of Iodine Excited with 185-nm Radiation. III. Reactions with Hydrogen, Methane, Trifluoromethane, Fluoromethane, Chloromethane, and Oxygen. Mechanistic Tests	L. C. Glasgow and J. E. Willard*	1585
Substituent Parameters for Carbon-13 Chemical Shifts of 1,2-Disubstituted Ethanes	L. Simeral and G. E. Maciel*	1590

### COMMUNICATIONS TO THE EDITOR

Nuclear Magnetic Relaxation of Sodium-23 in Polyphosphate Solutions	H. S. Kielman and J. C. Leyte*	1593
Effect of 2-Butanol on the Activity of Sodium Sulfate in Aqueous Solutions. Implications for Electrosorption Studies	David M. Mohilner* and Hisamitsu Nakadomari	1594
Substituent Effects on Excited-State Acidities of Some Substituted 8-Hydroxyquinolinium Cations	M. P. Bratzel, J. J. Aaron, J. D. Winefordner,* S. G. Schulman, and H. Gershon	1595
Reply to the Comments of Desnoyers on the Paper, "Ionic Solvation Numbers from Compressibilities and Ionic Vibration Potentials Measurements"	J. O'M. Bockris* and P. P. S. Saluja	1598
Gaseous Thallium(I) Metaborate and Thallium(I) Aluminum Fluoride	David H. Feather and Alfred Büchler*	1599

■ Supplementary material for this paper is available separately, in photocopy or microfiche form. Ordering information is given in the paper.

\* In papers with more than one author, the asterisk indicates the name of the author to whom inquiries about the paper should be addressed.

### AUTHOR INDEX

Aaron, J. J., 1595	Fujiwara, S., 1497	Leyden, D. E., 1562	Robinson, D. J., 1552
Baybarz, R. D., 1528	Fuwa, K., 1497	Leyte, J. C., 1593	Ryan, J. L., 1528
Bloor, J. E., 1520	Gardner, M. P., 1557	MacFadden, K. O., 1475	Saluja, P. P. S., 1598
Bockris, J. O'M., 1598	Gershon, H., 1595	Maciel, G. E., 1590	Schulman, S. G., 1595
Bogan, C. M., 1491	Glasgow, L. C., 1585	Maksic, Z. B., 1520	Searcy, A. W., 1578
Bos, A., 1513	Goldwhite, H., 1506	Mazzola, E., 1506	Simeral, L., 1590
Bragin, J., 1506	Graceffa, P., 1566	Mittal, J. P., 1482	Skinner, H. B., 1578
Bratzel, M. P., 1595	Green, M. E., 1567	Mittal, L. J., 1482	Stern, S. H., 1567
Büchler, A., 1599	Haraguchi, H., 1497	Mohilner, D. M., 1594	Sutter, J. R., 1547
Burnett, J. L., 1528	Hayon, E., 1482	Morrison, G., 1572	Svirbely, W. J., 1552
Cavanaugh, J. R., 1501	Jensen, J. L., 1557	Nakadomari, H., 1594	Testa, A. C., 1487
Chan, S., 1506	Kielman, H. S., 1593	Nugent, L. J., 1528	Thyryon, F. C., 1478
Channell, R. E., 1562	Kispert, L. D., 1491	Ogden, J. S., 1513	Tschuikow-Roux, E., 1475
Chen, C.-H., 1540	Kundell, F. A., 1552	Pruitt, G. L., 1572	Tuttle, T. R., Jr., 1566
Cu, A., 1487	Lawani, S. A., 1547	Purcell, J. M., 1501	Willard, J. E., 1585
Feather, D. H., 1599		Ramirez, J. E., 1501	Winefordner J. D., 1595
Frank, H. S., 1540			Wold, L. E., Jr., 1572

# THE JOURNAL OF PHYSICAL CHEMISTRY

Registered in U. S. Patent Office © Copyright, 1973, by the American Chemical Society

VOLUME 77, NUMBER 12 JUNE 7, 1973

## Spectrophotometric Determination of the Rate of Dissociation of Nitrogen Trifluoride behind Shock Waves<sup>1a</sup>

K. O. MacFadden<sup>1b</sup> and E. Tschuikow-Roux\*

Department of Chemistry, University of Calgary, Calgary, Alberta T2N 1N4, Canada (Received November 14, 1972)

The rate of dissociation of nitrogen trifluoride in excess argon has been determined by measuring the rate of formation of  $\text{NF}_2$  in the temperature range 1050–1390°K using a shock tube-spectrophotometric technique. In the range of 2.7–6.0 atm total pressure the reaction was found to be first order in both  $\text{NF}_3$  and Ar concentrations. The reaction may be represented by  $\text{NF}_3 + \text{M} \rightleftharpoons \text{NF}_2 + \text{F} + \text{M}$  ( $k_M; k_{-M}$ ) and for small conversions, other reactions are shown to be unimportant. The temperature dependence of the bimolecular rate constants can be described by  $k_M$  ( $\text{M}^{-1} \text{sec}^{-1}$ ) =  $10^{10.10 \pm 0.02} \exp[-(30.1 \pm 2.3 \text{ kcal mol}^{-1})/RT]$  where it is noted that the *apparent* activation energy is significantly lower than the bond dissociation energy,  $D(\text{NF}_2\text{-F})$ .

### Introduction

The species  $\text{NF}_2$ ,  $\text{NF}_3$ , and  $\text{N}_2\text{F}_4$  are prototypes of the classical  $\text{XY}_2$ ,  $\text{XY}_3$ , and  $\text{X}_2\text{Y}_4$  molecules. The structure determination and the physical properties of these molecules have been the subject of numerous investigations and reviews.<sup>2,3</sup> In contrast, kinetic data on the thermal decomposition of these compounds are relatively scarce. The only decomposition studies reported hitherto are those on tetrafluorohydrazine<sup>4-6</sup> and the  $\text{NF}_2$  radical.<sup>7-9</sup> The kinetic parameters for the decomposition of  $\text{NF}_3$ ,  $\text{HNF}_2$ , and  $\text{ClNF}_2$  have apparently not been reported.

In this communication we report on the kinetics of the shock-induced thermal decomposition of  $\text{NF}_3$  in the presence of inert gas at temperatures in the range 1050–1390°K and total pressures 2.7–6.0 atm.

### Experimental Section

A detailed description of the experimental apparatus has been reported elsewhere.<sup>6</sup> An aluminum shock tube (80 mm i.d.), designed for cold driver operation, was used to heat dilute mixtures of  $\text{NF}_3$  in argon. In these experiments, the driver section was 305 cm and the expansion channel 417 cm long. Helium as driver gas and aluminum diaphragms were used to obtain the desired shock strengths. The incident shock velocity was measured by three pressure transducers of 1- $\mu\text{sec}$  risetime (Kistler, Model 603A/623F) located 40, 60, and 80 cm from the

endplate. The signals from the transducers were amplified and fed to two universal counters (Hewlett-Packard, Model 5325 A) which provided a direct readout of the transit times of the shock wave.

The reaction kinetics were monitored by following the  $\text{NF}_2$  radical concentration in absorption at 260 nm. The optical observation station, placed perpendicular to the shock tube axis, was located in the vicinity of the last pressure transducer, 36 cm from the endplate. It consisted of a xenon arc lamp (Hanovia, Model 538 C-1), a pair of quartz lenses to spatially define the light beam, a light chopper to produce a reference signal for 100% absorption, followed by a 0.3-m plane grating monochromator (McPherson, Model 218) and a high-gain photomultiplier (EMI-9635 QB). The output of the photomultiplier, after passing through a variable load resistor, was displayed on the face of an oscilloscope and recorded photographically.

- (1) (a) Work supported by the Defence Research Board of Canada, under DRB Grant No. 9530-107. (b) Postdoctorate Fellow, 1971–1973.
- (2) (a) C. J. Hoffman and R. G. Neville, *Chem. Rev.*, **62**, 1 (1962); (b) A. V. Pankratov, *Usp. Khim.*, **32**, 336 (1963).
- (3) C. B. Colburn, *Endeavour*, **24**, 138 (1965).
- (4) L. M. Brown and B. de B. Darwent, *J. Chem. Phys.*, **42**, 2158 (1965).
- (5) A. P. Modica and D. F. Hornig, *J. Chem. Phys.*, **49**, 629 (1968).
- (6) E. Tschuikow-Roux, K. O. MacFadden, K. H. Jung, and D. A. Armstrong, *J. Phys. Chem.*, **77**, 734 (1973).
- (7) A. P. Modica and D. F. Hornig, *J. Chem. Phys.*, **43**, 2739 (1965).
- (8) R. W. Diesen, *J. Chem. Phys.*, **41**, 3256 (1964).
- (9) R. W. Diesen, *J. Chem. Phys.*, **45**, 759 (1966).

ห้องสมุด กรมวิทยาศาสตร์  
24 ส.ค. 2516

Nitrogen trifluoride of 99.8% purity was obtained from the Air Products Co. and used without further purification. Reaction mixtures of 1 and 2%  $\text{NF}_3$  in research grade argon were prepared in stainless steel tanks and allowed to mix prior to use.

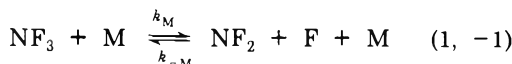
The temperature and density conditions behind the shock wave were calculated from the Rankine-Hugoniot equations, modified to account for the enthalpy of dissociation.<sup>6</sup> These calculations were made using data from the JANAF Tables.<sup>10</sup>

**Absorption Coefficient of  $\text{NF}_2$ .** Above 500°K, the absorption coefficient of the  $\text{NF}_2$  radical has been shown to be slightly temperature dependent.<sup>7</sup> In the present study, the absorption coefficient was redetermined by shock heating a 1% mixture of  $\text{N}_2\text{F}_4$  in argon to temperatures between 800 and 1400°K. In this temperature range the  $\text{N}_2\text{F}_4$  is completely dissociated and the  $\text{NF}_2$  concentration can be calculated from the known equilibrium constant,<sup>5,6</sup> since the  $\text{NF}_2$  should be stable with respect to decomposition under conditions of the experiment.<sup>7</sup> This was confirmed by observing that the  $\text{NF}_2$  concentration reached its equilibrium value very rapidly and no further change in concentration occurred during the time of these experiments (150  $\mu\text{sec}$ ). The absorption coefficient was evaluated from the Beer-Lambert law in the form

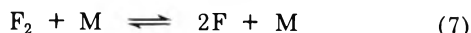
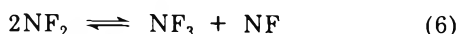
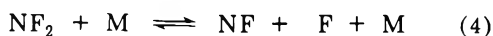
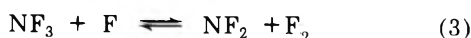
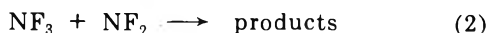
$$\epsilon = \ln [H/(H - h_{\text{eq}})]/L[\text{NF}_2] \quad (\text{I})$$

where  $H$  is the deflection of the oscilloscope trace for 100% absorption produced by the light chopper;  $h_{\text{eq}}$  is the deflection due to  $\text{NF}_2$  absorption at equilibrium; and  $L$  is the optical path length. The  $\text{NF}_2$  concentration is given by  $[\text{NF}_2] = 2\alpha'\rho_{21}[\text{N}_2\text{F}_4]_{01}$ , where  $\rho_{21}$  is the density ratio across the shock front,  $[\text{N}_2\text{F}_4]_{01}$  is the initial  $\text{N}_2\text{F}_4$  concentration ahead of the shock, and  $\alpha'$  is the fraction of  $\text{N}_2\text{F}_4$  dissociated ( $\alpha' \approx 1$ ). The absorption coefficient was found to change very little with temperature, and the average value over this temperature range,  $\epsilon = 603 \text{ M}^{-1} \text{ cm}^{-1}$ , was used for all calculations.

**Kinetics.** In contrast to the situation in  $\text{NH}_3$ , the first N-F bond in  $\text{NF}_3$  is broken more easily than the second and third. The strength of the first N-F bond is 57 kcal  $\text{mol}^{-1}$ <sup>11</sup> while the average strength of the latter two bonds is 71 kcal  $\text{mol}^{-1}$ .<sup>11,12</sup> The most likely mode of decomposition is therefore *via* N-F bond scission, and the reaction is reversible



Secondary reactions which must also be considered may include



The rate parameters for reactions 3-7 are summarized in Table I; those for reaction 2 are not known. The feasibility of reaction 2 was explored by shock heating a mixture of 1%  $\text{NF}_3$  and 0.5%  $\text{N}_2\text{F}_4$  in argon to temperatures between 950 and 1120°K. In this temperature range virtually all of

TABLE I: Arrhenius Parameters

Reaction	A, $\text{M}^{-1} \text{sec}^{-1}$	E, kcal $\text{mol}^{-1}$	Ref.
3	$8.8 \times 10^{10}$	35.6	a
4	$6.0 \times 10^{11}$	52.0	9
-5	$3.6 \times 10^{13}$	15.3	6
6	$4.3 \times 10^6$	$\sim 0$	b
7	$2.0 \times 10^{10}$	35.0	13

<sup>a</sup> Computed from the reverse reaction (ref 13) and the equilibrium constant using data in ref 10. <sup>b</sup>  $k_6$  was assumed to be equal to  $0.1k_5'$  where  $k_5'$  is the rate constant for  $\text{NF}_2$  radical recombination in the limit of high pressures. The latter was deduced from the reverse dissociation rate constant,  $k_{-5}$  (ref 6) and the equilibrium constant using data in ref 10.

the  $\text{N}_2\text{F}_4$  is converted to  $\text{NF}_2$  while very little of the  $\text{NF}_3$  decomposes. The  $\text{NF}_2$  concentration was observed to reach a maximum in less than 50  $\mu\text{sec}$  and then remain constant over the observation period (1 msec). A 0.5% mixture of  $\text{N}_2\text{F}_4$  in argon was then heated to the same temperatures yielding identical results. Based on this evidence it was concluded that reaction 2 is not significant under the conditions of the  $\text{NF}_3$  decomposition experiments.

In order to determine the rate parameters for the  $\text{NF}_3$  dissociation reaction it was next assumed (to be justified later) that over the temperature-time regime of this study reactions 3-7 were negligible in comparison to the  $\text{NF}_3$  decomposition rate. Since for reaction 1 the equilibrium constant is much less than unity over the entire temperature range,  $K_c = k_M/k_{-M} \ll 1$ , the reverse reaction is formally included and the rate of decomposition is given by

$$-d[\text{NF}_3]/dt_p = k_M[\text{M}][\text{NF}_3] - k_{-M}[\text{NF}_2][\text{F}][\text{M}] \quad (\text{II})$$

where the concentrations refer to the region behind the incident shock and the independent variable refers to particle time. Substituting  $\alpha$  for the fraction of  $\text{NF}_3$  molecules dissociated ( $\alpha = [\text{NF}_2]/[\text{NF}_3]_0 = [\text{NF}_2]/\rho_{21}[\text{NF}_3]_{01}$ ), and making the identification  $t_p = \rho_{21}t$ , where  $t$  is the laboratory time, gives

$$d\alpha/dt = k_M\rho_{21}^2[\text{M}]_1(1 - \alpha) - k_{-M}\rho_{21}^3[\text{M}]_1[\text{NF}_3]_{01}\alpha^2 \quad (\text{III})$$

where  $\rho_{21} = \rho_2/\rho_1$ , is the density ratio across the shock front, and  $[\text{NF}_3]_{01}$  and  $[\text{M}]_1$  are, respectively, the initial nitrogen trifluoride and total gas concentrations prior to shock compression. Integration of eq III yields

$$\ln \left[ \frac{1 + \alpha\psi^{-1}}{1 - \alpha\phi^{-1}} \right] = a\rho_{21}^2[\text{M}]_1k_Mt \quad (\alpha < \phi) \quad (\text{IV})$$

where  $a = (1 + 4/b)^{1/2}$ ,  $b = K_c/\rho_{21}[\text{NF}_3]_{01}$ ,  $\psi = (a + 1)b/2$ , and  $\phi = (a - 1)b/2$ . When the experimental data were plotted as  $\ln \{(1 + \alpha\psi^{-1})/(1 - \alpha\phi^{-1})\}$  vs.  $t$ , linear plots were obtained for small values of  $\alpha$ , and second-order rate constants,  $k_M$ , were evaluated from the slopes of such plots for  $\alpha < 0.1$ . For larger values of  $\alpha$  the plots become nonlinear as secondary reactions become important and eq IV is no longer obeyed. This onset of curvature was used as a cut-off point for rate data evaluation. The results of this study are listed in Table II<sup>13</sup> where  $W_1$  denotes the shock Mach number,  $T_2$  the reaction temper-

(10) JANAF Thermochemical Tables, Nat. Stand. Ref. Data Ser., Nat. Bur. Stand., No. 37 (1971).

(11) A. Kennedy and C. E. Colburn, J. Chem. Phys., 35, 1892 (1961).

(12) D. A. Armstrong and C. L. Holmes, Comp. Chem. Kin., 4, 178 (1972).

(13) R. W. Diesen, J. Phys. Chem., 72, 108 (1968).

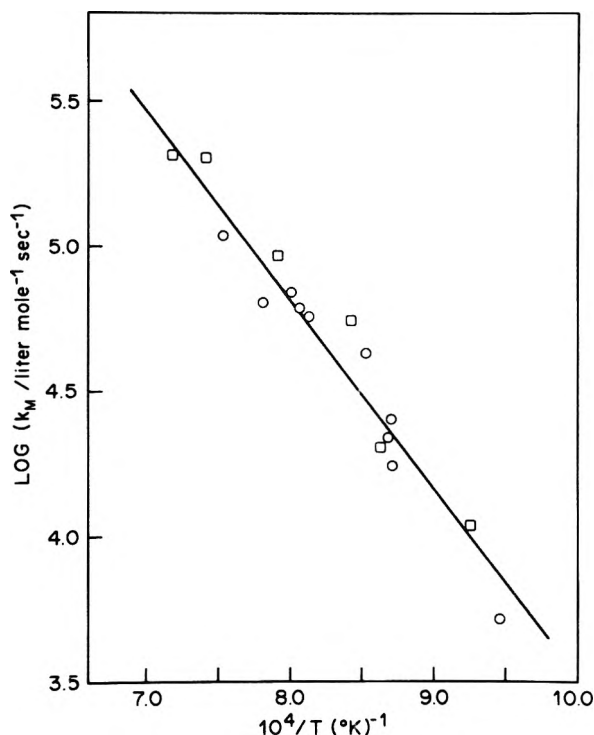


Figure 1. Temperature dependence of the second-order rate constants,  $k_M$ : squares, experiments with 1% NF<sub>3</sub> in argon; circles, experiments with 2% NF<sub>3</sub> in argon.

TABLE II: Kinetic Data

Run	$W_1$	$T_2, ^\circ\text{K}$	$\rho_{21}$	$10^2[M], M$	$10^{-4}k_M, M^{-1} \text{sec}^{-1}$
NF <sub>3</sub> /Ar = 0.01					
1	2.90	1080	3.07	4.65	1.11
2	3.20	1159	3.16	4.95	2.04
3	3.28	1184	3.16	3.01	5.50
4	3.60	1263	3.25	3.10	9.43
5	3.90	1349	3.35	3.06	19.98
6	4.07	1389	3.35	3.10	21.06
NF <sub>3</sub> /Ar = 0.02					
7	2.86	1057	3.14	6.93	0.52
8	3.19	1147	3.25	3.09	1.74
9	3.20	1148	3.26	3.13	2.56
10	3.22	1153	3.27	3.12	2.22
11	3.28	1170	3.28	3.14	4.28
12	3.49	1229	3.33	3.13	5.88
13	3.54	1238	3.34	3.21	6.11
14	3.58	1248	3.37	3.21	7.00
15	3.68	1280	3.37	3.18	6.58
16	3.87	1328	3.43	3.23	11.02

ature, and  $[M]$  is the total concentration of the shocked gas.

The temperature dependence of the rate constants is shown in Figure 1, and the least-squares line gives the Arrhenius equation  $k_M (M^{-1} \text{sec}^{-1}) = 10^{10.10 \pm 0.02} \exp[-(30.1 \pm 2.3 \text{ kcal mol}^{-1})/RT]$  where the error limits are standard deviations. The reaction order with respect to argon concentration was determined from a plot of  $\log k_1$  vs.  $\log [M]$  at constant temperature, where  $k_1$  is now a first-order rate constant obtained by multiplying  $k_M$  by total concentration ( $k_1 = k_M[M]$ ). For this purpose the rate constants in Table II at differing concentrations were corrected to the reference temperature of 1146°K using the

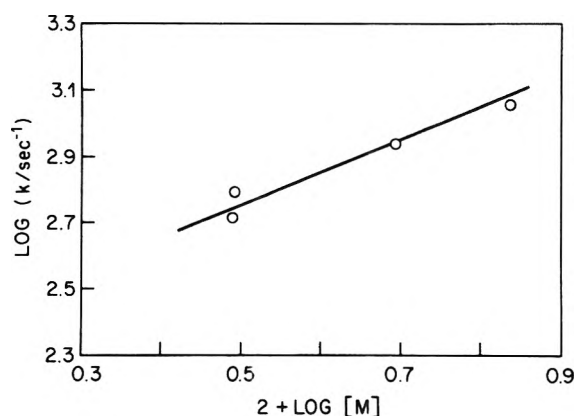


Figure 2. The dependence of the first-order rate constants  $k_1$ , on the concentration  $[M]$  ( $M$ ) at 1146°K.

activation energy determined in Figure 1. The slope of the data in Figure 2 indicates an approximate first-order dependence on argon (slope = 0.93). It may be noted that the pressure range in this study was limited by low absorption signals below 2.7 atm and by pressure limitations of the shock tube above 6.0 atm commensurate with high temperatures.

## Discussion

The validity of the assumption that secondary reactions are negligible over the temperature-time regime of this study was checked by numerical integration of the coupled differential rate equations corresponding to reaction 1 and reactions 3-7, using the Treanor-Runge-Kutta (TRK) method. For this calculation rate coefficients listed in Table I and the rate constant for reaction 1 determined in this study were used. The time dependence of the predicted NF<sub>2</sub> concentration was then compared with the experimental results. This comparison is shown as the solid line in Figure 3. As can be seen, for short times and hence small  $\alpha$  the agreement is good which confirms that the rate constant determined is that for NF<sub>3</sub> decomposition. Variation of the rate constants for reactions 3-7 by a factor of 2 had little effect on the calculated "theoretical" line for short times ( $t \leq 30 \mu\text{sec}$ ). Larger variations in the rate constants do, of course, produce a departure from linearity at somewhat shorter times. Perhaps the most uncertain value in Table I is the disproportionation rate constant, reaction 6, which was arbitrarily chosen as  $1/10$  of the recombination rate in the limit of high pressures. Since disproportionation/recombination ratios are usually less than unity, an upper limit for the disproportionation rate constant is obtained by setting it equal to the recombination rate,  $k_6 = K_5 k_{-5}^\infty \approx 4.3 \times 10^7 M^{-1} \text{sec}^{-1}$ , where  $K_5$  is the equilibrium constant for reaction 5 and  $k_{-5}^\infty$  is the rate constant for dissociation of N<sub>2</sub>F<sub>4</sub> in the high-pressure limit.<sup>6</sup> Using this value of  $k_6$  the TRK calculations showed a departure from linearity of the plot in Figure 3 at  $\sim 20 \mu\text{sec}$ , where the experimental data is linear. This further confirms the validity of the assumption that secondary reactions are unimportant in this system for reaction times  $t \leq 30 \mu\text{sec}$ .

The apparent activation energy of 30 kcal mol<sup>-1</sup> is well below the N-F bond dissociation energy in NF<sub>3</sub>. This is not an uncommon feature for small molecules;<sup>14,15</sup> for ex-

(14) J. H. Kiefer, *J. Chem. Phys.*, **57**, 1938 (1972).

(15) R. L. Belford and R. A. Strehlow, *Annu. Rev. Phys. Chem.*, **20**, 247 (1969).

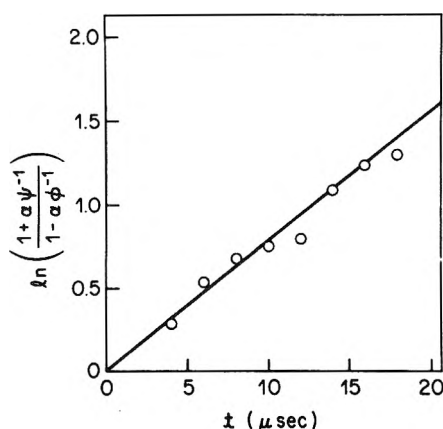


Figure 3. Plot of the integrated rate expression, eq IV: circles, experimental data from experiment 10; solid line, theoretical computation using Treanor-Runge-Kutta method (see text).

ample, this trend has also been observed in the decomposition of the triatomic  $\text{NF}_2^7$  and the tetratomic  $\text{C}_2\text{N}_2$ .<sup>16</sup> Although a decrease in activation energy in the second-order region is predicted by all theories of unimolecular reactions, the energy difference in these cases is larger than can be accounted for by these theories.

For example, when the  $\text{NF}_3$  bimolecular rate constants are fitted to the classical collision theory expression in the form<sup>17</sup>

$$k_M = [PZT^{1/2}/(n/2!)](E_0/RT)^{n/2} \exp(-E_0/RT)$$

with a critical energy of  $E_0 \approx 57 \text{ kcal mol}^{-1}$ , a value of  $n = 24$  is obtained for the number of square terms of internal energy effective in dissociation which exceeds the theoretical maximum value of 15. Alternatively, with  $n = 15$  the predicted dissociation energy is found to be  $46 \text{ kcal mol}^{-1}$  which is too low to be attributed to experimental error.

In a recent paper by Kiefer,<sup>14</sup> similarly low apparent activation energies in diatomic molecules were treated theoretically. His results indicated that the apparent low activation energy can be attributed to the effect of vibrational to vibrational energy transfer which causes a serious depression in the rate at high temperatures and a slight increase in the rate at low temperatures. It was also pointed out that such intermolecular relaxation processes could account for low apparent activation energies in small polyatomic molecules. However, a theoretical treatment does not appear feasible at present, since the participation of the additional vibrational modes greatly complicates the problem.

It is, therefore, concluded that the observed apparent activation energy bears no direct relation to any theoretical thermochemical quantity but is to be viewed strictly as an empirical kinetic parameter, which is useful in describing the dissociation of small molecules.

(16) M. W. Slack, E. S. Fishburne, and A. R. Johnson, *J. Chem. Phys.*, **54**, 1652 (1971).

(17) R. Fowler and E. A. Guggenheim, "Statistical Thermodynamics," Cambridge University Press, Cambridge, England, 1956.

## Flash Photolysis of Aromatic Sulfur Molecules<sup>1</sup>

F. C. Thyron<sup>2</sup>

Davy Faraday Research Laboratory of the Royal Institution, London W 1X 4 BS, England (Received December 22, 1972)

Publication costs assisted by Louvain University

A transient absorption spectrum with a maximum at 297 nm and a continuous band up to 520 nm has been observed after flash photolysis of thiophenol and unsubstituted sulfides in solution and has been attributed to the phenylsulfur radical. Substituted sulfides show similar transients with a shift to longer wavelengths. Sulfoxides displayed a spectrum with a short wavelength band at 312 nm. Absorption spectra of the triplet states of thionaphthene, dibenzothiophene, thioxanthene, and thianthrene have been recorded. Kinetic studies of the radicals reactivity and triplet decay are described.

Many attempts to detect organic sulfur radicals have been already reported.<sup>3</sup> Some of them were based on determinations of molecular weight, light absorption, and magnetism by the monovalent sulfur radicals after thermal or photochemical dissociation of disulfides. The results were not convincing since the analytical methods used to detect the expected small amounts of free radicals were too inaccurate.

More recently Schmidt and coworkers<sup>4</sup> succeeded in isolating several arylsulfur radicals by photolysis of aro-

matic disulfides or mercaptans in the gaseous state followed by quenching at 77 K.

Photolysis of diaryl disulfides in solution has shown the interaction of two PhS fragments to form thiophenyl-thio-

(1) Presented at the 5th Symposium on Organic Sulfur Chemistry, Lund, 1972.

(2) Present address: département de chimie, Université de Louvain, B-1348 Louvain-la-Neuve, Belgium.

(3) See M. J. Janssen in "Organosulfur Chemistry," Interscience, New York, N.Y., 1967, and references therein.

(4) U. Schmidt, A. Müller, and K. Markau, *Chem. Ber.*, **97**, 405 (1964).



phenol type compounds  $\text{PhSC}_6\text{H}_4\text{SH}$ .<sup>5</sup> Mercaptans and disulfides are well-established dehydrogenating agents. They inhibit, for instance, radiation-induced reduction of benzophenone by 2-propanol.<sup>6</sup> The mechanism would imply the existence of a thiyl radical. In the gas phase, an absorption band at wavelengths lower than 310 nm was attributed to the phenylsulfur radical by several authors.<sup>7,8</sup> All these features indicate the existence of PhS but, in contrast to phenoxy radicals, no observations have so far been reported of such species stable at room temperature.

We have applied the method of flash spectroscopy to further studies of the photochemical dissociations of aromatic sulfides and mercaptans. The absorption spectrum of the phenylsulfur radical may be unequivocally identified by studies of the changes produced in its spectrum by substitution of chlorine and amino groups. The results have been compared with those obtained in flash photolysis of diphenyl disulfide and several sulfoxides. In order to verify the stability of the C-S bond in a ring, the transient spectra of several polycyclic molecules were recorded.

### Experimental Section

Experiments were conducted in solutions aerated or thoroughly degassed by successive freezing and evacuation. To prevent oxidation of oxygen sensitive compounds, the solvents used were flushed with pure nitrogen. The purity of substances was checked by their absorption, fluorescence spectra (spectrofluorimeter MPF2A, Perkin-Elmer), or melting point. Furthermore, the absorption spectrum of each solution was taken before and after flashing. When decomposition was too high, a new solution was prepared before each flash. Solutions of various pH were prepared with sulfuric acid, potassium mono or dihydrogen orthophosphate, sodium hydrogen carbonate, and sodium hydroxide. pH values were checked with a potentiometer. The flash photolysis apparatus employed two rare gas filled photolysis lamps in series with a flash duration of 4-5  $\mu\text{sec}$  and a discharge energy of 1000 J in a 20-cm path length cell. The spectra were photometered on a Joyce-Loeble microdensitometer. Optical density calibration was carried out with a density wedge. Kinetics were studied using a quartz-iodine lamp and two photolysis lamps in series with a flash duration of 5  $\mu\text{sec}$  and a discharge energy of 220 J.

### Results and Discussion

*I. Aryl Derivatives. A. Transient Spectra. 1. Thiophenols.* Flash photolysis of outgassed solutions of thiophenol in various solvents resulted in the appearance of a transient absorption with a short wavelength maximum near 297 nm and a continuous band up to 520 nm (Figure 1a). Increasing the pH from 3 M  $\text{H}_2\text{SO}_4$  solutions to pH 10 slightly increased the optical density without modifying the shape of the absorption.

*p*-Chloro- and *p*-aminothiophenol displayed a spectrum with a more intense long wavelength band (Figure 1b,c). The solvent effect was rather pronounced in the case of the amino compound.

Absorption spectra in aerated solutions were identical but generally less intense than those of outgassed solutions and the intensities of the spectra reached a maximum during or immediately after the flash.

The half-life was about 200  $\mu\text{sec}$ .

*2. Sulfides.* Methyl phenyl sulfide showed nearly the same absorption spectrum as thiophenol (Figure 2a). Di-

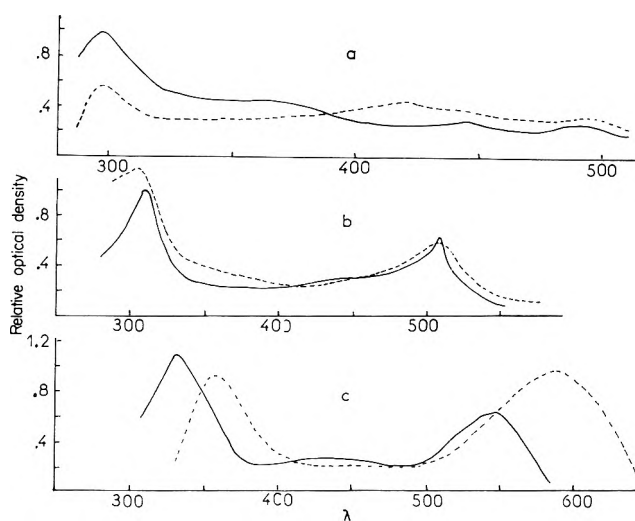


Figure 1. Transients observed from thiophenol (a), *p*-chlorothiophenol (b), and *p*-aminothiophenol (c) in  $\text{C}_6\text{H}_{12}$  (—) and EtOH (---).

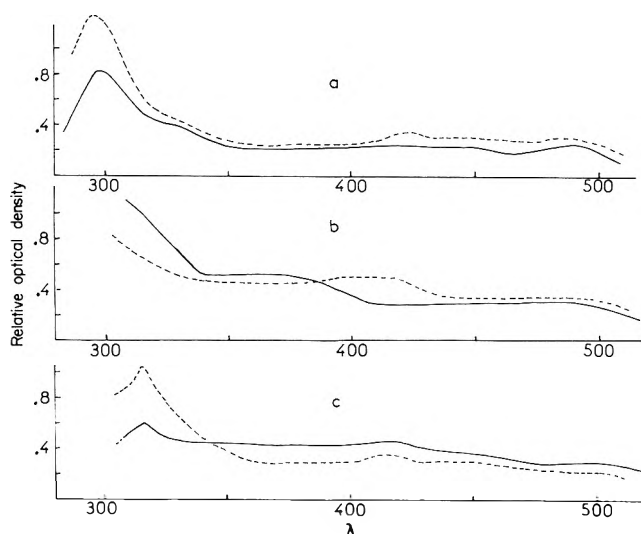


Figure 2. Transients observed from methyl phenyl sulfide (a), diphenyl sulfide (b), and benzyl phenyl sulfide (c) in  $\text{C}_6\text{H}_{12}$  (—) and EtOH (---).

phenyl and benzyl phenyl sulfides (Figure 2b,c) did not display the maximum at 297 nm due to absorption of the parent compounds. Benzyl phenyl sulfide showed an additional sharp band at 317 nm which disappeared quite rapidly in outgassed solutions ( $\sim 50 \mu\text{sec}$ ) and was absent in aerated solutions. From previous work,<sup>9</sup> this band can be attributed to the benzyl radical.

*3. Diphenyl Disulfide.* Diphenyl disulfide displayed a band at 352 nm, insensitive to pH and hardly visible in thiophenol and diphenyl sulfide (Figure 3a).

*4. Triphenylsulfonium Chloride.* The absorption spectrum was observed from 340 nm and consisted of a broad maximum at 370 nm and a continuous absorption up to 620 nm (Figure 3b). The decay time was shorter than 50  $\mu\text{sec}$ .

- (5) Scheafsmu, A. F. Bickel, and E. C. Kooyman, *Tetrahedron*, **10**, 76 (1960).
- (6) W. V. Sherman and S. G. Cohen, *J. Phys. Chem.*, **70**, 178 (1966).
- (7) G. Porter and F. J. Wright, *Trans. Faraday Soc.*, **51**, 1469 (1955).
- (8) R. G. W. Norrish and A. P. Zeelenberg, *Proc. Roy. Soc., Ser. A*, **240**, 293 (1967).
- (9) G. Porter and M. W. Winsor, *Nature (London)*, **180**, 187 (1957).

TABLE I: Second-Order Decay Constants of Transients

Parent molecule	Solvent	$k/\epsilon$ , $\text{cm sec}^{-1}$	$k$ , $M^{-1} \text{sec}^{-2}$ ( $\epsilon = 340$ )	$k_c = 8RT/$ $3000\eta$
Diphenyl sulfide	$C_6H_{14}$	$8.2 \times 10^6$	$2.8 \times 10^9$	$2 \times 10^{10}$
Benzyl phenyl sulfide	$C_6H_{14}$	$1.5 \times 10^7$	$5.1 \times 10^9$	$2 \times 10^{10}$
	EtOH-H <sub>2</sub> O (1:1)	$4 \times 10^6$	$1.4 \times 10^9$	$5.9 \times 10^9$
	EtOH	$3.4 \times 10^6$	$1.2 \times 10^9$	$5.4 \times 10^9$
	Glycerol (95%) or	$6 \times 10^5$ $3.5 \times 10^4$		
Diphenyl sulfoxide	EtOH	$4.5 \times 10^6$		
4,4'-Ditolyl sulfoxide	EtOH	$3 \times 10^6$		

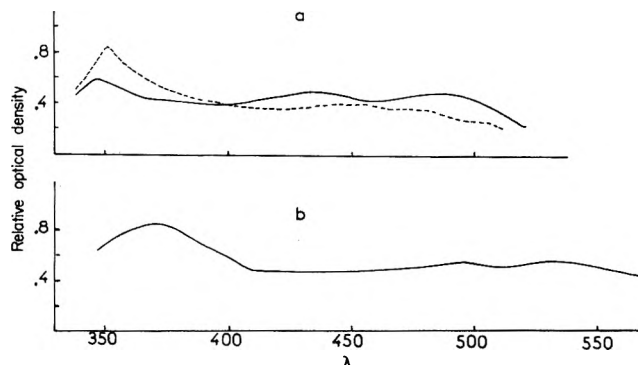


Figure 3. Transients observed from diphenyl disulfide (a) in  $C_6H_{12}$  (—) and EtOH-H<sub>2</sub>O 1:1 (---) and from triphenylsulfonium chloride (b) in H<sub>2</sub>O.

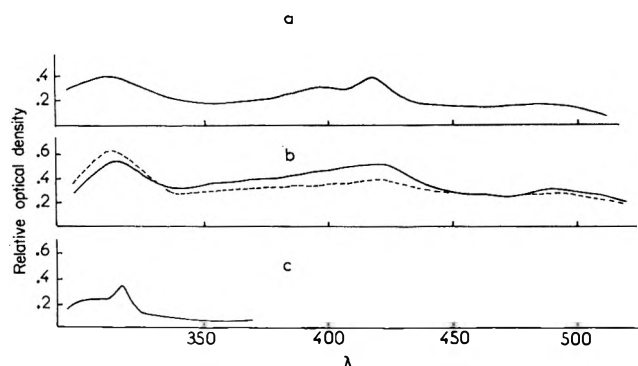


Figure 4. Transients observed from diphenyl sulfoxide (a) in EtOH, 4,4'-ditolyl sulfoxide (b) in  $C_6H_{12}$  (—) and EtOH (---), and dibenzyl sulfoxide (c) in EtOH.

5. *Sulfoxides.* On photolysis, outgassed solutions of diphenyl and 4,4'-ditolyl sulfoxides produced slightly different spectra (Figure 4a,b) while aerated solutions showed a very weak absorption. The common absorption maximum in polar and nonpolar solvents were localized at 312 and 420 nm. Dibenzyl sulfoxide (Figure 4c) exhibited only one band at 317 nm which is assigned to the benzyl radical.

*B. Decay Kinetics.* We studied the decay of transients at room temperature by following the change in light absorption at their 420–450-nm absorption using the photoelectric flash-photolysis apparatus. The decay curves of intermediates derived upon flashing sulfides and sulfoxides gave excellent second-order plots. Some second-order rate constants are collected in Table I. Both  $k$  values in glycerol solution of benzyl phenyl sulfide were calculated assuming a two component decay curve (Figure 5, lower

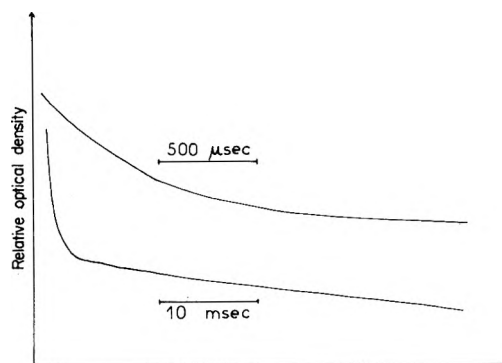


Figure 5. Decay of transient observed at 450 nm from benzyl phenyl sulfide in 95% glycerol solution.

curve). The initial rate of decay (upper curve) was many times faster than the rate of total decay. If the system is initially populated with a random distribution of radicals, some pairs of radicals will be situated close together and will react rapidly. Hence, the measured initial rate constant will be high and will decrease with time as such pairs are consumed. Ultimately, a steady state will be established in which the rate of reaction is limited by the rate of diffusion of radicals toward one another. In this case, we should be able to estimate the extinction coefficient of the radical assuming a diffusion-limited reaction. This hypothesis gave the molar extinction coefficient at 450 nm as 340 in 95% glycerol solution at room temperature. This value allows us to determine the recombination rate constants  $k$  assuming that the extinction coefficient is the same in all solvents. The diffusion-controlled rate constants,  $k_c$ , calculated using the Debye formula  $k_c = 8RT/3000\eta M^{-1} \text{sec}^{-1}$  are also given for comparison. The difference between the experimental and the diffusion-controlled rates may be attributed to a small activation energy of recombination.

*C. Assignment of the Transient Spectra.* The two most probable assignments for the transient spectra in sulfides would be to the phenylsulfur radical  $C_6H_5S\cdot$  or to a phenylsulfur radical ion. The observed independence of solvent, pH, and ionic strength argues against a radical-ion assignment. The absorption spectrum is attributed to the neutral phenylsulfur radical for the following reasons.

(a) The position of its absorption is similar to the spectra of isoelectronic radicals such as benzyl, phenoxy, and anilino. The absorption spectra of these radicals consist of two separate systems: a sharp band around 300 nm and another transition near 400 nm of varying intensity and sharpness for the three types of radicals.

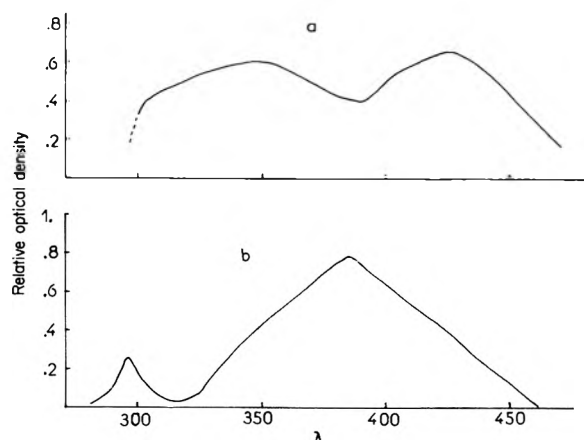


Figure 6. Transients absorption spectra: (a) benzothiophene,  $2 \times 10^{-5} M$  in EtOH, (b) dibenzothiophene,  $5 \times 10^{-6} M$  in EtOH.

(b) The absorption is common to the photolysis of different molecules.

(c) The longer wavelength light absorption of the *p*-aminophenylsulfur radical is attributed to the stabilization of the radical by an electron-donating group in para position.<sup>4</sup>

(d) All the sulfides showed a permanent absorption at  $\lambda < 340$  nm after flashing. This absorption which was much stronger in polar media and in concentrated solutions of the parent compounds has been identified with the absorption spectrum of diphenyl disulfide. In the case of thiophenol, however, the permanent absorption was more intense in cyclohexane. It has been estimated that about 10% of the original  $5 \times 10^{-4} M$  of mercaptan reacted to form disulfide.

The assignment of the absorption bands to a phenylsulfur radical is in contradiction with that postulated by Gaspari and Granzow<sup>10</sup> who observed a transient spectrum with maximum at  $\sim 420$  nm identified as arising from the  $RSSR^-$  radical anion upon photolyzing aqueous solutions of thiophenol.

A few more comments are necessary in the case of *p*-aminothiophenol. The half-life was about ten times higher in ethanol ( $\sim 500 \mu\text{sec}$ ) than in cyclohexane. The permanent absorption was intense in cyclohexane but quite low in ethanol. Furthermore, a reversible decrease in optical density of the parent compound at 295 nm has been related to the simultaneous appearance of strong optical density at 360 nm in ethanol solutions. If the parent compound undergoes only decomposition to the thiyl radical under flash photolysis, this would give 9000 as the maximum value of  $\epsilon$  at 360 nm.

The assignment of radical spectra in 4,4'-ditolyl and diphenyl sulfoxides will be now considered. These spectra show a common band at 312 and 420 nm and a shape similar to that observed in sulfides. We assume, then, that the absorbing species is isoelectronic to that observed in sulfides. The slight difference observed in radical absorption when irradiating sulfoxides and the oxygen effect as well as the absence of the common absorption spectrum in the case of dibenzyl sulfoxide led us to conclude that the radical species was not the thiophenyl radical but could be attributed to the sulfinyl radical  $C_6H_5SO\cdot$ . Several results from mass spectrometry<sup>11</sup> and classical photolysis<sup>12</sup> of sulfoxides suggested the existence of the sulfinyl radical which was thought to be rather stable by analogy with the isoelectronic nitroxide radical  $R_2NO\cdot$ .

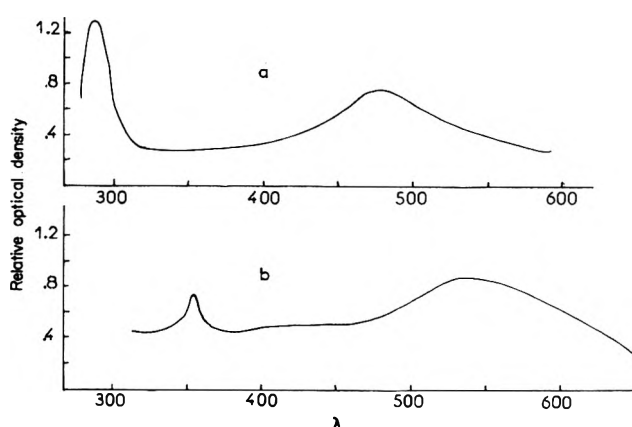


Figure 7. Transients absorption spectra of (a) thianthrene,  $2 \times 10^{-6} M$ , in EtOH, and (b) thioxanthene,  $2 \times 10^{-5} M$ , in EtOH.

**II. S-Containing Polycyclic Molecules.** Strong absorptions were recorded in carefully outgassed solutions of thionaphthene, dibenzothiophene, thioxanthene, and thianthrene (Figures 6 and 7). From spectrographic experiments the lifetimes seemed to be the same at both maxima excepting thioxanthene where the lifetime at 355 nm was five-ten times longer. The decay of transients was studied with the photoelectric apparatus and followed a first-order process with the lifetimes indicated in Table II. Thioxanthene, however, showed a second-order decay at 355 nm. Since this band was always observed in conjunction with the long wavelength band, this absorption could be due to a radical species arising from the decomposition of the triplet state or of another state which gives rise to the triplet state.

The nature of the transient was identified as a triplet state by the following spectrographic flash photolysis experiment. With a solution containing both sulfur compound and anthracene, the transient absorption disappeared and the triplet-triplet absorption of anthracene was observed. From the results of Table II, it can be seen that the lifetimes in ethanol solutions decrease with the number of sulfur atoms and the number of rings. In the last column of Table II are listed the triplet lifetimes found by Bonnier and Jardon<sup>13,14</sup> who studied the phosphorescence of biacetyl or benzil sensitized by various concentrations of S heterocyclic molecules in cyclohexane. There is only a maximum factor of 4 between the two series of values.

TABLE II:  $\lambda_{\text{max}}$  and Mean Lifetimes of Transients in Some S Heterocyclic Molecules

	$M^{-1}$ (in EtOH)	$\lambda_{\text{max}}$	Transients	
			$\tau$ , $\mu\text{sec}$	$\tau$ , <sup>a</sup> $\mu\text{sec}$
Thionaphthene	$1.4 \times 10^{-5}$	343, 425	108	232
Dibenzothiophene	$5 \times 10^{-6}$	296, 384	86	20.3
Thioxanthene	$2 \times 10^{-5}$	355, 535	58 (535 nm)	40.4
Thianthrene	$5 \times 10^{-6}$	287, 475	49	172

<sup>a</sup> References 13 and 14.

- (10) G. Gaspari and A. Granzow, *J. Phys. Chem.*, **74**, 836 (1970).
- (11) C. Nolde, J. Masden, S. O. Lawesson, and J. H. Bowie, *Ark. Kemi.*, **31**, 481 (1969).
- (12) D. K. Emerson, Ph D. Thesis, Case Western University, 1968.
- (13) J.-M. Bonnier and P. Jardon, *J. Chim. Phys.*, **66**, 1506 (1969).
- (14) J.-M. Bonnier and P. Jardon, *J. Chim. Phys.*, **68**, 432 (1971).
- (15) F. W. Lampe and R. N. Noyes, *J. Amer. Chem. Soc.*, **76**, 2140 (1954).
- (16) D. C. Frost, F. G. Herring, A. Katrib, C. A. McDowell, and R. A. N. McLean, *J. Phys. Chem.*, **76**, 1030 (1972).

## Conclusions

Photolysis of sulfides results in a bond scission generally confined to the C-S bond, except in the case of thiophenol where S-H scission is favored probably due to the solvent cage effect.<sup>15</sup> The phenylsulfur radical seems more stable than the benzyl radical. It has been recognized that the sulfur lone pair in thiophenol exhibits a considerable amount of  $\pi$  interaction with the adjacent benzene ring<sup>16</sup> and this interaction should stabilize the thiyl radical. The stability of PhS is increased when electron-donating

groups are substituted in the para position. It is rather insensitive to oxygen while the sulfinyl radical PhSO is more sensitive. Irradiation of S heterocyclic compounds produces triplet states with lower lifetimes than those of their aromatic analogs. This observation agrees with the smaller degree of conjugation and stabilization of the  $\pi$  systems across the heteroatom junction.

*Acknowledgments.* The author is grateful to Professor G. Porter for hospitality at the Davy Faraday Laboratory and for fruitful discussions with him and his coworkers.

## Photo-Induced Decarboxylation of Aliphatic Acids and Esters in Solution. Dependence upon State of Protonation of the Carboxyl Group

Lalitha J. Mittal,<sup>1a,b</sup> J. P. Mittal,<sup>1a</sup> and E. Hayon\*

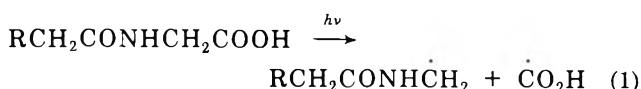
Pioneering Research Laboratory, U. S. Army Natick Laboratories, Natick, Massachusetts 01760 (Received November 10, 1972)

Publication costs assisted by U. S. Army Natick Laboratories

The flash photolysis of oxygen-free aqueous solutions of simple aliphatic acids and esters has been studied. Acetic acid, malonic acid, dimethyl malonate, and diethyl malonate have been examined in detail. In all these cases, the major photolytic process observed was the rupture of the C-COOH or C-COOR bond. The  $\cdot\text{COOH}$  radical was observed from acetic acid, the  $\cdot\text{COOH}$  and  $\cdot\text{CH}_2\text{COOH}$  radicals from malonic acid, and the  $\cdot\text{CH}_2\text{COOR}^1$  radical from dimethyl and diethyl malonate:  $\text{RCOOH} + h\nu \rightarrow \text{R}\cdot + \cdot\text{COOH}$ ;  $\text{RCOOR}^1 + h\nu \rightarrow \text{R}\cdot + \cdot\text{COOR}^1$ . The  $\cdot\text{COOR}^1$  radicals decay very fast, with  $\tau < 10 \mu\text{sec}$  in water, to give  $\text{R}\cdot$  and  $\text{CO}_2$ . On ionization of these acids the quantum yield for this photolytic process is reduced to zero. For acetic acid the  $\phi$  was found to follow exactly the  $\text{p}K_a = 4.76$  of the ground-state molecule, and for malonic acid the  $\phi$  follows the first  $\text{p}K_a = 2.83$  of the ground-state molecule. While photodecomposition of the dissociated acids occurs in aqueous solution, no transient absorption could be observed. The  $\phi$  for the decomposition of the esters was independent of pH in the examined range 1.5–8.0. The photolysis of diethyl malonate produced strong absorptions with  $\lambda_{\text{max}} \sim 268 \text{ nm}$  suggested to be the result of a Norrish type II reaction. The intermediates produced from the flash photolysis of the keto acids, pyruvic, ethyl pyruvate, and benzoylformic acids are briefly described. No intermediates were observed from the photolysis of acetamide and malonamide.

## Introduction

In the study of the action of uv light on peptides and proteins, the photochemistry of end groups (*e.g.*, the carboxyl group) may play a significant role in the inactivation of enzymes. This is of particular interest since it was recently found<sup>2</sup> that  $\text{CH}_3\text{COOH}$  and  $\text{HCOOH}$  in water phosphoresce at 77°K and have a triplet energy level (0,0) of  $\sim 80 \text{ kcal}$ . Furthermore, in a study of the direct optical excitation of aliphatic amino acids and peptides in aqueous solution it was found<sup>3</sup> that the major intermediates observed on flash photolysis were formed from a photo-induced decarboxylation reaction



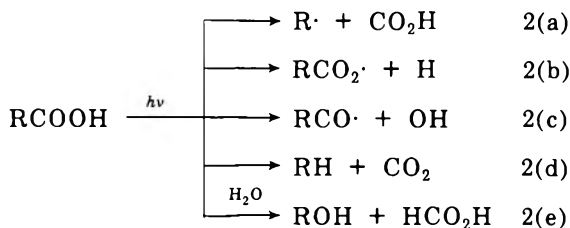
Very little work appears to have been done on the photochemistry of simple aliphatic acids and esters and their corresponding salts in solution.<sup>4</sup> None of the primary processes have been established, the nature of the excited state precursors are not known, and indeed the electronic transitions which these molecules undergo have not been clearly defined. One of the reasons for this lack of information must be due to the fact that the carboxyl group

- (1) (a) Permanent address, Bhabha Atomic Research Center, Trombay, Bombay, India. (b) This work is based on a dissertation to be submitted in partial fulfillment of the Ph.D. degree, University of Bombay, Bombay, India.
- (2) L. W. Johnson, H. J. Maria, and S. P. McGlynn, *J. Chem. Phys.*, **54**, 3823 (1971).
- (3) L. J. Mittal, J. P. Mittal, and E. Hayon, *Photochem. Photobiol.*, submitted for publication.
- (4) J. G. Calvert and J. N. Pitts, Jr. in "Photochemistry," Wiley, New York, N. Y., 1966, p 427.

absorbs in the far-uv region, a hitherto experimentally difficult region.

The absorption spectra<sup>5-8</sup> of aliphatic acids and esters (e.g.,  $\text{CH}_3\text{COOH}$  and  $\text{CH}_3\text{COOC}_2\text{H}_5$ ) in aqueous solution show a maxima at  $\sim 204$  nm, whereas the sodium salts (e.g.,  $\text{CH}_3\text{COONa}$ ) have a slightly lower absorption down to  $\sim 215$  nm, show no maxima at  $\sim 204$  nm, and continue to absorb strongly at shorter wavelengths ( $\lambda_{\text{max}} < 180$  nm). The weak absorption of  $\text{RCOOH}$  and  $\text{RCOOR}^1$  compounds from  $\sim 250$  nm, and increasing with decrease in wavelength, is associated with  $n \rightarrow \pi^*$  singlet-singlet excitation involving a nonbonding electron on the carbonyl linkage, and the intense absorption at  $\sim 205$  nm is thought to be associated with a  $\pi \rightarrow \pi^*$  excitation. The absorption spectrum of  $\text{HCOO}^-$  has been suggested<sup>2,8</sup> to be a  $n \rightarrow \pi^*$  electronic transition.

The photochemistry of unsubstituted aliphatic carboxylic acids has been explained on the basis of one or more of the primary processes 2a-e. None of these reactions have been established. In the photolysis of aqueous solutions of acetic acid, methane, carbon dioxide, methanol, and formic acid have been found<sup>9-11</sup> among the permanent products.



In this work, the intermediates formed on flash photolysis of oxygen-free aqueous solutions of acetic acid, malonic acid, malonamide, dimethyl malonate, and diethyl malonate have been observed. The dependence of the formation of these intermediates upon the acid-base properties of the carboxyl group has been investigated. The dependence of the concentration of these intermediates upon the intensity of the exciting light has also been studied to determine whether one or two photons are required for their formation. Finally, preliminary results on the flash photolysis of some keto acids in aqueous solution are reported.

### Experimental Section

The flash photolysis set-up used for this investigation has been described elsewhere.<sup>12</sup> Briefly, the flash has a lifetime  $\tau_{1/2} \sim 10$   $\mu\text{sec}$  and an intensity of 2000 J. The light output has been shown to be directly proportional to the charging voltage at constant capacitance. The test for the monophotonic-biphotonic nature of the intermediates observed was done by varying the voltage across the flash lamps from  $\sim 17$ -23 kV. The values of  $I$  given below and in the figures are proportional to light intensity and refer to the (voltage)<sup>2</sup> (e.g.,  $I = 290$  or  $I^2 = 784$ , the  $10^3$  (or  $10^6$ ) V factor was dropped for convenience).

Jacketed quartz optical cells were used, with an optical path length of 20 cm. Water was placed in the outer jacket of the cells. Solutions were prepared using triply distilled water which was further purified by radiolysis and photolysis. Degassing of the solutions was done by bubbling prepurified nitrogen gas through a glass frit in a bubbler for  $\sim 45$  min.

All the chemicals used were the highest grade commercially available. Diethyl malonate was redistilled. Chemi-

cals were supplied by Eastman Chemicals, Baker and Adamson, and Mallinckrodt. Solutions were buffered with perchloric acid, phosphates ( $\sim 1$  mM), tetraborate ( $\sim 1$  mM), and potassium hydroxide.

### Results and Discussion

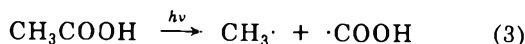
It should be stated at the outset that the observation of the absorption spectra of free radicals and intermediates using the technique of flash photolysis does not necessarily reveal all the photolytic processes which a molecule undergoes. Free radicals with very low extinction coefficients, short lifetimes, or absorption in the far uv or near ir may not be detected due to experimental limitations.

Unless stated otherwise, all the systems examined have been photolyzed using  $1 \times 10^{-2}$  M concentration of the acids, the same light intensity from the flash lamps, and a water filter in the outer jacket of the quartz optical cell.

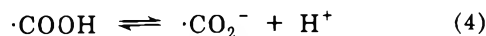
#### Acetic Acid

The flash photolysis of oxygen-free  $1 \times 10^{-2}$  M aqueous solutions of acetic acid ( $\text{p}K_a = 4.76$ ) at pH 1.95 gives rise to a transient absorption which increases rapidly below 300 nm, see Figure 1. Due to the absorption of the ground-state acetic acid and the 20-cm optical path of the cell used, it was not possible to record the transient spectrum below 255 nm. The spectrum in Figure 1 resembles the absorption spectrum of the  $\cdot\text{CO}_2\text{H}$  radical obtained<sup>13</sup> from the pulse radiolysis studies, with  $\lambda_{\text{max}}$  235 nm and  $\epsilon_{\text{max}}$   $3.0 \times 10^3$   $M^{-1}$   $\text{cm}^{-1}$ . On normalization of the  $\cdot\text{CO}_2\text{H}$  spectrum upon the spectrum obtained in the flash photolysis of acetic acid, a perfect agreement can be observed (see Figure 1).

The occurrence of reaction 3 is therefore demonstrated



The carboxyl radical undergoes acid-base reactions and has<sup>14</sup> a  $\text{p}K_a \sim 1.4$ .



The optical spectra of the  $\cdot\text{COOH}$  and  $\text{CO}_2^-$  radicals have been found<sup>13</sup> to be experimentally indistinguishable. From the extinction coefficient obtained<sup>13</sup> for this radical, the bimolecular decay kinetics of the  $\cdot\text{COOH}$  radical was found to be  $2k = 2.0 \times 10^9$   $M^{-1}$   $\text{sec}^{-1}$  (see Table I), in good agreement with the value of  $1.5 \times 10^9$   $M^{-1}$   $\text{sec}^{-1}$  determined<sup>13</sup> in the pulse radiolysis work. Based<sup>13</sup> on  $\epsilon_{270}$   $1700$   $M^{-1}$   $\text{cm}^{-1}$  for  $\cdot\text{COOH}$ , the concentration of  $\cdot\text{COOH}$  produced per flash under the experimental conditions used is  $0.74$   $\mu\text{M}$ .

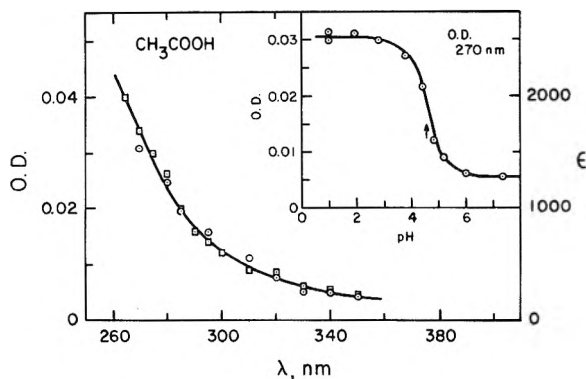
On flash photolysis of  $1 \times 10^{-2}$  M sodium acetate at pH 7.5 an extremely weak absorption was observed. By following the change with pH of the absorbance of the radical at 270 nm, a "titration-type" curve was obtained (see insert to Figure 1) from which a  $\text{p}K = 4.65 \pm 0.1$  was de-

- (5) H. Ley and B. Arends, *Z. Phys. Chem.*, **B4**, 234 (1929).
- (6) L. J. Sidel, *Arch. Biochem. Biophys.*, **54**, 184 (1955).
- (7) E. E. Barnes and W. T. Simpson, *J. Chem. Phys.*, **39**, 670 (1963).
- (8) H. Basch, M. B. Robin, and N. A. Kuebler, *J. Chem. Phys.*, **49**, 5007 (1968).
- (9) L. Farkas and O. H. Wansbrough-Jones, *Z. Phys. Chem.*, **B18**, 124 (1932).
- (10) L. Farkas, *Z. Phys. Chem.*, **B23**, 89 (1933).
- (11) A. D. McLaren and D. Shugar, "Photochemistry of Proteins and Nucleic Acids," Pergamon Press, New York, N. Y., 1964, p 90.
- (12) L. Dogliotti and E. Hayon, *J. Phys. Chem.*, **71**, 2511 (1967); M. Langmuir and E. Hayon, *ibid.*, **71**, 3808 (1967).
- (13) P. Neta, M. Simic and E. Hayon, *J. Phys. Chem.*, **73**, 4207 (1969).
- (14) G. V. Buxton and R. M. Sellers, *J. Chem. Soc., Faraday Trans. 1*, **69**, 555 (1973).

**TABLE I: Absorption Maxima and Decay Kinetics of Radicals Produced in the Photolysis of Aliphatic Carboxylic Acids and Esters in Aqueous Solution**

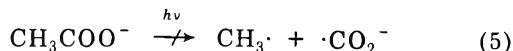
System <sup>a</sup>	pH	$\lambda_{\max}$ , nm	Suggested radical	Decay, $2k/\epsilon^b$	$\epsilon$ , $M^{-1} \text{ cm}^{-1} \text{ c}$	Decay, $2k, M^{-1} \text{ sec}^{-1}$
Acetic acid	2.2	235	$\dot{\text{C}}\text{O}_2\text{H} + \dot{\text{C}}\text{O}_2^-$	$1.2 \times 10^6$ (270)	1700 <sup>d</sup>	$2.0 \times 10^9$
Malonic acid	0.8	315	$\dot{\text{C}}\text{H}_2\text{CO}_2\text{H} + \dot{\text{C}}\text{O}_2\text{H}$	$2.5 \times 10^6$ (310)		<i>e</i>
				$1.0 \times 10^6$ (270)		<i>e</i>
Dimethyl maionate	8.0	320	$\dot{\text{C}}\text{H}_2\text{CO}_2\text{CH}_3$	$3.6 \times 10^6$ (320)	800 <sup>f</sup>	$2.9 \times 10^9$
	2.0	320	$\dot{\text{C}}\text{H}_2\text{CO}_2\text{CH}_3$	$3.8 \times 10^6$ (320)	800 <sup>f</sup>	$3.0 \times 10^9$
Glutaric acid	1.8	235	$\dot{\text{C}}\text{O}_2\text{H} + \dot{\text{C}}\text{O}_2^-$	$1.3 \times 10^6$ (270)	1700 <sup>d</sup>	$2.2 \times 10^9$

<sup>a</sup>  $10^{-2} M$  oxygen-free solutions used. <sup>b</sup> Wavelength at which second-order decay kinetics was measured is given in parentheses. <sup>c</sup>  $\epsilon$  value at wavelength where decay kinetics were measured. <sup>d</sup> From ref 13. <sup>e</sup> Mixed radicals. <sup>f</sup> From ref 22.



**Figure 1.** Transient spectrum observed on flash photolysis of  $\text{O}_2$ -free  $1 \times 10^{-2} M$  aqueous solutions of acetic acid at pH 1.95 (O). Symbols ( $\square$ ) represent normalized spectrum of the  $\text{CO}_2^-$  radical obtained from ref 13. Insert shows dependence upon pH of the absorbance at 270 nm.

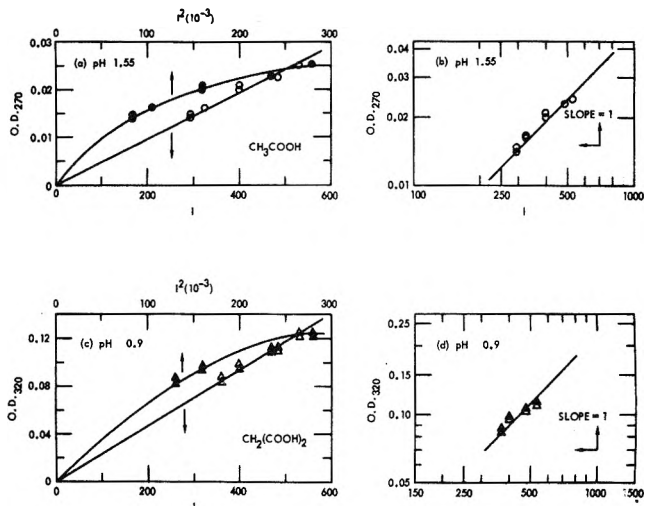
rived. This value is to be compared with the  $pK_a = 4.76$  of acetic acid. It follows from these results that the optical excitation of  $\text{CH}_3\text{COO}^-$  does not rupture the C-C bond according to



Other photolytic reactions are taking place since methane and carbon dioxide are among the products formed<sup>9,10</sup> on photolysis of  $\text{CH}_3\text{COONa}$  at pH 8.5. The reduction in the yield of reaction 3 can be seen, therefore, to follow the change in the concentration of the undissociated acetic acid.

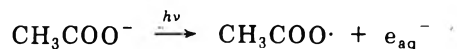
The phosphorescence from both acetic acid and acetate salts in water at 77°K has been reported,<sup>2</sup> with  $\phi_p < 0.01$ . Since the concentration of  $\cdot\text{COOH}$  is relatively high and is apparently formed from the photolysis of  $\text{CH}_3\text{COOH}$  but not from the dissociated acid, it seems unlikely that triplet excited states are involved. However, in the flash photolysis of aliphatic amino acids and peptides it was found<sup>3</sup> that the formation of some of the radicals formed by photodissociation occurred *via* a biphotonic process, indicating the role of the triplet excited state of these molecules as the precursor. The dependence of the  $[\cdot\text{COOH}]$  upon the light intensity from the flash lamps was determined and is shown in Figure 2. The OD at 270 nm *vs.*  $I$  and  $I^2$  is plotted in a linear (curve a) and a log-log (curve b) scale. A slope of 1 was found indicating a monophotonic process for reaction 3. The precursor could still, however, be either a singlet or a triplet excited state.

The absorption of  $\text{CH}_3\text{COO}^-$  has been suggested<sup>5,9</sup> to be an "electron affinity spectrum." The electron affinity of the  $\text{CH}_3\text{COO}\cdot$  radical is 3.2 eV (76 kcal).<sup>15</sup> On flash



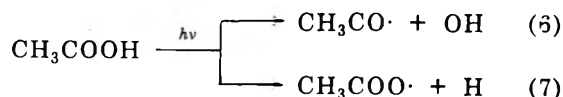
**Figure 2.** Dependence upon light intensity of the concentration of intermediates produced on flash photolysis of  $1 \times 10^{-2} M$  solutions of acetic acid at pH 1.55 (curves a and b, at 270 nm) and malonic acid at pH 0.9 (curves c and d, at 320 nm). Linear and log-log plots are shown for better representation of the experimental data.

photolysis of  $\text{O}_2$ -free  $5 \times 10^{-2} M$  sodium acetate at pH 8.0, no transient absorption at 700 nm due to the hydrated electron,  $e_{\text{aq}}^-$ , could be observed, indicating that on optical excitation at  $\lambda > 200$  nm the reaction

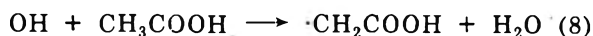


does not occur. Photoionization of the dissociated acid in the far uv (*i.e.*, below 200 nm) could still take place.

Reactions 6 and 7 have also been suggested<sup>9,10</sup>

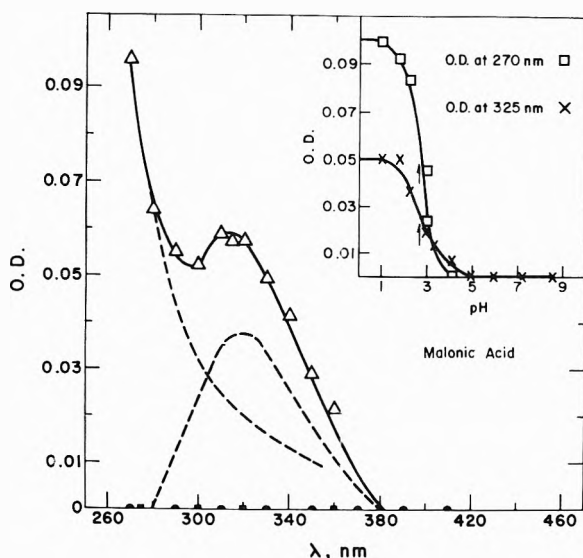


Under the conditions of the experiments, the OH radicals produced would react with acetic acid



with  $k_8 = 2.8 \times 10^7 M^{-1} \text{ sec}^{-1}$  (ref 16). The  $\cdot\text{CH}_2\text{COOH}$  radical has<sup>13</sup> an absorption maximum at 320 nm and  $\epsilon$  650  $M^{-1} \text{ cm}^{-1}$ . No absorption at 320 nm due to this radical could be seen, making the quantum yield of process 6 close to zero. The  $\text{CH}_3\text{COO-H}$  bond is 112 kcal<sup>17</sup> while

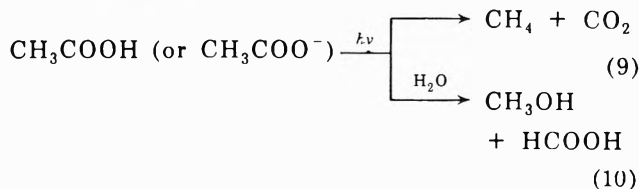
- (15) S. Tsuda and W. H. Hamill, *Advan. Mass Spectrom.*, Pergamon Press, New York, N. Y., 1965.  
 (16) M. Anbar and P. Neta, *Int. J. Appl. Radiat. Isotopes*, **98**, 493 (1967).  
 (17) J. A. Kerr, *Chem. Rev.*, **66**, 496 (1966).



**Figure 3.** Transient spectra observed on flash photolysis of  $O_2$ -free  $1 \times 10^{-2} M$  aqueous solutions of malonic acid at pH 0.8 ( $\Delta$ ) and 9.2 ( $\circ$ ). Spectrum of the  $\cdot CH_2COOH$  (---) and  $CO_2^{\cdot -}$  (---) radicals used to synthesize the experimental curve. Inset shows dependence upon pH of the absorbance at 325 and 270 nm. Symbols ( $\blacksquare$ ) represent results obtained from flash photolysis of  $O_2$ -free  $1 \times 10^{-2} M$  malonamide at pH 6.0.

the C-C bond in  $CH_3-COOH$  is 82.2 kcal,<sup>18</sup> suggesting that process 7 might not be very favorable. However, no experiments could be devised to prove or disprove the presence of process 7.

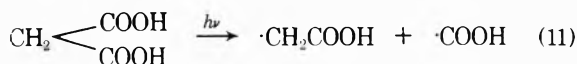
Since  $CH_4$ ,  $CO_2$ ,  $CH_3OH$ , and  $HCOOH$  have been found<sup>9-11</sup> as products in the photolysis of both  $CH_3COOH$  and  $CH_3COO^-$ , these are probably formed *via* reactions



Unfortunately no information is available on the pH dependence of the quantum yields of these products.

### Malonic Acid

The absorption spectrum of malonic acid ( $pK_{a1} = 2.83$ ,  $pK_{a2} = 5.69$ ) in water at pH 0.8 was found to have a maximum at 207 nm,  $\epsilon_{207} 88 M^{-1} cm^{-1}$  and  $\epsilon_{240} 6.0 M^{-1} cm^{-1}$ . Based on the results presented above for the flash photolysis of acetic acid, one would expect a C-C bond rupture, leading to the formation of  $\cdot CH_2COOH$  and  $\cdot COOH$  radicals

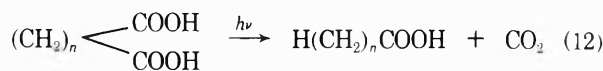


The spectrum produced on flash photolysis of  $1 \times 10^{-2} M$  malonic acid at pH 0.8 is shown in Figure 3. This spectrum is made up of the sum of the absorptions of the  $\cdot CH_2COOH$  and  $\cdot COOH$  radicals; indeed the experimental curve was synthesized from equimolar concentrations of these two radicals (see Figure 3), based on spectra obtained<sup>13</sup> independently. From these results,  $[\cdot CH_2COOH] = [\cdot COOH] = 2.3 \mu M$ .

On photolysis of the dianion of malonate at pH 9.2, no transient absorption could be seen (Figure 3). The change in absorbance with pH was monitored at 325 nm (where

the absorption of the  $\cdot CH_2COOH$  radical predominates) and at 270 nm (due mainly to the absorption of  $\cdot COOH$ ) and the "titration" curves obtained are shown in Figure 3. From these curves  $pK$  values of  $2.75 \pm 0.1$  (at 270 nm) and  $2.65 \pm 0.1$  (at 325 nm) can be derived, in close agreement with the  $pK_{a1} = 2.83$  of malonic acid. It is interesting to note that on ionization of the *first* carboxyl group process 11 does not occur, since only *one* step was observed (Figure 3) on monitoring the pH dependence for the formation of either  $\cdot COOH$  or  $\cdot CH_2COOH$  radicals.

Support for reaction 11 can be obtained from the nature of the final products measured. Succinic, acetic, and oxalic acids have been observed<sup>9,19</sup> in addition to  $CO_2$ . These products are produced from the bimolecular recombination of  $\cdot CH_2COOH$  and  $\cdot COOH$ . Recent<sup>20</sup> esr results on the direct photolysis of aqueous solutions of malonic acid at 20° have confirmed reaction 11. In general, one of the main photolytic reactions of dibasic acids and their anions can be expressed as

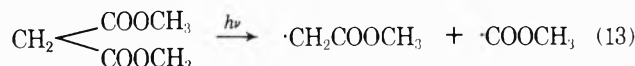


The dependence of the concentration\* of the radicals produced upon the intensity of the light is shown in Figure 2. In this case, as for acetic acid, the reaction is monophotonic. After the addition of 5 mM  $Ni(ClO_4)_2$  (a quencher of triplet excited states) under conditions where only ~1-2% of the light above 210 nm is absorbed by the quencher, no change in the  $OD_{320}$  or in the decay kinetics of the radical could be seen. This result probably means (a) that the quenching rate is relatively low, (b) that the triplet excited state precursor is very short lived, or (c) that the precursor is a singlet excited state.

On flash photolysis of  $1 \times 10^{-2} M$  malonamide,  $CH_2(CONH_2)_2$ , at pH 9.2 and at 5.0 no transient absorption could be seen (Figure 3). These results are in keeping with the absence of short-lived intermediates from the flash photolysis of aqueous solutions of aliphatic amides<sup>21</sup> and of the amide derivatives of amino acids and peptides.<sup>3</sup>

### Dimethyl Malonate

The photochemistry of undissociated acids leads, among other processes, to the rupture of the C-COOH bond. In addition to acetic and malonic acids described above, glutaric acid is photolyzed to produce also the  $\cdot COOH$  radicals. On ionization of glutaric acid beyond the first  $pK_a$ , no transient absorption can be observed. The photolysis of the esters can be expected to be similar to the photolysis of the corresponding undissociated acids. Figure 4 shows the transient spectrum obtained on flash photolysis of dimethyl malonate at pH 2.0 and 8.0. Identical spectra are obtained, indicating the absence of a dependence upon the pH of the solution. The spectrum has a maximum at 320 nm and corresponds to the absorption of the  $\cdot CH_2COOCH_3$  radical.



This radical has already been observed and identified,<sup>22</sup>

- (18) R. T. Sanderson, "Chemical Bonds and Bond Energy," Academic Press, New York, N. Y., 1971, p 203.  
 (19) I. D. S. Rao, *J. Univ. Bombay, Part 3*, **9**, 94 (1940); A. Miotati and G. Semeraro, *Atti. Inst. Veneto Sci., Part II*, **100**, 167 (1941).  
 (20) C. E. Burchill and P. W. Jones, *Can. J. Chem.*, **49**, 4005 (1971).  
 (21) M. Nakashima and E. Hayon, *J. Phys. Chem.*, **75**, 1910 (1971).  
 (22) M. Simic and E. Hayon, *Radiat. Res.*, **48**, 244 (1971).

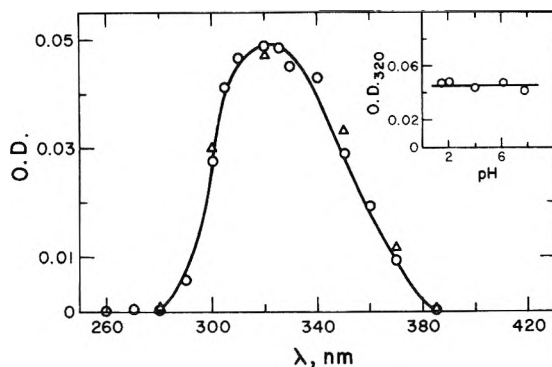
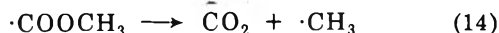


Figure 4. Transient spectra observed on flash photolysis of  $O_2$ -free  $1 \times 10^{-2} M$  dimethyl malonate at pH 2.0 (O) and 8.0 ( $\Delta$ ). Insert shows dependence upon pH of the absorbance at 320 nm.

$\lambda_{\max}$  320 nm and  $\epsilon_{320}$   $800 M^{-1} \text{ cm}^{-1}$ . Based on this extinction coefficient, the radical concentration produced per flash is  $3.1 \mu M$ . This quantum yield is about the same as that obtained for malonic acid.

The absence of an absorption due to the  $\cdot\text{COOCH}_3$  radical is due to its relatively short lifetime ( $<10 \mu\text{sec}$ ), probably decomposing unimolecularly to give  $\text{CO}_2$

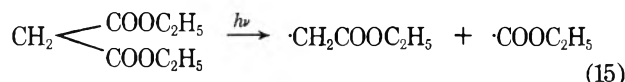


The absorption spectrum of the methyl radical is expected to be below  $\sim 220$  nm.

The  $\cdot\text{CH}_2\text{COOCH}_3$  radical decays bimolecularly to give a rate  $2k = 3.0 \times 10^9 M^{-1} \text{ sec}^{-1}$ , in fair agreement to the reported<sup>22</sup> decay kinetics of this radical.

### Diethyl Malonate

The photochemistry of aqueous solutions of diethyl malonate (DEM) was expected to give results similar to those obtained for dimethyl malonate. On flash photolysis of DEM solutions at pH 5.3 and 7.9, a transient absorption with  $\lambda_{\max}$  at  $\sim 320$  nm was observed (Figure 5) due probably to the  $\cdot\text{CH}_2\text{COOC}_2\text{H}_5$  radical



The  $[\cdot\text{CH}_2\text{COOC}_2\text{H}_5] = 0.78 \mu M$  compared to  $[\cdot\text{CH}_2\text{COOCH}_3] = 3.1 \mu M$  from the photolysis of dimethyl malonate. The  $\cdot\text{COOC}_2\text{H}_5$  radical is also considered to decay rapidly to give  $\text{CO}_2$  and  $\cdot\text{C}_2\text{H}_5$ . The fate of the ethyl radicals is not known but, due to its relatively low rate for H atom abstraction, probably decays bimolecularly to give  $\text{C}_4\text{H}_{10}$ .

In addition to the  $\cdot\text{CH}_2\text{COOC}_2\text{H}_5$  radical, a more intense absorption is also observed at pH 5.3 and 7.9, see Figure 5, with a maximum at  $\leq 265$  nm. This transient absorption decays "back to baseline" following second-order kinetics, with  $2k/\epsilon = 2.6 \times 10^2 \text{ cm sec}^{-1}$  at both pH values.

At pH 5.3, no absorption due to a permanent product is observed. At pH 7.9, a new intense absorption (B) was found to "grow in" (see Figure 5) slowly with a rate of  $7 \times 10^{-1} \text{ sec}^{-1}$  and a  $\lambda_{\max} \sim 268$  nm. An intermediate A is formed following the decay of the primary produced transients which is the precursor of B, but is not observable. At pH 7.9 absorption B decays with a  $k = 1.23 \times 10^{-1} \text{ sec}^{-1}$  to give another similar absorption C which is stable in presence of  $O_2$ , and whose spectrum was reproduced on a spectrophotometer. The spectrum of C increases in ab-

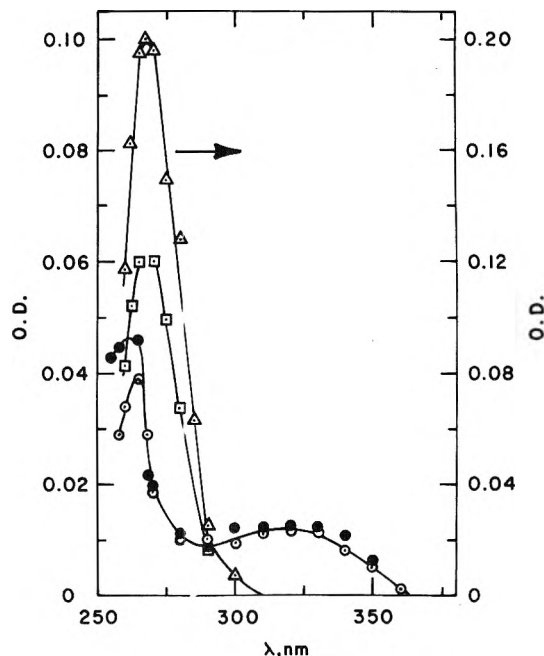


Figure 5. Intermediates observed on flash photolysis of  $1 \times 10^{-2} M$  aqueous solutions of diethyl malonate,  $N_2$ , at pH 5.3 (O) and 7.9 (O) read at  $\sim 10 \mu\text{sec}$  after the flash. Long-lived intermediate formed at pH 7.9, read at  $\sim 0.8 \text{ sec}$  after the flash and  $\sim 5 \text{ min}$  ( $\square$ ) later.

sorption with time (from 1 to 24 hr) and on increase of the pH subsequent to flash photolysis. Similarly, on increasing the pH of the solution initially flashed at pH 5.3 a similar absorption with  $\lambda_{\max} \sim 268$  nm grows in, which increased further on going from pH 8.3 to 9.2. The spectrum of the unirradiated solution remains unchanged under otherwise similar conditions.

The nature of the intermediates A, B, and C is unknown, but it is suggested that a Norrish type II reaction is possibly occurring. It is interesting to note that the absorption spectrum of ethyl acetoacetate,  $\text{CH}_3\text{COCH}_2\text{COOC}_2\text{H}_5$ , gives at pH 6.0 an absorption with  $\lambda_{\max} \sim 260$  nm which increases strongly at pH 9.2 (a keto-enol tautomerism accounts for this change). It is tentatively suggested that intermediate A is undergoing a similar reaction.

### Keto Acids

The photochemistry of keto acids is more complicated due to the combined electronic transitions of the carbonyl and carboxyl groups. The results obtained from pyruvic acid, ethyl pyruvate, and benzoylformic acid are briefly described.

On flash photolysis of  $O_2$ -free 5 mM aqueous solutions of pyruvic acid ( $pK_a = 2.5$ ) at pH 0.8 using a Co-Ni solution filter or a 218-nm cut-off filter, a transient absorption increasing strongly from  $\sim 350$  to 270 nm is observed. No absorption could be seen from 350 to 630 nm. This absorption is too strong to be due to the  $\cdot\text{COOH}$  radical only, and is thought to be due in addition to the  $\text{CH}_3\text{CO}\cdot$  radical or its hydrated form



The quantum yield of decomposition of pyruvic acid is<sup>23</sup>  $\sim 0.79$ , and its yield was found<sup>23</sup> to decrease to near zero in neutral solutions. The spectrum of the acetyl radical in

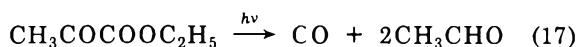
(23) S. Noda, K. Fueki, and Z. Kuri, *J. Chem. Phys.*, **49**, 3287 (1968).



organic glasses at 77°K has been reported.<sup>23</sup> The absorption observed in aqueous solution is quite different and may be due to its reaction with water. The esr spectrum of CH<sub>3</sub>CO in ice matrices has been determined.<sup>24</sup>

On flash photolysis of 5 mM sodium pyruvate at pH 6.2, a very weak but similar transient absorption was found. On monitoring the decrease in the absorption at 280 nm with increase in pH, a "titration" curve is obtained with a pK ~ 2.5. On increasing the pH of the solution above pH 5.0, an enhanced transient absorption was observed. The nature of this reaction is not clear.

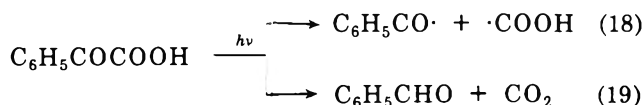
The flash photolysis of O<sub>2</sub>-free 2 mM solutions of ethyl pyruvate (using a 218-nm cut-off filter) at pH 3.9 produced a very strong transient absorption, similar to that formed on photolysis of pyruvic acid. The photolysis of ethyl pyruvate in inert solvents<sup>25</sup> gives carbon monoxide and acetaldehyde



This reaction proceeds *via* the triplet excited state ( $E_T = 65 \text{ kcal/mol}$ ) with a quantum yield<sup>25</sup> of 0.17.

On flash photolysis of  $2-5 \times 10^{-5} \text{ M}$  O<sub>2</sub>-free benzoylformic acid solutions at pH 0.8, using a 218-nm cut-off filter, transient absorptions with maxima at ~395, 320, and <280 nm were observed. No absorption from ~430 to 650 nm could be seen, and due to the absorption of

C<sub>6</sub>H<sub>5</sub>COCOOH itself none could be observed below ~280 nm. No transients were observed at pH 6.8. Reactions 18 and 19 are suggested to occur



Carbon dioxide and benzaldehyde have been observed<sup>26,27</sup> as products. The transient absorption found is tentatively assigned to the C<sub>6</sub>H<sub>5</sub>CO· radical in water.

### Conclusions

The above experiments on the flash photolysis of oxygen-free aqueous solutions of simple aliphatic carboxylic acids and esters have revealed that (a) the only major observable photolytic process is the rupture of C-COOH and C-COOR bonds; (b) the quantum yield of this process follows the pK<sub>a</sub> of the ground state of the carboxylic acids, *i.e.*, the presence of undissociated acid; (c) the decarboxylation reactions are found to be monophotonic.

- (24) J. E. Bennett and B. Mile, *Trans. Faraday Soc.*, **67**, 1587 (1971).  
 (25) G. S. Hammond, P. A. Leermakers, and N. J. Turro, *J. Amer. Chem. Soc.*, **83**, 2395 (1961).  
 (26) P. A. Leermakers and G. F. Vesley, *J. Amer. Chem. Soc.*, **85**, 3776 (1963).  
 (27) A. Schonberg, N. Latif, R. Moubasher, and A. Sina, *J. Chem. Soc.*, 1364 (1951).

## Photochemistry of 4-Nitropyridine in Acid Solutions

A. Cu and A. C. Testa\*

Department of Chemistry, St. John's University, Jamaica, New York 11432 (Received January 8, 1973)

The photoreduction of 4-nitropyridine to 4-hydroxylaminopyridine has been studied in acidic solutions of 2-propanol in the range 0.1–6 M HCl. The quantum yields show an unusual dependence on hydrogen ion concentration which is suggested to involve the following proton transfer in the excited triplet state, ( $^+ \text{HNC}_6\text{H}_4\text{NO}_2$ )\*<sup>3</sup> → (NC<sub>6</sub>H<sub>4</sub>NO<sub>2</sub>H<sup>+</sup>)\*<sup>3</sup>, with only the nitropyridinium ion being photochemically active. A limiting quantum yield of  $0.65 \pm 0.05$  occurs in the acid concentration range 0.5–2 M HCl, but  $\Phi$  decreases on either side of this range. This limiting value of  $\Phi$  is presumed to be the triplet yield of the molecule. Despite high photochemical yields no phosphorescence is observed at 77°K in acidic solutions of isopropyl alcohol or in a 1:2 ethylene glycol-water mixture. Quantum yield data for degassed and air-saturated solutions indicate that the 4-nitropyridinium triplet is more sensitive to oxygen quenching than the nitrobenzene triplet. Repeats of the experiments of Hashimoto, *et al.*, indicate that their quantum yields are too large, and probably due to their analytical method. The photoreduction in acidic solutions proceeds through the <sup>3</sup>n,π\* state of the 4-nitropyridinium ion and parallels our previous photochemical studies with nitrobenzene.

### Introduction

The photoreduction of nitrobenzene in degassed isopropyl alcohol with 366-nm excitation proceeds cleanly to phenylhydroxylamine, with a quantum yield of  $1.14 \pm 0.08 \times 10^{-2}$ , which results from hydrogen abstraction by the n,π\* triplet.<sup>1</sup> The presence of other molecules, such as nitrosobenzene, azoxybenzene, and other related mole-

cules, in photolysis experiments of aromatic nitro compounds is due to dark reactions and does not represent the photochemical behavior of the nitrobenzene molecule. Enhancement of the photoreduction of nitrobenzene and 1-nitronaphthalene in acid solutions was demonstrated in

(1) R. Hurley and A. C. Testa, *J. Amer. Chem. Soc.*, **88**, 4330 (1966).

previous reports.<sup>2,3</sup> As an extension of our interest in the photochemical behavior of aromatic nitro compounds we have investigated the photochemistry of 4-nitropyridine with the aim of studying the influence of the nonbonding electron pair of the pyridine ring on the photoreduction of an aromatic nitro compound. There are in this molecule two interesting cases to consider, *i.e.*, (a) the neutral molecule and (b) the nitropyridinium ion. The latter case should exhibit photochemical behavior similar to that of nitrobenzene, since the nonbonding electrons on pyridine are not readily available for excitation when protonated. Kaneko, *et al.*,<sup>4</sup> and Hata, *et al.*,<sup>5</sup> demonstrated that the photoreduction of 4-nitropyridine *N*-oxide in ethanol with 313-nm excitation results in 4-hydroxylaminopyridine *N*-oxide in quantitative yield; however, no quantum yield data were presented. Hashimoto, *et al.*,<sup>6</sup> have studied the photoreduction of 4-nitropyridine in 2-propanol with and without HCl and concluded that in acid solutions 4,4'-azopyridine is formed, which is presumed to originate from 4-hydroxylaminopyridinium hydrochloride which was destroyed in work-up procedures. In 100% 2-propanol the photochemical reaction is different and the process has not yet been elucidated. Recently, Hashimoto, *et al.*,<sup>7</sup> reported that the photoreduction of 4-nitropyridine in hydrochloric acid-isopropyl alcohol solutions proceeds from its  $n,\pi^*$  triplet to give 4-hydroxylaminopyridine. Their measured quantum yields ( $\Phi = 0.27-0.94$ ) increased with acid concentration and attained a maximum value for (HCl)  $\geq 3.6 \times 10^{-2} M$ . An enhancement of  $\Phi$  in acid solutions was observed in our photochemical studies with nitrobenzene, but what is surprising is that their quantum yield reaches an upper limit, which levels off at 0.94. In contrast to this behavior the triplet lifetime of nitrobenzene at room temperature is  $\sim 10^{-9}$  sec and its triplet yield is 0.67;<sup>8</sup> consequently, the upper value of 0.94 which they report may be in error. Furthermore, their determination of quantum yields was made by a spectrophotometric method, which is not well suited for nitro compounds because of accompanying dark reactions, which make a quantitative analysis uncertain. Our experiences have convinced us that the polarographic method for determining the photochemical depletion of aromatic nitro compounds is significantly better than the spectrophotometric method.<sup>1</sup> We have investigated the photochemistry of 4-nitropyridine in hydrochloric acid-isopropyl alcohol solutions and our quantum yield results differ significantly from those of Hashimoto, *et al.*<sup>7</sup> Our quantum yield data were obtained for vacuum degassed and air-saturated solutions in order to assess the importance of oxygen on the photochemical process. Quantitative depletion of 4-nitropyridine was determined by polarography.

### Experimental Section

**Materials.** 4-Nitropyridine was prepared by the method of Ochiai,<sup>9</sup> purified by vacuum sublimation, and then recrystallized from petroleum ether (mp 46.5–48°). The purity of the sample was checked by gas and thin layer chromatography. Quantum yield measurements were obtained from freshly prepared solutions in order to minimize any dark reactions that may occur prior to photolysis. Spectrograde isopropyl alcohol from Matheson Coleman and Bell was used as received. Glass distilled water and reagent grade (Baker Chemical Co.) hydrochloric acid were used for aqueous solutions.

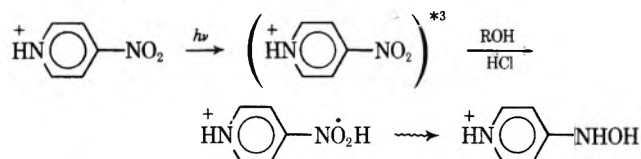
**Equipment.** All quantitative photolysis experiments were performed in 1-cm spectrophotometric quartz cells,

connected with a graded seal to Pyrex for connection to a vacuum system. The cells were sealed off at  $<10^{-4}$  mm, after three or more freeze-pump-thaw cycles. The isolation of 313-nm excitation from an Osram high-pressure mercury arc (HBO 100W/2) was achieved with a Schott interference filter (6-nm half-bandwidth) from Fish-Schurman Corp., New Rochelle, N. Y. Light intensities were determined with the potassium ferrioxalate actinometer,<sup>10</sup> and were typically  $3.88 \times 10^{15}$  quanta/sec. The disappearance of 4-nitropyridine was determined by polarographic analysis of buffered acetic acid-sodium acetate solutions (pH 4.7) before and after photolysis, and experiments were designed to keep the per cent depletion of 4-nitropyridine at  $\leq 15\%$ .

Large scale photolyses were performed through a Pyrex sleeve with an Hanovia 450-W medium-pressure mercury immersion lamp (type 679A-36) and separation was made on preparative thin layer chromatographic plates, using ethanol as the eluent. In a typical large scale photolysis 1.22 g of 4-nitropyridine was dissolved in 700 ml of isopropyl alcohol, 0.1 M in HCl, and irradiated for approximately 10 hr. The originally colorless solution was yellow at the end of the experiment. Evidence for the presence of 4-hydroxylaminopyridine was obtained by recording nmr spectra (Varian A60A) in DMSO- $d_6$  and ir (Beckman IR-8) spectra.

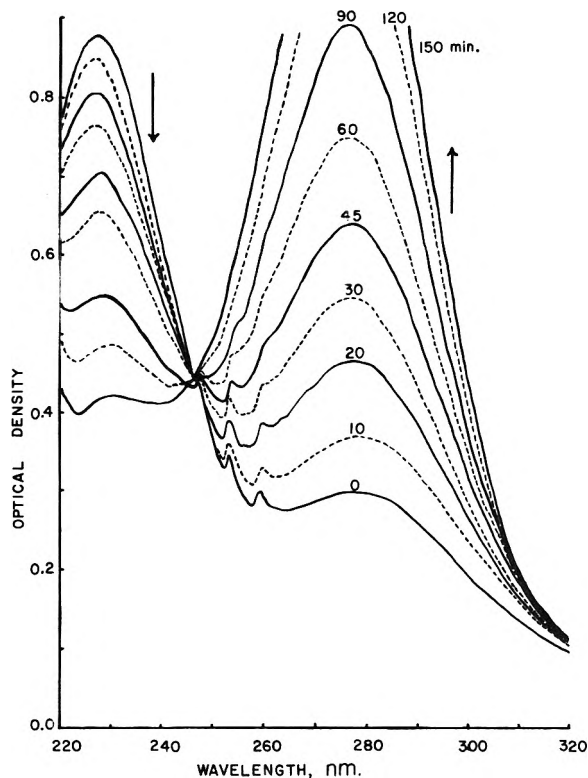
### Results

The 313-nm photochemical disappearance of  $1.0 \times 10^{-4} M$  4-nitropyridine in isopropyl alcohol, 0.1 M in HCl, after degassing, is shown in Figure 1. The spectral changes indicate a growth of absorption in the region of 280 nm with an isosbestic point at 244 nm which agrees with the results of Hashimoto, *et al.*<sup>7</sup> The ir of the isolated photoproduct exhibited bands at 2.9 and 3.2  $\mu$ , typical of amine hydrochlorides, and a sharp band at 8.4  $\mu$ , which is seen in pyridinium salts. The nmr bands for the ring hydrogen were observed at 6.75 (two hydrogens near amine) and 8.08  $\delta$  (two hydrogens near heteroatom), while -OH and -NH appeared at 11.2 and 12.9  $\delta$ , respectively. Subsequent shaking of the sample with D<sub>2</sub>O afforded the disappearance of these two exchangeable hydrogens, whereas the ring protons remained intact. Thus as in the photoreduction of nitrobenzene the hydroxylamine appears as the only primary product, *i.e.*



In the nmr spectra there was also evidence for some 4-aminopyridine, which exhibited a relatively broad singlet at 5.74  $\delta$ ; however, its presence is most likely due to a

- (2) R. Hurley and A. C. Testa, *J. Amer. Chem. Soc.*, **89**, 6917 (1967).
- (3) W. Trotter and A. C. Testa, *J. Phys. Chem.*, **74**, 845 (1970).
- (4) C. Kaneko, S. Yamada, and I. Yokoe, *Tetrahedron Lett.*, 4729 (1966).
- (5) N. Hata, E. Okutsu, and I. Tanaka, *Bull. Chem. Soc. Jap.*, **41**, 1769 (1968).
- (6) S. Hashimoto, K. Kano, and K. Ueda, *Tetrahedron Lett.*, 2733 (1969).
- (7) S. Hashimoto, K. Kano, and K. Ueda, *Bull. Chem. Soc. Jap.*, **44**, 1102 (1971).
- (8) R. Hurley and A. C. Testa, *J. Amer. Chem. Soc.*, **90**, 1949 (1968).
- (9) E. Ochiai, *J. Org. Chem.*, **18**, 534 (1953).
- (10) C. G. Hatchard and C. A. Parker, *Proc. Roy. Soc., Ser. A*, **235**, 518 (1956).

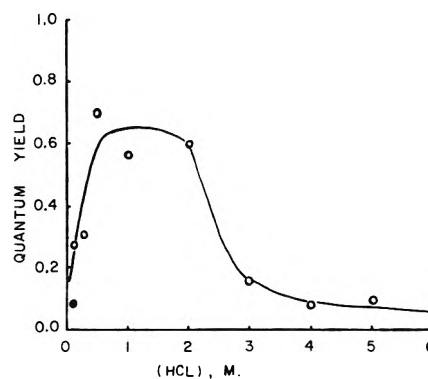


**Figure 1.** Uv spectral changes occurring during the 313-nm photolysis of degassed 4-nitropyridine ( $1.0 \times 10^{-4} M$ ) in isopropyl alcohol containing 0.1 M HCl. The intensity of light was  $\sim 3.9 \times 10^{15}$  quanta/sec.

dark reaction or a secondary photochemical event. This band was also observed to exchange upon addition of  $D_2O$ .

The quantum yield for the 313-nm photochemical disappearance of  $7.79 \times 10^{-3} M$  4-nitropyridine in isopropyl alcohol, after degassing, was studied in the acid concentration range 0.1–6 M HCl. The photolysis in 100% isopropyl alcohol was not investigated, since Hashimoto has indicated that the photochemistry in the absence of acid is different from the photoreduction which occurs in acid solutions.<sup>6,7</sup> The results of the present investigation are summarized in Figure 2. Of particular interest is that the quantum yield increases for dilute acid, appears to level off to a maximum value and then decreases again in more acidic solutions. The quantum yields plotted are the average of three or more measurements. This type of quantum yield dependence with acid is generally not observed in photochemical studies, but has been observed in the pH dependence of the fluorescence of certain heterocyclic molecules.<sup>11</sup> Thus, it is an inviting possibility to attribute the variation of quantum yield with  $(H^+)$  to protonation and ionization phenomena.

The measured quantum yields of the present study are in all cases significantly lower than the value of 0.94, which is reported by Hashimoto, *et al.*<sup>7</sup> Their photolyses were performed under a nitrogen atmosphere, whereas vacuum degassing procedures ( $<10^{-4}$  mm) employed in this study should more effectively exclude oxygen. They report that the 316-nm photolysis of  $1 \times 10^{-3} M$  4-nitropyridine in 80% isopropyl alcohol–20% water solutions containing  $\geq 0.04 M$  HCl has a quantum yield of 0.94. We have repeated Hashimoto's experiment, using 0.06 M HCl, and have obtained a value of  $\Phi_{deg} = 0.023 \pm 0.004$ . The disagreement between their results and those of this investigation suggest that their spectrophotometric meth-



**Figure 2.** Disappearance quantum yields for the photoreduction of  $7.79 \times 10^{-3} M$  4-nitropyridine in degassed isopropyl alcohol with varying concentrations of hydrochloric acid ( $\lambda_{exc}$  313 nm,  $I_a \sim 3.9 \times 10^{15}$  quanta/sec). The darkened circle at 0.1 M HCl is the result for the degassed photolysis in 50% isopropyl alcohol–water.

od is not very reliable. They unfortunately did not provide details concerning the wavelengths at which the optical densities were measured for the determination of  $\Phi$ . On the other hand, the polarograms of 4-nitropyridine in acetic acid–sodium acetate buffer solutions exhibit reproducible, well-defined polarographic reduction waves for the nitro group, which overcome the uncertainty of dark reactions and secondary photochemical events in spectrophotometric absorption measurements. Hashimoto, *et al.*,<sup>7</sup> did attempt polarographic analysis for the estimation of the disappearance of 4-nitropyridine, but stated that they were unable to obtain "satisfying data" by this method. It should be pointed out that the polarographic analysis of aromatic nitro compounds is well documented and that the polarography of 4-nitropyridine has been studied by Holubek and Volke<sup>12</sup> and Emerson and Rees.<sup>13</sup>

The quantum yields for the disappearance of 4-nitropyridine in 0.1 M HCl solutions, where protonation of the pyridine ring is not complete, were found to show some dependence on the water content of the solution. The degassed quantum yield in isopropyl alcohol containing 0.1 M HCl is  $0.27 \pm 0.03$ , while for the photolysis of a degassed 50% isopropyl alcohol–water solution containing 0.1 M HCl  $\Phi = 0.076 \pm 0.009$ . A similar behavior was observed by Cohen and Siddiqui<sup>14</sup> for the photoreduction of *p*-dimethylaminobenzophenone (DMAB) in aqueous acidic isopropyl alcohol, *i.e.*, the photoreduction of DMAB decreases upon addition of up to 10% water, but the effect levels off upon further addition of water. The decrease in  $\Phi$  for photolysis of 50% isopropyl alcohol–water, 0.1 M in HCl, is shown in Figure 2 as the darkened circle. The photochemical disappearance yield of 4-nitropyridine in pure isopropyl alcohol was determined to be  $0.013 \pm 0.003$ , but since the process is different from that which occurs in acid solutions, no further measurements were made.

The photoreduction of  $7.79 \pm 10^{-3} M$  4-nitropyridine in isopropyl alcohol with varying HCl concentration exhibited lower quantum yields in air-saturated solutions than when degassed. In Table I are presented the quantum yields for air-saturated and vacuum-degassed solutions

(11) H. Borresen, *Acta Chem. Scand.*, **17**, 921 (1963).

(12) J. Holubek and J. Volke, *Collect. Czech. Chem. Commun.*, **25**, 3286 (1960).

(13) T. R. Emerson and C. W. Rees, *J. Chem. Soc.*, 1923 (1962).

(14) S. G. Cohen and M. N. Siddiqui, *J. Amer. Chem. Soc.*, **89**, 5409 (1967).

**TABLE I: Quantum Yields for Disappearance of  $7.79 \times 10^{-3} M$  4-Nitropyridine in Isopropyl Alcohol with Varying HCl Concentration ( $\lambda_{\text{exc}} 313 \text{ nm}$ )**

HCl concn, $M$	$\Phi_{\text{deg}}$	$\Phi_{\text{air}}$	$\Phi_{\text{deg}}/\Phi_{\text{air}}$
0.1	$0.27 \pm 0.03$	$0.084 \pm 0.02$	3.2
0.3	$0.31 \pm 0.03$	$0.11 \pm 0.01$	2.8
0.5	$0.70 \pm 0.08$	$0.14 \pm 0.02$	5.8
1.0	$0.56 \pm 0.03$	$0.087 \pm 0.02$	6.4
2.0	$0.59 \pm 0.02$	$0.10 \pm 0.01$	5.9
3.0	$0.16 \pm 0.02$	$0.084 \pm 0.01$	1.9
4.0	$0.082 \pm 0.01$	0.081	1.0
6.0	$0.055 \pm 0.007$	$0.063 \pm 0.005$	0.9

and the ratio  $\Phi_{\text{deg}}/\Phi_{\text{air}}$ . It is seen that in the range where the ratio is the largest the dominant species present in solution is the 4-nitropyridinium ion formed by protonation in the ground state of the ring nitrogen. It is noteworthy that the air-saturated quantum yields are approximately constant and relatively insensitive to acid concentration. This behavior suggests that there may be two different paths by which the hydrogen abstraction process occurs.

The apparent constancy of  $\Phi_{\text{air}}$  as a function of HCl concentration indicates that the largest value of  $\Phi_{\text{deg}}/\Phi_{\text{air}}$  coincides with the largest photoreduction yield observed in degassed acid solutions. This result implies that the triplet state of the nitropyridinium ion is very sensitive to oxygen quenching, showing the greatest effect when all the molecules are protonated. The ratio decreases to unity in 4 M HCl in isopropyl alcohol, which probably involves proton transfer to the nitro group. The enhanced photoreduction of nitrobenzene in acidic solutions ( $>3 M$  HCl) of 50% isopropyl alcohol-water is also insensitive to oxygen.<sup>2</sup>

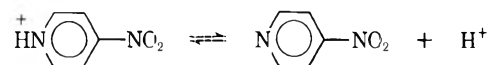
In view of the high photochemical quantum yields observed in the range 0.5–2.0 M HCl in isopropyl alcohol, we have attempted phosphorescence measurements, with the aim of directly demonstrating a large triplet population. We were unable to see any phosphorescence ( $\phi_p < 10^{-3}$ ) from 4-nitropyridine dissolved in acidic solutions of isopropyl alcohol or in 1:2 ethylene glycol-water upon irradiation with 313 nm at 77°K. This result is surprising in view of the large oxygen effect in the photolysis of degassed acid solutions. On the other hand, since neither nitrobenzene nor pyridine phosphoresces, it is very unlikely that 4-nitropyridine should phosphoresce.

## Discussion

It is seen from the results that the photoreduction of 4-nitropyridine occurs in acidic solutions of isopropyl alcohol with the formation of 4-hydroxylaminopyridine, provided the ring nitrogen is protonated. The photochemical behavior is in agreement with the results of Hashimoto, *et al.*,<sup>7</sup> however, comparison of their quantum yield results with those of this investigation indicates an unusually large disparity. In trying to account for part of the discrepancy we have noticed that Hashimoto and Kano<sup>15</sup> reported a value of 0.03 for the disappearance of nitrobenzene in isopropyl alcohol, which is approximately three times larger than the value of  $1.14 \pm 0.08 \times 10^{-2}$ , which we have determined by two completely independent methods.<sup>1</sup> Their determination of  $\Phi$  relies on measuring an optical density, which is not advisable in nitro group photochemistry, where dark reactions make it difficult to know the exact composition at any time. Also the fact

that the triplet yields of nitrobenzene and 1-nitronaphthalene are known to be  $0.67 \pm 0.10$  and  $0.63 \pm 0.10$ ,<sup>8</sup> respectively, suggest that the upper quantum yield limit they report may be larger than the triplet yield of the molecule, *i.e.*, it is reasonable to expect that the triplet yield of nitrobenzene and 4-nitropyridinium ion are similar. Although there is no simple justification that the triplet yield of nitrobenzene and the 4-nitropyridinium ion should be comparable, it is noteworthy that removal of the nonbonding electrons on the ring nitrogen by protonation does lead to a photochemical behavior similar to that of nitrobenzene. It is interesting to note that our limiting quantum yield value for 4-nitropyridine disappearance in acidic isopropyl alcohol solutions (0.5–2.0 M HCl) is  $0.65 \pm 0.05$ , and agrees within experimental error with the triplet yield determination of nitrobenzene.<sup>8</sup> Thus it is reasonable to conclude that  $\Phi_{\text{max}} = \Phi_T$  for 4-nitropyridine.

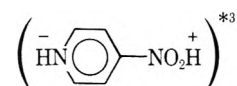
The increasing quantum yield for photoreduction in the range  $(H^+) = 0.1\text{--}0.5 M$  is probably due to increasing protonation of the pyridine nitrogen. If we consider that  $\Phi = (1/2)\Phi_{\text{max}} \approx 0.32$ , when  $(H^+) \approx 0.2 M$ , corresponds to the presence of  $\sim 50\%$  pyridinium ions in solution, the apparent  $pK_a$  for the process



is estimated to be 0.7. The  $pK_a$  for this process in aqueous solutions has been reported to be 1.61<sup>16</sup> and 1.4.<sup>17</sup> Since the medium in our photochemical studies was primarily isopropyl alcohol, a comparison with the literature value is difficult due to variation of solvent. In the range 0.5–2.0 M HCl the quantum yield remains constant since the pyridine nitrogen is totally protonated. When  $(\text{HCl}) > 2 M$ , the quantum yield again falls off which is suggested to be due to the following proton transfer in the excited triplet state, *i.e.*



The latter species may be expected to exhibit lower reactivity, since no significant photoreduction is observed unless the nonbonding electron pair on the ring nitrogen is protonated. To add support to this interpretation it is noteworthy that the enhanced photochemistry of nitrobenzene in 50% isopropyl alcohol-water for  $(H^+) \geq 3 M$  suggested protonation of the nitro group in the excited state;<sup>2</sup> consequently, the decreasing  $\Phi$  values could be due to a proton transfer from the ring nitrogen to the nitro group. Alternatively, it is also possible that the dication



forms in the excited state and is rapidly deactivated. A less likely possibility is that the decrease in  $\Phi$  when  $(H^+) > 2 M$  is due to enhanced deprotonation of 4-nitropyridinium upon addition of water.

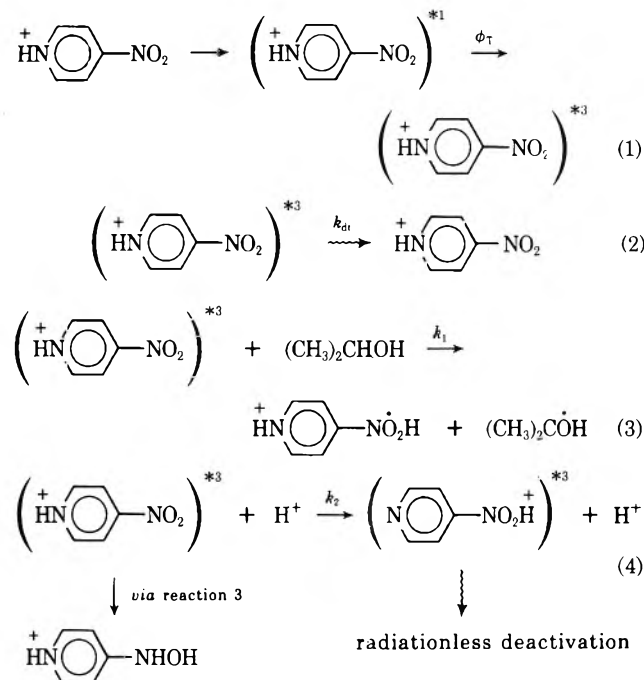
In view of the results which indicate that the photoreactive species is the triplet 4-nitropyridinium ion, the photochemical behavior in degassed acid solutions may be

(15) S. Hashimoto and K. Kano, *Tetrahedron Lett.*, 3509 (1970).

(16) J. M. Essery and K. Schofield, *J. Chem. Soc.*, 2225 (1963).

(17) A. Fischer, W. J. Galway, and J. Vaughan, *J. Chem. Soc.*, 3591 (1964).

described by reactions 1-4 in which reaction 3 is the



source of photochemistry, reaching an upper limit when

all the molecules exist as 4-nitropyridinium ions and  $k_2$  is the rate constant for the proton transfer in the excited state which results in some rapid radiationless decay. Reaction 3 may proceed *via* an electron transfer to the nitro group followed by protonation; however, the results obtained do not definitively answer this question. For reactions 1-4  $\Phi = \alpha\phi_T k_1(\text{ROH})/[k_1(\text{ROH}) + k_2(\text{H}^+)]$  where  $\alpha$  represents the fraction of 4-nitropyridine molecules that are protonated at the ring nitrogen. Reaction 2 is assumed to make a negligible contribution compared to reactions 3 and 4 in the acid range 0.5-2.0 M HCl. It is readily seen that when an upper limit to photoreduction is achieved  $\alpha = 1$ , and  $\Phi_{\text{max}} = \phi_T$ .

In conclusion the photoreduction of 4-nitropyridine proceeds efficiently in dilute acid solutions of isopropyl alcohol, provided the ring nitrogen is protonated. The large quantum yields reported by Hashimoto, *et al.*,<sup>7</sup> are attributed to uncertainties in the composition of photolyzed solutions, arising from dark reactions during photolysis. The results presented suggest enhanced photochemistry arising from protonation of the pyridine nitrogen and that proton transfer to the nitro group leads to a species which decays rapidly through some unknown radiationless path.<sup>18</sup>

(18) Note Added in Proof. In a recent publication, G. Wybbels, *et al.*, *J. Amer. Chem. Soc.*, **95**, 1281 (1973), have implicated the chloride ion as an electron donor in the photoreduction of nitrobenzene in hydrochloric acid solutions. A similar mechanism may be operative in the photoreduction of 4-nitropyridine and is currently under investigation.

## Analysis of the Temperature Dependence of the Electron Spin Resonance Spectrum of $-\text{OOCF}_2\dot{\text{C}}\text{FCOO}^-$ Using Density Matrix Techniques<sup>1</sup>

Carolyn M. Bogan<sup>2</sup> and Lowell D. Kispert\*

Department of Chemistry, The University of Alabama, Tuscaloosa, Alabama 35486 (Received November 21, 1972)

Publication costs assisted by The University of Alabama

The temperature dependence of the  $\alpha$  and  $\beta$  fluorines splittings in  $-\text{OOCF}_2\dot{\text{C}}\text{FCOO}^-$  (from irradiated single crystals of sodium perfluorosuccinate) has been examined using density matrix techniques. The temperature dependence of the  $\alpha$ -fluorine hyperfine splittings arises from a torsional oscillatory motion of the  $\alpha$  fluorine about the  $\text{C}_\alpha\text{-C}_\beta$  bond which averages the two crystallographically nonequivalent radicals observed at 77°K into a single radical at 300°K. The temperature dependence of the  $\beta$ -fluorine hyperfine tensors results from a nonadiabatic spin exchange,  $\tau^{-1} = 9.9 \times 10^{12} \exp(-3680 \text{ cal}/RT) \text{ rad sec}^{-1}$ , occurring as a direct consequence of the  $\alpha$ -fluorine torsional oscillation coupled with a shift in the  $\beta$ -fluorine position.

### Introduction

At 300°K, Rogers and Whiffen<sup>3</sup> reported that the esr spectrum of irradiated sodium perfluorosuccinate with the magnetic field along the  $b$  axis was primarily due to a single  $-\text{OOCF}_2\dot{\text{C}}\text{FCOO}^-$  radical (PFS). When the crystals were cooled below 130°K, Kispert and Rogers<sup>4</sup> have shown that the radicals, observed with  $b$  parallel to  $H$ , occupy two crystallographically nonequivalent positions (radicals I and II). This appeared to be the result of a freezing out

of some motion which led to the observation of an averaged esr spectrum at higher temperatures.

This temperature-dependent behavior is not atypical for  $\beta$  protons in the radicals found in irradiated single crys-

(1) This research was supported by the U. S. Atomic Energy Commission under Contract No. AT-(40-1)-4062 and this is AEC Document No. ORO-4062-11.

(2) AAUW Fellowship holder 1970-1971.

(3) M. T. Rogers and D. H. Whiffen, *J. Chem. Phys.*, **40**, 2662 (1964).

(4) L. D. Kispert and M. T. Rogers, *J. Chem. Phys.*, **54**, 3326 (1971).

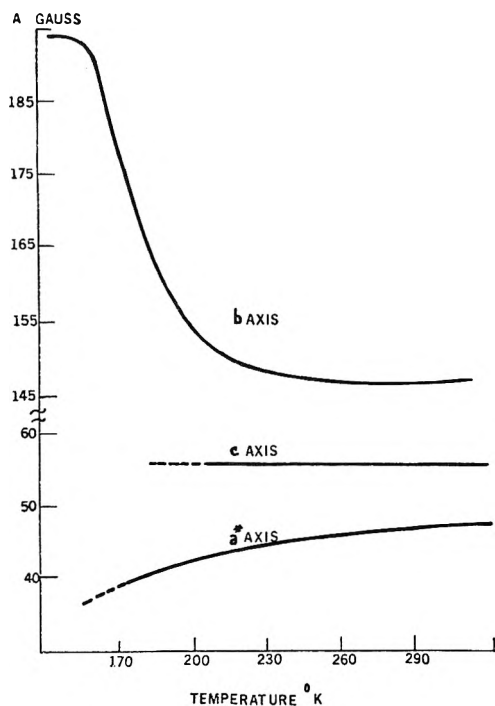


Figure 1. Experimental temperature dependence of the  $\alpha$ -fluorine hyperfine splittings of the 300°K radical along the *b*, *c*, and *a\** crystal axis of ref 3 and 4.

tals of aliphatic carboxylic acids.<sup>5</sup> Even though the  $\beta$ -proton splittings vary considerably from radical to radical, the temperature dependence of the  $\beta$ -proton splittings is well understood in terms of restricted internal motion about the  $C_{\alpha}$ - $C_{\beta}$  bond axis.<sup>6</sup> On the other hand, the  $\alpha$ -proton splittings in these radicals change little from matrix to matrix and show very little temperature dependence.

The behavior of the  $\alpha$ - and  $\beta$ -fluorine hyperfine interaction in fluorine-substituted aliphatic radicals is not as well understood. The temperature dependence of the isotropic and anisotropic splittings has only been documented for  $-\text{CF}_2\text{CF}-$ <sup>7</sup> and for  $\dot{\text{C}}\text{F}_2\text{CONH}_2$ .<sup>8,9</sup>

Recently, the temperature dependence of the esr spectrum of  $\text{CF}_2\text{CONH}_2$  has been analyzed.<sup>9</sup> The large anisotropy of the  $\alpha$  fluorines permitted the torsional motion to be understood from the temperature-dependent changes in the  $\alpha$ -fluorine splittings. Nonadiabatic effects were clearly evident in the esr spectrum as a result of the non-parallel fluorine p orbitals which caused the central peak ( $m_1 = 0$ ) to be split at low temperatures.

Kispert and Rogers<sup>4</sup> were able to approximate the temperature dependence of the  $\alpha$  fluorines in PFS in the two sites by averaging the two hyperfine tensors (I and II) and suggested that the averaging was due to an oscillation about the central C-C bond. They accounted for the observed line broadening by correlating the observed esr lines at 77°K with those observed at 300°K. A detailed examination of the line broadening and a determination of the motion responsible for the averaging process was not attempted.

In this work, a mechanism is proposed to account for the temperature dependence of the  $\alpha$ - and  $\beta$ -fluorines splittings and line width variations in PFS. The behavior of the  $\alpha$ -fluorine splittings is suggestive of a motional effect similar to that seen for the  $\alpha$  fluorines in  $\text{CF}_2\text{CONH}_2$ . In analogy to  $\text{CF}_2\text{CONH}_2$ , the  $\alpha$  fluorine in PFS is assumed to be oscillating between the two equilibrium posi-

tions observed at 77°K. Furthermore, any motion of the  $\alpha$  fluorine will cause a change to occur in the overlap of the  $\beta$ -fluorine p orbitals with the  $\alpha$ -carbon and  $\alpha$ -fluorine p orbitals, resulting in  $\beta$ -fluorine spin exchange effects.<sup>10a,b</sup> These spin exchange effects will be observed as line broadening and shifts in the esr peaks associated with  $\beta$  splittings. This is to be contrasted with the  $\text{CF}_2\text{CONH}_2$  case where the central peaks coalesced with little apparent line broadening as a result of the spin exchange of the  $\alpha$  fluorine.

The time-dependent nature of exchange in the presence of the motion of spins can be handled in a nearly exact manner using the density matrix formulation<sup>10</sup> of quantum mechanics. However, the size and complexity of the exact solution for a four spin system such as PFS severely limits the usefulness of the density matrix methods. Several approximations have been made to reduce the dimensions of the problem for the case of PFS. The first is to assume that the averaging of the  $\alpha$ -fluorine hyperfine splittings can be done in a semiclassical manner. The second approximation is that the  $\beta$ -fluorine spin exchange can be simulated using density matrix equations which include the torsionally averaged  $\alpha$ -fluorine hyperfine tensors. Other approximations have been used to reduce the dimensions of the transition basis set and these will be discussed in detail below.

#### $\alpha$ -Fluorine Torsional Oscillation

*Type of Motion.* The temperature dependence of the  $\alpha$ -fluorine hyperfine splitting<sup>4</sup> is most apparent when the magnetic field is parallel to the *b* crystal axis (Figure 1) where the *a\**, *b*, and *c* axes are the same as those used in ref 3 and 4. This is because the direction of the maximum component of the  $\alpha$ -fluorine hyperfine tensors lies near the *b* axis at low temperatures and any small change is more clearly seen than along the *c* or *a\** axis where the smaller  $\alpha$  hyperfine tensor components result in overlapped lines as the temperature is lowered. The 300°K hyperfine tensor for the  $\alpha$  fluorine is not axially symmetric as would be expected in the case of unrestricted rotation about the C-C bond. In fact, such rotation would have to involve motion of a large part of the radical which would be unlikely to occur in a crystal lattice.

If this temperature dependence is a motional effect, it would then be expected to be due to a torsional motion. Torsional motion can be analyzed in a straightforward manner.<sup>6,9,11,12</sup>

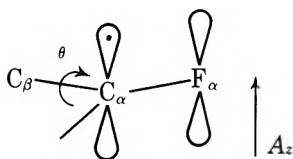
*Simple  $(1 - 3 \cos^2 \theta)$  Relationship.* Since the experimental temperature dependences of the  $\alpha$ -fluorine hyperfine splittings are so apparent along the *b* axis, these splittings were used to obtain an estimation of the barrier height by comparing them with those calculated using a simplified model. The torsional motion was approximated by a semiclassical averaging of the  $\alpha$ -fluorine p-orbital anisotropy<sup>9</sup> in a manner similar to that used for  $\beta$  protons.<sup>6</sup>

- (5) J. R. Morton, *Chem. Rev.*, **64**, 453 (1964).
- (6) (a) O. H. Griffith, *J. Chem. Phys.*, **41**, 1093 (1964); (b) P. J. Krusic, P. Meakin, and J. P. Jesson, *J. Phys. Chem.*, **75**, 3438 (1971).
- (7) M. Iwasaki and K. Toriyama, *J. Chem. Phys.*, **46**, 2852 (1967).
- (8) M. T. Rogers and L. D. Kispert, *J. Chem. Phys.*, **46**, 3193 (1967).
- (9) C. M. Bogan and L. D. Kispert, *J. Chem. Phys.*, **57**, 3109 (1972).
- (10) (a) A. Abragam, "The Principles of Nuclear Magnetism," Clarendon Press, Oxford, 1961; (b) C. S. Johnson, *Advan. Magn. Resonance*, **1**, 33 (1965); (c) U. Fano in "Lectures on the Many-Body Problem," Vol. II, E. R. Caianiello, Ed., Academic Press, New York, N. Y., 1964, pp 217-239.
- (11) N. L. Bauld, R. Gordon, and J. Zoeller, Jr., *J. Amer. Chem. Soc.*, **89**, 3948 (1967).
- (12) E. W. Stone and A. H. Maki, *J. Chem. Phys.*, **37**, 1326 (1962).

The observed hyperfine splitting thus reflects the torsional averaging of the dipolar interactions between the  $\alpha$ -fluorine p orbital and the partially occupied carbon p orbital. Along the direction of the partially occupied carbon p orbital ( $z$ ), this averaging has the functional form  $\langle 1 - 3 \cos^2 \theta \rangle$  where  $\langle \rangle$  indicates an expectation value and  $\theta$  is the torsional angle. Since the value of this function depends upon the value of the potential barrier height,  $V_0$ , this model can be used to estimate  $V_0$ .

In order to calculate  $\langle 1 - 3 \cos^2 \theta \rangle$ , it is necessary to know the value of the reduced moment of inertia,  $I$ . Since the crystal structure of PFS is not known, an exact value for  $I$  cannot be obtained. However, this is not a serious problem because the calculations which require  $I$  are not very sensitive to large variations in  $I$ . An approximate value of  $I$  was obtained by assuming the same basic crystal structure as has been reported for succinic acid.<sup>13</sup> The value of  $\langle 1 - 3 \cos^2 \theta \rangle$  was then calculated for several values of  $V_0$ , the potential barrier height, using a torsional Hamiltonian.<sup>6,11,12</sup> A simpler method, giving similar results, assumed a Boltzmann probability that the radical was in a torsional state of energy  $V(\theta)$ , at an angle of twist  $\theta$ .<sup>6b</sup>

The calculated splittings were in poor agreement with the experimental results (Figure 2). Several factors contributed to this. The experimental data were taken along the  $b$  axis which is near but not along either of the maximum  $\alpha$ -fluorine components. For  $\alpha$  fluorine, the  $A_z$  direction has been shown to be along the axis of the fluorine p orbital containing the unpaired spin population which is generally parallel to the carbon  $2p_z$  orbital.<sup>14</sup> There are two radicals with one  $\alpha$  fluorine in each radical. For PFS, the  $b$  axis is some  $30^\circ$  away from each of the  $\alpha$ -fluorine  $A_z$  directions. The function  $\langle 1 - 3 \cos^2 \theta \rangle$  is a valid description of the averaging only in the direction of the p orbital. The nonlinear temperature dependence of the splittings along  $b$  (Figure 1) is probably an indication that  $b$  is too far from  $A_z$  to use only the simple  $\langle 1 - 3 \cos^2 \theta \rangle$  function.



Despite this poor agreement, the value of  $V_0$  deduced from this treatment of a torsional oscillator is approximately 3000 cal. This is consistent with the estimate of the upper limit of 5500 cal calculated from the line width variation with temperature.<sup>4</sup>

A more complete treatment of the torsional motion has to include the averaging of the hyperfine tensors for both  $\alpha$  fluorines (I and II).

**Torsional Oscillation.** The undiagonalized  $\alpha$ -fluorine hyperfine tensors were averaged in a manner similar to that used for  $\text{CF}_2\text{CONH}_2$ .<sup>9</sup> Some of the results of this "torsional oscillation" of the low-temperature (77°K)  $\alpha$ -fluorine hyperfine tensors are given in Table I.<sup>15</sup> As expected, the simulated torsional averaging decreased the anisotropic components of the hyperfine interaction and left the magnitude of the isotropic component unchanged. Experimentally, the  $\alpha$ -fluorine isotropic splittings decrease over the temperature range of interest.<sup>4</sup> This decrease could be the result of a slight structural change or of orbital-following effects.<sup>16</sup> In order to compare the torsionally averaged splittings and the experimental splittings at 300°K, a correction for the change in isotropic

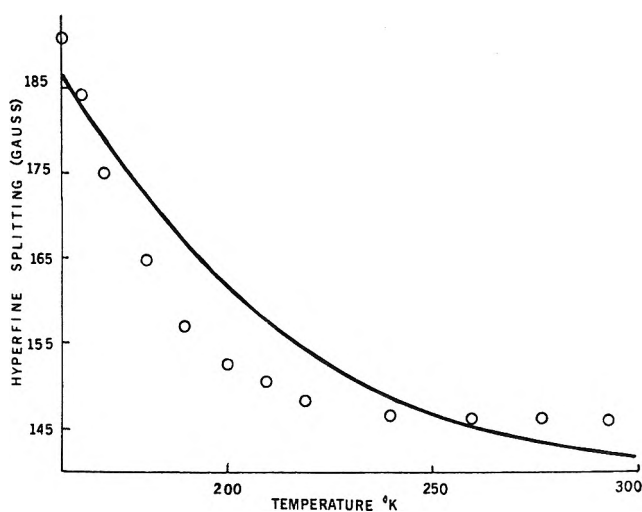


Figure 2. Calculated and experimentally observed hyperfine splittings for the  $\alpha$  fluorine in  $^-\text{OOC}\text{CF}_2\text{CF}\text{COO}^-$  vs. temperature. The experimental splittings (O) were measured along the  $b$  axis. The calculated splittings were obtained using the method of ref 6a (—).

TABLE I: Calculated and Observed  $\alpha$ -Fluorine Splittings (G) for  $^-\text{OOC}\text{CF}_2\text{CF}\text{COO}^-$  Assuming that the  $\alpha$  Fluorine Undergoes a Torsional Oscillation<sup>a</sup> with  $V_0 = 3000$  cal/mol

		$a^*$	$b$	$c$
Observed 77°K	Radical I	18	189	104
	Radical II	84	164	126
Calculated 300°K		58.3	153.6	57.8
Calculated 300°K corrected		50.0	148.0	51
Observed 300°K		45	145	56

<sup>a</sup> The potential function for the torsional motion was taken to have two equally populated minima.

splittings was subtracted from the calculated torsionally averaged splittings. This correction was calculated by subtracting the undiagonalized 300°K tensor from the average of the undiagonalized 77°K tensors. This difference tensor was used to calculate the correction for a given crystal orientation. The corrected splittings are also given in Table I.

Obviously, this treatment of the  $\alpha$  fluorines alone is not the complete explanation of the temperature dependence of the esr spectra. There is a considerable amount of line broadening around 130°K which seems to be related to the  $\beta$  fluorines.<sup>4</sup> In order to treat both the  $\alpha$  and the  $\beta$  fluo-

(13) J. S. Broadley, D. W. J. Cruickshank, J. D. Morrison, J. W. Robertson, and H. M. M. Shearer, *Proc. Roy. Soc., Ser. A*, **251**, 441 (1959).

(14) D. I. Beveridge, P. A. Dobosh, and J. A. Pople, *J. Chem. Phys.*, **48**, 4802 (1968).

(15) Since there are two magnetically nonequivalent sites corresponding to each of the two  $\alpha$  fluorines, there is a slight ambiguity in the assignment of the phases ( $\varphi$  in Table I of ref 4) of the direction cosines. It is assumed that if the  $\alpha$  fluorines are related by a simple torsional motion, the motion has a small amplitude because otherwise a large part of the radical would have to undergo a substantial motion which would be unreasonable in a crystal lattice. The average amplitude of the motion must also be such that the  $\alpha$ -fluorine splittings are drastically affected by the motion (see Discussion). To account for the expected amplitude of the motion, all phases were chosen to be those of the upper signs in Table I of ref 4, except that of  $\alpha$ -fluorine I which was inverted through the center of the coordinate system (i.e.,  $\theta = 61.3^\circ$ ,  $\varphi = -95.6^\circ$  changed to  $\theta = 119.7^\circ$ ,  $\varphi = 84.4^\circ$ ).

(16) R. W. Fessenden, *J. Phys. Chem.*, **71**, 74 (1967).

rines in the two sites, the torsionally averaged  $\alpha$ -fluorine hyperfine tensors were included in a density matrix treatment of the  $\beta$ -fluorine spin exchange.

### Density Matrix Treatment of Spin Exchange

The general theory for using the density matrix formalism for magnetic resonance has been developed.<sup>10</sup> Here it will only be necessary to discuss the particular form of the treatment which is best suited to this problem.

For magnetic resonance calculations, the general method of solution of the density matrix equations involves a transformation from an eigenstate space (Hilbert space) into Liouville space. Thus, as the number of spins increases, it becomes increasingly important to find methods of reducing the dimension of the Liouville space representation. The use of a contracted Liouville space, a transition space,<sup>17</sup> can sometimes reduce the dimensions of the matrices involved to the number of spectral lines.

A Liouville space basis set can be constructed from the eigenstate basis set for PFS, a four spin system with three ( $I = \frac{1}{2}$ ) spins and one ( $S = \frac{1}{2}$ ) spin. The simple product basis set is used for the eigenstate space. There will be  $2^4$  eigenstates (i.e.,  $\alpha_1\alpha_2\alpha_3\alpha_{e1}$ ,  $\alpha_1\alpha_2\beta_3\alpha_{e1}$ ,  $\alpha_1\beta_2\alpha_3\alpha_{e1}$ , etc.). If this eigenstate basis set were to be transformed into Liouville space without any approximations, it would become necessary to invert (or diagonalize) a complex  $256 \times 256$  matrix. Obviously, time and storage factors would limit the feasibility of simulating spectra in such a manner.

The first approximation which can be made to reduce the dimensions of the problem is to ignore the terms in the esr Hamiltonian which involve  $S_x$  or  $S_y$ .<sup>18</sup> This approximation effectively removes all Liouville basis states in which the basis eigenstates have the same electron spin quantum number,  $m_s$ .

The second approximation is to retain only those Liouville bases in which the two basis eigenstates differ by no more than one individual nuclear spin. This reduces the dimension of the Liouville space to 8 bases which connect states differing only in  $m_s$  and 24 bases which connect states differing in one individual nuclear spin and  $m_s$ .

The transition bases which are eliminated by this "contraction" are either nmr active or are forbidden transitions with  $m_1 \geq 1$ . These transitions would have been eliminated effectively by the  $\sigma$  vector (eq 17, ref 17). These approximations have reduced the size of the  $L_0$  matrix from a  $256 \times 256$  matrix to a  $32 \times 32$  matrix which is a more reasonable dimension.

To represent intramolecular exchange with a transition basis set, the concept of an exchange of sites is introduced. Exchange sites have been used extensively in some nmr and esr solution studies.<sup>17,19</sup> Radical I is designated as site I and radical II is designated as site II. This is not to be confused with the two magnetically nonequivalent sites occupied by each radical. Exchange sites are used to designate different orientations of a spin within a radical. Each orientation of the spin or exchange site has different splittings,  $g$  values, etc. The introduction of  $n$  sites increases the dimension of the  $L_0$  matrix by a factor of  $n$ .

Using the general equations for intramolecular exchange between magnetic environments derived by Alexander,<sup>20</sup> the exchange term can be written; however, this equation was derived for the general case where all of the nuclei are involved in mutual exchange. For PFS a correlation diagram can be drawn (ref 4, Figure 4) which indicates that only the  $\beta$  fluorines are exchanging and that the  $\alpha$  fluorines are not affected by the exchange.

The exchange matrix can then be written for only  $\beta$ -fluorine exchange. The Hamiltonian for the eigenstate basis set can be written<sup>10</sup> (using the torsionally averaged hyperfine tensors derived in the previous sections) and subsequently transformed into the Liouville space formulation using eq 3 of ref 17. Relaxation can be assumed<sup>17</sup> to arise from a single transverse relaxation time,  $T_2$ .

The form of the  $64 \times 64$  matrix (2 sites, 32 dimensional  $L_0$  for each) to be diagonalized is such for PFS that ALLMAT<sup>21</sup> is often quite unstable and it is not always possible to find the eigenvectors. An alternative way of solving for the elements of  $\rho$  is to invert the  $M_0$  matrix directly as in eq 18, ref 17. The only drawback in this approach is that the inversion is very time consuming. Several limited calculations were performed to show that this method of simulating exchange effects does reproduce the experimentally observed line widths and the shifts in the peak positions.

To circumvent this computational problem, the choice of the basis set was reexamined. A general product basis set was chosen as is customary in all density matrix calculations and a choice of a quantization axis was possible with the single restriction that the hyperfine and  $g$  tensors must be referenced to the same axis.

*Energy Representation in Hilbert Space.* If the eigenvectors which diagonalized the Hamiltonian (written in terms of the torsionally averaged hyperfine tensors) are chosen as the basis vectors then the  $L_0$ <sup>17</sup> matrix will be diagonal.  $L_0$  can then be reduced to two  $8 \times 8$  diagonal subblocks where each of the elements of  $L_0$  is associated with a transition which gives rise to a line in the first-order esr spectrum.

The addition of exchange between the sites causes severe complications if the basis set is not a simple product basis. When the Hamiltonian is diagonalized, the eigenvectors are found to be complicated functions of the simple product functions. When the exchange is formulated in the eigenvector basis set and then put into Liouville space, the exchange matrix cannot be reduced to two  $8 \times 8$  subblocks as was the Hamiltonian. However, an approximation can be made for the exchange matrix. If the quantization axis of the product basis set is the static magnetic field, it is only second-order corrections which couple the product bases in the eigenfunctions. Although this coupling cannot be ignored for the Hamiltonian, in some cases it can be ignored for the exchange matrix. Ignoring this coupling amounts to saying that the product basis set and the eigenvectors exchange in the same manner.

The test of the validity of this approximation is the comparison with the more complete calculation with the  $64 \times 64$  matrices. The validity of this approximation is expected to be a function of the magnitude of the hyperfine splittings for each orientation of the crystal. It was tested for the  $b$  and  $c$  crystal axes for PFS since along these axes the most accurate experimental data were available.

*Results of the Density Matrix Calculations.* The calculated  $\alpha$ - and  $\beta$ -fluorine splittings were in good agreement

- (17) G. Binsch, *J. Amer. Chem. Soc.*, **91**, 1304 (1969).
- (18) R. G. Hayes, D. J. Steible, W. M. Tolles, and J. W. Hunt, *J. Chem. Phys.*, **53**, 4466 (1970).
- (19) J. Heinzer, *Mol. Phys.*, **22**, 167 (1971).
- (20) S. Alexander, *J. Chem. Phys.*, **37**, 967, 974 (1962); **38**, 1787 (1963); **40**, 2741 (1964).
- (21) D. A. Kleier and G. Binsch, Program No. 165, Quantum Chemistry Program Exchange, Indiana University, 1970.



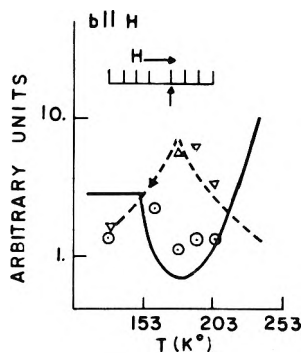


Figure 3. Calculated esr line heights (O) and widths ( $\Delta$ ) vs. temperature for  $-\text{OOCF}_2\text{CF}_2\text{COO}^-$  using the 32 dimensional transition basis set compared to the experimental heights (—) and widths (---).

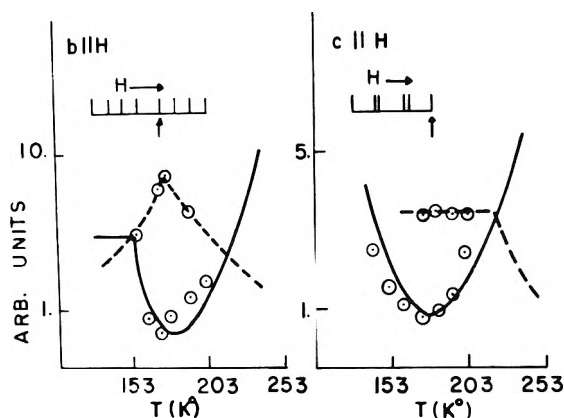


Figure 4. Calculated (O) and experimental esr line heights (—) and widths (---) vs. temperature for  $-\text{OOCF}_2\text{CF}_2\text{COO}^-$  along  $b$  parallel to  $H$  and  $c$  parallel to  $H$  using the eight dimension basis set.

with those observed experimentally. Reasonable agreement was also found for the temperature variation of the upfield line heights and widths along the  $b$  and  $c$  axes and a comparison is given in Figures 3 and 4.

The more complete ( $64 \times 64$ ) calculations were done for the spectrum along the  $b$  axis from about 60 to 45 G upfield from the center of the spectrum and along the  $c$  axis from about 98 to 117 G. The results are shown in Figure 3. The errors involved in assigning a peak height or width from a minimum number of points are rather large. The points here were calculated every 0.5–0.7 G with a line width in the absence of exchange of 1.1 G. Although an accurate value for a calculated line width is difficult to extrapolate from such a spectrum, comparison of a series of spectra can show the definite qualitative trends. Also the comparison with the simpler calculation ( $16 \times 16$ ) indicates the validity of the simple approximate calculation especially when the shifts in peak positions are compared.

The more complete calculation indicates that the exchange rate  $\tau^{-1}$  should be of the form  $\tau^{-1} = 10^{13} \exp(-3500/RT) \text{ sec}^{-1}$ . This is definitely an order of magnitude calculation because of the limited number of calculations. The simpler calculation could be done for many values of  $\tau^{-1}$  and a more accurate temperature dependence can be constructed. The results of some of the calculations are given in Figure 4 for orientations along the  $b$  and  $c$  axes. The simpler calculation indicates that the value of  $\tau^{-1}$  which fits the experimental data is  $\tau^{-1} = 9.9 \times 10^{12} \exp(-3680 \text{ cal}/RT) \text{ sec}^{-1}$ . Standard deviations have not been calculated because of the difficulty in determining a peak

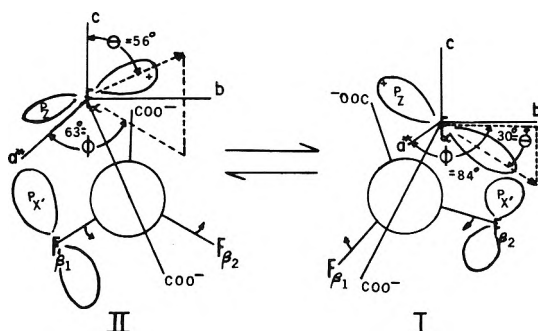


Figure 5. Newman projections along the  $\text{C}_{\alpha}\text{-C}_{\beta}$  bond showing the two configurations of the PFS radicals I and II which exist below  $130^\circ\text{K}$ . Rapid exchange between confirmation I and II lead to the room temperature configuration reported in ref 3. As a point of reference, the  $a^*$ ,  $b$ , and  $c$  axes are drawn relative to the  $\alpha$ -fluorine  $p_z$  orbital.

height or width from digitized spectra and the large errors in the experimental numbers.<sup>22</sup>

The results of the simpler ( $16 \times 16$ ) calculations agree quite well with those of the more complete ( $64 \times 64$ ) calculation. This indicates that the simpler calculation can be used to simulate the spectrum with a little loss of accuracy and rigor but with great saving in calculation time and complexity.

## Discussion

From the previous examination of the temperature-dependent hyperfine splittings of PFS,<sup>4</sup> it was suggested that the averaging process could result from a counterclockwise rotation of the direction normal to the plane of the radical by  $70^\circ$  while the  $\text{CF}_2(\beta)$  group moved about  $30^\circ$  clockwise. Alternative motions were also suggested including the possibility that the  $\alpha$  fluorine might exchange between two positions  $120^\circ$  apart, followed by some adjustments in structure. It now appears from the present calculation that the counterclockwise  $\alpha$ -fluorine rotation and the clockwise rotation of one  $\beta$  fluorine is a reasonable description of the motion.

Experimentally, the directions parallel to the largest  $\alpha$ -fluorine hyperfine splitting in each of the two PFS radicals were separated by a torsional angle of  $114^\circ$ . An approximate dihedral angle can be calculated from the average or expectation value of  $\cos^2 \theta$  obtained from the simulation of the  $\alpha$ -fluorine torsional oscillations. To gain a simple picture of the motion it is useful to assume that  $\arccos((\cos^2 \theta)^{1/2}) = \theta$ . This is, of course, a very rough approximation but it can be used to gain some physical insight into the extent of the motion. For PFS at  $300^\circ\text{K}$ ,  $\theta = 28^\circ$ . If this is the average displacement from an equilibrium position, this number must be multiplied by four to get a qualitative idea of the maximum extent of the motion. For PFS, the  $\alpha$  fluorines appear to be oscillating through an angle of about  $112^\circ$  in reasonable agreement with the experiment.

Inspection of the torsional oscillator calculation using the correct rotation of tensors shows that the averaging process is approximately as given in Figure 5. The principal direction of the largest  $\alpha$ -fluorine splitting ( $z$ ) (and thus the fluorine  $p$ -orbital direction) for radical II lies in a

(22) At temperatures above approximately  $220^\circ\text{K}$ , part or all of the spectrum could not be calculated because of the number of degeneracies in the eigenvalues generated by ALLMAT.<sup>21</sup> Because of this restriction on the temperature range of the calculations, the parameters used in the expression for  $\tau^{-1}$  have to be considered as giving only qualitatively correct results at higher temperatures.

plane above the  $a^*b$  plane ( $\theta = 56^\circ$ ,  $\varphi = 63^\circ$ , where  $\theta$  and  $\varphi$  are the spherical directions defined in Figure 5). When radical II undergoes torsional oscillation, the p orbital rotates to a direction below the  $a^*b$  plane corresponding to a direction parallel to the  $\alpha$ -fluorine principal axis ( $z$ ) of radical I ( $\theta = 119.7^\circ$ ,  $\varphi = 84.4^\circ$ ). Rapid oscillation gives rise to an  $\alpha$ -fluorine principal direction which lies near the  $a^*b$  plane at room temperature. This motion corresponds to an oscillation of the C-F $_{\alpha}$  group of approximately  $66^\circ$  which is the complement of  $114^\circ$ , the dihedral angle between the positive lobes of the fluorine p orbital. During the  $\alpha$ -fluorine torsional clockwise motion, the  $\beta$ -CF $_2$  group rotates in a counterclockwise motion by about  $30^\circ$  as deduced by the experimental direction cosines of  $\beta$ -fluorine hyperfine splittings. At the extreme ends of this motion exist two conformations in which the overlap of one  $\beta$ -fluorine  $2p_{xz}$  orbital with the  $\alpha$ -fluorine and carbon  $2p_{xz}$  orbitals is near a maximum, while the overlap with the second  $\beta$ -fluorine  $2p_{xz}$  orbital is near a minimum.

In order to determine the possible electron distribution for PFS, an INDO molecular orbital calculation<sup>23</sup> was carried out using standard bond lengths and angles for the carboxyl groups and standard bond lengths for the C $_{\beta}$ -F $_{\beta}$ , C $_{\alpha}$ -F $_{\alpha}$ , and C $_{\alpha}$ -C $_{\beta}$  bonds according to procedures reported previously.<sup>23</sup> The remaining angles were varied until a minimum in the energy was obtained.

Inspection of the calculated (INDO) optimized geometry of PFS showed that two radical conformations with the same minimum energy were possible. In the first conformation (see Figure 5, radical II), the F $_{\beta 2}$  (fluorine with the smallest splitting), C $_{\beta}$ , C $_{\alpha}$ , F $_{\alpha}$ , and the carboxyl group of atoms attached to the  $\alpha$  fluorine were found to lie in the XY plane where the X axis was defined to be parallel to the  $\alpha$ -carbon-carboxyl carbon bond. The carboxyl group attached to the  $\beta$  carbon and the  $\beta_1$  fluorine were found to lie nearly in the XZ plane. A second conformation (radical I, Figure 5) was obtained from the first conformation by a counterclockwise rotation of  $120^\circ$  about the C $_{\alpha}$ -C $_{\beta}$  bond and a clockwise rotation about the C $_{\beta}$ -carboxyl carbon. Essentially, only the role of the  $\beta$  fluorines was interchanged between the two conformations. These conformations agreed with those conformations deduced from esr measurements.<sup>4</sup>

The largest unpaired spin density (radical II) was found as expected in the C $_{\alpha}$  p $_z$  (0.733) and F $_{\alpha}$  p $_z$  orbital (0.073) while the unpaired spin density in the s orbitals of the  $\alpha$  carbon,  $\beta_1$  fluorine, and  $\beta_2$  fluorine contained (0.001), (0.004), and (0.0001) unpaired electrons, respectively. The fact that the  $\beta_2$ -fluorine atom lies nearly in the nodal plane of the C $_{\alpha}$ -F $_{\alpha}$  p $_z$  orbitals results in a very small unpaired density in the  $\beta_2$ -fluorine p orbitals (radical II), in fact, the spin density  $\rho^x(\text{F}_{\beta 2}) = 0.003$ ;  $\rho^y(\text{F}_{\beta 2}) = -0.0015$ ;  $\rho^z(\text{F}_{\beta 2}) = -0.0018$ . On the other hand, a significant unpaired spin density resides in the p orbitals on the  $\beta_1$ -fluorine atom ( $\rho^x(\text{F}_{\beta 1}) = 0.0002$ ;  $\rho^y(\text{F}_{\beta 1}) = 0.0360$ ;  $\rho^z(\text{F}_{\beta 1}) = 0.0150$ ). Since the XYZ axes are not parallel or perpendicular to the C $_{\beta}$ F $_{\beta}$  bonds, these densities do not correspond to the spin densities assigned to the normal p orbitals placed orthogonal to the C $_{\beta}$ F $_{\beta}$  bond. However, the above spin densities suggest considerable p-orbital unpaired spin density in the XZ plane. This effect agrees with what is depicted in Figure 5 as direct overlap of the Z and X' orbitals, suggesting that a mixture of  $\pi$ - $\pi$  and p- $\pi$  overlap exists between the  $\beta$  and  $\alpha$  fluorine and  $\alpha$  carbon. Experimentally the direction of the largest  $\beta_1$ -fluorine splitting tensor with respect to the directions of the largest  $\alpha$ -fluo-

rine and  $\alpha$ -carbon splitting tensor indicated considerable p- $\pi$  overlap. The calculated  $\beta$ -isotropic fluorine splittings of 4 and 179.5 G, although agreeing with the experimentally observed large and small splittings, failed to agree in magnitude.<sup>4</sup>

Calculations such as those done by Iwasaki<sup>24</sup> also indicate that the overlap of the  $\alpha$ -carbon and  $\alpha$ -fluorine p $_z$  orbitals with the p orbital of the  $\beta_1$  fluorine is a maximum while the  $\beta_2$ -fluorine p orbital is in a nodal plane of the p $_z$  orbitals of the  $\alpha$  fluorine and the  $\alpha$ -carbon. When the  $\alpha$  fluorine oscillates between its conformation in radical I and its conformation in radical II the overlap with each of the  $\beta$  fluorines changes from a maximum to a minimum. Even so, the origin of  $\beta$ -fluorine coupling constants is somewhat in doubt. Iwasaki<sup>24</sup> did a careful calculation of the expected hyperfine coupling constants for  $\beta$  fluorines as a function of the  $\beta$ -fluorine p orbital orientation with respect to the carbon p $_z$  orbital containing the unpaired spin. He concluded that most of the interaction arose because of the direct overlap of the fluorine p orbitals containing the lone pair and the carbon p $_z$  orbital. However, the experimentally observed  $\beta$ -fluorine couplings at 77°K for PFS fall outside of his calculated range of possible hyperfine couplings for  $\beta$  fluorines. Iwasaki's calculation did not include the effects of rotational averaging or any overlap with the  $\alpha$ -fluorine p orbital which may be the causes of this difference.

A similar restricted torsional motion was previously reported to occur about the C $_{\alpha}$ -C $_{\beta}$  bond for HOOC-CH $_2$ CHCOOH trapped in a mixed crystal of urea-fumaric acid.<sup>25</sup> The potential function for the torsional motion was also shown to have two equally populated minima. Analysis of the line shapes by use of the Bloch equations indicated that the potential barrier was approximately 2 kcal/mol. The somewhat higher barrier (3.7 kcal/mol) found for PFS could be a result of the difference between the  $\pi$  bonding present in PFS and the hyperconjugation present in the HOOCCH $_2$ CHCOOH radical. A host lattice dependence could also have an important influence.

In conclusion, the PFS radical exists in two conformations at 77°K due to the two possible ways in which strong overlap between the  $\alpha$ -fluorine and carbon  $2p_{xz}$  orbitals and one  $\beta$ -fluorine  $2p_{xz}$  orbital can occur. Upon raising the temperature, the PFS radical undergoes a torsional oscillation of the  $\alpha$  fluorine coupled to a motion of small amplitude involving the  $\beta$  fluorines. The torsional oscillation of the  $\alpha$  fluorine as determined from the temperature dependent  $\alpha$ -fluorine hyperfine splittings is responsible for the spin exchange effects as seen by the line width variations in the  $\beta$ -fluorine lines. The amount of torsion is such that in one orientation the  $\beta_1$  fluorine has a large hyperfine splitting and the  $\beta_2$  fluorine has a small splitting. As the  $\alpha$  fluorine rotates, this is reversed and the  $\beta$  fluorines appear to be averaged at 300°K.

*Acknowledgments.* We wish to acknowledge the Physics Department at the University of Alabama for use of their X-ray machine and to the University of Alabama Computing Center for a generous amount of computer time. Special thanks goes to H. Copeland for the help given on the density matrix calculations.

- (23) L. D. Kispert, C. U. Pittman, Jr., D. L. Allison, T. B. Patterson, Jr., C. W. Gilbert, Jr., C. F. Hains, and J. Prather, *J. Amer. Chem. Soc.*, **94**, 5979 (1972), and references cited therein.
- (24) M. Iwasaki, *Mol. Phys.*, **20**, 503 (1971).
- (25) C. Corvaja, *J. Chem. Phys.*, **44**, 1958 (1966).

# Indium-115 Nuclear Magnetic Resonance Study of Indium Complexes in Solvent Extraction System

Hiroki Haraguchi,\* Keiichiro Fuwa,

Department of Agricultural Chemistry, Faculty of Agriculture, The University of Tokyo, Yayoi, Bunkyo-ku, Tokyo 113, Japan

and Shizuo Fujiwara

Department of Chemistry, Faculty of Science, The University of Tokyo, Hongo, Bunkyo-ku, Tokyo 113, Japan

(Received December 7, 1972)

Indium-115 nuclear magnetic resonance spectra of indium-halogen complexes have been observed in solution. Chemical shifts of indium-115 vary with the kinds of coordination atoms in the order of  $\text{InCl}_4^- < \text{InBr}_4^- < \text{In}(\text{H}_2\text{O})_6^{3+} < \text{InI}_4^-$  from low to high magnetic field. The indium-115 line widths are mainly determined by quadrupole relaxation, which reflects the symmetry of complexes. The line widths are used along with the chemical shifts to elucidate the chemical equilibria and the chemical exchange of indium-halogen complexes in HCl, HBr, and HI aqueous solutions. When indium is extracted with various organic solvents from HCl, HBr, and HI solutions, the species in the organic solvents are tetrahedral complexes, examined from their data of the line widths and the chemical shifts of indium-115 nuclear magnetic resonance. In addition, the existence of the ion pair such as  $\text{H}^+ \cdots \text{InX}_4^-$  ( $\text{X} = \text{Cl}, \text{Br}, \text{and I}$ ) in the organic solvents has been determined by proton and indium-115 nuclear magnetic resonance.

## Introduction

Cannon and Richards showed that indium-115 nuclear magnetic resonance (nmr) is a very useful technique for the determination of the species and their structures in solution.<sup>1</sup> They investigated the species in various hydrogen acids in detail, and found that indium ion in  $\text{HNO}_3$  and  $\text{HClO}_4$  aqueous solutions exists as the hexaquoindium ion,  $\text{In}(\text{H}_2\text{O})_6^{3+}$ , which has octahedral symmetry.  $^{115}\text{In}$  nmr has not, however, been investigated in solution since their study. This may be due to the fact that  $^{115}\text{In}$  nmr gives relatively broad line widths even for the species with a high symmetry, as indium-115 nucleus has a large quadrupole moment.

According to solvent extraction studies, indium can be extracted as indium-halogen complexes with various organic solvents from HCl, HBr, and HI aqueous solutions.<sup>2-8</sup> Moreover, it has been suggested by Raman spectroscopy that the species extracted with ethyl ether from HCl, HBr, and HI aqueous solutions are tetrachloro-, tetrabromo-, and tetraiodoindium complexes with tetrahedral symmetry, respectively.<sup>9-11</sup> Hence  $^{115}\text{In}$  nmr seems to be useful for the investigation of these solvent extraction systems.

In the present work, line widths and chemical shifts of  $^{115}\text{In}$  nmr are measured for indium-halogen complexes in solution. These data are used to discuss the chemical equilibria and the chemical exchanges in acidic aqueous solutions, and along with those data obtained by proton nmr to identify the extracted species and their structures in organic solvents.

## Experimental Section

$\text{In}_2\text{O}_3$  (99.9%) and  $\text{In}(\text{NO}_3)_3 \cdot x\text{H}_2\text{O}$  were obtained from Mitsuwa Chemical Ind. Co. When  $\text{In}(\text{NO}_3)_3 \cdot x\text{H}_2\text{O}$  was used, the concentration of indium was determined by EDTA (ethylenediaminetetraacetic acid) titration. Organic solvents of reagent grade were used for solvent extraction without further purification. Samples of indium-

halogen complexes in organic solvents were obtained by extracting those complexes with organic solvents from the same volume of HCl, HBr, and HI aqueous solutions of indium, respectively, the concentrations of which are shown in Table I.

Spectra of  $^{115}\text{In}$  nmr were observed at 13.557 MHz using a bridge-type spectrometer, which was described previously,<sup>12</sup> and the peak-to-peak line widths were measured using 35-Hz modulation frequency, the amplitude of which was set to be small compared to the observed line widths. The sweep field was calibrated using a side-band technique. Sample tubes of 9 mm o.d. were used throughout the present experiment. For the measurement of chemical shifts, indium-bromine complex extracted with methyl isobutyl ketone (MIBK) from 5.5 N HBr solution was used as the external standard. The MIBK solution was enclosed in a small capillary and inserted into a sample tube. All measurements were carried out at 25°.

Proton magnetic resonance was observed on a JEOLCO 4H-100 100-MHz nmr spectrometer. In this case, tetramethylsilane (TMS) was used as the internal standard for the measurement of chemical shifts.

## Results and Discussion

Indium-115 line widths and chemical shifts of indium complexes observed by  $^{115}\text{In}$  nmr are listed in Table I. As

- (1) T. H. Cannon and R. E. Richards, *Trans. Faraday Soc.*, **62**, 1378 (1966).
- (2) H. M. Irving and F. J. C. Rossotti, *J. Chem. Soc.*, 2475 (1952).
- (3) G. N. Sundermann, I. B. Ackermann, and W. W. Meike, *Anal. Chem.*, **31**, 40 (1959).
- (4) L. Koste and J. Hoste, *Mikrochim. Acta*, **416**, 790 (1956).
- (5) J. Hoste and H. van den Berghe, *Mikrochim. Acta*, **416**, 797 (1956).
- (6) H. Hartlump and H. Specker, *Angew. Chem.*, **68**, 678 (1956).
- (7) H. Irving and F. J. C. Rossotti, *J. Chem. Soc.*, 2475 (1956).
- (8) B. S. Tsyvina and V. M. Vladimirova, *Zavod. Lab.*, **24**, 278 (1958).
- (9) L. A. Woodward and M. J. Taylor, *J. Chem. Soc.*, 4473 (1960).
- (10) L. A. Woodward and P. T. Bill, *J. Chem. Soc.*, 1699 (1955).
- (11) L. A. Woodward and G. H. Singer, *J. Chem. Soc.*, 716 (1958).
- (12) T. Yamamoto, H. Haraguchi, and S. Fujiwara, *J. Phys. Chem.*, **74**, 4369 (1970).

TABLE I:  $^{115}\text{In}$  Nmr Line Widths and Chemical Shifts of Indium Complexes

Complex	Indium concn, $M$	Acid concn	Solvent <sup>a</sup>	Line width, Hz	Chemical <sup>b</sup> shift, ppm
$\text{InCl}_4^-$	1.5	Concentrated HCl	MIBK	745	-239
			EE	1,255	-239
			<i>i</i> PE	675	-241
			<i>n</i> BA	2,030	<i>d</i>
			CH	<i>d</i>	<i>d</i>
			EAA	2070	-236
$\text{In}(\text{H}_2\text{O})_{6-x}\text{Cl}_x^{3-x}$	1.5	Concentrated HCl	Water	Broad	<i>d</i>
				(8,100) <sup>c</sup>	
$\text{InBr}_4^-$	1.0	Concentrated HBr	MIBK	490	~0
			EE	540	~0
			<i>i</i> PE	690	~0
			<i>n</i> BA	750	~0
			CH	<i>d</i>	<i>d</i>
			EAA	<i>d</i>	<i>d</i>
$\text{InBr}_4^-$	0.5	5.5 <i>N</i> HBr	MIBK	540	0 (ref)
			EE	660	~0
			<i>i</i> PE	470	~0
			<i>n</i> BA	850	~0
			CH	<i>d</i>	<i>d</i>
			EAA	1,040	~0
$\text{In}(\text{H}_2\text{O})_6^{3+}$	0.6	1 <i>N</i> $\text{HNO}_3$	Water	1,470	+180
$\text{In}(\text{H}_2\text{O})_{6-x}\text{Br}_x^{3-x}$	1.0	Concentrated HBr	Water	Broad	<i>d</i>
				(11,300) <sup>c</sup>	
$\text{InI}_4^-$	0.5	Concentrated HI	Water	850	+620
$\text{In}(\text{H}_2\text{O})_{6-x}\text{I}_x^{3-x}$	0.5	4.8 <i>N</i> HI	Water	4,800	+650
$\text{InI}_4^-$	0.2	2.0 <i>N</i> HI	MIBK	380	+650
			EE	405	+650
			<i>i</i> PE	535	+650
			<i>n</i> BA	1,980	+670
			CH	480	+655
			EAA	445	+650

<sup>a</sup> MIBK = methyl isobutyl ketone, EE = ethyl ether, *i*PE = isopropyl ether, *n*BA = *n*-butyl acetate, CH = cyclohexanone, EAA = ethyl acetoacetate. <sup>b</sup> The chemical shifts are defined as follows:  $\delta = [(H_c - H_r)/H_r]10^6$  (ppm), where  $H_r$  is the magnetic resonance field for  $\text{InBr}_4^-$  in MIBK, which was extracted from 5.5 *N* HBr solution, and  $H_c$  is the resonance field for the complexes for which  $\delta$  is given. Estimated accuracy,  $\pm 5$  ppm. <sup>c</sup> Reference 1. <sup>d</sup> Not detected because of line broadening, or samples not obtained because of the dissolution of the organic solvent into acidic aqueous solution.

shown in Table I, the hexacoordinated complex of  $\text{In}(\text{H}_2\text{O})_6^{3+}$  and the tetraordinated ones of  $\text{InCl}_4^-$ ,  $\text{InBr}_4^-$ , and  $\text{InI}_4^-$  can be distinguished from each other by their chemical shifts.<sup>13</sup> The order of the chemical shifts is  $\text{InCl}_4^- < \text{InBr}_4^- < \text{In}(\text{H}_2\text{O})_6^{3+} < \text{InI}_4^-$  from low to high magnetic field. This order is the same as those of aluminum and gallium complexes observed by  $^{27}\text{Al}$  and  $^{71}\text{Ga}$  nmr, respectively, although the chemical shifts of indium-115 are larger.<sup>15,16</sup> This can be attributed to the fact that the chemical shift of indium-115 is mainly determined by the paramagnetic shielding effect of the 5p electron.

If the line width of the indium complex is mainly determined by quadrupole relaxation, it may be qualitatively expressed as

$$\Delta\nu = \frac{8\sqrt{3}\pi^2}{125}(e^2Qq/h)^2\tau_c + \Delta\nu' \quad (1)$$

where  $\Delta\nu$  is the observed line widths in hertz,  $e^2Qq/h$  the quadrupole coupling constant in hertz,  $\tau_c$  the rotational correlation time in seconds, and  $\Delta\nu'$  the inhomogeneity of the magnetic field in hertz. The inhomogeneity is about 250 Hz at the magnetic field used, which is contained in the line widths shown in Table I. According to the Debye's rigid sphere model,  $\tau_c$  is expressed as

$$\tau_c = 4\pi r^3\eta/3kT \quad (2)$$

where  $r$  is a molecular radius,  $\eta$  the viscosity of the sample solution,  $k$  Boltzmann's constant, and  $T$  the absolute temperature. If the molecular radius of  $\text{In}(\text{H}_2\text{O})_6^{3+}$ , which is known as an octahedral complex,<sup>1</sup> is taken as 3 Å, the quadrupole coupling constant in 1 *N*  $\text{HNO}_3$  solution is calculated as 45 MHz from eq 1-2, where  $\eta$  is assumed to be 2 cP.

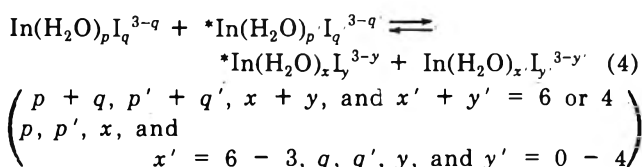
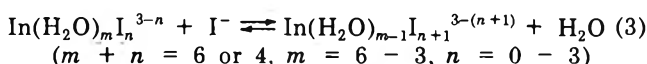
As shown in Table I, almost all the line widths of  $\text{InCl}_4^-$ ,  $\text{InBr}_4^-$ , and  $\text{InI}_4^-$  in various organic solvents used are smaller than that of  $\text{In}(\text{H}_2\text{O})_6^{3+}$  with octahedral symmetry. In ethyl ether, the tetraordinated complexes give line widths of 1255, 540, and 405 Hz, respectively. These results suggest that  $\text{InCl}_4^-$ ,  $\text{InBr}_4^-$ , and  $\text{InI}_4^-$  are tetrahedral. This coincides with the conclusion obtained by Raman spectroscopy.<sup>9-11</sup>

*Complexes in HCl, HBr, and HI Aqueous Solutions.* The line widths of indium-115 in the concentrated HCl

- (13) Dimeric species such as  $\text{In}_2\text{X}_6$  may not be present in the organic solvents, because such species exist only in the case of anhydrous metal halides dissolved in anhydrous organic solvents. In addition, when anhydrous indium iodide was dissolved in ethyl ether, no signal could be observed. This suggests that a dominant species in this solution is an adduct compound such as  $(\text{C}_2\text{H}_5)_2\text{O}\cdot\text{InI}_3$  rather than dimeric species  $\text{In}_2\text{I}_6$ . Similar adduct compounds have been known for indium bromide<sup>14</sup> and aluminum halides.<sup>15</sup>
- (14) I. A. Sheka, *Zh. Obshch. Khim.*, **26**, 26 (1956); *Chem. Abstr.*, **49**, 11748e (1956).
- (15) H. Haraguchi and S. Fujiwara, *J. Phys. Chem.*, **73**, 3467 (1969).
- (16) J. W. Akitt, N. N. Greenwood, and A. Storr, *J. Chem. Soc.*, 4410 (1965).

and HBr aqueous solutions could not be observed because of the very broad line width. This suggests that the complexes with low symmetry are dominant in these solutions. They may be mixed complexes as shown by  $\text{In}(\text{H}_2\text{O})_{6-x}\text{Cl}_x^{3-x}$  or  $\text{In}(\text{H}_2\text{O})_{6-x}\text{Br}_x^{3-x}$ .<sup>17</sup>

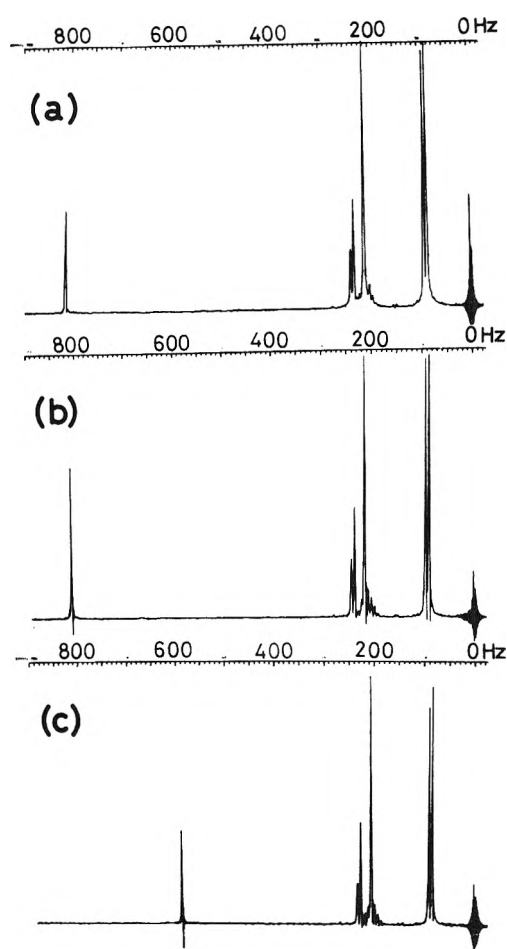
On the other hand, indium in HI aqueous solution gives an observable signal. As shown in Table I, the line width and the chemical shift of indium in concentrated HI solution are 850 Hz and +620 ppm, respectively, which are almost similar to those of  $\text{InI}_4^-$  in ethyl ether. This fact indicates the existence of  $\text{InI}_4^-$  of tetrahedral symmetry in this solution. The small difference of the chemical shift of  $\text{InI}_4^-$  in this solution from that in ethyl ether may be due to the solvent effect. When the concentration of HI is 4.8 N, the line width of indium becomes very broad, and its chemical shift changes to the higher magnetic field. The broadening of the line width in the case of 4.8 N HI solution is ascribed to the formation of the mixed complex such as  $\text{In}(\text{H}_2\text{O})_{6-x}\text{I}_x^{3-x}$  with low symmetry. Cannon and Richards reported -180 and +300 ppm as the chemical shifts for  $\text{In}(\text{H}_2\text{O})_{6-x}\text{Cl}_x^{3-x}$  and  $\text{In}(\text{H}_2\text{O})_{6-x}\text{Br}_x^{3-x}$ , respectively, and -440 and -180 ppm for  $\text{InCl}_4^-$  and  $\text{InBr}_4^-$  in ethyl ether, respectively, using  $\text{In}(\text{H}_2\text{O})_6^{3+}$  as the external standard.<sup>1</sup> According to their results for the mixed chlorine and bromine complexes, the chemical shift for the mixed iodine complex can also be explained by the formation of the mixed complex. Moreover, the fact that the line width of indium becomes broader as the concentration of HI decreases indicates the existences of the following chemical equilibria and fast chemical exchange in solution, shown by eq 3 and 4, respectively.<sup>18</sup>



The similar chemical equilibria and chemical exchanges may exist in the case of indium in HCl or HBr solution, although the formation of tetrahedral complex occurs to only a slight extent.

**Indium-Halogen Complexes in Organic Solvents.** The data of <sup>115</sup>In nmr line widths and chemical shifts of indium-halogen complexes in various organic solvents are summarized in Table I, where the concentrations of HCl, HBr, and HI, and those of indium in acidic aqueous solutions are also described. In the case of the indium-bromine complex, the dependences of the line widths and the chemical shifts on the concentrations of both indium and HBr were examined, and these results are also shown in Table I. As can be seen from these results, the line widths and the chemical shifts do not strongly depend on the concentrations of indium and HBr, although the line widths are slightly different in two cases. Therefore, such concentration dependences of the line widths and the chemical shifts were not examined in the cases of indium-chlorine and -iodine complexes.

As previously mentioned,  $\text{InCl}_4^-$ ,  $\text{InBr}_4^-$ , and  $\text{InI}_4^-$  are distinguished from each other by the differences in their chemical shifts. In such a case, each complex shows the similar chemical shift in the different organic solvents within the experimental error of  $\pm 5$  ppm. In addition, almost all the complexes in the organic solvents give line



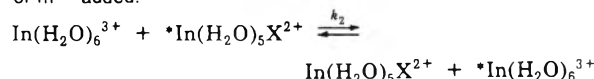
**Figure 1.** Proton nmr spectra of  $\text{H}^+ \cdots \text{InX}_4^-$  in MIBK at 100 MHz: (a)  $\text{H}^+ \cdots \text{InCl}_4^-$  ( $[\text{In}] = 1.5 \text{ M}$  in concentrated HCl); (b)  $\text{H}^+ \cdots \text{InBr}_4^-$  ( $[\text{In}] = 1.0 \text{ M}$  in concentrated HBr); (c)  $\text{H}^+ \cdots \text{InI}_4^-$  ( $[\text{In}] = 0.2 \text{ M}$  in 2.0 N HI).

widths of the same order as or smaller than that of  $\text{In}(\text{H}_2\text{O})_6^{3+}$ . These results indicate that all these complexes are essentially tetrahedral in all the organic solvents investigated in this work.

When the results shown in Table I are examined in more detail, the line widths of indium-halogen complexes generally become narrower in the order  $\text{InCl}_4^- > \text{InBr}_4^- > \text{InI}_4^-$ . These results suggest that another factor besides a molecular radius should be considered for the determination of their line widths, although the molecular radius is also important as can be shown from eq 1-2. Such a

(17) Cannon and Richards reported 8100 and 11,300 Hz as the line widths of these mixed complexes, respectively.<sup>1</sup>

(18) Cannon and Richards calculated the exchange rates in the following reactions, assuming the fast exchange due to the fact that <sup>115</sup>In nmr line widths are linearly dependent on the concentration of  $\text{X}^-$  or  $\text{In}^{3+}$  added.<sup>1</sup>

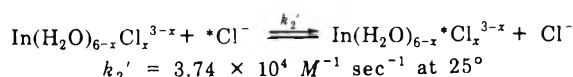


$$k_2 = 8.5 \times 10^3 \text{ M}^{-1} \text{ sec}^{-1} \text{ for } \text{X} = \text{Cl}$$

$$= 8.6 \times 10^3 \text{ M}^{-1} \text{ sec}^{-1} \text{ for } \text{X} = \text{Br}$$

$$= 2.2 \times 10^3 \text{ M}^{-1} \text{ sec}^{-1} \text{ for } \text{X} = \text{I at } 25^\circ,$$

where  $[\text{In}] = 0.405 \text{ M}$  and  $[\text{X}^-]/[\text{In}] < 1$ , and



where  $[\text{Cl}^-] = 2 \text{ M}$  and  $[\text{In}]/[\text{Cl}] < 1$ .

TABLE II: Chemical Shifts of Proton Magnetic Resonance of  $H^+ \cdots InX_4^-$  in Organic Solvents<sup>a</sup>

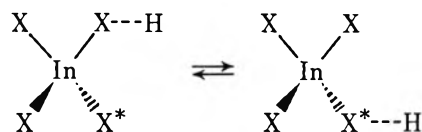
Solvent <sup>b</sup>	HCl concn, M (1.5 M) <sup>c</sup>	HBr concn, M (1.0 M) <sup>c</sup>	HBr concn, M (0.5 M) <sup>c</sup>	5.5 N HBr (1.0 M) <sup>c</sup>	5.5 N HBr (0.5 M) <sup>c</sup>	2 N HI (0.2 M) <sup>c</sup>
MIBK	8.16	8.13	8.12	6.62	6.74	5.95
EE	8.10	7.88	<i>d</i>	<i>d</i>	6.58	6.10
<i>i</i> PE	8.63	8.38	<i>d</i>	<i>d</i>	7.59	6.75
<i>n</i> BA	7.98	8.06	<i>d</i>	<i>d</i>	7.04	6.63
CH	8.02	7.73	<i>d</i>	<i>d</i>	6.28	5.51
EAA	7.61	7.27	<i>d</i>	<i>d</i>	6.23	5.34

<sup>a</sup> All data are expressed in ppm from TMS. <sup>b</sup> Abbreviation of the solvents is the same as that shown in Table I. <sup>c</sup> Concentration of indium in acidic aqueous solution. <sup>d</sup> Not investigated.

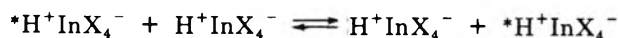
factor may be the electric field gradient produced by the proton in the organic solvents. When indium-halogen complexes are extracted into the organic solvents, protons are also transferred in order to maintain the electric charge neutrality condition. Therefore, the above results may be ascribed to the formation of an ion pair between proton and indium-halogen complex such as  $H^+ \cdots InX_4^-$ . As for the present experimental system, the existence of protons in the organic solvents was examined by proton magnetic resonance. The spectra of proton magnetic resonance in the case of MIBK solutions are shown in Figure 1a-c. As can be seen from the spectra, the existence of a proton in MIBK is clearly recognized as for the respective solvent extraction system. The results of proton magnetic resonance are summarized in Table II. If the ion pair suggested above is formed in the organic solvent, the tetrahedral symmetry about the indium nucleus may be broken down due to the electric charge of proton. Since the electric field gradient is proportional to  $r^{-5}$ , where  $r$  is the distance from the proton to the indium nucleus, the field gradient is larger the smaller the size of the complex. Therefore, the  $^{115}In$  nmr line width is expected to decrease in the order  $InCl_4^- > InBr_4^- > InI_4^-$ . This relation is generally realized in the results shown in Table I. The effect of protons on the  $^{115}In$  nmr line width is supported by the fact that the same indium-halogen complex gives considerably different line widths in different organic solvents. For example,  $^{115}In$  nmr line widths

of indium-iodine complexes in the organic solvents increase in the order MIBK < EE < EAA < CH < *i*PE < *n*BA. This result indicates that the distances between proton and indium nucleus in  $H^+ \cdots InI_4^-$  are different in those solvents. While it may be considered that such distances are mainly affected by the dielectric constants of the solvents, the correlation between  $^{115}In$  nmr line width and the dielectric constant could not be recognized in the present results. This may be due to the effects of the acids and water dissolved into the organic solvents. Those effects of the acids can be seen from the result, as is shown in Table II, that the chemical shifts of proton nmr depend on the concentration of HBr rather than that of indium in the case of the HBr-MIBK system.

In order for ion pairing between  $H^+$  and  $InX_4^-$  to be the major factor in the quadrupole relaxation, as proposed above, it is required that intra- and intermolecular proton exchange such as



or



should be relatively slow. Otherwise exchange effects may contribute to the observed line width.

# Rotational Isomerism of the Phenylalanine Anion in Mixed Aqueous Solvents by Nuclear Magnetic Resonance<sup>1</sup>

J. M. Purcell, J. E. Ramirez,<sup>2</sup> and J. R. Cavanaugh\*

Eastern Regional Research Laboratory,<sup>3</sup> Philadelphia, Pennsylvania 19118 (Received December 14, 1972)

Publication costs assisted by the U. S. Department of Agriculture

The chemical shifts and coupling constants for the aliphatic protons of the phenylalanine anion in mixed aqueous solvents have been obtained as a function of temperature and solvent composition. In general, the vicinal coupling constants diverge as the mole fraction of the nonaqueous component increases. The effect increases in the series urea < ethylene glycol, acetamide < methanol < dimethyl sulfoxide < acetone, urea causing even a mild convergence with increasing concentration. For those solvent mixtures for which the vicinal coupling constants diverge, the divergence of the coupling constants with temperature is reduced. With aqueous urea as solvent, on the other hand, the results are almost identical with pure water. These variations are interpreted in terms of the conformational stability of the staggered rotamers, the less favorable rotamers becoming less stable as the proportion of the nonaqueous component increases. The rotamer stabilities appear to be generally related to solubility and dielectric properties of the mixed aqueous solvents, but no correlation can be found between variations in the coupling constants and the "water-like" character of these solvents.

In a series of investigations,<sup>4</sup> the nmr spectra of the aromatic amino acids have been obtained in aqueous solution as a function of temperature and amino acid concentration. The results have been interpreted in terms of variations of the relative energies of the classical staggered rotamers. It appears that the rotamer energies are influenced by temperature and concentration-dependent solute-solute and solute-solvent interactions. The nature of these interactions is as yet unclear but, undoubtedly, the structure of water plays an important role. In order to vary systematically the properties of the water system, we have employed as solvents, mixtures of a variety of organic reagents with water at different concentrations. The effects of these mixed aqueous solvents on the rotational isomerism of the phenylalanine anion form the basis of the present communication.

## Experimental Section

The nmr spectra were recorded on a Varian Associates DA-60 IL spectrometer,<sup>5</sup> equipped with a variable temperature probe and operated at 60 MHz in the internal-lock, frequency-sweep mode. The frequency sweep was calibrated in the vicinity of each resonance peak by counting the difference between the fixed and swept oscillators. Line positions were calculated as the averages of at least four recordings taken with alternate upfield and downfield sweeps. Precision of the measurements was better than 0.1 Hz. The temperature in the probe was measured directly using a thermistor thermometer placed inside an empty nmr sample tube at the location of the transmitter-receiver coils. The probe assembly was fitted with a standard pressure cap through which the leads from the thermistor were led to a resistance bridge for measurement. The temperature could be measured to within 0.5° and remained stable to  $\pm 1^\circ$  during the course of the nmr measurements.

The amino acids and the solvents were obtained commercially and were of the highest purity obtainable. Acet-

amide and urea were recrystallized from methanol solution; ethylene glycol was twice redistilled; the other compounds were used without further purification. The samples were prepared with the mole fraction of phenylalanine kept constant at 1/55.5 (corresponding to 1 mol of phenylalanine per liter of solvent for pure water) while the composition of the solvent was varied. Solvent compositions are reported in terms of mole fraction of the organic reagent with regard to the solvent. Sufficient NaOH was included in the mixture to ensure that the phenylalanine was in the anionic state. *tert*-Butyl alcohol (2% v/v) was added as an internal standard.

The solubilities were determined gravimetrically by the dry weight method described previously<sup>6</sup> with the following modifications and exceptions. Additional water was added to the solutions of alanine and phenylalanine in dimethyl sulfoxide-water and the samples were dried by lyophilization before oven drying at 110°. For alanine in acetamide-water systems, water was first removed by rotary evaporation at 50°, the acetamide was separated by extraction with chloroform, and the alanine residue was finally dried at 110°. Runs carried out with known amounts of alanine showed that the method was quantitative. The concentration of phenylalanine in acetamide-water solutions was determined spectrophotometrically.<sup>6</sup> As a further check on the dry weight method, the solubilities of alanine and phenylalanine in pure water were determined; results were in excellent agreement with those reported previously.<sup>6</sup>

- (1) Presented in part at the 162nd National Meeting of the American Chemical Society, Washington, D. C., Sept 12-17, 1971.
- (2) Research performed under tenure of an NRC-ARS Postdoctoral Research Associateship. Present address, McKesson Laboratories, Fairfield, Conn. 06430.
- (3) Agricultural Research Service, U. S. Department of Agriculture.
- (4) (a) J. R. Cavanaugh, *J. Amer. Chem. Soc.*, **89**, 1558 (1967); (b) *ibid.*, **90**, 4533 (1968); (c) *ibid.*, **92**, 1488 (1970).
- (5) Mention of commercial products does not constitute an endorsement by the U. S. Department of Agriculture over others of a similar nature not mentioned.
- (6) Y. Nozaki and C. Tanford, *J. Biol. Chem.*, **238**, 4074 (1963).

## Results and Discussion

Spectral analysis and the calculation of chemical shifts and coupling constants were performed as discussed previously.<sup>4</sup> The results are presented in Table I.

*Framework for the Interpretation of the Variations in the Vicinal Coupling Constants.* It has become well established that the rotational isomerism of amino acids is adequately represented in the classical manner, that is, by an equilibrium mixture of the three staggered rotamers obtained by internal rotation about the  $\alpha$  carbon- $\beta$  carbon bond. The staggered rotamers are illustrated in Figure 1 for a substituted alanine. Since the internal rotation is sufficiently rapid, the observed coupling constants are weighted averages over those corresponding to the individual rotamers. The vicinal coupling constants are assumed to obey the form of the Karplus equation;<sup>7</sup> that is, the coupling constants of protons gauche or trans to one another are assumed to have the same value regardless of the particular conformation. The averaged vicinal coupling constants,  $J_{12}$  and  $J_{13}$ , are then simply given by

$$\begin{aligned} J_{12} &= (a + c)J_g + bJ_t \\ J_{13} &= (a + b)J_g + cJ_t \end{aligned} \quad (1)$$

where  $a$ ,  $b$ , and  $c$  are the normalized populations of rotamers A, B, and C, respectively, and  $J_g$  and  $J_t$  are the coupling constants of protons gauche or trans to one another. The populations are governed by the usual Boltzmann distribution; that is

$$a : b : c = e^{-F_A/RT} : e^{-F_B/RT} : e^{-F_C/RT} \quad (2)$$

where  $F_i$  is the appropriate rotamer free energy.

The rotational isomerism of the aromatic amino acids could not be explained simply in this fashion. The vicinal coupling constants diverged with increasing temperature in direct opposition to the expected trend toward equalization of the rotamer populations through the Boltzmann factor. The cause of the anomalous variations was interpreted<sup>8</sup> as arising from changes in the rotamer energies themselves with temperature; the two less favorable rotamers, A and B, became less stable as the temperature increased. Concentration effects were also in evidence. Apparently, the rotamer energies were being influenced by temperature and concentration-dependent solute-solute and solute-solvent interactions.

*Vicinal Coupling Constants as a Function of Composition and Temperature.* The variations in the vicinal coupling constants for the phenylalanine anion as a function of the composition of the mixed aqueous solvents are illustrated in Figure 2.<sup>9</sup> The values shown represent the data at 28° for all solvent systems except ethylene glycol. The viscosity of ethylene glycol at room temperature causes sufficient deterioration of spectral resolution that higher temperatures were required for accurate measurements. The data for pure water were interpolated from the data in ref 4a at 28°. The values for acetamide and ethylene glycol actually differ slightly even though they are shown as superimposable in Figure 2 for clarity of presentation.

In general, the coupling constants diverge with increasing fraction of the nonaqueous component. The effect is largest for acetone and ranges down through the series dimethyl sulfoxide, methanol, acetamide, ethylene glycol, and urea. The results for urea exhibit even a slight convergence with increasing urea concentration.

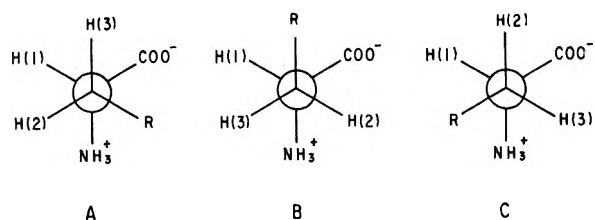


Figure 1. Newmann projections of the staggered rotamers of an R-substituted alanine (dipolar ion).

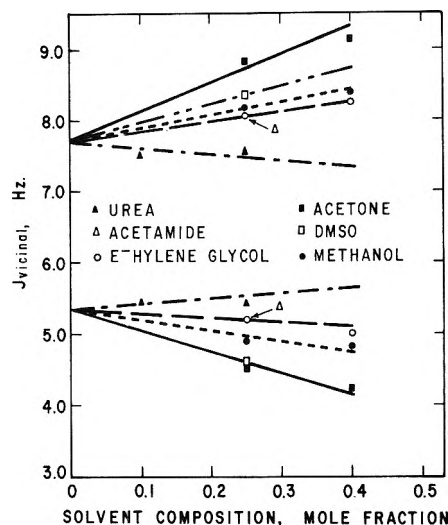


Figure 2. Variations of the phenylalanine anion vicinal coupling constants with solvent composition.

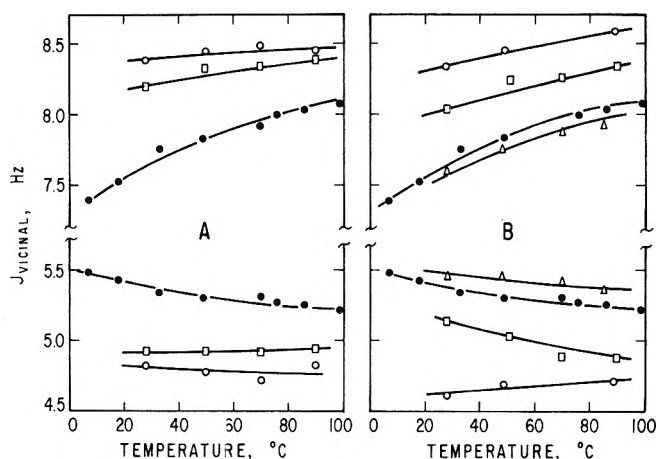


Figure 3. Temperature variations of the phenylalanine anion vicinal coupling constants in various solvent mixtures: ●, water; (A) □, 0.25 mol fraction methanol; ○, 0.4 mol fraction methanol; (B) △, 0.25 mol fraction urea; □, 0.25 mol fraction acetamide; ○, 0.25 mol fraction ethylene glycol.

The temperature variations of the coupling constants appropriate to some of these systems are shown in Figure 3. Included for comparison are the corresponding data for the phenylalanine anion in aqueous solution. The results for the alcohol-water system for two concentrations are displayed in Figure 3A, the outer curves representing the more concentrated alcohol system. Both curves exhibit

(7) M. Karplus, *J. Chem. Phys.*, **30**, 11 (1959).

(8) Cf. ref 4 for details of the experimental results and for the argumentation leading to the interpretations outlined here.

(9) The lines shown are hand drawn and intended simply to distinguish trends.



TABLE I: Chemical Shifts<sup>a</sup> and Coupling Constants<sup>b</sup> for the Phenylalanine Anion<sup>c</sup>

Nonaqueous component	Concn <sup>c</sup>	Temp <sup>e</sup>	$J_R$	$J_V^f$	$\Delta\nu_\alpha$	$\Delta\nu_\beta$		
Methanol- <i>d</i> <sub>4</sub>	0.25	28	-13.50	4.92	8.20	134.80	110.72	92.07
		50	-13.54	4.92	8.32	135.15	111.87	91.49
		70	-13.61	4.92	8.34	135.31	112.49	91.26
		90	-13.71	4.94	8.39	135.40	113.00	90.78
	0.4	28	-13.52	4.82	8.38	134.72	112.11	91.54
		50	-13.57	4.77	8.44	135.12	113.02	91.15
		70	-13.49	4.72	8.49	135.32	113.71	90.84
		90	-13.64	4.83	8.45	135.37	114.15	90.76
Urea	0.1	28	-13.43	5.46	7.53	134.67	105.73	93.29
		28	-13.47	5.46	7.60	136.19	106.67	94.22
	0.25	48	-13.50	5.45	7.75	136.30	107.94	93.41
		70	-13.60	5.42	7.87	136.81	109.23	93.41
		85	-13.70	5.36	7.92	136.83	109.60	92.61
Acetamide	0.25	28	-13.39	5.14	8.04	133.63	112.37	94.35
		51	-13.47	5.03	8.24	133.60	112.47	92.93
		70	-13.58	4.89	8.26	133.19	112.68	92.17
		90	-13.63	4.88	8.34	133.14	113.21	91.65
Dimethyl- <i>d</i> <sub>6</sub> sulfoxide	0.25	28	-13.67	4.61	8.34	129.61	110.86	89.11
		49	-13.52	4.69	8.45	129.66	111.37	88.64
		89	-13.62	4.71	8.59	129.73	112.12	88.00
Acetone	0.25	28	-13.45	4.55	8.86	134.85	113.54	89.08
	0.40	28	-13.46	4.25	9.18	134.69	115.30	87.39
Ethylene glycol	0.25	52	-13.58	5.25	8.07	135.66	110.38	92.86
	0.40	52	-13.58	4.99	8.26	138.30	110.99	92.47

<sup>a</sup> In Hz at 60-MHz downfield from *tert*-butyl alcohol (methyl resonance). <sup>b</sup> In Hz. <sup>c</sup> The concentration of the phenylalanine anion was kept constant at 1 mol per 55.5 mol of solvent mixture. <sup>d</sup> The concentration of the nonaqueous component in mole fraction units. <sup>e</sup> In °C. <sup>f</sup> The smaller of the two vicinal coupling constants is associated with the  $\beta$  proton resonance at lower field.

less divergence with increasing temperature than that shown for the water solution.

Some of the other systems are illustrated in Figure 3B. The curves for acetamide and dimethyl sulfoxide are similar to those for the methyl alcohol system with some variations. The smaller coupling constant for the acetamide-water system, for example, decreases slightly more rapidly with increasing temperature than that for pure water. On the other hand, the smaller coupling constant for the dimethyl sulfoxide system actually increases with increasing temperature. The urea system, for which there is little variation in the coupling constants with urea concentration, yields results remarkably close to those for pure water.

Qualitatively, the overall results may be summarized as follows: the larger the concentration divergent effect of the nonaqueous component on the averaged coupling constants, the more the anomalous temperature dependence appropriate to the aqueous solutions is attenuated. If the nonaqueous component has little effect on the coupling constants, the temperature dependence is not appreciably altered.

The variations in the coupling constants with solvent composition exhibited here must find their origin in variations in the rotamer populations. Even though it is conceivable that the proton-proton vicinal coupling constants in the staggered rotamers are themselves affected by changes in the solvent, the evidence against such a dependence on solvent medium is by now very secure, the best evidence coming from the invariance of the coupling con-

stants in conformationally rigid molecules.<sup>10</sup> Furthermore, classical electrostatic theory has been very successfully applied to rotational isomerism<sup>11</sup> by treating the variations in proton-proton vicinal coupling constants as arising solely from medium effects on the rotamer energies.

Changes in the rotamer populations and in the relative rotamer energies can be related to changes in the coupling constants by means of eq 1 and 2. Numerical values are assigned to  $J_R$  and  $J_V$ , and the populations and energies calculated from the experimentally observed coupling constants.<sup>12</sup> According to this interpretation, C is the most favorable rotamer for the phenylalanine anion with a population at room temperature in pure water of about 0.5. As the coupling constants diverge with solvent composition, the less favorable rotamers, A and B, became even less favorable and rotamer C increases in population.

The temperature dependence for the mixed solvent systems is consistent with this interpretation. Those nonaqueous solvents that cause a divergence of the coupling constants bring about an increase in the relative energies of the unfavorable A and B rotamers. In these mixed solvents at room temperature, the rotamer energies are already increased, any further increase with temperature is correspondingly reduced, and the divergence of the cou-

(10) A. M. Ibragimov and S. L. Smith, *J. Amer. Chem. Soc.*, **94**, 34 (1972); S. L. Smith and R. H. Cox, *J. Phys. Chem.*, **72**, 198 (1968); S. L. Smith and A. M. Ibragimov, *J. Chem. Phys.*, **46**, 1181 (1967).

(11) R. J. Abraham and R. H. Kemp, *J. Chem. Soc. B*, 1240 (1971). This paper is the eleventh in the series. The series can be generated by referring in turn to each preceding issue.

pling constants with increasing temperature is thereby diminished.

The actual values calculated for the populations and the relative rotamer energies are of course contingent on the values chosen for  $J_g$  and  $J_t$  and on the assumption that a single  $J_g$  is adequate to describe the system. Nevertheless, interpretations developed here will be based on changes in these parameters and the relationship of these changes to the physical systems. Therefore, even though the relative rotamer energies may not be very accurately known, variations in the rotamer energies can be carefully assessed.

*Variations in the Vicinal Coupling Constants and Properties of the Mixed Aqueous Solvents.* The changes in the vicinal coupling constants as they relate to variations in the rotamer energies can be conveniently discussed in terms of the quantity,  $\Delta J = J_{13} - J_{12}$ , the difference in the two coupling constants.  $\Delta J$  measures the divergence of the coupling constants and according to eq 1 can be expressed as a linear function of  $(c - b)$ , the difference in the populations of the C and B rotamers. Therefore, it takes into account variations in two of the populations and provides a more general description of the system than could be obtained by either of the coupling constants individually.

The variations in the rotamer energies observed here are apparently the result of variations in (the as yet imprecisely defined) solute-solvent interactions. Such interactions are likewise responsible for many of the bulk properties of these mixed solvent systems. In this section, three of these properties will be discussed in relation to variations in  $\Delta J$ . These properties are the solubility of phenylalanine in the mixed solvents, their dielectric constants, and the free energy of transfer of the phenyl group from water into the mixed solvents. The first and last properties are intimately connected with the effects of solute-solvent interactions; the dielectric constant is a general measure of the polar nature of the solvent, indicative of the kinds of solvent interactions possible.

A number of the appropriate data, especially the dielectric constants, are readily available in the literature. Data on solubilities are more limited and it was necessary to measure them directly for the acetone-, acetamide-, and dimethyl sulfoxide-water systems. These results and the pertinent literature information are collected in Table II.<sup>13-20</sup> Details of the measurements can be found in the Experimental Section.

The solubility of phenylalanine in the mixed solvents of composition 0.25 mol fraction in the nonaqueous component is plotted in Figure 4A *vs.* the phenylalanine anion  $\Delta J$  appropriate to the same solvents. The values of  $\Delta J$  are taken from Table I at 28° for all solvent systems except ethylene glycol-water for which the temperature is 52°. The value for pure water was interpolated from the data in ref 4a for 25°.

As illustrated by Figure 4A, the increasing divergence of the coupling constants roughly correlates with decreasing phenylalanine solubility. The point for water falls well below, while the point for acetone rises above the trend established by the other points. Nevertheless, despite the inexactness of the relationship, these results suggest that the solute-solvent interactions responsible for the increase in solubility of the phenylalanine molecule are related to the solute-solvent interactions that enhance the stability of the A and B rotamers.<sup>21</sup>

TABLE II: Amino Acid Solubilities and Dielectric Constants for the Mixed Aqueous Solvents

Solvent <sup>a</sup>	Solubility <sup>b</sup>		Dielectric constant <sup>c</sup>
	Alanine	Phenylalanine	
Water	0.0326 <sup>f</sup>	0.00302 <sup>f</sup>	78.5 <sup>j</sup>
Ethylene glycol	(-552) <sup>d</sup>	0.00320 <sup>g</sup>	61.9 <sup>k</sup>
Urea	(-740) <sup>e</sup>	0.00857 <sup>h</sup>	100.4 <sup>j</sup>
Methyl alcohol	0.0116 <sup>i</sup>	0.00232 <sup>i</sup>	60.9 <sup>k</sup>
Acetone	0.00423	0.00193	47.0 <sup>k</sup>
Acetamide	0.00709	0.00412	71.3 <sup>l</sup>
Dimethyl sulfoxide	0.00163	0.00092	73.6 <sup>m</sup>

<sup>a</sup> Composition of the mixed solvents is 0.25 mol fraction in the nonaqueous component. <sup>b</sup> In mole fraction units at 25°. Entries without a reference are experimental results (see text). <sup>c</sup> At 25° unless stated otherwise. <sup>d</sup> Free energy of transfer of the phenyl group interpolated directly from the data in ref 13 (n cal/mol). <sup>e</sup> Free energy of transfer of the phenyl group extrapolated directly to 10.0 M from the data in ref 6 (in cal/mol). <sup>f</sup> Reference 13. <sup>g</sup> Reference 14. <sup>h</sup> Reference 15. <sup>i</sup> Reference 16. <sup>j</sup> Reference 17. <sup>k</sup> Reference 18. <sup>l</sup> Reference 19. <sup>m</sup> Reference 20.

Dielectric constant *vs.*  $\Delta J$  is illustrated in Figure 4B. A general but inexact correlation is found between decreasing  $\Delta J$  and increasing dielectric constant. It appears that the more polar the solvent mixture, the more are enhanced the A and B rotamer stabilities. This interpretation is consistent with the observed temperature and concentration dependence of the rotamer energies of the phenylalanine anion in pure water.<sup>4b</sup> There, also, increases in the dielectric constant of the solution brought about an increase in the stability of the A and B rotamers. The lack of a more precise correlation here precludes a more quantitative development at this time.

Finally,  $\Delta J$  is compared to the free energies of transfer of the phenyl group in Figure 4C. The values are calculated from the following<sup>6,13</sup>

$$\delta g_{t,(\text{phenyl group})} \approx RT \left[ \ln \frac{N_{PA,W}}{N_{PA,S}} - \ln \frac{N_{A,W}}{N_{A,S}} \right] \quad (3)$$

where  $N_{i,j}$  is the concentration in mole fraction units of substance *i* in a saturated solution in solvent *j* and where PA, A, W, and S refer to phenylalanine, alanine, water, and mixed solvent, respectively. Activity coefficient corrections have been ignored in our calculations because the differences between estimates for phenylalanine and ala-

(12)  $J_g$  and  $J_t$  are assigned values of 2.60 and 13.56 Hz, respectively. Cf. K. G. R. Pachler, *Spectrochim. Acta*, **20**, 581 (1964). Representative values obtained for the relative rotamer energies can be found in ref 4. The limits of validity of this interpretation are discussed later.

(13) Y. Nozaki and C. Tanford, *J. Biol. Chem.*, **240**, 3568 (1965).

(14) Linearly interpolated from the data in ref 13.

(15) Value obtained by extrapolation to 10.0 M from the data in ref 6.

(16) T. E. Needham, A. N. Paruta, and R. J. Gerraughty, *J. Pharm. Sci.*, **60**, 258 (1971). Input for the equations in M/l obtained from density data given in "Handbook of Chemistry and Physics," 47th ed, Chemical Rubber Publishing Company, Cleveland, Ohio, 1966.

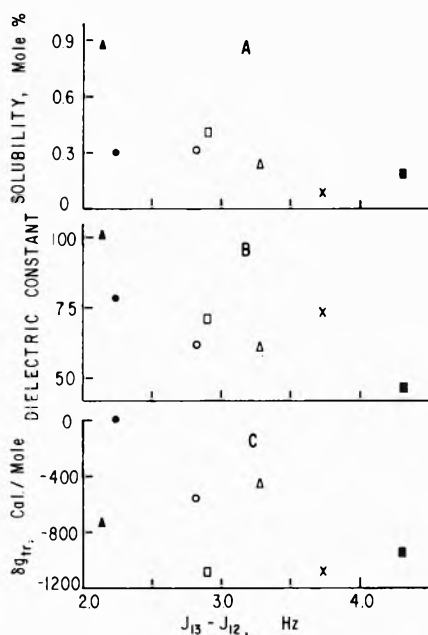
(17) J. Wyman, *J. Amer. Chem. Soc.*, **55**, 4116 (1933). Figure for urea-water system obtained by linear interpolation.

(18) G. Akerloff, *J. Amer. Chem. Soc.*, **54**, 4125 (1932). Values obtained by linear interpolation.

(19) J. Wyman, *Chem. Rev.*, **19**, 213 (1936). Result calculated assuming a linear decrement for a 9.1 M solution.

(20) Y. Doucet, F. Calmes-Perrault, and M. T. Durand, *C. R. Acad. Sci.*, **260**, 1878 (1965); at 27°.

(21) It should be pointed out that the precision of the relationship obtained depends on the units chosen for the solubility. Had the solubility been expressed in moles/liter of solvent or grams/100 grams of solvent, the correlation would have been somewhat improved. However, since there is as yet no well-founded theoretical justification for preferring one system of units over the other, the figure in its present form suffices to show the general trend.



**Figure 4.** Comparisons of  $\Delta J$  with properties of the mixed aqueous solvents of composition 0.25 mol fraction:  $\blacktriangle$ , urea;  $\bullet$ , water;  $\circ$ , ethylene glycol;  $\square$ , acetamide;  $\Delta$ , methanol;  $\times$ , dimethyl sulfoxide;  $\blacksquare$ , acetone. (A)  $\Delta J$  vs. the solubility of phenylalanine in the mixed solvents. (B)  $\Delta J$  vs. the dielectric constants of the mixed solvents. (C)  $\Delta J$  vs. the free energy of transfer of the phenyl group from water into the mixed solvents.

nine in urea<sup>6</sup> and ethylene glycol<sup>13</sup> solutions are sufficiently small (3–30 cal).

The results illustrated in Figure 4C show no regularity whatever. It was anticipated that the free energy of transfer of the phenyl group, which can be considered a measure of the "water-like" nature of the mixed solvent systems, would show a negative correlation with  $\Delta J$ . The expected interpretation would have been that the enhanced stability of the A and B rotamers (decreasing  $\Delta J$ ) would be associated with water-like solute-solvent interactions connected with water structure. The results obtained

here, however, suggest that the interactions influencing the rotamers are not simply related to hydrophobic interactions.

### Conclusion

The nonaqueous solvents appear to disrupt or diminish the solute-solvent interactions favoring the A and B rotamers of the phenylalanine anion in aqueous solution at low temperature, the intensity of the effect varying with the particular solvent employed. These results are closely related to those observed with studies of the concentration dependence of the nmr spectrum of the phenylalanine anion in pure water,<sup>4b</sup> the addition of nonaqueous component having a similar effect as an increase in the concentration of the anion in pure water. Both decrease the ratio of the number of water molecules available *per* phenylalanine anion molecule. The degree of the enhancement of the A and B rotamer stabilities undoubtedly is intimately connected with the solvation of the rotamers which in turn depends on this ratio. The nonaqueous solvents present the additional capability of themselves participating in the solvation presumably as a function of whether they are more or less water-like. It had been anticipated that the nmr results would have displayed regularities with the properties of the aqueous solutions which could be used as a basis for developing these concepts. However, the lack of a precise relationship with both the dielectric and solubility properties and the lack of any clear relationship with the free energies of transfer indicate that the solvation must be represented in a highly complex fashion. It is probable that major advances in the theoretical understanding of solute-solvent interactions in aqueous media will be required in order to explain adequately these phenomena. Hopefully, the rotational isomerism of amino acids will provide a convenient framework against which to test such developments.

*Acknowledgment.* The technical assistance of Messrs. L. B. Gordon and K. S. Schweizer and Miss M. H. Shelus is gratefully acknowledged.

# Vibrational Spectra, Structure, and Nature of the Phosphorus-Nitrogen Bond in *N,P,P,P*-Tetramethylphosphine Imide and *N*-Methyl-*d*<sub>3</sub>-*P,P,P*-trimethylphosphine Imide

J. Bragin,\* S. Chan, E. Mazzola, and H. Goldwhite

Department of Chemistry, California State University, Los Angeles, Los Angeles, California 90032 (Received January 17, 1973)

Publication costs assisted by California State University, Los Angeles

The vibrational spectra of the compound *N,P,P,P*-tetramethylphosphine imide and its *N*-methyl-*d*<sub>3</sub> analog have been found to be consistent only with a *C*<sub>s</sub> structure the vibrational *potential function* of which exhibits large deviations from local *C*<sub>3v</sub> symmetry at both phosphorus and nitrogen. All 48 vibrational fundamentals expected under *C*<sub>s</sub> molecular point symmetry have been assigned based on group frequencies, isotopic frequency shifts, and Raman depolarization measurements. The P:N torsional modes have been assigned at 112 and 100 cm<sup>-1</sup> in the light and heavy molecules, respectively, and threefold barriers of 2.06 and 2.42 kcal/mol, respectively, have been calculated from these assignments. The unusually low barrier to rotation around the formally double P:N bond confirms the results of low-temperature pmr studies of phosphine imides which indicate that the barrier to internal rotation in these molecules is *below* values reported for PN bond internal rotation in aminophosphines. The infrared spectrum of (CH<sub>3</sub>)<sub>3</sub>PNCH<sub>3</sub> liquid at room temperature (4000–300 cm<sup>-1</sup>) and solid at -175° (4000–200 cm<sup>-1</sup>) and the Raman spectra of the light and *N*-methyl-*d*<sub>3</sub> liquids are presented and these show no evidence of the existence of dimers in either the solid or liquid states.

## Introduction

There has been considerable recent interest in conformation at group V atoms and in the relative importance of electronic and steric factors as determinants of structure.<sup>1-8</sup> Molecules of the type X<sub>3</sub>PNY provide a unique opportunity for assessing the contributions of these factors to the barrier to rotation about a formal PN double bond at pentavalent phosphorus. In addition, the structure and bonding in phosphine imides are of interest because these molecules are the monomeric analogs of the cyclic phosphazenes, (PNX<sub>2</sub>)<sub>n</sub>, about which much has been written of late.<sup>9</sup> Despite these intriguing features there has been little in the way of detailed structural investigation of phosphine imides, hence the present work. The tetramethyl compounds were chosen for study here rather than the halides since X<sub>3</sub>PNY compounds with electronegative substituents on phosphorus are known to be dimeric.<sup>9</sup>

## Experimental Section

*N,P,P,P*-Tetramethylphosphine imide was prepared from trimethylphosphine<sup>10</sup> and methyl azide. The latter was synthesized by adding dimethyl sulfate to 30% aqueous sodium azide and purified by vacuum fractionation through traps at -46, -95, and -190°. A portion of the middle fraction (82% methyl azide, 18% diethyl ether as determined by pmr) sufficient to provide 100% mole excess of methyl azide was transferred *in vacuo* to a flask containing trimethylphosphine (0.50 g) in diethyl ether (5 ml). The solution was refluxed on a cold finger (-80°) for 1.5 hr and purified by successive fractionations through traps at -35, -80, and -190°. After two fractionations of its contents the -35° trap contained pure *N,P,P,P*-tetramethylphosphine imide in 70% yield (0.48 g).

Anal. Calcd for C<sub>4</sub>H<sub>12</sub>NP: C, 45.7; H, 11.4; P, 29.5%. Found: C, 45.5; H, 11.6; P, 30.2%.

(CH<sub>3</sub>)<sub>3</sub>PNCD<sub>3</sub> was prepared from methyl azide-*d*<sub>3</sub> and

trimethylphosphine by the same procedure. Methyl azide-*d*<sub>3</sub> was prepared from commercially available dimethyl-*d*<sub>6</sub> sulfate, in 52% yield, by reaction with sodium azide in H<sub>2</sub>O solution. The product was judged, by pmr, to contain less than 1% (CH<sub>3</sub>)<sub>3</sub>PNCHD<sub>2</sub> and no other detectable impurities.

Infrared spectra were recorded on a Beckman IR-12 double-beam grating spectrophotometer which was purged with a continuous stream of dry nitrogen gas and calibrated in the usual manner.<sup>11</sup> Solid (CH<sub>3</sub>)<sub>3</sub>PNCH<sub>3</sub> was examined using a modified Wagner-Hornig cold cell<sup>12</sup> in which the vapors were permitted to slowly distill onto a CsI substrate in good thermal contact with a dewar flask of boiling nitrogen. The solid samples were repeatedly annealed to -50° until no further change in the spectrum was observed. Several depositions gave identical spectra and no evidence of decomposition could be found. The ir spectrum of solid (CH<sub>3</sub>)<sub>3</sub>PNCH<sub>3</sub> is shown in Figure 1. The spectrum of liquid (CH<sub>3</sub>)<sub>3</sub>PNCH<sub>3</sub> was recorded for the sample contained in a 0.1-mm KBr liquid cell and is shown in Figure 2. The frequencies of sharp bands are ex-

- (1) J. R. Durig, J. W. Thompson, and J. D. Witt, *Inorg. Chem.*, **11**, 2477 (1972).
- (2) J. R. Durig and J. M. Casper, *J. Chem. Phys.*, **55**, 198 (1971).
- (3) J. R. Durig and J. S. DiYorio, *Inorg. Chem.*, **8**, 2796 (1969).
- (4) M. P. Simonnin, C. Charrier, and R. Burgada, *Org. Magn. Resonance*, **4**, 113 (1972).
- (5) A. H. Cowley, M. J. S. Dewar, W. R. Jackson, and W. B. Jennings, *J. Amer. Chem. Soc.*, **92**, 5206 (1970).
- (6) D. Imbery and H. Friebolin, *Z. Naturforsch. B.*, **23**, 759 (1968).
- (7) H. Goldwhite and D. G. Rowsell, *Chem. Commun.*, 713 (1969).
- (8) A. Rauk, L. C. Allen, and K. Mislow, *Angew. Chem., Int. Ed. Engl.*, **9**, 400 (1970).
- (9) D. E. C. Corbridge, *Top. Phosphorus Chem.*, **3**, 57 (1966).
- (10) F. G. Mann and A. F. Wells, *J. Chem. Soc.*, 702 (1938).
- (11) (a) IUPAC, "Tables of Wavenumbers for the Calibration of Infrared Spectrometers," Butterworths, Washington, D. C., 1961; (b) R. T. Hall and J. M. Dowling, *J. Chem. Phys.*, **47**, 2454 (1967); **52**, 1161 (1970).
- (12) E. L. Wagner and D. F. Hornig, *J. Chem. Phys.*, **18**, 296 (1950).

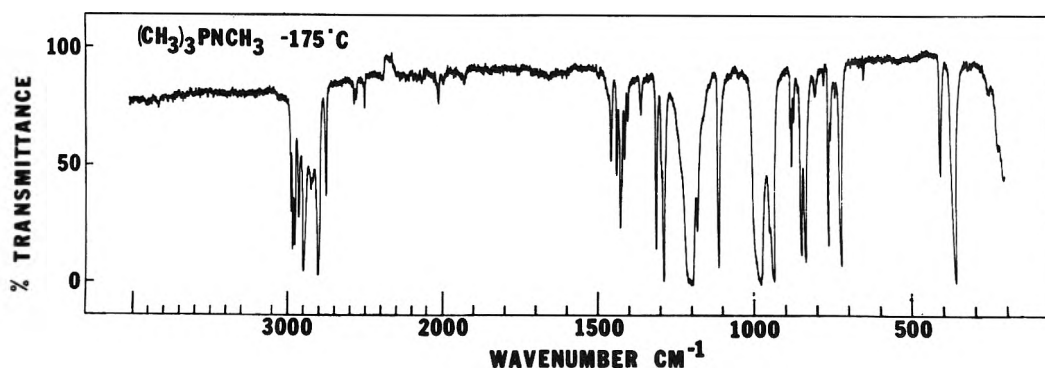


Figure 1. Infrared spectrum of polycrystalline  $(\text{CH}_3)_3\text{PNCH}_3$  at  $-175^\circ$ .

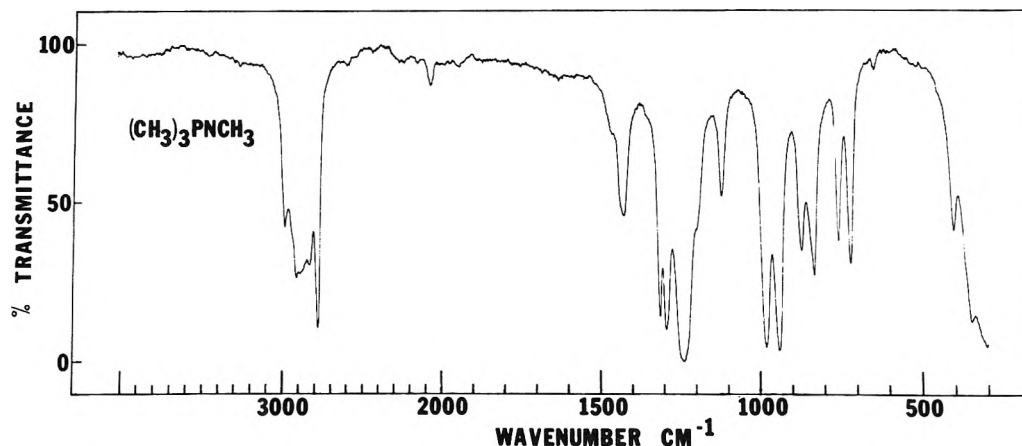


Figure 2. Infrared spectrum of liquid  $(\text{CH}_3)_3\text{PNCH}_3$ , 0.1-mm path.

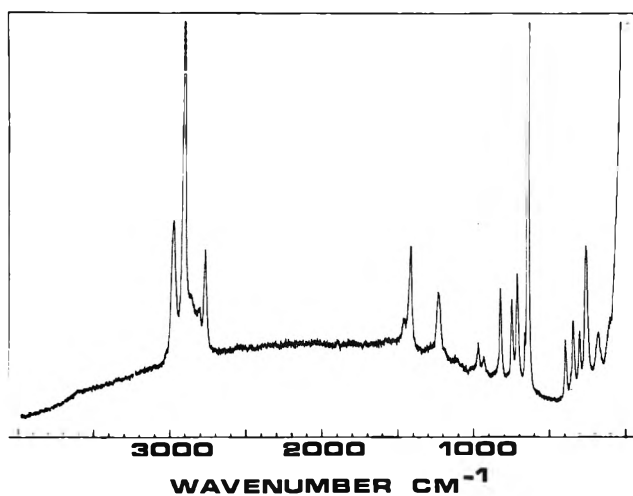


Figure 3. Raman spectrum of liquid  $(\text{CH}_3)_3\text{PNCH}_3$  (488-nm excitation).

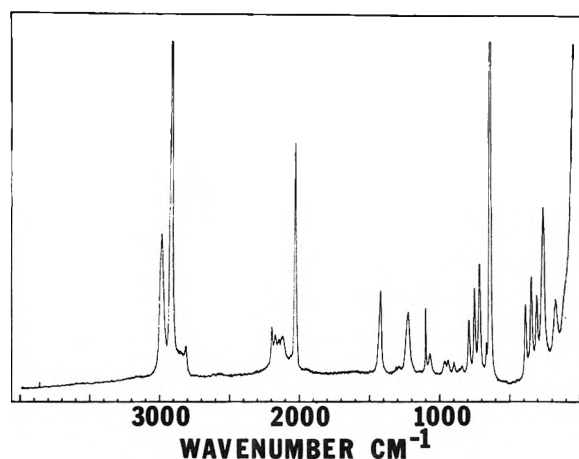


Figure 4. Raman spectrum of liquid  $(\text{CH}_3)_3\text{PNCD}_3$  (488-nm excitation).

pected to be accurate to  $\pm 0.5 \text{ cm}^{-1}$  below  $2000 \text{ cm}^{-1}$  and  $\pm 1 \text{ cm}^{-1}$  between  $4000$  and  $2000 \text{ cm}^{-1}$ .

The Raman spectra of the liquid compounds, degassed and sealed under vacuum in glass capillaries, were excited using 50 mW of 488-nm radiation from a Spectra Physics 164-03  $\text{Ar}^+$  laser and were recorded on a Beckman Model 700 laser-Raman spectrometer which was calibrated against atomic emission lines. The sample tubes were illuminated and viewed normal to their long axes and depolarization ratios were obtained by rotating a piece of polaroid in the scattered beam which subsequently passed through a polarization scrambler before entering the

monochromator. The Raman spectra of  $(\text{CH}_3)_3\text{PNCH}_3$  and  $(\text{CH}_3)_3\text{PNCD}_3$  are shown in Figures 3 and 4, respectively. Raman frequencies are expected to be accurate to  $\pm 2 \text{ cm}^{-1}$ . The measured frequencies of both molecules are given in Table I.

The imide reacts with  $\text{CDCl}_3$  at room temperature but reaction with vinyl chloride is slow enough to permit its use as a low-temperature nmr solvent. At ambient temperature the pmr spectrum of the imide consists of two doublets at  $\delta = 1.57 \text{ ppm}$ , downfield from internal TMS ( $\text{CH}_3\text{-P}$ ;  $^2J_{\text{HCP}} = 12.8 \text{ Hz}$ ), and  $\delta = 2.78 \text{ ppm}$  ( $\text{CH}_3\text{-N:P}$ ;  $^3J_{\text{HCNP}} = 23.6 \text{ Hz}$ ). Low-temperature pmr spectra were

TABLE I: Vibrational Spectra of Phosphine Imides

(CH <sub>3</sub> ) <sub>3</sub> PNCH <sub>3</sub>					(CH <sub>3</sub> ) <sub>3</sub> PNCD <sub>3</sub>				Assignment	
I <sub>r</sub> (liquid)		r (solid, -175°)		Raman (liquid)			Raman (liquid)			
$\tilde{\nu}^a$	I <sup>b</sup>	$\tilde{\nu}$	I	$\tilde{\nu}$	I	$\rho^c$	$\tilde{\nu}$	I		$\rho$
		2985								$\nu_1, \nu_2, \nu_3,$
2980 m,sh		2972 m		2977	10	0.67	2977	9	0.75	$\nu_{28}, \nu_{29},$
		2961								$\nu_{30}$
2930 sh		2935 m								$\nu_{31}$
2908 m		2900 s		2904	40	0.00	2907	40	0.00	$\nu_4, \nu_5, \nu_{32}$
2860 w,brd		2855 w		2864	0.2,sh	p				$\nu_8 + \nu_9$
2825 m		2805 s		2807	1,sh	dp	2804	1		$\nu_6$
2776 s		2759 m		2767	6	0.00				$\nu_7$
		2575 w								$2\nu_{13}$
		2565								$\nu_{38} + \nu_{33}$
		2510 w								$\nu_{38} + \nu_{34}$
							2191	2	sp	$\nu_6$
							2166	1	dp	$\nu_{31}$
							2143	1	p	$\nu_8 + \nu_{33}$
							2114	1	sp	$2\nu_{33}$
		2030 w								$\nu_{20} + \nu_{15}$
							2023	19	0.00	$\nu_7$
		1933 w								$\nu_{22} + \nu_{13}$
1465 w,sh		1459 m		1456	1	dp				$\nu_8, \nu_{33}$
		1440								$\nu_9$
		1428								
		1424 m								
		1415		1410	7	0.70	1414	7	0.71	$\nu_{10}, \nu_{11}, \nu_{12},$
1425 m		1404								$\nu_{34}, \nu_{35}, \nu_{36}$
		1363 w								$\nu_{21} + \nu_{22}$
1314 m		1312								$\nu_{37}$
1293 m		1295 w,sh		1290	0.1,brd		1284	0.1,brd		$\nu_{13}, \nu_{14}$
		1288 s								
1239 vs,brd		1201 vs,brd		1239	5	0.00	1220	5	0.10	$\nu_{15}$
1196 m,sh		1179 m		1191	0.1,brd,sh					$\nu_{38}$
1117 m		1111 s		1116	0.2,brd	dp				$\nu_{16}$
							1093	5	0.23	$\nu_8, \nu_9$
							1062	5	0.75	$\nu_{33}$
980 s		978 vs,brd		980	2	sp	960	1	p	$\nu_{17}$
939 s		946 w,sh		945	1	dp	933	1	p	$\nu_{18}, \nu_{39}$
		935 s								
							892	1	p	$\nu_{16}$
868 m		883								
		877 m								$\nu_{19}, \nu_{40}, \nu_{41}$
		871								
		860 vw								$\nu_{42} + \nu_{45}$
829 m		845 s		818	7	0.12	835	0.1		$\nu_{36}$
		832 s					786	4	0.22	$\nu_{20},$
		803 w								$\nu_{26} + \nu_{22}$
		777 w								$2\nu_{23},$
753 m		759 s		743	5	0.75	745	5	0.75	$\nu_{22} + \nu_{45}$
		753 w,sh								$\nu_{42},$
715 m		720 s		706	7	0.75	709	7	0.75	$\nu_{23} + \nu_{43}$
644 w		649 vw		634	50	0.00	635	50	0.00	$\nu_{21}$
399 m,sh		401 m		394	4	0.46	382	5	0.54	$\nu_{22}$
348 m,sh		358 s		343	5	0.75	340	6	0.75	$\nu_{23}$
				301	4	0.67	300	5	0.75	$\nu_{43}$
		249 vw,sh		256	9	0.75	254	11	0.75	$\nu_{24}$
				178	3	0.50	165	3	0.53	$\nu_{25}, \nu_{44}$
				112	0.2,sh		~100	sh		$\nu_{26}$
										$\nu_{45}$

<sup>a</sup>  $\nu$  = frequency in cm<sup>-1</sup>. <sup>b</sup> I = relative intensity: s = strong, m = medium, w = weak, vw = very weak, sh = shoulder, brd = broad. <sup>c</sup>  $\rho$  = approximate depolarization ratio: sp = strongly polarized, p = polarized, dp = depolarized.

recorded with a Varian A-60 spectrometer equipped with a variable temperature probe.

### Assignment

A large PNC angle in  $(\text{CH}_3)_3\text{PNCH}_3$ , approaching but not quite equalling  $180^\circ$ , would result in near degeneracy of the components of perpendicular modes with dipole changes lying in and out of the molecular symmetry plane. In this case analysis of the vibrational spectrum under  $C_{3v}$  molecular point symmetry would be appropriate assuming a threefold symmetric  $C_3\text{PN}$  framework. A maximum of 28 different ir and Raman frequencies would then be expected with as many as 11 polarized Raman lines. Smaller PNC angles would tend to remove the degeneracy of the components of the perpendicular modes.  $C_s$  point symmetry would be more appropriate in this case and a maximum of 48 unique ir and Raman frequencies could be observed of which as many as 27 could correspond to polarized Raman lines.

The skeletal modes are expected to be particularly sensitive to conformational changes. Under  $C_{3v}$  point symmetry only six ( $2a_1$ ,  $4e$ ) fundamental frequencies of  $(\text{CH}_3)_3\text{PNCH}_3$  (exclusive of the methyl torsions) are expected below  $800\text{ cm}^{-1}$  whereas four polarized and five depolarized Raman lines have been observed in this frequency range (cf. Figure 3 and Table I). The spectra of both  $(\text{CH}_3)_3\text{PNCH}_3$  and  $(\text{CH}_3)_3\text{PNCD}_3$  have, therefore, been assigned on the basis of a molecular structure with only a plane of symmetry in which the vibrational potential energy at both phosphorus and nitrogen shows considerable departure from local,  $C_{3v}$  symmetry.

**Methyl Group Modes.** The internal motions of the (P) methyl and (N) methyl groups may be assigned by analogy with corresponding modes in trimethylphosphine and methylamine. The (P) methyl CH stretching modes are expected to be mechanically isolated by the relatively massive phosphorus atom and to exhibit a high degree of degeneracy. These modes are assigned to the strong Raman lines at 2977 and  $2904\text{ cm}^{-1}$  which are insensitive to (N)C deuteration. Park and Hendra<sup>13</sup> assign the corresponding (P)CH stretches in  $(\text{CH}_3)_3\text{P}$  to strong Raman lines at 2969, 2954, and  $2894\text{ cm}^{-1}$  and Goubeau and Burger<sup>14</sup> assign corresponding modes in  $(\text{CH}_3)_3\text{PO}$  at 2980 and  $2910\text{ cm}^{-1}$ .

The local  $C_{3v}$  symmetry of the (N)CH<sub>3</sub> group in  $(\text{CH}_3)_3\text{PNCH}_3$  should be perturbed to a significant extent by the molecular frame as has been observed for  $\text{CH}_3\text{NH}_2$ . Durig, *et al.*,<sup>15</sup> assign the (N)CH stretching frequencies in  $\text{CH}_3\text{NH}_2$  at 2946, 2885,  $2807\text{ cm}^{-1}$  and the corresponding modes in  $\text{CD}_3\text{NH}_2$  at 2266, 2198, and  $2067\text{ cm}^{-1}$ . By analogy the corresponding modes in the phosphine imides are assigned at 2930, 2807, and  $2767\text{ cm}^{-1}$  in the light compound and 2166, 2191, and  $2023\text{ cm}^{-1}$  in the (N)CD<sub>3</sub> molecule. The (N)CH and (N)CD stretching assignments in the phosphine imides should be considered tentative since Fermi resonance of these fundamentals with overtones of the (N) methyl deformations may significantly perturb the upper state energies.

The medium intensity feature at  $1410\text{ cm}^{-1}$  and the weak feature at  $1290\text{ cm}^{-1}$  in the Raman spectrum of  $(\text{CH}_3)_3\text{PNCH}_3$  have been assigned to the (P)CH<sub>3</sub> deformations in good agreement with the assignments of similar features at 1421 and  $1293\text{ cm}^{-1}$  in the Raman spectrum of  $(\text{CH}_3)_3\text{P}$ .<sup>13</sup> These Raman lines are insensitive to (N)C deuteration appearing essentially unshifted in  $(\text{CH}_3)_3\text{PNCD}_3$  at 1414 and  $1284\text{ cm}^{-1}$ , respectively. An

additional (P)CH<sub>3</sub> deformation frequency was observed at  $1314\text{ cm}^{-1}$  in the infrared spectrum of liquid  $(\text{CH}_3)_3\text{PNCH}_3$  and this band is assigned by analogy with the assignment of the  $1312\text{--}1325\text{ cm}^{-1}$  doublet in the infrared spectrum of gaseous  $(\text{CH}_3)_3\text{P}$ .<sup>13</sup> In the  $C_s$  molecule,  $(\text{CH}_3)_2\text{POCl}$ , (P)CH<sub>3</sub> deformations have been assigned to ir bands at 1412, 1410, 1303, and  $1292\text{ cm}^{-1}$ <sup>16</sup> and in  $(\text{CH}_3)_3\text{PO}$  the frequencies of these modes have been put at 1430 and  $1324\text{ cm}^{-1}$ <sup>14</sup> providing additional support of the present assignment.

Of the modes as yet unassigned only the (N)CH<sub>3</sub> deformations are expected in the range  $1400\text{--}1500\text{ cm}^{-1}$ . In  $\text{CH}_3\text{NH}_2$  these modes are assigned to Raman lines at 1464 and  $1429\text{ cm}^{-1}$  which shift to 1060 and  $1135\text{ cm}^{-1}$ , respectively, in  $\text{CD}_3\text{NH}_2$ .<sup>15</sup> By analogy, the Raman line at  $1456\text{ cm}^{-1}$  and the infrared counterpart at  $1465\text{ cm}^{-1}$  in the spectrum of liquid  $(\text{CH}_3)_3\text{PNCH}_3$  are assigned as (N)CH<sub>3</sub> deformations. The sharp line at  $1093\text{ cm}^{-1}$  and the neighboring broad feature at  $1062\text{ cm}^{-1}$  in the Raman spectrum of  $(\text{CH}_3)_3\text{PNCD}_3$  must be due to the (N)CD<sub>3</sub> deformations in good agreement with the (N)C deuteration shifts observed for these modes in methylamine.

Only the  $a'$  (N)CH<sub>3</sub> rocking modes have been observed directly for  $\text{CH}_3\text{NH}_2$  ( $1130\text{ cm}^{-1}$ ) and  $\text{CD}_3\text{NH}_2$  ( $913\text{ cm}^{-1}$ ). Dellepiane and Zerbi<sup>17</sup> have recently reviewed the assignments for these compounds and although they agree with previous workers in putting the  $a''$  (N)CH<sub>3</sub> rocking frequency at  $1195\text{ cm}^{-1}$  in  $\text{CH}_3\text{NH}_2$  they calculate the frequency of this mode in  $\text{CD}_3\text{NH}_2$  as  $829\text{ cm}^{-1}$ . Only a weak broad feature is observed in the range of the (N)CH<sub>3</sub> rocking frequency in the Raman spectrum of  $(\text{CH}_3)_3\text{PNCH}_3$  but the infrared spectrum of the liquid exhibits moderately intense features at 1196 and  $1117\text{ cm}^{-1}$ . New features appear in the Raman spectrum of  $(\text{CH}_3)_3\text{PNCD}_3$  at 892 (polarized) and  $835\text{ cm}^{-1}$ . The assignment of these features to the  $a'$  and  $a''$  (N) methyl rocking modes, respectively, is in excellent agreement with the corresponding assignments for  $\text{CH}_3\text{NH}_2$  and  $\text{CD}_3\text{NH}_2$  proposed by Dellepiane and Zerbi.

The only methyl internal motions remaining unassigned are the (P)CH<sub>3</sub> rocking modes. In  $(\text{CH}_3)_3\text{P}$  these modes have been assigned to weak Raman lines at 973 and  $948\text{ cm}^{-1}$ <sup>13</sup> and in  $(\text{CH}_3)_2\text{POCl}$  moderately strong infrared bands at 930, 906, and  $865\text{ cm}^{-1}$  have been attributed to P(CH<sub>3</sub>) rocking motions.<sup>16</sup> In  $(\text{CH}_3)_3\text{PNCH}_3$  there are three moderately intense infrared bands in the frequency range of the P(CH<sub>3</sub>) rocking modes at 939, 868, and  $829\text{ cm}^{-1}$ . Corresponding Raman lines are observed for two of these bands at 945 and  $818\text{ cm}^{-1}$ . In the Raman spectrum of  $(\text{CH}_3)_3\text{PNCD}_3$  these lines appear at 933 and  $786\text{ cm}^{-1}$ . These frequencies are too high to be attributed to skeletal deformations or PC<sub>3</sub> stretching motions and too low to be due to P:N or CN stretching modes and can only be assigned to (P)CH<sub>3</sub> rocking vibrations.

**Skeletal Stretching Motions.**  $(\text{CH}_3)_3\text{PNCH}_3$  is expected to exhibit four characteristic skeletal stretching frequencies. The range for  $\nu_{\text{P:N}}$  in compounds containing the group  $\text{R}_3\text{P}=\text{N}$  (R = alkyl) has been given by Wiedegrabe and Bock as  $1140\text{--}1375\text{ cm}^{-1}$ .<sup>18</sup> In addition, Roesky and

(13) P. J. D. Park and P. J. Hendra, *Spectrochim. Acta, Part A*, **24**, 2081 (1968).

(14) J. Goubeau and W. Burger, *Z. Anorg. Chem.*, **304**, 147 (1960).

(15) J. R. Durig, S. F. Bush, and F. G. Baglin, *J. Chem. Phys.*, **49**, 2106 (1968).

(16) J. R. Durig, D. W. Wertz, B. R. Mitchell, F. Block, and J. M. Greene, *J. Phys. Chem.*, **71**, 3815 (1967).

(17) G. Dellepiane and G. Zerbi, *J. Chem. Phys.*, **48**, 3573 (1968).

(18) W. Wiedegrabe and H. Bock, *Chem. Ber.*, **101**, 1414 (1968).

Grimm have shown  $\nu_{P:N}$  to increase with electronegativity of the substituents on phosphorus.<sup>19</sup> Thus,  $(\text{CH}_3)_3\text{PNCH}_3$  should exhibit a broad intense ir band characteristic of the P:N bond in the neighborhood of  $1200\text{ cm}^{-1}$ . Such a feature is indeed observed at  $1239\text{ cm}^{-1}$ . A moderately intense completely polarized counterpart is observed at the same frequency in the Raman spectrum of  $(\text{CH}_3)_3\text{PNCH}_3$  and at  $1220\text{ cm}^{-1}$  in the Raman spectrum of  $(\text{CH}_3)_3\text{PNCD}_3$ .

The CN stretching frequency in  $\text{CH}_3\text{NH}_2$  has been assigned at  $1040\text{ cm}^{-1}$ .<sup>15</sup> The only frequency in this region of the vibrational spectrum of  $(\text{CH}_3)_3\text{PNCH}_3$  as yet unassigned is the strong feature observed at  $980\text{ cm}^{-1}$  in the ir spectrum of the liquid with a strongly polarized counterpart appearing weakly in the Raman spectrum at the same frequency. A polarized line at  $960\text{ cm}^{-1}$  in the Raman spectrum of  $(\text{CH}_3)_3\text{PNCD}_3$  is in reasonable agreement with the expected deuteration shift ( $-39\text{ cm}^{-1}$ ) calculated from the ratio of the reduced masses for the N- $\text{CH}_3$  and N- $\text{CD}_3$  units.

The  $\text{PC}_3$  modes are the only skeletal stretches as yet unassigned and these are well characterized as falling in the range  $620\text{--}780\text{ cm}^{-1}$ .<sup>20</sup> The symmetric  $\text{PC}_3$  component typically gives rise to a very intense strongly polarized Raman line near  $650\text{ cm}^{-1}$  with a vanishingly weak infrared counterpart whereas the antisymmetric component gives rise to moderately strong features in both the infrared and Raman spectra at higher frequencies.<sup>13,16</sup> In the phosphine imides the symmetric  $\text{PC}_3$  stretching motion can only be assigned to the strong Raman lines at  $634$  and  $635\text{ cm}^{-1}$  in the light and (N)C deuterated molecules, respectively. The only unassigned frequencies remaining in the range of the  $\text{PC}_3$  stretching modes are the moderately intense, depolarized lines at  $743$  and  $706\text{ cm}^{-1}$  in the Raman spectrum of  $(\text{CH}_3)_3\text{PNCH}_3$  with medium infrared counterparts at  $753$  and  $715\text{ cm}^{-1}$ . In the Raman spectrum of  $(\text{CH}_3)_3\text{PNCD}_3$  these lines appear virtually unshifted at  $745$  and  $709\text{ cm}^{-1}$ , respectively. These frequencies may be confidently assigned to the  $a''$  and  $a'$  components of the asymmetric  $\text{PC}_3$  stretches which have been split by the presence of the imide moiety. Schmidbaur and Jonas have reported the infrared spectrum of  $(\text{CH}_3)_3\text{PNH}$  and have observed moderately intense infrared features at  $722$  and  $745\text{ cm}^{-1}$ .<sup>21</sup> These bands must correspond to the  $a'$  and  $a''$  antisymmetric  $\text{PC}_3$  stretches in that molecule providing additional support for the present assignment.

**Skeletal Deformations.** The (P) and (N) methyl torsions are known to give rise to extremely weak features in both ir and Raman spectra<sup>22</sup> and these modes have not been observed in the present work. Investigation of the corresponding torsional motions in amines and phosphines<sup>23</sup> has shown that these modes have well-characterized frequencies and this is the basis for the tentative assignments of Table II. The remaining skeletal deformations fall into three groups: CPN (2),  $\text{PC}_3$  (3), PNC (2). Of these, the three  $\text{PC}_3$  modes are best characterized, giving rise to moderately intense features in the Raman spectrum of  $(\text{CH}_3)_3\text{P}$  at  $305$  (polarized) and  $263\text{ cm}^{-1}$ .<sup>13</sup> In the spectrum of  $(\text{CH}_3)_3\text{PO}$ , bands at  $311$  and  $265\text{ cm}^{-1}$ <sup>24</sup> are undoubtedly due to the  $a_1$  and  $e$   $\text{PC}_3$  deformation vibrations. In the less symmetric molecule,  $(\text{CH}_3)_2\text{POCl}$ , the corresponding motions have been assigned to the two moderately intense Raman lines at  $234$  (depolarized) and  $297\text{ cm}^{-1}$  (polarized).<sup>16</sup> Thus, the symmetric and antisymmetric  $\text{PC}_3$  deformation modes in  $(\text{CH}_3)_3\text{PNCH}_3$

may be confidently assigned to the Raman lines at  $301$  (polarized) and  $256\text{ cm}^{-1}$  (depolarized), respectively. The corresponding assignments in the Raman spectrum of  $(\text{CH}_3)_3\text{PNCD}_3$  are  $300$  and  $254\text{ cm}^{-1}$ .

The two remaining groups of skeletal deformations are both doubly degenerate under  $C_{3v}$  molecular point symmetry and may be designated CPN and PNC deformations. The out of plane component of the latter corresponds to twisting about the P:N bond and is, therefore, dependent on the variation of P:N bond energy with CPNC dihedral angle. Two groups of frequencies remain unassigned in the Raman spectrum of  $(\text{CH}_3)_3\text{PNCH}_3$ :  $392$  (polarized)- $343$  (depolarized) and  $178$  (polarized)- $112\text{ cm}^{-1}$ . Extensive low-temperature pmr studies of phosphine imides (see following paragraph) are incompatible with the assignment of the PNC deformations to the higher frequencies since an upper limit of  $8\text{ kcal/mol}$  for  $\Delta G^*$  of P:N internal rotation has been set for these molecules. For comparison, the C:C torsion has been assigned at  $440\text{ cm}^{-1}$  in 2-methyl-2-butene<sup>25</sup> and in this molecule the barrier must be an order of magnitude greater than  $8\text{ kcal/mol}$  due to the stabilization of the planar conformation by  $p_\pi$ - $p_\pi$  overlap. Thus it is unlikely that the frequency of the corresponding mode in  $(\text{CH}_3)_3\text{PNCH}_3$  would be of comparable magnitude. The  $a'$  and  $a''$  PNC deformations in  $(\text{CH}_3)_3\text{PNCH}_3$  have, therefore, been assigned to the Raman lines at  $178$  (polarized) and  $112\text{ cm}^{-1}$ , respectively. The isotopic frequency shift factors for the low-frequency Raman lines ( $178\text{ cm}^{-1} = 1.08$ ;  $112\text{ cm}^{-1} = 1.1$ ) are in good agreement with the present assignment. (The square root of the mass ratios of the  $\text{CH}_3$  and  $\text{CD}_3$  groups is 1:1.) The shift factors for the  $394$ - ( $1.03$ ) and  $343\text{-cm}^{-1}$  ( $1.01$ ) Raman lines of  $(\text{CH}_3)_3\text{PNCH}_3$  are much lower than the values expected for the PNC deformations and these frequencies have been assigned to the  $a'$  and  $a''$  CPN deformations, respectively. For comparison, the degenerate CPO bending in  $(\text{CH}_3)_3\text{PO}$  has been observed at  $369\text{ cm}^{-1}$ <sup>24</sup> and the corresponding motions (*tert*-butyl rocks) in  $(\text{CH}_3)_3\text{CCN}$  and  $(\text{CH}_3)_3\text{CCCH}$  have been assigned at  $527$  and  $542\text{ cm}^{-1}$ ,<sup>23</sup> respectively.

### Low-Temperature Pmr Studies

At temperatures down to  $-100^\circ$ , the lowest temperature studied, there is no major change in the pmr spectrum of  $(\text{CH}_3)_3\text{PNCH}_3$  apart from a slight broadening of the peaks at the lowest temperatures studied. If rotation about the P:N bond were slow on the nmr time scale at low temperatures, the methyl groups on phosphorus would become diastereotopic since the P:N-C skeleton is nonlinear, and an increase in complexity of the  $\text{CH}_3$ -P signal would be expected.

There are two possible explanations for the failure to observe this phenomenon. First, it might be that, although the methyl groups are diastereotopic, the chemical shift difference is so small ( $<0.5\text{ Hz}$ ) that it becomes

- (19) H. W. Roesky and L. F. Grimm, *Angew. Chem., Int. Ed. Engl.*, **9**, 244 (1970).
- (20) D. E. C. Corbridge, *Top. Phosphorus Chem.*, **6**, 237 (1969).
- (21) H. Schmidbaur and G. Jonas, *Chem. Ber.*, **101**, 1271 (1968).
- (22) J. R. Durig, J. Bragin, S. M. Craven, C. M. Player, Jr., and Y. S. Li in "Developments in Applied Spectroscopy," Vol. 9, A. L. Perkins and E. L. Grove, Ed., Plenum Press, New York, N. Y., 1971, pp 23-72.
- (23) J. R. Durig, S. M. Craven, and J. Bragin, *J. Chem. Phys.*, **53**, 38 (1970).
- (24) S. T. King and R. A. Nyquist, *Spectrochim. Acta, Part A*, **26**, 1481 (1970).
- (25) J. R. Durig, C. W. Hawley, and J. Bragin, *J. Chem. Phys.*, **57**, 1426 (1972).



TABLE II: Summary of Fundamental Frequencies<sup>a</sup> for Phosphine Imides

Description	Assignment $C_{3v}^b$	$C_s^c$	$(CH_3)_3PNCH_3$ $\bar{\nu}, cm^{-1}$	$(CH_3)_3PNCD_3$ $\bar{\nu}, cm^{-1}$
(P)CH stretch	$a_1$ — $a'$ $a_2$ — $a''$ $e(2)$ — $a''$	1,2,3 28,29,30	2977	2977
(N)CH stretch	$e$ — $a''$	31	2930 <sup>d</sup>	2166
(P)CH stretch	$a_1$ — $a'$ $e$ — $a''$ $a'$	4,5 32 6	2904 2807	2907 2191
(N)CH stretch	$a$ — $a'$	7	2767	2023
(N)CH deformation	$e$ — $a''$ $a'$	33 8	1456	1062
(N)CH deformation	$a_1$ — $a'$	9	1425 <sup>d</sup>	1093
(P)CH deformation	$a_1$ — $a'$ $a_2$ — $a''$ $e(2)$ — $a''$	10,11,12 34,35,36	1410	1414
	$e$ — $a''$ $a_1$ — $a'$	37 13,14	1314 <sup>d</sup> 1290	1284
PN stretch	$a_1$ — $a'$	15	1239	1220
(N)CH <sub>3</sub> rock	$e$ — $a''$ $a'$	38 16	1191 1116	835 892
CN stretch	$\epsilon_1$ — $a'$	17	980	960
	$e$ — $a''$ $a'$	39 18	945	933
(P)CH <sub>3</sub> rock	$a_2$ — $a''$ $e$ — $a'$ $a_1$ — $a'$	40,41 19 20	868 <sup>d</sup>	786
PC <sub>3</sub> stretch	$e$ — $a''$ $a_1$ — $a'$	42 21 22	743 706 634	745 709 635
CPN deformation	$e$ — $a''$ $a'$	23 43	394 343	382 340
PC <sub>3</sub> deformation	$a_1$ — $a'$ $e$ — $a''$ $a'$	24 25 44	301 256	300 254
PNC deformation	$e$ — $a''$ $a'$	26 45	178 112	165 ~100
(P)CH <sub>3</sub> torsion	$e$ — $a''$ $a'$	46 27	(250) <sup>e</sup>	
(N)CH <sub>3</sub> torsion	$a_2$ — $a''$	47	(225) <sup>e</sup>	
(P)CH <sub>3</sub> torsion	$a_2$ — $a''$	48	(200) <sup>e</sup>	

<sup>a</sup> Frequencies obtained from the Raman spectrum of the liquid unless otherwise noted. <sup>b</sup> Local symmetry of  $(CH_3)_3P$  and  $CH_3(N)$  moieties. <sup>c</sup> Molecular point symmetry. Mode numbering follows standard convention. <sup>d</sup> Ir of liquid. <sup>e</sup> Unobserved; estimated from data of ref 23.

unobservable. In rebuttal to this, it may be pointed out that similar negative results have been obtained<sup>26</sup> for a wide variety of other P:N compounds of types  $(RO)_3P:NR'$ ,  $R(RO)_2P:NR'$ ,  $(R_2N)_3P:NR'$ , and  $R(R'_2N)_2P:NR''$  and these results suggest that the lack of positive observations is a genuine property of the P:N bond, rather than the specific groups attached to it.

The second explanation is that the barrier to rotation around the P:N bond in the imide is low. If  $-100^\circ$  is

taken as the upper limit for the coalescence temperature for this compound, then it can be calculated<sup>27</sup> that  $\Delta G^*$  for the rotational process is less than 8 kcal/mol. Thus it appears that the rotational barrier about this formal phosphorus-nitrogen "multiple" bond is lower than that observed around some phosphorus-nitrogen "single" bonds.

(26) H. Goldwhite and P. Gysegem, unpublished observation.

(27) J. E. Anderson and J. M. Lehn, *Tetrahedron*, **24**, 123 (1968).

For example,  $\Delta G^*$  for rotation about the PN bond in  $C_6H_5P(Cl)N(CH_3)_2$  is 10.8 kcal/mol.<sup>4</sup>

### Barrier to P:N Torsion

The threefold barrier to P:N torsion in phosphine imides was calculated from the assignments of Table II by transferring geometrical parameters from  $(CH_3)_3P$ ,<sup>28</sup>  $CH_3NH_2$ ,<sup>29</sup> and  $(NP(CH_3)_2)_3$ .<sup>9</sup> For a PNC angle of 120° the reduced moments of inertia result in the  $F$  values of 2.11 and 1.40  $cm^{-1}$  for  $(CH_3)_3PNCH_3$  and  $(CH_3)_3PNCD_3$ , respectively. The corresponding threefold barriers to P:N bond rotation calculated from these values by using Tables of Mathieu Function eigenvalues<sup>30</sup> are 2.06 and 2.42 kcal/mol, respectively.

There are two principal sources of error in this calculation: the assumed geometry and the center frequencies of the bands assigned to the P:N torsional modes. Variation of the PNC angle changes the reduced moment of inertia resulting in a change in the threefold periodic barrier to P:N torsion of approximately 0.07 kcal/degree for each molecule. Since the features assigned to P:N torsions are shoulders on the Rayleigh line in the Raman spectra of both phosphine imides there may be as much as 10–15  $cm^{-1}$  error in the line center frequencies given in Table II. This could introduce errors of as much as  $\pm 0.6$ –0.7 kcal in  $V_3(P:N)$  over and above the error due to geometrical parameters.

Vibrational mixing involving the P:N torsions is unlikely since the next lowest frequency depolarized line is observed at more than double the torsional frequency in the Raman spectra of both  $(CH_3)_3PNCH_3$  and  $(CH_3)_3PNCD_3$  and these  $a''$  frequencies show no significant (N)CH<sub>3</sub> deuteration shift.

### Discussion

Both vibrational and pmr studies support an unusually low dihedral angular dependence for the P:N bond energy in  $(CH_3)_3PNCH_3$  yet the vibrational assignment for  $\bar{\nu}_{P:N}$  (1239  $cm^{-1}$ ) in this molecule is far higher than the range given for the stretching of a formally single PN bond (650–850  $cm^{-1}$ ).<sup>20</sup> These observations are consistent with the theoretical results of Dewar, *et al.*, for the cyclic phosphazenes,  $(PNCl_2)_n$ ,<sup>31</sup> in which it was pointed out that it is always possible to select two hybrid d orbitals the orientation of which matches that of adjacent nitrogen p orbitals thereby permitting  $d_{\pi}-p_{\pi}$  overlap with little angular dependence. More recently Cowley, *et al.*,<sup>5</sup> have suggested that the finite torsional barriers observed around the formally single PN bond in amino phosphines may be attributed to  $p_{\pi}-d_{\pi}$  interaction if participation of  $d_{xz}$  and  $d_{yz}$  orbitals in the  $\sigma_z$  bonds of these molecules results in unequal availability of these d orbitals for participation in  $p_{\pi}-d_{\pi}$  overlap. Mixing of  $\sigma$  and  $\pi$  orbitals may be symmetry allowed in molecules capable of  $p_{\pi}-d_{\pi}$  inter-

action whereas such mixing is symmetry forbidden for  $p_{\pi}-p_{\pi}$  systems. However, the failure to observe diastereotopic P(CH<sub>3</sub>) groups in asymmetric imides<sup>26</sup> would seem to argue against a decisive role for symmetry effects in determining barriers to P:N bond rotation. Further work is in progress to attempt to clarify this point.

$Ir^{32}$  and nmr<sup>33</sup> spectra of  $Cl_3PNCH_3$  have been interpreted in terms of a cyclic dimer in which some delocalization of electrons in ring orbitals may occur. In support of this interpretation the infrared workers cite as evidence the low intensity of the ir active NC stretching mode at the quarternary nitrogen of the polar structure. The NC stretching mode in  $(CH_3)_3PNCH_3$  is comparable in intensity to the very strong P:N stretch and such an interpretation is not possible here. In addition, cyclic dimerization of an  $X_3PNY$  molecule would create a four-membered ring with six degrees of skeletal vibrational freedom. Two of these dimer skeletal modes would result from in- and out-of-phase coupling of the P:N stretching motions. If the dimer were centrosymmetric the ir and Raman bands corresponding to these motions would be singlets appearing at different frequencies in the two spectra. A non-centrosymmetric dimer might exhibit doublets of unequal intensity in each spectrum. For liquid  $(CH_3)_3PNCH_3$  the P:N stretching frequency gives rise to a strong ir singlet and a moderately intense strongly polarized Raman singlet at exactly the same frequency. Thus, the existence of cyclic  $(CH_3)_3PNCH_3$  dimers would require complete decoupling of the ring bond stretching motions, an extremely unlikely possibility. Furthermore, of the four additional ring modes which would be created by cyclic dimerization three are deformations and are expected below 400  $cm^{-1}$ . No unassigned ir or Raman features have been observed in this region of the spectrum of either molecule and whereas some of the modes in question might have escaped detection by being weak or obscured this is unlikely to be the case for all three. Finally, simultaneous symmetric stretching of all four ring bonds (ring breathing) should give rise to an extremely intense, strongly polarized Raman line in the range 650–1375  $cm^{-1}$ . No such line is observed for either molecule.

*Acknowledgment.* This work was supported in part by Public Health Service Grant No. CA-07182 from the National Cancer Institute.

(28) L. S. Bartell and L. C. Brockway, *J. Chem. Phys.*, **32**, 512 (1960).

(29) T. Itoh, *J. Phys. Soc. Jap.*, **11**, 264 (1956).

(30) W. G. Fateley, F. A. Miller, and R. E. Witkowski, Air Force Materials Laboratory Technical Report No. AFML-TR-66-408. Wright-Patterson Air Force Base, Ohio.

(31) M. J. S. Dewar, E. A. Lucken, and M. A. Whitehead, *J. Chem. Soc.*, 2423 (1960).

(32) A. C. Chapman, W. S. Holmes, N. L. Paddock, and H. Y. Searle, *J. Chem. Soc.*, 1825 (1961).

(33) E. Fluck, *Z. Anorg. Allg. Chem.*, **320**, 64 (1963).

# Matrix Isolation Infrared Study of the Reaction between Tin Vapor and Molecular Oxygen. The Characterization of Molecular Tin Dioxide

A. Bos<sup>1</sup> and J. S. Ogden\*

*Inorganic Chemistry Laboratory, South Parks Road, Oxford, England (Received January 26, 1973)*

When tin vapor is cocondensed at 20°K with krypton or nitrogen matrices containing a few mole per cent of oxygen, the molecular species SnO<sub>2</sub> and Sn<sub>2</sub>O<sub>2</sub> (*D*<sub>2h</sub>) are found to be major reaction products. Small amounts of O<sub>3</sub>, SnO, Sn<sub>3</sub>O<sub>3</sub>, and other tin oxide species are also produced, and it is found that the chemical reactions taking place are very dependent on matrix deposition rates and, to a lesser extent, upon the nature of the matrix gas. A normal coordinate analysis based upon a large number of tin and oxygen isotope frequencies indicates that SnO<sub>2</sub> is linear (*D*<sub>∞h</sub>) with a principal Sn–O stretching constant of 5.36 mdyne/Å in krypton matrices. The use of unscrambled <sup>16</sup>O<sub>2</sub>–<sup>18</sup>O<sub>2</sub> isotope mixtures indicates that the SnO<sub>2</sub> is formed by the direct insertion of a tin atom into an oxygen molecule, and that the major route to Sn<sub>2</sub>O<sub>2</sub> appears to be the subsequent reaction of SnO<sub>2</sub> with a second tin atom. Matrix isolation may thus be used to study the mechanisms of metal atom–oxygen reactions.

## Introduction

Matrix isolation is now well established as a technique for studying high-temperature chemical species,<sup>2a</sup> and in particular the ir spectra of matrix isolated SnO, Sn<sub>2</sub>O<sub>2</sub>, Sn<sub>3</sub>O<sub>3</sub>, and Sn<sub>4</sub>O<sub>4</sub> have recently been obtained.<sup>2b</sup> These molecules are known to be present in the vapor above heated tin oxide,<sup>3</sup> and it is interesting to examine whether the same species are equally important in the oxidation of tin vapor.

Although metal vapor–oxygen reactions may be studied by fast-flow techniques in the gas phase,<sup>4–6</sup> it is usually only possible to recover the thermodynamically stable end products in these experiments, and information concerning the stoichiometry of any reaction intermediate is generally inferred from kinetic data. By carrying out the metal vapor–oxygen reaction under matrix isolation conditions, in which the products of a reaction are rapidly quenched at low temperatures, it should be possible to characterize many reaction intermediates spectroscopically. Thus Andrews, in a series of papers<sup>7–10</sup> on alkali metal atom–oxygen reactions in matrices, has confirmed that molecular NaO<sub>2</sub> is formed in the Na atom–O<sub>2</sub> reaction by observing both the ir<sup>9</sup> and Raman<sup>10</sup> spectra of this species.

In an earlier communication,<sup>11</sup> we presented evidence which suggested that the linear molecule SnO<sub>2</sub> is an important product of the tin atom–O<sub>2</sub> matrix reaction. This paper describes in detail our characterization of molecular SnO<sub>2</sub>, and also shows how the use of <sup>18</sup>O enrichment can provide information about the mechanism of the oxidation.

## Experimental Section

The Knudsen furnace and low-temperature cryotip used for our matrix isolation studies have been described previously.<sup>12</sup> In these experiments, tin metal (99.999%) was heated to ~1350°K in tantalum or alumina sample holders and the vapor deposited on a cooled CsI window with an excess of krypton or nitrogen containing between 1 and 20 mol % of oxygen.

Research grade <sup>16</sup>O<sub>2</sub>, Kr, and N<sub>2</sub> gases were obtained from the British Oxygen Co. and <sup>18</sup>O enriched oxygen gas

(84% <sup>18</sup>O<sub>2</sub>, 16% <sup>16</sup>O<sup>18</sup>O) was supplied by Miles Laboratories Inc. In all <sup>18</sup>O enrichment experiments, this gas was initially mixed with an approximately equimolar amount of <sup>16</sup>O<sub>2</sub>. This mixture could then be diluted with matrix gas (Kr or N<sub>2</sub>) and used directly, or alternatively could be irradiated with light from a high-pressure xenon lamp before dilution. The purpose of this was to produce two different types of oxygen sample: an “unscrambled mixture” which before dilution contained approximately equimolar amounts of <sup>16</sup>O<sub>2</sub> and <sup>18</sup>O<sub>2</sub> and only a small proportion of the mixed molecule <sup>16</sup>O<sup>18</sup>O (~8%), and a “scrambled mixture” which as a result of irradiation contained 50% <sup>16</sup>O<sup>18</sup>O.

A few experiments were attempted using pure <sup>16</sup>O<sub>2</sub> as a matrix gas, but these were unsuccessful, and the results described were all obtained using dilution factors (Kr or N<sub>2</sub>:total O<sub>2</sub>) of between 5 and 100. As might be expected, relatively long deposition times were required when the proportion of O<sub>2</sub> in the matrix gas was low and, although the 1% O<sub>2</sub> experiments eventually yielded satisfactory <sup>16</sup>O spectra under moderate resolution, it was not possible to build up sufficient intensity at this dilution to carry out high-resolution <sup>18</sup>O and Sn isotope studies. The majority of experiments were carried out using matrix gases containing higher proportions of O<sub>2</sub> (typically 10%) where it was found that relatively intense peaks could be produced without a significant loss in overall transmission.

- (1) Present address, Research School of Chemistry, Australian National University, P.O. Canberra, A. C. T., 2600, Australia.
- (2) (a) W. Weltner, Jr., *Advan. High Temp. Chem.*, **2**, 85 (1969); (b) J. S. Ogden and M. J. Ricks, *J. Chem. Phys.*, **53**, 896 (1970).
- (3) R. Colin, J. Drowart, and G. Verhaegen, *Trans. Faraday Soc.*, **61**, 1364 (1965).
- (4) P. R. Ryason and E. A. Smith, *J. Phys. Chem.*, **75**, 2259 (1971).
- (5) M. J. McEwan and L. F. Phillips, *Trans. Faraday Soc.*, **62**, 1717 (1966).
- (6) R. Carabetta and W. E. Kaskan, *J. Phys. Chem.*, **72**, 2483 (1968).
- (7) D. A. Hatzenbuehler and L. Andrews, *J. Chem. Phys.*, **56**, 3398 (1972).
- (8) L. Andrews, *J. Chem. Phys.*, **54**, 4935 (1971).
- (9) L. Andrews, *J. Phys. Chem.*, **73**, 3922 (1969).
- (10) R. R. Smarzewski and L. Andrews, *J. Chem. Phys.*, **57**, 1327 (1972).
- (11) J. S. Anderson, A. Bos, and J. S. Ogden, *Chem. Commun.*, 1381 (1971).
- (12) J. S. Anderson and J. S. Ogden, *J. Chem. Phys.*, **51**, 4189 (1969).

Gas samples were made up using a Toepler pump, and flow rates were varied between 2 and 15 mmol/hr. The optimum spray-on rate was found to be  $\sim 10$  mmol/hr, and moderately intense peaks were produced after  $\sim 1$ -2-hr deposition. It may be significant that at flow rates below  $\sim 5$  mmol/hr, new peaks grew extremely slowly even though the tin vapor deposition rate remained unaltered. The matrix ratio in these experiments was estimated by combining the measured weight loss of the tin (typically  $\sim 0.1$  g per experiment) with the known Clausing and geometric factors for the system, and at the optimum gas flow rate was  $\sim 500:1$ . The cooled CsI window could be maintained at any fixed temperature between 15 and  $25^\circ\text{K}$  during deposition. Controlled diffusion reactions were carried out up to  $\sim 55^\circ\text{K}$ , and a high-pressure mercury lamp was used in the photolysis studies. Ir spectra were recorded at  $20^\circ\text{K}$  using a Perkin-Elmer 225 spectrophotometer, and the full range of this instrument ( $5000$ – $200\text{ cm}^{-1}$ ) was available through efficient dry air purging.

## Results

Experiments were carried out in both krypton and nitrogen matrices. However, spectral resolution was better in krypton, and the frequencies quoted in the text refer to krypton matrix experiments unless otherwise stated. No significant differences were observed between the spectra of samples deposited at  $15^\circ\text{K}$  and those deposited at  $25^\circ\text{K}$ .

A typical ir spectrum obtained after cocondensing tin vapor with a large excess of krypton containing  $\sim 15\%$   $^{16}\text{O}_2$  is shown in Figure 1. Two prominent bands are observed at  $863.1$  and  $611.7\text{ cm}^{-1}$ , and several weaker features are also present at  $1034.6$ ,  $812.0$ ,  $804.3$ ,  $763$ ,  $744.9$ ,  $615.1$ ,  $577.7$ ,  $524.4$ , and  $501.9\text{ cm}^{-1}$ . Small amounts of matrix isolated  $\text{H}_2\text{O}$ ,  $\text{CO}$ , and  $\text{CO}_2$  were generally present, and the feature labeled X at  $880\text{ cm}^{-1}$  is due to an impurity in the cesium iodide window material. In nitrogen matrices, the two most prominent bands appeared at  $877.8$  and  $612.4\text{ cm}^{-1}$ , and weaker features were also noted at  $746.5$ ,  $523$ , and  $506.9\text{ cm}^{-1}$ . Apart from small changes in frequency, the only significant difference between the nitrogen and krypton results was that in nitrogen matrices, features corresponding to the bands at  $1034.6$ ,  $812.0$ , and  $804.3\text{ cm}^{-1}$  were not observed. These three bands, which are prominent in Figure 1, became relatively less intense in krypton matrices containing smaller amounts of oxygen, and the  $1034.6\text{-cm}^{-1}$  band was not observed in matrices containing less than  $\sim 8\%$   $\text{O}_2$ . Decreasing the oxygen concentration also produced other significant changes in relative band intensities and, in particular, the  $611.7$ - and  $524.4\text{-cm}^{-1}$  bands were found to be less intense in comparison with the  $863.1\text{-cm}^{-1}$  band.

Photolysis and diffusion experiments were generally carried out in an attempt to determine the number of different chemical species present. After irradiation with unfiltered uv light for  $\sim 15$  min, the bands at  $744.9$  and  $501.9\text{ cm}^{-1}$  decreased in intensity by typically  $50\%$ , while the  $577.7\text{-cm}^{-1}$  band increased in intensity. The remaining features in the spectrum showed little or no change. Diffusion experiments carried out up to  $\sim 40^\circ\text{K}$  resulted in a modest decrease in intensity ( $\sim 30\%$ ) of the  $863.1$ -,  $804.3$ -,  $611.7$ -, and  $524.4\text{-cm}^{-1}$  bands and the complete disappearance of the other bands in the spectrum. Two broad features centered at  $640$  and  $560\text{ cm}^{-1}$  remained at  $\sim 55^\circ\text{K}$ .

Thus as a result of varying experimental conditions, at least five different chemical species characterised by ir

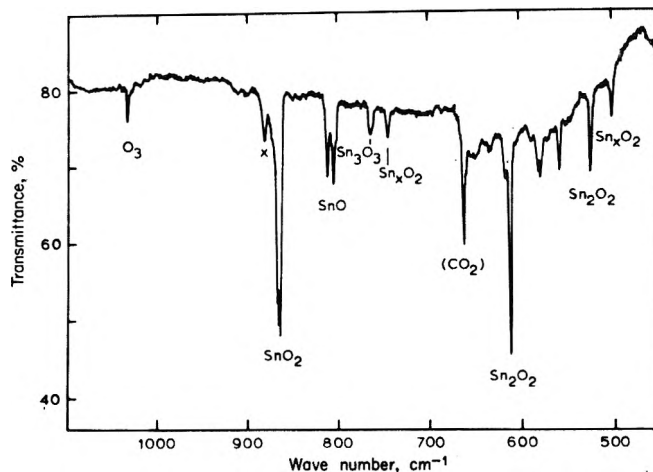


Figure 1. Ir spectrum obtained after cocondensing tin vapor with krypton containing 15% oxygen at  $20^\circ\text{K}$ .

TABLE I: Ir Bands Observed after Cocondensing Tin Vapor with Nitrogen or Krypton Matrices Containing Oxygen

Frequency, $\text{cm}^{-1}$ <sup>a</sup>				Assignment
$\text{N}_2$ - $^{16}\text{O}_2$	$\text{N}_2$ - $^{16}\text{O}_2$ , $^{16}\text{O}^{18}\text{O}$ , $^{18}\text{O}_2$	$\text{Kr}$ - $^{16}\text{O}_2$	$\text{Kr}$ - $^{16}\text{O}_2$ , $^{16}\text{O}^{18}\text{O}$ , $^{18}\text{O}_2$	
877.8	877.8	863.1	863.1	$\Sigma_u^+ ^{16}\text{O}^{120}\text{Sn}^{16}\text{O}$
	861.4		847.2	$\Sigma^+ ^{16}\text{O}^{120}\text{Sn}^{18}\text{O}$
	838.3		824.7	$\Sigma_u^+ ^{18}\text{O}^{120}\text{Sn}^{18}\text{O}$
612.4	612.4	611.7	611.7 <sup>b</sup>	$B_{2u} \text{Sn}_2^{16}\text{O}_2$
	598.2		597.8 <sup>b</sup>	$B_2 \text{Sn}_2^{16}\text{O}^{18}\text{O}$
	581.9		581.3 <sup>b</sup>	$B_{2u} \text{Sn}_2^{18}\text{O}_2$
523	523	524.4	524.4	$B_{3u} \text{Sn}_2^{16}\text{O}_2$
			508.3	$A_1 \text{Sn}_2^{16}\text{O}^{18}\text{O}$
			498.5	$B_{3u} \text{Sn}_2^{18}\text{O}_2$
		812.0	812.0	$\text{Sn}^{16}\text{O}$
		804.3	804.3	$\text{Sn}^{16}\text{O} (?)$
			771.4	$\text{Sn}^{18}\text{O}$
			764.5	$\text{Sn}^{18}\text{O} (?)$
746.5	746.5	744.9	744.9	$\text{Sn}_x^{16}\text{O}_2$ $x = 2 ?$
	728		727	$\text{Sn}_x^{16}\text{O}^{18}\text{O}$
	706		705	$\text{Sn}_x^{18}\text{O}_2$
506.9	506.9	501.9	501.9	$\text{Sn}_x^{16}\text{O}_2$
			489	$\text{Sn}_x^{16}\text{O}^{18}\text{O}$
			479	$\text{Sn}_x^{18}\text{O}_2$
		763	763	$\text{Sn}_3^{16}\text{O}_3$
		1034.6		$^{16}\text{O}_3$
		615.1	615.1	$\text{Sn}_x^{16}\text{O}$ $x = 2 ?$
			587.4	$\text{Sn}_x^{18}\text{O}$
		577.7		Not assigned
		557.7		Not assigned

<sup>a</sup> Absolute frequency accuracy  $\pm 0.3\text{ cm}^{-1}$  for  $\text{SnO}_2$  and  $\text{SnO}$  in both matrices,  $\pm 1.0\text{ cm}^{-1}$  for all other peaks. <sup>b</sup> These three peaks had shoulders at  $609.7$ ,  $596.1$ , and  $579.5\text{ cm}^{-1}$ , respectively.

absorptions at  $1034.6$ ,  $863.1$ ,  $812.0$ ,  $744.9$ , and  $611.7\text{ cm}^{-1}$  are observed. Further examination of a large number of spectra shows that the  $524.4$ - and  $611.7\text{-cm}^{-1}$  bands are always present in approximately the same relative intensity, and these two bands are therefore assigned to the same chemical species. The  $501.9\text{-cm}^{-1}$  band was similarly associated with the  $744.9\text{-cm}^{-1}$  band over a wide range of experimental conditions.

Oxygen-18 isotope enrichment experiments were carried out using  $90\%$   $\text{Kr}$ - $10\%$  total  $\text{O}_2$  mixtures, and it was only possible to obtain  $^{16}\text{O}$ - $^{18}\text{O}$  isotope patterns for the more

TABLE II: Observed Frequencies (cm<sup>-1</sup>) and Isotope Assignments for Matrix Isolated SnO<sub>2</sub><sup>a</sup>

Oxygen isotopes		Tin isotopes						
		116	117 <sup>b</sup>	118	119 <sup>b</sup>	120	122	124
Σ <sub>u</sub> <sup>+</sup> <sup>16</sup> OSn <sup>16</sup> O	Kr matrix	866.1	865.1	864.6	863.6	863.1	861.5	860.1
	N <sub>2</sub> matrix	881.0	880.4	879.5	879.0	877.8	876.4	874.8
Σ <sup>+</sup> <sup>16</sup> OSn <sup>18</sup> O	Kr matrix	850.2	849.2	848.7	847.6	847.2	845.6	844.3
	N <sub>2</sub> matrix	864.4		863.0		861.4		858.4
Σ <sub>u</sub> <sup>+</sup> <sup>18</sup> OSn <sup>18</sup> O	Kr matrix	828.0	827.0	826.3	825.2	824.7	823.1	821.6
	N <sub>2</sub> matrix	841.6		840.1		838.3		835.2

<sup>a</sup> Absolute frequency accuracy ±0.3 cm<sup>-1</sup>. Relative frequency accuracy ±0.1 cm<sup>-1</sup> for all frequencies except those involving tin isotopes 117 and 119, for which the relative frequency accuracy is ±0.2 cm<sup>-1</sup>. <sup>b</sup> These bands appeared as incompletely resolved shoulders.

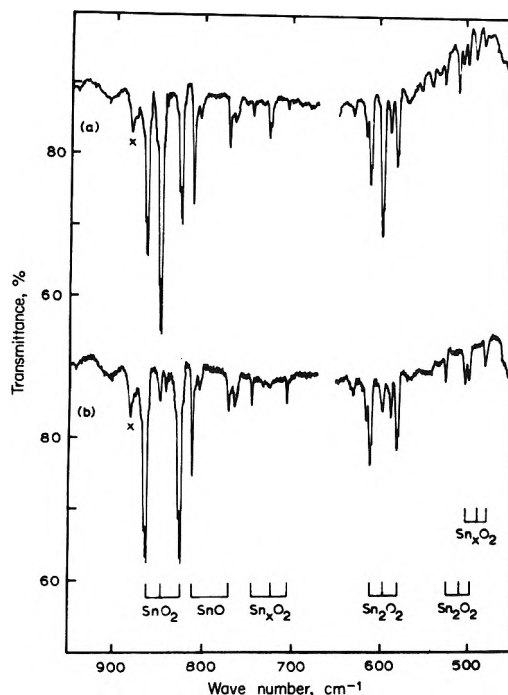


Figure 2. Ir spectra of tin vapor cocondensed with krypton containing 10% total oxygen: (a) using scrambled oxygen 90% Kr, 2.2% <sup>16</sup>O<sub>2</sub>, 5.3% <sup>16</sup>O<sup>18</sup>O, 2.5% <sup>18</sup>O<sub>2</sub>; (b) using unscrambled oxygen 90% Kr, 4.5% <sup>16</sup>O<sub>2</sub>, 0.8% <sup>16</sup>O<sup>18</sup>O, 4.7% <sup>18</sup>O<sub>2</sub>. Note the reduced intensity in b of the central peak of the SnO<sub>2</sub> and Sn<sub>2</sub>O<sub>2</sub> triplets.

prominent absorptions. A typical spectrum obtained after cocondensing tin vapor with krypton containing 10% scrambled oxygen (2.2% <sup>16</sup>O<sub>2</sub>, 5.5% <sup>16</sup>O<sup>18</sup>O, 2.5% <sup>18</sup>O<sub>2</sub>) is shown in Figure 2a. A very prominent triplet is observed at 863.1, 847.2, and 824.7 cm<sup>-1</sup>, and it is evident that each of the bands at 744.9, 611.7, 524.4, and 501.9 cm<sup>-1</sup> also appears as the highest frequency component of a triplet structure. In contrast, the peaks at 812.0, 804.3, and 615.1 cm<sup>-1</sup> have only a single extra band associated with them. Figure 2b shows the spectrum obtained using a corresponding unscrambled krypton-oxygen mixture (90% Kr, 4.5% <sup>16</sup>O<sub>2</sub>, 4.7% <sup>18</sup>O<sub>2</sub>, 0.8% <sup>13</sup>O<sup>18</sup>O). All the peaks observed in Figure 2a are present, but the central components of the five triplets are considerably reduced in intensity. In particular, the central band of the 863.1-cm<sup>-1</sup> triplet is now only ~8% of the total intensity in the group, whereas for the 611.7-cm<sup>-1</sup> triplet, it is ~20%. In the experiments involving scrambled oxygen, these central bands account for ~50% of the total intensity.

Tables I and II list the frequencies of all the bands observed in krypton and nitrogen matrices.

In addition to these <sup>16</sup>O-<sup>18</sup>O isotope patterns, all peaks were examined under optimum resolution conditions (~0.1 cm<sup>-1</sup>) in an attempt to observe fine structure due to the natural abundance of tin isotopes. Under these conditions, the peaks at 812.0 and 771.4 cm<sup>-1</sup> (Table I) gave partially resolved triplets at 812.0, 812.6, and 813.3 cm<sup>-1</sup>, and at 771.4, 772.0, and 772.7 cm<sup>-1</sup> respectively, while the peaks at 863.1, 847.2, and 824.7 cm<sup>-1</sup> were each shown to consist of seven components. Figure 3 shows these three multiplets under high resolution, and the five components corresponding to Sn = 116, 118, 120, 122, and 124 are visible on each band. Under optimum resolution, two additional partially resolved shoulders appear on either side of the Sn = 118 component. These are assigned to the Sn = 117 and Sn = 119 components, and the frequencies of all these bands are listed in Table II. In nitrogen matrices, the basic triplet appears at 877.8, 861.4, and 838.3 cm<sup>-1</sup> and, although resolution was not as good, some fine structure was visible, and these peaks are included in Table II. No tin isotope fine structure was observed on the remaining bands listed in Table I.

### Spectral Interpretation

Previous ir studies<sup>2b</sup> on molecular tin oxides trapped in pure argon matrices have established that diatomic Sn<sup>16</sup>O absorbs at 811 cm<sup>-1</sup>, and that Sn<sub>2</sub><sup>16</sup>O<sub>2</sub> has two strong bands at 611.3 and 522.2 cm<sup>-1</sup>. A weaker feature at 762 cm<sup>-1</sup> was assigned to Sn<sub>3</sub>O<sub>3</sub>. Subsequent experiments have shown<sup>13</sup> that these species have corresponding absorptions at 811.4 cm<sup>-1</sup> (SnO), 611.1 and 523.9 cm<sup>-1</sup> (Sn<sub>2</sub>O<sub>2</sub>), and 763.2 cm<sup>-1</sup> (Sn<sub>3</sub>O<sub>3</sub>) in pure krypton matrices. The bands observed in this work at 812.0, 611.7, 524.4, and 763 cm<sup>-1</sup> (Table I) are thus readily assigned to these molecules on the basis of frequency position, and in the case of SnO and Sn<sub>2</sub>O<sub>2</sub>, this assignment is completely confirmed by the additional bands observed in <sup>18</sup>O enrichment experiments.

The weak feature at 1034.6 cm<sup>-1</sup> is assigned to <sup>16</sup>O<sub>3</sub>. In their paper describing the reaction of calcium atoms with oxygen in krypton matrices, Brewer and Wang<sup>14</sup> observe a prominent band due to matrix isolated <sup>16</sup>O<sub>3</sub> at 1035 cm<sup>-1</sup>. Our assignment is made partly on the basis of this work, and also as a result of isotopic substitution patterns obtained in this region in other metal atom-oxygen matrix reactions.<sup>15</sup>

Four bands thus remain for which isotope data are available, and these occur at 863.1, 744.9, 615.1, and 501.9

(13) A. Bos, unpublished observations.

(14) L. Brewer and J. L. F. Wang, *J. Chem. Phys.*, **56**, 759 (1972).

(15) A. Bos, J. S. Ogden, and L. Orgee, to be published.

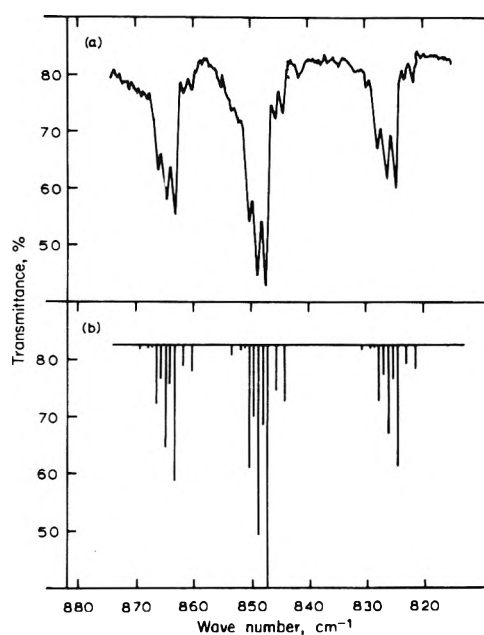


Figure 3. (a) Ir spectrum of  $\text{SnO}_2$  in krypton-10% scrambled oxygen under high resolution. (b) Ir spectrum of  $\text{SnO}_2$  calculated on the basis of known isotopic abundances and using  $F_r = 5.36$  mdyn/Å and  $F_{rr} = -0.18$  mdyn/Å.

$\text{cm}^{-1}$  (Table I). None of these bands was observed in the previous tin oxide matrix isolation work, but evidence was recently presented<sup>11</sup> suggesting that the  $863.1\text{-cm}^{-1}$  band is the  $\Sigma_u^+$  vibration of the linear  $\text{SnO}_2$  molecule. This assignment may now be discussed in detail.

$\text{SnO}_2$ . The relative intensities of the three bands at  $863.1$ ,  $847.2$ , and  $824.7\text{ cm}^{-1}$  are  $\sim 1:2:1$  when isotopically scrambled oxygen mixtures are used, and this indicates that the species responsible contains two equivalent atoms of oxygen. Under high resolution, each band is found to consist of seven components, the intensities of which reflect the isotopic abundances expected for a molecule containing one atom of tin. This species is thus identified as molecular  $\text{SnO}_2$ , and, with two equivalent oxygen atoms, must have either  $C_{2v}$  or  $D_{\infty h}$  symmetry.

For a linear structure, the symmetric stretching vibration ( $\Sigma_g^+$ ) is not ir active, and the  $863.1\text{-cm}^{-1}$  band would therefore be assigned as the antisymmetric stretch ( $\Sigma_u^+$ ) of  $\text{Sn}^{16}\text{O}_2$ . The bending mode in this molecule is also ir active, but it is expected to be considerably lower in frequency, and may lie below the limit of our spectrometer ( $200\text{ cm}^{-1}$ ). For  $C_{2v}$  symmetry, the symmetric stretch is now ir active ( $A_1$ ), but is expected to be less intense than the antisymmetric stretch ( $B_2$ ), and the bending mode will again lie at much lower frequencies. The observed band is therefore assigned to the antisymmetric Sn-O stretching mode for either symmetry.

If one assumes that molecular vibrations are completely harmonic, then the antisymmetric stretching frequency  $\omega_3$  for either of these symmetries is related<sup>16</sup> to the molecular geometry of a general  $\text{XY}_2$  species by

$$4\pi^2\omega_3^2 = (F_r - F_{rr})(\mu_Y + 2\mu_X \sin^2 \alpha)$$

where  $\mu$  is the reciprocal mass, and  $2\alpha$  is the angle  $\angle \text{YXY}$ .  $F_r$  and  $F_{rr}$  are the principal and interaction X-Y stretching constants, respectively. This equation indicates that if  $\omega_3$  is known for two different isotopic molecules  $\text{XY}_2$  and  $\overline{\text{XY}}_2$ , the angle  $\alpha$  may be calculated from the

frequency ratio  $R_3$  and the known atomic masses *via*

$$R_3 = \omega_3/\overline{\omega}_3 = (\mu_Y + 2\mu_X \sin^2 \alpha)^{1/2}/(\mu_{\overline{Y}} + 2\mu_{\overline{X}} \sin^2 \alpha)^{1/2}$$

In general, however,  $\omega$  values are not directly obtainable from matrix isolation studies, and experiments yield absorption frequencies  $\nu$  which differ slightly from  $\omega$  as a result of matrix perturbations and the neglect of anharmonicity. In this event, the observed frequency ratio  $R_3' = \nu_3/\overline{\nu}_3$  is often taken<sup>17</sup> to be sufficiently close to  $R_3$  to allow a reasonable estimate of  $\alpha$  to be made. The errors introduced by neglecting anharmonicity have been summarized by Overend,<sup>17</sup> and in particular, Allavena, *et al.*<sup>18</sup> have shown that if anharmonicity constants are positive, the use of  $R_3'$  rather than  $R_3$  will give a value of  $\sin \alpha$  which is lower than the true value when isotopic substitution takes place at the central atom only (*i.e.*, using the pair of molecules  $\text{XY}_2$  and  $\overline{\text{XY}}_2$ ), whereas substitution at the terminal atoms ( $\text{XY}_2$  and  $\overline{\text{XY}}_2$ ) gives a value which is too high. For a linear  $\text{XY}_2$  molecule, isotopic substitution at X should therefore yield a value of  $2\alpha$  which is less than  $180^\circ$ , and it is probable that isotopic substitution at Y will give an imaginary value of  $\alpha$  corresponding to  $\sin \alpha > 1.0$ .

In Table III we compare the observed frequency ratios  $R_3'$  of selected pairs of  $\text{SnO}_2$  molecules with the corresponding ratios  $R_3$  calculated first for a linear model and second for a  $C_{2v}$  structure with  $2\alpha = 150^\circ$ . It can be seen that for pairs of molecules such as  $^{116}\text{Sn}^{16}\text{O}_2$ - $^{124}\text{Sn}^{16}\text{O}_2$ , which involve changes in the tin isotope mass, the observed ratios indicate an almost linear structure, whereas a pair of molecules such as  $^{120}\text{Sn}^{16}\text{O}_2$ - $^{120}\text{Sn}^{18}\text{O}_2$  yields a value of  $R_3'$  which is significantly less than the theoretical minimum at  $2\alpha = 180^\circ$ , and in fact gives a value of  $\sin \alpha = 1.02$ . Both Sn and O isotope substitution therefore strongly suggest that  $\text{SnO}_2$  is a linear  $D_{\infty h}$  molecule isostructural with  $\text{CO}_2$ .

The frequencies of the partially substituted species  $\text{Sn}^{16}\text{O}^{18}\text{O}$  may be used in conjunction with those of  $\text{Sn}^{16}\text{O}_2$  or  $\text{Sn}^{18}\text{O}_2$  to obtain values<sup>19</sup> for both  $F_r$  and  $F_{rr}$ . Slightly different values are obtained for krypton and nitrogen matrices as a result of the small frequency differences, but in both cases,  $F_r$  is close to the stretching constant in diatomic SnO (Table IV) and considerably higher than the stretching constants previously observed for Sn-O bonds. In addition to being isostructural with  $\text{CO}_2$ , molecular  $\text{SnO}_2$  therefore appears to show a significant amount of multiple bonding, and this is reflected in the bond length estimates which are available through the Herschbach and Laurie relationship<sup>20</sup>

$$r = 2.36 - 0.76 \log F_r$$

This equation is moderately successful in estimating a bond length of  $1.79\text{ Å}$  for diatomic SnO from a krypton matrix frequency of  $812.0\text{ cm}^{-1}$  (microwave studies in the gas phase give  $r_{\text{Sn-O}} = 1.8325\text{ Å}$ ), and the corresponding

- (16) G. Herzberg, "Molecular Spectra and Molecular Structure," Vol. II, Van Nostrand, New York, N. Y., 1959.
- (17) J. Overend, *Annu. Rev. Phys. Chem.*, **21**, 265 (1970).
- (18) M. Allavena, R. Rysnik, D. White, V. Calder, and D. E. Mann, *J. Chem. Phys.*, **50**, 3393 (1969).
- (19) J. L. Griggs, Jr., K. N. Rao, L. H. Jones, and R. M. Potter, *J. Mol. Spectrosc.*, **18**, 212 (1965).
- (20) D. R. Herschbach and V. W. Laurie, *J. Chem. Phys.*, **35**, 453 (1961).
- (21) F. J. Lovas and D. R. Lide, Jr., *Advan. High Temp. Chem.*, **3**, 177 (1971).

TABLE III: Observed and Calculated Frequency Ratios for Isotopic SnO<sub>2</sub> Species

Species	N <sub>2</sub> matrices		Kr matrices			Calculated ratio (R <sub>3</sub> )	
	Obsd frequency	Obsd ratio	Obsd frequency	Obsd ratio <sup>a</sup>	sin α <sup>b</sup>	D <sub>∞h</sub> (α = 90°)	C <sub>2v</sub> (α = 75°)
<sup>16</sup> O <sup>120</sup> Sn <sup>16</sup> O	877.8		863.1				
<sup>18</sup> O <sup>120</sup> Sn <sup>18</sup> O	838.3	1.0471	824.7	1.04655	1.020	1.0470	1.0477
<sup>16</sup> O <sup>116</sup> Sn <sup>16</sup> O	881.0		866.1				
<sup>16</sup> O <sup>124</sup> Sn <sup>16</sup> O	874.8	1.0071	860.1	1.0070	0.999	1.0071	1.0067
<sup>18</sup> O <sup>116</sup> Sn <sup>18</sup> O	841.6		828.0				
<sup>18</sup> O <sup>124</sup> Sn <sup>18</sup> O	835.2	1.0077	821.6	1.0078	1.001	1.0077	1.0073

<sup>a</sup> Error limits ±0.0001. <sup>b</sup> Error limits ±0.003.

TABLE IV: Comparison of Molecular Parameters Found in Tin Oxides

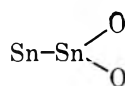
	Molecular SnO <sub>2</sub>				
	N <sub>2</sub> matrix	Kr matrix	Diatomic SnO	Sn <sub>2</sub> O <sub>2</sub>	Solid SnO <sub>2</sub>
Principal force constant, mdyn/Å	5.57	5.36	5.62 <sup>a</sup>	2.59 <sup>b</sup>	
Interaction force constant, mdyn/Å	-0.16	-0.18			
Bond length, r <sub>Sn-O</sub> , Å	1.79 <sup>c</sup>	1.81 <sup>c</sup>	1.83 <sup>d</sup>	2.05 <sup>b</sup>	2.05 <sup>e</sup>

<sup>a</sup> Calculated from the gas-phase frequency.<sup>23</sup> <sup>b</sup> Reference 2. <sup>c</sup> Estimated from Herschbach-Laurie relationship.<sup>20</sup> <sup>d</sup> Reference 21. <sup>e</sup> Shortest Sn-O distance.<sup>22</sup>

estimate for SnO<sub>2</sub> is 1.81 Å. Table IV<sup>21,22</sup> summarizes various molecular parameters obtained for tin oxides.

Using the calculated values of  $F_r$  and  $F_{rr}$ , it is possible to predict the frequencies of the symmetric Sn-O stretching vibrations using standard equations.<sup>23</sup> These frequencies are listed in Table V together with the observed and calculated antisymmetric frequencies, and Figure 3 shows that the agreement between the observed and calculated SnO<sub>2</sub> spectrum is very satisfactory. A careful search was made under optimum conditions for the low-frequency  $\pi_u$  bending mode, but no absorption was observed when the  $\nu_3$  band in Sn<sup>16</sup>O<sub>2</sub> had an optical density of ~0.5.

*The 744.9- and 501.9-cm<sup>-1</sup> Bands.* The two bands at 744.9 and 501.9 cm<sup>-1</sup> were initially present in all spectra, but rapidly decreased in intensity on photolysis. Under high resolution, the bands were ~2 cm<sup>-1</sup> wide, and it was not possible to resolve any tin isotope fine structure. Experiments with <sup>18</sup>O enriched oxygen produced triplet patterns characteristic of a molecule containing two equivalent oxygen atoms (for scrambled mixtures), and in view of the identical behavior of these bands over a wide range of experimental conditions, they are assigned to a single species Sn<sub>x</sub>O<sub>2</sub>. The triplet patterns produced from unscrambled oxygen isotope mixtures were very similar to those observed for SnO<sub>2</sub>. It is not possible to determine  $x$  from these experiments, but the lack of any tin isotope fine structure, particularly on the higher band, indicates that  $x \geq 2$ . Both bands lie within the expected frequency range for Sn-O stretching vibrations (~900-400 cm<sup>-1</sup>), and one model which is consistent with the frequency data and with the proposed mechanism of formation (see below) is the C<sub>2v</sub> structure



in which it is assumed that  $x = 2$ . This molecule would have two ir active Sn-O stretching vibrations (A<sub>1</sub> + B<sub>2</sub>) and although the remaining vibrations are all ir active, they would be expected to lie below this region of the spectrum.

*Remaining Features.* The four remaining bands at 804.3, 615.1, 577.7, and 557.7 cm<sup>-1</sup> are weaker than the principal absorptions (Figure 1), but they were observed in nearly all spectra. The 804.3-cm<sup>-1</sup> band would appear to lie in the Sn=O stretching region, and may even be due to molecular SnO trapped in a different matrix environment. Isotope enrichment suggests that only one atom of oxygen is present in the species, and the <sup>18</sup>O counterpart of this band is shown at 764.5 cm<sup>-1</sup> in Figure 2. The frequency shift 804.3 → 764.5 cm<sup>-1</sup> is consistent with molecular SnO, but it is evident in Figure 2b that the lower component is more intense than would be expected on the basis of the known proportion of <sup>18</sup>O present. Although this anomaly is probably due to overlap with the Sn<sub>3</sub>O<sub>3</sub> absorption at 763 cm<sup>-1</sup>, the assignment of this feature as a matrix effect therefore remains tentative.

The 615.1-cm<sup>-1</sup> absorption also produces a single new band at 587.4 cm<sup>-1</sup> on <sup>18</sup>O enrichment. This band also lies in the Sn-O stretching region, and although no specific assignment is made, a cyclic structure such as



would be a possible model for this species. No attempt is made to assign the two features at 577.7 and 557.7 cm<sup>-1</sup>. This region of the spectrum showed several very weak features on <sup>18</sup>O enrichment (Figure 2) but it was not possible to correlate them with the parent <sup>16</sup>O absorptions.

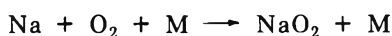
### Reaction Mechanisms

The conditions under which metal atoms react with oxygen in matrix isolation studies are in some ways similar to those in classical gas-phase fast-flow techniques. In both types of experiment, the partial pressures of the reacting species are low, and the presence of the matrix gas adequately fulfills the role of the inert "third body"

(22) W. H. Baur, *Acta Crystallogr.*, **9**, 515 (1956).

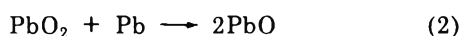
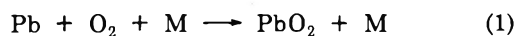
(23) G. Herzberg, "Molecular Spectra and Molecular Structure," Vol. I, Van Nostrand, Princeton, N. J., 1959.

necessary in many gas-phase studies. The main difference is that in the matrix isolation experiment, one is quenching a chemical reaction very rapidly in the hope of isolating a reaction intermediate, and as temperature is an important factor in determining both the rates and products of chemical reactions, one might anticipate some differences between gas-phase reactions and parallel matrix isolation studies. However, the experiments so far carried out on sodium or potassium atom-O<sub>2</sub> reactions in the presence of a third body M indicate that

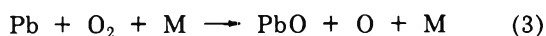


occurs both in the gas phase<sup>5,6</sup> and under matrix isolation conditions.<sup>9,10</sup> Tin vapor is predominantly monatomic,<sup>24</sup> and although there is no kinetic data published on the tin atom-O<sub>2</sub> reaction, Ryason and Smith have studied the gas-phase oxidation of lead vapor,<sup>4</sup> and it is interesting to compare their conclusions with the results obtained here.

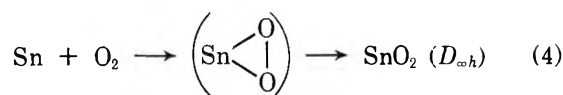
In their paper, Ryason and Smith show that the kinetics of the Pb atom-O<sub>2</sub> gas-phase reaction are consistent with the formation and decay of molecular PbO<sub>2</sub> according to



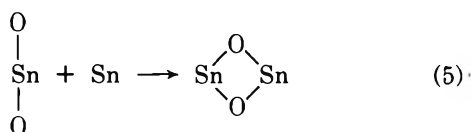
and point out that the reaction



is thermodynamically unfavorable. In this tin atom work, the most significant result of the <sup>18</sup>O enrichment experiments is the observation that only small amounts of Sn<sup>16</sup>O<sup>18</sup>O and Sn<sub>2</sub><sup>16</sup>O<sup>18</sup>O are produced from unscrambled oxygen mixtures. The simplest interpretation of this is that tin atoms react with molecular oxygen by an insertion mechanism in which the O-O bond is retained in the transition state



Molecular SnO<sub>2</sub> may then further react with tin atoms to form the cyclic molecule Sn<sub>2</sub>O<sub>2</sub>



and in this way, the oxygen isotope patterns in SnO<sub>2</sub> and Sn<sub>2</sub>O<sub>2</sub> would reflect the abundances present in the original mixture. This proposed scheme differs from the lead atom-O<sub>2</sub> reaction in the final stage, where we propose an addition mechanism, and Ryason and Smith imply an abstraction mechanism. However, this is probably not a real disagreement, since Ryason and Smith are not primarily concerned with the nature of vapor phase PbO. This has been shown to consist of several<sup>25</sup> molecular species (PbO)<sub>1-6</sub>, and kinetic studies based on the rate of reaction of the metal atoms would be unable to distinguish between reactions 2 and 5.

The reactions of tin and lead atoms with molecular oxygen present an interesting contrast with the gas-phase studies<sup>26</sup> on the atomic carbon-O<sub>2</sub> reaction, in which only CO + O is observed, and there is no evidence for an insertion mechanism to produce CO<sub>2</sub>.

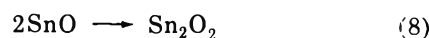
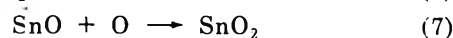
An alternative route to SnO<sub>2</sub> or Sn<sub>2</sub>O<sub>2</sub> is provided by

TABLE V: Comparison of Observed and Calculated Frequencies (cm<sup>-1</sup>) for Molecular SnO<sub>2</sub>

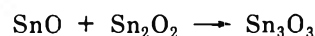
Species	N <sub>2</sub> matrices		Kr matrices	
	Obsd	Calcd <sup>a</sup>	Obsd	Calcd <sup>b</sup>
Σ <sub>u</sub> + <sup>16</sup> O <sup>124</sup> Sn <sup>16</sup> O	874.8	874.8	860.1	860.3
Σ <sub>u</sub> + <sup>16</sup> O <sup>120</sup> Sn <sup>16</sup> O	877.8	877.7	863.1	863.3
Σ <sub>u</sub> + <sup>16</sup> O <sup>116</sup> Sn <sup>16</sup> O	881.0	880.9	866.1	866.4
Σ <sub>g</sub> + <sup>16</sup> O <sup>124</sup> Sn <sup>18</sup> O	858.4	858.4	844.3	844.2
Σ <sub>g</sub> + <sup>16</sup> O <sup>120</sup> Sn <sup>18</sup> O	861.4	861.4	847.2	847.2
Σ <sub>g</sub> + <sup>16</sup> O <sup>116</sup> Sn <sup>18</sup> O	864.4	864.6	850.2	850.3
Σ <sub>u</sub> + <sup>18</sup> O <sup>124</sup> Sn <sup>18</sup> O	835.2	835.2	821.6	821.5
Σ <sub>u</sub> + <sup>18</sup> O <sup>120</sup> Sn <sup>18</sup> O	838.3	838.4	824.7	824.5
Σ <sub>u</sub> + <sup>18</sup> O <sup>116</sup> Sn <sup>18</sup> O	841.6	841.7	828.0	827.8
Σ <sub>g</sub> + <sup>16</sup> OSn <sup>16</sup> O		757.3		743.1
Σ <sub>g</sub> + <sup>16</sup> OSn <sup>18</sup> O		732.3		718.6
Σ <sub>g</sub> + <sup>18</sup> OSn <sup>18</sup> O		714.0		700.5

<sup>a</sup> Values calculated for a linear model using  $F_r = 5.568 \text{ mdy}/\text{\AA}$ ,  $F_{rr} = -0.164 \text{ mdy}/\text{\AA}$ . <sup>b</sup>  $F_r = 5.363 \text{ mdy}/\text{\AA}$ ,  $F_{rr} = -0.181 \text{ mdy}/\text{\AA}$ . The Σ<sub>g</sub><sup>+</sup> vibrations are independent of the tin isotope mass.

the reaction scheme

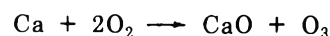


and this sequence must be considered in any discussion of the mechanism, as reaction 6 is thermodynamically favorable for tin atoms ( $D_{\text{SnO}} > D_{\text{O}_2}$ ),<sup>27</sup> and the majority of spectra showed small amounts of molecular SnO. However, if this were an important route to the species SnO<sub>2</sub> or Sn<sub>2</sub>O<sub>2</sub>, one would expect to observe considerable amounts of Sn<sup>16</sup>O<sup>18</sup>O and Sn<sub>2</sub><sup>16</sup>O<sup>18</sup>O in the experiments with unscrambled <sup>16</sup>O<sub>2</sub>-<sup>18</sup>O<sub>2</sub> mixtures, as these reactions provide an opportunity for complete isotope scrambling. In practice, our experiments indicate that although there is no evidence for (7), the proportion of Sn<sub>2</sub><sup>16</sup>O<sup>18</sup>O observed in unscrambled oxygen experiments is ~20% and thus significantly higher than the 8% which would be expected solely on the basis of (5). Reaction 8 does therefore appear to take place to a small extent, and a limited amount of further polymerization

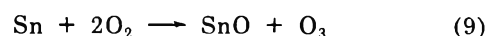


would account for the traces of Sn<sub>3</sub>O<sub>3</sub> observed.

In addition to producing SnO, reaction 6 is also a source of oxygen atoms, and it is significant that in krypton matrices containing >10% O<sub>2</sub>, small amounts of ozone were observed. Brewer and Wang observed molecular CaO and ozone as principal reaction products in their study<sup>14</sup> of the calcium atom-O<sub>2</sub> matrix reaction, and suggested that it proceeded *via*



From our experiments, it is not possible to decide whether SnO and O<sub>3</sub> are produced by the analogous three body reaction



(24) R. E. Honig, *J. Chem. Phys.*, **21**, 573 (1953).

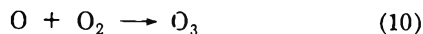
(25) J. Drowart, R. Colin, and G. Exsteen, *Trans. Faraday Soc.*, **61**, 1376 (1965); D. M. Chizhikov, E. K. Kazenas, and Y. V. Tsvetkov, *Izv. Akad. Nauk. SSSR Metal.*, **5**, 57 (1969).

(26) R. F. Peterson, Jr., and R. Wolfgang, *Advan. High Temp. Chem.*, **4**, 43 (1971).

(27) J. Drowart and P. Goldfinger, *Angew. Chem., Int. Ed. Engl.*, **6**, 581 (1967).



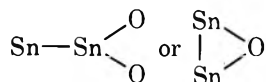
or by reaction 6 followed by



but it is significant that ozone was only observed under conditions where two oxygen molecules have a high probability of being trapped on adjacent sites in the matrix. The situation in nitrogen matrices, however, is rather different. Both ozone and molecular SnO were noticeably absent from the spectra even at N<sub>2</sub>:O<sub>2</sub> ratios of 5:1, and this implies that reaction 6 does not take place to a significant extent in nitrogen matrices. The reason for this is not clear, but it is known from gas-phase studies that the nature of the third body M can significantly affect the rates of chemical reactions.<sup>28</sup>

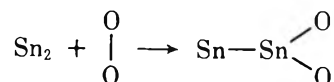
We therefore propose that tin atoms can undergo two basic types of chemical reaction when cocondensed at low temperatures with matrices containing oxygen, and that the relative importance of these depends upon the nature of the matrix gas. The first reaction is a simple insertion and results in the formation of molecular SnO<sub>2</sub> according to (4), and this may then further react to produce Sn<sub>2</sub>O<sub>2</sub> (5). In krypton matrices, an abstraction reaction becomes significant and results in the formation of SnO and O<sub>3</sub> (reactions 6, 9, and 10). A limited amount of molecular diffusion also takes place to produce traces of higher polymers.

These reactions therefore account for the formation of five of the species listed in Table I, but a number of additional bands are also observed. It has been suggested that these might be assigned to species such as



and although these molecules could be formed by the reaction of tin atoms with SnO<sub>2</sub> or SnO, they might alternatively be formed by reactions involving molecular Sn<sub>2</sub>. The proportion of Sn<sub>2</sub> in tin vapor is low,<sup>24</sup> but it is possible that as a result of diffusion during quenching, significant concentrations may be produced in the matrix and may undergo reaction with oxygen. In particular, the two bands at 744.9 and 501.9 cm<sup>-1</sup> have been assigned to a C<sub>2v</sub> isomer of Sn<sub>2</sub>O<sub>2</sub>, and both these bands produce triplet patterns similar to SnO<sub>2</sub> on <sup>18</sup>O enrichment. This species could be formed by the insertion of Sn<sub>2</sub> into an oxygen

molecule in a similar way to the formation of SnO<sub>2</sub>



and this mechanism would allow retention of the O-O bond in the transition state as suggested by the unscrambled <sup>18</sup>O results.

All the above reaction schemes proposed for tin vapor-O<sub>2</sub> would be expected to be thermodynamically favorable on the basis of available bond energy data.<sup>27</sup>

### Conclusion

These experiments show that when tin vapor is cocondensed at low temperatures with matrices containing oxygen, the major reaction products are molecular SnO<sub>2</sub> and Sn<sub>2</sub>O<sub>2</sub> (*D*<sub>2h</sub>). Small amounts of SnO and O<sub>3</sub> are sometimes observed together with a number of other tin oxide species which could not be completely characterized. A normal coordinate analysis based upon the large number of available isotope frequencies indicates that SnO<sub>2</sub> is linear (*D*<sub>∞h</sub>). This molecule therefore appears to be isostructural with CO<sub>2</sub>, and the value of the principal Sn-O force constant suggests that there is considerable multiple bonding present.

As well as providing additional vibration frequencies, <sup>18</sup>O enrichment experiments suggest that the primary reaction Sn + O<sub>2</sub> → SnO<sub>2</sub> proceeds through a transition state in which the O-O bond is retained, and that the majority of the Sn<sub>2</sub>O<sub>2</sub> produced comes from the secondary reaction Sn + SnO<sub>2</sub> → Sn<sub>2</sub>O<sub>2</sub>. These mechanisms differ significantly from the reactions of atomic carbon with oxygen, but are consistent with parallel gas-phase kinetic studies on the lead atom-O<sub>2</sub> reaction, and it is possible that matrix isolation could become an important technique in studying the mechanisms of a large number of metal atom-oxygen reactions.

*Acknowledgments.* We gratefully acknowledge the financial support of the Science Research Council and the Central Electricity Generating Board for this work, and also wish to thank Professor J. S. Anderson for much cooperation and discussion.

(28) F. Kaufman and J. R. Kelso, *J. Chem. Phys.*, **46**, 4541 (1967).

# An Additivity Equation for Calculating Second Moments of the Electronic Charge Distribution

Z. B. Maksić and J. E. Bloor\*<sup>1</sup>

*Institute "Ruder Bosković," 41001 Zagreb, Croatia, Yugoslavia and the Department of Chemistry, The University of Tennessee, Knoxville, Tennessee 37916 (Received December 29, 1972)*

The additivity equation previously proposed for calculating the diamagnetic susceptibilities of hydrocarbons has been extended to the calculation of second moments and of diamagnetic susceptibilities of molecules containing atoms of the second and third rows of the periodic table and the higher halogens. An analysis in terms of CNDO/2D wave functions of the different orbital contributions to second moments is presented. It is shown that the success of methods of representing second moments as a sum of atomic contributions is dependent on a cancelling out of opposing factors rather than on a lack of charge polarization on molecule formation.

## Introduction

Recent developments in the area of experimental microwave spectroscopy have made available experimental values of molecular quadrupole moments, diamagnetic and paramagnetic susceptibilities, and the individual components of the second moments of the electronic charge distributions.<sup>2a</sup> The analysis of these experimental results by Blickensderfer, *et al.*,<sup>2b</sup> led to the development of empirical rules for the out-of-plane second moments,  $\langle c^2 \rangle_e$  for planar molecules containing first row atoms and hydrogens. These empirical findings were rationalized<sup>3</sup> in terms of CNDO/2 molecular orbital calculations, which showed that  $\langle c^2 \rangle_e$  could be written as a sum of the second moments of the atomic orbitals on each atom multiplied by the corresponding orbital populations

$$\langle c^2 \rangle_e = \sum_A \sum_{\mu} \sum_{\nu} P_{\mu\nu}^A \langle \phi_{\mu}^A | c_A^2 | \phi_{\nu}^A \rangle \quad (1)$$

where  $P_{\mu\nu}^A$  is the bond order between atomic orbitals (AO)  $\phi_{\mu}$ , and  $\phi_{\nu}$  on atom A,  $\langle \phi_{\mu}^A | c_A^2 | \phi_{\nu}^A \rangle$  is a one-center second moment integral calculated with the coordinate origin of the second moment operator  $c_A^2$  placed on atom A.

Further analysis<sup>3</sup> of the way this expression changed with the nature of the atom A showed that, for the first row of the periodic table, there were two opposing effects.  $P_{\mu\mu}^A$  was, as expected, found to be strongly dependent on the electronegativity of atom A; *i.e.*, as the electronegativity increased so did  $P_{\mu\mu}^A$ . Opposing this effect, however, were the concomitant changes in the Slater shielding exponents. These increased as the electronegativity increased resulting in a contraction of the AO's and a smaller value for the integral  $\langle \phi_{\mu}^A | c^2 | \phi_{\mu}^A \rangle$ . The net result, after correcting for the hybridization terms ( $\mu \neq \nu$ ), was a constant contribution of  $1 \times 10^{-16}$  cm<sup>2</sup>/atom to  $\langle c^2 \rangle_e$  independent of the nature of the atom. This is exactly the value found empirically by Blickensderfer, *et al.*<sup>2b</sup>

In a subsequent study<sup>4</sup> it was shown that for hydrocarbons the second moments along all three principal inertial axes (*a*, *b*, and *c*) could be written in terms of a contribution depending only on the geometry of the molecule plus a contribution from each atom. This latter term was assumed to be independent of the molecular environment, *i.e.*, local atomic anisotropic effects were neglected. In the present work we extend this model to include the second

moments and diamagnetic susceptibilities of molecules containing atoms other than carbon and hydrogen, including atoms of the second row of the periodic table. We also discuss the relationship between our model and the results of semiempirical MO theory,<sup>3,5,6</sup> and also its relationship to a recently reported empirical method for calculating dipole and quadrupole moments.<sup>7</sup>

## Methods of Calculation

The second moments of the electronic charge distribution are defined as

$$\langle \alpha^2 \rangle_e = \langle 0 | \sum \alpha_i^2 | 0 \rangle \quad \alpha = a, b, \text{ or } c \quad (2)$$

where  $\langle 0 | | 0 \rangle$  indicates the average value over the ground-state single-determinantal wave function, the summation is extended over all the electrons in a molecule and  $\alpha^2$  denotes the second moment operator along one of the three principal inertial axes, *a*, *b*, and *c*. The corresponding expressions along the cartesian coordinate axes of a molecule,  $\langle v^2 \rangle_e$ ,  $v = x, y, \text{ or } z$ , can be expanded over contributions from integrals over AO's.

$$\langle v^2 \rangle_e = \sum_A \sum_{\mu} P_{\mu\mu}^A \langle \phi_{\mu}^A | v^2 | \phi_{\mu}^A \rangle + 2 \sum_{\mu < \nu} \sum_{\nu} P_{\mu\nu}^A \langle \phi_{\mu}^A | v^2 | \phi_{\nu}^A \rangle + 2 \sum_{A < B} \sum_{\mu < \nu} \sum_{\nu} P_{\mu\nu}^{AB} \langle \phi_{\mu}^A | v^2 | \phi_{\nu}^B \rangle \quad (3)$$

where  $\phi_{\mu}^A$  is a Slater type atomic orbital (STO) on center A and  $P_{\mu\nu}^A$  and  $P_{\mu\nu}^{AB}$  are one and two center elements, respectively, of the first-order density matrix.

The first two terms in eq 3 represent the sum of atomic contributions to the molecular second moments involving AO's on one atomic center, while the third term is a sum of the bonding and nonbonding contributions in which the AO's are on two atomic centers. It can be shown that the

- (1) Department of Chemistry, University of Tennessee.
- (2) (a) W. H. Flygare and R. C. Benson, *Mol. Phys.*, **20**, 225 (1971), and references cited therein; (b) R. P. Blickensderfer, Y. H. S. Wang, and W. H. Flygare, *J. Chem. Phys.*, **51**, 3196 (1971).
- (3) J. E. Bloor and Z. B. Maksić, *Mol. Phys.*, **22**, 351 (1971).
- (4) Z. B. Maksić and J. E. Bloor, *Chem. Phys. Lett.*, **13**, 571 (1972).
- (5) J. E. Bloor and Z. B. Maksić, *J. Chem. Phys.*, in press.
- (6) (a) R. Rein, G. R. Pack, and J. R. Rabinowitz, *J. Mag. Resonance*, **6**, 360 (1972); (b) J. R. Rabinowitz and R. Rein, *Int. J. Quantum Chem.*, **6**, 669 (1972).
- (7) T. D. Gierke, H. L. Tigelaar, and W. H. Flygare, *J. Amer. Chem. Soc.*, **94**, 331 (1972).

third term is generally small and may be dropped from further consideration (*vide infra*). Equation 3 can be simplified by transforming the coordinate system in which the integrals are evaluated, from a molecular coordinate system,  $v_i$ , to individual coordinate systems,  $v_A^1$  centered on each atom. The two are related by

$$v_A = V_A + v_A^1$$

where  $V_A$  is one of the coordinates of atom A. If we then make the assumptions that (i) the 1s AO's on different atoms are orthogonal, (ii) that the 1s inner core electrons are unpolarizable on molecule formation and can be treated as point charges, and (iii) that the third term of eq 3 can be neglected, then eq 3 reduces to

$$\langle v^2 \rangle_e = \sum_{\mu} \sum_{\nu} P_{\mu\nu}^A V_A^2 + \sum_{\mu} P_{\mu\mu}^A \langle \phi_{\mu}^A | (v_A^1)^2 | \phi_{\mu}^A \rangle + 4 \sum_{\mu < \nu} \sum_{\mu, \nu} P_{\mu\nu}^A V_A \langle \phi_{\mu}^A | v_A^1 | \phi_{\nu}^A \rangle \quad (4)$$

The one center integrals occurring in eq 4 are easily calculated for the first row atoms in terms of STO's using eq 5-8.

$$\alpha_A = \langle 1s^A | (v_A^1)^2 | 1s^A \rangle = a_0^2 / \zeta_{1s}^A \quad (5)$$

$$\beta_A = \langle 2s^A | (v_A^1)^2 | 2s^A \rangle = 10a_0^2 / (\zeta_{2s}^A)^2 \quad (6)$$

In these equations  $a_0$  is the Bohr radius, and  $v_A^1$  represents  $x$ ,  $y$ , and  $z$  coordinates of the electron, relative to nucleus A, noting that the directions of  $x$ ,  $y$ , and  $z$  were fixed by the molecular coordinate system. This coordinate system is usually chosen, purely for calculational convenience, to coincide with the principal axes system of the second moment, which also, for many of the molecules studied here, coincides with the principal inertial axis system.  $\xi_{\mu}$  is the shielding exponent for the STO,  $\phi_{\mu}$ . If we now assume that  $\xi_{2s} = \xi_{2p}$  then the integrals for  $2p_v$  and  $2p_w$  STO's (where  $w, v = x, y, \text{ and } z$  and  $w \neq v$ ) may be written as

$$2p_v^A | (v_A^1)^2 | 2p_v^A \rangle = 3 \langle 2p_w^A | (v_A^1)^2 | 2p_w^A \rangle = a_0 / 5\beta_A \quad (v \neq w) \quad (7)$$

The only other integrals required are the one-center atomic dipole integrals  $\alpha_A$  where  $\alpha_A$  is defined by

$$\alpha_A = \langle 2s^A | (v_A^1) | 2p_v^A \rangle = 5\sqrt{3}a_0 / 3\xi_{2s}^A \quad (8)$$

we may then use these equations to write an approximate equation for the second moment

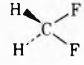
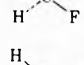
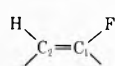
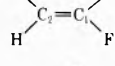
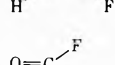
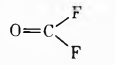
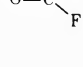
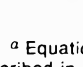
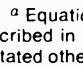
$$\langle v^2 \rangle_e \cong \sum_A \{ P^A V_A^2 + 2\alpha_A + [P_{2s2s}^A + 1.8P_{p_x2p_x}^A + 0.6(P_{2p_y2p_y}^A + P_{2p_z2p_z}^A)]\beta_A + 4V_A \sum_{\substack{v=x \\ y,z}} P_{2s2p_v}^A \langle 2s^A | v_A^1 | 2p_v^A \rangle \} \quad (9)$$

In eq 9  $P^A$  is the total charge density on atom A, including a contribution of 2 from the 1s electrons whereas terms such as  $P_{2s2s}^A$  represent the charge density in a particular AO specified by the subscript. The values of the different terms in eq 9 calculated using CNDO/2D wave functions are given for three molecules containing C, H, F, and O in Tables I and II. In Table I we also compare the second moments calculated using eq 3 and 9 with the results calculated using an extension of the additivity relationship we previously reported for calculating the second moments of hydrocarbons.<sup>4</sup> This new additivity relationship, which is valid for molecules containing hydrogen and any atom from the first row of the periodic table, is

$$\langle v^2 \rangle_e = \sum_A (Z_A V_A^2 + K_A n_A) \quad (10)$$

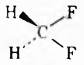
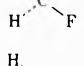
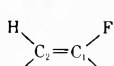
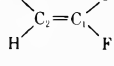
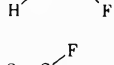
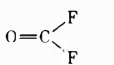
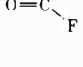
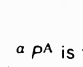
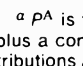
where  $Z_A$  is the atomic number of atom A,  $n_A$  is the number of atoms, and  $K_A$  is a constant depending on the nature of atom A. For atoms of the first row we used  $K_A = 1.0 \times 10^{-16} \text{ cm}^2$  and for hydrogen we used  $K_H = 0.2 \times 10^{-16} \text{ cm}^2$ . (In our earlier work<sup>4</sup> we used 0.95 and 0.19 for carbon and hydrogen.) The values calculated using eq 10

TABLE I: Comparison between Difference Methods of Calculating Electronic Second Moments of Difluoromethane, 1,1-Difluoroethylene, and Carbonyl Fluoride

Molecule	$\langle v^2 \rangle_e$ ( $10^{-16} \text{ cm}^2$ )			Expt <sup>d</sup>
	Full CNDO/2D <sup>a</sup>	One center CNDO/2D <sup>b</sup>	Additivity equation <sup>c</sup>	
	7.93	8.64	9.0	9.0 ± 0.7
	4.53	4.53	5.0	5.0
	23.06	26.09	25.2	25.8 ± 0.7
	31.96	32.31	32.2	31.7 ± 0.6
	27.23	28.28	27.1	27.1 ± 0.6
	4.09	4.07	4.4	4.5
	25.6	26.54	25.1	26.1 ± 0.5
	24.36	25.04	24.3	24.8 ± 0.5
	3.24	3.26	4.0	4.0

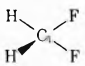
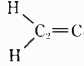
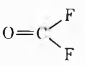
<sup>a</sup> Equation 3 used with all many centered integrals included as described in ref 3. <sup>b</sup> Equation 9 was used. <sup>c</sup> Equation 10 was used. <sup>d</sup> Unless stated otherwise experimental data is from ref 2.

TABLE II: Breakdown of Contributions to the Electronic Second Moment using CNDO/2D Wave Functions

Molecule	$\sum_A Z_A X_A^2$	$\sum_A P^A X_A^2$	Orbital contributions for individual atoms <sup>b</sup>				
			H	C(1)	C(2)	F	O
	5.61	5.43	0.19	0.98		0.79	
	1.64	1.59	0.19	0.98		0.77	
	21.79	22.38	0.19	0.93		0.73	
	27.78	27.60	0.17	0.93	1.08	0.75	
	22.69	23.10	0.17	0.87	1.10	0.73	
	0.00	0.00	0.17	0.96	1.17	0.77	
	21.13	21.74		0.84		0.75	0.81
	20.26	20.85		0.81		0.73	0.92
	0.0	0.0		0.85		0.77	0.83

<sup>a</sup>  $P^A$  is the sum of the electron densities of all valence AO's on atom A plus a contribution of 2 for the 1s electrons. <sup>b</sup> The one center orbital contributions are the second and third terms in eq 9.

TABLE III: Hybridization Contributions to the Second Moments Calculated using CNDO/2D Wave Functions<sup>a</sup>

Atom			
C <sub>1</sub>	0.094 (X)	0.041 (X)	0.034 (X)
C <sub>2</sub>		0.401 (Y)	1.107 (X)
F	0.069 (X)	0.175 (X)	0.178 (X)
	0.457 (Z)	0.676 (Y)	0.473 (Y)
O			1.107 (X)


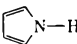
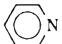
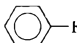
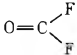
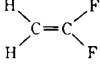
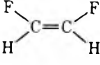
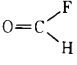
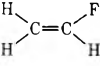
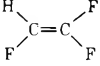
<sup>a</sup> Only nonzero contributions of the valence electrons are given. The principal axis is given in parentheses after the value. The 1s shell contributions for C<sub>1</sub>, F, and O are 0.017, 0.007, and  $0.009 \times 10^{-16} \text{ cm}^2$ , respectively.

TABLE IV: Calculated and Experimental Molecular Second Moments and Diamagnetic Susceptibilities

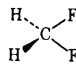
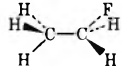
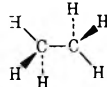
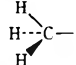
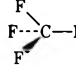
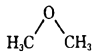
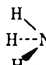
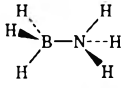
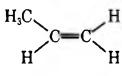
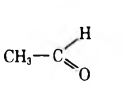
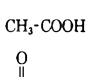
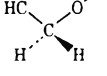
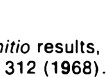
Molecule	Nuclear moment, $\sum Z_A a_A^2$	Electronic moment, ( $10^{-16} \text{ cm}^2$ )		Diamagnetic Susceptibility, ( $10^{-6} \text{ cm}^3 \text{ mol}^{-1}$ )	
		$\langle a^2 \rangle_e$ $\langle b^2 \rangle_e$ Calcd	Expt	$\chi_{  }^d$ $\chi_{\perp}^d$ Calcd	Expt <sup>a</sup>
N≡N	4.22	6.2	6.6	17.0	17.8
		2.0	2.1	34.8	36.9
O=O	5.83	7.8	8.2	17.0	19.5
		2.0	2.3	41.6	44.5
F-F	9.05	11.1	10.7 <sup>b</sup>	17.0	17.7 <sup>a</sup>
		2.0	1.5	55.6	51.8
N=N=O	20.08	23.1	24.1	25.5	25.5
		3.0	3.0	110.7	115.0
O=C=O	21.53	24.5	25.5	25.5	24.6
		3.0	2.9	116.7	120.5
F-C≡C-H	28.34	31.5	31.0	27.2	29.7
		3.2	3.5	147.2	146.4
CH <sub>3</sub> -C≡N	30.77	34.4	34.7 ± 0.4	44.1	44.2 ± 0.5
		5.2	5.2 ± 0.3	168.0	169.4 ± 1.1
H-C≡N	10.49	12.8	13.09	18.7	20.7 <sup>c</sup>
		2.2	2.44	63.6	59.9

<sup>a</sup> In this table and Tables V-X experimental data are taken from the compilation of ref 2 unless otherwise stated. <sup>b</sup> CNDO/2D calculations from ref 3. <sup>c</sup> *Ab initio* calculation by R. Bonaccorsi, C. Petrongolo, E. Scrocco, and J. Tamasi, *J. Chem. Phys.*, **48**, 1500 (1968).

TABLE V: Molecular Second Moments and Diamagnetic Susceptibilities of Cyclic and Noncyclic Planar Molecules

Molecule	Nuclear moments $\sum Z_a a_a^2$ $\sum Z_b b_b^2$	Electronic moments, ( $10^{-16} \text{ cm}^2$ )		Diamagnetic susceptibilities, ( $10^{-6} \text{ cm}^3 \text{ mol}^{-1}$ )	
		$\langle a^2 \rangle_e$ $\langle b^2 \rangle_e$ $\langle c^2 \rangle_e$ Calcd	Expt	$\chi_{aa}^d$ $\chi_{bb}^d$ $\chi_{cc}^d$ Calcd	Expt
	30.20	36.0	36.2 ± 0.7	$\chi_{aa}^d = 187.5$ $\chi_{bb}^d = 177.3$ $\chi_{cc}^d = 315.6$	189.5
	32.62	38.4	37.8 ± 0.7		182.5
		5.8	6.8 ± 0.7		313.9
	34.25	40.3	39.1 ± 0.6	193.9	195.7 ± 1.1
	33.69	39.7	38.6 ± 0.6	196.4	197.6 ± 1.3
		6.0	7.4 ± 0.6	339.4	329.8 ± 0.2
	50.56	57.6	57.1 ± 0.8	270.2	271.9
	49.66	56.7	56.2 ± 0.8	274.0	275.7
		7.0	7.9 ± 0.8	484.9	480.6
	101.06	109.1	111.8 ± 0.7	295.7	293.3 ± 1.7
	53.70	61.7	60.8 ± 0.7	496.8	509.7 ± 3.6
		8.0	8.4 ± 0.7	724.6	732.4 ± 5.0
	21.13	25.1	26.1 ± 0.5	120.1	122.1
	20.26	24.3	24.8 ± 0.5	123.4	127.8
		4.0	4.0	209.6	216.2
	27.78	32.2	31.7 ± 0.6	133.6	133.8
	22.69	27.1	27.1 ± 0.6	155.3	153.5
		4.4	4.5	251.6	249.2
	41.65	46.1	46.7 ± 0.7	96.7	95.6
	14.03	18.4	18.1 ± 0.7	214.2	217.3
		4.4	4.5	273.6	274.9
	20.94	24.1	24.4 ± 2.0	43.7	38.0 ± 4.7
	3.88	7.1	6.4 ± 2.0	115.8	114.6 ± 5.8
		3.2	2.6 ± 2.0	132.4	130.6 ± 5.9
	26.26	29.9	29.5 ± 1.6	56.0	52.6 ± 4.2
	6.01	9.6	8.8 ± 1.6	142.1	140.5 ± 4.5
		3.6	3.6 ± 1.6	167.6	162.5 ± 4.5
	62.40	67.6	68.3 ± 4.8	146.4	145.7 ± 10.6
	24.05	29.3	29.1 ± 4.8	308.8	312.1 ± 10
		5.2	5.3 ± 4.8	411.1	413.1 ± 10

**TABLE VI: Calculated and Experimental Molecular Second Moments and Diamagnetic Susceptibilities for Nonplanar Noncyclic Molecules**

Molecule	Nuclear moments $\sum Z_A^2 a_A^2$ $\sum Z_A b_A$ $\sum Z_A c_A^2$	Electronic moments, ( $10^{-16} \text{ cm}^2$ )		Diamagnetic susceptibilities, ( $10^{-6} \text{ cm}^3 \text{ mol}^{-1}$ )	
		$\langle a^2 \rangle_e$ $\langle b^2 \rangle_e$ $\langle c^2 \rangle_e$ Calcd	Expt	$\chi_a^d$ $\chi_b^d$ $\chi_c^d$ Calcd	Expt
	21.79	25.2	25.8 ± 0.7	59.4	59.2
	5.61	9.0	9.0 ± 0.7	128.1	130.7
	1.64	5.0	5.0	145.1	147.7
	28.79	32.8	33.2 ± 1.9	80.2	80.0 ± 4.7
	7.65	11.7	11.6 ± 1.9	169.7	171.6 ± 5.3
	3.16	7.2	7.2 ± 1.9	188.8	190.3 ± 5.3
	30.03	34.8	34.8 ± 5.2	160.4	161.5 ± 12.8
	23.30	28.1	28.6 ± 5.2	188.8	187.9 ± 12.8
	4.66	9.7	9.5 ± 5.2	266.8	268.9 ± 12.9
	1.6	4.2	4.0 <sup>a</sup>	35.6	33.9 <sup>a</sup>
	10.6	13.2	13.2	73.8	73.0
	21.7	25.3	26.3 <sup>a</sup>	214.6	223.1 <sup>a</sup>
	3.3	7.5	6.9	139.1	140.8
	23.9	25.9	26.6 <sup>a</sup>	109.9	112.8 <sup>a</sup>
	30.31	34.5	33.9	77.2	78.5
	6.63	10.8	11.0	177.7	175.7
	3.20	7.4	7.5	192.2	190.6
	1.34	2.9	2.6 ± 0.4	24.6	22.0 ± 1.4
	0.31	1.9	1.9 ± 0.4	20.4	19.3 ± 1.4
	3.33	6.5	6.74 <sup>b</sup>	120.1	121.03 <sup>b</sup>
	3.33	6.5	121.03	120.1	6.74
	18.61	21.8	21.79	55.2	57.18
	3				
	53.52	37.7	37.5	74.2	73.3 ± 1.3
	7.58	11.8	11.2 ± 0.5	184.1	184.8 ± 1.6
	1.54	5.7	6.1 ± 0.5	209.9	206.6 ± 1.7
	28.9	32.7	32.3 ± 0.5	61.9	64.1 ± 1.4
	5.5	9.3	9.6 ± 0.4	161.2	160.4 ± 1.8
	1.5	5.3	5.6 ± 0.5	178.2	177.4 ± 1.8
	40.4	45.2	45.6 ± 1.5 <sup>c</sup>	106.9	108.0 ± 2.4 <sup>c</sup>
	14.0	18.8	19.0 ± 1.5	218.9	221.2 ± 3.8
	1.6	6.4	6.5 ± 1.5	271.5	274.3 ± 4.5
	40.3	45.1	46.0	116.7	114.5 ± 6.2
	16.3	21.2	20.7	218.5	221.7 ± 7.3
	1.6	6.9	6.3	280.8	282.9 ± 8.3

<sup>a</sup> *Ab initio* results, C. R. Brundle, M. B. Robin, and H. Basch, *J. Chem. Phys.*, **53**, 2196 (1970). <sup>b</sup> *Ab initio* results, S. D. Peyerimhoff, and R. J. Buenker, *ibid.*, **49**, 312 (1968). <sup>c</sup> Corrected experimental values given by J. H. Wang and W. H. Flygare, *ibid.*, **55**, 3616 (1971).

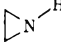
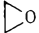


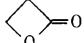
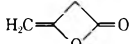
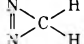
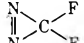
are compared with experimental and *ab initio* calculated values in Tables IV–VII for a wide variety of molecules. We have also extended eq 10 to molecules containing atoms of higher atomic number. These results are presented in Tables VIII–X.

## Results and Discussion

**1. Validity of Approximate Expressions for Second Moments.** In our previous work<sup>4</sup> on the second moments of hydrocarbons we derived our additivity equation by assuming nonpolar bonds. It is not possible to show purely on *a priori* fundamental grounds that the same type of expression would also be successful for molecules of greater polarity than hydrocarbons. In order to establish whether such an extension is possible we have carried out calculations

at different levels on the series  $\text{CH}_2\text{F}_2$ ,  $\text{C}_2\text{H}_2\text{F}_2$ , and  $\text{COF}_2$ , *i.e.*, using eq 3, 9, and 10. The results are compared in Table I with the corresponding experimental values. The close similarity between the first column of data, which were obtained by calculating all the many center integrals and using eq 3, and the second column, which was calculated including one center terms only using eq 9, demonstrates that second moment integrals between AO on different centers (the third term of eq 3) are relatively unimportant in calculating the total second moments. The reason for this can be seen from an examination of the two center terms after making the coordinate transformation to individual atomic coordinates. The contribution to eq 3 for AO's on different centers then becomes

TABLE VII: Molecular Second Moments and Diamagnetic Susceptibilities for Cyclic Nonplanar Molecules

Molecule	Nuclear moments $\sum Z_A a_A^2$ $\sum Z_A b_A^2$ $\sum Z_A c_A$	Electronic moments, ( $10^{-16} \text{ cm}^2$ )		Diamagnetic susceptibilities, ( $10^{-6} \text{ cm}^3 \text{ mol}^{-1}$ )	
		$(a^2)_e$ $(b^2)_e$ $(c^2)_e$ Calcd	Expt	$\chi_c^d$ $\sum \chi_c^d$ $\chi_c^d$ Calcd	Expt
	13.05	17.1	16.9	96.7	97.6
	10.30	14.3	14.7	108.6	107.0
	4.46	8.5	8.3	133.2	134.1
	12.90	16.7	$16.3 \pm 0.4$	84.8	$85.4 \pm 0.9$
	9.02	12.8	$13.3 \pm 0.4$	101.4	$97.7 \pm 1.1$
	3.38	7.2	$6.8 \pm 0.4$	125.1	$125.4 \pm 2.8$
	26.98	32.2	$31.9^a$	128.1	$130^a$
	10.71	15.9	16.4	197.3	195
	9.11	14.3	14.0	204.0	$205^a$
	22.10	27.3	28.3	166.3	166.4
	23.98	29.2	29.2	158.2	162.5
	4.83	10.0	10.0	239.7	244.0
	50.77	56.6	$57.2 \pm 4.0$	158.2	$158.9 \pm 6.0$
	22.51	28.3	$28.8 \pm 4.0$	278.3	$279.6 \pm 6.0$
	3.24	9.0	$8.6 \pm 4.0$	360.1	$365.5 \pm 6.0$
	100.00	106.8	$107.6 \pm 6.0$	170.5	$173.0 \pm 9.0$
	25.0	31.8	$32.1 \pm 6.0$	488.7	$493.7 \pm 18.7$
	1.6	8.4	$8.7 \pm 6.0$	587.9	$592.7 \pm 19.0$
	12.00	15.4	$15.49^b$	58.1	$62.53^b$
	5.23	8.6	9.66	86.97	87.26
	1.69	5.1	5.08	101.8	106.69
	31.88	36.9	$38.14^b$	162.9	$164.77^b$
	5.85	10.9	11.60	273.2	277.36
	22.52	27.5	27.24	202.8	211.01

<sup>a</sup> Estimated values using the empirical method of ref 7. <sup>b</sup> *Ab initio* results, M. B. Robin, H. Basch, N. A. Keubler, K. B. Wiberg, and G. B. Ellison, *J. Chem. Phys.*, 51, 45 (1969).

TABLE VIII: Molecular Second Moments and Diamagnetic Susceptibilities of Halogen-Containing Molecules

Molecule	Nuclear moments $\sum Z_A a_A^2$ $\sum Z_A b_A^2$	Electronic second moments, ( $10^{-16} \text{ cm}^2$ )		Diamagnetic susceptibilities, ( $10^{-6} \text{ cm}^3 \text{ mol}^{-1}$ )	
		Calcd	$(a^2)_e$ $(b^2)_e$ Expt	Calcd	$\chi_c^d$ $\chi_c^d$ $\chi_c^d$ Expt
CH <sub>3</sub> Cl	21.43	25.5	$25.0 \pm 0.64^a$	48.4	$46.9 \pm 3.1^a$
	1.63	(5.7)	$5.53 \pm 0.24$	132.4	$129.8 \pm 2.7$
CH <sub>3</sub> Br	30.6	35.7	$35.1 \pm 0.8^a$	56.8	$58.3 \pm 4.0$
	1.64	(6.7)	$6.9 \pm 0.3$	179.9	$178.2 \pm 3.7$
CH <sub>3</sub> I	39.8	46.9	$45.8 \pm 1.1^a$	73.8	$74.2 \pm 5.2$
	1.65	(8.7)	$8.7 \pm 0.3$	235.9	$231.2 \pm 5.0$
ClF	15.6	19.1	$19.2 \pm 0.4^b$	29.7	$30.6 \pm 1.7$
		3.5	$3.6 \pm 0.2$	95.9	$96.8 \pm 2.3$
BrF	22.24	26.7	$26.7 \pm 0.4^b$	38.2	$39.0 \pm 1.7$
		4.5	$4.6 \pm 0.2$	132.4	$133.3 \pm 2.3$
ClCN	41.81	46.3	$46.7 \pm 0.6^b$	38.2	$41.6 \pm 1.7^b$
		4.5	$4.9 \pm 0.3$	215.5	$219.0 \pm 2.9$
BrCN	59.68	65.2	$65.6 \pm 0.6^b$	46.7	$50.1 \pm 2.5^b$
		5.5	$5.9 \pm 0.3$	299.9	$303.5 \pm 3.2$
ICN	76.11	83.6	$84.0 \pm 0.6^b$	63.6	$67.1 \pm 2.5^b$
		7.5	$7.9 \pm 0.3$	386.4	$390.0 \pm 2.9$
H-Cl	1.56	4.3	$3.68^c$	22.9	$24.86^c$
		2.7	2.93	29.7	28.04

<sup>a</sup> Taken from ref 14. <sup>b</sup> J. J. Ewing, H. L. Tigelaar, and W. H. Flygare, *J. Chem. Phys.*, 56, 1957 (1972). <sup>c</sup> Taken from ref 12.

$$\sum_{A < B} \sum_{\mu} \sum_{\nu} P_{\mu\nu}^{AB} [V_A^2 \langle \phi_{\mu}^A | \phi_{\nu}^B \rangle + 2V_A \langle \phi_{\mu}^A | V_A | \phi_{\nu}^B \rangle + \langle \phi_{\mu}^A | (V_A^1)^2 | \phi_{\nu}^B \rangle] \quad (11)$$

The individual terms in this expression have appreciable values, especially the terms containing the coordinates ( $V_A^2$  and  $V_A$ ). These terms are, however, of opposite sign and therefore approximately cancel each other. However, these terms are very important for the calculation of molecular quadrupoles where the very fine details of the atomic charge distribution, particularly the anisotropy of the electron cloud, are decisive.<sup>3</sup> This conclusion has also been reached by Rein, *et al.*, on the basis of MO calculations<sup>6</sup> and by Flygare, *et al.*, using a very empirical model.<sup>7</sup>

The results obtained by the use of the extended additivity equation (eq 10) are given in data column three of Table I. These results are either as good or are in better agreement with the experimental results than are the previous two columns which were obtained by using actual semiempirical wave functions. In order to elucidate the factors responsible for this rather surprising success of the additivity eq 10 we have examined the relative magnitudes of the various contributions to eq 3. These results are compared with the first term of eq 10 ( $\sum_A Z^2 V_A^2$ ) in Table II. It becomes immediately clear that the agreement between this first term and the value of  $\sum_A P^A V_A^2$  is the main factor responsible for the success of the additivity relationship eq 10. The individual orbital contributions are also given in Table II. These terms are the second and third terms of eq 9 which involve  $\alpha_A$  and  $\beta_A$ . They vary from atom to atom with the more electronegative atoms

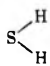
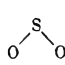
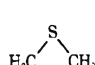
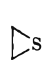
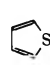
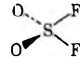
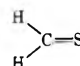
tending toward values less than unity. However, although, as can be seen by comparing the values for C(1) and C(2) in 1,1-difluoroethylene, there is individual variation of the orbital contributions, after adding in the hybridization contributions from Table III they average out to a contribution of one unit per atom as required by the additivity equation. Thus the net result of the averaging out process is that the second moment for the molecule appears to be a sum of contributions of the individual atoms, with very little anisotropy for each atom and with a very small amount of charge transfer. However, this is only an illusion since the individual contributions of each atom may vary considerably from molecule to molecule. Furthermore, there is considerable anisotropy, particularly with respect to the hybridization moments (Table III), for each individual atom, although again this is not apparent in the final result after summing over all the atoms.

2. *Second Moments and Magnetic Susceptibilities.* The second moments are related to the diagonal elements of the diamagnetic susceptibility tensor

$$\chi_{uv}^d = -(e^2 N / 4mc^2) [\langle w^2 \rangle_e + \langle (w^1)^2 \rangle_e] \quad (12)$$


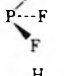
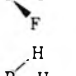
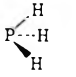
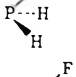
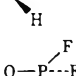
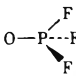
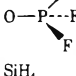
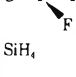
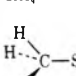
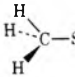
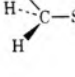
where the constants have their conventional meaning. The remaining diagonal elements are generated by the permutation of the coordinates  $v$ ,  $w$ , and  $w^1$ . By using formulas 10 and 12 and the known molecular geometries, the molecular second moments and diamagnetic susceptibilities are easily calculated. The results are compared with available experimental data and *ab initio* results in Tables IV–X for a very wide variety of polyatomic molecules. The agreement with both experiment and with the more

TABLE IX: Electronic Second Moments and Diamagnetic Susceptibilities of Sulfur-Containing Molecules

Molecule	Nuclear moments $\sum Z_A^2 V_A^2$ $\sum Z_B^2 V_B^2$ $\sum Z_C^2 V_C^2$	Electronic second moments, ( $10^{-16}$ cm <sup>2</sup> )		Diamagnetic susceptibilities, ( $10^{-6}$ cm <sup>3</sup> mol <sup>-1</sup> )	
		$\langle a^2 \rangle_e$ $\langle b^2 \rangle_e$ $\langle c^2 \rangle_e$ Calcd	Expt	$\chi_a^d$ $\chi_b^d$ $\chi_c^d$ Calcd	Expt
	1.55	4.45	4.36 <sup>a</sup>	32.4	33.39 <sup>a</sup>
	1.83	4.73	4.45	4.38	31.2
	24.61	29.1	30.0 ± 0.2	55.6	54.9 ± 0.3
	4.0	8.6	8.7 ± 0.2	142.5	145.1 ± 0.3
		4.5	4.2 ± 0.2	159.9	164.3 ± 0.5
	40.1	45.8	45.2	127.7	128.6
	15.5	21.2	21.3	232.0	230.0
	3.2	8.9	9.0	284.2	282.3
	26.72	32.0	29	113.7	108
	12.32	18.2	17	172.2	157
	3.34	8.6	8	212.9	195
	51.43	58.7	58.6 ± 1.3	224.0	225.3
	38.16	45.5	44.6 ± 1.2	280.0	284.6
	0	7.3	8.5 ± 1.2	42.0	437.8
	24.48	31.0	30.7 <sup>b</sup>	258.3	263.5
	23.27	29.8	31.4	263.4	260.0
	24.59	31.1	30.5	257.9	262.7
O=C=S	46.2	46.0	46.2 <sup>c</sup>	38.2	38.6 <sup>c</sup>
	0	4.5	4.5	214.2	215.5
	17.0	20.9	21.1 ± 0.6 <sup>d</sup>	40.3	47.5 ± 2.5 <sup>d</sup>
	1.7	5.6	6.6 ± 0.5	105.2	109.1 ± 3.0
	0	3.9	4.6 ± 0.4	112.4	117.6 ± 3.4

<sup>a</sup> Near Hartree-Fock calculations: S. Rothenberg, R. H. Young, and H. F. Schaefer, III, *J. Amer. Chem. Soc.*, **92**, 3243 (1970). <sup>b</sup> R. G. Stone and W. H. Flygare, *Inorg. Chem.*, **8**, 2647 (1969). <sup>c</sup> W. H. Flygare, W. Hüttner, R. L. Schoemaker, and P. D. Foster, *J. Chem. Phys.*, **50**, 1714 (1969). <sup>d</sup> S. L. Rock and W. H. Flygare, *ibid.*, **56**, 4723 (1972).

TABLE X: Electronic Second Moments and Diamagnetic Susceptibilities Phosphorus- and Silicon-Containing Molecules

Molecule	Nuclear moments $\sum Z_A a_A^2$ $\sum Z_A b_A^2$ $\sum Z_A c_A^2$	Electronic second moments, ( $10^{-16} \text{ cm}^2$ )		Diamagnetic susceptibilities, ( $10^{-6} \text{ cm}^3 \text{ mol}^{-1}$ )	
		$(a^2)_e$ $(b^2)_e$ $(c^2)_e$ Calcd	Expt	$\chi_a^d$ $\chi_b^d$ $\chi_c^d$ Calcd	Expt
	4.5	10.0	8.5 <sup>c</sup>	268.1	297.9
	26.1	31.6	35.1	176.5	184.9
	26.1	31.6	35.1	176.5	184.9
	1.54	4.6	4.87 ± 0.42	44.1	42.9 ± 1.4
	2.14	5.2	5.06 ± 0.42	41.6	42.1 ± 1.1
	2.14	5.2	5.06 ± 0.42	41.6	42.1 ± 1.1
	27.84	34.3	33.0 <sup>c</sup>	269.8	294.7
	25.29	31.8	34.7	280.4	287.4
	25.29	31.8	34.7	280.4	287.4
SiH <sub>4</sub>	2.92	6.2	6.40 <sup>a</sup>	52.6	54.3 <sup>a</sup>
	4.54	9.2	9.42 <sup>b</sup>	171.4	173.76 <sup>b</sup>
	4.54	9.2	9.42	171.4	173.76
	26.54	31.2	31.54	78.1	79.92

<sup>a</sup> Taken from ref 7. <sup>b</sup> D. H. Liskow and H. F. Schaeffer, III, *J. Amer. Chem. Soc.*, **94**, 6641 (1972).

TABLE XI: Comparison between  $[r_e^2]^{1/2}$  and the Effective Molecular Radius

Molecule	$\langle r^2 \rangle_e$	$[\langle r^2 \rangle_e]^{1/2}$ , $10^{-8} \text{ cm}$	$r_{\text{eff}}^a$ Å	$\langle r^2 \rangle^{1/2} / r_{\text{eff}}$
CH <sub>4</sub>	9.84	3.14	2.08	1.51
NH <sub>3</sub>	7.70	2.78	1.95	1.43
H <sub>2</sub> O	5.93	2.44	1.67	1.46
HF	2.09	2.09	1.43	1.46
SiH <sub>4</sub>	18.60	4.31	2.51	1.72
PH <sub>3</sub>	15.00	3.87	2.31	1.67
H <sub>2</sub> S	12.08	3.48	1.93	1.80
HCl	9.70	3.11	1.68	1.55

<sup>a</sup> The effective molecular radius,  $r_{\text{eff}}$ , is defined as a radius of a sphere which embraces 98% of the overall electronic charge, ref 18.

sophisticated calculations is very good indeed. The implication of this good agreement is that the second moments and diamagnetic susceptibilities depend almost entirely on the geometry of the molecule and the number of the constituent atoms. They are not dependent to any large extent on the bonding effect in any particular molecule or on the specific type of bonding between any two atoms. Thus our work is in full agreement with the view recently expressed by Rein, *et al.*,<sup>6</sup> that the second moments and diamagnetic susceptibilities are very insensitive, even for very polar molecules, to the finer details of the electronic structure of molecules and should, therefore, not be used as a test of quality of the molecular wave functions although they have been frequently used to differentiate between different *ab initio* calculations which employ varying basis set sizes.<sup>8,9</sup>

3. *Molecules Containing Second and Higher Row Elements.* Since the additivity equation works successfully for the first row elements of the periodic system the next step is obviously to try and generalize it in order to include heavier atoms. However, caution has to be exercised because of the greater importance of d AO's in these atoms. We can distinguish two classes of molecules: (1) those containing atoms with "inner" d orbitals ( $(n-1)d$ ,  $n_s$ ,  $np$ ), such as, the transition elements and (2) those

molecules containing atoms with "outer" d orbitals ( $ns$ ,  $np$ ,  $(n+1)d$ ) which are not occupied in the atomic ground state but which might become occupied, and so play a role in bonding, on molecule formation. Examples of such atoms are Si, P, S, Cl, Br, and I. In this study we will confine ourselves to the latter group for which extensive experimental data are available. There are in the literature several *ab initio* studies of molecules involving second row atoms. Unfortunately, the conclusions expressed in these works concerning the importance of d orbitals in determining the bonding differ with the size of basis set used. For instance, using minimal basis set STO (Slater type orbital) *ab initio* calculations Boyd, Boer, and Lipscomb<sup>10,11</sup> report the total populations of d orbitals SiH<sub>4</sub>, PH<sub>3</sub>, and H<sub>2</sub>S to be 0.447, 0.290, and 0.147 for Si, P, and S, respectively. Rothenberg, *et al.*,<sup>12</sup> on the other hand, used a bigger basis set for their calculations and found the corresponding populations to be 0.108, 0.082, and 0.063, respectively. They then concluded, as have other workers, that minimal basis set calculations overestimate 3d orbital populations due to the inability of the minimum basis set of s and p STO's to represent adequately the electron redistribution on molecule formation. In spite of the fact that Rothenberg, *et al.*,<sup>12</sup> found very low d orbital populations in SiH<sub>4</sub>, PH<sub>3</sub>, and H<sub>2</sub>S, the contribution of the d orbitals to the molecular second moments is expected to be significant because they are much more diffuse than s and p orbitals. Moreover, we would expect the d orbital contribution to the bonding to vary considerably from molecule to molecule. For instance, the d orbitals of sulfur in SO<sub>2</sub> have a much higher population than the corresponding orbitals in H<sub>2</sub>S since the heavier oxygen atoms perturb the spherical electron charge distribution of sulfur much more effectively than do hydrogen

(8) K. E. Banyard, *J. Chem. Phys.*, **33**, 832 (1960).

(9) D. N. Tripathi, P. T. Wari, and D. K. Rain, *Ind. J. Pure Appl. Phys.*, **7**, 707 (1969).

(10) D. B. Boyd and W. N. Lipscomb, *J. Chem. Phys.*, **46**, 910 (1967).

(11) F. P. Boer and W. N. Lipscomb, *J. Chem. Phys.*, **50**, 989 (1969).

(12) S. Rothenberg, R. H. Young, and H. F. Schaefer, III, *J. Amer. Chem. Soc.*, **92**, 3243 (1970).

(13) S. Rothenberg and H. F. Schaefer, III, *J. Chem. Phys.*, **53**, 3014 (1970).



atoms.<sup>13</sup> Thus it seems possible that this individual variation would render invalid the additivity property for molecules containing second row atoms. Nevertheless, because of the cancelling out effects we encountered in our calculations for the lighter elements, we have proceeded to extend additivity eq 10 to the prediction of the second moments of molecules containing heavier atoms.

The general equation tried was

$$\langle v^2 \rangle_e = \sum_A (Z_A V_A^2 + \sum_i K_i n_i) \quad (13)$$

where  $n_i$  is the number of atoms belonging to the  $i$ th period of the system of elements and  $K_i$  is the corresponding additivity constant. The additivity constants  $K_2$ ,  $K_3$ , and  $K_4$  are determined in order to match the experimental second moments of  $\text{CH}_3\text{Cl}$ ,  $\text{CH}_3\text{Br}$ , and  $\text{CH}_3\text{I}$ , respectively.<sup>14</sup> By using  $K_0 = K_{\text{H}} = 0.2$ ,  $K_1 = 1.0$  the values  $K_2 = 2.5$ ,  $K_3 = 3.5$ , and  $K_4 = 5.5$  (in units of  $10^{-16} \text{ cm}^2$ ) were obtained. These values were then used to calculate the second moments and diamagnetic susceptibilities for a number of molecules. These are compared with the available experimental data or with *ab initio* values in Tables VIII-X. The overall agreement is very good although there are some cases where the additivity rules are poor.

The molecules for which most deviation is experienced are  $\text{PF}_3$ ,  $\text{POF}_3$  (Table X), and  $\text{SO}_2\text{F}_2$  (Table IX). For these molecules *ab initio* calculations have demonstrated that d orbitals play a very important role.<sup>15-17</sup> Unfortunately no *ab initio* calculations of the second moments of the molecules have been reported so we cannot comment further on the possible cause of the deviations, except to note that for  $\text{SO}_2$ , a molecule for which it is fairly certain that d orbitals are important in the bonding, their inclusion in the basis set has very little effect on the calculated second moments.

**4. Calculation of Effective Molecular Radii.** It has recently been shown by Kammeyer and Whitman<sup>18</sup> that the van der Waals radii of atoms and molecules can be calculated reasonably well by assuming that the "van der Waals sphere" contains 98% of the electronic charge density. Such a calculation is limited to molecules for which a wave function is available. However, we have found that the value of  $\langle r^2 \rangle$  calculated by the additivity equation is linearly related to the effective values,  $r_{\text{eff}}$ , considered in ref 18. This is demonstrated by the constant values (within the same period of the periodic table) of the ratio  $\langle r^2 \rangle^{1/2}/r_{\text{eff}}$  given in data column 4 of Table XI. Thus by using the easily calculated  $\langle r^2 \rangle$  values one can obtain a value for an effective molecular size as accurately as those obtained from good molecular wave functions. Moreover, since we can also calculate the different components of  $\langle r^2 \rangle$ , it seems feasible that it might be possible to calcu-

late effective sizes of those molecules for which the assumption of spherical symmetry is not valid. Such an endeavor is in progress.

**5. Relationship to Other Work.** After our work was completed a paper by Gierke, Tigelaar, and Flygare<sup>7</sup> appeared in which dipole and quadrupole moments were calculated, with considerable accuracy, by using a set of atomic dipole terms obtained by fitting the experimental values of certain reference molecules to the corresponding theoretical expression. This method is more general than our method because the empirical parameter fitting procedure takes into consideration both the anisotropy of the atom dipoles and also allows different parameters to be chosen for an atom depending on the different molecular environment. This enables the method to be used for calculating quadrupole moments, for which the anisotropic terms and the dipole terms are very important. Its major disadvantage is the very large number of parameters necessary for each atom (three for each chosen environment). In our method which requires far fewer parameters we have assumed the second moments are sums of spherically symmetrical (*i.e.*, isotropic) contributions. The excellent agreement with experimental second moments justifies the use of this approximation for second moments, and, of course, for diamagnetic susceptibilities it is, however, inadequate for the quadrupole moments. Both our original empirical method<sup>4</sup> and that of ref 7 were derived on the assumption that the amount of charge polarization occurring on molecular formation is small. Our analysis of this assumption using semiempirical wave functions shows that this assumption is invalid and that the success of the methods is dependent on a cancelling out of a number of opposing factors in the total expression for the second moment.

We regard our method as a first step to producing an explanation of Pascal's rules for calculating total magnetic susceptibilities. Our analysis of the nature of the individual factors influencing the second moments also shows why phenomenological schemes such as those reviewed by Tatevskii<sup>19</sup> have been so successful.

**Acknowledgments.** This work was supported by the Air Force Office of Scientific Research through Grant No. AF-AFOSR-1184-67 and by a Faculty Research Grant from the University of Tennessee.

- (14) D. Van der Hart and W. H. Flygare, *Mol. Phys.*, **18**, 77 (1969).
- (15) I. Absar and J. R. Van Wazer, *J. Phys. Chem.*, **75**, 1360 (1971).
- (16) I. H. Hillier and V. R. Saunders, *J. Phys. Chem.*, **66**, 2401 (1970).
- (17) R. L. DeKock, D. R. Lloyds, I. H. Hillier, and V. R. Saunders, *Proc. Roy. Soc., Ser. A.*, **328**, 401 (1972).
- (18) C. W. Kammeyer and D. R. Whitman, *J. Chem. Phys.*, **56**, 4419 (1972).
- (19) V. M. Tatevskii, *Russ. J. Phys. Chem.*, **35**, 1027 (1961).

# Electron-Transfer and f-d Absorption Bands of Some Lanthanide and Actinide Complexes and the Standard (II-III) Oxidation Potential for Each Member of the Lanthanide and Actinide Series<sup>1</sup>

L. J. Nugent,\* R. D. Baybarz, J. L. Burnett,<sup>2</sup>

*Transuranium Research Laboratory, Oak Ridge National Laboratory, Oak Ridge, Tennessee 37830*

and J. L. Ryan

*Pacific Northwest Laboratories, Battelle Memorial Institute, Richland, Washington 99352 (Received January 5, 1973)*

*Publication costs assisted by the U.S. Atomic Energy Commission*

A powerful new correlation technique is introduced. It is based on the theoretical and experimental results of atomic spectroscopy, and it is shown to be generally applicable for intraseries correlations of various physical and chemical properties, such as oxidation potentials, first electron-transfer absorption-band energies, and first f-d absorption-band energies of the compounds and complexes of the lanthanide and actinide series. For many of the members of these series representative values of some of these properties were available from the literature; for others new measurements were made, so that sufficient data are available to provide a test of the general validity of the theory, and hence, to calculate many of these properties for all the members of both series. The most important new results of this work are the determination or verification of the following standard oxidation potentials:  $E^\circ\text{Sm(II-III)} = +1.55$ ,  $E^\circ\text{Eu(II-III)} = +0.35$ ,  $E^\circ\text{Tm(II-III)} = +2.3 \pm 0.2$ ,  $E^\circ\text{Yb(II-III)} = +1.15$ ,  $E^\circ\text{Am(II-III)} = +2.3 \pm 0.2$ ,  $E^\circ\text{Es(II-III)} = +1.2 \pm 0.2$ ,  $E^\circ\text{Fm(II-III)} = +1.1 \pm 0.2$ ,  $E^\circ\text{Md(II-III)} = +0.15$ , and  $E^\circ\text{No(II-III)} = -1.45$ , each in volts relative to the standard oxidation potential of the normal hydrogen electrode.

## 1. Introduction

In a previous paper<sup>3</sup> we related the first electron-transfer absorption-band energies of some lanthanide, Ln(IV), and actinide, An(IV), complexes, and the first f-d absorption-band energies of some Ln(III) and An(III) complexes, to the standard  $E^\circ\text{M(III-IV)}$  oxidation potentials of the metals M of these two inner transition series. Best values for the  $E^\circ\text{M(III-IV)}$  potentials were obtained from a variety of sources, namely, from direct electrode potential measurements reported in the literature, from linear plots of first electron-transfer absorption-band energies *vs.* the respective  $E^\circ\text{M(III-IV)}$  potentials, from linear plots of first f-d absorption-band energies *vs.* the respective  $E^\circ\text{M(III-IV)}$  potentials, and from theoretical correlations based on Jørgensen's refined-electron-spin-pairing-energy theory.

In the present paper, which develops in a similar fashion as above from an extension of the electron-transfer band work reported in a preliminary note,<sup>4</sup> we relate the first electron-transfer absorption-band energies of some of the Ln(III) and An(III) complexes, and the first f-d absorption-band energies of some of the Ln(II) and An(II) complexes, to the respective  $E^\circ\text{M(II-III)}$  oxidation potentials. We obtain best values for all of the  $E^\circ\text{M(II-III)}$  potentials from the same variety of sources, from direct electrode potential measurements reported in the literature, from linear plots of electron-transfer absorption-band energy *vs.* the respective  $E^\circ\text{M(II-III)}$  potential, and from theoretical correlations based on a newly modified and considerably improved version<sup>5,6</sup> of the refined-electron-spin-pairing-energy treatment.<sup>7-9</sup>

## 2. Experimental Results

In our preliminary work<sup>4</sup> on these  $E^\circ\text{M(II-III)}$  potentials, the first electron-transfer absorption bands of some

of the M(III) tribromides were measured in anhydrous ethanol solution. This solvent was chosen because it was the medium in which Jørgensen first analyzed the first electron-transfer bands and first f-d absorption bands of the Ln(III) tribromides. Unfortunately, however, because of strong competition from solvation, the metal halide species present when  $\text{MX}_3$  is dissolved in ethanol can be multicomponent, with relative concentrations unknown and variable as a function of atomic number across both the Ln(III) and An(III) series. So in each case any or all solvated  $\text{M}^{3+}$ ,  $\text{MX}_2^{2+}$ ,  $\text{MX}_2^{1+}$ , and/or  $\text{MX}_3$  species could be present in indeterminate concentrations. Such multicomponent and presently indeterminate species add an additional element of uncertainty to an already complex problem, because they effectively broaden and shift the observed absorption bands and thereby make the interpretation of the spectra unnecessarily complex.

In order to bypass the above multispecies complications, in the present work we report only the spectra of

- (1) Research sponsored by the U. S. Atomic Energy Commission under contract with the Union Carbide Corporation and under contract with Battelle Northwest Laboratory. Presented by L. J. Nugent in part at the Third International Transplutonium Element Symposium, Oct 20-22, 1971, Argonne National Laboratory, Argonne, Ill., and in part at the USSR Academy of Sciences Symposium on the Chemistry of the Transuranium Elements, Sept 4-8, 1972, Moscow.
- (2) Present address, Division of Physical Research, U. S. Atomic Energy Commission, Washington, D. C.
- (3) L. J. Nugent, R. D. Baybarz, J. L. Burnett, and J. L. Ryan, *J. Inorg. Nucl. Chem.*, **33**, 2533 (1971), and the references therein.
- (4) L. J. Nugent, R. D. Baybarz, and J. L. Burnett, *J. Phys. Chem.*, **73**, 1177 (1969), and the references therein.
- (5) L. J. Nugent and K. L. Vander Sluis, *J. Opt. Soc. Amer.*, **61**, 1112 (1971); *ibid.*, in press.
- (6) K. L. Vander Sluis and L. J. Nugent, *Phys. Rev. A*, **6**, 86 (1972).
- (7) C. K. Jørgensen, *Mol. Phys.*, **5**, 271 (1962).
- (8) J. L. Ryan and C. K. Jørgensen, *Mol. Phys.*, **7**, 17 (1963).
- (9) C. K. Jørgensen, *Chem. Phys. Lett.*, **2**, 549 (1968).

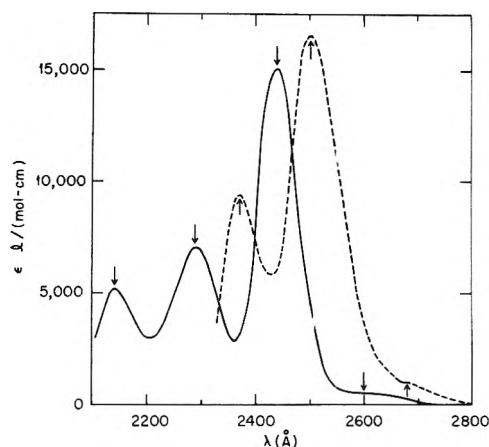


Figure 1. Absorption spectra of  $\text{AmCl}_6^{3-}$  (solid line) and  $\text{AmBr}_6^{3-}$  (dashed line) in the respective tetraethylammonium halide saturated acetonitrile solution at 298°K. These measurements were made in a 0.01-cm absorption cell.

the  $\text{MX}_6^{3-}$  complex, where  $\text{X}^- = \text{Cl}^-$  or  $\text{Br}^-$ . This octahedral  $\text{MX}_6^{3-}$  species is known to be the only significant metal complex present when  $\text{MX}_3$  is dissolved in the respective tetraethylammonium halide saturated anhydrous acetonitrile solution.<sup>10</sup> The measurements are made on a Cary 14 recording spectrophotometer with the solution at room temperature (298°K) and sufficiently dilute so that electron-transfer and f-d absorptions are observed but f-f absorptions, which are considerably weaker, are not observed. It is advantageous to perform all chemical manipulations in quartz labware in order to avoid contamination of the microgram lanthanide and actinide samples with uv absorbing impurities from Pyrex labware. Other details of the experimental techniques are described elsewhere.<sup>3,10</sup>

Radiolysis arising from the radioactivity of the actinide metals was troublesome only in the absorption measurements of  $\text{EsX}_6^{3-}$  ( $t_{1/2} = 20$  days for 6.63-MeV  $\alpha$  emission from  $^{253}\text{Es}$ ).<sup>11</sup> In these cases radiolysis effects were minimized by maintaining dilute ( $\sim 10^{-6}$  M)  $\text{EsX}_6^{3-}$  concentrations, by making rapid ( $\sim 3$  min) absorption measurements after introduction of the  $\text{EsX}_3$  into solution, and by remeasuring the absorption after introducing 4–5% by volume of water into solution. The latter hydrolyzes the  $\text{EsX}_6^{3-}$  species and thereby effectively erases the  $\text{EsX}_6^{3-}$  electron-transfer bands by removing the  $\text{X}^-$  ions from direct contact with the  $\text{Es(III)}$ . By taking the difference between the absorption of the unhydrolyzed and hydrolyzed solutions we were able to obtain an  $\text{EsX}_6^{3-}$  spectrum with a minimum of complications from radiolysis.

The absorption spectra of  $^{243}\text{AmCl}_6^{3-}$  and  $^{243}\text{AmBr}_6^{3-}$  are shown in Figure 1. These are the so-called f-d bands which, more precisely, should be designated  $5f^6 \rightarrow 5f^56d^1$ . Each spectrum shows broad-band structure marked by the arrows in Figure 1. The terminations of the  $\text{AmCl}_6^{3-}$  spectrum at 2110 Å and of the  $\text{AmBr}_6^{3-}$  spectrum at 2330 Å arise because of the onset of opacity in the respective  $(\text{C}_2\text{H}_5)_4\text{NX}$  saturated acetonitrile solutions over the 0.01-cm absorption-cell path length. There are very likely more  $\text{AmX}_6^{3-}$  bands at shorter wavelengths here but they cannot be conveniently measured because of the opacity of these solvents. The wave number at maximum absorption for each of the observed bands is listed in Table I with the corresponding molar absorptivity,  $\epsilon(\text{max})$ , and  $\delta(-)$  the half-width at half-maximum absorption on the low-wave number side.

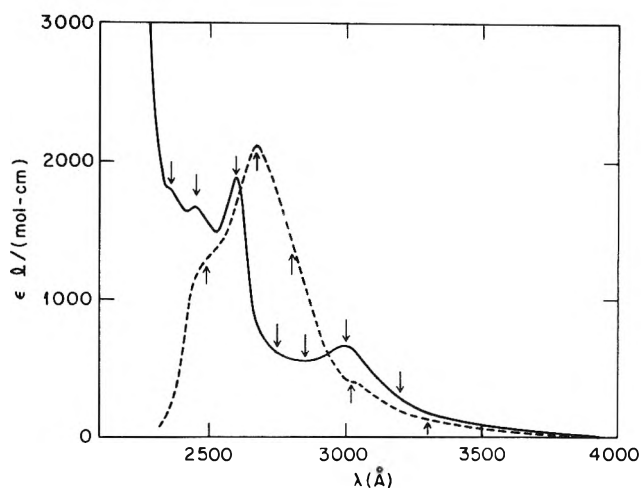


Figure 2. Absorption spectra of  $\text{BkCl}_6^{3-}$  (solid line) and  $\text{BkBr}_6^{3-}$  (dashed line) in the respective tetraethylammonium halide saturated acetonitrile solution at 298°K. These measurements were made in a 0.01-cm absorption cell.

TABLE I. 4f–5d Absorption Bands of Some Ln(III) Hexahalides and 5f–6d Absorption Bands of Some An(III) Hexahalides

Species	$hc/\lambda$ (f-d), $10^3 \text{ cm}^{-1}$	$\epsilon(\text{max})$ , $M^{-1} \text{ cm}^{-1}$	$\delta(-)$ , $10^3 \text{ cm}^{-1}$
$\text{CeCl}_6^{3- a}$	30.3	1,600	0.8
$\text{CeBr}_6^{3- a}$	29.15	1,600	1.05
$\text{PrCl}_6^{3-}$	42.0		
$\text{PrBr}_6^{3-}$	39.9	$\sim 1,600$	
	41.6	$\sim 800$	
$\text{TbCl}_6^{3- a}$	36.8	30	1.2
	42.75	1,500	0.7
$\text{TbBr}_6^{3- a}$	36.0	Weak	0.9
	$\sim 41.4$	Strong	0.9
$\text{UCl}_6^{3- b}$	15.6	1,400	
$\text{UBr}_6^{3- b}$	14.5 <sup>c</sup>		
$\text{AmCl}_6^{3-}$	38.5	500	1.2
	41.0	15,100	0.7
	43.7	7,100	1.0
	46.7	5,200	1.1
$\text{AmBr}_6^{3-}$	37.3	1,000	0.7
	40.0	16,600	1.1
	42.2	9,400	0.7
$\text{BkCl}_6^{3-}$	31.3	280	1.1
	33.3	470	1.1
	35.1	340	1.0
	36.4	340	1.1
	38.5	1,880	1.1
	40.8	1,680	1.1
	42.4	$\sim 1,000$	1.1
	45.5	8,600	1.1
	47.2	13,000	1.1
$\text{BkBr}_6^{3-}$	30.3	150	1.3
	33.1	290	1.4
	35.6	950	1.3
	37.5	1,720	1.1
	40.2	1,100	1.4

<sup>a</sup> Reference 10. <sup>b</sup> J. L. Ryan *MTP Int. Rev. Sci.*, **7**, 323 (1972). <sup>c</sup> We estimate this wave number by noting that the average  $\text{Cl}^-$ - $\text{Br}^-$  shift of the first f-d bands of  $\text{AmX}_6^{3-}$  and  $\text{BkX}_6^{3-}$  is  $1.1 \times 10^3 \text{ cm}^{-1}$  and by assuming that the same shift occurs in the  $\text{UX}_6^{3-}$  complexes.

- (10) J. L. Ryan and C. K. Jørgensen, *J. Phys. Chem.*, **70**, 2845 (1966); see also J. L. Ryan, *Advan. Chem. Ser.*, No. 71, 331 (1967).  
 (11) L. J. Nugent, J. L. Burnett, R. D. Baybarz, G. K. Werner, S. P. Tanner, J. R. Tarrant, and O. L. Keller, Jr., *J. Phys. Chem.*, **73**, 1540 (1969), and the references therein.

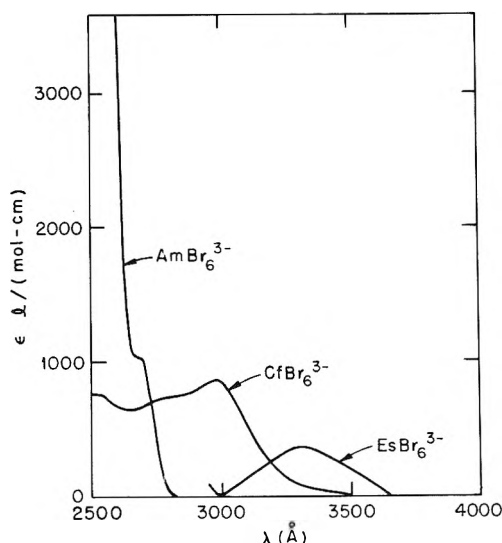


Figure 3. Absorption spectra of  $\text{AmBr}_6^{3-}$ ,  $\text{CfBr}_6^{3-}$ , and  $\text{EsBr}_6^{3-}$  in tetraethylammonium bromide saturated acetonitrile solution at 298°K. These measurements were made in a 1.0-cm absorption cell.

The near-uv absorption spectra of  $^{249}\text{BkCl}_6^{3-}$  and  $^{249}\text{BkBr}_6^{3-}$ , showing complex  $5f^8 \rightarrow 5f^7 6d^1$  band structure, are presented in Figure 2. Peak wave numbers,  $\epsilon(\text{max})$ , and  $\delta(-)$  values obtained with the aid of a Du Pont 310 curve resolver are recorded in Table I. The spectrum of  $\text{BkCl}_6^{3-}$  in Figure 2 is terminated in the uv somewhat before the corresponding  $\text{AmCl}_6^{3-}$  spectrum of Figure 1 because the opacity of the solution is slightly enhanced by radiolysis ( $t_{1/2} = 314$  days for 0.10-MeV  $\beta$  emission from  $^{249}\text{Bk}$ ).<sup>11</sup>

The near-uv absorption spectra of  $^{249}\text{CfBr}_6^{3-}$  and  $^{253}\text{EsBr}_6^{3-}$  are shown in Figure 3 with the spectrum of  $\text{AmBr}_6^{3-}$  to illustrate the difference between electron-transfer and f-d absorption bands. The  $\text{CfBr}_6^{3-}$  band peaks at 2985 Å with  $\delta(-)$  and band wave numbers as listed in Table II. This is the first electron-transfer band corresponding to the transition  $\text{Br}^- \text{Cf(III)} 5f^9 \rightarrow \text{Br}^0 \text{Cf(II)} 5f^{10}$  terminating on the lowest energy level of Cf(II). Similarly, the  $\text{EsBr}_6^{3-}$  absorption shows the corresponding first  $\text{Br}^- \text{Es(III)} 5f^{10} \rightarrow \text{Br}^0 \text{Es(II)} 5f^{11}$  electron-transfer band at 3300 Å with  $\delta(-)$  and band wave numbers as listed in Table II.

The  $\text{CfBr}_6^{3-}$  absorption spectrum of Figure 3 is terminated at 2500 Å because the present availability of only 50  $\mu\text{g}$  amounts of  $^{249}\text{Cf}$  prescribes that measurements be performed in a 1-cm absorption cell; for this cell length the reference solution becomes opaque just below 2500 Å. Similarly, the  $\text{EsBr}_6^{3-}$  spectrum is terminated near 2900 Å because radiolysis contributes to excessively strong absorption through the 1-cm cell at shorter wavelengths.

We see from Figures 1, 2, and 3 that a fundamental distinction, aside from the theoretical considerations, between electron-transfer and f-d absorption bands is the bandwidth. In the Table I listing of the  $\text{MX}_6^{3-}$  f-d band characteristics,  $\delta(-)$  ranges from  $0.8 \times 10^3$  to  $1.4 \times 10^3 \text{ cm}^{-1}$ , with a typical value of  $1.1 \times 10^3 \text{ cm}^{-1}$ , whereas in the Table II listing of the  $\text{MX}_6^{3-}$  first electron-transfer band characteristics,  $\delta(-)$  ranges from  $1.6 \times 10^3$  to  $2.4 \times 10^3 \text{ cm}^{-1}$ , with a typical value of  $2.0 \times 10^3 \text{ cm}^{-1}$ . Thus we observe that the electron-transfer bands are typically about twice as broad as the f-d bands in these complexes, and this is apparently more generally true for most lanthanide and actinide complexes.

TABLE II: First Electron-Transfer Absorption Bands for Some Ln(III) and An(III) Hexahalides at Room Temperature

Species	$hc/\lambda(\text{et}),$ $10^3 \text{ cm}^{-1}$	$\epsilon(\text{max}),$ $M^{-1} \text{ cm}^{-1}$	$\delta(-),$ $10^3 \text{ cm}^{-1}$
$\text{SmCl}_6^{3-}$ <sup>a</sup>	43.1	930	2.3
$\text{SmBr}_6^{3-}$ <sup>a</sup>	35.0	1050	2.4
$\text{EuCl}_6^{3-}$ <sup>a</sup>	33.2	400	2.1
$\text{EuBr}_6^{3-}$ <sup>a</sup>	24.5	250	2.0
$\text{TmCl}_6^{3-}$	46.8 <sup>b</sup>		
$\text{TmBr}_6^{3-}$ <sup>a</sup>	38.6	300	
$\text{YbCl}_6^{3-}$ <sup>a</sup>	36.7	160	1.7
$\text{YbBr}_6^{3-}$ <sup>a</sup>	29.2	105	2.4
$^{243}\text{AmCl}_6^{3-}$	$\geq 49.0$ <sup>b,c</sup>		
$^{243}\text{AmBr}_6^{3-}$	$\geq 40.8$ <sup>c</sup>		
$^{249}\text{CfCl}_6^{3-}$	42.1	1550	1.9
$^{249}\text{CfBr}_6^{3-}$	33.5	875	1.6
$^{253}\text{EsCl}_6^{3-}$	38.1	$\sim 500$	1.6
$^{253}\text{EsBr}_6^{3-}$	30.3	$\sim 400$	1.7

<sup>a</sup> Reference 10. <sup>b</sup> This electron-transfer band is not observed because it is beyond the uv cutoff. The wave number given here is an approximation based on the average ( $8.2 \times 10^3 \text{ cm}^{-1}$ ) hexabromide-hexachloride shift for Sm(III), Eu(III), Yb(III), Cf(III), and Es(III). <sup>c</sup> This electron-transfer band is not observed because it is obscured because of strong f-d bands. The wave number reported here is a lower limit.

### 3. Theoretical Considerations

*f-d Band Structure and Overview.* The band structures in Figures 1 and 2 arise primarily from the structure of the final  $5f^q 6d^1$  energy levels, rather than from the initial  $5f^{q+1}$  energy levels which are thermally populated only in the ground state and which are considerably more shielded and hence much less sensitive to environmental splitting. The  $5f^q 6d^1$  electron configurations in the free Am(III) ( $q = 5$ ) and Bk(III) ( $q = 7$ ) ions involve complex electronic structures with hundreds of energy levels not yet measured and classified. Each free-ion energy level in these  $5f^q 6d^1$  configurations is highly perturbed by the six  $X^-$  ions making up the octahedral ligand complex. The ligand field strongly splits the  $J$  degeneracy into components that can, in principle, be labeled according to the symmetry species of the  $O_h$  point group. However, because of the intrinsic complexity of these band structures, and the limited amount of experimental information presently available from the solution spectra of Figures 1 and 2, it is inopportune at present to attempt any detailed ligand-field or molecular-orbital analysis.

It is opportune, on the other hand, to make intraseries calculations and correlations of the first f-d band energies of these and other chemical complexes of the lanthanide and actinide series, so that the absorption band onsets can be identified for each member of any particular set of complexes. It is, in fact, the major theme of this paper to show that not only can such first f-d band energies be accurately correlated and calculated from the results of the analysis of similar transitions in the neutral free Ln and An atoms, where the experimental data are far more abundant, but so also can the  $E^\circ \text{M(II-III)}$  and  $E^\circ \text{M(III-IV)}$  oxidation potentials, which in most cases involve the same  $f^{q+1} - f^q$  configuration differences between the two states of interest as are involved in the f-d ( $f^{q+1} \rightarrow f^q d^1$ ) transitions.

*Previous Free Atom Work.* We recapitulate next the recent correlative analysis of  $\Delta_d E(q)$ , the energy differences between the lowest energy levels of the  $f^q d^1 s^2$  and  $f^{q+1} s^2$  electron configurations in the neutral Ln and An free

atoms.<sup>5,6</sup> If the term  $+(9/13)E^1$  implicit in the parameter  $A$  of  $(E - A)$  in eq 1 of ref 5 is expressed explicitly as  $A = A' + (9/13)E^1$ , then  $\Delta_d E(q)$  can be written to a good approximation as follows<sup>6</sup>

$$\Delta_d E(q) = W + (E - A')q - M(L)E^3 - P(S, L, J)\zeta_r \quad (1a)$$

$$0 \leq q < 7$$

$$\Delta E(q) = W + (E - A')q - 9E^1 - M(L)E^3 - P(S, L, J)\zeta_r \quad (1b)$$

$$7 \leq q \leq 13$$

where one set of parameters  $W$  and  $(E - A')$  is fitted, along with two additional parameters  $a$  and  $b$  defining  $E'$ , to the ten experimentally known  $\Delta_d E(q)$  values of the Ln series, and another set is fitted to the eight experimentally known  $\Delta_d E(q)$  of the An series. The parameter  $W$  is the value  $\Delta_d E(q)$  would have at the beginning of each series if there were no spin-orbit or relativistic interactions. The term  $E$  in the combined parameter  $(E - A')$  accounts for the increase in the effective nuclear charge felt by each electron as the actual nuclear charge  $Z$  (or  $q$ ) increases across each series; it is found to be constant across an entire series. The term  $A'$  accounts mainly for those inter f electron repulsions that arise *via* the Racah parameter  $E^0$ ; it is found to be effectively the same for both configurations and constant across an entire series. The term  $A'$  also accounts approximately for the effects of f-d interelectron repulsions. The Racah inter f electron repulsion parameters  $E^1$  and  $E^3$  are fitted to the experimental data and they are thus found to be effectively unchanged between both configurations. The latter parameters are determined as follows:  $E^3$  is taken to be  $0.1E^1$ , in the hydrogenic ratio, and  $E^1$  is assumed to be linear in  $q$ ,  $E^1 = a + bq$ , where the constants  $a$  and  $b$  are fitted by the method of least squares to the experimental  $\Delta E(q)$  data *via* eq 1 with the following inputs. The spin-orbit interaction parameters,  $\zeta_r$ , are taken to be the same in the  $f^{q+1}s^2$  and  $f^q d^1 s^2$  metal atom configurations as they are in the respective Ln(III) aquo ion or the respective An(III) ion in certain crystals. This is a good approximation because the contributions from these spin-orbit interaction terms are small enough such that the small differences in  $\zeta_r$  between the various media are not important. It was made because most of the metal atom values for  $\zeta_r$  are not known, whereas the corresponding Ln(III) aquo ion values and the An(III) crystal ion values are extensively known and conveniently tabulated in previous publications. Finally,  $M(L)$  and  $P(S, L, J)$  are integers or half-integers obtained from the theory and tabulated in a previous publication.<sup>3</sup>

The standard deviation between the experimentally determined and the calculated  $\Delta_d E(q)$  values above is  $0.62 \times 10^3 \text{ cm}^{-1}$  for the ten Ln experimental points, and it is  $0.75 \times 10^3 \text{ cm}^{-1}$  for the eight An experimental points. The numerical results for those terms in eq 1 which are nonlinear in  $q$ , *i.e.*, the sum of the  $E^3$ - and  $\zeta_r$ -dependent terms of eq 1a, and the sum of the  $E^1$ -,  $E^3$ -, and  $\zeta_r$ -dependent terms of eq 1b, are listed here in Table III. We show in the developments to follow that these numerical values,  $F_1(q)$  for the lanthanides and  $F_a(q)$  for the actinides, which account to within  $\pm 2 \times 10^3 \text{ cm}^{-1}$  for the nonlinear variations in  $\Delta_d E(q)$  in the neutral metal atoms, account as well for the corresponding nonlinear variations in the first f-d band energies [ $hc/\lambda(f-d)$ ] in all the chemical complexes of the M(II) and M(III) ions. Moreover, these same numerical values also account as well for the corresponding nonlinear variations in the  $E^\circ M(\text{II-III})$  and  $E^\circ M(\text{III-IV})$  oxidation potentials.

TABLE III: General f Electron Linearization Energies for the Lanthanides,  $F_1(q)$ , and Actinides,  $F_a(q)$

$q$	Ln <sup>a</sup>	$F_1(q), \text{V}^b$	An <sup>a</sup>	$F_a(q), \text{V}^b$
0	La	+0.11	Ac	+0.18
1	Ce	+0.63	Th	+0.53
2	Pr	+0.80	Pa	+0.63
3	Nd	0.00	U	0.00
4	Pm	-0.84	Np	-0.69
5	Sm	-0.74	Pu	-0.71
6	Eu	-0.32	Am	-0.65
7	Gd	-5.85	Cm	-3.93
8	Tb	-5.38	Bk	-3.68
9	Dy	-5.34	Cf	-3.76
10	Ho	-6.38	Es	-4.67
11	Er	-7.48	Fm	-5.63
12	Tm	-7.54	Md	-5.85
13	Yb	-7.17	No	-5.78

<sup>a</sup> Note that the elements and  $q$  values are properly aligned with respect to each other here for application to  $E^\circ M(\text{II-III})$  and to  $hc/\lambda(f-d)$  for M(II) ions. For application to  $E^\circ M(\text{III-IV})$  and to  $hc/\lambda(f-d)$  for M(III) ions all element symbols should be raised one row with respect to  $q$ .

<sup>b</sup> Note that the signs of  $F_1(q)$  and  $F_a(q)$  here are correct for application to  $E^\circ M(\text{II-III})$  and  $E^\circ M(\text{III-IV})$ ; for application to f-d bands of M(II) and M(III) ions all of these signs must be reversed and the numbers multiplied by  $8.06547 \times 10^3 \text{ cm}^{-1} \text{ V}^{-1}$  for conversion to  $\text{cm}^{-1}$ .

#### 4. Spectroscopic Determination of $E^\circ M(\text{II-III})$ Potentials

The fact that a roughly linear correlation exists between the first electron-transfer band energies of certain Ln(III) complexes and the corresponding  $E^\circ \text{Ln}(\text{II-III})$  oxidation potentials has been recognized for a long time, but only recently has the analogous correlation been demonstrated for the An series.<sup>3,4</sup> We proceed next to develop both of these correlations further on the basis of the first electron-transfer band data of the  $\text{MX}_6^{3-}$  complexes of Table II and the known  $E^\circ M(\text{II-III})$  oxidation potentials of Table IV. The oxidation potentials here and throughout this paper are all with reference to the normal hydrogen electrode (NHE), with the sign convention such that the greater the positive potential the more stable is the oxidized form.

The  $E^\circ M(\text{II-III})$  values are plotted against the corresponding first electron-transfer band energies for the  $\text{MBr}_6^{3-}$  complexes in Figure 4. Similarly, the  $E^\circ M(\text{II-III})$  values are plotted against the corresponding first electron-transfer band energies for the  $\text{MCl}_6^{3-}$  complexes in Figure 5. In both Figures 4 and 5 the known experimental points are for Eu, Yb, Sm, and Cf. It is clear that the experimental Ln points do *not* fit precisely any one straight line, but it is also clear from the following developments how these points can be linearized.

We show in the next section that the  $E^\circ \text{Ln}(\text{II-III})$  and the  $E^\circ \text{An}(\text{II-III})$  potentials of Table IV separately follow eq 1 with the same numerical values for the nonlinear terms as given in Table III. Furthermore, it can be shown that the corresponding first electron-transfer band energies also separately follow eq 1 with the same numerical values for the nonlinear terms as given in Table III, but with slightly different values for  $(E - A')$  and, of course, considerably different values for  $W$  than those obtained from the  $E^\circ M(\text{II-III})$  calculations. Thus it follows that we can transform the experimental Ln points of Figures 4 and 5 to a unit-slope straight line simply by adding a term  $+q\Delta(E - A')_{\text{Ln}}$  to the electron-transfer band energies,

TABLE IV:  $E^\circ M(\text{II-III})$  Oxidation Potentials for the Lanthanides and Actinides<sup>e</sup>

M	Measd	Calcd	M	Measd	Calcd
La		+3.1 ± 0.2	Ac		+4.9 ± 0.2
Ce		+3.2	Th		+4.9
Pr		+2.7	Pa		+4.7
Nd		+2.6	U		+4.7
Pm		+2.6	Np		+4.7
Sm	+1.55 <sup>a</sup>	+1.6	Pu		+3.5
Eu	+0.35 <sup>b</sup>	+0.3	Am		+2.3 (2.6) <sup>a,c</sup>
Gd		+3.9	Cm		+4.4 (5.0) <sup>a,c</sup>
Tb		+3.7	Bk		+2.8 (3.4) <sup>a,c</sup>
Dy		+2.6	Cf	1.6 ± 0.2 <sup>d</sup>	+1.6 (1.9) <sup>a,c</sup>
Ho		+2.9	Es	1.2 ± 0.2	+1.3 (1.6) <sup>a,c</sup>
Er		+3.1	Fm		+1.1 (1.3) <sup>a,c</sup>
Tm	+2.3 ± 0.2(2.2) <sup>a,c</sup>	+2.3	Md	+0.15 <sup>a</sup>	0.0
Yb	+1.15 <sup>a</sup>	+1.1	No	-1.45 <sup>a</sup>	-1.3

<sup>a</sup> Reference 4. <sup>b</sup> L. R. Morss and H. Haug, *J. Chem Thermodyn.*, in press. <sup>c</sup> These values from previous work are in general considered to be less accurate. <sup>d</sup> H. A. Friedman, J. R. Stokely, and R. D. Baybarz, *Inorg. Nucl. Chem. Lett.*, **8**, 433 (1972), have recently shown that the half-wave polarographic (III-II) reduction potentials for Sm(III) and for Cf(III) in anhydrous 0.1 M tetraethylammonium perchlorate-acetonitrile solution are essentially the same. This is good evidence that  $E^\circ \text{Cf}(\text{II-III})$  is equal to  $E^\circ \text{Sm}(\text{II-III})$ , or 1.6 V. The 1.6 V  $E^\circ \text{Cf}(\text{II-III})$  value is also supported by the work of N. B. Mikheev, of the Institute of Physical Chemistry, Moscow, USSR, on cocrystallization of Cf(II) and SmC<sub>2</sub> from alcohol solution. <sup>e</sup> Volts relative to NHE.

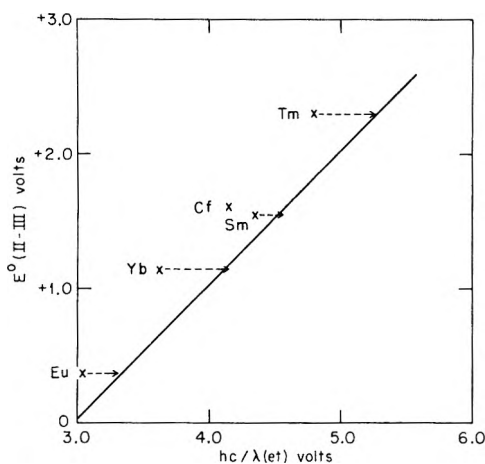


Figure 4.  $E^\circ(\text{II-III})$  vs.  $hc/\lambda(\text{et})$  for the lanthanide and actinide  $\text{MBr}_6^{3-}$  complexes.  $\Delta(E - A') = 0.040$  V. The points  $\times$  are measured values and the arrow tips represent values that have been linearized by adding  $+q\Delta(E - A')$  to the measured values.

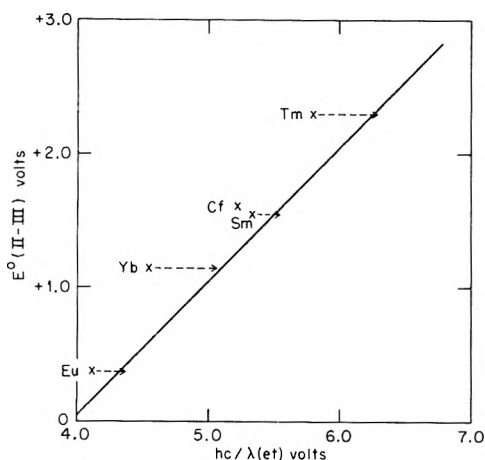


Figure 5.  $E^\circ(\text{II-III})$  vs.  $hc/\lambda(\text{et})$  for the actinide  $\text{MCl}_6^{3-}$  complexes.  $\Delta(E - A') = 0.040$  V. The points  $\times$  are measured values and the arrow tips represent values that have been linearized by adding  $+q\Delta(E - A')$  to the measured values.

where  $\Delta(E - A')_{\text{Ln}}$  is the difference between the  $(E - A')$  value obtained from the electron-transfer band calculations and the corresponding  $(E - A')$  value obtained from the  $E^\circ \text{Ln}(\text{II-III})$  calculations. The arrow tips in Figures 4 and 5 are the points so linearized, and  $\Delta(E - A')_{\text{Ln}}$  is determined from the linearization requirement to be +0.040 V for both the  $\text{LnBr}_6^{3-}$  and the  $\text{LnCl}_6^{3-}$  series.

From the unit-slope calibration lines in Figures 4 and 5, the  $\Delta(E - A')_{\text{Ln}}$  value above, and the measured first electron-transfer band energies of Table II, we obtain  $E^\circ \text{Tm}(\text{II-III}) = +2.3 \pm 0.2$  V, as reported in Table IV. Note that we obtain essentially the same  $E^\circ \text{Tm}(\text{II-III})$  potential in Figure 4 from the first electron-transfer band energy of the  $\text{TmBr}_6^{3-}$  complex as we obtain in Figure 5 from the first electron-transfer band energy of the  $\text{TmCl}_6^{3-}$  complex, as is of course required.

It follows that we can, in principle, transform the experimental An points of Figures 4 and 5 to unit-slope straight lines by adding a term  $+q\Delta(E - A')_{\text{An}}$  to the first electron-transfer band energies. However only the Cf points are known for these  $\text{AnX}_6^{3-}$  series, and so  $\Delta(E - A')_{\text{An}}$  is not determined here. Nevertheless we can obtain a value for  $E^\circ \text{Es}(\text{II-III})$  of  $+1.2 \pm 0.2$  V from the known  $E^\circ \text{Cf}(\text{II-III})$  potential of Table IV and the difference between the first electron-transfer band energies of the respective  $\text{CfX}_6^{3-}$  and  $\text{EsX}_6^{3-}$  complexes, from Table II, assuming that  $|\Delta(E - A')_{\text{An}}|$  is less than the 0.2 V error limit above. Since the corresponding parameter  $\Delta(E - A')_{\text{Ln}}$  is 0.040 V for the  $\text{LnX}_6^{3-}$  series, and the corresponding parameter  $\Delta(E - A')_{\text{An}}$  can be shown to be easily less than 0.04 V for the  $\text{AnX}_6^{2-}$  series,<sup>3</sup> very likely no significant error is introduced into  $E^\circ \text{Es}(\text{II-III})$  above due to the indeterminate  $\Delta(E - A')_{\text{An}}$  contribution. Additional support for this contention is also provided later in this section where it is shown that our  $E^\circ \text{Es}(\text{II-III})$  value correlates as expected with the known experimental values for  $E^\circ \text{Cf}(\text{II-III})$ ,  $E^\circ \text{Md}(\text{II-III})$ , and  $E^\circ \text{No}(\text{II-III})$ .

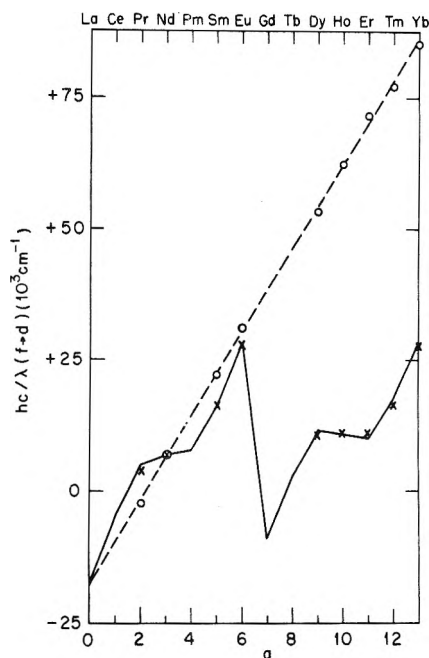
It is evident in the development of this paper that for various reasons the electron-transfer bands of all of the other members of these  $\text{LnX}_6^{3-}$  and  $\text{AnX}_6^{3-}$  series cannot at present be measured; so this exhausts our spectroscopic method for the determination of the Ln and An  $E^\circ M(\text{II-III})$  potentials.

## 5. Analysis

**First  $f-d$  Bands of  $M(II)$  in  $\text{CaF}_2$ .** McClure and Kiss<sup>12</sup> surveyed the room-temperature spectra of 13 of the Ln(II) ions in  $\text{CaF}_2$  crystalline hosts, obtained by  $\gamma$ -irradiation reduction of the corresponding Ln(III) doped  $\text{CaF}_2$  crystals, and they reported the first  $f-d$  band energies plotted here in Figure 6. We add the general  $f$  electron linearization energies  $F_1(q)$  of Table III to these experimental points in Figure 6, and we thereby generate the dashed straight line which fits the linearized points in Figure 6 to within  $\pm 2 \times 10^3 \text{ cm}^{-1}$ .<sup>13</sup> Conversely, the first  $f-d$  band energies for the entire Ln(II) series in  $\text{CaF}_2$  can now be generated from the dashed line of Figure 6 and the  $F_1(q)$  values of Table III. These calculated results are represented by the solid line in Figure 6. Thus we demonstrate that the  $f-d$  band data of Figure 6 fits eq 1 with  $(E - A') = 7.95 \times 10^3 \text{ cm}^{-1}$  and  $W = -17.5 \times 10^3 \text{ cm}^{-1}$ , and with values for the nonlinear terms taken directly from the previous atomic analysis. The fact that this simple analysis is as successful here as it is in the atomic cases demonstrates that contributions to these band energies arising from  $f-d$  interactions and ligand field interactions can, to a good approximation, be treated as linear functions of  $q$  and systematically accounted for by the  $W$  and  $(E - A')$  terms of eq 1.

It is important in the  $E^\circ\text{Ln(II-III)}$  analysis to follow to recognize that the first  $f-d$  band energies reported for  $\text{Sm(II)}_{\text{aq}}$  ( $17.9 \times 10^3 \text{ cm}^{-1}$ ),  $\text{Yb(II)}_{\text{aq}}$  ( $28.4 \times 10^3 \text{ cm}^{-1}$ ), and  $\text{Eu(II)}_{\text{aq}}$  ( $31.2 \times 10^3 \text{ cm}^{-1}$ ), the only members of the  $\text{Ln(II)}_{\text{aq}}$  series sufficiently stable to be measured, nearly match those of the respective  $\text{Sm(II)}$  ( $16.2 \times 10^3 \text{ cm}^{-1}$ ),  $\text{Y}_2\text{(II)}$  ( $27.5 \times 10^3 \text{ cm}^{-1}$ ), and  $\text{Eu(II)}$  ( $31.2 \times 10^3 \text{ cm}^{-1}$ ) ions in  $\text{CaF}_2$ .<sup>12,14</sup> This indicates that we can, to a good approximation, take the first  $f-d$  band energies for the entire  $\text{Ln(II)}_{\text{aq}}$  series to be the same as those of the  $\text{Ln(II)-CaF}_2$  ions of Figure 6. The negative energies in this figure show that the ground states of the highly unstable and essentially unmeasurable  $\text{La(II)}_{\text{aq}}$ ,  $\text{Ce(II)}_{\text{aq}}$ , and  $\text{Gd(II)}_{\text{aq}}$  ions are the lowest energy levels in  $f^q d$  electron configurations, and not in  $f^{q+1}$  configurations as are the other  $\text{Ln(II)}_{\text{aq}}$  ions of this series. Thus when we correlate  $E^\circ\text{Ln(II-III)}$  potentials on the basis of  $f^{q+1}$  electron configurations for the  $\text{Ln(II)}_{\text{aq}}$  ions and  $f^q$  electron configurations for the  $\text{Ln(III)}_{\text{aq}}$  ions, we must correct the potentials in the above exceptional  $\text{Ln(II)}_{\text{aq}}$  ion cases to account for the energy separation between the ground state  $f^q d$  electron configuration and the excited state  $f^{q+1}$  electron configuration. This correction is to a good approximation  $hc/\lambda(f-d)$  taken from Figure 6.

Exceptional  $f^q d$  ground state electron configurations also occur for some of the  $\text{An(II)}_{\text{aq}}$  ions, but we cannot at present directly measure the first  $hc/\lambda(f-d)$  values for any of these aquo ions. The problem here is that where the  $\text{An(II)}_{\text{aq}}$  ions are sufficiently stable for measurement,  $Z \geq 93$  for  $\text{Cf(II)}_{\text{aq}}$  and above, a sufficient amount of material for this measurement has not been available, and where a sufficient amount of material has been available for the measurement,  $Z \leq 97$  for  $\text{Bk(II)}_{\text{aq}}$  and below, the  $\text{An(II)}_{\text{aq}}$  ions are not sufficiently stable for measurement. Nevertheless, we can make good estimates of the first  $f-d$  band energies of the  $\text{An(II)}_{\text{aq}}$  ions from the corresponding measured data for the three presently known  $\text{An(II)-CaF}_2$  first  $f-d$  bands. The band onsets reported for the latter are  $\text{Am(II)-CaF}_2$  ( $15.4 \times 10^3 \text{ cm}^{-1}$ ),<sup>15</sup>  $\text{Cf(II)-CaF}_2$  ( $17.4 \times 10^3 \text{ cm}^{-1}$ ),<sup>16</sup> and  $\text{Es(II)-CaF}_2$  ( $24.4 \times 10^3 \text{ cm}^{-1}$ ).<sup>17</sup> Band centers are not accurately determined in these cases be-



**Figure 6.** First  $f-d$  band centers vs.  $q$  for the lanthanide(II) ions in  $\text{CaF}_2$ . The points  $\times$  are the measured values taken from ref 12 and 13. The points  $\circ$  are the linearized values defining the dashed straight line with slope  $(E - A') = 7.95 \times 10^3 \text{ cm}^{-1}$  and intercept  $W = -17.5 \times 10^3 \text{ cm}^{-1}$ . The solid line describes the calculated values.

cause the observed bands are broad and poorly defined, but, by analogy with the  $\text{Ln(II)-CaF}_2$  series, they should be about  $3 \times 10^3 \text{ cm}^{-1}$  greater in energy than the band onsets.

The above band onsets are plotted in Figure 7 where they are also linearized by the addition of the appropriate  $F_a(q)$  energy of Table III. Approximating the first  $f-d$  band energies of the  $\text{An(II)}_{\text{aq}}$  ions to be the same as these corresponding  $\text{An(II)-CaF}_2$  first  $f-d$  band energies, by analogy with the  $\text{Ln(II)}_{\text{aq}}$  and  $\text{Ln(II)-CaF}_2$  series, we see in Figure 7 that  $f^q d$  electron configurations are expected for the ground states of the  $\text{Ac(II)}_{\text{aq}}$ ,  $\text{Th(II)}_{\text{aq}}$ ,  $\text{Pa(II)}_{\text{aq}}$ ,  $\text{U(II)}_{\text{aq}}$ , and  $\text{Np(II)}_{\text{aq}}$  ions. Thus in the  $E^\circ\text{An(II-III)}$  analysis to follow, when we correlate  $E^\circ\text{An(II-III)}$  potentials across the  $\text{An}$  series on the basis of  $f^{q+1}$  electron configurations for the  $\text{An(II)}_{\text{aq}}$  ions and  $f^q$  electron configurations for the  $\text{An(III)}_{\text{aq}}$  ions, we must correct by the amount  $hc/\lambda(f-d)$  taken from Figure 7 (plus  $3 \times 10^3 \text{ cm}^{-1}$  to obtain the band center) in the cases of the above exceptional  $\text{An(II)}_{\text{aq}}$  ions.

It is worth noting that the actual measurement of the first  $f-d$  band for the  $\text{Ac(II)-CaF}_2$  species may be feasible when the  $\text{Ac}$  becomes available. This will be an important datum point in Figure 7 to check the theory and provide a more accurate correction to  $E^\circ\text{Ac(II-III)}$  for the  $d$ -electron stabilization of the ground state of the  $\text{Ac(II)}_{\text{aq}}$  ion. Also

- (12) D. S. McClure and Z. Kiss, *J. Chem. Phys.*, **39**, 3251 (1963).
- (13) We note that the first  $\text{Eu(II)-CaF}_2$   $f-d$  band, as shown in ref 12, is unusually wide on the low-energy side. Accordingly, we take the actual peak here to be not at the observed peak at 31 kK, but on the unresolved shoulder at 27.5 kK, in accord with K. E. Johnson and J. N. Sardo, *J. Chem. Soc. A*, 1694 (1969); A. A. Kaplyanskii and P. P. Feofilov, *Opt. Spectrosc.*, **13**, 129 (1962).
- (14) F. D. S. Butement, *Trans. Faraday Soc.*, **44**, 617 (1948). See also M. Faraggi and Y. Tendler, *J. Chem. Phys.*, **56**, 3287 (1972).
- (15) N. Edelstein, E. Easley, and R. McLaughlin, *J. Chem. Phys.*, **44**, 3130 (1966).
- (16) R. D. Baybarz, unpublished work.
- (17) N. Edelstein, J. G. Conway, D. Fujita, W. Dolbe, and R. McLaughlin, *J. Chem. Phys.*, **52**, 6425 (1970).

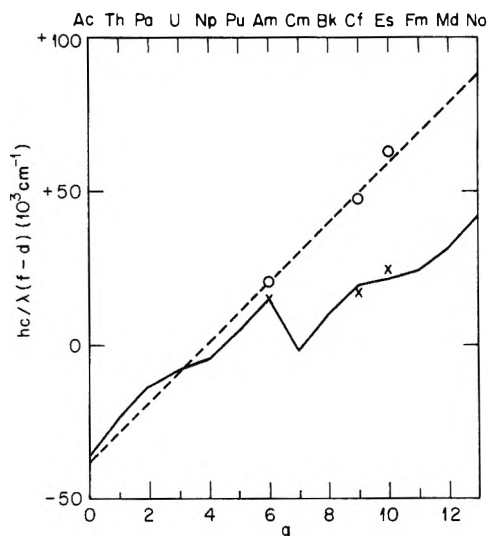


Figure 7. First  $f-d$  band onsets vs.  $q$  for the actinide(II) ions in  $\text{CaF}_2$ . The points  $\times$  are the measured values taken from ref 15-17. The points  $\circ$  are the linearized values defining the dashed line. The solid line describes the calculated values. ( $E - A'$ ) =  $9.7 \times 10^3 \text{ cm}^{-1}$ ,  $W = -37.5 \times 10^3 \text{ cm}^{-1}$ .

as  $^{249}\text{Cf}$  becomes available in greater than 100- $\mu\text{g}$  quantities, it will be helpful in this regard to measure directly the first  $f-d$  band for  $\text{Cf(II)}_{\text{aq}}$  in the same way as was done in the case of the chemically similar  $\text{Sm(II)}_{\text{aq}}$  ion.<sup>14</sup>

**First  $f-d$  Bands of the  $\text{MBr}_6^{3-}$  Complexes.** The measured wave numbers of the first strong  $f-d$  bands of  $\text{CeBr}_6^{3-}$ ,  $\text{PrBr}_6^{3-}$ , and  $\text{TbBr}_6^{3-}$ , taken from Table I, are plotted vs.  $q$  in Figure 8. These values are linearized by addition of the appropriate  $F_1(q)$  value of Table III, and this defines the dashed line in Figure 8. Here again we have a linear relationship in agreement with the theory. As before, the solid line in Figure 8 identifies the calculated values. We see there that all the other  $\text{LnBr}_6^{3-}$  complexes have first  $f-d$  band energies greater than  $48 \times 10^3 \text{ cm}^{-1}$ , so they cannot be readily measured because the bromide ligand absorption cutoff is at  $43 \times 10^3 \text{ cm}^{-1}$  and higher. Also, from the data of Table I we see that the  $\text{CeCl}_6^{3-}$ ,  $\text{PrCl}_6^{3-}$ , and  $\text{TbCl}_6^{3-}$  complexes have first strong  $f-d$  bands about  $1 \times 10^3$ - $2 \times 10^3 \text{ cm}^{-1}$  higher in energy than the corresponding  $\text{LnBr}_6^{3-}$  complexes. These  $\text{LnCl}_6^{3-}$  wave numbers can be similarly linearized, with the same slope as obtained for the  $\text{LnBr}_6^{3-}$  series, and from this the first  $f-d$  band wave numbers can be determined for the entire  $\text{LnCl}_6^{3-}$  series. Our results on this indicate that, similar to the  $\text{LnBr}_6^{3-}$  series, all  $\text{LnCl}_6^{3-}$  complexes other than those indicated above have first  $f-d$  bands higher than  $49 \times 10^3 \text{ cm}^{-1}$ , beyond the chloride ligand absorption cutoff at  $47 \times 10^3 \text{ cm}^{-1}$ , and so these  $f-d$  bands cannot be readily measured.

It should be noted above, in Figure 8 and in Table I, that although the weak  $f-d$  satellite band of  $\text{TbBr}_6^{3-}$  at  $36.0 \times 10^3 \text{ cm}^{-1}$ , and of  $\text{TbCl}_6^{3-}$  at  $36.8 \times 10^3 \text{ cm}^{-1}$ , is in each case at the lowest wave number, it does not directly fix the slope of the linearization in Figure 8. These so-called spin-forbidden satellites are peculiar to  $\text{Tb(III)}$ ,<sup>10</sup> as evidenced by the appearance of similar weak satellites at the lowest wave numbers in the absorption spectra of  $\text{Tb(III)}_{\text{aq}}$  and  $\text{Tb(III)-CaF}_2$ .<sup>18</sup> Our analysis of the  $\text{Ln(III)-CaF}_2$  system,<sup>18</sup> where more points are known across the series, indicates that the calculated wave number for  $\text{Tb(III)}$  should in general pass through the average wave

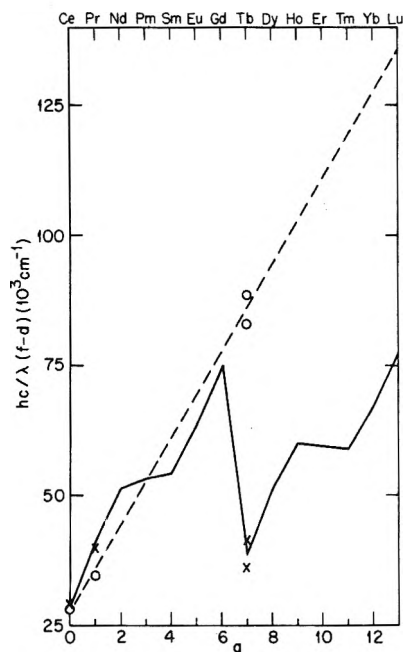


Figure 8.  $hc/\lambda(f-d)$  vs.  $q$  for the  $\text{LnBr}_6^{3-}$  complexes. The points  $\times$  are the measured values taken from Table I. The points  $\circ$  are the linearized values defining the dashed straight line. The solid line describes the calculated values. ( $E - A'$ ) =  $8.4 \times 10^3 \text{ cm}^{-1}$ ,  $W = +27.0 \times 10^3 \text{ cm}^{-1}$ .

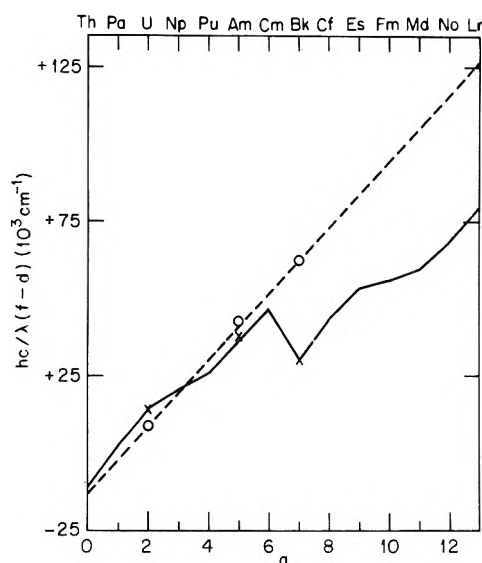
number of the first weak satellite band and the first strong band, and this, as shown in Figure 8, is how the slope of our linearization is fixed at the  $\text{TbBr}_6^{3-}$  points.

It should also be noted that the measured<sup>3</sup> first  $f-d$  bands of the corresponding  $\text{Ln(III)}_{\text{aq}}$  ions are all greater than those of the corresponding  $\text{LnBr}_6^{3-}$  ions of Figure 8. Since the latter are all greater than zero, this shows that the ground states of the  $\text{Ln(III)}_{\text{aq}}$  ions in no case involve  $f^q d$  electron configurations, they involve only  $f^{q+1}$  electron configurations. Thus there is no  $f^q d$  ground-state configuration for any of the  $\text{Ln(III)}_{\text{aq}}$  ions, and so no corrections to the  $\text{Ln } E^\circ(\text{II-III})$  potentials arise from this source as they do for the exceptional  $\text{Ln(II)}_{\text{aq}}$  ions discussed above.

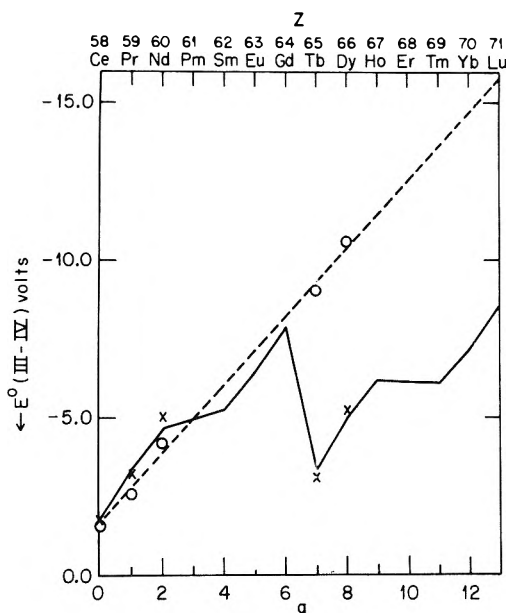
The wave numbers of the first  $f-d$  bands of  $\text{UBr}_6^{3-}$ ,  $\text{AmBr}_6^{3-}$ , and  $\text{BkBr}_6^{3-}$ , taken from Table I, are plotted vs.  $q$  in Figure 9. These values are linearized by addition of the appropriate  $F_a(q)$  value of Table III, and this defines the dashed line in Figure 9. Here again we have a linear relationship in agreement with the theory, and, as before, the solid line represents the calculated values. In this  $\text{AnBr}_6^{3-}$  series, neither  $\text{ThBr}_6^{3-}$ , nor  $\text{PaBr}_6^{3-}$  can be measured because they are highly unstable, whereas  $\text{CmBr}_6^{3-}$ ,  $\text{CfBr}_6^{3-}$ , and the other complexes to the right in this series have first  $f-d$  bands in and beyond the bromide cutoff and/or competing electron-transfer bands. The spectra of the other two complexes to the left in this series,  $\text{NpBr}_6^{3-}$  and  $\text{PuBr}_6^{3-}$ , could be measured; however, because of their marginal stability they were not measured in the present work. Also, from the data of Table I the  $\text{AnCl}_6^{3-}$  complexes have first  $f-d$  bands about  $1 \times 10^3 \text{ cm}^{-1}$  higher than those of the corresponding  $\text{AnBr}_6^{3-}$  complexes, so the former can be similarly linearized with the same slope as the latter, and remarks similar to those above for the  $\text{AnBr}_6^{3-}$  complexes also apply for the  $\text{AnCl}_6^{3-}$  complexes.

(18) J. L. Ryan, L. J. Nugent, and R. D. Baybarz, *J. Phys. Chem.*, to be submitted for publication.





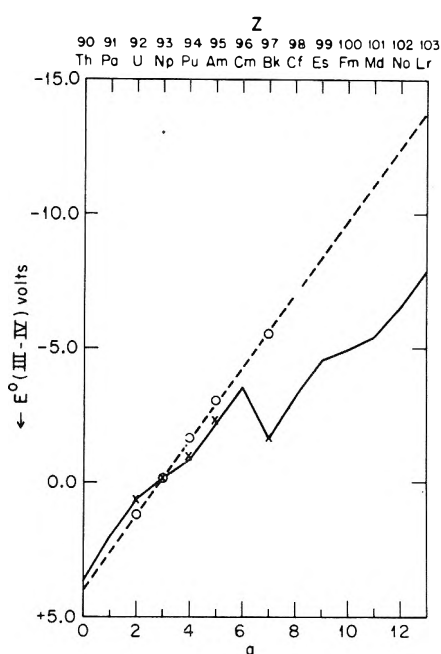
**Figure 9.**  $hc/\lambda(f-d)$  vs.  $q$  for the  $AnBr_6^{3-}$  complexes. The points X are the measured values taken from Table I. The points O are the linearized values defining the dashed straight line. The solid line describes the calculated values.  $(E - A') = 10.8 \times 10^3 \text{ cm}^{-1}$ ,  $W = -13.0 \times 10^3 \text{ cm}^{-1}$ .



**Figure 10.**  $E^\circ(\text{III-IV})$  vs.  $q$  for the lanthanide series. The points X are the measured values taken from Table V. The points O are the linearized values defining the dashed straight line. The solid line describes the calculated values.  $(E - A') = 1.07 \text{ V} = 8.63 \times 10^3 \text{ cm}^{-1}$ ,  $W = -1.80 \text{ V} = -14.5 \times 10^3 \text{ cm}^{-1}$ .

Finally, it should be noted that the measured<sup>3</sup> first f-d bands of the  $An(\text{III})_{aq}$  ions are each just  $11 \pm 2 \times 10^3 \text{ cm}^{-1}$  higher than those of the corresponding  $AnBr_6^{3-}$  complexes of Figure 9. Thus we see that all of the  $An(\text{III})_{aq}$  ions are in  $f^{q+1}$  ground-state electron configurations, and so no correction is required in our  $E^\circ An(\text{II-III})$  analysis due to irregular  $f^q d$  electron configurations entering into these ground states, as they do for some of the  $An(\text{II})_{aq}$  ions.

**$E^\circ M(\text{III-IV})$  Oxidation Potentials.** Previously we correlated the  $E^\circ M(\text{III-IV})$  potentials for the Ln and An series using Jørgensen's refined-electron-spin-pairing-energy theory.<sup>3</sup> Now we re-do these calculations on the basis of our newly modified and improved theoretical treatment.



**Figure 11.**  $E^\circ(\text{III-IV})$  vs.  $q$  for the actinide series. The points X are the measured values taken from Table V. The points O are the linearized values defining the dashed straight line. The solid line describes the calculated values.  $(E - A') = 1.37 \text{ V} = 11.1 \times 10^3 \text{ cm}^{-1}$ ,  $W = +4.0 \text{ V} = +32 \times 10^3 \text{ cm}^{-1}$ .

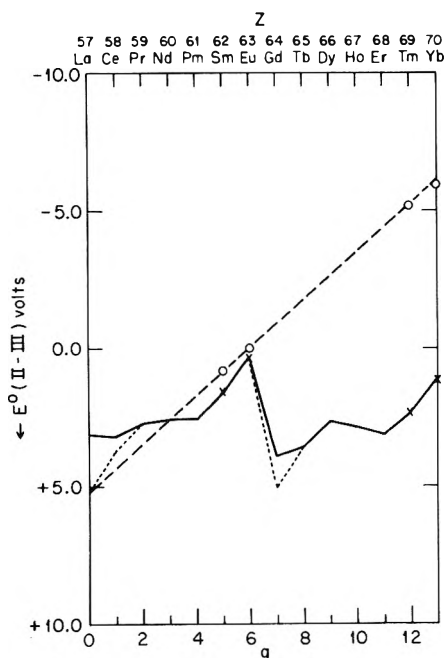
**TABLE V:  $E^\circ M(\text{III-IV})$  Oxidation Potentials for the Lanthanides and Actinides<sup>a</sup>**

M	Measd <sup>b</sup>	Calcd <sup>c</sup>	M	Measd <sup>b</sup>	Calcd <sup>c</sup>
Ce	-1.74	-1.8	Th		+3.7
Pr	-3.2 ± 0.2	-3.4	Pa		+2.0
Nd	-5.0 ± 0.4	-4.6	U	+0.63	+0.6
Pm		-4.9	Np	-0.15	-0.2
Sm		-5.2	Pu	-0.97	-0.8
Eu		-6.4	Am	-2.34	-2.2
Gd		-7.9	Cm	-3.1	-3.5
Tb	-3.1 ± 0.2	-3.3	Bk	-1.64	-1.6
Dy	-5.2 ± 0.4	-5.0	Cf		-3.2
Ho		-6.2	Es		-4.5
Er		-6.1	Fm		-4.9
Tm		-6.1	Md		-5.4
Yb		-7.1	No		-6.5
Lu		-8.5	Lr		-7.9

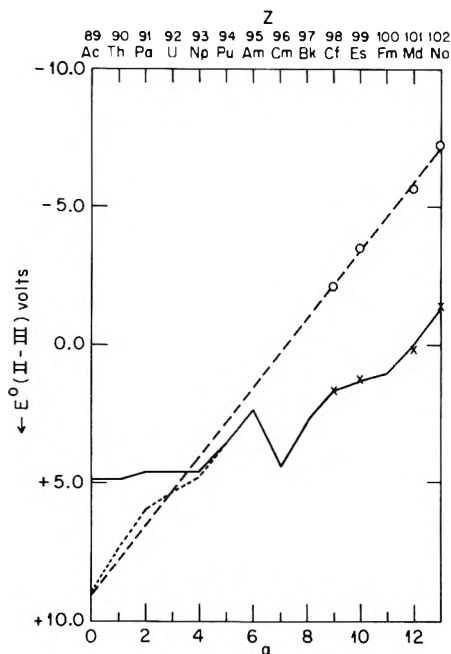
<sup>a</sup> Volts relative to the NHE. <sup>b</sup> Reference 3. <sup>c</sup> These values calculated in the present work are in general considered to be more accurate than the corresponding calculated values of ref 3 (see text).

The experimentally determined<sup>3</sup>  $E^\circ M(\text{III-IV})$  potentials are plotted vs.  $q$  in Figure 10 for the Ln series and in Figure 11 for the An series. These values are linearized by addition of the appropriate  $F_1(q)$  and  $F_a(q)$  values from Table III, and this defines the dashed lines in Figures 10 and 11. Here again we have a linear relationship showing that the irregular and the linear variations in these potentials can be separated according to the theory, and again the solid lines represent the new calculated values. All of the  $E^\circ M(\text{III-IV})$  potentials so determined are listed in Table V with the experimentally determined values.

There are essentially three new results coming out of the correlations in Figures 10 and 11. The first is that the  $E^\circ M(\text{III-IV})$  potentials for those elements on the far-right side of both series are now calculated to be somewhat smaller in absolute value than in the previous treatment;



**Figure 12.**  $E^\circ(\text{II-III})$  vs.  $q$  for the lanthanide series. The points X are the measured values taken from Table IV. The points O are the linearized values defining the dashed straight line. The solid line describes the calculated values.  $(E - A') = 0.87 \text{ V} = 7.02 \times 10^3 \text{ cm}^{-1}$ ,  $W = +5.12 \text{ V} = +41.3 \times 10^3 \text{ cm}^{-1}$ . For an explanation of the dotted line see text.



**Figure 13.**  $E^\circ(\text{II-III})$  vs.  $q$  for the actinide series. The points X are the measured values taken from Table IV. The points O are the linearized values defining the dashed straight line. The solid line describes the calculated values.  $(E - A') = 1.24 \text{ V} = 10.0 \times 10^3 \text{ cm}^{-1}$ ,  $W = +9.10 \text{ V} = +73.4 \times 10^3 \text{ cm}^{-1}$ . For the explanation of the dotted line see text.

e.g.,  $E^\circ\text{Lr(III-IV)}$  is now  $-7.9 \text{ V}$  compared to  $-9.0 \text{ V}$  before. The second is that whereas before  $E^\circ\text{Cm(III-IV)}$  was calculated to be  $-4.2 \text{ V}$ , which made it appear anomalous compared to the  $-3.1 \text{ V}$  estimated on the basis of relative chemical stabilities, it now is calculated to be  $-3.5 \text{ V}$ . Thus the anomaly is removed since the present difference between these calculated and experimental values is now

not out of range of the uncertainties. The third new result is that the values determined for  $(E - A')$  from the slopes of the dashed lines, and given in the captions to Figures 10 and 11, are now larger than before, mainly because the term  $(9/13)E^1$  is no longer included in the parameter  $A'$ .<sup>6</sup>

**$E^\circ\text{M(II-III)}$  Oxidation Potentials.** The experimentally determined  $E^\circ\text{M(II-III)}$  potentials from Table IV are plotted vs.  $q$  in Figure 12 for the Ln series and in Figure 13 for the An series. These values are linearized by addition of the appropriate  $F_1(q)$  and  $F_a(q)$  values from Table III, and this defines the dashed lines in Figures 12 and 13. Here again we obtain a linear relationship which shows that the irregular and the linear variations in these potentials can also be separated according to the theory, and again the solid lines represent the calculated values. It should be noted in these figures that dotted lines represent calculated potentials in those cases where the ground state of the  $\text{M(II)}_{\text{aq}}$  ion is not, in fact, in the  $f^{q+1}$  electron configuration, as assumed in the theory, but in the  $f^q d$  configuration. In these cases the solid line above the dotted line represents the true potential which is obtained by correcting the value on the dotted line by the  $f^q d$  electron stabilization energy, as estimated in the beginning of this section. All of the  $E^\circ\text{M(II-III)}$  potentials so determined are listed in Table IV with the experimentally determined values.

## 6. Discussion

We show in Figures 6-13, and in previous work,<sup>5,6</sup> that our systematic treatment provides a generally accurate description of physical and chemical properties of systems relating to electronic energy differences between atoms, ions, or chemical complexes involving  $f^q$  electron configurations and the corresponding atoms, ions, or chemical complexes involving  $f^{q+1}$  electron configurations. Furthermore, the nonlinear (in  $q$ ) irregularities in all such energy differences in the systems studied thus far are not seriously affected by the state of oxidation of the metal, or by the chemical bonding, whether present or absent, as might be expected for the relatively isolated  $f^q$  electrons. These nonlinear irregularities are to a good approximation ( $\pm 2 \times 10^3 \text{ cm}^{-1}$ , or  $\pm 0.2 \text{ V}$ ) the same for the same value of  $q$  in every system. The linear regularities, on the other hand, vary from system to system, as expected, but these variations are absorbed in the more or less loosely defined linearization parameters  $W$  and  $(E - A')$ . In addition to the energy contributions discussed previously, for those systems involving free atoms or ions,<sup>5,6</sup> the linearization parameters also reflect contributions from chemical bonding energies, ligand field energies, and entropy changes, where involved in the present systems. It is interesting to note in this regard that in systems involving oxidation potentials, which are of course free energy differences and which therefore depend both on energy differences and entropy differences, the nonlinear variations are accounted for by energy differences alone, the same energy differences as in the free atom systems. We are fortunate here that the effects of the corresponding entropy differences are accounted for, to a good approximation, by the linear parameters  $W$  and  $(E - A')$ , as are all other effects associated with chemical bonding, including the nonlinear tetrad effect which amounts to less than  $\pm 0.2 \text{ V}$ .<sup>19,20</sup>

It is noteworthy that in each actinide system studied thus far, whether it is chemical, gaseous atomic, or gas-

(19) C. K. Jørgensen, *J. Inorg. Nucl. Chem.*, **32**, 3127 (1970).

(20) L. J. Nugent, *J. Inorg. Nucl. Chem.*, **32**, 3485 (1970).

eous ionic, the value obtained for  $(E - A')_{An}$  is consistently larger than the corresponding value for  $(E - A')_{Ln}$  by a factor of  $1.3 \pm 0.1$ , with the exact ratio in this range depending on the particular system. Typical values are  $(E - A')_{An} \approx 10 \times 10^3 \text{ cm}^{-1}$  and  $(E - A')_{Ln} \approx 8 \times 10^3 \text{ cm}^{-1}$ , and deviations from these values occur for particular systems mainly in the next decimal place. In searching for the reasons for such consistency it is apparent that the dominant terms contributing to the parameters  $E$  and  $A'$  originate in the relatively isolated and shielded f electron cores. The contribution to  $E$  arises there due to inefficient mutual screening of the f electrons from the nuclear charge, whereas the contribution to  $A'$  arises there due to those parts of the inter f electron repulsions accounted for by the Racah parameter  $E^\circ$ . Relative to these dominant contributions, other contributions from chemical bonding energies, from entropy differences, from f valence-electron interactions, and from valence-electron-nuclear-charge interactions cannot be as important because they vary considerably from system to system yet the consistency stated above remains.

In the simple theory of the gaseous atoms the Racah inter f electron repulsion parameter  $E^\circ$  adds directly to  $A'$ , whereas the f electron contributions to the parameter  $E$  arise as follows. The lowest electronic energy level of each configuration, besides the electronic energy accounted for by the various Racah and spin-orbit interaction parameters, is assumed, by analogy with hydrogenic energetics, to be proportional to the square of the effective nuclear charge acting on the f electrons; *i.e.*, it is proportional to  $-Kq[Z_1(0) + (1-s)q]^2/n^{*2}$  for the  $f^q d^1 s^2$  configuration and proportional to  $-K(q+1)[Z_2(0) + (1-s)q]^2/n^{*2}$  for the  $f^{q+1} s^2$  configuration, where  $Z_1(0)$  and  $Z_2(0)$  are the effective nuclear charges of the respective configurations of the element at the beginning of the series ( $q = 0$ ), the parameter  $s$  is the mutual f electron Slater screening constant,  $n^*$  is an effective principle quantum number, and  $K$  is the constant of proportionality.<sup>21</sup> When energy differences are taken between these two configurations, the terms above yield three components: a constant component  $K[Z_2(0)]/n^{*2}$  which is absorbed by the parameter  $W$ , a linear (in  $q$ ) component  $qK[Z_2(0)^2 - Z_1(0)^2 + 2(1-s)Z_2(0)]/n^{*2}$  with the constant coefficient of  $q$  here absorbed by the shielding parameter  $E$  of  $(E - A')$ , and a relatively small quadratic component which can be ignored.

We can obtain some idea of the value of  $E$  for both series from the experimental  $(E - A')$  values above and the following estimates for the parameters  $E^\circ$ . We calculate  $(E^\circ/E^1)$  in the hydrogenic approximation to be 26.07 for 4f electrons;<sup>22</sup> from this ratio and the experimental value<sup>6</sup>  $E^1 = 5 \times 10^3 \text{ cm}^{-1}$ , we estimate  $E^\circ_{Ln}$  to be  $130 \times 10^3 \text{ cm}^{-1}$ . For our present purposes the corresponding parameters should not be importantly different for any of the Ln(III) ions, whether complexed or free, or for any of the other oxidation states of this series. Thus taking  $(E - A') \approx 8 \times 10^3 \text{ cm}^{-1}$  and  $A' \approx E^\circ_{Ln} \approx 130 \times 10^3 \text{ cm}^{-1}$  from above, we obtain  $E_{Ln} \approx 138 \times 10^3 \text{ cm}^{-1}$ . Similarly we estimate  $E^\circ_{An}$  at  $95 \times 10^3 \text{ cm}^{-1}$  by taking the ratio of the  $E^\circ$  values for the Ln and An series to be the same as the ratio (0.73) of the effective  $E^1$  values.<sup>6</sup> Thus taking  $(E - A')_{An} \approx 10 \times 10^3 \text{ cm}^{-1}$  and  $E^\circ_{An} \approx 95 \times 10^3 \text{ cm}^{-1}$ , as above, we obtain  $E_{An} \approx 105 \times 10^3 \text{ cm}^{-1}$ .

The relative values of the  $E$  and  $A'$  parameters above are important in understanding why divalent stability becomes progressively more pronounced toward the right-

hand side of the An(II) series than toward the right-hand side of the Ln(II) series. These differences in M(II) stabilities for the two series arise mainly because of the difference in the values of the  $(E - A')$  parameters, and, as indicated above, the latter differ mainly because the decrease in the Racah inter f electron repulsion parameters  $E^\circ$  between these two series is greater than the decrease in the shielding parameters  $E$ . Thus, for example, because of the greater decrease in inter f electron repulsion compared to shielding in the  $\text{No(II)}_{aq}$  ion relative to the  $\text{Yb(II)}_{aq}$  ion, the former is stable in aqueous solution whereas the latter is unstable relative to rapid conversion to the  $\text{Yb(III)}_{aq}$  ion. Likewise, the same argument applies to why  $(\text{Cf}?)$ , Es, Fm, Md, and No are divalent crystalline metals in the An series, but only Eu and Yb are divalent crystalline metals in the Ln series.<sup>23</sup>

In the correlation of the first f-d bands of the Ln(II)- $\text{CaF}_2$  system in Figure 6, it should be noted that the experimental points for La(II) at  $q = 0$ , for Ce(II) at  $q = 1$ , for Gd(II) at  $q = 7$ , and for Tb(II) at  $q = 8$  are missing. McClure and Kiss<sup>12</sup> show a room-temperature absorption spectrum for each member of this Ln(II)- $\text{CaF}_2$  system, including spectra for the four cases above. However, the spectra they claim for Ce(II)- $\text{CaF}_2$ , Gd(II)- $\text{CaF}_2$ , and Tb(II)- $\text{CaF}_2$  do not show first f-d band energies sufficiently near the calculated values of Figure 6 to make this claim believable.

More recent studies<sup>24,25</sup> have shown that the four systems above are in fact unique in the Ln(II)- $\text{CaF}_2$  series. Unlike the other members of this series except Lu(II)- $\text{CaF}_2$ , they are photochromic with unusually complicated absorption spectra; *i.e.*, the spectra change upon exposure to light. The photochromism appears in those cases involving a single d electron in or near the Ln(II)- $\text{CaF}_2$  ground state as can be seen from Figure 6. It is ascribed to photoreversible electron transfer to Ln(III) from a photochromic (PC) color center produced in the crystal during the attempted reduction; absorption of uv light by the PC center transfers an electron from it to an isolated Ln(III) and this converts the latter to Ln(II); the process is slowly reversed thermally, or more quickly by Ln(II) absorption of visible light.

The other Ln(II)- $\text{CaF}_2$  systems do not involve a d electron in or sufficiently near the ground state and they are not photochromic; upon reduction of Ln(III)- $\text{CaF}_2$ , either by  $\gamma$ -irradiation or by heating in the presence of Ca vapor, these Ln(II)- $\text{CaF}_2$  systems are produced directly without the intermediate of photoconversion.

It is not understood, beyond the apparent requirement of d-electron involvement, why the PC color center requires the intermediate of a uv photon to make the conversion from Ln(III)- $\text{CaF}_2$  to Ln(II)- $\text{CaF}_2$  in the former cases, whereas the corresponding conversion proceeds directly in the latter cases. We can obtain more understanding of this problem by examining the  $E^\circ M(\text{II-III})$  oxidation potentials of Table IV. Although these potentials relate strictly only to the metal aquo ion systems, the relative metal ion stabilities should not change significantly

- (21) H. Eyring, J. Walter, and G. E. Kimball, "Quantum Chemistry," Wiley, New York, N. Y., 1954, pp 84 and 163.  
 (22) B. R. Judd, "Operator Techniques in Atomic Spectroscopy," McGraw-Hill, New York, N. Y., 1963, Appendix 1.  
 (23) L. J. Nugent, J. L. Burnett, and L. R. Morss, *J. Chem. Thermodyn.*, in press.  
 (24) R. C. Alig, Z. J. Kiss, J. P. Brown, and D. S. McClure, *Phys. Rev.*, **186**, 276 (1969), and the references therein.  
 (25) D. L. Staebler and S. E. Schnatterly, *Phys. Rev. B*, **3**, 516 (1971), and the references therein.

in the  $\text{CaF}_2$  crystal systems. We see in Table IV that the photochromic  $\text{Ln(II)}$  species are the least stable of the series, with  $E^\circ\text{M(II-III)}$  potentials in the range 3.1–3.9 V. Thus the energetics are relatively more unfavorable for transition to the  $\text{Ln(II)-CaF}_2$  species in the photochromic cases, and this may help explain the need for the intervention of a uv photon.

It should also be noted in Table IV that  $E^\circ\text{Er(II-III)} = 3.1 \pm 0.2$  V, and this value is in the photochromic range quoted above; however,  $\text{Er(II)-CaF}_2$  does not involve a d electron in the ground state, as can be seen from Figure 6, and it is not reported to be photochromic. We do not know whether the  $\pm 0.2$  V uncertainty above provides that  $E^\circ\text{Er(II-III)}$  is actually less than 3.1 V, and this is why  $\text{Er(II)-CaF}_2$  is not photochromic; or whether d-electron involvement in the ground state is actually necessary for photochromism, and this is why  $\text{Er(II)-CaF}_2$  is not photochromic. In any event it may be worthwhile to reexamine this system to make sure that  $\text{Er(II)-CaF}_2$  is actually produced and that it is in fact not photochromic.

By analogy with the discussion above, the normal, non-photochromic, stable  $\text{An(II)-CaF}_2$  species are expected to be  $\text{Am(II)-CaF}_2$ ,  $\text{Bk(II)-CaF}_2$ ,  $\text{Cf(II)-CaF}_2$ ,  $\text{Es(II)-CaF}_2$ ,  $\text{Fm(II)-CaF}_2$ ,  $\text{Md(II)-CaF}_2$ , and  $\text{No(II)-CaF}_2$ . This has already been shown experimentally for  $\text{Am(II)-CaF}_2$ ,<sup>15</sup>  $\text{Cf(II)-CaF}_2$ ,<sup>16</sup> and for  $\text{Es(II)-CaF}_2$ .<sup>17</sup>

The other members of the  $\text{An(II)-CaF}_2$  series, including  $\text{Lr(II)-CaF}_2$ , involve a d electron in or near the  $\text{An(II)-CaF}_2$  ground state, as can be seen from Figure 7; so these are the photochromic candidates. However only  $\text{Pu(II)-CaF}_2$  falls within the photochromic oxidation potential range of 3.1–3.9 V discussed above for the  $\text{Ln(II)-CaF}_2$  series, i.e.,  $E^\circ\text{Pu(II-III)} = 3.5$  V from Table IV, and it remains to be seen whether  $\text{Pu(II)-CaF}_2$  can be stabilized, with the outcome probably dependent on the amount of d-electron involvement in the  $\text{Pu(II)-CaF}_2$  ground state.

Stacy, Edelstein, and McLaughlin<sup>26</sup> have recently reported the results of  $\gamma$ -irradiation of several  $\text{An(III)-CaF}_2$  systems. They see no spectroscopic evidence for the formation of  $\text{U(II)-CaF}_2$ ,  $\text{Np(II)-CaF}_2$ ,  $\text{Pu(II)-CaF}_2$ , or  $\text{Cm(II)-CaF}_2$ ; instead they observe these metals to be partially oxidized to the (IV) state. If these metals cannot in fact be reduced to the  $\text{An(II)-CaF}_2$  states, either by  $\gamma$ -irradiation or by heating in the presence of Ca vapor, it indicates that d-electron involvement in the ground state of  $\text{Pu(II)-CaF}_2$  does not occur, and that  $\text{U(II)}$ ,  $\text{Np(II)}$ , and  $\text{Cm(II)}$  are insufficiently stable as suggested by their  $E^\circ\text{M(II-III)}$  oxidation potential range of 4.4–4.7 V from Table IV.

Experimental work on these actinide photochromic candidates is not as yet definitive, however, and it remains to be seen whether we can reduce the corresponding  $\text{An(III)-CaF}_2$  crystals in the presence of hot Ca vapor, using low activity dopants such as  $^{248}\text{Cm}$  to minimize the effects of radiolysis, and obtain stable photochromic (II-III) systems. Very little hope can be entertained for the eventual stabilization of photochromic  $\text{Th(II)-CaF}_2$  or  $\text{Pa(II)-CaF}_2$  for two important reasons. The corresponding  $E^\circ\text{M(II-III)}$  values from Table IV indicate highly unstable  $\text{M(II)}$  states, and the corresponding  $E^\circ\text{M(III-IV)}$  values from Table V indicate highly unstable  $\text{M(III)}$  states. More hope may be entertained, on the other hand, for the eventual stabilization of photochromic  $\text{Ac(II)-CaF}_2$ , since  $\text{Ac(III)}$  is the most stable oxidation state, higher actinium oxidation states are essentially impossible in chemical systems, and the only important obstacle is the highly unstable  $\text{Ac(II)}$  species.

The  $E^\circ\text{M(II-III)}$  potentials of Figures 12 and 13 and of Table IV also serve as an indicator of the relative stabilities of the  $\text{MX}_2$  compounds of both series.<sup>27</sup> For those metals with  $E^\circ\text{M(II-III)}$  potentials below +1.6 V, the  $\text{MX}_3$  compounds can be reduced to the salt-like  $\text{MX}_2$  compounds *via* heating *in vacuo* or in a  $\text{H}_2$  or  $\text{HX}$  atmosphere.<sup>28</sup>  $\text{CfX}_3$  is a borderline case [ $E^\circ\text{Cf(II-III)} = +1.6$  V] with conversion of  $\text{CfBr}_3$  to  $\text{CfBr}_2$  occurring *via* heating *in vacuo* or in an  $\text{H}_2$  or  $\text{HBr}$  atmosphere, but no conversion of  $\text{CfCl}_3$  to  $\text{CfCl}_2$  upon heating *in vacuo* or in an  $\text{H}_2$  or  $\text{HCl}$  atmosphere.<sup>29</sup> For those metals with  $E^\circ\text{M(II-III)}$  potentials in the range from +1.7 to +2.7 V, the conversion to the salt-like  $\text{MX}_2$  compound requires heating of the  $\text{M} + \text{MX}_3$  or  $\text{M} + \text{HgX}_2$  systems; it does not proceed by heating *in vacuo* or in a  $\text{H}_2$  or  $\text{HX}$  atmosphere.<sup>28,30</sup> Finally, for those metals with  $E^\circ\text{M(II-III)}$  potentials greater than or equal to +2.7 V the  $\text{MX}_2$  compounds are unstable with respect to disproportionation to  $\text{M}$  and  $\text{MX}_3$ , or in some cases with respect to disproportionation to higher-valent compounds.<sup>31</sup>

Special cases not conforming to our indicator above arise for crystalline  $\text{LaI}_2$ ,  $\text{CeI}_2$ ,  $\text{PrI}_2$ , and  $\text{GdI}_2$ , which are stable enough for preparation, but which are known to be metallic conductors rather than salt-like insulators like all the other  $\text{LnX}_2$  compounds.<sup>28</sup> We see from the analogous  $\text{Ln(II)-CaF}_2$  cases in Figure 6 that these particular  $\text{Ln(II)}$  ions involve  $f^q d$  electron configurations in the ground state, or near the ground state in the case of  $\text{Pr(II)}$ . Moreover, the  $\text{LnI}_2$  compounds would be expected to have  $f^q d$  configurations even lower than those of Figure 6 by several thousand  $\text{cm}^{-1}$ , so the ground state would also be expected to be in the  $f^2 d$  electron configuration for  $\text{Pr(II)}$  in  $\text{PrI}_2$ . It appears, however, that these special cases are not true  $\text{M(II)I}_2$  compounds, but metallic  $\text{M(III)e}^- \text{I}_2$  compounds with the electron ( $e^-$ ) in the conduction band. This metallic character occurs, as suggested by Jørgensen<sup>32</sup> and others,<sup>28</sup> only when the  $\text{Ln(II)}$  ion would otherwise be expected to have a  $f^q d$  electronic ground state, so that the electron has mobility in an extended d orbital. It also appears that another requirement for the occurrence of the metallic state is that the associated anions,  $\text{I}^-$  in these cases, have relatively low electronegativity, since the analogous  $\text{MCl}_2$  compounds are not metallic but salt-like and unstable with respect to disproportionation.

A similar special case not conforming to the guide above arises in the actinide series for  $\text{ThI}_2$ , which is also metallic. The diamagnetic character of this compound suggests that it is best represented as  $\text{Th(IV)e}_2 \text{-I}_2$  with two electrons in the conduction band.<sup>28</sup> In this case the ground-state configuration of  $\text{Th(III)}$  should involve a d electron, and from Figure 9 we can see that this is true. Efforts have been made to prepare other metallic  $\text{AnI}_2$  compounds but they have so far been unsuccessful; e.g.,  $\text{U}_2$  is reported to be unstable,<sup>33</sup> but perhaps this is to be

- (26) J. J. Stacy, N. Edelstein, and R. D. McLaughlin, *J. Chem. Phys.*, **57**, 4980 (1972).
- (27) For an excellent discussion of the variations in the relative stabilities of the di-, tri-, and tetrapositive oxidation states of the lanthanides and actinides in terms of electronic structure and oxidation potentials see D. A. Johnson, *J. Chem. Soc. A*, 1528 (1969).
- (28) D. Brown, "Halides of the Lanthanides and Actinides," Wiley, New York, N. Y., 1968.
- (29) J. R. Peterson and R. D. Baybarz, *Inorg. Nucl. Chem. Lett.*, **8**, 423 (1972).
- (30) R. D. Baybarz, L. B. Asprey, C. E. Strouse, and E. Fukushima, *J. Inorg. Nucl. Chem.*, **34**, 3427 (1972).
- (31) D. A. Johnson, *J. Chem. Soc. A*, 2578 (1969).
- (32) C. K. Jørgensen, *Mol. Phys.*, **7**, 417 (1964).
- (33) J. D. Corbett, R. J. Clark, and T. F. Munday, *J. Inorg. Nucl. Chem.*, **25**, 1287 (1963).

expected since the ground state of U(III) does not involve a d electron, as can be seen in Figure 9. Besides Th(III) in the An(III) series, only the ground state of Pa(III) involves a d electron. On this basis we might also expect a stable metallic  $\text{PaI}_2$  compound, and possibly a stable metallic  $\text{AcI}_2$  compound, for the same reasons that  $\text{LaI}_2$  is stable and metallic, but we should not expect stable metallic compounds for any of the other actinides.

In conclusion it is appropriate to mention the pioneering work by Malý<sup>34</sup> and Cunningham,<sup>35</sup> and by David and Bouissières,<sup>36</sup> on the amalgamation behavior of Ln(III) and An(III) ions from aqueous solutions. They demonstrated that the ions of these series could be divided into two distinct classes: those that are systematically regular in their amalgamation rates from aqueous solution, and the others, Sm(III), Eu(III), Yb(III), Cf(III), Es(III), Fm(III), Md(III), and presumably No(III), which proceed irregularly fast in amalgamation from aqueous solution. It was postulated that the latter ions were amalgamated irregularly fast simply because the fast amalgamation involves a mechanism with a limiting rate dependent on the production and existence of the  $\text{M(II)}_{\text{aq}}$  ions.

Our results on the  $E^\circ\text{M(II-III)}$  potentials in Figures 12 and 13 clearly support this postulate. The critical potential which constitutes a dividing line between the two classes of ions above appears to be about 1.8 V, between  $E^\circ\text{Cf(II-III)}$  and  $E^\circ\text{Tm(II-III)}$ , with those elements with  $E^\circ\text{M(II-III)}$  potentials greater than 1.8 V constituting the regular amalgamation class, and those elements with  $E^\circ\text{M(II-III)}$  potentials less than 1.8 V constituting the fast amalgamation class. The  $\text{M(II)}_{\text{aq}}$  ions of the latter class have sufficient short-time stability to allow the amalgamation mechanism to proceed from  $\text{M(III)}_{\text{aq}}$  to  $\text{M(II)}_{\text{aq}}$  to M, whereas for the former class, where the  $\text{M(II)}_{\text{aq}}$  ions are essentially nonexistent, a slower amalgamation mechanism apparently proceeds from  $\text{M(III)}_{\text{aq}}$  directly to M.

In the more recent work of Musikas and Myasoyedov<sup>37</sup> on the polarography of Am(III) in anhydrous acetonitrile

solution, they observed a first half-wave potential at +1.4 V which they suggest may arise from the  $\text{Am(III)} + e^- \rightarrow \text{Am(II)}$  reaction. Making the assumption that the previously measured 0.82 V change in potential for the Eu(II-III) couple between acetonitrile and aqueous solution is the same as for the Am(II-III) couple, they tentatively estimated  $E^\circ\text{Am(II-III)}$  to be +2.2 V, and this is in agreement with our present value  $E^\circ\text{Am(II-III)} = +2.3 \pm 0.2$  V. However, recent preliminary work at our laboratory has indicated that the first half-wave potential in the polarographic measurement of the Am(III)-acetonitrile system is closer to +1.2 V, and that this half-wave may arise from the  $\text{Am(III)} + 3e^- \rightarrow \text{Am}$  reaction. We suggest, therefore, because of this fundamental disagreement, that the general acceptance of these Am(III) polarographic results await further verification.

Finally, the recent work of David<sup>38-41</sup> is worthy of note in that he uses results from amalgamation and polarographic measurements to make tentative estimates of some of the  $E^\circ\text{M(II-III)}$  potentials. It would appear to be more profitable now to reverse this approach and to reexamine his results from the point of view of some new interpretations in the light of our present knowledge of the Ln and An  $E^\circ\text{M(II-III)}$  potentials.

*Acknowledgments.* The authors take pleasure in acknowledging several helpful discussions with Professor C. K. Jørgensen, Dr. K. L. Vander Sluis, and Professor E. Y. Wong.

(34) J. Malý, *Inorg. Nucl. Chem. Lett.*, **3**, 373 (1967).

(35) J. Malý and B. B. Cunningham, *Inorg. Nucl. Chem. Lett.*, **3**, 445 (1967).

(36) F. David and G. Bouissières, *Inorg. Nucl. Chem. Lett.*, **4**, 153 (1968).

(37) C. Musikas and B. Myasoyedov, *Radiochem. Radioanal. Lett.*, **2**, 21 (1969).

(38) F. David, *Rev. Chim. Miner.*, **7**, 1 (1970).

(39) F. David, *Radiochem. Radioanal. Lett.*, **5**, 279 (1970).

(40) F. David, *C. R. Acad. Sci., Ser. C*, **270**, 2112 (1970).

(41) F. David, *C. R. Acad. Sci., Ser. C*, **271**, 440 (1970).

# Liquid Junction Potentials by Computer Simulation. II. The Lewis and Sargent Cell. A Harned's Rule for Single Ions

Chang-Hwei Chen and Henry S. Frank\*

Department of Chemistry, University of Pittsburgh, Pittsburgh, Pennsylvania 15213 (Received January 22, 1973)

Publication costs assisted by the Office of Saline Water, U.S. Department of the Interior

The method employed by Hafemann and by Goldberg and Frank for calculating liquid junction potentials by computer simulation has been extended to the so-called Lewis and Sargent junction  $\text{Ag}, \text{AgCl}; \text{MCl}(C_1) || \text{MCl}(C_2); \text{AgCl}, \text{Ag}$ ;  $\text{MCl}(C) || \text{NCl}(C); \text{AgCl}, \text{Ag}$ . This involved the use of additional conventions because the junction is now a mixture of  $\text{MCl}$  and  $\text{NCl}$  solutions. For the Onsager flux coefficients in the mixture the LN1 convention of Miller was used, and for the (assumed) single-ion activity values needed for calculation of thermodynamic driving forces on individual ions an extension of Harned's rule was devised. In the three cases studied [ $\text{HCl}:\text{KCl}$ ,  $\text{KCl}:\text{NaCl}$ ,  $\text{KCl}:\text{LiCl}$ , all at  $0.1\text{ M}$ ] calculated cell emf's agree with measured ones to a few tenths of a millivolt, and it is found that, as in the earlier case of concentration cells with transference, this agreement is equally good for any arbitrary (but self-consistent) set of assumptions regarding the single-ion activities. This leads to the expected conclusion that, for the Lewis and Sargent cell also, the measurement of a cell emf can give no single-ion information. Such a measurement, in contrast, could in principle be used to determine a Harned's rule coefficient, but it is found in practice that the sensitivity of a calculated cell emf to changes in these coefficients is too low for this purpose. Not only is there an unresolved discrepancy of tenths of millivolts between computed and measured cell emf's in known cases, but the uncertainty, of some hundredths of a millivolt, in the best present-day values of the measured cell emf's still corresponds to large percentage errors in the Harned  $\alpha$ 's.

## I. Introduction

Some years ago Hafemann<sup>1</sup> showed that a computer simulation process could be used in an approximate calculation of the liquid junction potentials in such electrochemical cells as



and



Recently the calculation for the concentration cell with transference, cell A, was amended by Goldberg and Frank<sup>2</sup> to (a) enable the Onsager transport formalism<sup>3</sup> to be used without truncation (*i.e.*, to include use of the off-diagonal coefficient  $l_{ij}$ , which represents the motion of ion  $i$  under the influence of a force of which the direct action is only on ion  $j$ ) and (b) gain greater flexibility in expressing assumptions about single-ion activities<sup>4</sup> (required in the evaluation of the "diffusion force" on an ion  $i$ ,  $-\partial\mu_i/\partial x$ , where  $\mu_i$  is its chemical potential and  $x$  the length coordinate along the junction). It was found that, with these generalizations, and using the numerical values of the Onsager transport coefficients given by Miller,<sup>5</sup> the calculation was able to give results for the over-all electromotive forces of several cells of type A in satisfactory agreement with experiment. It was also found that the same calculated cell emf was obtained for the same salt  $\text{MCl}$  between the same concentrations  $C_1$  and  $C_2$ , no matter what assumptions were inserted regarding the single-ion activity coefficients, so long only as the assumption regarding  $\text{M}^+$  and that regarding  $\text{Cl}^-$  satisfied a requirement of being mutually consistent. This finding, as was pointed out, does not call into question the reality of the single-ion activities involved, but simply gives alternative expression to a cancellation which occurs in the thermo-

dynamic derivation<sup>6</sup> of the expression for the cell emf  $E_A$ , and thus confirms that comparison of observed and calculated values of  $E_A$  can give no information regarding single-ion quantities taken separately.<sup>7</sup>

In the present paper this work has been further extended to the consideration of the so-called Lewis and Sargent<sup>8</sup> junction exemplified in cell B; *i.e.*, a junction in which solutions of different salts are in contact with each other, the solutions being of equal equivalent concentration, and the salts having in common the ion (here the

- (1) D. R. Hafemann, *J. Phys. Chem.*, **69**, 4226 (1965).
- (2) R. N. Goldberg and H. S. Frank, *J. Phys. Chem.*, **76**, 1758 (1972).
- (3) See, e.g., D. D. Fitts, "Non-Equilibrium Thermodynamics," McGraw-Hill, New York, N. Y., 1962.
- (4) H. S. Frank, *J. Phys. Chem.*, **67**, 1554 (1963). Shortly after this paper had appeared its author's attention was drawn to the earlier finding [C. H. Hale and T. DeVries, *J. Amer. Chem. Soc.*, **70**, 2473 (1948)] that abnormal behavior is observed when silver is made an anode in an aqueous tetraalkylammonium iodide solution. Potentiometric titration of  $\text{AgNO}_3$  into, say,  $0.1\text{ M Et}_4\text{NI}$  easily confirmed that the initial precipitate is white, somewhat flocculent, and of apparent composition  $\text{Et}_4\text{NAg}_2\text{I}_3$ . The yellow microcrystalline  $\text{AgI}$  appears only later after a break in the titration curve. This means that the  $\text{Ag}|\text{AgI}$  electrode can not be taken to be simply reversible to  $\text{I}^-$  in  $\text{R}_4\text{NI}$  solutions, so that the purported activity coefficients which were quoted in the present reference must be rejected. Developments in the mean time have, however, tended to confirm the usefulness of the concept of "structural salting in" and "salting out" introduced in that paper, as well as of the quantity there defined as "mean ionic activity deviation" as a tool in quantitative discussions, such as the present one, of single-ion activities and activity coefficients.
- (5) D. G. Miller, *J. Phys. Chem.*, **70**, 2639 (1966).
- (6) See, for example, D. A. MacInnes, "Principles of Electrochemistry," Dover Publications, New York, N. Y., 1961, pp 220-223.
- (7) In some modern work on polyelectrolyte solutions numbers are assigned to single-ion activities of either polyion or counterion [e.g., S. Lapanje, J. Haebig, H. T. Davis, and S. A. Rice, *J. Amer. Chem. Soc.*, **83**, 1590 (1961), or, more recently, M. M. Reddy, S. Amdur, and J. A. Marinsky, *ibid.*, **94**, 4087 (1972)] but these cases are simply new illustrations of the need to make extrathermodynamic assumptions to obtain estimates of single-ion quantities from thermodynamic measurements.
- (8) G. N. Lewis and L. W. Sargent, *J. Amer. Chem. Soc.*, **31**, 363 (1909).

anion) to which the electrodes are reversible. The fact that two salts are involved here meant that two additional formalisms had to be introduced to enable numbers to be arrived at for single-ion activities and for Onsager transport coefficients in the mixed electrolyte solutions of which the junction is made up. For the first of these (the activities) a self-consistent combination was worked out of Harned's rule<sup>9</sup> and the single-ion convention previously employed.<sup>2,4</sup> For the second, the transport coefficients, the assumption used is one of those tested by Miller,<sup>10</sup> designated by him the LN1 approximation. As will appear in what follows, the use of these conventions gives good results, and the calculated emf of a cell of type B is found, in several examples, to be within a few tenths of a millivolt of the measured value. It is indifferent, as with cells of type A, to the assumptions made regarding single-ion activity coefficients, and for a corresponding reason. The calculated emf of a type B cell does, however, depend upon the value used for the Harned's rule coefficient  $\alpha_{12}$  for MCl-NCl mixtures. It should thus be possible in principle to determine this coefficient by comparing the measured emf of the cell with the results of a series of calculations in which different  $\alpha_{12}$  values had been employed. In practice, however, this would require the calculated cell emf to be more sensitive than it is to changes in  $\alpha_{12}$ . That is, for this method to give an accuracy of 10% in a typical  $\alpha_{12}$  would require agreement between calculated and measured emf's to within a few microvolts (more than an order of magnitude better than we have been able to attain in cases where  $\alpha_{12}$  is known, and better also than the reproducibility to which our measured emf's can be counted on).

## II. Calculation

The electrostatic potential difference across the one-dimensional liquid junction, MCl:NCl, of cell B may be written<sup>1,2</sup>

$$E_J = \Phi_l - \Phi_0 = - \int_0^l dx_1 \int_0^{x_1} \frac{\rho(x)}{\epsilon} dx \quad (1)$$

where  $\Phi_x$  is the potential at  $x$ , and  $x$ , ranging from 0 to  $l$ , is the distance along the junction, values of 0 and  $l$  denoting positions in pure MCl and NCl solutions, respectively.  $\epsilon$  is the dielectric permittivity of the medium (see below) and  $\rho(x)$  is the distributed charge density in the junction and is given by

$$\rho(x) = \sum C_i(x) z_i = C_1(x) z_1 + C_2(x) z_2 + C_3(x) z_3 \quad (2)$$

where  $C_i(x)$  is the concentration of the ion  $i$  at  $x$ ,  $z_i$  is the valence, including sign, of ion  $i$ , and subscript 1 refers to  $M^+$ , 2 to  $N^+$ , and 3 to  $Cl^-$ .

Assuming that bulk flow can be neglected and choosing a solvent-fixed reference frame,<sup>5</sup> the variation with time of the concentration at  $x$  of ion  $i$  can be expressed as

$$\partial C_i / \partial t = - \partial J_i / \partial x \quad (3)$$

where  $J_i$  is the flux of ion  $i$ , given by<sup>5</sup>

$$J_i = \sum l_{ij} X_j \quad (4)$$

$X_j$  in eq 4 is the force acting on ion  $j$ , arising from gradients in chemical and electrostatic potentials, and the  $l_{ij}$  are the Onsager transport coefficients. More explicitly

$$X_j = - \frac{\partial \mu_j}{\partial x} - z_j F \frac{\partial \Phi}{\partial x} \quad (5)$$

where  $\mu_j$  is the chemical potential of an ion of type  $j$  and

$F$  is the Faraday, and

$$\begin{aligned} J_1 &= l_{11} X_1 + l_{12} X_2 + l_{13} X_3 \\ J_2 &= l_{21} X_1 + l_{22} X_2 + l_{23} X_3 \\ J_3 &= l_{31} X_1 + l_{32} X_2 + l_{33} X_3 \end{aligned} \quad (6)$$

Here also  $l_{ij} = l_{ji}$  by Onsager's reciprocity relation. For the present work, values of  $l_{ij}$  for pure solutions of KCl, HCl, NaCl, and LiCl, in the concentration ranges  $C = 0.005$ – $0.100$   $M$ , were taken from Miller's tables<sup>5</sup> and fitted to polynomial expressions in terms of concentration, for storage in the computer memory.

For mixtures such as those here of interest Miller<sup>10</sup> has tested several methods of formulating additivity rules for the  $l_{ij}$ . He found one such rule, which he designated the LN1 approximation, to give results which agreed well with experiment in the cases for which the necessary data were available to make the test, and it is the one chosen for use in the present study. By this means the computer was enabled to supply, within the composition ranges involved, any  $l_{ij}$  for a mixture of any total concentration, in which MX and NX were present in any ratio.

If, as is customary,<sup>6</sup>  $\mu_i$  is taken to equal  $\mu_i^\circ + RT \ln a_i$ , where  $\mu_i^\circ$  refers to a standard state (here a hypothetical molar solution) and  $a_i$  is  $C_i f_i$ ,  $f_i$  being the single-ion activity coefficient on the molar scale,<sup>2,11</sup> the gradient of the chemical potential of ion  $i$ ,  $\partial \mu_i / \partial x$ , can be written

$$\frac{\partial \mu_i}{\partial x} = RT \frac{\partial \ln C_i}{\partial x} + RT \frac{\partial \ln f_i}{\partial \bar{C}} \frac{\partial \bar{C}}{\partial x} \quad (7)$$

where  $\bar{C} = \frac{1}{2}(C_1 + C_2 + C_3)$ . The condition of electroneutrality can not be assumed to hold across the liquid junction;<sup>12</sup> therefore, in order to have numbers to use, the activity and transport coefficients at any  $x$  are assigned as though the solution were made up of  $C_1$  mole/liter of MCl and  $C_2$  mole/liter of NCl. The mean ionic activity coefficients of MCl and NCl in these mixed solution are then assumed to follow Harned's rule, *i.e.*, to be given by<sup>9,13</sup>

$$\begin{aligned} \log f_{\pm MCl} &= \log f_{\pm MCl}^\circ - \alpha_{12} C(1 - y) \\ \log f_{\pm NCl} &= \log f_{\pm NCl}^\circ - \alpha_{21} C y \end{aligned} \quad (8)$$

where the  $f^\circ$ 's refer to pure salt solutions at constant total

(9) See, *e.g.*, H. S. Harned and B. B. Owen, "The Physical Chemistry of Electrolyte Solutions," 3rd ed, Reinhold, New York, N. Y., 1958, pp 602 ff.

(10) D. G. Miller, *J. Phys. Chem.*, **71**, 616 (1967).

(11) In ref 2 the practice of Harned and Owen (ref 9) was followed, of using the letter  $y$  to refer to the activity coefficient defined on a molar (as opposed to molal) scale. Since we have used the letter  $y$  for a different purpose the letter  $l$  will be employed here for the molar activity coefficient (*cf.* ref 6).

(12) It is precisely because differential diffusion of ions within the junction produces local charge separations that the junction potential comes into being (*cf.* ref 1). In the regions thus produced where the condition of electroneutrality is not met it is, strictly, inappropriate to use thermodynamic or transport quantities which are defined for neutral systems. This does not, however, obviate the necessity of using such quantities in such regions as input if the attempt is to be made to calculate the junction potential by the computer simulation method here employed. The present calculations, therefore, as well as those of ref 1 and 2, are subject to an unavoidable logical inconsistency on this score. It will be concluded later in the text that the magnitude of the numerical error which this introduces into the final results is too small to vitiate their acceptability, but the formal inconsistency in principle remains.

(13) Another formal inaccuracy is introduced into eq 8 and 9 by using concentrations in them instead of the molalities in terms of which (8) was postulated and (3) derived. At constant total concentrations of 0.1  $M$  or less, however, the errors so produced seem certain to be very small. So, in most cases, do those produced by neglect of possible departures from linearity in Harned's rule (*i.e.*, the quadratic terms that are needed in stronger, or less "simple" solutions).

concentration  $C$ , and  $y$  (a function of  $x$ ) is the "quasi-mole fraction" of MCl in the salt mixture and is defined as  $C_1/(C_1 + C_2)$ , i.e., the concentration, or quasiconcentration, of MCl is  $Cy$ .  $\alpha_{12}$  and  $\alpha_{21}$  are the Harned's rule coefficients. The activity coefficients of KCl (0.005–0.20  $M$ ) are taken from Shedlovsky and MacInnes;<sup>14</sup> of HCl (0.001–0.10  $M$ ) from Bates and Bower;<sup>15</sup> of NaCl (0.005–0.10  $M$ ) from Brown and MacInnes;<sup>16</sup> and of LiCl (0.004–0.10  $M$ ) as recalculated from Scatchard's data.<sup>17</sup> These quantities are also stored in the computer in the form of polynomials in terms of concentration. Combining Harned's rule and the Gibbs-Duhem equation gives a relation between  $\alpha_{12}$  and  $\alpha_{21}$ , namely<sup>9,13</sup>

$$\alpha_{12} = \alpha_{21} + \frac{2}{2.303C}(\phi_{\text{NCl}^\circ} - \phi_{\text{MCl}^\circ}) \quad (9)$$

where  $\phi_{\text{MCl}^\circ}$  and  $\phi_{\text{NCl}^\circ}$  are the osmotic coefficients of the pure salts at concentration  $C$ . Osmotic coefficients of KCl, HCl, NaCl, and LiCl at  $C = 0.10 M$ , 0.927, 0.943, 0.932, and 0.939, respectively, are taken from the tables of Robinson and Stokes.<sup>18</sup>  $\alpha_{12}$ 's for the pairs HCl:KCl, KCl:NaCl, KCl:LiCl, all at  $C = 0.10 M$ , were taken from Harned and Owen,<sup>9</sup> Robinson,<sup>19</sup> and Robinson and Lim,<sup>20</sup> and equal 0.077,  $-0.016$ , and  $-0.041$ , respectively.

### III. Harned's Rule for Single Ions

In order to obtain the numerical values for  $f_i$  required in eq 7, the concept of the mean ionic activity deviation,<sup>4</sup>  $\delta_{\pm}$ , is introduced into the calculation. This is the ratio of the (appropriately weighted) single-ion activity coefficients of the cation and anion in solutions of a single salt,  $\delta_{\pm} = (f_+^{\nu_+}/f_-^{\nu_-})^{1/\nu}$ , so that

$$\nu \ln \delta_{\pm} = \nu_+ \ln f_+ - \nu_- \ln f_- \quad (10)$$

the  $\nu$ 's being ion numbers per formula of salt.  $\delta_{\pm}$  supplements the mean ionic activity coefficient,  $f_{\pm} = (f_+^{\nu_+}f_-^{\nu_-})^{1/\nu}$ , in such sense that the single-ion activities of a salt in solution are conveniently expressed in terms of its  $f_{\pm}$  and  $\delta_{\pm}$  values. In the 1-1 cases here considered

$$\begin{aligned} \ln f_+ &= \ln f_{\pm} + \ln \delta_{\pm} \\ \ln f_- &= \ln f_{\pm} - \ln \delta_{\pm} \end{aligned} \quad (11)$$

Assumptions regarding the single-ion activity coefficients in any pure salt solution can therefore be made in the form of assumptions regarding its  $\delta_{\pm}$ , since its  $f_{\pm}$  values are or can be known.

The assumption here made for the relation between  $\delta_{\pm}$  and  $C$  in a pure salt solution is, as before<sup>2</sup>

$$\begin{aligned} \ln \delta_{\pm\text{MCl}}^\circ &= B_{\text{MCl}}C \\ \ln \delta_{\pm\text{NCl}}^\circ &= B_{\text{NCl}}C \end{aligned} \quad (12)$$

so that assumed values of the  $B$ 's make it possible to compute the  $\delta^\circ$ 's for the pure solutions of any given concentrations.

In mixed solutions, a new assumption regarding  $\delta_{\pm}$  is introduced, namely, that it obeys an analog of Harned's rule for  $f_{\pm}$ , in which equations of the form (8) are written with coefficients  $\beta$  corresponding to the Harned's rule  $\alpha$ 's. That is, we adopt the convention

$$\begin{aligned} \log \delta_{\pm\text{MCl}} &= \log \delta_{\pm\text{MCl}}^\circ - \beta_{12}C(1 - y) \\ \log \delta_{\pm\text{MCl}} &= \log \delta_{\pm\text{NCl}}^\circ - \beta_{21}Cy \end{aligned} \quad (13)$$

Upon the eq 8, 11, 12, and 13, a self-consistency requirement can be imposed, that  $f_{\text{Cl}}$  in the mixture be the same

when derived from MCl as when obtained from NCl. For this to be true it is easy to show that the  $\beta$ 's must be connected to the  $\alpha$ 's by the relations

$$\alpha_{12} + \alpha_{21} = \beta_{12} + \beta_{21} \quad (14)$$

and

$$\alpha_{12} - \beta_{12} = \frac{1}{2}[\log(f_{\pm\text{MCl}}^\circ/f_{\pm\text{NCl}}^\circ) - \log(\delta_{\pm\text{MCl}}^\circ/\delta_{\pm\text{NCl}}^\circ)] \quad (15)$$

Thus, for given experimental values of activity and osmotic coefficients, assumed values of  $B$  parameters for the pure salt solutions, and known Harned's rule  $\alpha$ 's for the mixtures in question,  $\beta$ 's can be computed from eq 14 and 15,  $f_i$  can be obtained from eq 8, 13, and 11, and the corresponding  $\partial\mu_i/\partial x$  from eq 7, numerical values for the properties of the pure salts being assigned in accordance with the quasineutrality procedure described above.

The computer simulation method used here was essentially the same as the one described in the previous papers.<sup>1,2</sup> The junction is treated as infinite and uniform in the  $y$  and  $z$  directions, so that all variations take place along the  $x$  axis, and no edge effects are considered. For purposes of digital computation distance in the  $x$  direction is divided into numbered cells of equal thickness  $d$ , within which the concentrations  $C_i$  and the potentials  $\Phi$  and  $\mu_i$  are taken as constant. Except where otherwise noted, the cell thickness  $d$  employed in this paper is the same as was used in ref 2, namely,  $1 \times 10^{-9}$  m.<sup>21</sup> The calculation of derivatives and of integrals was, as in that paper, performed as described by Hafemann.<sup>1</sup> The calculations were carried out in part on a CDC 1604 computer in Mellon Institute of Science of Carnegie-Mellon University and in part on IBM 360/50 and DEC system-1055 computers of the Computer Center of the University of Pittsburgh.

In carrying out the calculation of an  $E_J$  value, an assumed initial concentration profile of the neutral salts across the junction is used to compute the gradients of the  $\mu_i(x)$ , and, from these and the  $l_{ij}$ , the initial motions of the ions are calculated. After these motions have proceeded for a time interval  $\Delta t$ , which was  $10^{-10}$  sec unless otherwise noted, stock is taken of the new ionic composition profiles,  $C_i(x)$ , which have been produced, from which a gradient in  $\phi(x)$  and new gradients in the  $\mu_i(x)$  are computed. These, with the appropriate new  $l_{ij}$ , give rise to a new set of fluxes  $J_i(x)$ , resulting, after another  $\Delta t$  in a third set of  $C_i(x)$ . This process is repeated until quasi-steady-state profiles are approached, and the calculated electrostatic potential across the junction,  $E_J = \Phi_l - \Phi_0$ , begins to level off. By this time  $E_J(t)$  is observed to vary linearly with respect to  $1/t^3$ , as had been found in ref 2. This usually requires about 100 iterations. The steady-state potential is taken as that given by the linear extrapolation of  $E_J$  to  $1/t^3 = 0$ . The extrapolation customarily involves a further growth in (the absolute value of)  $E_J$  no

(14) T. Shedlovsky and D. A. MacInnes, *J. Amer. Chem. Soc.*, **59**, 503 (1937).

(15) R. G. Bates and V. E. Bower, *J. Res. Nat. Bur. Stand.*, **53**, 283 (1954).

(16) A. S. Brown and D. A. MacInnes, *J. Amer. Chem. Soc.*, **57**, 1356 (1935).

(17) P. T. Thompson, Ph.D. Thesis, University of Pittsburgh, 1956.

(18) R. G. Robinson and R. H. Stokes, "Electrolyte Solutions," Butterworths, London, 1959, pp 483 and 484.

(19) R. A. Robinson, *J. Phys. Chem.*, **65**, 662 (1961).

(20) R. A. Robinson and C. K. Lim, *Trans. Faraday Soc.*, **49**, 1144 (1953).

(21) By an unfortunate oversight the statement appears on p 1760 of ref 2 that the length increment used in that work was  $10^{-10}$  m. The length actually used was  $10^{-9}$  m.



larger than a few hundredths of a millivolt. Figure 1 shows the computed concentration profiles for the ions  $H^+$ ,  $K^+$ , and  $Cl^-$  in the HCl:KCl cell where  $C = 0.10 M$ ,  $B_{HCl} = 1.023$ ,  $B_{KCl} = 0$ , and the number of iterations was 100. These curves will be seen to be qualitatively similar to the ones derived earlier by Taylor,<sup>22</sup> using the less powerful methods which were available when he worked, and to a corresponding set for the KCl:NaCl junction given in ref 1. It is interesting that the similarity between the profiles displayed in Figure 1 and those published by Hafemann extends to the occurrence, in both sets, of step-wise and partly retrograde (zig-zag) dependences of concentration upon the distance  $x$ . This is, of course, an artifact of the simulation and is presumably related both to the early stage of approach to a steady state (for this purpose, 100 iterations is a small number) and to the particular combination of  $d$  and  $\Delta t$  employed. The dependence of our results on these parameters is discussed below.

#### IV. Results and Discussion

The cell potential of the Lewis and Sargent cell  $B$  is given by<sup>6</sup>

$$E_B = RT \ln \frac{a_{Cl^-(MCl)}}{a_{Cl^-(NCl)}} + E_{JB} \quad (16)$$

which, by use of eq 11 and 12, may be rewritten

$$E_B = \frac{RT}{F} \ln \frac{f_{\pm(MCl)}}{f_{\pm(NCl)}} + \frac{RT}{F} (B_{NCl} - B_{MCl})C + E_{JB} \quad (17)$$

For any set of assumed values of the  $B$ 's therefore, not only  $E_{JB}$ , but  $E_B$  itself, may be calculated, using once more the tabulated values of the  $f_{\pm}$  (see above). When this is done for three solution pairs, HCl:KCl, KCl:NaCl, and KCl:LiCl, all at 0.1  $M$ , results are obtained which are presented in Table I. Here again as in ref 2, it is seen that while the calculated  $E_J$  values are, as they should be, dependent upon the choices of the  $B$ 's, this dependence is no longer present in  $E_B$  itself, the spread in the latter being no greater than 0.029, 0.014, and 0.004 mV, respectively, as compared with spreads of 5.283, 1.541, and 1.542 mV in the  $E_J$ 's for the particular range of  $B$ 's tested. This means, as will be seen below, that the  $E_B$  are constant, well within the limits to be expected considering the possible uncertainties in input data.

This constancy can be accounted for in the same way as in the simpler case studied by Goldberg.<sup>2</sup> In the present instance the fundamental thermodynamic equation for the junction is<sup>6</sup>

$$dE_{JB} = \frac{RT}{F} [t_{M^+} d \ln a_{M^+} + t_{N^+} d \ln a_{N^+} - t_{Cl^-} d \ln a_{Cl^-}] \quad (18)$$

which, using the conservation condition  $t_{M^+} + t_{N^+} + t_{Cl^-} = 1$ , integrates to

$$E_{JB} = \frac{RT}{F} \left[ \ln \frac{a_{Cl^-(NCl)}}{a_{Cl^-(MCl)}} - 2 \int_{MCl}^{NCl} t_{M^+} d \ln a_{\pm(MCl)} - 2 \int_{MCl}^{NCl} t_{N^+} d \ln a_{\pm(NCl)} \right] \quad (19)$$

so that, again, when the over-all cell potential is computed, using eq 16, the terms which contain the single-ion activity ratio (*i.e.*, depend on the assumed  $B$ 's) cancel out, and  $E_B$  is incapable of being used to obtain information about single-ion properties. That this cancellation should

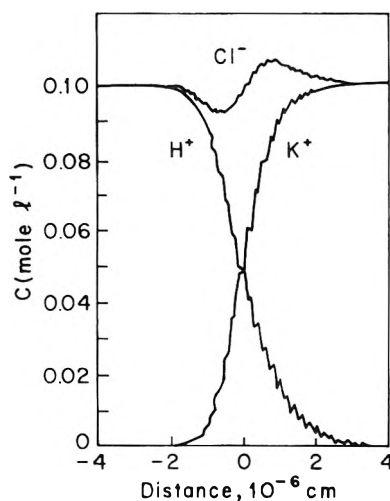


Figure 1. Computed profiles, after  $10^{-8}$  sec (100 iterations), of ionic concentrations across the Lewis and Sargent junction HCl:KCl at  $C = 0.10 M$ ,  $B_1 = 1.023$ , and  $B_2 = 0$ . For discussion of charge separation in this junction and of oscillations in the curves, see text.

be so accurately reflected in the machine calculation, in spite of the ostensibly very different logical content of the latter, again<sup>2</sup> speaks well both for the appropriateness of the formalisms employed and for the accuracy of the numbers in Miller's tables.<sup>5,10</sup>

Another compensation phenomenon which was observed in the work of both ref 1 and 2 also occurs here, namely, a lack of effect upon  $E_J$  of changing the assumed value of the dielectric permittivity of the solution. In the present work the value used was that corresponding to the dielectric constant of water at 25°, but several test runs were also made in which the permittivity was halved or doubled without making any detectable difference in the extrapolated steady-state value of  $E_J$ . In the latter cases, however, changes did appear in its time rise, as had been observed and remarked upon in ref 1. The whole subject of dielectric permittivity in cells such as these remains, in any case, somewhat obscure.<sup>23</sup>

In contrast to  $\epsilon$  and the  $B$ 's,  $\alpha_{12}$  and the  $l_{ij}$  are quantities of which changes in the input values do produce changes in the calculated value of  $E_B$ . How sensitive the latter is to variations in these quantities was studied by subjecting some of their accepted values to arbitrary alterations and observing the results. These are recorded in Table II for changes in two  $l_{11}$ 's and in Table III, for changes in three  $\alpha_{12}$ 's. It will be seen that, in the cases studied, a change of 0.1 mV in the calculated  $E_B$  is produced by a change of the order of 1% in an  $l_{11}$  or by a change of about 0.1 unit in an  $\alpha_{12}$ .

In order to know what an uncertainty of 0.1 mV in a calculated  $E_B$  means in practical terms it is necessary to consider how accurately a measured value of this quantity can be known. This question has recently been discussed,<sup>24</sup> and experimental values presented for five Lewis and Sargent junctions, including the three on which calculations are reported in the present study. From those experiments it appears that a measured emf of this type can be reproduced to a few hundredths (in favorable cases less than one hundredth) of a millivolt. Assuming that

(22) P. B. Taylor, *J. Phys. Chem.*, **31**, 1478 (1927).

(23) See footnote 17 of ref 2.

(24) C. H. Chen, *J. Chem. Eng. Data*, **17**, 473 (1972).

TABLE I: Results of Computer Simulation Calculation of Lewis and Sargent Cells at  $C = 0.10 M$  for Different Assumed Values of  $B$

Cell	Assumed $B$ 's		Calculated potentials, mV		Measured cell <sup>a</sup> emf, mV, $E_B$
	$B_1$	$B_2$	$E_J$	$E_B$	
HCl:KCl $\alpha_{12} = 0.077$	-1.023	0	25.512	28.991	
	0	0	28.154	29.006	
	0.230	0	28.749	29.009	
	1.023	0	30.795	29.020	
	0	1.023	25.512	28.991	
	0	0.230	27.559	28.998	
	0	-1.023	30.795	29.020	
				Av $E_B = 29.005$	28.545
KCl:NaCl $\alpha_{12} = -0.016$	0	0	4.984	4.677	
	0	0.170	4.547	4.677	
	0	0.300	4.213	4.674	
	0.022	0.160	4.629	4.676	
	-0.300	0.079	4.022	4.684	
	0.300	0.079	5.563	4.688	
	0.022	0.079	4.847	4.682	
				Av $E_B = 4.679$	4.585
KCl:LiCl $\alpha_{12} = -0.041$	0	-0.30	8.060	7.315	
	0	0	7.288	7.312	
	0	0.110	7.004	7.311	
	0	0.30	6.518	7.311	

<sup>a</sup> Measured cell emf's from ref 24.

TABLE II: Effect of Changes in Assumed  $I_{ij}$  on Calculated  $E_J$  at  $C = 0.10 M$

Cell	Assumed $B_1$	Assumed $B_2$	Assumption regarding $I_{ij}$	$E_{J(\text{calcd})}$ , mV
HCl:KCl $\alpha_{12} = 0.077$	0	0.022	a	27.979
	0	0.022	b	30.082
	1.023	0.022	a	30.620
	1.023	0.022	b	32.722
	-1.023	0.022	a	25.346
KCl:NaCl $\alpha_{12} = -0.016$	-1.023	0.022	b	27.443
	0.022	0.160	a	4.629
	0.022	0.160	c	4.525
	0.022	0.160	d	4.402

<sup>a</sup> Miller's values. <sup>b</sup> Miller's values but with  $I_{H-H}$  increased by 10%. <sup>c</sup> Miller's values but with  $I_{Na-Na}$  increased by 1%. <sup>d</sup> Miller's values but with  $I_{Na-Na}$  increased by 2%.

TABLE III: Sensitivity of  $E_B$  to Assumed Value of  $\alpha_{12}$  at  $C = 0.10 M$  and at Fixed Values of  $B_1$  and  $B_2$ <sup>a</sup>

Cell	$\alpha_{12}$	$E_{J(\text{calcd})}$	$E_{B(\text{calcd})}$	$\Delta E_B$	$\Delta \alpha_{12}$	$\Delta E_B / \Delta \alpha_{12}$
HCl:KCl $B_1 = 0.230; B_2 = 0$	0.577	31.199	31.459	-2.450	-0.500	4.90
	0.077	28.749	29.009	-0.750	-0.154	4.87
	-0.077	27.999	28.259	-2.409	-0.500	4.82
	-0.577	25.590	25.850			
KCl:NaCl $B_1 = 0; B_2 = 0$	0.014	5.013	4.706	-0.029	-0.030	0.967
	-0.016	4.984	4.677	-0.054	-0.055	0.982
	-0.071	4.930	4.623	-0.028	-0.030	0.933
	-0.101	4.902	4.595			
$B_1 = 0.022; B_2 = 0.160$	0.014	4.656	4.703	-0.027	-0.030	0.900
	-0.016	4.629	4.676	-0.055	-0.055	1.000
	-0.071	4.574	4.621	-0.028	-0.030	0.933
	-0.101	4.546	4.593			
KCl:LiCl $B_1 = 0; B_2 = 0$	0.541	8.183	8.207	-0.395	-0.581	1.54
	-0.041	7.288	7.312	-0.720	-0.499	1.44
	-0.540	6.548	6.572			

<sup>a</sup>  $E$ 's in mV.

there are no systematic errors in the experiments, this means that it would be worthwhile to be able, if possible, to account for calculated  $E_B$  values to an accuracy corresponding to a few tenths of a per cent in the  $l_{ii}$  and a few hundredths of a unit in the  $\alpha_{12}$  values used in the calculations.

In the case of the  $\alpha_{12}$ 's, it seems almost certain that the values here employed do come up to this standard since the accepted values of these  $\alpha_{12}$ 's do not exceed 0.1 in absolute magnitude. For the  $l_{ii}$  the required accuracy seems at first glance rather more difficult to count on when one considers the simplicity of the assumptions upon which they were obtained. On the other hand, inspection of Table I makes the  $l_{ij}$  look very good, in the light of the fact that changing the assumed value of a  $B$  changes the weightings with which the various  $l_{ij}$  and activity coefficients enter into the calculation. That under these circumstances changes in  $B$ 's produce such small changes in the calculated  $E_B$ 's must be regarded as noteworthy. It is all the more so when considered in the light of the discrepancies between the calculated  $E_B$ 's and the experimental emf's. These are also shown in Table I and are seen to amount, for the cells HCl:KCl, KCl:NaCl, and KCl:LiCl, to 0.460, 0.094, and 0.175 mV, respectively, and thus to fall well outside the limits discussed above. The question of the source of these disagreements thus invites further attention.

One possibility is that the discrepancies result from the presence of some systematic error in the measured  $E_B$  but we are inclined, at least tentatively, to reject this explanation on two grounds. First, the same cell, with similarly prepared electrodes and a junction formed in the same way, has been used to make emf measurements on concentration cells with transference, with successful results.<sup>25-27</sup> In one case where these measurements were on a system for which high-quality literature values were available, namely, with dilute KCl solutions,<sup>14</sup> the agreement with the latter was much better than within 0.10 mV.

The second reason for not as yet finding it necessary to blame the measured emf's for the discrepancies is that scrutiny of our computer simulation procedure reveals some possible alternative causes. Among the several logical loopholes through which errors may in principle be able to enter the following seem worthy of mention.

(1) The use, remarked upon above, of literature values of  $\alpha_{12}$  and  $\alpha_{21}$  which had been measured in (or computed for) mixtures of constant total molality (molarity) whereas here, as Figure 1 illustrates, the total molarity at various positions in the junction is sometimes higher and sometimes lower than the constant value of 0.1  $M$  prevailing in the end solutions.<sup>28</sup>

(2) The failure of electroneutrality in certain regions across the junction and the consequent failure of the effective activity or transport coefficients in these regions to correspond in definition to the quantities employed as input data in the calculation.

(3) The somewhat casual use of an assumed empirical  $1/t^3$  law for extrapolation from computer runs that represent extremely short intervals in real time.

(4) The ignoring of the possibility that the choice of the time interval,  $\Delta t$ , and/or of the length interval,  $d$ , might not be optimal.

Of these possible sources of error, the first seems unlikely to be serious in practice. Not only, as mentioned above, is the difference between molality and molarity

very small at these low concentrations of the substances in question, but these are also substances which form mixtures in which the importance of the nonlinear terms in the generalized Harned's rule is known to be small.<sup>9,29</sup> Related to the latter fact<sup>9,29</sup> is the slow variation with total molality which  $\alpha_{12}$  and  $\alpha_{21}$  display in these mixtures, so that the departures from constant molarity across the junction would also be expected to have only a trivial effect on the accuracy of the present calculation even if they did not tend to be ironed out as the steady state is approached (see below). The same is true *a fortiori* of the very small variations in molarity which must in principle be present as a result of the small volume changes on mixing which these solutions display.<sup>30</sup>

The failure of electroneutrality raises more interesting questions, for we find, in agreement with Hafemann, that under certain conditions it can be sizeable in magnitude. In Figure 1, for instance  $C_{Cl^-}$ , at the point where it is a minimum (0.09209  $M$ ) is about 2% higher than the sum of  $C_{H^+}$  and  $C_{K^+}$ , and where it is a maximum (0.10605  $M$ ), it is about 1% less than the total concentration of positive ions. These are large enough amounts of excess charge that, if they persisted in time, they might, at least logically, be sources of worry. It will be remembered, however, that the configuration of Figure 1 is that calculated as existing instantaneously after 100 iterations, *i.e.*, at a time only  $1 \times 10^{-8}$  sec after the junction had been formed. And Hafemann has shown,<sup>1</sup> in a comparable example, that the excesses and deficiencies of  $Cl^-$  (in comparison with the "constant" concentration and with the concentration of positive charge) change very rapidly in this time regime, drifting apart in position and decaying in amount, so that long before a measurement could be made on the cell all local departures from electroneutrality and from constancy of total concentration will have become completely negligible.<sup>1</sup> If it could be assumed, therefore, that a good extrapolation could be made, *i.e.*, one which accurately reproduced the changes in  $E_j$  between the 100 iterations of our machine runs and the steady state,<sup>31</sup> no further separate attention would need to be given to the electroneutrality question.

Unfortunately, although the  $1/t^3$  extrapolation, which we borrowed from Goldberg,<sup>2</sup> was adequate for his requirements, it loses much of its attractiveness for the

(25) R. E. Verrall, to be submitted for publication.

(26) J. Paul Rupert, Ph.D. Thesis, University of Pittsburgh, 1969.

(27) J. C. Ku, Ph.D. Thesis, University of Pittsburgh, 1971.

(28) Along this same line, the conventions by which  $\delta_{\pm}$  was introduced and assumed to vary with composition in a mixed solution could also, in principle, produce errors in the gradients of chemical potential. It seems likely, however, that if they did these would be gross errors, rather than the small ones that we are here trying to trace down. Still other logically possible sources of error in this connection are the data used for activity coefficients of pure salts. These are, however, among the best activity coefficient data that exist, and it is highly likely that their absolute values are in error by less than 0.001 in  $\log f_{\pm}$  at 0.1  $M$ , and that corresponding accuracy can be claimed for  $\partial \ln f_{\pm} / \partial C$ . (The LiCl data may not quite come up to this standard, but the cell containing LiCl is not the one which shows the largest "error.")

(29) See, for example, H. S. Harned and R. A. Robinson, "Multicomponent Electrolyte Solutions," Pergamon Press, Oxford, 1969, p 35.

(30) See, for example, T. F. Young and M. B. Smith, *J. Phys. Chem.*, **58**, 716 (1954). This reference also gives data on the heat effect which accompanies the mixing of KCl and NaCl solutions. Here is another general phenomenon [T. F. Young, Y. C. Wu, and A. A. Krawetz, *Disc. Faraday Soc.*, **24**, 37 (1957)] which could in principle cause the true junction to differ from the simulated junction of our calculation which is, since no provision is made for anything different, strictly isothermal. In the steady state, however, it would seem that the rate at which heat is generated or absorbed in the real junction must be small compared with the rate at which the thermostat carries it off or supplies it.

present purpose when examined from the standpoint of the last item in the above list of logical loopholes, namely, the question of optimal values of  $\Delta t$  and of  $d$ . Our attempt to study this question was empirical,<sup>32</sup> and consisted of making runs with various  $\Delta t$ 's while holding  $d$  constant, and with various  $d$ 's while holding  $\Delta t$  constant, in the hope that somewhere in the  $d, \Delta t$  plane a region could be found within which the calculated  $E_J$  would be independent of changes in these variables. For the HCl:KCl cell at 0.10  $M$ , with  $B_1 = 1.023$  and  $B_2 = 0$ , there is some indication that when  $d = 1.3 \times 10^{-9}$  m,  $E_J$  is nearly constant at 30.81 mV, between the limits of  $2 \times 10^{-11}$  and  $1.6 \times 10^{-10}$  sec in  $\Delta t$ , but this whole study turned out to be unsatisfactory in an important respect. In order to be able to make as many runs as we needed to cover the field adequately, we had to restrict each run to 100 iterations, and this meant using the  $1/t^3$  extrapolation for each  $d, \Delta t$  point. In this process, however, we found two new and undesirable features, which had not appeared while  $\Delta t$  and  $d$  were kept at the values ( $1 \times 10^{-10}$  sec;  $1 \times 10^{-9}$  m) which we had borrowed from Goldberg,<sup>2</sup> and he, in turn from Hafemann.<sup>32</sup> First, the extrapolation in the general case sometimes was to higher and sometimes to lower absolute values of  $E_J$  (this confirms another of Hafemann's findings<sup>1</sup>), and second, the amount of the extrapolation "correction" was no longer always small. These shortcomings in the extrapolation procedure seem to us to mean that another study, involving a large number of runs, each to a large number of iterations (perhaps 1000?) will be necessary before the question of optimal choice of  $\Delta t$  and  $d$  values can be settled, and therefore before it will be possible to say whether such a choice (if one can be identified) would yield computed  $E_B$  values which agree with measured ones within the accuracy attainable in the latter. We would be greatly interested to see the results of such a study but are not at present prepared to undertake it.

A few longer runs have, however, been made with the standard values of  $\Delta t = 1 \times 10^{-10}$  sec and  $d = 1 \times 10^{-9}$  m, and it was verified that under these conditions the  $1/t^3$  plot does indeed give a good extrapolation. It thus appears that it is only when the highest absolute accuracy in a calculated  $E_B$  is in question that doubts need be felt either about the choices of  $\Delta t$  and of  $d$  or about the extrapolation. When, instead, the question is one of relative accuracy, as in the studies reported in Tables I, II, and III, of the effects of changing  $B, l_{ii}$ , and  $\alpha_{12}$ , the methods used in the present work seem to be satisfactory, and we therefore consider that the results reported and discussed above are, at least provisionally, reliable.

Returning, finally, to the question raised in the Introduction of using such calculations as these to determine  $\alpha_{12}$ , it is necessary to answer this in the negative. Even if the calculated  $E_B$  could be made as accurate as desired,

the uncertainty in our best measured  $E_B$  values still corresponds to uncertainties, in the simple cases here studied, that are large fractions of the  $\alpha_{12}$ 's themselves. And although there are cases, e.g., mixtures of tetraalkylammonium halides with alkali halides, where the  $\alpha_{12}$ 's seem to be large enough to circumvent this difficulty,<sup>33</sup> these are also cases where the simple form of Harned's rule can no longer be expected to hold (i.e., the change in  $\log \gamma_{\pm}$  is presumably no longer linear in  $y$  and for such mixtures an acceptable formalism for dependence of  $\log \delta_{\pm}$  on  $y$  has yet to be developed.

*Acknowledgment.* Grateful acknowledgment is made of the support of this work by the Office of Saline Water, U. S. Department of the Interior.

- (31) The term "steady state" as used here refers to the period of several hours during which, experimentally, the emf of a "good" cell is constant except for random fluctuations of a few microvolts amplitude (cf. ref 24). The permanently steady state would not be reached, of course, until the solution throughout the cell had come to be of uniform composition, and the cell emf was therefore identically zero.
- (32) This interval question is discussed by Hafemann (ref 1), who gives a prescription based in part on theoretical considerations and in part (we assume) on practical convenience and the acceptability of the results to which it led. The theoretical argument that "the ratio  $\Delta t/d^2$  must be such that  $d$  is approximately equal to the root-mean-square distance a molecule travels in a time  $\Delta t$ ," and that "for diffusion of uncharged species  $\Delta t/d^2 = 0(D^{-1})$ " ( $D$  = diffusion coefficient) leads, taking account of the fact that the effective diffusion coefficient of an ion will also be influenced by the charge distribution, to a choice of  $1 \times 10^4$  sec  $\text{cm}^{-2}$  as the optimum value for the ratio  $\Delta t/d^2$ .  $\Delta t = 10^{-10}$  sec was chosen as "short compared with the rise-time of  $E_J$ ," but not so short as to require an unreasonably large amount of computing time to get a sufficient number of iterations. Hafemann seems also to have experimented with other values of  $\Delta t/d^2$  for he concludes "If  $\Delta t/d^2$  is too large the calculation will be unstable and lead to meaningless results." An example of what he seems to mean by a meaningless result is shown in his Figure 4 where, for a very low dielectric constant ( $\epsilon$  19.53), the time-rise curve of  $E_J$  overshoots its steady-state value and approaches it from above. This behavior is ascribed to  $\Delta t/d^2$  being too large in this case.
- In our view, the use of the ratio  $\Delta t/d^2$  implies the invoking of the distance-time relationship which characterizes the "random walk" nature of diffusive motion [see, for example, S. Chandrasekhar, *Rev. Mod. Phys.*, **15** 1 (1943)] and is inconsistent with the use of the Onsager formalism, which is written in terms of ion fluxes based on "conductive" behavior [Hafemann's eq 9; our eq 4 and 6]. The latter presupposes a continuum model of sorts, in which an ion is pulled smoothly forward so as to describe a motion which is represented as uniform and rectilinear under the influence of a force which, during the interval  $\Delta t$ , is treated as constant in magnitude and direction. For the next  $\Delta t$ , moreover, each force is still in the same direction as before and differs predictably in magnitude producing, therefore, a new displacement which is continuous with the previous one in direction and differs from it in length in the exact ratio of the magnitudes of the forces at work in the two time intervals. Under these circumstances an appropriate ratio would be  $\Delta t/d$  rather than  $\Delta t/d^2$ . That " $\Delta t/d$  motion" does not describe the details of what individual ions actually do in a real solution may legitimately raise questions about the applicability of the formalism, but not about the relationship to each other of features within the model. In this sense the use of the ratio  $\Delta t/d^2$  must be considered logically foreign to the theory of this computer simulation, and the success that Hafemann achieved while keeping it constant would seem to be the result of felicitous empirical experimentation.
- (33) This inference follows from the comparatively large values of free energies of mixing reported for these systems by W. Y. Wen, K. Miyajima, and A. Otsuka, *J. Phys. Chem.*, **75**, 2148 (1971).

## Kinetic Studies of Permanganate Oxidation Reactions. IV. Reaction with Bromide Ion

Samuel A. Lawani<sup>1</sup> and John R. Sutter\*

Department of Chemistry, Howard University, Washington, D. C. 20001 (Received January 29, 1973)

The kinetics of the permanganate-bromide redox reaction has been studied in acid medium at 25.1° using a stopped-flow spectrophotometer. The disappearance of permanganate,  $\text{MnO}_4^- + 5\text{Br}^- + 8\text{H}^+ \rightarrow \text{Mn}^{2+} + \frac{5}{2}\text{Br}_2 + 4\text{H}_2\text{O}$ , was followed at 520 nm and the production of  $\text{Br}_3^-$ ,  $\text{Br}_2 + \text{Br}^- \rightleftharpoons \text{Br}_3^-$  ( $K$ ), was monitored at 267 nm. It was found that the observed absorbance,  $D$ , can be represented at either wavelength by the equation  $(D - D_\infty) = B \exp(-\lambda_3 t) \pm A \exp(-\lambda_2 t)$ . The positive sign applies to kinetics performed at high excess of bromide ion or hydrogen ion concentration. Plots of  $\log(D - D_\infty)$  vs. time become first order, being curved at the beginning of the reaction concave up. The negative sign applies at lower excesses, where first-order linearity develops from a concave down beginning. A mechanism consistent with the data is  $\text{H}^+ + \text{Br}^- + \text{MnO}_4^- \rightleftharpoons (\text{HO}_3\text{MnOBr})^-$  ( $k_1; k_{-1}$ ),  $(\text{HO}_3\text{MnOBr})^- + \text{H}_3\text{O}^+ \rightarrow \text{HOBr} + \text{H}_3\text{MnO}_4$  ( $k_2$ ),  $(\text{HO}_3\text{MnOBr})^- + \text{H}_2\text{O} \rightarrow \text{HOBr} + \text{H}_2\text{MnO}_4^-$  ( $k_3$ ). The enthalpy and entropy values obtained from the temperature dependence of  $k_1$  are  $\Delta H_1^* = 6.2 \pm 0.6$  kcal/mol and  $\Delta S_1^* = -29.7 \pm 2.2$  eu, respectively;  $k_2$  seems to be very nearly temperature independent.

## Introduction

The reaction between permanganate and bromide ion affords further opportunity to study permanganate reactions and in particular to compare the results with those of the iodide system previously reported.<sup>2</sup> A kinetic path involving a permanganate to manganate transformation through a reaction with bromide ion to form either  $\text{Br}_2$  or  $\text{HOBr}$  as a first step in the overall five equivalent reduction is thermodynamically forbidden. The reaction is, however, fairly fast and involves protons in such a way as to give rise to a set of coupled pseudo-first-order reactions in a mechanism involving a 2-equiv reduction of  $\text{Mn(VII)}$  to  $\text{Mn(V)}$ .

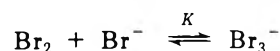
## Experimental Section

The Baker Analyzed reagent grade potassium permanganate used was handled as previously described.<sup>2,3</sup> The extinction coefficients found for permanganate were  $2234 \pm 9$  and  $483 \pm 3 \text{ M}^{-1} \text{ cm}^{-1}$  at 520 and 267 nm, respectively. Baker Analyzed reagent grade potassium bromide was used as the reducing agent while potassium sulfate from the same source was used to control the ionic strength. Both reagents were recrystallized three times in distilled water, dried at 110° for 4 days, and kept in a desiccator above silica gel. The Baker Analyzed reagent grade sulfuric acid used was standardized with sodium hydroxide of known concentration.

The following procedure was followed to determine the extinction coefficients of bromine and tribromide ion, which are two of the final products of the reaction.

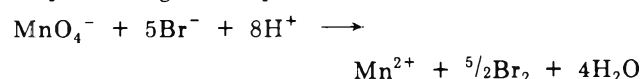
Five different concentrations of bromine in 0.5 M sulfuric acid were prepared, and the absorbances taken on a standard Beckman DU spectrophotometer at 400, 267, and 520 nm, the wavelengths for bromine, tribromide ion, and permanganate ion, respectively. The concentration of bromine in the solutions was calculated using the extinctions coefficients for  $\text{Br}_2$  at 400 nm.<sup>4</sup> The absorbances at each wavelength were plotted against the concentrations, which ranged from  $0.124 \times 10^{-3}$  to  $2.162 \times 10^{-3} \text{ M}$ . The extinction coefficients were found to be  $\epsilon(\text{Br}_2)_{520\text{nm}} 20.5 \pm 0.5$  and  $\epsilon(\text{Br}_2)_{267\text{nm}} 100 \pm 2 \text{ M}^{-1} \text{ cm}^{-1}$ .

To obtain the extinction coefficients of the tribromide ion, the following procedure was followed: five different solutions of bromine, ranging in concentration from  $0.439 \times 10^{-4}$  to  $8.18 \times 10^{-4} \text{ M}$ , were prepared and 1 ml of each was pipeted into separate 50-ml volumetric flasks. A weighed quantity (11.9016 g) of solid potassium bromide was placed in each of the 50-ml volumetric flasks, and the solutions were brought to mark with distilled water. The initial concentrations of the bromine solutions ranged from  $0.878 \times 10^{-6}$  to  $1.64 \times 10^{-5} \text{ M}$ , and the bromide ion concentration was 2 M. Under these conditions practically all the bromine was in the form  $\text{Br}_3^-$ ; the absorbance was taken at 267, 400, and 520 nm and the concentrations of tribromide ion calculated from the equilibrium



using 16.21 as the value of  $K$  at 25°.<sup>5</sup> A plot of the absorbance against  $[\text{Br}_3^-]$  gave  $\epsilon(\text{Br}_3^-)_{267\text{nm}}$  as  $3.47 \times 10^4 \pm 100 \text{ M}^{-1} \text{ cm}^{-1}$ .

To determine the stoichiometry of the reaction permanganate solutions of known concentrations and volumes were injected into the bromide solutions using a rapid mixing device.<sup>6</sup> The absorbances at 267 and 400 nm were read; using the molar extinction coefficients at these wavelengths with the equilibrium constant for the reaction between bromine and bromide ion, the concentration of the total bromine for each run was calculated. The ratio of total bromine to initial permanganate was found to be 2.5, indicating the reaction proceeds stoichiometrically according to the equation



(1) This paper is based on a dissertation submitted by S. A. Lawani to the faculty of Howard University in partial fulfillment of the requirements for the Ph.D. degree.

(2) L. J. Kirschenbaum and J. R. Sutter, *J. Phys. Chem.*, **70**, 3863 (1966).

(3) M. A. Rawoof and J. R. Sutter, *J. Phys. Chem.*, **71**, 2767 (1967).

(4) H. A. Young, *J. Amer. Chem. Soc.*, **72**, 3310 (1950).

(5) G. N. Lewis and M. Randall, *J. Amer. Chem. Soc.*, **38**, 2354 (1916).

(6) R. Thompson and G. Gordon, *J. Sci. Instrum.*, **41**, 480 (1964).

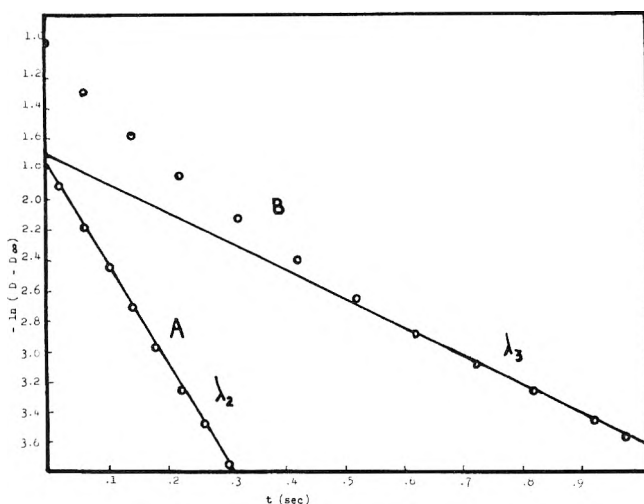


Figure 1. Concave upward first-order plot:  $[\text{Br}^-] = 0.40 \text{ M}$ ;  $[\text{MnO}_4^-]_0 = 9.251 \times 10^{-5} \text{ M}$ ;  $[\text{H}_2\text{SO}_4] = 0.20 \text{ M}$ ;  $T = 25.1^\circ$ ;  $I = 0.919 \text{ M}$ ; wavelength 520 nm.

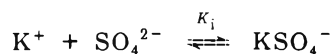
TABLE I: Dependence of the Rate Constants on Bromide Ion Concentration<sup>a</sup>

$[\text{Br}^-], \text{M}$	$\lambda_3$	$\lambda_2$	$\lambda_2 + \lambda_3$	$\lambda_2\lambda_3$
0.8	2.60	12.57	15.17	32.69
0.6	2.48	9.70	12.18	24.02
0.4	2.17	6.61	8.78	14.38
0.2	1.73	4.18	5.91	7.21
0.1	1.36	2.91	4.27	3.95
0.06	1.04			
0.05	0.905	2.28	3.19	2.07
0.04	0.809	2.03	2.84	1.64

<sup>a</sup>  $[\text{H}^+] = 0.265 \text{ M}$ ;  $[\text{H}_2\text{SO}_4] = 0.20 \text{ M}$ ;  $[\text{MnO}_4^-]_0 = 9.251 \times 10^{-5} \text{ M}$ ; temperature =  $25.1^\circ$ ; ionic strength =  $0.919 \text{ M}$ ; 520 nm.

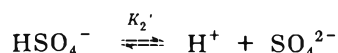
A modified Durrum-Gibson stopped-flow spectrophotometer (Durrum Instruments Corp., Palo Alto, Calif.) was used for the kinetic runs. This apparatus, along with the procedure for obtaining the necessary raw data, has been previously described.<sup>7</sup>

Bromide solutions of a given concentration were made up by weight. Potassium sulfate was used to keep the ionic strength constant at  $0.919 \text{ M}$ . For the sulfuric acid solutions the  $[\text{HSO}_4^-]$ ,  $[\text{SO}_4^{2-}]$ , and in particular, the  $[\text{H}^+]$  were calculated. The calculations took into account that potassium ion associates with sulfate ion to form an ion pair



where  $K_1$  has a value of 9.120 at zero ionic strength and  $25^\circ$ .<sup>8</sup> Using the Davies equation to calculate (approximate) activity coefficients,<sup>9</sup> a value of  $K_1$  of 2 is found at the ionic strength used in this work (i.e.,  $0.919 \text{ M}$ ).

In addition, the second dissociation constant of sulfuric acid



was corrected for ionic strength effects using Kerker's<sup>10</sup> experimental values of  $K_2'$  which are reported as a function of both ionic strength and temperature.

Finally, the amount of potassium sulfate necessary to maintain constant ionic strength in both bromide and

TABLE II: Dependence of the Rate Constants on Bromide Ion Concentration<sup>a</sup>

$[\text{Br}^-], \text{M}$	$\lambda_3$	$\lambda_2$	$\lambda_2 + \lambda_3$	$\lambda_2\lambda_3$
0.600	1.62	5.10	6.72	8.26
0.400	1.48	3.63	5.11	5.38
0.300	1.21	2.96	4.17	3.59
0.040	0.537	0.988	1.52	0.530

<sup>a</sup>  $[\text{H}^+] = 0.145 \text{ M}$ ;  $[\text{H}_2\text{SO}_4] = 0.10 \text{ M}$ ;  $[\text{MnO}_4^-]_0 = 9.251 \times 10^{-5} \text{ M}$ ; temperature =  $25.1^\circ$ ; ionic strength =  $0.919 \text{ M}$ ; 520 nm.

TABLE III: Dependence of the Rate Constants on Hydrogen Ion Concentration<sup>a</sup>

$[\text{H}_2\text{SO}_4], \text{M}$	$[\text{H}^+], \text{M}$	$\lambda_3$	$\lambda_2$	$\lambda_2 + \lambda_3$	$\lambda_2\lambda_3$
0.7	0.972	2.58	10.52	13.10	27.19
0.5	0.685	1.78	7.52	9.30	13.41
0.3	0.407	1.09	4.85	5.94	5.29
0.1	0.132	0.690	1.92	2.61	1.32
0.06	0.079	0.373	1.42	1.78	0.527

<sup>a</sup>  $[\text{Br}^-] = 0.10 \text{ M}$ ;  $[\text{MnO}_4^-]_0 = 1.079 \times 10^{-4} \text{ M}$ ; temperature =  $25.1^\circ$ ; ionic strength =  $0.919 \text{ M}$ ; 520 nm.

TABLE IV: Dependence of the Rate Constants of Hydrogen Ion Concentration<sup>a</sup>

$[\text{H}_2\text{SO}_4], \text{M}$	$[\text{H}^+], \text{M}$	$\lambda_3$	$\lambda_2$	$\lambda_2 + \lambda_3$	$\lambda_2\lambda_3$
0.5	0.711	2.56	10.75	13.31	27.47
0.3	0.424	1.69	6.59	8.28	11.17
0.1	0.139	0.99	2.43	3.42	2.42
0.06	0.084	0.619	1.61	2.23	1.00
0.04	0.057	0.418	1.38	1.80	0.575

<sup>a</sup>  $[\text{Br}^-] = 0.2 \text{ M}$ ;  $[\text{MnO}_4^-]_0 = 1.079 \times 10^{-4} \text{ M}$ ; temperature =  $25.1^\circ$ ; ionic strength =  $0.919 \text{ M}$ ; 520 nm.

permanganate solutions was calculated by successive approximations. These corrections, in particular the effect of ionic strength on the value of  $K_2'$ , are responsible for the hydrogen ion concentration being considerably greater than the concentration of sulfuric acid in Tables I-IV.

Photographs of the kinetic runs obtained from the oscilloscope were read and, with the help of a computer, the raw data were transformed to the absolute value of the optical density term,  $\ln(D - D_\infty)$  (absolute values were used since  $(D - D_\infty)$  would have the opposite sign at 520 and 267 nm, where  $\text{MnO}_4^-$  and  $\text{Br}_3^-$  absorb, respectively). Plots of  $\ln(D - D_\infty)$  against time were curved at the beginning but became linear after a length of time which depended on the reaction conditions (see Figure 1). These will be referred to as first-order plots. The situation was analyzed by means of a difference plot, which was done using the following procedure.

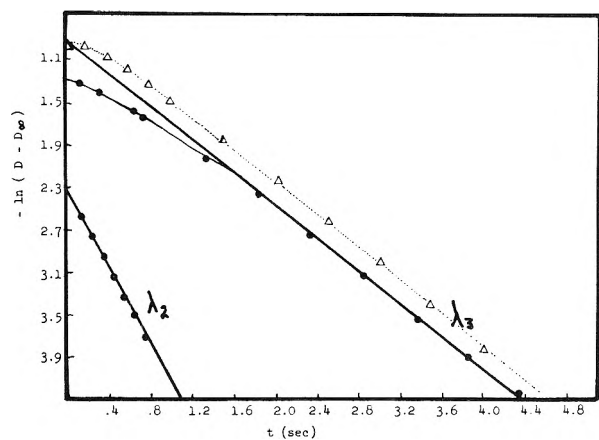
A straight line was drawn through the linear portion of the first-order plot (plot B of Figure 1), and calculations were performed to obtain the values of  $(D_\infty - D)$  extrapo-

(7) K. W. Hicks and J. R. Sutter, *J. Phys. Chem.*, **75**, 1107 (1971).

(8) I. L. Jenkins and C. B. Monk, *J. Amer. Chem. Soc.*, **72**, 2695 (1950).

(9) C. W. Davies, "Ion Association," Butterworths, Washington, D. C., 1962, p 39.

(10) M. Kerker, *J. Amer. Chem. Soc.*, **79**, 3665 (1957).



**Figure 2.** Concave downward first-order plot;  $[\text{Br}^-] = 4.00 \times 10^{-2} \text{ M}$ ;  $[\text{MnO}_4^-]_0 = 9.251 \times 10^{-5} \text{ M}$ ;  $[\text{H}_2\text{SO}_4] = 0.2 \text{ M}$ ;  $T = 25.1^\circ$ ;  $l = 0.919 \text{ M}$ ; wavelength 520 nm: upper curve, ●, experimental values; Δ, calculated from eq 4.

lated to the beginning of the reaction. These calculated values were designated as  $(D_\infty - D)'$ . The difference between these values and the experimentally observed  $(D_\infty - D)$  values were used in the form of  $\ln [(D_\infty - D)' - (D_\infty - D)]$  and plotted against time,  $t$ . This gave the second straight line, A, in Figure 1. This last plot will be referred to as the difference plot. The rate constant obtained from the slopes of the lines A and B are designated  $\lambda_2$  and  $\lambda_3$ , respectively. A set of instructions for obtaining the difference plot was incorporated into the computer program. At high concentrations of bromide or acid, the plot was concave up, but concave down at low concentrations of either (see Figure 2). All kinetic runs were pseudo first order with respect to permanganate.

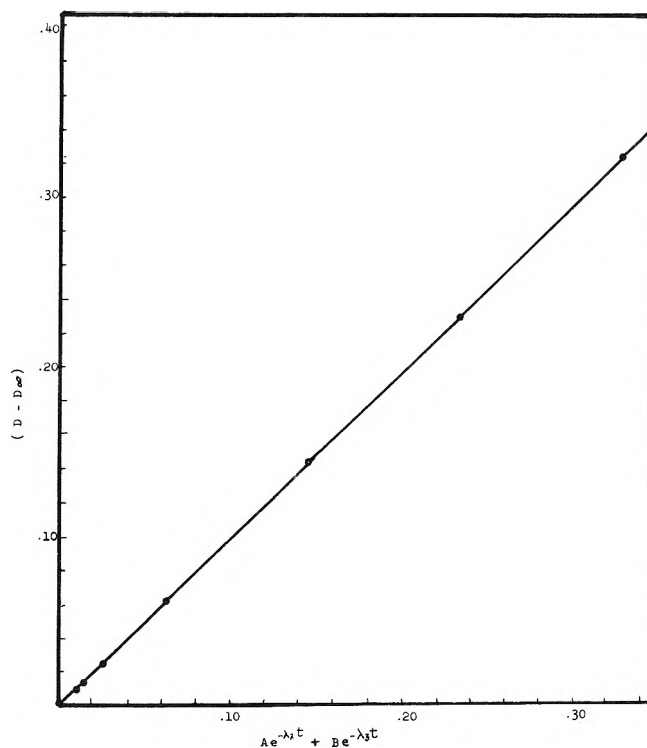
## Results and Discussion

Experimental results show that the observed absorbance can be expressed as a sum or difference of two exponential functions of the form

$$(D - D_\infty) = Be^{-\lambda_3 t} \pm Ae^{-\lambda_2 t}$$

where  $D$  is the absorbance at any time,  $t$ ;  $D_\infty$  is the absorbance at infinite time;  $A$  and  $B$  are preexponential constants, while  $\lambda_2$  and  $\lambda_3$  are the observed rate constants. (The last four quantities are functions of the bromide and hydrogen ion concentrations as well as the true rate constants. The value of  $A$  was obtained by extrapolating the difference plot to zero time and  $B$  by extrapolating the linear portion of the first-order plot to zero time;  $\lambda_2$  and  $\lambda_3$  are the slopes of the two straight lines.) The results of calculations made using this equation are plotted in Figure 3. The positive sign is required for concave up plots, and the negative sign for concave down plots. The experimental values of the intercepts,  $A$  and  $B$ , were not used in the calculation of the true rate constants of the reaction. They were used, instead, to convince us that  $(D - D_\infty)$  could indeed be represented as a sum or difference of exponentials. Equation 4 shows the complexity of  $A$  and  $B$  which precludes their use for calculating precise values of the individual rate constants. These rate constants, as will be shown, were determined solely from  $\lambda_2$  and  $\lambda_3$ .

Kinetic runs show that bromide and acid have a similar effect on the shapes of the first-order plots. Using a given permanganate concentration and keeping the acid con-



**Figure 3.** Test of the equation  $(D - D_\infty) = A \exp(-\lambda_2 t) + B \exp(-\lambda_3 t)$  at  $25.1^\circ$ :  $[\text{Br}^-] = 0.20 \text{ M}$ ;  $[\text{H}_2\text{SO}_4] = 0.30 \text{ M}$ ;  $[\text{MnO}_4^-] = 1.079 \times 10^{-4} \text{ M}$ ;  $l = 0.919 \text{ M}$ ; wavelength 520 nm.

**TABLE V: Comparison of  $\lambda$  Values at 520 and 267 nm<sup>a</sup>**

[Br <sup>-</sup> ], M	$\lambda_2$		$\lambda_3$	
	520 nm	267 nm	520 nm	267 nm
0.15	3.13	3.73	1.09	1.00
0.03	0.99	0.96	0.54	0.50
0.02	0.58	0.52	0.36	0.34

<sup>a</sup>  $[\text{MnO}_4^-]_0 = 5.44 \times 10^{-5} \text{ M}$ ;  $[\text{H}_2\text{SO}_4] = 0.2 \text{ M}$ .

stant, say at 0.2 M, one gets plots of  $\ln(D_\infty - D)$  against time which are concave up, becoming linear toward the end of the reaction at high bromide concentrations. As the bromide concentrations are lowered, a critical stage is reached at which the plot is entirely first order. As the bromide concentrations are lowered further, the plots become concave down, turning first order toward the end of the reaction. The same situation holds if one keeps the initial permanganate and bromide concentrations constant and varies the acid concentrations. Tables I-IV show the concentration dependence of the observed pseudo rate constants  $\lambda_2$  and  $\lambda_3$ . All entries are the average of replicate values. Table V shows a comparison of the eigenvalues  $\lambda_2$  and  $\lambda_3$  obtained at the two wavelengths studied (520 nm for permanganate disappearances, and 267 nm for bromine appearance).

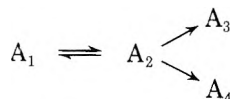
It was found convenient to analyze the rate parameters by means of functions of the  $\lambda$  values and not in terms of the individual  $\lambda$ 's themselves. Linear plots of  $\lambda_2 + \lambda_3$  and of  $\lambda_2 \lambda_3$  vs. the various concentrations were obtained and all of the experimental data were found to obey equations of the form

$$(\lambda_2 + \lambda_3) = C_1[\text{Br}^-][\text{H}^+] + C_2[\text{H}^+] + C_3$$

and

$$(\lambda_2\lambda_3) = C_4[\text{Br}^-][\text{H}^+]^2 + C_5[\text{Br}^-][\text{H}^+]$$

Thus, plots, as for instance,  $\lambda_2 + \lambda_3$  vs.  $\text{Br}^-$  or  $\text{H}^+$  (with one being constant at a time), are all linear. For the hydrogen ion concentration dependence in  $\lambda_2\lambda_3$ , plots of  $\lambda_2\lambda_3/\text{H}^+$  vs.  $[\text{H}^+]$  are quite linear. Clearly,  $\lambda_2$  and  $\lambda_3$ , alone, are not simple functions of the concentrations. These functions of  $\lambda_2$  and  $\lambda_3$  are solutions to the set of coupled first-order rate equations<sup>11</sup> (in our case, pseudo first order) arising from the analysis of a mechanism of the general type



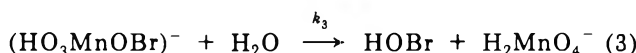
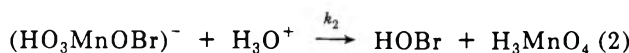
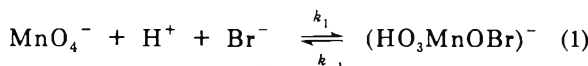
This mechanism leads to a secular determinant, the eigenvalues of which are the  $\lambda$ 's. In our case  $\lambda_2$  and  $\lambda_3$  appear as the pair of roots to a quadratic expression making the handling of the square root term analytically awkward. The sum and product of the  $\lambda$ 's, however, are in general easy to handle<sup>12</sup> although the error resulting in multiplying  $\lambda$ 's can be sizeable. At 25.1° all of our data are consistent with the equations

$$\lambda_2 + \lambda_3 = (59.8 \pm 1)[\text{Br}^-][\text{H}^+] + (6.48 \pm 0.25)[\text{H}^+] + (0.71 \pm 0.09)$$

$$\lambda_2\lambda_3 = (356 \pm 59)[\text{Br}^-][\text{H}^+]^2 + (29 \pm 10)[\text{Br}^-][\text{H}^+]$$

The larger errors in  $C_4$  and  $C_5$  arise in part from the multiplication of the two eigenfunctions and from the uncertainties in the hydrogen ion concentration, a calculated quantity.

All runs were made under pseudo-kinetic conditions with the hydrogen ion and bromide ion always in large excess over the permanganate. The simplest mechanism consistent with the above data is



Thus

$$\lambda_2 + \lambda_3 = k_1[\text{H}^+][\text{Br}^-] + k_2[\text{H}^+] + k_3 + k_{-1}$$

$$\lambda_2\lambda_3 - k_1k_2[\text{H}^+]^2[\text{Br}^-] + k_1k_3[\text{H}^+][\text{Br}^-]$$

Further analysis of the above set of coupled first-order equations leads to the following representations of the dependence of permanganate concentration on time<sup>11</sup>

$$[\text{MnO}_4^-] = \frac{(k_{-1} + k_2[\text{H}^+] + k_3 - \lambda_2)}{\lambda_3 - \lambda_2} C_0^0 e^{-\lambda_2 t} + \frac{(k_{-1} + k_2[\text{H}^+] + k_3 - \lambda_3)}{\lambda_2 - \lambda_3} C_0^0 e^{-\lambda_3 t} \quad (4)$$

where  $C_0^0$  is the initial concentration of permanganate at  $t = 0$ . At 520 nm, where permanganate is the only absorbing species of interest

$$[\text{MnO}_4^-] = (D - D_\infty)/\epsilon l$$

may be substituted. It may be seen that at a hydrogen ion

TABLE VI: Temperature Dependence of  $\lambda_2$  and  $\lambda_3$  as a Function of Bromide Ion Concentration<sup>a</sup>

[Br <sup>-</sup> ], M	T = 20.6°		T = 16.1°		T = 11.9°	
	$\lambda_3$	$\lambda_2$	$\lambda_3$	$\lambda_2$	$\lambda_3$	$\lambda_2$
0.8	2.39	11.05	2.36	9.07	2.33	7.14
0.6	2.36	8.15	2.28	6.84	2.14	5.42
0.4	2.17	5.48	2.07	4.67	1.94	3.53
0.2	1.75	3.09	1.58	2.98		
0.1	1.32	2.47	1.31	2.14	1.27	1.72
0.06	1.08	1.68	1.00	1.62	0.92	1.53

<sup>a</sup>  $[\text{H}^+] = 0.265 \text{ M}$ ;  $[\text{MnO}_4^-]_0 = 1.495 \times 10^{-4} \text{ M}$ ; ionic strength = 0.919 M.

concentration of 0.265 M the curvature should change from concave up to concave down when the bromide ion concentration is lower than about 0.05 M, in agreement with the observed behavior. In the runs at fixed bromide ion concentration, with hydrogen ion concentration varying it should be noted that the predicted change in curvature occurs at a hydrogen ion concentration slightly lower than observed. Allowing permanganate to be the only absorbing species at 520 nm leads to the simplest interpretation of the change in curvature. One could, of course, allow the intermediate,  $(\text{HO}_3\text{MnOBr})^-$ , to absorb also, with the extinction coefficient  $\epsilon'$ , a to be determined parameter. This seems to be unnecessary in the present case.

From the above data the rate constants at 25.1° may be evaluated. The values are  $k_1 = 59.8 \text{ M}^{-2} \text{ sec}^{-1}$ ,  $k_2 = 6.48 \text{ M}^{-1} \text{ sec}^{-1}$ ,  $k_{-1} = 0.2 \text{ sec}^{-1}$ , and  $k_3 = 0.5 \text{ sec}^{-1}$ . As an example, these values of the rate constants along with the experimental values of  $\lambda_2$  and  $\lambda_3$  for the run pictured in Figure 2 (see last entry, Table I) were used to calculate the preexponential terms of eq 4. Further, using the  $\epsilon(\text{MnO}_4^-)$  and a 2-cm path length, there results

$$(D - D_\infty)_{\text{calcd}} = -0.131e^{-2.03t} + 0.54e^{-0.809t}$$

These  $(D - D_\infty)_{\text{calcd}}$  values are displayed, for comparison, in Figure 2. Considering the complexity of the preexponentials, the agreement is quite good.

The temperature dependence of the eigenvalues was determined as a function of bromide concentration at a fixed hydrogen ion concentration of 0.265 M. The results are given in Table VI. The value of the  $\lambda$ 's at 25.1° may be found in Table II.

Plots of  $\lambda_2 + \lambda_3$  vs. bromide were again linear and  $k_1$  was obtained from the slope of the line directly. The intercept, however, within experimental error, was independent of temperature. This suggests that  $k_2$ , the principal contributor to the intercept, has an extremely low apparent activation energy.

The values of  $k_1$  at 25.1, 20.6, 16.1, and 11.9° are respectively 59.8, 53.2, 43.8, and 35.5  $\text{M}^{-2} \text{ sec}^{-1}$ . From these data one calculates  $\Delta H^* = (6.15 \pm 0.64) \times 10^3 \text{ cal}$  and  $\Delta S^* = -29.7 \pm 2.2 \text{ eu}$ .

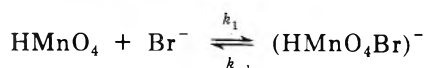
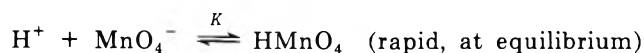
Kinetic runs were conducted with added acrylonitrile (10 vol %) in order to test for a radical mechanism, i.e., the production of Br·. Solutions whose concentrations were the same as those used in the kinetic runs were

- (11) S. W. Benson, "The Foundations of Chemical Kinetics," McGraw-Hill, New York, N. Y., 1960, p 39.  
 (12) H. Margeneau and G. M. Murphy, "The Mathematics of Physics and Chemistry," Van Nostrand, New York, N. Y., 1943, p 304.



made containing (a) permanganate, acid, and acrylonitrile, (b) permanganate, acid, acrylonitrile, and bromide, and (c) acid, acrylonitrile, and bromide. In only solution a did a precipitate of polymerized acrylonitrile form, due to the initiated oxidation of acrylonitrile by permanganate.<sup>13</sup> Apparently then in solution b the permanganate-bromide reaction proceeds at a rate much faster than the polymerization reaction and, in addition, no species is formed during the course of the reaction which would polymerize the acrylonitrile, suggesting that  $\text{Br}^-$  is not oxidized by permanganate to  $\text{Br}\cdot$  and, for instance,  $\text{MnO}_4^{2-}$ . This result cannot rule out conclusively a radical mechanism as either a major or a minor path in this reaction, but it does suggest that such a course is not in operation under the conditions of our experiments.

Any reaction in which permanganate is reduced to manganate while  $\text{Br}^-$  is oxidized to either bromine or  $\text{HOBr}$  is quite thermodynamically forbidden. To overcome the low oxidizing power of the  $\text{MnO}_4^-$  to  $\text{MnO}_4^{2-}$  couple, it appears that a proton is involved, perhaps to form  $\text{HMnO}_4$ , which is then capable of carrying out the oxidation



This would be kinetically the same as the mechanism suggested in eq 1-3,  $(\text{HMnO}_4\text{Br})^-$  would then decompose by either a protonated or a nonprotonated path. It is supposed, however, that the  $(\text{HMnO}_4\text{Br})^-$  complex consists of  $\text{Mn(V)}$  and  $\text{Br(I)}$ , and that this is probably the redox step, with the second proton, or water, facilitating the breaking up of the complex and anticipating a highly protonated  $\text{Mn(V)}$  species. (A highly protonated  $\text{Mn(V)}$ ,  $\text{H}_2\text{MnO}_4^-$ , etc., would be in keeping with our finding, unpublished, of a predominant  $\text{HMnO}_4^-$  species in the disproportionation of manganate ion in acid medium.) The

low activation enthalpy would tend to substantiate this. Indeed, although the number of reactions studied is small, it appears that in general if the potential for the oxidation couple (*i.e.*,  $\text{I}^-|\text{I}_2$  and  $\text{Fe}(\text{CN})_6^{4-}|\text{Fe}(\text{CN})_6^{3-}$ ) is less than the +0.564 V for the  $\text{MnO}_4^-|\text{MnO}_4^{2-}$  couple, the reaction may proceed without a proton dependence and by a relatively uncomplicated mechanism, but if the oxidation couple is more negative than about -0.56 V (*i.e.*,  $\text{Br}^-|\text{Br}_2$ ,  $\text{Fephen}_3^{2+}|\text{Fephen}_3^{3+}$  and  $\text{Ce(III)}|\text{Ce(IV)}$ )<sup>14</sup> the reaction will take on a proton dependence and the mechanism will become more complicated in order to bypass this unfavorable first step.

The mechanism of the present reaction is seen to be formally identical with the mechanism presented for the permanganate-iodide reaction.<sup>2</sup> The difference between them is the important extra proton functioning in the first step of the bromide reaction (eq 1) and, of course, the reversibility of step 1. If the bromide and iodide reactions are the same, then the function of the hydrogen ion in the iodide reaction is to assist in the breakup of the  $(\text{MnO}_4\text{I})^{2-}$  complex, with  $\text{HMnO}_4$  not being important in the kinetics. The differences, then, between the iodide and bromide reactions may be attributed to the change in the thermodynamics associated with the ease of oxidation of the respective halide ions.

Lastly, it must be pointed out that reversible step 1 is a necessity. No other mechanism except one that offers "feedback" to the permanganate ion will account for the curvature in the first-order plots for the disappearance of this ion.

*Acknowledgment.* The authors wish to acknowledge partial support of this research under the National Science Foundation Grant No. GP 8097.

- (13) L. F. Fieser and M. Fieser, "Organic Chemistry," 4th ed, D. C. Heath, Boston, Mass., 1960, p 67.  
 (14) R. J. Isabel, Dissertation submitted to Howard University, 1970.

# Kinetics of Twelve-Step Competitive-Consecutive Second-Order Reactions. The Alkaline Hydrolysis of Triethyl Citrate

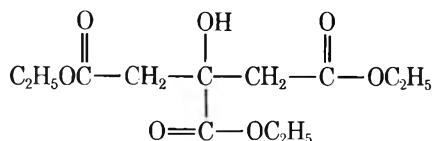
F. A. Kundell,<sup>1</sup> D. J. Robinson,<sup>1</sup> and W. J. Svirbely\*

Chemistry Department, University of Maryland, College Park, Maryland 20742 (Received January 17, 1973)

The kinetic process for a twelve-step competitive-consecutive second-order reaction involving an unsymmetrical trifunctional molecule, B, reacting with a common reagent, A, can be written as  $A + B \rightarrow C + P$ ,  $A + B \rightarrow D + P$ ,  $A + B \rightarrow E + P$ ,  $A + C \rightarrow F + P$ ,  $A + C \rightarrow G + P$ ,  $A + D \rightarrow F + P$ ,  $A + D \rightarrow H + P$ ,  $A + E \rightarrow G + P$ ,  $A + E \rightarrow H + P$ ,  $A + F \rightarrow I + P$ ,  $A + G \rightarrow I + P$ ,  $A + H \rightarrow I + P$  having the rate constants  $k_1, k_2, \dots, k_{12}$ , respectively. The rate equations have been solved in terms of the variable  $\lambda$ , where  $\lambda = \int_0^t A dt$ . The solution is of the form  $\beta = \sum_{i=1}^7 G_i e^{-S_i \lambda}$  where  $\beta = (A - A_0)/B_0 + 3$  and  $G_i$  and the  $S_i$  are constants involving various combinations of the twelve rate constants. If the trifunctional compound has a reaction plane of symmetry, as is the case for triethyl citrate, some of the reaction steps are indistinguishable from others. As a result, the twelve-step case can be treated mathematically as a seven-step case and it becomes a problem of determining seven parameters only. A least-squares solution can be used to calculate these seven rate constants. This procedure was used to determine the  $k$  values for the alkaline hydrolysis of triethyl citrate in dioxane-water mixtures of varying composition at 15°.

## Introduction

The last paper in the series concerned with the kinetics of hydrolysis of multifunctional compounds dealt with the alkaline hydrolysis of diethyl malate, an unsymmetrical difunctional compound.<sup>2</sup> In this paper, we shall report on the alkaline hydrolysis of triethyl citrate, an unsymmetrical trifunctional compound. Triethyl citrate may be represented by the formula

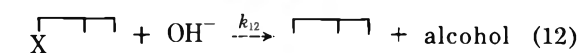
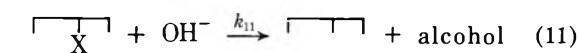
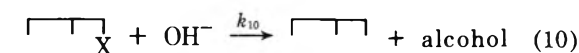
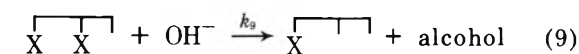
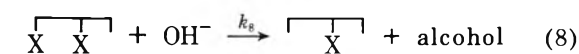
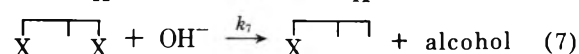
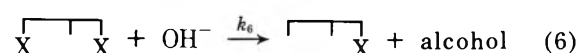
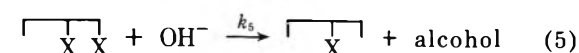
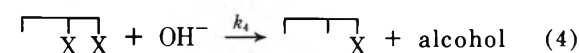
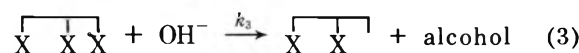
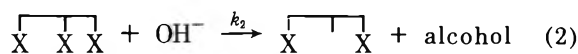
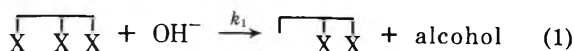


It is apparent that, as a result of a reaction plane of symmetry passing through the central carbon atom in the formula, the reactions of the two terminal ester groups with a common reactant will be indistinguishable from one another. Thus, the saponification of triethyl citrate will be a special case of the more general one involving an unsymmetrical molecule which does not have a reaction plane of symmetry. One expects, therefore, seven different reaction steps only for this special case rather than the twelve steps which normally would exist for the saponification of an unsymmetrical triester.

A study of the alkaline hydrolysis of triethyl citrate was made in various dioxane-water media at 15° in order to (a) demonstrate the validity of the apparent seven-step kinetic process for this reaction, (b) relate each of the final twelve rate constants to a mechanistic rationalization of the reaction, and (c) extend computer techniques for handling the calculations for such a complex system.

## Mathematical Analysis

The alkaline hydrolysis of an unsymmetrical trifunctional compound can be represented schematically by the following twelve-step process.



If one uses the definitions

$A = [\text{OH}^-]$  = the concentration of base

$B = \left[ \begin{array}{c} \text{X} \quad \text{X} \quad \text{X} \\ | \quad | \quad | \\ \text{X} \quad \text{X} \quad \text{X} \end{array} \right]$  = the concentration of the triester

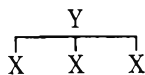
$C = \left[ \begin{array}{c} \text{X} \quad \text{X} \\ | \quad | \\ \text{X} \quad \text{X} \end{array} \right]$  = the concentration of the first diester ion

$D = \left[ \begin{array}{c} \text{X} \\ | \\ \text{X} \end{array} \right]$  = the concentration of the second diester ion

(1) Abstracted in part from the Ph.D. Theses of F. A. K. and D. J. R.  
(2) W. J. Svirbely and F. A. Kundell, *J. Amer. Chem. Soc.*, **89**, 5354 (1967).



As stated in the introduction, triethyl citrate has a reaction plane of symmetry. Schematically, the triester may be represented by the symbol



It is apparent that because of the reaction plane of symmetry, the reactions of the terminal ester groups with a common reagent would be mathematically indistinguishable from each other. The same situation would exist in several of the succeeding steps. In terms of the symbolism used in eq 1-12 this is tantamount to saying that if  $k_3$ ,  $k_7$ ,  $k_8$ ,  $k_9$ , and  $k_{12}$  are set equal to zero, then the twelve-step case can be treated mathematically as a seven-step mechanism. Then, after these seven constants  $k(i)$  have been determined from the data, the rate constants for the twelve-step mechanism can easily be calculated in accordance with the following definitions:  $k_1 = k_3 = k(1)/2$ ;  $k_2 = k(2)$ ;  $k_4 = k_9 = k(4)/2$ ;  $k_5 = k_8 = k(5)/2$ ;  $k_6 = k_7 = k(6)/2$ ;  $k_{10} = k_{12} = k(10)/2$ ;  $k_{11} = k(11)$ .

The procedure for evaluating the constants  $k(1)$ ,  $k(2)$ ,  $k(4)$ ,  $k(5)$ ,  $k(6)$ ,  $k(10)$ , and  $k(11)$  through the direct use of eq 30 is in principle the same as the one which has already been described.<sup>2</sup> In practice, however, complications arise.

### Materials and Apparatus

**Triethyl Citrate.** Research grade triethyl citrate was purchased from Aldrich Chemical Co. The ester was vacuum distilled several times, the center cut being saved. The saponification equivalent indicated a purity of  $100 \pm 0.1\%$ . A chromatographic analysis yielded one maximum only. Information on an infrared analysis indicated that no impurities were present.<sup>3</sup>  $n_{20}^D$  was 1.4426.

**Other Details.** The apparatus, procedure, and other pertinent factors have already been described.<sup>2</sup> Starting concentrations of the triester and of the sodium hydroxide were adjusted so that equivalent amounts were used (*i.e.*,  $A_0 = 3B_0$ , where  $A_0$  and  $B_0$  are the concentrations in moles per liter of hydroxide and triester, respectively). This restriction is not a necessity but merely a convenience.

Triplicate runs were made under identical conditions and the data were pooled for calculation purposes.

A partial saponification of triethyl citrate was carried out. The product was a very viscous, syrupy liquid. At low temperatures it formed a clear glassy solid. From this product a solid which was insoluble in *N,N*-dimethylformamide was recrystallized. Following saponification equivalent determination, it was concluded that the product recovered was disodium ethyl citrate, a monoester. The rate of hydrolysis of this solid was determined at  $15^\circ$  in 30 wt % dioxane-water. The rate constant was  $0.0195 M^{-1} \text{min}^{-1}$ . We will comment on this data later.

### Data, Calculations, and Discussion

**Computing Program.** A program<sup>4</sup> for the solution of competitive-consecutive second-order rate equations using a least-squares procedure was developed. The cases considered were one-step through three-step reactions involving both symmetrical and unsymmetrical molecules and a four-step reaction involving a symmetrical molecule. The coding for the system has been done in a "neutral" Fortran IV.

**Evaluation of Rate Constants.** In the least-squares fitting procedure one starts with estimated values for the

seven rate constants to be determined. Equation 30 is then expanded around these initial guesses by a Taylor's expansion. However, when so many parameters are involved the success of the convergence of the  $k(i)$  values to their true values using the iterative method depends on a good choice for these estimates.

One avenue of approach is to utilize a routine in the computer program called SIMPLEX. This is a least-squares trial and error procedure for generating a set of the desired number of rate constants which are consistent with the kinetic data. While this proved successful in cases where four or less constants were involved, it was not successful in generating *seven* rate constants which could be used as estimates which would later lead to convergence and reproduction of the data. Our estimated value for  $k(1)$ , which is quite large, did, however, come from this approach.

Another possibility is to attempt to calculate the rate constants utilizing structure factors for the various compounds. Considerable effort has been expended in the past to generalize existing data and to predict the reaction rates of similar compounds for which no data exists.<sup>5</sup> Among the most successful of these has been the Hammett equation which was used to predict rate constants for meta- and para-substituted benzene derivatives. Hammett's equation was extended by Taft to include aliphatic compounds. Taft also attempted to account for differences in steric hindrance by introduction of a steric factor. Hancock modified Taft's equation by separation of the Taft steric factor into steric and hyperconjugative contributions. Hancock's equation is

$$\log k/k_0 = \sigma^* \rho^* + \delta E_s^c + h(n - 3) \quad (39)$$

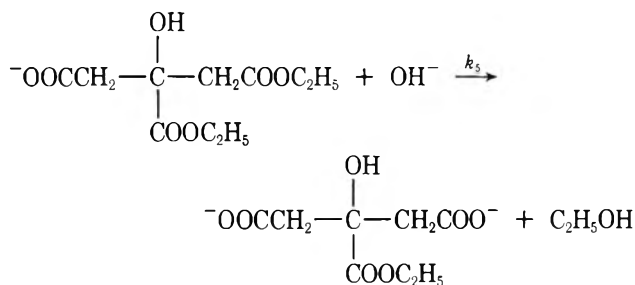
where  $\sigma^*$  is a substituent constant specific for the substituent regardless of the reaction under consideration and  $\rho^*$  is a reaction coefficient and is dependent upon the type of reaction and the reaction conditions; the product of these two describes the polar or inductive contribution.  $\delta$  and  $h$  are steric and hyperconjugative factors, respectively, which are reaction dependent,  $E_s^c$  is a corrected steric factor which is substituent dependent,  $n$  is the number of hydrogen atoms on the carbon  $\alpha$  to the reaction site, and  $k/k_0$  is the ratio of rate constants for the compound containing a particular substituent and a reference compound, which in our case was ethyl acetate. On referring to Table I, one can see that within the structural formula for triethyl citrate one can locate the substituents analogous to diethyl glutarate, diethyl 3-hydroxyglutarate, diethyl succinate, and diethyl malate. From recent studies made in our laboratory<sup>6</sup> on these and other compounds and from data in the literature<sup>2,7,8</sup> we were able to obtain values for the  $\sigma^*$ ,  $\rho^*$ ,  $E_s^c$ ,  $\delta$ , and  $h$  factors for the substituents on the various species involved in the different reacting steps of the citrate reaction. This permitted us to cal-

- (3) Private communication from the supplier, "A very careful infrared analysis indicates no impurities present."
- (4) F. A. Kundell, W. J. Svirbely, and J. M. Stewart, Technical Report No. 68-69, Kinetics 68, Computer Science Center, University of Maryland.
- (5) (a) L. P. Hammett, *Chem. Rev.*, **17**, 125 (1935); (b) R. W. Taft, Jr., M. S. Newman, and F. H. Verhoek, *J. Amer. Chem. Soc.*, **72**, 4511 (1950); R. W. Taft, Jr., *ibid.*, **74**, 3120 (1952); (c) C. K. Hancock, E. A. Meyers, and B. J. Yager, *ibid.*, **83**, 4211 (1961).
- (6) Kinetic studies on the alkaline hydrolysis of ethyl acetate, ethyl propionate, ethyl valerate, ethyl hexanoate, diethyl 3-hydroxyglutarate, diethyl glutarate, diethyl 2-methylglutarate, diethyl 3-methylglutarate, and diethyl 3,3-dimethylglutarate will be the subject of another paper.
- (7) W. J. Svirbely and A. D. Kuchta, *J. Phys. Chem.*, **65**, 1333 (1961).
- (8) E. Tommila, A. Koivisto, J. P. Lyyra, and S. Heimo, *Ann. Acad. Sci. Fenn., Ser. A2*, **47** (1952).

**TABLE I: Structural Formulas for Triethyl Citrate and Esters which Can Be Considered as Its Substituents**

$\begin{array}{c} \text{OH} \\   \\ \text{H}_3\text{C}_2\text{OOCCH}_2\text{CCH}_2\text{COOC}_2\text{H}_5 \\   \\ \text{COOC}_2\text{H}_5 \end{array}$	Triethyl citrate
$\text{H}_3\text{C}_2\text{OOCCH}_2\text{CH}_2\text{CH}_2\text{COOC}_2\text{H}_5$	Diethyl glutarate
$\begin{array}{c} \text{OH} \\   \\ \text{H}_3\text{C}_2\text{OOCCH}_2\text{CHCH}_2\text{COOC}_2\text{H}_5 \\   \\ \text{CH}_2\text{CH}_2\text{COOC}_2\text{H}_5 \\   \\ \text{COOC}_2\text{H}_5 \end{array}$	Diethyl 3-hydroxyglutarate
$\begin{array}{c} \text{OH} \\   \\ \text{CH}_2\text{CH}_2\text{COOC}_2\text{H}_5 \\   \\ \text{COOC}_2\text{H}_5 \end{array}$	Diethyl succinate
$\begin{array}{c} \text{OH} \\   \\ \text{CHCH}_2\text{COOC}_2\text{H}_5 \\   \\ \text{COOC}_2\text{H}_5 \end{array}$	Diethyl malate

culate an approximate value of a rate constant through the use of Hancock's equation. That number then became our estimate for that particular step which would be used in the iterative procedure of our computing program. For example, consider the hydrolysis step



The polar substituent contribution is the summation of the contributions of the carboxylate ion in the glutarate position,  $-0.208$ , the ester substituent in the succinate position,  $0.199$ , and the hydroxyl group one methylene group removed from the reaction site,  $0.198$ .  $\sigma^*$  therefore is the sum of these, or  $0.189$ .

$E_s^c$  was originally estimated from the value for the reaction involving a terminal ester group and an assumption that the steric contributions of the various substituents are additive. The original estimate was revised by an iterative procedure and for the above step calculated as  $-1.91$ .

The values of  $\rho^* = 2.22$ ,  $\delta = 0.567$ , and  $h = +0.012$  were obtained using regression analysis on the data from the hydrolysis of other esters in this same solvent system at the same temperature.

There are two hydrogen atoms on the carbon  $\alpha$  to the reacting carbonyl carbon of the ester described by eq 5. Therefore  $n - 3 = -1$ . Making these substitutions in the Hancock equation, together with the value of  $\log k_0^6$  (ethyl acetate is the reference compound), one calculates  $k_5 = 0.625$  in 30% dioxane at  $15.07^\circ$ . The same procedure was used to obtain  $k_2$ ,  $k_4$ ,  $k_6$ , and  $k_{10}$ . The SIMPLEX routine gave  $k_1 = 26.59$  and  $k_{11}$  had been determined in this research. However,  $k(1) = 2k_1$ ,  $k(2) = k_2$ ,  $k(4) = 2k_4$ ,  $k(5) = 2k_5$ ,  $k(6) = 2k_6$ ,  $k(10) = 2k_{10}$ , and  $k(11) = k_{11}$ . The values of the  $k(i)$ 's obtained by this procedure were used as initial guesses in the least-squares program and are listed in the second column of Table II.

A typical set of time-concentration data is shown in the first two columns of Table III. Using this data and the estimates given in Table II, the values of the rate constants were determined by the least-squares procedure. These are listed in the third column of Table II. The values of  $\alpha$

**TABLE II: Estimates and Least-Squares Values**

Rate Constant	Estimates	Least-squares values
$k(1)$	53.18	$49.6 \pm 1.2$
$k(2)$	8.49	$2.92 \pm 1.1$
$k(4)$	1.11	$0.49 \pm 0.19$
$k(5)$	1.25	$1.1 \pm 0.17$
$k(6)$	12.6	$7.4 \pm 1.4$
$k(10)$	0.018	$0.14 \pm 0.15$
$k(11)$	0.02	$0.011 \pm 0.006$

**TABLE III: Data<sup>a</sup> Obtained at  $15.07^\circ$  in 30 wt% Dioxane-Water Mixture<sup>b</sup>**

Time, min	$\alpha$ (expt), $\alpha = A/A_0$	$\alpha$ (calcd)	% deviation
0.000	1.0000	1.000	0.00
1.08	0.8409	0.8426	-0.21
2.00	0.7787	0.7731	0.72
3.00	0.7281	0.7270	0.15
4.01	0.7008	0.6974	0.48
5.00	0.6788	0.6779	0.13
6.00	0.6632	0.6634	-0.10
7.00	0.6528	0.6534	-0.10
8.00	0.6463	0.6453	0.16
9.00	0.6411	0.6386	0.40
11.00	0.6254	0.6279	0.24
13.00	0.62C4	0.6192	0.20
15.00	0.6126	0.6115	0.18
17.00	0.6055	0.6045	-0.16
19.00	0.5970	0.5979	-0.15
21.00	0.5905	0.5917	-0.19
23.00	0.5840	0.5857	-0.29
30.00	0.5633	0.5665	-0.57
40.00	0.5472	0.5428	-0.30
50.00	0.5243	0.5224	0.35
60.00	0.5075	0.5045	0.56
70.00	0.4906	0.4891	0.31
80.00	0.4750	0.4754	-0.07
90.00	0.4634	0.4632	0.05
100.00	0.4576	0.4522	-0.11
110.00	0.4426	0.4424	0.05
120.00	0.4335	0.4335	0.00
140.00	0.4180	0.4181	-0.02
150.00	0.4115	0.4114	-0.02
180	0.3946	0.3946	0.000
200	0.3855	0.3855	0.000
210	0.3803	0.3814	-0.30

<sup>a</sup> Only about half of the experimental data for this run are shown. <sup>b</sup>  $D = 54.74$ ;  $A_0 = 0.01214 M$ ;  $B_0 = \frac{1}{3} A_0$ . QME of fit is 0.70%.

(calcd) in column three of Table III were obtained through use of eq 30 and 31 using the final values of the  $k$ 's. The fourth column in Table III represents the deviation between  $\alpha$  (expt) and  $\alpha$  (calcd) and is thus a measure of the reproducibility of the experimental data. The agreement is excellent and the random plus and minus deviations lend credibility to this procedure as a solution for the triethyl citrate problem.

The program allows for the calculation of the intermediate concentrations of each of the reacting species at each of the recorded times. Figure 1 shows a plot of the intermediate concentrations. One observation from examining this graph is that Pinnow<sup>9</sup> was correct in his state-

(9) J. Pinnow, *Z. Elektrochem.*, **24**, 21 (1918).

TABLE IV: Summary of the  $k(i)$  Values at 15.07° in Various Dioxane–Water Mixtures

	Dioxane, wt %				
	20.0	30.0	50.0	70.0	80.0
	Dielectric constant				
	63.97	54.74	36.25	18.71	11.27
$k(1)$	57.4	49.6 ± 1.2	37.2	36.7	46.4
$k(2)$	1.54	2.92 ± 1.1	6.4	3.9	5.1
$k(4)$	0.78	0.49 ± 0.19	0.90	3.0	20
$k(5)$	1.12	1.1 ± 0.17	0.62	4.2	5.4
$k(6)$	56.2	7.4 ± 1.4	8.2	3.8	1.5
$k(10)$	0.030	0.14 ± 0.15	0.022	0.11	2.1
$k(11)$	0.007	0.011 ± 0.006	0.0058	0.093	0.24
% QME of fit	0.63	0.70	0.50	0.83	1.8

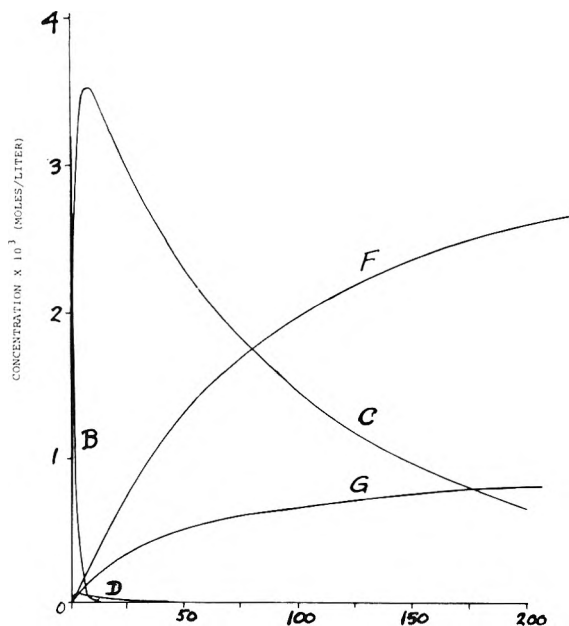


Figure 1. Plot of intermediate concentrations of the reacting species vs. time (min).

ment that the first step of the alkaline hydrolysis of triethyl citrate involves one of the side groups and that the reaction essentially proceeds to completion before the next step begins. Another observation is that species F and G are present in reasonably large quantities and this mixture is most probably what we isolated in our partial saponification of triethyl citrate and it was on this mixture of isomers of disodium ethyl citrate that we ran our hydrolysis measurements to determine a rate constant.

We used existing data<sup>2</sup> and a computer program for regression analysis to calculate the three Hancock reaction parameters  $\rho^*$ ,  $\delta$ , and  $h$  for three additional solvent systems, 20, 50, and 70% dioxane. Using these values, the substituent parameters  $\sigma^*$  and  $E_s^c$  which had previously been determined and values of  $\log k_0$  determined from the work of Tommila<sup>8</sup> we then calculated, with aid of the Hancock equation, trial values for the  $k$ 's for each of the three new solvent compositions. Using these trial  $k$ 's the calculations quite quickly converged to the values shown in columns 2, 4, and 5 of Table IV.

Extrapolation of plots of  $\log k$  vs.  $100/D$  then permitted us to extend all of our data to the 80% dioxane solvent system. Reaction parameters were calculated and trial  $k$ 's were calculated and after some 120 iterations the calculations converged to the values listed in the sixth column of Table IV.

TABLE V: Test for Uniqueness of the  $k$  Values in the 30% Dioxane–Water System

Rate constant	Accepted value	Trial value	New value	% difference
$k(1)$	49.6	40	50.6	2
$k(2)$	2.92	3	2.28	22
$k(4)$	0.49	0.5	0.47	4
$k(5)$	1.1	1.0	1.06	4
$k(6)$	7.4	2.0	7.85	6
$k(10)$	0.14	0.05	0.038	17
$k(11)$	0.011	0.01	0.0051	54
QME	0.70		0.50	

TABLE VI: Summary of Rate Constants<sup>a</sup> at 15.07° in Various Dioxane–Water Mixtures

	Dielectric constant				
	63.97	54.74	36.25	18.71	11.27
	Dioxane, wt %				
	20.0	30.0	50.0	70.0	80.0
$k_1$	28.7	24.8	18.6	18.4	23.2
$k_2$	1.54	2.92	6.4	3.9	5.1
$k_3$	28.7	24.8	18.6	18.4	23.2
$k_4$	0.39	0.25	0.45	1.5	10.0
$k_5$	0.56	0.55	0.31	2.1	2.7
$k_6$	28.1	3.70	4.1	1.9	0.75
$k_7$	28.1	3.70	4.1	1.9	0.75
$k_8$	0.56	0.55	0.31	2.1	2.7
$k_9$	0.39	0.25	0.45	1.5	10.0
$k_{10}$	0.015	0.07	0.011	0.055	1.05
$k_{11}$	0.007	0.011	0.006	0.093	0.24
$k_{12}$	0.015	0.07	0.011	0.055	1.05

<sup>a</sup> In units of  $l. mol^{-1} min^{-1}$ .

Reference to the fifth column of Table IV shows that in 70% dioxane the magnitudes of  $k(2)$ ,  $k(4)$ ,  $k(5)$ , and  $k(6)$  are all nearly the same. Similarly the values for  $k(10)$  and  $k(11)$  are also very similar. These conditions tend to cause singularities in the matrices involved in the least-squares calculations. Original difficulties in getting convergence in the calculations for this solvent system are now explainable.

It was desirable to see if the seven constants calculated for a triethyl citrate run are unique, or if some other set might be found which would fit the experimental data equally well. We had set as criteria of acceptability of rate constants the following conditions.

(1) The quadratic mean error (QME) of fit. This was set to be less than 1% and we have succeeded in most cases in obtaining it.

(2) The experimental data must be reproducible with only small scale and random plus and minus variations between the values for the experimental concentration and the calculated concentration obtained at each of the experimental times.

The uniqueness of a particular set of rate constants was checked in the following way. For the 30% dioxane-water solvent system, we changed the time- $\alpha$  input data for 25 of the 54 data points in a roughly Gaussian distribution about 3.5 times the standard deviations for these points to see what would be the effect of these changes on the rate constants. We used trial  $k(i)$ 's which were quite far from those we believed to be the true values (but still within what we believed to be the convergence sphere). The new set of rate constants obtained is shown in Table V along with the "estimates" and with the "accepted values" listed in Table IV for ease of comparison. It can be seen from Table V that while the value for  $k(1)$ ,  $k(4)$ , and  $k(5)$  remained essentially unchanged, the values of the other rate constants were changed from 6% to as much as 54% of their original values. The QME of fit was improved. These "new" values are therefore no less reliable from the standpoint of our criteria than are the accepted values. However, the overall picture of the kinetic steps in terms of magnitude of the rate constants is essentially the same. We therefore believe that our results are unique and represent a true picture.

There is an option in the computer program which allows for grouping one or more rate constants together and refining by the iterative process successively on the members of these groups in turn, instead of allowing all of the rate constants to be varied simultaneously during each iteration. This process is slower, but it avoids the possibility of missing the minimum in the least-squares fit and

very often aids in convergence, particularly if singularities in the matrices could occur. Group refinement was used in all of the triethyl citrate calculations. The members of the groups were changed from run to run and between cycles to avoid any bias in the results.

Table VI is the final summary of our rate constants in terms of the twelve steps postulated for the reaction. The effect of solvent variation on each step is very apparent. However, an analysis of the solvent effect is not easy to evaluate. We believe that in addition to polar and ionic effects which have been commonly observed, both steric and hyperconjugation effects make themselves more felt as the dioxane concentration increases. Steps leading to the rate constants  $k_2$ ,  $k_4$ ,  $k_9$ , and  $k_{11}$  have reactant species in which there are no hydrogen atoms on the carbon  $\alpha$  to the carbonyl carbon. These steps therefore would preclude any contribution from  $\alpha$  hydrogen bonding and consequently no hyperconjugation effects. These are also the steps when the reactant species are most highly steric hindered due to the ester group on the center carbon. It is possible that in high dioxane concentration media, the above-mentioned effects override the polar effects. In the steps leading to the rate constants  $k_1$ ,  $k_3$ ,  $k_6$ , and  $k_7$ , polar effects predominate and the general behavior is similar to what has been previously observed in studies involving simple molecule-ion and ion-ion reactions as a function of the dielectric constant. In the steps leading to the rate constants  $k_5$ ,  $k_8$ ,  $k_{10}$ , and  $k_{12}$  an inductive effect is added to the polar effect. This type of behavior we had reported previously.<sup>2</sup>

*Acknowledgments.* We wish to express our appreciation to the Computer Science Center of the University of Maryland and the National Aeronautics and Space Administration Grant No. NSG-398 for computer time, and to Professor James Stewart for helpful discussions relative to the computer program.

## Solvent Isotope Effects on $pK_a$ of Anilinium Ions in Aqueous Sulfuric Acid

J. L. Jensen\* and M. P. Gardner

Department of Chemistry, California State University, Long Beach, California 90840 (Received December 13, 1972)

Publication costs assisted by the California State University, Long Beach Foundation

Solvent isotope effects on  $K_a$  of a variety of anilinium ions are reported. As anilinium ion  $pK_a$  changes from 5 to -6.5,  $K_a(\text{H}_2\text{O})/K_a(\text{D}_2\text{O})$  changes from 4.6 to 1.4. These isotope effects consist of primary, secondary, and solvation isotope effects. In buffer solutions of constant ionic strength, it appears that changes in secondary isotope effect predominate over changes in primary isotope effect with changing substituents on the aryl group of the aniline. The solvation isotope effect does not appear to be extractable from the secondary isotope effect, except perhaps in the case of 2,4-dinitroaniline.

Two investigations of Hammett indicator behavior in deuteriosulfuric acid have recently been reported.<sup>1,2</sup> It is now established that the Hammett acidity function determined using primary anilines as Hammett indicators in

aqueous sulfuric acid,  $H_0'$ , is virtually identical with the analogous function,  $D_0$ , determined in deuteriosulfuric

- (1) E. Hogfeldt and J. Bigelsen, *J. Amer. Chem. Soc.*, **82**, 15 (1960).  
(2) J. Serrra, M. Ojeda, and P. A. Wyatt, *J. Chem. Soc.*, 1570 (1970).

acid (up to 90% w/w acid). In the course of establishing the  $D_0$  acidity scale,  $pK_a$  values for a variety of anilines were measured in sulfuric and deuteriosulfuric acids. The equilibrium solvent isotope effects thus obtained were expressed as  $\Delta pK_a$  ( $\Delta pK_a = pK_a(D_2O) - pK_a(H_2O)$ ) and varied between 0.1 and 0.6. This corresponds to a  $K_a(H_2O)/K_a(D_2O)$  ratio range of 1.5–4.0, a significant change in equilibrium solvent isotope effect. Data obtained in more dilute sulfuric acid or acetic acid–sodium acetate buffers indicated an approximate correlation between  $pK_a$  and  $\Delta pK_a$  ( $\Delta pK_a$  decreasing as  $pK_a$  decreases); however, the data obtained in more concentrated acid did not bear out this correlation. Due to the vast changes in medium and aniline structure, it is not possible to conclude much from the changes in  $\Delta pK_a$ .

The major purpose of our investigation was to acquire data which would allow meaningful discussion of medium and structural effects. Consequently, we wish to report the equilibrium solvent isotope effect,  $K_a(H_2O)/K_a(D_2O)$ , for a variety of anilinium ions. Experiments were also carried out on both primary and tertiary anilinium ions at constant ionic strength.

### Experimental Section

The variety of problems encountered in attempting accurate reproducible measurement of  $pK_a$  for substituted anilinium ions in solutions of mineral acids has been reported and reviewed in considerable detail.<sup>3,4</sup> The procedure used in the present investigation closely resembles that of Jorgenson and Harter<sup>4</sup> and is summarized below.

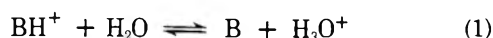
**Materials.** Deuterium oxide and deuteriosulfuric acid were obtained from Stohler Isotope Chemicals and were used without further purification. Anilines obtained commercially were recrystallized from aqueous methanol or vacuum distilled until a constant melting point/boiling point and quantitative ultraviolet spectrum were obtained. Some anilines were purchased from Aldrich Chemicals as Hammett indicators and were certified analytically pure. These indicators were used without further purification.

**Solutions.** A methanolic stock solution of each aniline was prepared. Appropriate quantities of these solutions were diluted to achieve aniline concentrations of  $10^{-3}$ – $10^{-5}$  M in 0.1 N NaOH, acetic acid–sodium acetate buffers (ionic strength maintained at 0.1 using NaCl), or aqueous sulfuric acid. In all cases the final concentration of methanol in the aqueous solutions was 0.75% w/w or less. Deuterated solutions were prepared from  $D_2O$  and NaOH, acetic acid, or deuteriosulfuric acid; however, in all cases the final solutions were at least 99 atom % deuterium.

**Method.** Solutions were placed in a 1-cm silica cell and the visible and/or ultraviolet spectrum recorded on a Beckman DK-2A recording spectrophotometer. The cell compartment was thermostated at  $23 \pm 2^\circ$ . After recording the spectrum, solutions were titrated or the pH was measured (Corning Model 12 research pH meter, expanded scale), as appropriate.

### Results

Determination of  $pK_a$  values were carried out using the following relationships



$$pK_a = -\log \frac{[B][H_3O^+]}{[BH^+]} \frac{f(B)f(H_3O^+)}{f(BH^+)} \quad (2)$$

$$\frac{[B]}{[BH^+]} = \frac{\epsilon(e) - \epsilon(BH^+)}{\epsilon(B) - \epsilon(e)} \quad (3)$$

where values in brackets are molarities,  $f$  represents activity coefficient,  $\epsilon$  represents molar absorptivity (e.g.,  $\epsilon(e)$  is the molar absorptivity of an equilibrium mixture of B and  $BH^+$  of comparable concentrations), and all values of  $\epsilon$  in eq 3 are at the same wavelength.

When the value of  $[H_3O^+]$  was obtained from the measured pH, activity coefficient ratio terms were assumed to follow Debye–Hückel theory and approximate unity. In deuterated solvents, pD was determined using the relationship<sup>5</sup>

$$pD = pH \text{ (measured)} + 0.41$$

In aqueous sulfuric acid solutions,  $H_0$  was used as a measure of  $[H_3O^+]/(f(H_3O^+)f(B)/f(BH^+))$ .<sup>1-4</sup> Measurements of  $[B]/[BH^+]$  rely on the accurate determinations of molar absorptivities,  $\epsilon$ , of the various species. Since molar absorptivities are notoriously medium dependent (as well as  $\lambda^{\max}$ ), the ratio  $[B]/[BH^+]$  was determined at two or three wavelengths in the region of  $\lambda_B^{\max}$ . The reported  $pK_a$  values are averages of these measurements (all done in triplicate). The method of Jorgenson and Harter<sup>4,6</sup> was followed exactly in several instances and found to yield an identical value for  $pK_a$ .

Measurement of  $\epsilon(BH^+)$  and  $\epsilon(B)$  were made in solutions 2 pH or  $H_0$  units different from the  $pK_a$ . In the cases studied, changes in medium over this range did not affect the spectrum sufficiently to affect  $pK_a$  determinations significantly, as shown by the noninterdependence of calculated  $pK_a$  and  $[B]/[BH^+]$  measurement wavelength. In all cases wavelengths were chosen for measurement such that  $\epsilon(BH^+)$  drops out of eq 2; i.e.,  $\epsilon(e)$  and  $\epsilon(B) \gg \epsilon(BH^+)$ .

Table I displays the data in several ways. Values of  $pK_a$  in  $H_2O$  solution ( $pK_a(H_2O)$ ) are reported in column two. Literature values of  $pK_a(H_2O)$  are listed in column three. Since a variety of values have been previously reported for most anilines studied, the values quoted are representative of the ranges which exist in the literature. Values of  $pK_a$  in  $D_2O$  solution are reported in column four; the few literature values are listed in column five (the closeness of these values to ours indicates that consistency in technique and use of more sophisticated equipment helps to eliminate "laboratory dependence" of this type of data). The solvent isotope effect,  $\Delta pK_a$ , is the difference between values in columns two and four; i.e.,  $\Delta pK_a = pK_a(D_2O) - pK_a(H_2O)$ . These values are listed since the few literature values which do exist were reported in this fashion; however, it is more direct to consider the solvent isotope effect not as a log function but in the typical ratio fashion. Therefore the solvent isotope reported as  $K_a(H_2O)/K_a(D_2O)$  is given in column seven of Table I. The discussion to follow centers about the change in solvent isotope effect,  $K_a(H_2O)/K_a(D_2O)$ , with change in aniline structure and/or with change in medium.

(3) M. A. Paul and R. A. Long, *Chem. Rev.*, **57**, 1 (1957).

(4) M. J. Jorgenson and D. R. Harter, *J. Amer. Chem. Soc.*, **85**, 878 (1963).

(5) A. K. Covington, M. Paabo, R. A. Robinson, and R. G. Bates, *Anal. Chem.*, **40**, 700 (1968).

(6) M. J. Jorgenson and D. S. Noyce, *J. Amer. Chem. Soc.*, **83**, 2525 (1961).



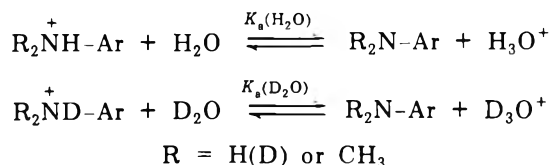
TABLE I: Anilinium Ion  $pK_a$ 

Compound	$pK_a(\text{H}_2\text{O})^a$	Lit. $pK_a(\text{H}_2\text{O})$	$pK_a(\text{D}_2\text{O})^a$	Lit. $pK_a(\text{D}_2\text{O})$	$\Delta pK_a$	$K_a(\text{H}_2\text{O})/K_a(\text{D}_2\text{O})$
2-Methoxyaniline	4.59 ± 0.00		5.11 ± 0.01		0.52	3.27 <sup>b</sup>
Aniline	4.59 ± 0.02	4.60, <sup>c</sup> 4.58 <sup>d</sup>	5.15 ± 0.01		0.56	3.60 <sup>b</sup>
<i>N</i> -Methylaniline	4.82 ± 0.01	4.84, <sup>e</sup> 4.85 <sup>f</sup>	5.49 ± 0.02		0.67	4.70 <sup>b</sup>
<i>N,N</i> -Dimethylaniline	5.12 ± 0.02	5.12, <sup>g</sup> 5.15 <sup>f</sup>	5.78 ± 0.01		0.66	4.58 <sup>b</sup>
2,6-Diethylaniline	3.73 ± 0.02		4.37 ± 0.02		0.64	4.28 <sup>b</sup>
3-Nitroaniline	2.48 ± 0.03	2.47, <sup>h</sup> 2.50 <sup>i</sup>	3.14 ± 0.01		0.66	4.55 <sup>b</sup>
4-Nitroaniline	0.98 ± 0.01	1.00, <sup>j</sup> 0.99 <sup>k</sup>	1.58 ± 0.01		0.60	3.99 <sup>b</sup>
<i>N,N</i> -Dimethyl-4-nitroaniline	0.68 ± 0.00 <sup>u</sup>	0.67, <sup>l</sup> 0.66 <sup>m</sup>	1.28 ± 0.02		0.60	4.07 <sup>b</sup>
2-Nitroaniline	-0.29 ± 0.01	-0.29, <sup>n</sup> 0.29 <sup>o</sup>	0.27 ± 0.02		0.56	3.63
<i>N,N</i> -Dimethyl-2-nitroaniline	2.77 ± 0.02		3.45 ± 0.02		0.68	4.78 <sup>b</sup>
2-Chloro-4-nitroaniline	-0.91 ± 0.01		-0.39 ± 0.01		0.52	3.30
2-Nitro-4-chloroaniline	-0.98 ± 0.01	-0.97, <sup>p</sup> -1.02 <sup>q</sup>	-0.46 ± 0.01	-0.46 <sup>q</sup>	0.52	3.36
2,4-Dichloro-6-nitroaniline	-3.13 ± 0.03	-3.16, <sup>q</sup> -3.79 <sup>n</sup>	-2.76 ± 0.01	-2.73 <sup>q</sup>	0.37	2.32
2,6-Dichloro-4-nitroaniline	-3.25 ± 0.02	-3.24 <sup>r</sup>	-2.89 ± 0.02	-2.96 <sup>s</sup>	0.36	2.28
2,4-Dinitroaniline	-4.43 ± 0.02	-4.42, <sup>q</sup> -4.53 <sup>t</sup>	-4.02 ± 0.00	-4.03 <sup>q</sup>	0.41	2.58
<i>N,N</i> -Dimethyl-2,4,6-trinitroaniline	-4.46 ± 0.03 <sup>u</sup>	-6.55 <sup>m</sup>	-6.31 ± 0.02 <sup>u</sup>		0.15	1.41
	-4.99 ± 0.03 <sup>v</sup>	-4.98 <sup>q</sup>	-4.61 ± 0.02 <sup>v</sup>	-4.67 <sup>q</sup>		

<sup>a</sup> Mean values of replicate determinations ± average deviation. <sup>b</sup> Ionic strength held constant at 0.1 using NaCl. <sup>c</sup> R. A. Benkeser and H. R. Krysiak, *J. Amer. Chem. Soc.*, **75**, 2421 (1953). <sup>d</sup> R. N. Beale, *J. Chem. Soc.*, 4494 (1954). <sup>e</sup> B. Gutbezahl and E. Grunwald, *J. Amer. Chem. Soc.*, **75**, 559 (1953). <sup>f</sup> A. L. Bacarella, E. Grunwald, H. P. Marshall, and E. L. Purlee, *J. Org. Chem.*, **20**, 747 (1955). <sup>g</sup> A. Ebrother, E. Jucher, A. Lindenmann, E. Rissi, R. Steiner, R. Sless, and A. Vogel, *Helv. Chim. Acta*, **42**, 533 (1959). <sup>h</sup> M. M. Ficking, A. Fischer, B. R. Mann, J. Packer, and J. Vaughan, *J. Amer. Chem. Soc.*, **81**, 4226 (1959). <sup>i</sup> K. N. Bascombe and R. P. Bell, *J. Chem. Soc.*, 1096 (1959). <sup>j</sup> A. I. Biggs and R. A. Robinson, *ibid.*, 388 (1961). <sup>k</sup> M. Kilpatrick and C. A. Arenberg, *J. Amer. Chem. Soc.*, **75**, 3812 (1953). <sup>l</sup> A. V. Willi, *Helv. Chim. Acta*, **40**, 2019 (1957). <sup>m</sup> E. M. Arnett and G. W. Mach, *J. Amer. Chem. Soc.*, **86**, 2671 (1964). <sup>n</sup> N. F. Hall and W. F. Sprengeman, *ibid.*, **62**, 2487 (1940). <sup>o</sup> H. Suzuki, "Electronic Absorption Spectra and Geometry of Organic Molecules," Academic Press, New York, N. Y., 1967. <sup>p</sup> Reference 3. <sup>q</sup> E. Hogfelct and J. Bigelaisen, *J. Amer. Chem. Soc.*, **82**, 15 (1960). <sup>r</sup> R. H. Boyd, *ibid.*, **85**, 1553 (1963). <sup>s</sup> Reference 2. <sup>t</sup> L. P. Hammett and M. A. Paul, *ibid.*, **56**, 827 (1934). <sup>u</sup>  $H_0'''$  used to calculate  $pK_a$  ( $D_0'''$  assumed to equal  $H_0'''$ ). <sup>v</sup>  $H_0'$  used to calculate  $pK_a$ .

## Discussion

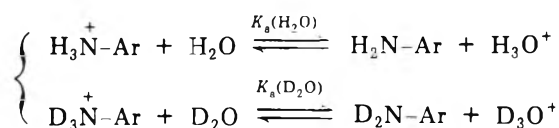
The solvent isotope effect on the  $K_a$  of anilinium ions is a composite isotope effect. In many instances, composite isotope effects are not resolvable into the various parts; in this investigation the results are partially resolvable experimentally and totally resolvable conceptually.



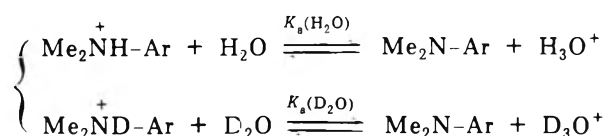
In the equilibria above, three types of isotope effects make up the overall solvent isotope effect. (1) Primary isotope effect—the equilibrium involves the transfer of a proton (deuteron) from nitrogen to solvent. (2) Solvation isotope effect<sup>7,8</sup>— $K_a(\text{H}_2\text{O})$  is determined in  $\text{H}_2\text{O}$  solvent and  $K_a(\text{D}_2\text{O})$  is determined in  $\text{D}_2\text{O}$  solvent. These two solvents ( $\text{H}_2\text{O}$  and  $\text{D}_2\text{O}$ ) differ slightly in dielectric constant, solvating ability, etc. (3) Secondary isotope effect of the first kind—this isotope effect exists only for primary and secondary anilinium ions, where  $\text{R} = \text{H(D)}$ . It arises because of the impossibility of retaining  $\text{ArNH}_2$  or  $\text{ArNH}_3^+$  in a solution of  $\text{D}_2\text{O}$ . Overall, then, we are comparing the transfer of a proton from, say,  $\text{ArNH}_3^+$  to  $\text{H}_2\text{O}$  in  $\text{H}_2\text{O}$  to the transfer of a deuteron from  $\text{ArND}_3^+$  to  $\text{D}_2\text{O}$  in  $\text{D}_2\text{O}$ . These three effects will be related to experimental data in subsequent sections.

**Primary vs. Tertiary Anilinium Ion  $K_a(\text{H}_2\text{O})/K_a(\text{D}_2\text{O})$ .** Following the convention established by Arnett and Mach,<sup>9</sup> we denote the solvent isotope effect on primary anilinium ions as  $(K_a(\text{H}_2\text{O})/K_a(\text{D}_2\text{O}))'$  and the solvent isotope effect on tertiary anilinium ions as  $(K_a(\text{H}_2\text{O})/K_a(\text{D}_2\text{O}))'''$  based on the following two sets of equilibria.

$$(K_a(\text{H}_2\text{O})/K_a(\text{D}_2\text{O}))'$$

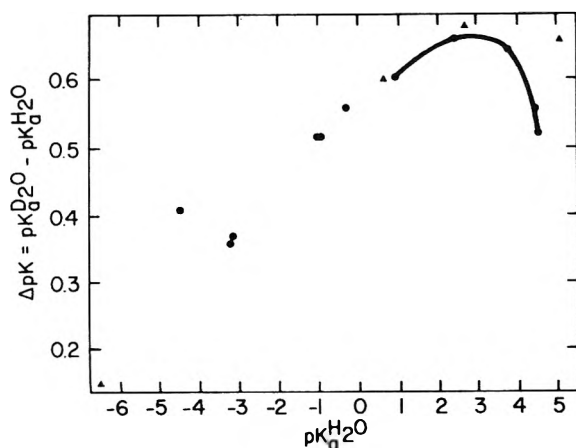


$$(K_a(\text{H}_2\text{O})/K_a(\text{D}_2\text{O}))'''$$



$(K_a(\text{H}_2\text{O})/K_a(\text{D}_2\text{O}))'$  is a composite isotope effect comprised of a solvation isotope effect, a primary isotope effect, and a secondary isotope effect of the first kind.  $(K_a(\text{H}_2\text{O})/K_a(\text{D}_2\text{O}))'''$  is a composite isotope effect comprised of a solvation isotope effect and a primary isotope effect. If it could be assumed that the solvation isotope effect and the primary isotope effect were the same for a given pair of primary and tertiary anilinium ions, the following considerations would be considerably simplified. However, while such an assumption is probably approxi-

- (7) The term solvent isotope effect is used to denote an isotope effect arising due to an isotopic change in the solvent used for a particular measurement. However, as noted above, such isotope effects are often composite in nature and in major part may be due to the presence of a primary isotope effect. Solvent isotope effects are so named based on the type of experiment performed. Consequently, a term other than solvent isotope effect must be used when discussing an isotope effect arising solely from differences in solvating ability, dielectric constant, etc. between isotopic solvents. The term "solvation isotope effect" lends clarity to these discussions.<sup>8</sup>
- (8) E. K. Thornton and E. R. Thornton in "Isotope Effects in Chemical Reactions," C. J. Collins and N. S. Bowman, Ed., Van Nostrand-Reinhold, New York, N. Y., 1970, Chapter 4.
- (9) See discussion pertaining to tertiary anilinium ion data from Table III.



**Figure 1.** Solvent isotope effects,  $\Delta pK$ , plotted vs.  $pK_a(H_2O)$ . Solid curve indicates region of constant ionic strength (0.1). ● indicates primary anilinium ions, ▲ indicates tertiary anilinium ions.

**TABLE II: Solvent Isotope Effects on Primary and Tertiary Anilinium Ion  $K_a$**

Compound	$K_a(H_2O)/K_a(D_2O)$
Aniline	3.6
<i>N,N</i> -Dimethylaniline	4.6
4-Nitroaniline	4.0
<i>N,N</i> -Dimethyl-4-nitroaniline	4.1
2-Nitroaniline	3.6 <sup>a</sup>
<i>N,N</i> -Dimethyl-2-nitroaniline	4.8

<sup>a</sup> Ionic strength is 0.6. for all the other measurements,  $\mu = 0.1$ .

mately true for the solvation isotope effect, it certainly is not even approximately true for the primary isotope effect.

An hypothesis which needs to be considered is that the primary isotope effect *difference* in one pair of primary and tertiary anilinium ions is close to that *difference* in another pair. Such an hypothesis assumes that the effect of replacing two hydrogens by methyls is about the same, regardless of the substitution on the aryl group. If this hypothesis were correct, the differences between  $(K_a(H_2O)/K_a(D_2O))'$  and  $(K_a(H_2O)/K_a(D_2O))''$  listed in Table II should be nearly constant, which obviously they are not (if the hypothesis were approximately true for the large primary isotope effect, it would surely be true for the much smaller secondary isotope effect). Consequently, we are left with the inescapable conclusion that the differences between the pairs listed in Table II arise mainly from changes in primary isotope effect.

The data in Table II clearly show, then, that  $(K_a(H_2O)/K_a(D_2O))''$  and  $(K_a(H_2O)/K_a(D_2O))'$  differ (for a given pair of primary and tertiary anilinium ions) due to differences in primary isotope effects *and* secondary isotope effects of the first kind. Differences in primary isotope effects appear to predominate and the magnitude of the secondary isotope effect cannot be extracted.

It is interesting to note that the large steric effect in *N,N*-dimethyl-2-nitroaniline is reflected not only in  $pK_a$  but also rather dramatically in the difference between  $(K_a(H_2O)/K_a(D_2O))'$  and  $(K_a(H_2O)/K_a(D_2O))''$ . Aside from the steric effect, it seems reasonable to expect that the 2-nitro- and 4-nitro-substituted anilinium ions might exhibit similar  $(K_a(H_2O)/K_a(D_2O))'$  and  $(K_a(H_2O)/$

**TABLE III: Solvent Isotope Effects at Constant Ionic Strength (0.1)**

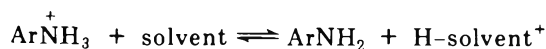
Compound <sup>a</sup>	$K_a(H_2O)/K_a(D_2O)$
2-Methoxyaniline	3.3
Aniline	3.6
2,6-Diethylaniline	4.3
3-Nitroaniline	4.6
4-Nitroaniline	4.0
<i>N,N</i> -Dimethylaniline	4.6
<i>N,N</i> -Dimethyl-2-nitroaniline	4.8
<i>N,N</i> -Dimethyl-4-nitroaniline	4.1

<sup>a</sup> Each series is listed in order of increasing anilinium ion acidity (increasing  $K_a$ , decreasing  $pK_a$ ).

$K_a(D_2O))''$  differences, which from Table II is clearly not the case at all. This is the first instance of "steric inhibition of resonance" demonstrated in isotope effects.

$K_a(H_2O)/K_a(D_2O)$  at Constant Ionic Strength. Maintaining constant ionic strength minimizes the solvation isotope effect.<sup>7</sup> The solvation isotope effect will not be constant since as the nature of the solute changes, solute-solvent interactions (solvation) changes, resulting in some change in the solvation isotope effect. However, for the ensuing discussion this change will be assumed reasonably regular and smaller in comparison with the primary and secondary effects (a more complete discussion is presented in the subsequent section).

For anilinium ion-aniline equilibria in aqueous solution, the primary and secondary isotope effects are functions of the same quantity, the overall change in force constants between the N-H bonds of anilinium ion and the N-H bonds of aniline and the solvent-H bond.



Changes in solvent isotope effect on tertiary anilinium ion  $K_a$  essentially reflect changes in primary isotope effect which reflect change in force constant of the N-H bond of the anilinium ion. Changes in solvent isotope effect on primary anilinium ion  $K_a$  reflect changes in primary *and* secondary isotope effects. These data are summarized in Table III and are reported graphically in Figure 1 (log-log plots allow greater changes to be displayed, therefore  $pK_a(D_2O) - pK_a(H_2O)$  is plotted vs.  $pK_a(H_2O)$ ). The data pertaining to this discussion are connected by the solid line in Figure 1.

Data for the tertiary anilinium ions is explained in a straightforward fashion. As  $pK_a$  decreases (acidity increases) the primary isotope effect decreases, in accord with a decreasing force constant for the N-H anilinium ion bond.  $K_a(H_2O)/K_a(D_2O)$  for *N,N*-dimethylaniline and *N,N*-dimethyl-2-nitroaniline (4.6 and 4.8, respectively) are constant within our experimental error, but the value of 4.1 for *N,N*-dimethyl-4-nitroaniline is definitely lower.

For the primary anilinium ions of 3-nitroaniline and 4-nitroaniline the above explanation also fits. However, the decrease in  $K_a(H_2O)/K_a(D_2O)$  as electron-attracting substituents are replaced by electron-repelling substituents on the aryl group is striking. This appears as a maximum for the curve plotted in Figure 1 (at about  $pK_a(H_2O) = 3$ ).

The large isotope effect observed on anilinium ion  $K_a$  is indication of an overall bond "loosening" (net decrease in

TABLE IV: Solvent Isotope Effects in Sulfuric Acid Solutions

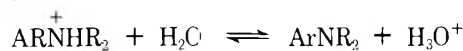
Compound	$pK_a(\text{H}_2\text{O})$	$K_a(\text{H}_2\text{O})/K_a(\text{D}_2\text{O})$	$[\text{H}_2\text{SO}_4], M^a$
2-Nitroaniline	-0.29	3.6	0.6
2-Chloro-4-nitroaniline	-0.91	3.3	2
2-Nitro-4-chloroaniline	-0.98	3.4	2
2,4-Dichloro-6-nitroaniline	-3.13	2.3	6
2,6-Dichloro-4-nitroaniline	-3.25	2.3	6
2,4-Dinitroaniline	-4.43	2.6	8
<i>N,N</i> -Dimethyl-2,4,6-trinitroaniline	-6.46	1.4	10

<sup>a</sup> Approximate molarity of sulfuric acid solution in which  $K_a$  was measured.

force constant) for isotopically substituted bonds. It was demonstrated in the previous section that  $K_a(\text{H}_2\text{O})/K_a(\text{D}_2\text{O})$  decreases with increasing  $K_a$  due primarily to a decreasing primary isotope effect (which arises from a loosening of the anilinium ion N-H bond). However, for primary anilinium ion  $K_a$ ,  $K_a(\text{H}_2\text{O})/K_a(\text{D}_2\text{O})$  increases with increasing  $K_a$  when  $K_a < 10^{-3}$ . This behavior may be explained as follows. As  $K_a$  increases (due to relative -I, -R substitution on Ar) two things happen. (1) Anilinium ion N-H bonds "loosen."<sup>9</sup> (2) Aniline N-H bonds "tighten."<sup>10</sup> If electron-contributing substituents affect 2 much more than 1 then the secondary isotope effect predominates over the primary, giving rise to the observed curve. This appears plausible since the secondary effect arises from the net force constant change introduced by changing two anilinium ion N-H bonds into two aniline N-H bonds. It is also significant that the curve in Figure 1 has a steeper slope in the low  $K_a$  region; this is consistent with a sizeable change in secondary isotope effect predominating change over the primary isotope effect change when  $K_a < 10^{-3}$  (in the region where the primary effect has reached its maximum value) and the change in secondary isotope effect somewhat compensating for the sizeable change in primary isotope effect when  $K_a < 10^{-3}$ . That the primary isotope effect is maximized at about  $K_a = 10^{-3}$  is substantiated by the constancy of  $K_a(\text{H}_2\text{O})/K_a(\text{D}_2\text{O})$  for tertiary anilinium ions over the region  $K_a = 10^{-2.8}$ - $10^{-5.1}$ .

**Solvent Isotope Effects in Strong Acid Solutions.** As  $K_a$  increases beyond  $10^{-1}$ , the medium in which it is measured changes. For example,  $K_a$  of the anilinium ions of 2-nitroaniline, 2-chloro-4-nitroaniline, 2,4-dichloro-6-nitroaniline, and 2,4-dinitroaniline were measured in 0.6, 2, 6, and 8 M sulfuric acid, respectively. The nature of the solvent is clearly changing as the medium changes from 0.6 to 8 M sulfuric acid. Probably the most significant change is a marked decrease in the activity of water, resulting in a decreasingly effective solvation of solutes via hydrogen bonding. The more strongly solvated a solute, the more solvation energy it loses as the activity of water is decreased. Clearly the nitro-substituted anilinium ions are more strongly solvated (via specific hydrogen bonding) than the nitro-substituted anilines, due primarily to strong and specific solvation at the anilinium ion N-H protons. This solvent change, then, has a net effect of increasing  $K_a$  (i.e., the solvent change influences  $K_a$  in the

same direction as the substituent effect on the aryl group of the anilinium ion). Consequently, since solvation is more effective in  $\text{H}_2\text{O}$  than in  $\text{D}_2\text{O}$ ,<sup>8,12,13</sup> the overall solvation effect is to increase  $K_a(\text{H}_2\text{O})$  more than  $K_a(\text{D}_2\text{O})$  with decreasing activity of water, resulting in  $K_a(\text{H}_2\text{O})/K_a(\text{D}_2\text{O})$  increasing. In opposition to this solute-solvent solvation effect is the loosening of  $\text{H}_2\text{O}$  (or  $\text{D}_2\text{O}$ ) bonds as acidity is increased. The appropriate data are summarized in Table IV and Figure 1 (the points not connected by the solid line).



$K_a(\text{H}_2\text{O})/K_a(\text{D}_2\text{O}) > 1$  because the above reaction proceeds with overall bond loosening. As acidity is increased, then, (1) the solute-solvent solvation forces favor an increase in  $K_a(\text{H}_2\text{O})/K_a(\text{D}_2\text{O})$  (see previous paragraph), (2)  $\text{H}_2\text{O}$  (or  $\text{D}_2\text{O}$ ) bonds are loosening, favoring a decrease in  $K_a(\text{H}_2\text{O})/K_a(\text{D}_2\text{O})$ , and (3)  $\text{H}_3\text{O}^+$  (or  $\text{D}_3\text{O}^+$ ) bonds are loosening, favoring an increase in  $K_a(\text{H}_2\text{O})/K_a(\text{D}_2\text{O})$ . Whether the net result should be to increase or decrease  $K_a(\text{H}_2\text{O})/K_a(\text{D}_2\text{O})$  is not possible to completely determine. However, it may be that the increase in  $K_a(\text{H}_2\text{O})/K_a(\text{D}_2\text{O})$  noted by others in very high acid molarities<sup>2</sup> arises from 1 becoming predominant as more specific solvation sites are introduced and as the solvating agent becomes a  $(\text{H}_3\text{O}^+)(\text{H}_2\text{O})$  moiety.

As is evident from Table II and especially Figure 1, the solvent isotope effect decreases fairly regularly with decreasing  $pK_a$  which is consistent with a large decrease in primary isotope effect predominating over smaller decreases in secondary and changes in solvation isotope effects. The lone but notable exception is 2,4-dinitroaniline; although an anilinium ion is more acidic by a factor of 10 than the dichloronitroanilines, the solvent isotope effect is significantly larger. Although the data do not permit a definitive solution to this problem, an attractive postulate is that introduction of a second nitro group increases solvation of the aniline sufficiently so as to cause this significant rise in  $K_a(\text{H}_2\text{O})/K_a(\text{D}_2\text{O})$ . It is probable that the nitro groups of the aniline are more strongly solvated than the nitro group of an anilinium ion and, as the second nitro group is placed in conjugation with the amino group, the N-H amine protons may become significantly solvated as well. This is consistent with recent work pertaining to the  $sp^2$  hybrid nature of nitrogen in conjugated nitroanilines.<sup>14</sup>

## Summary

Solvent isotope effects on  $K_a$  of tertiary anilinium ions at constant ionic strength have shown that the primary isotope effect does not depend upon anilinium ion structure when  $K_a < 10^{-3}$ . Solvent isotope effects on  $K_a$  of primary anilinium ions at constant ionic strength have shown that the secondary isotope effect is strongly dependent upon anilinium ion structure. Indeed, when  $K_a < 10^{-3}$ , changes in secondary isotope effect predominate over changes in

(10) As electron-withdrawing substituents are placed on the aryl group of aniline  $\nu_{\text{NH}}$  increases and as electron-contributing substituents are placed on Ar,  $\nu_{\text{NH}}$  decreases.<sup>11</sup>

(11) L. S. Bellamy, "Advances in Infrared Group Frequencies," Methuen, London, 1968, p 95.

(12) C. A. Bunton and V. J. Shiner, *J. Amer. Chem. Soc.*, **83**, 42, 3207, 3214 (1961).

(13) J. L. Jensen and M. P. Gardner, *J. Phys. Chem.*, in press.

(14) J. W. Eastes, M. H. Aldredge, R. R. Minesinger, and M. J. Kamlet, *J. Org. Chem.*, **36**, 3847 (1971).

primary isotope effect, giving rise to a maximum in the curved plotted in Figure 1,  $pK_a(\text{H}_2\text{O})$  vs.  $pK_a(\text{D}_2\text{O}) - pK_a(\text{H}_2\text{O})$ .

Change in medium (acid molarity) affect the solvent isotope effect. As acidity is increased, the solvent isotope

effect should decrease due to solute-solvent solvation changes but increase due to a net loosening of  $\text{H}_2\text{O}$  (or  $\text{D}_2\text{O}$ ) bonds. The only factor which may be sorted out is that nitro groups are strongly and specifically solvated in strongly acidic medium.

## Protolysis and Nitrogen Inversion of Anilines in Sulfuric Acid<sup>1</sup>

Donald E. Leyden\* and Ronald E. Channell

Department of Chemistry, University of Georgia, Athens, Georgia 30601 (Received August 17, 1972)

The protolysis and nitrogen inversion kinetics of several substituted anilines have been studied using water-sulfuric acid as the solvent. Line shape analysis of the high-resolution nmr spectra of the amines was used to determine the rate of reaction. The studies were performed in the 50–90° range to reduce line broadening because of the high solution viscosity. An acidity function was used as a measure of acidity. Results indicate the principal mechanism of proton exchange is similar to that of alkyl amines, but with larger rate constants. The rate constant for breaking of an amine-water hydrogen bond decreases with increasing size of the *N*-alkyl substituents. The rate of the nitrogen inversion process is closely related to the protolysis rate.

### Introduction

Recently the kinetic analysis of proton exchange between ammonium ions and aqueous acid has been extensively studied.<sup>2–8</sup> Both high-resolution<sup>2,3,5,7,8</sup> and pulsed<sup>4,6,7</sup> nuclear magnetic resonance techniques have been employed, and data are available over a wide range of acid and ammonium ion concentrations. A rather extensive study has also been conducted in the area of nitrogen inversion in aliphatic amines.<sup>9,10</sup> However, there has been very little study of the proton exchange of aromatic amines such as anilines,<sup>11</sup> and essentially no work has been done in the area of nitrogen inversion of aniline compounds.<sup>12</sup> In previous studies, a similar kinetic scheme appears to prevail over a wide range of acid and/or amine concentrations<sup>6,13</sup> as well as amine structures. Apparently, the variations in the rate constants of the exchange and inversion reactions are not simply related to the basicity of the amines or steric factors.<sup>6</sup> This paper is a report of the results of an investigation of the proton exchange kinetics of *N*-methylaniline (I), *N,N*-dimethylaniline (II), *N*-methyl-*N*-ethylaniline (III), *N*-benzylaniline (IV), *N*-methyl-*N*-benzylaniline (V), *N*-ethyl-*N*-benzylaniline (VI), and *N*-methyl-*N*-benzyl-*p*-anisidine (VII). The results of an investigation of nitrogen inversion of V, VI, and VII in sulfuric acid and deuteriosulfuric acid are also discussed.

Although extensive use of high-resolution nmr for studies of the type reported here have been described repeatedly, a brief discussion of the basis of the method is given for clarity. In the case of proton exchange, it is most convenient to use the broadening and eventual coalescence of a multiplet resulting from spin-spin coupling between the labile N-H proton and protons of an *N*-alkyl group such as a methyl group.<sup>2</sup> In the case of tertiary methyl amines,

a simple doublet is observed for the methyl protons. To detect inversion of the nitrogen atom, some type of diastereotropic probe is required. Most convenient is the benzyl group because the methylene protons give rise to a clean AB pattern in the limit of slow interchange between the enantiomers. Because the magnetic environments of the two methylene protons interchange upon inversion of the amine nitrogen atom, the AB pattern will broaden and eventually coalesce in the limit of fast inversion. Because nonlabile protons are observed, and coupling to the exchanging proton is not desired, these studies may be performed in deuterium solvents.

### Experimental Section

All anilines with the exception of VII were obtained from Aldrich Chemical Co. or Eastman Organic Chemical Co. and were purified by vacuum distillation. VII was prepared from *p*-anisidine which was obtained from Eastman Organic Chemical Co. *N*-Benzyl-*p*-anisidine was prepared

- (1) This investigation was supported in part by Public Health Service Grant No. GM-13935 from the National Institutes of Health.
- (2) E. Grunwald, A. Loewenstein, and S. Meiboom, *J. Chem. Phys.*, **27**, 630 (1957).
- (3) A. Loewenstein and S. Meiboom, *J. Chem. Phys.*, **27**, 1067 (1957).
- (4) E. K. Ralph, III, and E. Grunwald, *J. Amer. Chem. Soc.*, **89**, 2963 (1967).
- (5) R. J. Day and C. N. Reilley, *J. Phys. Chem.*, **71**, 1588 (1967).
- (6) E. Grunwald and E. K. Ralph, III, *J. Amer. Chem. Soc.*, **89**, 4405 (1967).
- (7) E. Grunwald and A. Y. Ku, *J. Amer. Chem. Soc.*, **90**, 29 (1968).
- (8) D. E. Leyden and W. R. Morgan, *J. Phys. Chem.*, **73**, 2924 (1969).
- (9) W. R. Morgan and D. E. Leyden, *J. Amer. Chem. Soc.*, **92**, 4527 (1970).
- (10) D. E. Leyden and W. R. Morgan, *J. Phys. Chem.*, **75**, 3190 (1971).
- (11) E. Grunwald, R. L. Lipnick, and E. K. Ralph, *J. Amer. Chem. Soc.*, **91**, 4333 (1969).
- (12) H. Kessler and D. Leibfritz, *Tetrahedron*, **25**, 5127 (1969).
- (13) M. Emerson, E. Grunwald, M. Kaplan, and R. Kromhout, *J. Amer. Chem. Soc.*, **82**, 6307 (1960).

by treating *p*-anisidine with benzaldehyde to prepare the corresponding Schiff base, which subsequently was reduced with sodium borohydride.<sup>14</sup> VII was then prepared by treating *N*-benzyl-*p*-anisidine with formic acid,<sup>15</sup> followed by the reduction of the resulting amide with lithium aluminum hydride. The product was confirmed by nmr. Stock solutions were prepared from the anilines and sulfuric acid and were diluted to the desired aniline and/or acid concentrations. Each solution was then analyzed by potentiometric titration. Aniline concentrations ranged from 1.0 to 0.25 *M* with excess sulfuric acid present from 60 to 40%. Deuteriosulfuric acid was prepared by reaction of phosphorus pentoxide with fuming sulfuric acid under a nitrogen atmosphere. The resulting sulfur trioxide was bubbled through deuterium oxide. The per cent H in the solution was determined by standard addition of H<sub>2</sub>O to the solution followed by integration of the HDO nuclear magnetic resonance line. Back extrapolation of the plot of area *vs.* added H<sub>2</sub>O yielded the per cent H present in the D<sub>2</sub>SO<sub>4</sub> which was found to be less than 0.3%. Dissociation constants were determined at 50° by differential potentiometric titration.<sup>16</sup> Nmr measurements were made at 50° for I, II, and III, at 70° for V and VII, and at 90° for IV and VI. These temperatures were selected in order to avoid viscosity broadening of the nmr lines.

Nuclear magnetic resonance data were obtained on a Hitachi Perkin-Elmer R-20 nuclear magnetic resonance spectrometer operated under slow passage conditions. Routine checks were made to ensure against saturation. The temperature was regulated to within ±1° using a standard R-20 variable temperature probe.

Exchange rate parameters were obtained by comparison of computer-simulated line shapes with experimental ones. The simulated mean residence time,  $\tau$ , of a proton on a given aniline molecule was adjusted so that a minimum standard deviation between computed and experimental points on the spectrum was obtained. The program used was prepared using equations similar to those given by Arnold<sup>17</sup> for spin-coupled systems in which the coupling is small compared with the chemical shifts of the coupled nuclei. The simulated residence time of a proton before A-B interchange was used to obtain the inversion rate parameters and was also adjusted so that a minimum standard deviation between computed and experimental points in the spectra was obtained. The program was prepared utilizing the equations of Alexander.<sup>18</sup> In both cases the natural line width was taken from the line width at half height of the group under study in solutions of low acidity in which the exchange or inversion is very rapid and was found to approximately 0.5 Hz in most cases. This measurement was made for each experimental point and the value was assumed to be controlled by inhomogeneities in the magnetic field. Although this line width is not a measurement of  $T_2$  as desired, there were reasons for this choice as an approximation of  $T_2$ . First, in sufficiently acidic solutions to achieve "nonexchanging" conditions for more accurate  $T_2$  measurements, viscosity caused serious line broadening. It was apparent that attempts to correct this phenomenon would introduce considerable errors. Experimental points were not taken in this region of acidity. Second, a comparison of the line widths of aliphatic amines in the slow exchange limit in aqueous acid gave values within 0.1 Hz. This observation implies that factors other than a pure  $T_2$  relaxation are controlling the line width. Finally, considering that data

TABLE I: Nmr Spectral Parameters for Compounds Studied

Amine	$J_{AX}^a$	$J_{AB}^a$	$\Delta_{AB}^b$
I	5.67		
II	5.16		
III	5.15		
IV	4.96		
V	5.16	12.70	11.48
VI	3.89, (7.44 <sup>c</sup> )	12.84	15.41
VII	5.00	12.75	13.47

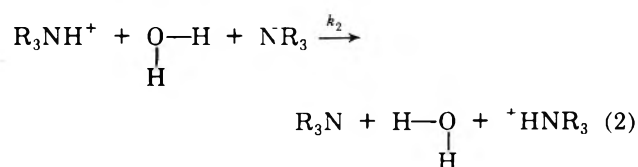
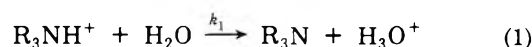
<sup>a</sup> All in Hz. <sup>b</sup> All in Hz at 60 MHz. <sup>c</sup>  $J_{BX}$  in Hz.

were taken only from the middle of the nmr kinetic window (*i.e.*, extensive line broadening), errors caused by  $T_2$  estimation should be minimal. Thus, the choice was made to use the line width at the fast exchange limit as the best available source of a natural line width. The spin-coupling constants  $J$  between the N-H proton and the group under study in the various compounds are given in Table I. The spectral parameters for the A-B pattern are also given in Table I.

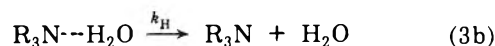
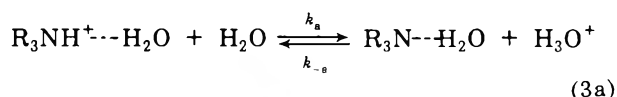
The sulfuric acid concentration required for these studies was in the range of 40–60%. Rate data were plotted *vs.* the Hammett acidity for tertiary amines given by Arnett and Mach.<sup>19</sup> All data were treated with standard least-squares techniques. The precision of the data for both exchange and inversion processes varied between 5 and 10% relative standard deviation. When data repeated on different runs are included, an estimate of 15% relative standard deviation is obtained. This is reasonably typical of nmr kinetic data.

## Results

There are several possible mechanisms of proton exchange in the H<sub>2</sub>SO<sub>4</sub>-H<sub>2</sub>O solvent system that have evolved in previous investigations.<sup>6,7,13,20</sup> However, eq 1 and 2 represent those which repeatedly have been shown to be the predominant mechanisms in acidic solutions.<sup>6,8,13</sup>



Reaction 1 has been shown to occur in two steps.<sup>6,13</sup> These are given as



By applying a steady-state approximation to the concen-

- (14) S. Yamada and S. Ikegami, *Chem. Pharm. Bull.*, **14**, 1382 (1966).
- (15) "Organic Synthesis," Collect. Vol. III, Wiley, New York, N. Y., 1964, p 590.
- (16) A. L. Bacarella, E. Grunwald, H. P. Marshall, and E. L. Purlee, *J. Org. Chem.*, **20**, 747 (1955).
- (17) J. T. Arnold, *Phys. Rev.*, **102**, 136 (1956).
- (18) S. Alexander, *J. Chem. Phys.*, **37**, 967 (1962).
- (19) E. M. Arnett and G. W. Mach, *J. Amer. Chem. Soc.*, **86**, 2671 (1964).
- (20) D. E. Leyden and J. F. Whicby, *J. Phys. Chem.*, **73**, 3076 (1969).

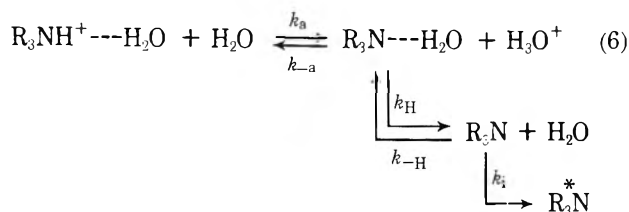
tration of  $R_3N \cdot H_2O$  in reaction 3 and combining the result with reaction 2 a total rate equation may be obtained.<sup>6,8,9,13,20</sup> This is given by

$$1/\tau = \text{rate}/[R_3NH^+] = \frac{k_H k_a}{k_H + k_{-a}[H^+]} + \frac{k_2 K_a [R_3NH^+]}{[H^+]} \quad (4)$$

This equation has been widely and successfully used to explain the protolysis kinetics of a variety of amines. Although many combinations of values of the parameters of eq 4 are possible, the most general case predicts first an increase of the proton exchange rate with a decrease in acidity, followed by an acid-independent region where  $k_H \gg k_{-a}[H^+]$  and the second-order term is negligible, and finally an increase in rate with a decrease in acidity as the second term in the equation becomes large compared with  $k_a$ . However, for each aniline compound studied, a plot of  $1/\tau$  vs.  $1/h_0'''$  was linear over the entire acid range employed and none of the anilines exhibited second-order dependence in this acid range. The exchange phenomenon may be represented by eq 5 where  $k_a/k_{-a}$  is assumed to equal  $K_a$ , the dissociation constant for the anilinium ion. The value of  $[H^+]$  must be represented in terms of an acidity function.

$$1/\tau = \text{rate}/[R_3NH^+] = \frac{k_H k_a}{k_{-a}[H^+]} = \frac{k_H K_a}{[H^+]} \quad (5)$$

A scheme for the nitrogen inversion of amines in acid solution has been proposed as<sup>9,10,21</sup>



where  $R_3^*N$  represents an inverted species of  $R_3N$ . The rate of inversion is described in eq 7 in which  $1/\tau_i$  represents the observed rate of A-B interchange,  $k_i$  is the inversion rate constant and  $k_{-H}$  is the pseudo-first-order rate constant of rehydration (and/or) reprotonation of the amine. In eq 7,  $f = k_i/(k_i + k_{-H})$  or the fraction of dehy-

$$1/\tau_i = \frac{\text{rate}}{[BH^+]} = \left( \frac{f k_a K_H}{k_{Hf} + k_{-a}[H^+]} \right) \quad (7)$$

drated amine molecules which undergo nitrogen inversion before reprotonation or rehydration. In this scheme it is assumed that neither protonated or hydrated ( $R_3N \cdot H_2O$ ) amine molecules can invert at a rate comparable to the free amine. In concentrated sulfuric acid  $k_H \ll k_{-a}[H^+]$ . If  $k_i$  is much less than  $k_{-H}$ , the observed rate of A-B interchange will be some fraction of the rate of proton exchange given by the mechanism represented by eq 3. In other words, only a fraction of the molecules which undergo proton exchange, breaking the  $R_3N \cdot H_2O$  bond, will also undergo nitrogen inversion. On the other hand, if  $k_i$  is much greater than  $k_{-H}$ , eq 7 becomes identical with the first term in eq 4; the rate of inversion will be equal to the rate of proton exchange executed by the first-order mechanism. If  $k_i = k_{-H}$ , the observed rate of A-B interchange will be half the rate of proton exchange given by the mechanism represented by eq 3. Qualitatively it can be

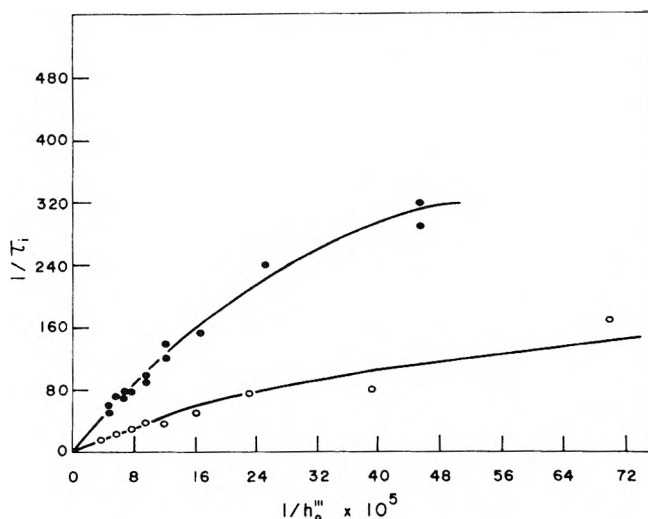


Figure 1. Plot of  $1/\tau_i$  (A-B interchange) vs.  $1/h_0'''$  for *N*-benzyl-*N*-methyl-*p*-anisidine: ●,  $H_2SO_4$  solvent; ○,  $D_2SO_4$  solvent.

recognized that if many inversions occur before the aniline is rehydrated (and reprotonated), there is an equal probability of obtaining the original and inverted enantiomer. This is also true if the planar state is resonance stabilized, since there is an equal probability of rehydration (and reprotonation) of either invertomer. Under these conditions, the observed rate of A-B interchange will be one-half the rate of proton exchange. In this event,  $k_i$  cannot be evaluated. In any case  $k_i/(k_i + k_{-H})$  can only be evaluated as a value representing some fraction of the rate of proton exchange. The principal reason for this is the lack of data on the value of  $k_{-H}$ .

We became interested in studying the proton exchange and nitrogen inversion of aniline compounds because of the ability of unprotonated nitrogen to participate in resonance interactions with the benzene ring. Such an interaction may stabilize a planar transition state. The rate of nitrogen inversion may then be somewhat faster in the aniline compounds than in the case of aliphatic amines. For each compound a plot of  $1/\tau_i$  vs.  $1/h_0'''$  was linear initially, but began to approach a slope of apparently zero as  $k_H$  became significant or larger than  $k_{-a}[H^+]$  in the denominator of the first term in eq 7. An example is shown in Figure 1 for VII utilizing both  $H_2SO_4$  and  $D_2SO_4$  solvent systems.

Results from the proton exchange studies are given in Table II. Because of the variations in viscosity of the solutions, different temperatures were required for the various compounds. The data were extrapolated to 50° in all cases, and 25° in some cases by performing temperature studies over ranges of 20–30°. Extrapolation errors limit the accuracy of these values. The values of  $k_H$  reported in Table II are similar or higher than aliphatic amines of comparable molecular volume.<sup>6</sup> The value of  $k_H$  at 25° has been determined to be  $6.6 \times 10^9 \text{ sec}^{-1}$  for *N,N*-diethyl-*m*-toluidine studied in a water-*tert*-butyl alcohol mixture.<sup>11</sup> The values for compounds in Table II are in fair agreement considering the differences in solvent and experimental method. There is some internal consistency in the data as well. The decreasing values of  $k_H$  in the series I, II, III, and the series IV, V, VI, and VII is consistent

(21) T. P. Pitner and R. B. Martin, *J. Amer. Chem. Soc.*, **93**, 4400 (1971).

TABLE II: Exchange Rate Data

Compd	Temp (°C) at which data were taken	$pK_a^H$ at 50°	$k_H \times 10^{-10}$ sec <sup>-1</sup> at 50°	$pK_a^H$ at 25°	$k_H \times 10^{-10}$ sec <sup>-1</sup> at 25°
I	50	4.5	11.9	4.85 <sup>b</sup>	4.32 <sup>c,d</sup>
II	50	4.9	8.9	5.10 <sup>b</sup>	1.45 <sup>c</sup>
III	50	5.5	8.5	6.08 <sup>b</sup>	3.45 <sup>c</sup>
IV	90	3.8	1.0 <sup>a,d</sup>		
V	70	3.4	0.4 <sup>a</sup>		
VI	90	4.1	1.0 <sup>a</sup>		
VII	70	4.6	0.5 <sup>a</sup>		

<sup>a</sup> Calculated at 50° from temperature dependence. <sup>b</sup> D. D. Perrin, "Dissociation Constants of Organic Bases in Aqueous Solutions," Butterworths, London, 1965, Table IV. <sup>c</sup> Calculated at 25° from temperature dependence. <sup>d</sup> Corrected for statistical effects of two exchanging protons.

TABLE III: Data Obtained from AB Interchange (50°)

Compd	$pK_a^H$	$pK_a^D$	$k_a^H$ , sec <sup>-1</sup> × 10 <sup>-2</sup>	$k_a^D$ , sec <sup>-1</sup> × 10 <sup>-2</sup>	$k_{-a}^H$ , sec <sup>-1</sup> × 10 <sup>-6</sup>	$k_{-a}^D$ , sec <sup>-1</sup> × 10 <sup>-6</sup>	$f$
V	3.4	4.1	5.2	2.5	1.31	0.94	0.67
VI	4.1	4.6	6.5	3.8	8.2	5.82	1.01
VII	4.6	5.1	6.6	2.5	26.3	18.8	0.84

with the theory of Grunwald and Ralph that dispersion forces between the hydrogen bonded water molecule and the alkyl substituents influence the value of  $k_H$ .<sup>6</sup> In addition the sharp decrease in  $k_H$  from secondary to tertiary anilines may be related to the "aniline hydration effect" proposed by Condon.<sup>22</sup> The proposal that hydration energies may be closely related to  $k_H$  values is partially substantiated by the fact that a plot of  $\log k_H$  vs. the  $\Delta H$  of solution for three aliphatic amines is linear and curves smoothly to the diffusion-controlled limit of exchange of ammonia.<sup>23</sup> The apparently anomalous value of  $k_H$  for VI may in fact be due to inaccuracy in its measurement. The line shape analysis of the benzyl CH<sub>2</sub> protons which was used to obtain proton exchange data consisted of an ABX pattern coalescing to an AB pattern. This complication introduced errors which could be as large as 100% in the determination of  $\tau$  values. The values of  $k_a$  and  $k_{-a}$  could not be determined directly in the highly acidic solutions.

These will be discussed as an indirect determination resulting from the study of the nitrogen inversion process.

Figure 1 shows a plot of  $1/\tau_i$  (A-B interchange as a result of nitrogen inversion) vs.  $1/h_0'''$  for VII. Plots for the other compounds are very similar to Figure 1 and not given. The general shape of these plots is similar to those obtained for aliphatic amines and predicted by eq 7. Taking  $k_H$  from Table III,  $k_a$  is estimated from the low acidity values of  $1/\tau_i$ . The ratio of  $k_a/k_{-a}$  is taken equal to  $K_a$ . The value of  $f$  is varied in eq 7 to obtain the best least-squares fit to the experimental data. The results are shown in Table III. Once these parameters are obtained, kinetic isotope effects are applied to  $k_H$ ,  $k_a$ ,  $k_{-a}$ , and the curve shown for the D<sub>2</sub>O-D<sub>2</sub>SO<sub>4</sub> solvent system calculated using eq 7. The isotope effect on  $k_H$  and  $k_{-a}$  was taken as 1.4.<sup>9</sup> The isotope effect on  $k_a$  was calculated from the  $K_a^H/K_a^D$  ratio determined experimentally and 1.4 for  $k_{-a}$ . The line calculated in this way is in excellent agreement with the data obtained using the D<sub>2</sub>O-D<sub>2</sub>SO<sub>4</sub> solvent.

VII was studied to determine whether there was a significant influence of the strongly electron-donating properties of the *p*-methoxy group upon the exchange or inversion rate. Comparison of  $k_H$  values for V and VII show there is little or no influence by this substitution. Surprisingly, there is a 30% increase in the value of  $k_a$  upon substitution of the methoxy group. The increase in basicity of VII over V is reflected in the value of  $k_{-a}$ . The only apparent conclusion is that the increased electron density at the nitrogen is more important in the efficiency of the protonation step than in the slower dissociation of the proton from the hydrated amine cation.

The  $f$  values obtained from the inversion studies are shown in Table III. Because no value of  $k_{-H}$  is available, only the  $f$  values may be reported. However, if  $k_{-H} > k_{-a}$ , then  $k_i \approx 10^6$ - $10^7$  sec<sup>-1</sup>.<sup>9</sup>

The conclusions from this work are that the value of  $k_H$  for substituted aniline compounds is comparable or larger than those for aliphatic compounds of similar molecular size. The value of  $k_H$  decreases with increasing size of substituents. The value of  $k_H$  is significantly larger for secondary anilines than tertiary anilines. As in the case of aliphatic amines, the rate of inversion of the nitrogen is limited by the rate of proton exchange, and a lower estimate for the rate of nitrogen inversion is  $10^6$ - $10^7$  sec<sup>-1</sup>.

(22) F. E. Condon, *J. Amer. Chem. Soc.*, **87**, 4485 (1965).

(23) D. E. Leyden, unpublished results.

## Determination of Ion-Pairing Dissociation Constants Using Electron Spin Resonance Spectroscopy

Philip Graceffa and T. R. Tuttle, Jr.\*

Department of Chemistry, Brandeis University, Waltham, Massachusetts 02154 (Received December 1, 1972)

Ion-pairing dissociation constants for sodium naphthalenide dissolved in THF have been determined using esr spectroscopy. Values of  $K_D$  obtained agree with those derived from electrical conductivity measurements. The discrepancy between  $K_D$  from electrical conductivity and earlier esr measurements is interpreted in terms of potassium impurity. A value of  $K_D$  obtained for sodium biphenylide in THF is judged to be consistent with the values of  $K_D$  from electrical conductivity measurements. However, contrary to expectation, no evidence of ion is found in sodium biphenylide solutions whose esr spectra display sodium hyperfine splittings.

The method of determining ion-pairing dissociation constants using esr spectroscopy was exemplified by Atherton and Weissman<sup>1</sup> in their measurements on sodium naphthalenide prepared in tetrahydrofuran (THF) and in other organic ethers. A subsequent determination<sup>2</sup> of this dissociation constant,  $K_D$ , through electrical conductivity measurements yielded a value about a factor of 10 lower than the esr measurements. It was suggested that the esr spectrum attributed to the ion actually arose only partly from the ion and that an appreciable portion of this spectrum came from solvent-separated ion pairs. A recent report<sup>3</sup> raises the possibility that potassium impurity in esr experiments may be responsible for the different results obtained for  $K_D$  with the two different methods. In order to resolve this difference we have remeasured with esr spectroscopy  $K_D$  for sodium naphthalenide in THF. In addition we have measured  $K_D$  for sodium biphenylide in THF to provide another comparison between the two methods. In all our experiments special care was taken to remove nonvolatile impurities, including potassium, from solution on which measurements were taken.<sup>4</sup>

Values of  $K_D$  for sodium naphthalenide in THF based on spectra in which hyperfine components due to ion and ion pair were used to estimate concentrations are plotted in Figure 1. The rather large uncertainties in  $K_D$  obtained in this way reflect the uncertainties due to overlap and line shapes which affect the estimations of concentrations. These values of  $K_D$  are still a bit larger than the corresponding values determined by electrical conductivity measurements, but probably do not differ from the latter within the rather large experimental uncertainties.

For sodium biphenylide in THF no evidence of free ion was found in any of the solutions studied in which a sodium hyperfine splitting,  $a_{Na}$ , was detected. Below about 20°,  $a_{Na} = 0$  so that ion and ion pair could not be distinguished. However, at room temperature and at a concentration of biphenylide of  $\sim 10^{-5}$  M spectra were obtained which clearly demonstrate the presence of ion pair, but which show no trace of ion. A straightforward calculation based on  $K_D$  from conductivity measurements gives a value of the ratio of ion to ion pair,  $R = 1$ , at the biphenylide concentration studied. It is hard to understand why

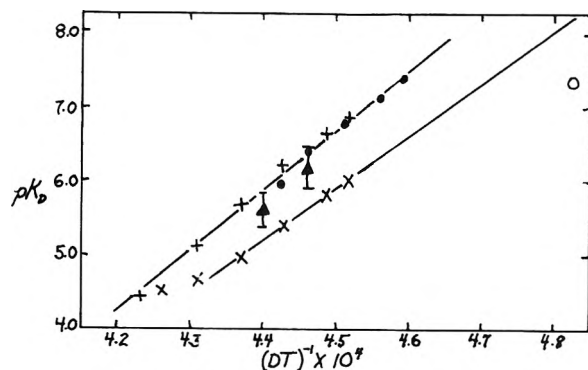
no ion was detected in the esr spectrum in view of this high value of  $R$ .

For more accurate determinations of  $K_D$  using esr measurements, spectra were obtained under conditions such that hyperfine splittings were averaged by electron exchange between neutral hydrocarbon and its anion. Under these conditions simple spectra consisting of two lines were obtained<sup>5</sup> (see Figure 2). The narrower of the two lines became relatively more important at lower hydrocarbon concentrations and at lower temperatures. For sodium naphthalenide- $d_8$  in THF- $d_8$  the broader of the two lines split up into four equally spaced, equally intense lines at higher temperatures. Consequently, the narrow line was assigned to the ion and the broad line to the ion pair. The values of  $pK_D$  obtained by analyzing such spectra for sodium naphthalenide solutions are plotted in Figure 1. Clearly, the correlation between these  $pK_D$  values and those determined by electrical conductivity<sup>2</sup> is excellent.

Spectra of sodium biphenylide- $d_{10}$  in THF- $d_8$  in the presence of excess hydrocarbon also displayed two lines as shown for naphthalenide in Figure 2. As in the case of the naphthalenide system, the narrow line increased in relative importance at lower radical concentrations and at lower temperatures. From these data  $pK_D = 7.37$  at 58° in a solution 0.97 M in biphenyl. A correlation of this value of  $pK_D$  with the values from conductivity is shown in Figure 1. The value of  $pK_D$  from esr measurements is about a factor of 2 larger than the value obtained from the linear extrapolation of the conductivity data<sup>2</sup> shown in Figure 1. This difference is probably not significant. The results derived from measurements on solutions containing excess hydrocarbon are essentially in agreement with conductivity results for this system. This agreement makes our failure to observe ion lines in spectra in which hyperfine lines due to sodium are well resolved all the more puzzling. Microwave saturation, excessive line broadening, or suppres-

- (1) N. M. Atherton and S. I. Weissman, *J. Amer. Chem. Soc.*, **83**, 1330 (1961).
- (2) P. Chang, R. V. Slaters, and M. Szwarc, *J. Phys. Chem.*, **70**, 3180 (1966).
- (3) P. Graceffa and T. R. Tuttle, Jr., *J. Chem. Phys.*, **50**, 1908 (1969).
- (4) P. Graceffa, Ph.D. Thesis, Brandeis University, 1972.
- (5) R. Chang and C. S. Johnson, *J. Amer. Chem. Soc.*, **88**, 2338 (1966).

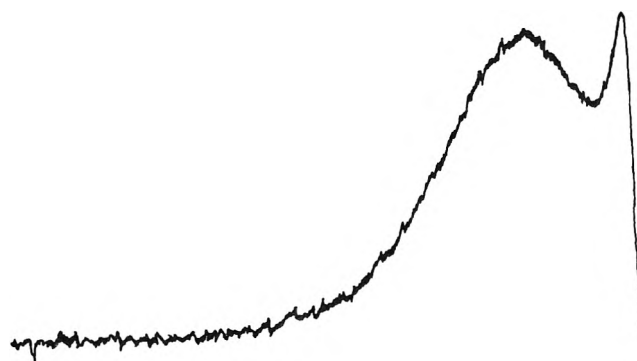




**Figure 1.** Correlation of  $pK_D$  values: ●, sodium naphthalenide- $d_8$  in THF- $d_8$  with excess hydrocarbon; ▲, Na naphthalenide in THF (by esr); +, Na naphthalenide in THF (by electrical conductivity<sup>2</sup>); O, sodium biphenylide- $d_{10}$  in THF- $d_{10}$  with excess hydrocarbon (by esr) ×, Na biphenylide in THF (by electrical conductivity).

sion of the ion-pairing dissociation reaction are all possible causes for our failure to observe ion lines. However, special precautions were taken to minimize each of these possible causes. The reason for our failure to observe ion in the absence of excess hydrocarbon remains a mystery.

Apart from this one point which remains to be resolved the esr and conductivity methods appear to yield concordant results for ion-pairing dissociation constant without the necessity of assigning some of an ion line to solvent-



**Figure 2.** ESR spectrum of sodium naphthalenide- $d_8$  in THF- $d_8$  solution 0.136 M in naphthalene- $d_8$ . Naphthalenide concentration is  $4.05 \times 10^{-4}$  M.  $dx''/dH$  is plotted vs.  $H$ . Only half of the spectrum is shown.

separated or loose ion pairs. For sodium naphthalenide the loose ion pair, according to Hirota,<sup>6</sup> is in rapid equilibrium with the tight ion pair in order to account for the temperature dependence of  $a_{Na}$ . Under these circumstances the loose ion pair could not contribute to the intensity of the ion lines.

*Acknowledgment.* The authors gratefully acknowledge the financial support of The National Science Foundation.

(6) N. Hirota, *J. Phys. Chem.*, **71**, 127 (1967).

## Noise Generated during Sodium and Hydrogen Ion Transport across a Cation Exchange Membrane<sup>1</sup>

Stephen H. Stern and Michael E. Green\*

Department of Chemistry, City College of the City University of New York, New York, New York 10031  
(Received October 5, 1972)

Publication costs assisted by the City University of New York

Measurements on the noise spectrum of solutions containing  $Na^+$  ion and  $H^+$  ion, taken during transport across a cation exchange membrane, are reported. The measurements were taken as a function of concentration, flux, and temperature. Two types of noise sources are indicated, which would correspond to two transport mechanisms in the solution on the diluate side of the membrane. The nature of these mechanisms is discussed qualitatively, together with certain quantitative characteristics.

### Introduction

In previous papers on ion transport noise, Yafuso and Green presented studies on noise generated during transport of several ions across cation exchange membranes,<sup>2</sup> followed by more detailed work on HCl noise spectra.<sup>3</sup> (These papers will be referred to as I and II, respectively.) Studies on noise in biological systems have been carried out by several workers,<sup>4,5</sup> and it is becoming apparent

that noise can be a valuable tool in understanding transport across biological membranes. By studying noise spec-

- (1) S. H. Stern, Doctoral Dissertation, City University of New York, 1973 (paper based in part upon dissertation).
- (2) (a) M. E. Green and M. Yafuso, *J. Phys. Chem.*, **72**, 4072 (1968); (b) *ibid.*, **73**, 1626 (1969).
- (3) M. Yafuso and M. E. Green, *J. Phys. Chem.*, **75**, 654 (1971).
- (4) (a) H. E. Derksen and A. A. Verveen, *Science*, **151**, 1388 (1965); (b) A. A. Verveen, H. E. Derksen, and K. L. Schick, *Nature (London)*, **316**, 688 (1967).
- (5) H. M. Fishman, *Biophys. Abstr.*, **119e**, SaAM-E4 (1971).

tra, one may be able to obtain information on processes more rapid than the rate-determining step.

With ion-exchange membranes at low currents, diffusion and drift to the membrane surface supply adequate current. Above a critical current density (CCD), these are inadequate, so a new mechanism must be found. In this paper, we discuss several possibilities for transport mechanisms. By consideration of noise spectra measured during  $\text{Na}^+$  and  $\text{H}^+$  transport, we are able to reach a tentative conclusion as to noise sources, and therefore make a suggestion regarding the transport process. This extends the work presented in I and II, in which it was only possible to determine that the noise source was near the membrane surface in the dilute solution.

### Experimental Section

The electrical measurements were similar to those described in II, but there were several modifications.

(1) The magnetically shielded box containing the cell and preamplifier was shock mounted. This made possible the measurement of low-frequency spectra at currents close to the CCD, with total noise (defined below) less than 3 dB above background.

(2) The preamplifier was an Applied Cybernetics Model LA260V, with total noise of  $1.4 \mu\text{V}$ .

(3) Total noise was monitored continuously, rather than before and after, with Hewlett-Packard 3400A true root mean square voltmeter. The bandwidth was  $10 \text{ Hz} < f < 300 \text{ kHz}$ , determined by the preamplifier response.

In addition to changes in the electrical measurements, the Ionac MC3142 membrane was used in place of MC3235. The differences in noise spectra between these two membranes are too small to concern us. Additional precautions to avoid possible impurity effects, especially from surfactants, were taken in this work. The water was treated by the method of Christodolou and Rosano.<sup>6</sup> The membrane was only touched by clean tweezers. Finally, the cell was cleaned with X-100 detergent (Rohm and Haas) plus  $\text{Na}_2\text{CO}_3$ . This detergent can be easily rinsed out, and the cell was extensively rinsed with water treated as mentioned above. None of these extra precautions had any observable effect, confirming that surfactants are not likely to be affecting the results.

Solutions were prepared from NaOH (Amend) and  $\text{H}_3\text{PO}_4$  (J.T. Baker), both reagent grade and used without further purification. A standard  $\text{Na}_2\text{HPO}_4$  solution was prepared by titrating the  $\text{H}_3\text{PO}_4$  with the NaOH, and the  $\text{Na}^+$  solutions used in this work were prepared by dilution from this. Solutions were 0.010, 0.020, 0.040, and 0.060  $M$  in  $\text{Na}^+$  ion (pH 7.19, 7.20, 7.12, and 7.02, respectively). The only anion present in appreciable concentration is  $\text{HPO}_4^{2-}$ , with the exception of the dimer  $\text{H}_5\text{P}_2\text{O}_8^-$ , which at most may be present to the order of 1%.<sup>7</sup>

The  $\text{H}_3\text{PO}_4$  solutions were 0.008, 0.010, 0.016, and 0.021  $M$  in  $\text{H}^+$  ion (pH 2.08, 1.99, 1.80, and 1.69). All pH measurements were made with the Corning Model 5 pH meter, and were  $\pm 0.03$  pH units.

### Results

Noise spectra were measured at several temperatures, concentrations, and fluxes. The  $\text{H}_3\text{PO}_4$  spectra resembled the HCl spectra reported in II, while with  $\text{Na}_2\text{HPO}_4$  the spectra had shallower slopes; an example was reported in I. In this work, detailed results have been obtained, especially with spectra measured at currents near the CCD,

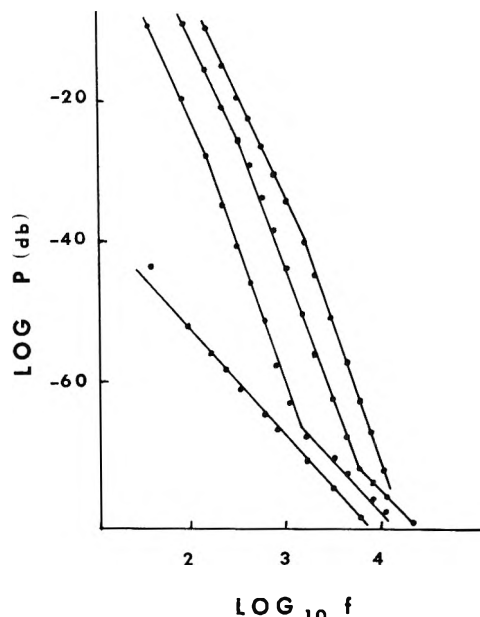


Figure 1. Power spectra of  $\text{H}_3\text{PO}_4$ , 0.016  $M$  in  $\text{H}^+$  ion, at  $283^\circ\text{K}$ . Curves from top to bottom, fluxes in  $\text{A}/\text{m}^2$ : 758, 558, 395, 322.

and thus at low total noise. With no current, background noise for the system is  $3 \mu\text{V}$  at all temperatures and concentrations.

A typical set of  $\text{H}_3\text{PO}_4$  spectra is shown in Figure 1. Note that at the lowest current the spectrum is qualitatively different. This type of spectrum was not found in II, very possibly because of lack of shock mounting. Its frequency dependence is  $f^{-1.5}$  (i.e.,  $d \log P/d \log f = -1.5$ , where  $P$  = power spectral density in  $\text{V}^2/\text{Hz}$ ), and a high-frequency tail with  $f^{-1.5}$  slope is observed on two of the steeper spectra.

In the higher current region, there is a linear relation between the frequency of intersection of the two steep lines and the current. (This frequency is obtained by extrapolating the two straight line portions.) As in II, we may write

$$J = \kappa f_B + \beta \quad (1)$$

where  $f_B$  is the frequency at the point of intersection,  $J$  is the current density, and  $\kappa$  and  $\beta$  are constants. Figure 2 shows one set of  $J$  vs.  $f_B$  curves.

An evidently fundamental parameter is total noise; a plot of total noise vs.  $f_B$  allows points for all concentrations at one temperature to be combined on a single line, as shown in Figure 3. There are slight differences as a function of temperature.

More generally, the essential features of the spectra can be described as in the schematic representation of Figure 4a, where the slopes are labeled  $a$ ,  $b$ , and  $c$ , together with the total noise at which spectra of the particular type are found. Table I describes the essential features of a sample of these spectra.

In II, it was argued that  $\beta$  of eq 1 should represent the diffusion flux. A plot of  $\log \beta$  vs.  $1/T$  was used to determine an activation energy for  $\beta$ , which could be compared to an activation energy of diffusion. In this work, we have

(6) A. P. Christodolou and H. L. Rosano, *Advan. Chem. Ser.*, No. 84 (1968).

(7) K. L. Elmore, J. C. Hatfield, R. L. Dunn, and A. D. Jones, *J. Phys. Chem.*, 69, 3520 (1965).

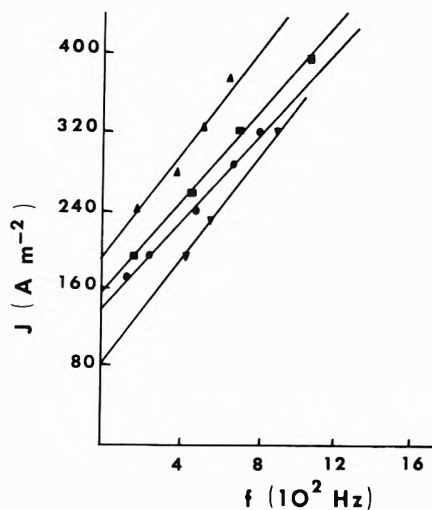


Figure 2. Plot of frequency of intersection of straight line slopes vs. flux for phosphoric acid. Curves from top to bottom (concentrations for  $H^+$  ion): 0.010 M at 313°K; 0.010 M at 283°K; 0.008 M at 310°K; 0.008 M at 318°K.

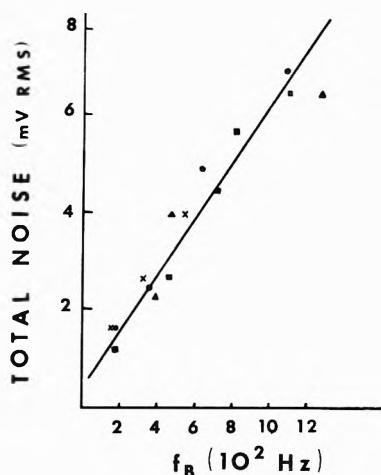


Figure 3. Total noise vs. break frequency for phosphoric acid at 283°K (concentrations for  $H^+$  ion): ●, 0.008 M; ■, 0.010 M; ▲, 0.016 M; ×, 0.021 M.

used lower concentrations of  $H^+$ , and have found that this apparent activation energy is a strong function of concentration. In II, with only two points ( $[H^+] = 0.025$  and  $0.050 M$ ), it seemed most reasonable to attribute any differences to experimental error, although the error did seem larger than expected. By combining those points with the  $H_3PO_4$  points from this work (Figure 5), it becomes evident that there is a decrease in apparent activation energy at low concentration.

We will see that an interpretation of  $\kappa$  depends on a calculation of convection outside the diffusion layer. We shall, therefore, have further comments concerning this in the Discussion section.

**$Na_2HPO_4$  Spectra.** At the three higher concentrations (0.020, 0.040, and 0.060 M), these spectra appear different from the  $H_3PO_4$  spectra; examples are shown in Figure 6. Clearly, the spectra are not always simply two straight line portions meeting at a reasonably well-defined point. Again,  $f^{-1.5}$  sections appear at low noise, with current density near the CCD. In spite of the fact that a curved region is commonly found, much of the spectrum does consist of straight line regions; we therefore use the nota-

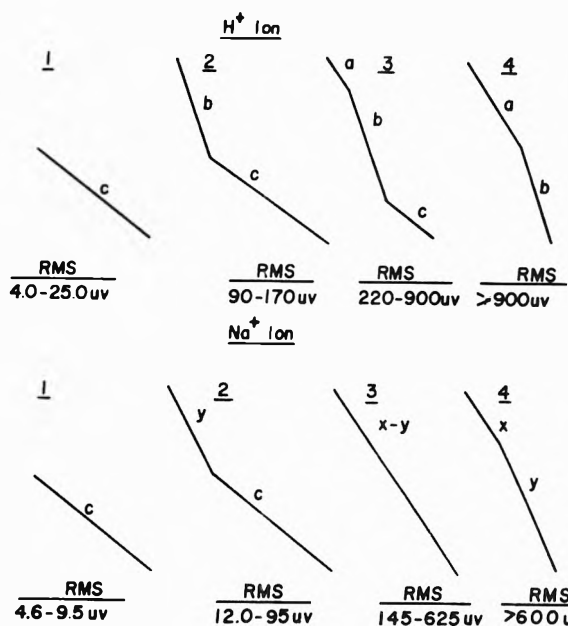


Figure 4. Schematic representation of types of power spectra observed, with corresponding ranges total noise.  $a$ ,  $b$ ,  $c$ ,  $x$ , and  $y$  represent slopes ( $d$  in  $P/d$  in  $f$ ). Only two examples of type 2  $H^+$  spectra, and only four examples of  $Na^+$  type 1 spectra, were found.

TABLE I: Characteristics of Spectra with 0.008 M  $H^+$  Ion

$T, ^\circ K$	$J, A/m^2$	Total noise, $\mu V, rms$	$f_B, Hz$	$d \log P/d \log f$		
				$a$	$b$	$c$
283	106	15	$a$			1.49
283	121	425	94	3.28	5.06	1.58
283	255	5000	615	2.88	4.53	
283	322	7000	1060	3.05	4.65	
283	395	9000	1290	3.08	4.71	
313	121	22	$a$			1.52
313	255	2700	530	2.65	4.76	1.64
313	395	7900	1060	$b$	3.88	1.64
313	525	17000	3160	2.76	4.82	
318	191	2450	334	2.42	4.60	
318	223	5500	630	2.58	4.60	

<sup>a</sup> No  $f_B$ ;  $c$  slope only. <sup>b</sup>  $a$  slope not reliable.

tion indicated in Figure 4b. The characteristics of the spectra are given in the microfilm edition of this journal.<sup>8</sup>

With the  $H^+$  spectra, the values of  $\beta$  (eq 1) were close to the CCD, as expected if both represent the diffusion-limited current density. For  $Na^+$  ( $c \geq 0.02 M$ ), it is difficult to find  $\beta$ . We can define  $\beta'$  as the current density at which measurable noise first appears, and use this to find an activation energy. This was done for 0.040 M  $Na^+$ , to give  $E_a = 4.0$  kcal/mol.

Finally, the 0.010 M  $Na^+$  solutions present a possibly instructive case. The spectra resemble the  $H^+$  spectra almost as much as they do the other  $Na^+$  spectra, in that they follow eq 1, and show the characteristic two slope pattern, with a well-defined break. However, the frequen-

(8) Complete tables giving characteristics of these spectra will appear following these pages in the microfilm edition of this volume of the journal. Single copies may be obtained from the Business Operations Office, Books and Journals Division, American Chemical Society, 1155 Sixteenth St., N.W., Washington, D. C. 20036. Remit check or money order for \$3.00 for photocopy or \$2.00 for microfiche, referring to code number JPC-73-1567.

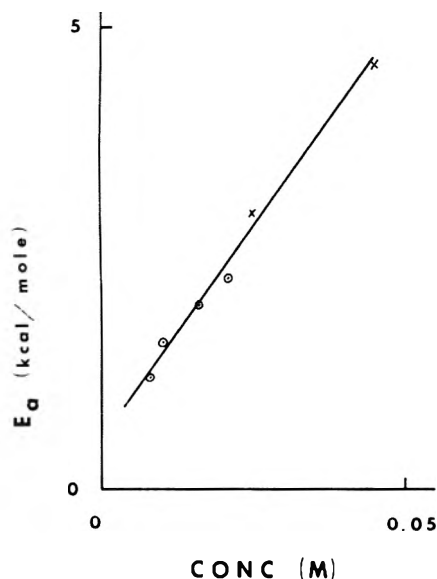


Figure 5. Activation energy of  $\beta$  (eq 1) as a function of concentration: X, HCl points; O,  $\text{H}_3\text{PO}_4$  points.

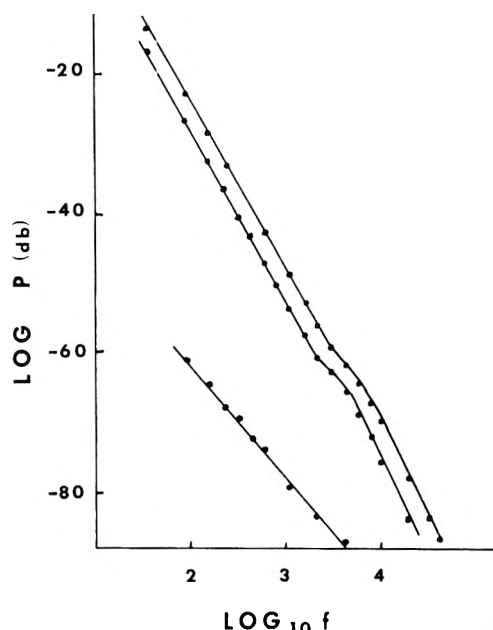


Figure 6. Power spectra of  $\text{Na}_2\text{HPO}_4$ , 0.060 M in  $\text{Na}^+$  ion, at  $313^\circ\text{K}$ . Curves from top to bottom, fluxes in  $\text{A}/\text{m}^2$ : 249, 196, 116.

cy range extends approximately one decade higher than with  $\text{H}^+$ , the value of  $\kappa$  is about an order of magnitude less, and the CCD is low as appropriate for the relatively low mobility of the  $\text{Na}^+$  ion. The absolute values of the slopes are steeper than for the higher  $\text{Na}^+$  concentrations, but lower than any  $\text{H}^+$  slopes. In particular the  $b$  slope of  $\text{H}^+$  ions is typically 4.6 at the lowest concentrations, dropping to 3.9 at  $0.021\text{ M H}^+$ . The steeper  $\text{Na}^+$  slope,  $y$ , at the higher concentrations, is about 2.7–2.8. The  $y$  slope for  $0.010\text{ M Na}^+$  averages 3.4. The shallower slopes are about 2.8 ( $\text{H}^+$ ) vs. 2.3 ( $\text{Na}^+$ ,  $c \geq 0.02\text{ M}$ ), and about 2.7 for  $0.010\text{ M Na}^+$ . Furthermore, the absolute values of  $f_B$  for  $0.010\text{ M Na}^+$  can be well below  $10^3\text{ Hz}$ , though values as high as  $10^4\text{ Hz}$  are found. For higher  $\text{Na}^+$  concentrations, where the value may be less well defined because of curvature, we find  $f_B > 3 \times 10^3\text{ Hz}$ . For  $\text{H}^+$ , this frequency represents an approximate upper limit. It appears that

$0.010\text{ M Na}^+$  behaved somewhat as an intermediate case between the  $\text{H}^+$  ion solutions and the more concentrated  $\text{Na}^+$  ion solutions.

## Discussion

The data presented here enable us to revise and extend the conclusions presented in II. To summarize, the data were there interpreted as showing the noise to depend on a diffusion part ( $\beta$  of eq 1) and on the dissociation of water. The steepness of the spectra was postulated to be possibly dependent on an internal filter; however, there were difficulties in explaining the magnitude of capacitance which would have been required. Our data now allow us to conclude that there is indeed noise due to diffusion starting at currents just below the CCD. At higher currents a different process dominates the noise, but this depends on convective flow of solution rather than dissociation.

The current-voltage characteristics of systems similar to those we have studied have presented workers in the field with a puzzle. There is a low current ohmic region, then a sharp rise in voltage when diffusion of ions to the membrane can no longer supply the current. However, at the highest flux densities, the voltage no longer rises so rapidly with increasing current, so that an alternate current carrying mechanism must exist at high flux densities. The possibilities include dissociation of water, as discussed in II, and transport of coions. One or both of these suggestions has been criticized by Cooke,<sup>9,10</sup> Frilette,<sup>11</sup> and Block and Kitchener.<sup>12</sup> Dissociation under high field should have produced pH changes, which were not found,<sup>9-11</sup> and no evidence was found for coion transport.<sup>9,10,12</sup> Another possibility, electroosmotic flow, was also ruled out.<sup>11,12</sup>

Before we can continue, we must consider the possibility that the membrane surface does not become depleted of ions uniformly. Cooke<sup>9,10</sup> found evidence to suggest that the outer edge of the membrane could have an ionic concentration approaching its minimum value, while the inner portion was not yet depleted. Our data do not bear on the question of which portion of the membrane depletes first, but do suggest that there may be initial partial depletion, preceding complete depletion. Sata, *et al.*,<sup>13</sup> accepted this interpretation. There is a well-defined current density  $J_N$  at which noise first appears above background. At each  $c$  and  $T$ ,  $J_N$  values were always less than the flux needed to see depletion chronopotentiometrically at the same concentration.<sup>1</sup> The noise at  $J_N$ , although only a few decibels above background, is sufficient to measure a spectrum, and this is always a diffusion spectrum. At a higher current density, the chronopotentiometric curve indicates depletion, and the high current density noise spectrum appears; the total noise is at least two orders of magnitude greater than background. The increase in total noise with current density is huge; see Figure 1 of I, where the initial region was not found, but the increase is shown clearly. The intermediate noise range, 25–200  $\mu\text{V}$ , is rarely found with  $\text{H}^+$  (see Figure 4a). The  $\text{Na}^+$  solutions show fewer representatives of the pure dif-

(9) B. A. Cooke, *Electrochim. Acta*, **3**, 307 (1961).

(10) B. A. Cooke, *Electrochim. Acta*, **4**, 179 (1961).

(11) V. J. Frilette, *J. Phys. Chem.*, **61**, 168 (1957).

(12) M. Block and J. A. Kitchener, *J. Electrochem. Soc.*, **113**, 947 (1966).

(13) T. Sata, R. Yamane, and Y. Mizutani, *Bull. Chem. Soc. Jap.*, **42**, 279 (1969).

**TABLE II: Relation of Noise Spectra to Chronopotentiometric Measurements**

Concn, <i>M</i>	<i>T</i> , °K	<i>J<sub>N</sub></i> , A/m <sup>2a</sup>	<i>J<sub>VT</sub></i> , A/m <sup>2b</sup>	<i>J<sub>N2</sub></i> , A/m <sup>2c</sup>
0.008 H <sup>+</sup>	283	106	121	121
0.008 H <sup>+</sup>	313	121	172	156
0.016 H <sup>+</sup>	283	325	366	360
0.021 H <sup>+</sup>	283	462	608	557
0.021 H <sup>+</sup>	313	690	758	795
0.020 Na <sup>+</sup>	283	19.3	20.4	24
0.020 Na <sup>+</sup>	313	30.6	35.7	35
0.040 Na <sup>+</sup>	301	51.0	56.0	56
0.060 Na <sup>+</sup>	313	116	127	156

<sup>a</sup> *J<sub>N</sub>* = lowest *J* values at which noise appears. <sup>b</sup> *J<sub>VT</sub>* = lowest *J* values where chronopotentiometry shows membrane polarization. <sup>c</sup> *J<sub>N2</sub>* = *J* value at which steep slope first appears. All *J* values ±10%.

fusion spectra, but some more in the transitional range. Table II relates the chronopotentiometric and noise spectral data for a representative selection of concentrations and temperatures. With both H<sup>+</sup> and Na<sup>+</sup>, there is a clear transition; this type of transition is strong evidence for the existence of two types of noise source, and therefore two mechanisms of flux maintenance. One is diffusion, at the lower values of flux; the other is almost certainly associated with the bulk flow of solution, and will be discussed below. The diffusion slope, after the appearance of the spectra with steep slopes, still survives at high frequencies. This indicates that both mechanisms must be able to exist simultaneously. The values of  $\beta$  are close to *J<sub>N</sub>*. Since eq 1 is a straight line,  $\beta$  must be constant, and diffusion must not be altered above the CCD; however, at high currents diffusion noise is largely obscured by the more powerful second noise source.

**Second Noise Source.** We have noted that other workers have found evidence against possible alternate current sources, except for bulk flow. However, Block and Kitchener,<sup>12</sup> using Schlieren techniques, have observed both laminar flow and turbulence in systems similar to ours. One of the membranes they used, Ionac MC 3142, is the membrane used here. They found turbulence only in the diluate layer, with the membrane horizontal and counterions passing upward (conditions favoring stagnation). Under these conditions, they also observed that chronopotentiometric curves continued to show a rise in voltage after the initial sharp rise upon depletion (at the Sand's law transition time). Under other conditions, the voltage decreased and no turbulence was observed.

All of our experiments were carried out using vertical mounting for the membrane; however, the membrane surface in contact with solution was only a small part of an infinite plane. This contrasts with Block and Kitchener's geometry, where the membrane surface covered the complete cross section of a tube 1 cm in diameter. They found that turbulence did not occur in much smaller tubes.

Further support for turbulence comes from the noise spectra themselves. The H<sup>+</sup> spectra have two intersecting lines with slopes which can approach  $f^{-3}$  and  $f^{-5}$ . A theory of plasma turbulence developed recently by Tchen<sup>14</sup> predicts slopes of  $f^{-3}$ ,  $f^{-1}$ , and  $f^{-5}$  (from low to high frequency) with the possibility that the middle frequency range with  $f^{-1}$  slope could collapse to zero. Since similar approximations to those used by Tchen for the plasma case with regard to Debye length should hold here, the resulting  $f^{-3}$ ,  $f^{-5}$  spectrum at least suggests turbulence.

A very brief description of the basic assumptions of the theory is needed to understand the principle physical processes involved; in addition, this will enable us to understand better the parameter  $\kappa$  in eq 1. The starting point is the hydrodynamic equation of motion, in which the acceleration of unit mass of fluid is equated to the forces on the fluid, including those arising from electrical, thermal, and concentration gradients. The Poisson equation is also required; however, for the relatively low-frequency range involved here, an assumption of quasi-neutrality is valid. Another necessary condition can be expressed in terms of frequency,  $f_D \gg f_{max}$ , where  $f_D$  is the ratio of the characteristic velocity ( $(kT/m)^{1/2}$  for plasmas) to the Debye length, and  $f_{max}$  is the highest frequency to which the theory is applied. For ionic solutions,  $(kT/m)^{1/2}$  should be replaced by the ratio of a distance characteristic of charge separation in the solution to the time needed to diffuse this distance. If the distance is of the order of the Debye length, then  $f_D \sim 10^9$  Hz, and the condition is easily satisfied for frequencies of the order of  $10^5$  Hz.

The theory predicts that, in a given frequency range, one of three processes dominates the noise power spectrum. At low frequencies, the process is a production of turbulence due to drift, in an unstable region (one in which a driving force (electric field, for instance) goes in the opposite direction to the concentration gradient) and it provides an  $f^{-3}$  spectrum. At high frequencies, molecular dissipation of local concentration fluctuations provides an  $f^{-5}$  spectrum. At intermediate frequencies, inertial terms resulting from the nonlinear coupling between modes of fluctuations, for example, due to concentrations and fields, produces an  $f^{-1}$  spectrum. However, this section can be small or nonexistent. The boundary between  $-3$  and  $-1$  slopes comes at a frequency

$$f_s \propto (\Gamma(\nabla c)^2/D(\nabla(\delta c))^2)^{1/2} \quad (2a)$$

and that between  $-5$  and  $-1$  slopes at

$$f_L \propto (\Gamma/D)^{1/2} \quad (2b)$$

with the same proportionality constant for both frequencies.  $\Gamma \propto \nabla E$ , where  $E$  = electric field;  $\nabla c$  = concentration gradient;  $\nabla(\delta c)$  = gradient of concentration fluctuation; and  $D$  = diffusion coefficient.

For the inertial region to collapse to zero,  $f_s \leq f_L$ . Then  $f_B$  of eq 1 is defined by the point where the two regions cross. If  $f_s = f_L$ , then  $\nabla c = \nabla(\delta c)$ ; that is, the average fluctuation gradient is as large as the overall concentration gradient, a situation which is not uncommon if there is turbulence. Further,  $f_3$  should be proportional to the square root of the field gradient by eq 2, while experimentally it is proportional to the average current. Unfortunately, the relation between the local field gradient and the average current is not yet known for our case, although one does expect them to both change in the same direction. Therefore,  $\kappa$  of eq 1 should be proportional to the square root of the field gradient and the inverse of the diffusion coefficient. In this point, theory and experiment are not inconsistent, but further work is needed to show quantitative agreement.

The Na<sup>+</sup> spectra are less steep, and do not consist of two straight lines (except 0.010 *M*). As with the chronopotentiometric data, the noise spectral evidence does not argue as strongly for turbulence in the Na<sup>+</sup> case as in the H<sup>+</sup> case.

(14) C. M. Tchen, *Phys. Rev. A*, in press.

*Diffusion Activation Energies.* In II, plotting  $\log \beta$  vs.  $1/T$ , we obtained activation energies of 3.0 (0.025  $M$   $H^+$ ) and 4.6 kcal/mol (0.050  $M$   $H^+$ ). Lacking a reason to suspect concentration dependence, we reported an activation energy of  $3.8 \pm 0.8$  kcal/mol. However, by combining those results with the present  $H^+$  results ( $H_2PO_4^-$  coion), we get an unambiguous decrease of activation energy with decreasing concentration (Figure 5). As we might expect from the Nernst-Planck equation,<sup>15</sup> the field should be larger at lower concentration. In II, we took the field to be high enough to cause significant dissociation of water; we now believe that the field is not quite so high. The decrease in activation energy of diffusion required at the lowest concentration is about 3 kcal/mol (4.7 kcal/mol for phosphoric acid<sup>16</sup> vs. approximately 1.5 kcal/mol observed for 0.008  $M$   $H^+$  here). It is known that in some circumstances a high field can affect the activation energy of diffusion of ions in solids.<sup>17</sup> Our situation is slightly different; it also differs from the field affected activation energy of charge transfer at an electrode.<sup>18</sup> It does appear that the decrease in activation energy is mediated by an increase in field.

*Location of Noise Sources.* Since the two noise sources can evidently coexist, they must not interfere with each other. For convection and diffusion, this can only happen if the noise sources are spatially separated. It is known<sup>19</sup> that near electrodes, the outer edge of the diffusion layer is always blurred by convection. Furthermore, convection, especially if turbulent, requires a volume of solution larger than the diffusion layer. The drop in activation energy with concentration suggests that this process (diffusion) occurs in a high-field region; this high field should be possible only in a narrow region near the membrane surface. We appear therefore to have two spatially distinct noise

sources, one close to the membrane (diffusion), and the other responsible for transport to this stagnant layer (convection, sometimes apparently turbulent).

### Summary

- (1) Noise spectra of transport of  $Na^+$  and  $H^+$  ions across a cation exchange membrane are presented.
- (2) Two types of noise source appear to be present, diffusion and convection.
- (3) Diffusion activation energies are found to fall to relatively low values at low concentrations. This is postulated to be due to an increase in electric field.
- (4) The convection, in the case of  $H^+$  at least, appears to be turbulent.
- (5) The two noise sources coexist, and must be spatially separated.

*Acknowledgments.* We are grateful to Professor H. Rosano for helpful discussions with regard to experimental problems, and for supplying purified water. We also wish to thank Professor T. C. Tchen for discussions of turbulence, and Professor H. Hoyer for useful conversations.

This work was supported in part by City University Faculty Research Grants to M. E. G.

- (15) F. Helferrich, "Ion Exchange," McGraw-Hill, New York, N. Y., 1962, p 134.
- (16) Value based on ionic mobility data assuming,  $\mu(HPO_4^{2-}) \approx \mu(H_2PO_4^-)$ , which are published in (a) R. A. Robinson and R. H. Stokes, "Electrolyte Solutions," Butterworths, London, 1959; (b) L. G. Longworth, "Electrochemistry in Biology and Medicine," T. Shedlovsky, Ed., Wiley, New York, N. Y., 1956.
- (17) B. E. Conway, "Theory and Principles of Electrode Processes," Ronald Press, New York, N. Y., 1965, p 99.
- (18) K. J. Vetter, "Electrochemical Kinetics," Academic Press, New York, N. Y., 1967, pp 113-115.
- (19) Reference 18, p 160.

## The Shape of the Coexistence Curve of Ternary Liquid Mixtures near the Plait Point

L. E. Wold, Jr., G. L. Pruitt, and G. Morrison\*<sup>1</sup>

St. Olaf College, Northfield, Minnesota 55057 (Received November 13, 1972)

Publication costs assisted by the Research Corporation

The coexistence curve in the immediate region of the plait point for the ternary liquid system water-acetic acid-carbon tetrachloride was determined for temperatures at 2-deg intervals from 26 to 40°. According to "scaling law" notation for coexistence curves near a critical point, these curves should have a functional form of degree  $d = (1 - \alpha')/\beta$ . The value of  $d$  was found to be  $2.72 \pm 0.12$ , which is in close agreement with the values of  $\alpha'$  and  $\beta$  for single-component systems. The diameter of the coexistence curve near the plait point was also studied; within experimental error, it shows a tendency to be tangent to the curve at the plait point.

### Introduction

A mixture of two liquids which are only partially miscible (referred to as the immiscible pair) and a third which is completely miscible in each of the first two will form

one or two liquid phases, depending upon the total composition.<sup>2</sup> The addition of the third liquid causes the im-

- (1) Enquiries should be directed to this author at the Department of Chemistry, University of Exeter, Exeter EX4 4QD, U. K.

miscible pair to become more soluble in one another; with sufficient dilution by the third component, the mixture will form a single phase. The effect of the third component is to attenuate the forces between both like and unlike molecules of the immiscible pair so that what appears as repulsion between the unlike molecules is diluted, destroyed, or radically altered. The exact mechanism is dependent on the nature of the molecules; its interpretation can vary considerably from system to system. A discussion of this aspect of ternary liquid mixtures is not the purpose of this paper; one is referred to other works for details on specific systems.<sup>3</sup>

Ternary systems are represented at constant temperature and pressure on an equilateral triangle: the vertices are the pure components; the sides are the respective binary mixtures; and the interior is the ternary system. Such a diagram can be found in any physical chemistry text. Because only two of the three composition variables are independent, the composition may be represented on a cartesian coordinate system; the equilateral triangle becomes a right isosceles triangle. If the dimensions along the legs of the triangle are the compositions of the immiscible pair, the coexistence curve will end on the hypotenuse; this curve can thus be expressed as a function of one of the composition variables. Temperature or pressure may be added to this representation by constructing a right prism; either of these two variables changes along the length of the prism. The addition of  $T$  or  $p$  to the representation generates a coexistence surface.

A mixture whose total composition falls within the region surrounded by the coexistence curve and the hypotenuse forms two phases of unique composition which are connected by a tie line. If the total composition of the mixture is systematically varied so that the equilibrium phases become more alike, the tie lines will become shorter and ultimately vanish at a unique point called the plait point, an isothermal, isobaric critical mixing point; this point is a true critical point.<sup>4</sup> A mixture whose composition is outside the coexistence curve forms a single phase. Recent experiments<sup>5</sup> on single-component systems near the liquid-vapor critical point and systems which show other kinds of critical points have shown a behavior in the coexistence curve that is significantly different from the parabolic curve predicted by the van der Waals equation of state or any other "classical" equation of state. The reason for this difference and the nonclassical behavior of other thermodynamic properties near a critical point is that the expansion of the free energy as an analytical function around the critical point is incapable of generating equations of state that will describe the "nonclassical" behavior.<sup>6</sup> The three-component system can be related to the properties of a single-component reference system<sup>7</sup> so that the functional form of the coexistence curve may be predicted; its degree around the plait point is

$$d = \frac{1 - \alpha'}{\beta} \quad (1)$$

$\alpha'$  and  $\beta$  are the exponents related to the divergence of the specific heat at constant volume and the degree of the coexistence curve for the reference system, respectively.<sup>8</sup>  $\beta$  has the value of nearly  $1/3$ , a value which has been used for some time for comparison of pure fluids around the critical point.<sup>9a</sup> The factor  $1 - \alpha'$  is due to the renormalization of the critical exponents;<sup>9b</sup> it arises in lattice gas models of ternary mixtures<sup>7</sup> and in considerations of the

"scaling law" properties of the critical exponents for mixtures.<sup>10</sup>

Data for coexistence curves exist for several thousand ternary systems;<sup>11</sup> however, all these data either lack the necessary precision or avoid the critical region because of the long times required for equilibration. A recent paper<sup>12</sup> reports a value for  $d$  for the system chloroform-ethanol-water; the value,  $d = 2.67 \pm 0.12$ , is for the locus of points resulting from the intersection of the coexistence surface,  $X_1, X_2, T$  and the vertical plane tangent to an isothermal coexistence curve at the plait point. The value of  $d$  for the experiment described in this paper, for isothermal coexistence curves of the system water-acetic acid-carbon tetrachloride, was found to be  $2.72 \pm 0.12$ .

The classical technique for locating the critical point of a single-component system has been the "law of rectilinear diameters."<sup>13</sup> This approach depends upon the almost linear behavior of the locus of midpoints of the tie lines with respect to temperature. Analogous techniques have been used for binary and ternary systems. Although the diameter may no longer be linear, it is generally a smooth curve which is extrapolated to an intersection with the coexistence curve. Recently, a number of papers have indicated that the law of rectilinear diameters may be inconsistent with nonclassical behavior near the critical point,<sup>14</sup> and that the diameter should be tangent to the coexistence curve at the critical point. Within experimental error, such behavior was found for the ternary system reported here. Although the diameter approached the coexistence curve near the plait point at a very small angle, a detectable change of direction within 0.001 mass fraction of the coexistence curve altered the location of the plait point by 0.005 mass fraction  $\text{CCl}_4$  and 0.001 mass fraction  $\text{H}_2\text{O}$  so that the tangent appeared to become tangent to the coexistence curve.

The system carbon tetrachloride-acetic acid-water was chosen because of the large differences in the refractive index and density of the coexisting phases, even near the plait point. The components are readily available in highly purified form, are easily purified further, and do not react with one another over long periods of time. The plait

- (2) Immiscibility in any of the pairs is not essential, however: a classic example of such a system is water-phenol-acetone above  $66.8^\circ$  in which the two-phase region is a closed loop. F. A. H. Schreinemakers, *Z. Phys. Chem.*, **33**, 78 (1900).
- (3) (a) A. W. Francis, "Liquid-Liquid Equilibrium," Interscience, New York, N. Y., 1963, pp 25-102; (b) A. Findley, "The Phase Rule," 5th ed, Dover Publications, New York, N. Y., 1951, pp 282-402.
- (4) I. Prigogine and R. Defay, "Chemical Thermodynamics," Longmans, London, 1954, pp 254-261.
- (5) (a) P. Heller, *Rep. Progr. Phys.*, **30**, 731 (1967); (b) J. M. H. Levelt Sengers, J. Straub, and M. Vincentini-Missoni, *J. Chem. Phys.*, **54**, 5034 (1971).
- (6) (a) J. S. Rowlinson, "Liquids and Liquid Mixtures," 2nd ed, Butterworths, London, 1969, pp 75-90; (b) M. G. Fisher, *J. Math. Phys.*, **5**, 944 (1964).
- (7) B. Widom, *J. Chem. Phys.*, **46**, 3324 (1967).
- (8) M. E. Fisher, *Nat. Bur. Stand. (U. S.) Misc. Publ.*, **No. 273**, 21 (1966).
- (9) (a) E. A. Guggenheim, *J. Chem. Phys.*, **13**, 253 (1945); (b) M. E. Fisher, *Rep. Progr. Phys.*, **13**, 253 (1945).
- (10) E. Helfand and F. H. Sturlinger, Jr., *J. Chem. Phys.*, **49**, 1232 (1968).
- (11) (a) H. Stephen and T. Stephen, "Solubilities of Inorganic and Organic Compounds," Vol. 2, Pergamon, London, 1964; (b) A. Seidell and W. F. Linke, "Solubilities of Inorganic and Organic Compounds," Suppl. to 3rd ed, American Chemical Society, Washington, D. C., 1952.
- (12) J. A. Zollweg, *J. Chem. Phys.*, **55**, 1430 (1971).
- (13) L. Cailliet and E. C. Mathias, *Seanc. Acad. Sci. (Paris)*, **102**, 1202 (1886); **104**, 1563 (1887).
- (14) (a) B. Widom and J. S. Rowlinson, *J. Chem. Phys.*, **52**, 1670 (1970); (b) M. S. Green, M. J. Cooper, and J. M. H. Levelt Sengers, *Phys. Rev. Lett.*, **26**, 492 (1971); (c) G. Stell and P. C. Hemmer, *J. Chem. Phys.*, **56**, 4274 (1972).

point is well to the carbon tetrachloride side of the phase diagram, a property which enhances the precision of the titration technique.

The coexistence curve was determined by titration of previously weighed mixtures of carbon tetrachloride and water to clarity. The plait point was located by relating the densities of the coexistent liquid pairs to the densities of the mixtures prepared from the titration. The experimental error incumbent in this particular technique, and the efforts made to minimize these errors, are discussed in the Experimental Section. The results and discussion and conclusions are found in the succeeding sections.

### Experimental Section

The acetic acid and carbon tetrachloride were prepared from commercially available analytical reagent grade materials. Analysis by gas chromatography on a Poropak Q column, a preparation that separates molecules by size and shape, indicated a single impurity of about 0.1% in the acetic acid. This could not be removed by either by treatment with  $\text{Cr}_2\text{O}_3$ <sup>15</sup> or triacetyl borate<sup>16</sup> and subsequent distillation; the chromic oxide treatment increased the amount of the impurity. By comparing the retention times on the column, the molecular size of the impurity was found to be smaller than that of acetic acid but larger than water. Retention time was comparable to those for formaldehyde and formic acid. The acetic acid was dried with triacetyl borate and distilled. The carbon tetrachloride was refluxed over dried alumina and distilled. Except for the one impurity in the acetic acid, no other impurities were detected in either the acetic acid or the carbon tetrachloride by gas chromatography. Both were sparged with 99.999% dry argon and stored in desiccators away from light.

The water was prepared by a sixfold distillation of deionized water in an argon atmosphere; the second and third distillations were made from basic potassium permanganate solutions. All the distillations were done in a glass apparatus that had been thoroughly washed with a detergent, rinsed with copious amounts of deionized water, and finally steam. The water was saturated with 99.999% argon and stored in glass vessels that had been cleaned in the same manner as the still and then washed with each of the subsequent distillations.

Two series of mixtures were prepared at 2-deg intervals from 26 to 40°. One series, for the location of the plait point, was prepared so that the overall composition was in the two-phase region. These mixtures were stirred continually for 1 hr in a thermostated bath and then allowed to settle for at least 3 hr; for mixtures very near the plait point, settling times of over 24 hr were necessary. The density of each of the phases was measured with a 10-cm<sup>3</sup> or 15-cm<sup>3</sup> Lipkin pycnometer calibrated with water at  $25.000 \pm 0.001^\circ$ ; the usual buoyancy and thermal expansion corrections for the pycnometer were made. At least 12 pairs were prepared for each temperature.

The second series of mixtures, for the location of the coexistence curve, was prepared by titrating mixtures of water and carbon tetrachloride with acetic acid. The acid was added to the continuously stirred mixture until the meniscus disappeared. For mixtures near the plait point, the final solutions were very cloudy; even under these conditions, however, the presence of the continually agitated interface was easily observed. The mass of each component was determined to the nearest tenth of a milligram; evaporation losses were eliminated as much as pos-

sible by preparing the mixtures beginning with the water and by performing the titrations in an argon atmosphere saturated with carbon tetrachloride and acetic acid vapors. The composition was determined by the directly measured masses rather than by titration of the acetic acid with a standardized base or by gas-phase chromatography. Titration of weighed aliquots of the mixtures produced acetic acid compositions that were approximately 0.2% too large; this discrepancy can be explained by evaporation losses on transferring the solution. These mixtures are not readily analyzed by gas chromatographic methods because both acetic acid and water are highly associated, even in the vapor phase;<sup>17</sup> the relative response of the chromatograph changes with both the size and the composition of the sample. As an example, the sensitivity of the chromatograph to water in the system water-ethanol-ethyl ether changed by 10% by changing the mole fraction of water from 0.3 to 0.6.

The bottle for the titration and the pycnometers were kept in a water bath controlled to  $\pm 0.001^\circ$  by a proportional temperature controller; the temperature was continually monitored by a Hewlett-Packard thermometer to the nearest 0.001°. The titration buret, which had a Teflon stopcock, was enclosed in a water jacket at a temperature approximately 0.5° above that of the titration vessel. The temperature of the water jacket was controlled to  $\pm 0.01^\circ$  by a mercury regulator. The several reasons for the slightly warmer temperature for the water jacket will be explained below. The entire system was isolated from the atmosphere, filled with 99.999% argon, and allowed to come to equilibrium with vapors from reservoirs of pure carbon tetrachloride and acetic acid.

The precision of the titration is controlled by four factors: the diffuseness of the end point; the minimum amount of acetic acid that could be added at any one time; the path of the titration with respect to the coexistence curve; and the state of thermal equilibrium in the mixtures. Errors due to diffuseness in the end point seemed to be well below the others; the disappearance of the meniscus was readily determined within one drop of acetic acid. The volume of a single drop, approximately 0.02 cm<sup>3</sup>, was the smallest amount of acetic acid that could be reproducibly delivered; an error of one drop in a total volume of about 12 cm<sup>3</sup> of the acid leads to an error of 0.17% in the location of the coexistence curve. In this system, however, the plait point is well to one side of the phase diagram; the actual error due to one drop should be  $0.17 \sin \theta$ , where  $\theta$  is the angle between the coexistence curve and the titration path. With  $\theta \approx 15^\circ$ , the error becomes 0.05%. This value agrees well with the random variation from the curves used to fit the data. The last factor affecting the precision of the titration is the temperature of the system. There is a positive enthalpy of mixing of the three components; continuous rapid stirring and the warmer temperature of the acetic acid counteract the lowering of the temperature upon mixing of the components. An overcompensation of the temperature is easily corrected; after the mixture separates into two phases upon cooling to the bath temperature, the titration can be continued. That such separations appeared after the titra-

(15) A. W. Hutchinson and G. C. Chandler, *J. Amer. Chem. Soc.*, **53**, 2881 (1931).

(16) K. Hess, *Ber. Deut. Chem. Ges.*, **63**, 518 (1930).

(17) (a) O. R. Foz Gazella and J. M. Vidal, *An. Soc. esp. Fis. Quim.*, **43**, 842 (1947); (b) E. W. Johnson and L. K. Nash, *J. Amer. Chem. Soc.*, **72**, 547 (1952); (c) H. L. Ritter and J. H. Simons, *J. Amer. Chem. Soc.*, **67**, 757 (1945).



tion apparently had been completed and that the addition of a small amount of acetic acid recovered the end point indicates that sufficient compensation had been made. To not have compensated for the enthalpy of mixing would have led to an apparent coexistence curve outside the actual curve. Each isotherm contained at least 30 points in the range  $\pm 0.20$  mass fraction carbon tetrachloride from the plait point.

An added reason for the second bath was to facilitate transferring the mixtures from the titration bottle to the pycnometers. In addition to the normal methods practiced for the analytical transfer of liquids, it was necessary to keep the syringes and the pycnometers slightly warmer than the temperature at which the mixtures were prepared. Since the mixtures were on the coexistence curve, any cooling would cause a phase separation. Once this separation occurs it is impossible to recover the original mixture, not only because of the slowness of diffusion in liquids and the difficulty of efficient mixing in the pycnometers, but also because of the lack of certainty that the entire amount of both phases had been transferred. The result would be a new mixture of unknown composition. This procedure also facilitated the filling of the pycnometers which were filled to the upper part of the calibration grating; cooling of  $0.5^\circ$  would cause the liquid to contract but not below the calibration marks. The pycnometer was thus opened only at the time of filling; errors due to evaporation were thus minimized.

Although errors arose in the experimental techniques and the exact location of the coexistence curve might be slightly inaccurate, the primary effort was directed toward maintaining the same conditions for all the mixtures so that the data for each temperature were internally consistent. The precision of the data was such that rogue points were immediately detectable. For the interpretation of the data, such random points were dropped before serious interpretation was attempted; these points represent about 5% of the total data.

## Results

The information from the two sets of data described in the Experimental Section can be combined to locate the plait point. The data arising from the densities of the coexisting phases provide the density of the plait point mixture; the data from the titrations yield a density-composition map for the coexistence curve. Thus the composition of the plait point can be readily deduced. Figure 1 shows the coexistence curves for 26 and  $40^\circ$  and the plait points at 2-deg intervals; the data for  $26^\circ$  are given in Table I<sup>18</sup> to show the kind of information necessary to produce Figures 1 and 3. The curves over so small a temperature range are nearly the same; it thus suffices to show the behavior of one in detail. One immediately notes that the plait points do not fall on a smooth curve; however, the variation from a straight line between the 26 and  $40^\circ$  plait points is  $\pm 0.5\%$  in the mass fractions of the immiscible pair. The probable reason for this variation is explained later.

The coexistence curve is characterized by its behavior relative to the tangent at the plait point; the coordinate system is altered so that the tangent becomes the abscissa and the plait point becomes the origin. It has been pointed out<sup>7</sup> that there are a number of slightly different coordinate systems arising from this convention but that they are equivalent near the origin. Figure 2 shows the coordinate system used for this analysis.  $\Delta w_{\text{CCl}_4}$  is the difference

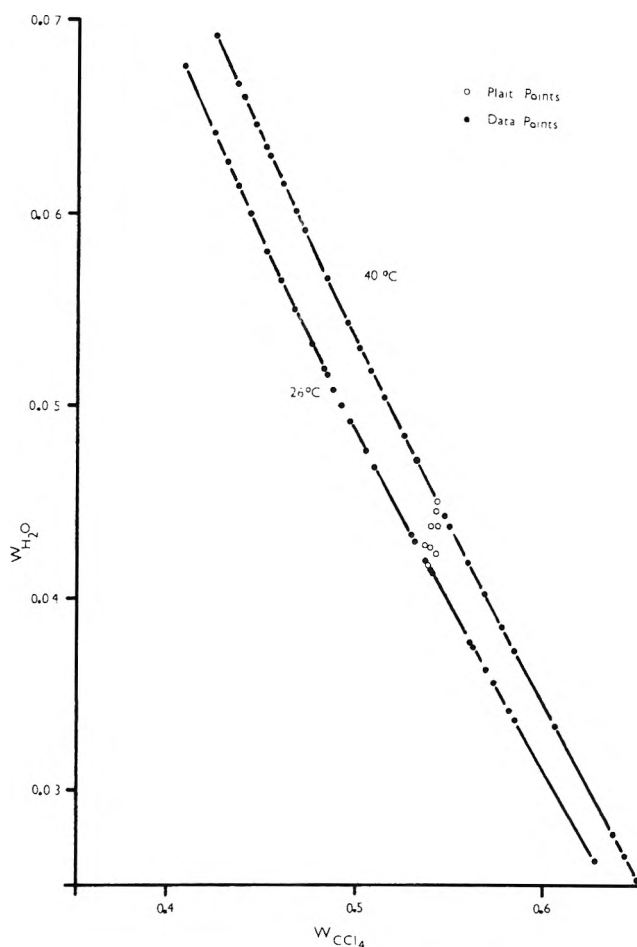


Figure 1. The coexistence curves for 26 and  $40^\circ$ . The open circles show the plait points at 2-deg intervals from 26 to  $40^\circ$ .

between any value of  $w_{\text{CCl}_4}$ , the mass fraction of carbon tetrachloride, and the plait point value;  $\Delta w_{\text{H}_2\text{O}}$  is the difference between  $w_{\text{H}_2\text{O}}$  on the coexistence curve and  $w_{\text{H}_2\text{O}}$  on the tangent for any  $w_{\text{CCl}_4}$ . The degree of the curve is determined by the expression

$$\Delta w_{\text{H}_2\text{O}} = A|\Delta w_{\text{CCl}_4}|^d \quad (2)$$

In the region of the plait point, the mass density is nearly a linear function of the mass fraction so that eq 2 is equivalent to the function as it usually appears in a number density space.

$$\Delta \rho_{\text{H}_2\text{O}} = A'|\Delta \rho_{\text{CCl}_4}|^d \quad (3)$$

$$A' = AL^{d-1} \frac{m_{\text{H}_2\text{O}}(2m_{\text{CCl}_4}w_{\text{p}(\text{CCl}_4)} + b_{\text{CCl}_4})^d}{m_{\text{CCl}_4}^d(2m_{\text{H}_2\text{O}}w_{\text{p}(\text{H}_2\text{O})} + b_{\text{H}_2\text{O}})} \quad (4)$$

It is then possible to use the mass fraction directly to determine  $d$ ; thus errors in density, however small, do not enter into the analysis.  $d$  is determined by plotting  $\log(\Delta w_{\text{H}_2\text{O}})$  as a function of  $\log(|\Delta w_{\text{CCl}_4}|)$ . Although it is possible to determine the plait point and the tangent experimentally, the shape of the log-log plot is dramatically affected by even small changes in the slope of the tangent and its tangent point. It is necessary to refine this experimental line by moving it slightly, but within the limits of

(18) Table I will appear following these pages in the microfilm edition of this volume of the journal. Single copies may be obtained from the Business Operations Office, Books and Journals Division, American Chemical Society, 1155 Sixteenth St., N.W., Washington, D. C. 20036. Remit check or money order for \$3.00 for photocopy or \$2.00 for microfiche, referring to code number JPC-73-1572.

TABLE II

$T, ^\circ\text{C} \pm 0.0001$	$(w_{\text{H}_2\text{O}}, w_{\text{CCl}_4})$	Slope of tangent	$d$	$A$
26.000	0.04167, 0.5368	0.1829	$2.75 \pm 0.02$	$0.7708 \pm 0.0008$
28.000	0.04277, 0.5354	0.1827	$2.65 \pm 0.03$	$0.6318 \pm 0.0010$
30.000	0.04260, 0.5379	0.1837	$2.78 \pm 0.04$	$0.6998 \pm 0.0012$
32.000	0.04233, 0.5408	0.1850	$2.71 \pm 0.05$	$0.6974 \pm 0.0016$
34.000	0.04382, 0.5386	0.1883	$2.76 \pm 0.05$	$0.7185 \pm 0.0016$
36.000	0.04369, 0.5413	0.1897	$2.70 \pm 0.06$	$0.6830 \pm 0.0018$
38.000	0.04459, 0.5407	0.1890	$2.69 \pm 0.04$	$0.6654 \pm 0.0012$
40.000	0.04520, 0.5418	0.1919	$2.69 \pm 0.05$	$0.7233 \pm 0.0017$

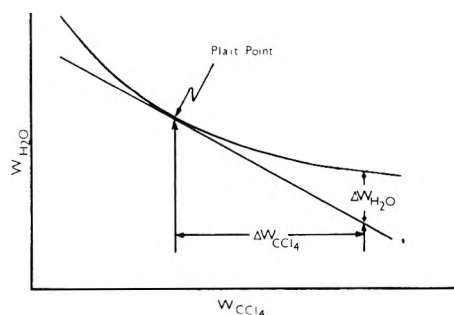


Figure 2. The transformation of variables and coordinates for the analysis of the coexistence curve.

experimental error, to determine the "best" tangent, the one for which the least-squares straight-line fit to the log-log plot has the smallest standard deviation. The slopes of these log-log plots are the values for  $d$  which are reported in Table II. Figure 3 shows the plots for 26 and 40°. These two, as well as those for the other temperatures, are essentially identical; this is unsurprising for the small temperature range at a temperature well below the upper consolute critical point of the system. This method for evaluating  $d$  is less haphazard than it might appear; the values of  $\log \Delta w_{\text{H}_2\text{O}}$  at large values of  $|\Delta w_{\text{CCl}_4}|$  are relatively unchanged even for large variations of the tangent. At small values of  $|\Delta w_{\text{CCl}_4}|$ , the log-log plot varies wildly with shifts in the position of the tangent; thus, there is a quite small range of variation in the tangents that will produce straight lines for the log-log plot in the region of  $|\Delta w_{\text{CCl}_4}| = 0$ . The errors attributed to  $A$  and  $d$  are the extremes in these parameters that will produce curves within the error envelope surrounding the best fit to the data in the range of the experiment.

The plait point was experimentally located by determining the limiting value of the average density of the coexisting phases by a graphical technique; the values of the densities of the two phases were plotted as a function of the average of the densities. The graphs for 26 and 32° are shown in Figure 4. The unexpected property of these graphs is that the average density does not vary monotonically as the plait point is reached. Since there is no unusual behavior in the coexistence curve or in the density-composition variation along the curve, this behavior can be attributed either to very slow reactions between the components during the long times necessary to separate the two phases in the plait point region or to changes in the tie lines and hence the diameter. The densities of mixtures of the three components measured over periods of several days remained constant so that one can conclude that a chemical reaction was not the cause of this behavior. The second unexpected property of these plots was the large difference in the depth of the indentation

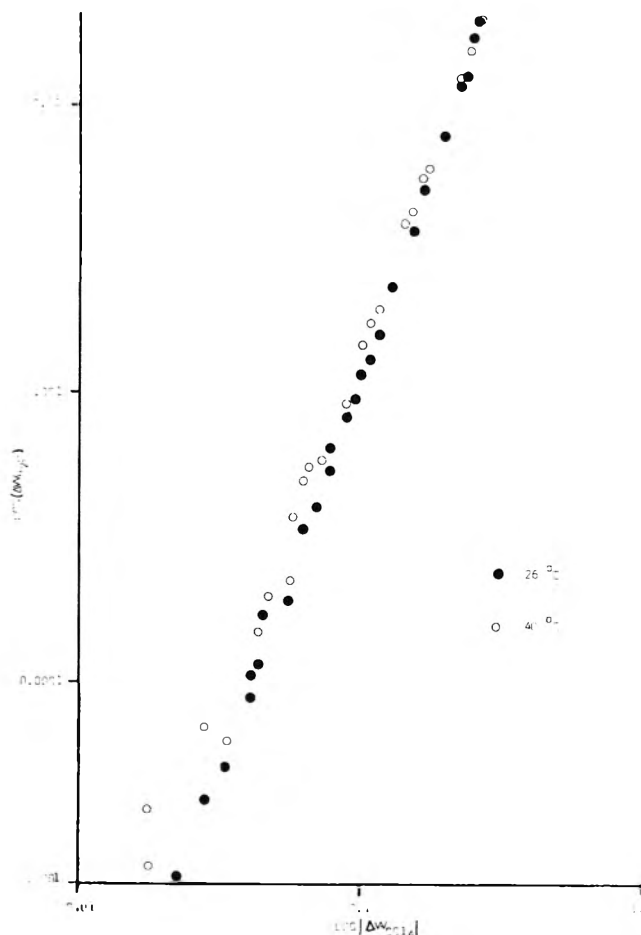


Figure 3. The plot  $\log(\Delta w_{\text{H}_2\text{O}})$  vs.  $\log|\Delta w_{\text{CCl}_4}|$  for the 26 and 40° coexistence curves.

from temperature to temperature. Although some of this variation can be attributed to experimental error, a significant part must be attributed to the difficulty of obtaining the necessary data in the plait point region; the shallowness of the coexistence curve makes the appropriate mixture very difficult to prepare. The more shallow indentations are likely the result of lack of data closer to the plait point. The differences in the depth of the indentation causes scatter in the locus of plait points.

Figure 4 shows the extremes in the anomalous behavior of the average density as the plait point is approached; Figure 5 shows the diameter for the 26° isotherm. The diameter ending at  $A$  is the one corresponding to the plot in Figure 4;  $B$  terminates the diameter as if there were as large an indentation as in the 32° plot.  $C$  shows the diameter extrapolated from outside the region of the indentation. Although the diameter would intersect the coexis-

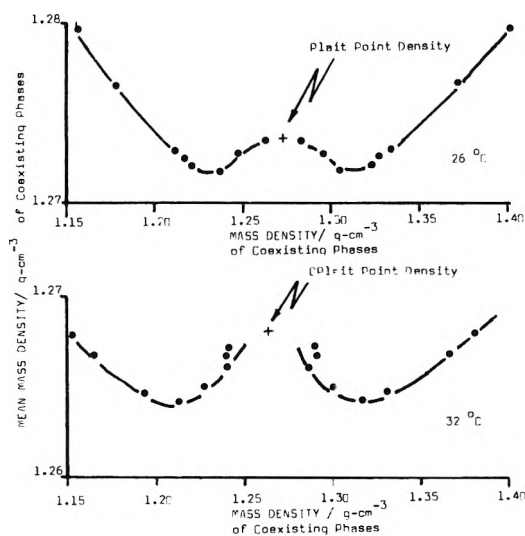


Figure 4. The plot of the mass densities of the coexisting phases against the mean of the mass densities for the location of the plait point for 26 and 32°.

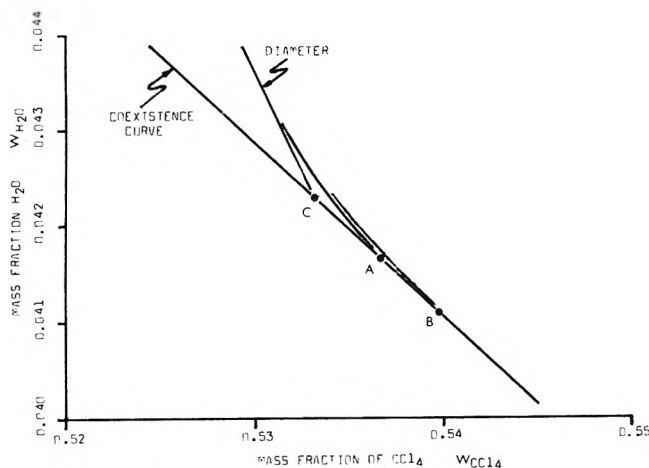


Figure 5. The extremes in the variation of the diameter for the 26° coexistence curve.

tence curve at a very small angle in any case, the indentation further diminishes the size of the angle of intersection; indeed, in the case of diameter B, the intersection appears a tangent point.

## Discussion

The value for  $d$ ,  $2.72 \pm 0.12$ , agrees within the experimental error with the known values of  $\alpha'$  and  $\beta$  for binary liquid systems having critical mixing points and for liquid-vapor critical points in single-component systems where quantum effects are not important. The value is unambiguously different from the classical value of  $d = 2$ ; it is close to the value predicted by the approximate solution to the three-dimensional Ising lattice for which  $\alpha = 1/16$  to  $1/8$ ,  $\beta = 5/16$ , and  $d = 3$  to 2.8.<sup>19</sup> One of the unfortunate aspects of this experiment is that it is not possible to measure  $\beta$  for the binary mixture water-carbon tetrachloride at atmospheric pressure; the mixture boils at 67°, but even at this temperature, the two components are almost totally immiscible. If one assumes that  $\beta$  is the same as the generally accepted value of  $\beta$ , it is possible to determine the value of  $\alpha'$ . For  $\beta = 0.350 \pm 0.005$ ,<sup>20</sup>  $\alpha' = 0.047 \pm 0.041$ . This indicates that  $\alpha'$  has a value in the middle of the gen-

erally accepted range of experimentally determined values, 0.0 to 0.125.<sup>21</sup>

The recent theoretical discoveries<sup>14</sup> of the anomalous behavior in the diameter are specifically for single-component systems. It is necessary to invoke certain symmetry properties in mixtures so that any solution might result at all. An example of such a symmetry requirement is in the decorated lattice theory of ternary mixtures; the plait point must be on the half-occupied composition line of the primary lattice, and this line must be the diameter. Such results indicate that the absence of the anomaly in the multicomponent system may not be inconsistent with nonclassical behavior; indeed in perhaps the only real binary system that fulfills such stringent symmetry requirements, the array of spins on a lattice where  $H = 0$ , the rectilinear diameter of the magnetization is a straight line as a function of temperature. Practically all other mixtures do not possess this symmetry; one reflection of this is a curved diameter, perhaps possessing a singularity.

It suffices to say that in single-component systems, the singularity in the diameter at the critical point has not yet been observed. Even in binary and ternary mixtures, there is very little information about the diameter in the immediate region of the critical mixing points; however, Haselden, *et al.*,<sup>22</sup> note that the law of rectilinear diameters appears to break down for the CO<sub>2</sub>-propylene system, albeit for a liquid-vapor critical point. The diameter of the 2,6-dimethylpyridine-water system, which has a highly asymmetric coexistence curve and yet has a functional form of  $\beta \approx 1/3$ , is bowed near the lower critical mixing point; the l.c.m.p. determined by a diameter extrapolation technique is in error by approximately 1% in the mole fraction.<sup>23</sup> The phenomenon of dramatic bending in the diameter is not isolated to systems of complicated polar molecules, however; the diameter of the solid-solid immiscibility curve of the mixture Ar-CH<sub>4</sub> bends sharply to the argon rich side of the phase diagram as the critical point at 63 K is approached.<sup>24</sup>

The observation in this experiment and in the others noted that the diameter of the coexistence curve of a multicomponent system behaves differently in the region of the critical mixing point gives credence to the theory that there is a singularity in the diameter for one-component systems. Considerable analysis of the properties of this anomalous behavior, even in multicomponent systems, remains to be done.

*Acknowledgments.* This work was made possible by the generosity of the Research Corporation, who provided funds for much of the equipment through a Cottrell Grant, and grants made to the Department of Chemistry at St. Olaf College from the NSF-URP program, and from the E. I. du Pont de Nemours Co.

## Appendix. Glossary of Terms

$\alpha'$  = the critical exponent describing the behavior of  $C_v$  near the critical point on the path  $T > T_c$

- (19) H. E. Stanley, "Introduction to Phase Transitions and Critical Phenomena," Oxford, 1971, pp. 11, 47.
- (20) J. S. Rowlinson, *Ber. Bunsenges. Phys. Chem.*, **76**, 281 (1972).
- (21) R. L. Scott, *Ber. Bunsenges. Phys. Chem.*, **76**, 296 (1972).
- (22) G. C. Haselden, F. A. Holland, M. B. King, and R. F. Strickland-Constable, *Proc. Roy. Soc. Ser. A*, **240**, 1 (1957).
- (23) J. D. Cox and E. F. G. Herington, *Trans. Faraday Soc.*, **52**, 926 (1956).
- (24) S. C. Greer, L. Meyer, and C. S. Barrett, *J. Chem. Phys.*, **50**, 4299 (1969).

$\beta$	= the critical exponent describing the shape of the coexistence curve of a single-component system	$M_A$	= relative molar mass of component A
$w_A$ and $w_{pA}$	= the mass fraction of A and the mass fraction of A at the plait point	$m_A$ and $b_A$	= the slope and intercept of the straight line relation of the mass fraction of component A and the mass density
$\rho_A$	= number density of component A	$L$	= Avogadro's number
		$H$	= magnetic field
		$K$	= the kelvin, unit of thermodynamic temperature

## Mass Spectrometric Studies of Gaseous Oxides of Rhenium

Harry B. Skinner and Alan W. Searcy\*

*Inorganic Materials Research Division, Lawrence Berkeley Laboratory and Department of Materials Science and Engineering, College of Engineering, University of California, Berkeley, California (Received November 2, 1972)*

*Publication costs assisted by the U. S. Atomic Energy Commission*

Effusion cell mass spectrometry has been employed to study vapor species of the rhenium-oxygen system. The equilibrium partial pressure of  $\text{Re}_2\text{O}_7(\text{g})$  above a mixture of  $\text{Re}_2\text{O}_7(\text{s})$  and  $\text{ReO}_3(\text{s})$  from 327 to 463°K is given by  $\log P(\text{Re}_2\text{O}_7) = -(7.44 \pm 0.08)10^3/T + (12.35 \pm 0.21)$  where the pressure is in atmospheres. The enthalpy of sublimation at 430°K is  $34.0 \pm 2$  kcal/mol. Weight loss measurements show the probable composition of the dirhenium heptoxide phase in equilibrium with  $\text{ReO}_3(\text{s})$  at 400°K to be  $\text{Re}_2\text{O}_{6.98 \pm 0.02}$ . The reaction of rhenium with zinc oxide at 1047 at 1267°K produces  $\text{Re}_2\text{O}_7(\text{g})$ ,  $\text{ReO}_3(\text{g})$ , and possibly  $\text{Re}_2\text{O}_6(\text{g})$ . Reaction of rhenium with magnesium oxide from 1770 to 2143°K produces principally  $\text{ReO}_3(\text{g})$ . The enthalpy of formation of  $\text{ReO}_3(\text{g})$  is  $-67.0 \pm 4$  kcal/mol at 298°K and that of  $\text{Re}_2\text{O}_6(\text{g})$  is  $\geq -212 \pm 20$  kcal/mol at 298°K.  $\text{Re}_2\text{O}_5(\text{g})$ ,  $\text{ReO}_2(\text{g})$ , and  $\text{ReO}(\text{g})$  are not present at measurable concentrations under any of the conditions of study. The heats of formation of  $\text{ReO}(\text{g})$  and  $\text{ReO}_2(\text{g})$  are more positive than  $-10$  and  $+48$  kcal/mol, respectively.

### Introduction

The vapor pressure for the reaction  $\text{Re}_2\text{O}_7(\text{s}) \rightarrow \text{Re}_2\text{O}_7(\text{g})$  was measured by Ogawa,<sup>1</sup> by Smith, Line, and Bell,<sup>2</sup> and more recently by Glemser, Muller, and Stocke.<sup>3</sup> A mass spectrometer investigation of vapors from the solids  $\text{ReO}_3$  and  $\text{ReO}_2$  was first made by Semenov and Ovchinnikov,<sup>4</sup> who reported that both  $\text{ReO}_3(\text{g})$  and  $\text{Re}_2\text{O}_7(\text{g})$  are important species in vaporization of both phases. However, Battles, Gundersen, and Edwards<sup>5</sup> showed that  $\text{ReO}_3(\text{s})$  and  $\text{ReO}_2(\text{s})$  do not vaporize congruently as reported by Semenov and Ovchinnikov<sup>4</sup> and that  $\text{Re}_2\text{O}_7(\text{g})$  was the only major vapor species over the solid-phase mixtures  $\text{ReO}_3\text{-ReO}_2$  and  $\text{ReO}_2\text{-Re}$ . Norman, Winchell, and Staley<sup>6</sup> were able to study the reaction of rhenium metal with oxygen to form  $\text{ReO}_3(\text{g})$  but obtained conflicting measurements of its stability.

This paper reports mass spectrometer investigations of vaporization of  $\text{Re}_2\text{O}_7\text{-ReO}_3$  solid mixtures, of  $\text{Re-ZnO}$  solid mixtures, and of  $\text{Re-MgO}$  solid mixtures which were undertaken to obtain, if possible, more precise data for  $\text{ReO}_3(\text{g})$  and to determine if additional gaseous rhenium oxides could be identified and studied. In the course of the work it was discovered that solid  $\text{Re}_2\text{O}_7$  does not vaporize congruently *in vacuo* but has a low partial pressure of oxygen.

### Dirhenium Heptoxide Vaporization

*Experimental Section.* This study was carried out with a 60° sector, 1-ft radius, magnetic deflection mass spectrometer built by Nuclide Analysis Associates. The dirhenium heptoxide obtained from Alfa Inorganics Co. had Mg as the only impurity detectable by spectroscopic analysis.

The sample was resistively heated by nichrome wire wound closely around an anodized aluminum effusion cell. The interior of the cell was gold plated and a gold lid and liner were installed to prevent any contact of the rhenium heptoxide sample with the aluminum.

The sample color changed after prolonged heating, which suggested that some reaction other than simple congruent sublimation was occurring. X-Ray diffraction measurements demonstrated that a residue of  $\text{ReO}_3(\text{s})$  re-

- (1) E. Ogawa, *Bull. Chem. Soc. Jap.*, **7**, 265 (1932).
- (2) W. T. Smith, L. E. Line, Jr., and W. A. Bell, *J. Amer. Chem. Soc.*, **74**, 4964 (1952).
- (3) O. Glemser, A. Muller, and U. Stocke, *Z. Anorg. Allg. Chem.*, **333**, 25 (1964).
- (4) G. A. Semenov and K. V. Ovchinnikov, *J. Gen. Chem. USSR*, **35**, 1517 (1965).
- (5) J. E. Battles, G. E. Gundersen, and R. K. Edwards, *J. Phys. Chem.*, **72**, 3963 (1968).
- (6) J. H. Norman, P. Winchell, and H. G. Staley, G. A. 8472, OCB Work No. 3111A, T. O. No. 3110 (67) (1968).

**TABLE I: Relative Intensities of Ions Formed from the Vapor, from  $\text{Re}_2\text{O}_7(\text{s})$ , and from the  $\text{Re} + \text{ZnO}$  and  $\text{Re} + \text{MgO}$  Reactions at 70 eV and Their Appearance Potentials**

Ion	Intensity and standard deviation			Appearance potentials, eV		
	$\text{Re}_2\text{O}_7(\text{s})$	$\text{Re} + \text{ZnO}$	$\text{Re} + \text{MgO}$	$\text{Re}_2\text{O}_7(\text{s})$	$\text{Re} + \text{ZnO}$	$\text{Re} + \text{MgO}$
$\text{Re}_2\text{O}_7^+$	1000	1000	<1	$12.7 \pm 0.2$	$13.6 \pm 0.8$	
$\text{Re}_2\text{O}_6^+$	$91 \pm 2$	$131 \pm 12$	<1	$16.2 \pm 0.5$	$16.1 \pm 0.6$	
$\text{Re}_2\text{O}_5^+$	$17.4 \pm 0.4$	$23 \pm 2$	<1	$17.5 \pm 0.2$	$16.1 \pm 0.8$	
$\text{ReO}_3^+$	$276 \pm 11$	$720 \pm 260$	1000	$16.2 \pm 0.5$	$14.7 \pm 0.6$	$12.5 \pm 0.4$
$\text{ReO}_2^+$	$154 \pm 9$	$218 \pm 52$	320	$21.9 \pm 1.0$	$18.0 \pm 0.8$	$14.4 \pm 1.0$
$\text{ReO}^+$			100			$\sim 18$

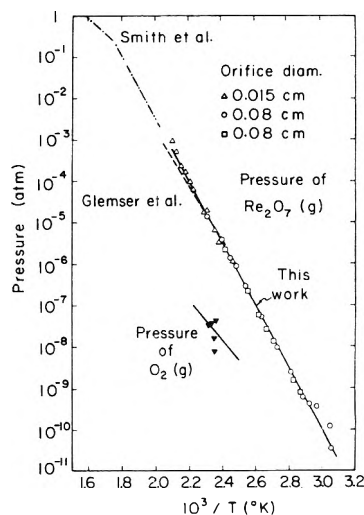
mained after long heating of  $\text{Re}_2\text{O}_7(\text{s})$ . To determine the fraction of  $\text{Re}_2\text{O}_7(\text{s})$  that decomposed to  $\text{ReO}_3(\text{s})$ , 0.5-g samples were heated to constant weight at about 430°K in a separate vacuum system capable of  $\sim 2 \times 10^{-6}$  Torr using the effusion cell and liner from the mass spectrometric experiments. Heating times of 60–150 hr were required. Spectroscopically detectable impurities in the  $\text{ReO}_3(\text{s})$  residue were Mg, Si, and Fe, all present at less than 2% of the Re concentration.

Bombardment of the vapor from the  $\text{Re}_2\text{O}_7$ – $\text{ReO}_3$  solid mixtures by 70-eV electrons produced  $\text{Re}_2\text{O}_7^+$ ,  $\text{Re}_2\text{O}_6^+$ ,  $\text{Re}_2\text{O}_5^+$ ,  $\text{ReO}_3^+$ , and  $\text{ReO}_2^+$ , which were each measured seven or more times over a 7-day period while the rhenium heptoxide was held at about 404°K. Appearance potentials were measured by the method of extrapolated differences with the mercury ion intensity used as the reference. Analysis of these data and comparison with data for the same ions produced by reaction of rhenium metal with metal oxides showed all the ions found in  $\text{Re}_2\text{O}_7(\text{s})$  vaporization to arise from an  $\text{Re}_2\text{O}_7(\text{g})$  parent molecule. (See Discussion section.)

The intensity of the  $\text{Re}_2\text{O}_7^+$  ion was followed as a function of temperature from 327 to 463°K. Three runs were made, with several datum points being taken in each run in a random manner allowing 0.5 hr or more for equilibrium to be obtained. A 0.0762-cm diameter effusion orifice was used for two of the runs and a 0.014-cm orifice for a higher temperature run. Channel lengths were about equal to the orifice diameters. The temperature was continuously monitored and readings were taken after at least 15 min had passed with the temperature constant to within 0.5°. One 5-mil chromel–alumel thermocouple was clamped against the junction of the gold cell lid and the gold cell lip; another was clamped to the cell 1.6 mm from the bottom. The two thermocouples read to within 0.25° of each other. The thermocouples were calibrated by determination of the melting point of 99.999% indium, 429.3°K.<sup>7</sup> They gave melting points of 430.0 and 430.3°K.

Since the heat of sublimation was to be determined from the temperature dependence of the measured ion intensities, the heat of sublimation of cadmium was measured by the same (second law) method to test the reliability of the apparatus and experimental techniques. Nine points were taken in random order over the temperature range 427–512°K. A least-squares enthalpy of  $26.72 \pm 0.52$  kcal/mol (where the quoted error is the standard deviation) was calculated from the data. The selected value of Hultgren, *et al.*,<sup>7</sup> at 469°K is  $26.41 \pm 0.15$  kcal/mol.

**Results.** The steady-state relative intensities of the major species observed for  $\text{Re}_2\text{O}_7(\text{s})$ – $\text{ReO}_3(\text{s})$  mixtures and appearance potentials are recorded in Table I. Intensities of  $\text{Re}_2\text{O}_6^+$  and  $\text{Re}_2\text{O}_5^+$  changed little relative to  $\text{Re}_2\text{O}_7^+$



**Figure 1.** The  $\text{Re}_2\text{O}_7(\text{s}) = \text{Re}_2\text{O}_7(\text{g})$  reaction as a function of temperature and the dissociation pressure for the reaction  $\text{Re}_2\text{O}_7(\text{s}) = 2\text{ReO}_3(\text{s}) + \frac{1}{2}\text{O}_2(\text{g})$  if  $\text{Re}_2\text{O}_7(\text{s})$  is stoichiometric. See text.

during the initial days of vaporization, but intensities of  $\text{ReO}_2^+$  decreased some 27% and of  $\text{ReO}_3^+$  decreased about 26%. These changes are attributed to gradual reduction in contamination by  $\text{HReO}_4$  from which  $\text{ReO}_3^+$  and  $\text{ReO}_2^+$  would arise through a fragmentation process.<sup>5</sup> A known  $\text{HReO}_4^+$  peak<sup>5</sup> was observed, but not monitored.

Data for the steady-state  $\text{Re}_2\text{O}_7^+$  ion are plotted in Figure 1, along with total pressures of Glemser, *et al.*,<sup>3</sup> and Smith, *et al.*<sup>2</sup> Glemser's conditions would be expected to give the  $\text{ReO}_3(\text{s})$ – $\text{Re}_2\text{O}_7(\text{s})$  invariant system.

The least-squares fit of  $\log [T I(\text{Re}_2\text{O}_7^+)]$  vs.  $1/T$  for each run was made to coincide at the average pressure of Glemser, *et al.*, and Smith, *et al.*, at 433.3°K (Figure 1). Enthalpies calculated from temperature dependence of intensities for the three runs were  $33.25 \pm 0.72$ ,  $35.30 \pm 0.15$ , and  $36.45 \pm 0.92$  kcal/mol. The least-squares fit of all the data normalized to this point yielded an enthalpy of sublimation of  $34.0 \pm 0.4$  and an entropy of sublimation of  $56.0 \pm 1.0$  eu/mol.

The partial pressure of  $\text{Re}_2\text{O}_7$  from 327 to 463°K is given by the equation

$$\log P_{\text{atm}} = -(7.44 \pm 0.08)10^3/T + (12.35 \pm 0.21) \quad (1)$$

where the quoted errors are the standard deviations from the least-squares fit.

(7) R. Hultgren, R. L. Orr, P. D. Anderson, and K. K. Kelley, "Selected Values of Thermodynamic Properties of Metals and Alloys," Wiley, New York, N. Y., 1963.

TABLE II:  $\Delta H^{\circ}_{298}$  Calculated from Weight Loss Data for the Reaction  $\text{Re}_2\text{O}_7(\text{s}) = 2\text{ReO}_3(\text{s}) + \frac{1}{2}\text{O}_2(\text{g})$

Temp. °K	$\Delta F^{\circ}_T$ , kcal	Orifice area, cm <sup>2</sup>	$-(\Delta F^{\circ}_T - \Delta H^{\circ}_{298})/T$	$\Delta H^{\circ}_{298}$ , kcal
430.9	7.38	0.01046	13.41	13.16
424.9	7.91	0.01046	13.42	13.61
424.6	7.60	0.034	13.42	13.30
423.7	7.16	0.001075	13.42	12.85
429.4	7.34	0.034	13.41	13.10

A limit to the composition of the phase  $\text{Re}_2\text{O}_7(\text{s})$  that was in equilibrium with  $\text{ReO}_3(\text{s})$  could be set from the ratio of moles of  $\text{Re}_2\text{O}_7(\text{s})$  heated to moles of  $\text{ReO}_3(\text{s})$  remaining after heating to constant weight. This ratio was about 22/1. Accordingly, if the oxygen dissociation pressure for the  $\text{Re}_2\text{O}_7(\text{s})$  phase was completely negligible, composition of the  $\text{ReO}_3(\text{s})$  phase boundary is calculated to be  $\text{Re}_2\text{O}_{6.98}$ . This calculation is insensitive to possible nonstoichiometry of  $\text{ReO}_3(\text{s})$  because the fraction of the dirhenium heptoxide converted to the  $\text{ReO}_3(\text{s})$  phase is small.

If it is assumed that dirhenium heptoxide is essentially stoichiometric, the oxygen dissociation pressure of  $\text{Re}_2\text{O}_7(\text{s})$  which would yield the  $\text{ReO}_3(\text{s})$  residue can be calculated from the Langmuir<sup>8</sup> equation. These oxygen pressures are plotted in Figure 1 and Gibbs free energies and  $\Delta H^{\circ}_{298}$  for the dissociation reaction are given in Table II.

The calculations assume the heat capacity for  $\text{Re}_2\text{O}_7(\text{s})$  to be linear from the values<sup>9</sup> at 298°K to the melting point where the  $C_p$  was estimated to be 7.0 cal/deg atom.<sup>10</sup> This gave  $C_p = 14.55 + 8.47 \times 10^{-2}T$ . King<sup>10</sup> and Cobble<sup>11</sup> have reported for  $\text{ReO}_3(\text{s})$   $S^{\circ}_{298} = 19.3$  eu/mol. The heat contents and entropy increases above 298°K for  $\text{ReO}_3(\text{s})$  were assumed to be the same as the values reported for  $\text{WO}_3(\text{s})$  in JANAF,<sup>12</sup> and JANAF data were used for  $\text{O}_2(\text{g})$ .

### Zinc Oxide-Rhenium Equilibrium

*Experimental Section.* Reagent grade zinc oxide supplied by Baker and Adamson, which was used in this part of the study, showed 0.15% Mn, 0.06% Si, and 0.025% Ca as the principal spectroscopically detectable impurities. The rhenium powder obtained from the Department of Chemistry, University of Tennessee, showed 0.015% Si as the principal impurity.

Mass spectrometer experiments were performed in a molybdenum or tantalum outer cell with either an alumina cell liner or a rhenium liner. A machined alumina cell was constructed for weight loss experiments. Orifice areas, 0.3 mm<sup>2</sup> were about one-tenth the cross sectional area shown to yield equilibrium data<sup>13</sup> in zinc oxide vaporization. Heating at lower temperatures was by radiation from two filaments positioned horizontally around the cell at top and bottom to minimize gradients along the length of the cell and at higher temperatures was by electron bombardment. The temperature was measured to the nearest degree with a platinum/platinum-10% rhodium thermocouple clamped to the bottom of the cell.

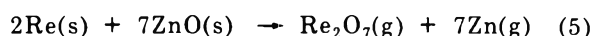
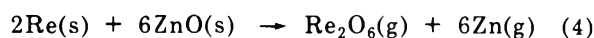
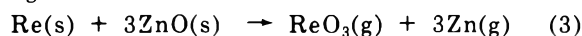
Temperature calibrations were checked by measuring the second-law enthalpy of sublimation of silver in the range 1051–1225°K. Fourteen measurements made in random order yielded a least-squares enthalpy of sublimation

of  $64.48 \pm 0.44$  kcal/mol at 1138°K. The value interpolated from Hultgren's<sup>7</sup> tabulation is  $66.49 \pm 0.20$  kcal/mol.

Mann's<sup>14</sup> cross sections for electron impact ionization were used with the assumption that atomic cross sections are additive. Measured electron multiplier gains relative to  $^{484}\text{Re}_2\text{O}_7 = 1$  were  $^{64}\text{Zn} = 0.86$ ,  $\text{ReO}_3 = 1.0$ ,  $\text{ReO}_2 = 1.0$ , and  $\text{Re}_2\text{O}_6 = 0.9$ . The relative gain for  $\text{Re}_2\text{O}_5$  was assumed to be 0.9.

The intensity of each ion produced with 70-eV electrons was followed as a function of temperature in five separate runs. After the temperature had stabilized, about 15 min was allowed for equilibrium to be obtained.

In all temperature variation experiments, a small portion of zinc metal was added to the Re-ZnO mixture. Measurement of the vapor pressure of zinc at low temperature provided a direct determination of the proportionality constant between  $I^+T$  and pressure for  $\text{Zn}(\text{g})$ . Several  $\text{Zn}^+$  intensities were measured, then the Zn was exhausted and the rhenium-zinc oxide equilibrium was measured. In addition, weight loss experiments were performed at constant temperature. The ion intensities of  $\text{Zn}^+$ ,  $\text{Re}_2\text{O}_7^+$ ,  $\text{ReO}_3^+$ , and  $\text{Re}_2\text{O}_6^+$  were measured several times during a run, then averaged and corrected for fragmentation in order to calculate equilibrium constants for the following reactions



Losses during heating and cooling were negligible.

To check the accuracy of the weight loss experiments, two weight loss measurements were made on silver. Measured silver pressures were found to be approximately 1.7 times higher than the pressures selected by Hultgren.<sup>7</sup> The measured total pressure in ZnO-Re weight loss experiments was reduced by this factor to correct for systematic errors.

Average appearance potentials measured for rhenium oxide ions produced from the vapor above ZnO-Re mixtures are given in the last column of Table I. One set of measurements was made using background mercury as a standard, another used  $\text{Zn}^+$  from the reduction of zinc oxide to zinc vapor.

A cell exhaustion experiment was made to determine if the  $\text{Re}_2\text{O}_6^+$  was all produced by fragmentation of  $\text{Re}_2\text{O}_7(\text{g})$  or if some arose from ionization of  $\text{Re}_2\text{O}_6(\text{g})$ . If  $\text{Re}_2\text{O}_6(\text{g})$  is present in significant amounts in the vapor above zinc oxide-rhenium mixtures, the  $\text{Re}_2\text{O}_6^+$  peak should decrease more slowly than the  $\text{Re}_2\text{O}_7^+$  peak. For this experiment, excess rhenium powder was mixed with a very small portion of zinc oxide powder. The mixture was heated to about 1186°K and held until the intensities began to drop. The intensities of  $\text{Re}_2\text{O}_7^+$  and  $\text{Re}_2\text{O}_6^+$  were followed as a function of time. When the intensities had dropped to about 1/10 of their initial values, the cell temperature was raised about 50°K causing the intensities

(8) K. D. Carlson in "The Characterization of High Temperature Vapors," J. L. Margrave, Ed., Wiley, New York, N. Y., 1967, Chapter 5.

(9) R. H. Busey, *J. Amer. Chem. Soc.*, **78**, 3263 (1956).

(10) K. K. Kelley, *U. S. Bur. Mines, Bull.*, No. 371 (1934).

(11) J. P. King and J. W. Cobble, *J. Amer. Chem. Soc.*, **79**, 1559 (1957).

(12) "JANAF Thermochemical Data," Dow Chemical Co., Midland, Mich., 1965.

(13) D. F. Anthrop and A. W. Searcy, *J. Phys. Chem.*, **68**, 2335 (1964).

(14) J. B. Mann, *J. Chem. Phys.*, **46**, 1646 (1967).

TABLE III: Weight Loss Data for ZnO-Re Experiments

	1	2	3
Temp, °K	1245	1177	1187
Time, sec	$4.00 \times 10^4$	$1.60 \times 10^5$	$1.75 \times 10^5$
Weight loss, g	0.0336	0.0265	0.0358
Clausing factor	0.4	0.4	0.4
Area, cm <sup>2</sup>	$6.42 \times 10^{-4}$	$6.42 \times 10^{-4}$	$6.42 \times 10^{-4}$
Corrected partial pressures, atm			
(1) Zn(g)	$1.55 \times 10^{-4}$	$3.02 \times 10^{-5}$	$4.59 \times 10^{-5}$
(2) Re <sub>2</sub> O <sub>7</sub> (g)	$9.15 \times 10^{-6}$	$1.68 \times 10^{-6}$	$2.66 \times 10^{-6}$
(3) ReO <sub>3</sub> (g)	$1.65 \times 10^{-6}$	$5.58 \times 10^{-7}$	$1.235 \times 10^{-6}$
(4) Re <sub>2</sub> O <sub>5</sub> (g)	$9.86 \times 10^{-8}$ <sup>a</sup>	$7.05 \times 10^{-8}$ <sup>a</sup>	$1.60 \times 10^{-7}$ <sup>a</sup>
Equilibrium constants			
Re(s) + 3ZnO(s) → ReO <sub>3</sub> (g) + 3Zn(g)	$6.2 \times 10^{-18}$	$1.5 \times 10^{-20}$	$1.2 \times 10^{-19}$
2Re(s) + 6ZnO(s) → Re <sub>2</sub> O <sub>6</sub> (g) + 6Zn(g)	$1.4 \times 10^{-30}$ <sup>a</sup>	$5.3 \times 10^{-35}$ <sup>a</sup>	$1.5 \times 10^{-33}$ <sup>a</sup>
2Re(s) + 7ZnO(s) → Re <sub>2</sub> O <sub>7</sub> (g) + 7Zn(g)	$2.0 \times 10^{-32}$	$3.8 \times 10^{-38}$	$1.1 \times 10^{-36}$

<sup>a</sup> These values must be viewed as upper limits, see text.

to increase. The intensity of each ion was again followed at constant temperature until the Re<sub>2</sub>O<sub>6</sub><sup>+</sup> intensity had dropped to a value which was difficult to measure in a time span of 1 min. This process was repeated until at about 1450°K the Re<sub>2</sub>O<sub>6</sub><sup>+</sup> ion intensity became too small for accurate measurements.

**Results.** The average of several separate measurements at 1200°K of the intensities of the major ions above the mixtures, Re<sub>2</sub>O<sub>7</sub>-ReO<sub>3</sub>, Re-ZnO, and Re-MgO, are given in Table I. The Re-ZnO and Re-MgO mixtures yield higher relative intensities of the lighter ions than were found for Re<sub>2</sub>O<sub>7</sub>-ReO<sub>3</sub> solid mixtures, and the appearance potentials measured for ReO<sub>3</sub><sup>+</sup> and ReO<sub>2</sub><sup>+</sup> are distinctly lower than values found from Re<sub>2</sub>O<sub>7</sub>(s) vaporization (Table I).

The cell exhaustion experiments were designed to decrease the oxygen activity as a function of time at constant temperature. If an ion of lower O/Re atom ratio arose exclusively from fragmentation of Re<sub>2</sub>O<sub>7</sub>, that ion should disappear at the same rate as Re<sub>2</sub>O<sub>7</sub><sup>+</sup>, but if it arose from an oxide of lower O/Re atom ratio than Re<sub>2</sub>O<sub>7</sub>, the lighter ion would decrease in intensity more slowly than did Re<sub>2</sub>O<sub>7</sub><sup>+</sup>. The Re<sub>2</sub>O<sub>6</sub><sup>+</sup>/Re<sub>2</sub>O<sub>7</sub><sup>+</sup> ratio showed a small, but steady, increase with time. When signals at a given temperature became weak, temperatures were raised until measurements again became possible. The ratio of Re<sub>2</sub>O<sub>6</sub><sup>+</sup> to Re<sub>2</sub>O<sub>7</sub><sup>+</sup> during the initial decline at 1186°K was 0.106. On increasing the temperature to 1235, 1298, 1353, and 1407°K, this ratio increased to 0.107, then 0.126, 0.133, and 0.139. At 1436°K, the Re<sub>2</sub>O<sub>6</sub><sup>+</sup>/Re<sub>2</sub>O<sub>7</sub><sup>+</sup> ratio was found to be ~0.154 and the ReO<sub>3</sub><sup>+</sup>/Re<sub>2</sub>O<sub>7</sub><sup>+</sup> ratio was found to be 10. The increases in Re<sub>2</sub>O<sub>6</sub><sup>+</sup>/Re<sub>2</sub>O<sub>7</sub><sup>+</sup> and ReO<sub>3</sub><sup>+</sup>/Re<sub>2</sub>O<sub>7</sub><sup>+</sup> ratios with time and temperature in the nonequilibrium run are to be contrasted with the equilibrium values of Table III that are independent of time and decrease with temperature.

The slopes of the log  $I^+T$  vs.  $1/T$  plots of a typical run at 70 eV for intersities with no fragmentation correction were for Re<sub>2</sub>O<sub>7</sub><sup>+</sup>,  $58.25 \pm 0.68$ ; Re<sub>2</sub>O<sub>6</sub><sup>+</sup>,  $59.53 \pm 0.92$ ; and ReO<sub>3</sub><sup>+</sup>,  $64.30 \pm 0.66$ , all in kcal/mol.

These results, plus comparison of ion intensities obtained under greater and less strongly reducing conditions (see Discussion), demonstrated that the important neutral

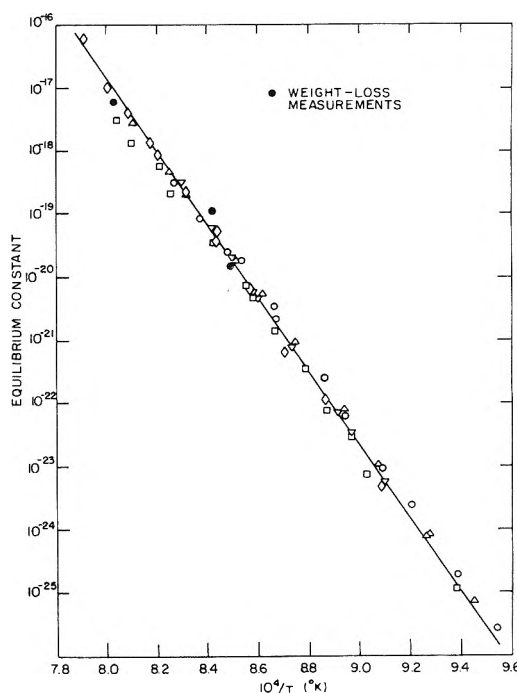


Figure 2. Equilibrium constant for the reaction  $\text{Re(s)} + 3\text{ZnO(s)} = \text{ReO}_3\text{(g)} + 3\text{Zn(g)}$  as a function of temperature.

precursors of the rhenium-containing ions in the rhenium metal-zinc oxide experiments were Re<sub>2</sub>O<sub>7</sub>(g), ReO<sub>3</sub>(g), and possibly Re<sub>2</sub>O<sub>6</sub>(g). To calculate pressures of these species, the ion currents for each run were corrected for differences in electron multiplier gain. The proportion of each ion current due to fragmentation of Re<sub>2</sub>O<sub>7</sub> (Table I) was subtracted from the total ion current for that ion. The currents were then multiplied by temperature and divided by cross sections to obtain pressure values.

The results of the weight loss experiments on rhenium-zinc oxide mixtures are shown in Table III and the equilibrium constants are plotted in Figure 2 for the reaction  $\text{Re(s)} + 3\text{ZnO(s)} = \text{ReO}_3\text{(g)} + 3\text{Zn(g)}$  for comparison with results of the temperature variation experiments. When the cross section measured for zinc by vaporization of zinc

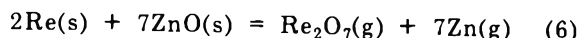
**TABLE IV: Enthalpies of Reaction and Entropies of Reaction Calculated from Mass Spectrometer Measurements for the Re-ZnO Reactions<sup>a</sup>**

Equilibrium	Experiment	Midpoint temp. °K	$\Delta H^\circ_T$ , (second-law), kcal
<b>Re(s) + 3ZnO(s) →</b>			
ReO <sub>3</sub> (g) + 3Zn(g)	1 (13 points)	1155	263.7 ± 3.7
	2 (11 points)	1145	266.7 ± 2.4
	3 (13 points)	1128	264.7 ± 3.0
	4 (12 points)	1189	275.9 ± 2.6
	5 (9 points)	1152	271.2 ± 2.1
	Av $\Delta S^\circ = 137.8 \pm 3.0$	Av $\Delta H^\circ = 268.2 \pm 3.0$	
<b>2Re(s) + 6ZnO(s) →</b>			
Re <sub>2</sub> O <sub>6</sub> (g) + 6Zn(g)	1 (13 points)	1155	452.0 ± 6.8
	2 (11 points)	1145	458.0 ± 5.8
	3 (12 points)	1128	453.5 ± 7.0
	4 (15 points)	1175	465.3 ± 6.2
	Av $\Delta S^\circ = 233.0 \pm 8.0$	Av $\Delta H^\circ = 457.9 \pm 6.0$	
<b>2Re(s) + 7ZnO(s) →</b>			
Re <sub>2</sub> O <sub>7</sub> (g) + 7Zn(g)	1 (13 points)	1155	514.4 ± 8.3
	2 (11 points)	1145	515.3 ± 4.6
	3 (13 points)	1128	516.3 ± 5.9
	4 (15 points)	1175	505.0 ± 6.3
	5 (10 points)	1152	538.9 ± 9.3
	Av $\Delta S^\circ = 267.8 \pm 7.8$	Av $\Delta H^\circ = 516.5 \pm 7.1$	

<sup>a</sup> Corrected to agree with the silver enthalpy measurements and weight loss results. Quoted errors are standard deviations from the least-squares fit.

metal was used, two of the five runs gave calculated zinc pressures about a factor of 5 lower than those measured in the weight loss experiments. Only small amounts of zinc were used and equilibrium zinc pressures probably were not developed in the cells during the calibration periods of these two runs. Each mass spectrometer run was normalized, therefore, to agree with the zinc loss of the weight loss experiments.

The enthalpies of equilibrium constant measurements for the reaction



were corrected for the error in temperature dependence of pressures found for silver. The correction for reaction 6 is  $+16.0 \pm 3.5$  kcal/mol, yielding an average enthalpy of 516.5 kcal/mol at 1156°K. An internal check on the corrected enthalpy can be made since the heat of formation of Re<sub>2</sub>O<sub>7</sub>(g) can be calculated from the heat of vaporization of Re<sub>2</sub>O<sub>7</sub>(g) and the heat of formation of Re<sub>2</sub>O<sub>7</sub>(s). When temperature corrections are made using data from Kelley<sup>15</sup> for Re(s), ZnO(s), and Zn(g) and the approximation that the heat content for Re<sub>2</sub>O<sub>7</sub>(g) is that given by JANAF<sup>12</sup> for W<sub>2</sub>O<sub>6</sub>(g) the heat for reaction 6 is calculated to be  $521.3 \pm 3.0$  kcal/mol, in fair agreement with the corrected value of 516.5 kcal/mol.

Enthalpies and average entropies calculated from the equilibrium constant measurements for the three equilibria, after correction of the error in the enthalpy of sublimation, are given in Table IV. The average enthalpies calculated by weighting each enthalpy by the number of points in that particular run were used to calculate the entropies of reaction using the weight loss measurements.

The heat of formation of ReO<sub>3</sub>(g) and Re<sub>2</sub>O<sub>6</sub>(g) at 298°K were calculated by the second- and third-law methods (Table V). For ReO<sub>3</sub>(g), estimated free energy func-

tion and heat content values were available.<sup>15</sup> For Re<sub>2</sub>O<sub>6</sub>, the thermochemical values given by JANAF<sup>12</sup> for W<sub>2</sub>O<sub>6</sub> were used. The heat of formation for zinc oxide employed in this calculation was  $-111.8$  kcal/mol at 1156°K. Additional auxiliary data for Re(s) and O<sub>2</sub>(g) were taken from Kelley,<sup>15</sup> and data for Zn(g) from Hultgren.<sup>7</sup>

### Magnesium Oxide-Rhenium Equilibrium

**Experimental Section.** The magnesium oxide used in this portion of the study was obtained from single crystals of unknown origin. Semiquantitative spectroscopic analysis revealed only the following impurities: Si 0.008%, Fe 0.007%, Ca 0.01%, Mn 0.001%, Al 0.001%, and Cr 0.001%. The crystals were ground in a silica mortar and pestle immediately before use. X-Ray diffraction measurements, after vaporization, showed no evidence of phases other than magnesium oxide and rhenium.

A tungsten outer cell and lid with a 0.08-cm orifice surrounded a rhenium cell liner. Three filaments were used, with the third being placed slightly above center to ensure that the lid was hotter than the cell bottom and to enable three blackbody holes (with length to diameter ratio of 4 to 1) to be seen with an optical pyrometer from outside the mass spectrometer. The optical pyrometer was calibrated through the window used in the experiments against a standard optical pyrometer by the Lawrence Berkeley Laboratory meter shop. To obtain a correction for temperature-dependent errors, the second-law enthalpy of sublimation of lanthanum metal was measured in the temperature range 1794–2103°K. Ten points yielded  $\Delta H^{1950} = 93.4 \pm 1.7$  kcal/mol, in only fair agreement with the value of  $99.7 \pm 1.0$  kcal/mol interpolated from Hultgren's tabulation.

Two temperature variation experiments were conducted in a manner similar to those used for zinc oxide and rhenium using 70-eV electrons. Appearance potentials were measured using background mercury as a standard for the extrapolated differences method.

**Results.** Ions identified as Mg<sup>+</sup>, ReO<sub>3</sub><sup>+</sup>, ReO<sub>2</sub><sup>+</sup>, and ReO<sup>+</sup> were observed. Relative intensities at 2080°K and appearance potentials are included in Table I.

Both ReO<sup>+</sup> and ReO<sub>2</sub><sup>+</sup> arise primarily from dissociative ionization of ReO<sub>3</sub>(g) (see Discussion), and quantitative data can be derived only from the ReO<sub>3</sub><sup>+</sup> measurements. The equilibrium constant for the reaction



is plotted in Figure 3. Least-squares analysis yielded  $425.9 \pm 5.1$  and  $429.1 \pm 5.7$  kcal/mol for the heat of reaction. The average of these enthalpies is  $452.7 \pm 5$  kcal/mol after the measured temperature dependence of the cell is corrected to make the measured second-law enthalpy of sublimation of lanthanum metal agree with the accepted value. When this average for eq 7 is combined with thermochemical enthalpy data for MgO and Mg(g),<sup>12</sup> the heat of formation of ReO<sub>3</sub>(g) at 1980°K is calculated to be  $-69.6 \pm 5$  kcal/mol.

### Discussion

In order to calculate partial pressures from mass spectrometry intensity measurements such as obtained in this study, it is necessary to establish the formulas of the vapor molecules from which the observed ions are produced. These neutral molecules may include species of

(15) K. K. Kelley, *U. S. Bur. Mines, Bull.*, No. 584 (1960).



TABLE V: Enthalpies of Formation of  $\text{ReO}_3(\text{g})$  and  $\text{Re}_2\text{O}_6(\text{g})$  at 298°K

Molecule	Method of calculation	$\Delta H_f, 298, \text{ kcal/mol}$			
		Ref 6	This work ZnO + Re	This work MgO + Re	Kinetic <sup>b</sup> limit
$\text{ReO}_3(\text{g})$	Second law	-75.8, -90.6 <sup>a</sup>	-66.6 ± 5	-67.7 ± 5	
	Third law	-62.7 <sup>a</sup>	-74.6 ± 2 <sup>c</sup>		≤ -78 ± 14 <sup>b</sup>
$\text{Re}_2\text{O}_6(\text{g})$	Second law		≤ -208.7 ± 20		
	Third law		≤ -216.8 ± 4 <sup>c</sup>		

<sup>a</sup> Recalculated from the data of Norman, *et al.*,<sup>6</sup> <sup>b</sup> Calculated from Weber, *et al.*,<sup>17,18</sup> by the method of Franklin and Stickney.<sup>16</sup> <sup>c</sup> This estimated uncertainty neglects the possible errors in estimated partition function. See text.

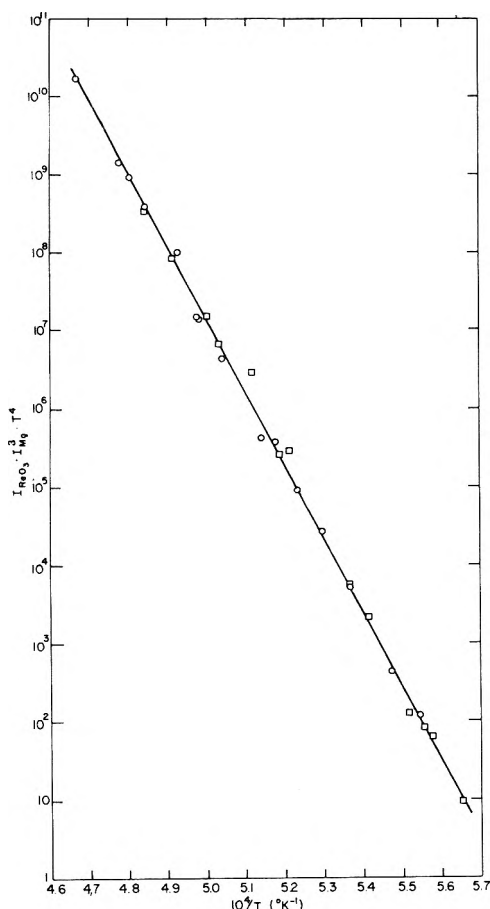


Figure 3. Intensity data as a function of temperature for the reaction  $3\text{MgO}(\text{s}) + \text{Re}(\text{s}) \rightarrow \text{ReO}_3(\text{g}) + 3\text{Mg}(\text{g})$ .

higher molecular weights than any of the ions observed in the mass spectrum for the vapor. For the rhenium oxygen system, however, significant concentrations of molecules of higher oxygen to rhenium atomic ratio than 7/2 are very unlikely on chemical grounds. Polymers of  $\text{Re}_2\text{O}_7(\text{g})$  are possible vapor species, but such polymers, if present at compositions comparable with the monomer, would almost certainly yield measurable concentrations of ions of greater mass than  $\text{Re}_2\text{O}_7^+$ . Since ions of higher mass than  $\text{Re}_2\text{O}_7^+$  were not observed, it is virtually certain that all the  $\text{Re}_2\text{O}_7^+$  ions were produced by simple ionization of  $\text{Re}_2\text{O}_7(\text{g})$ . The data collected for  $\text{Re}_2\text{O}_7^+$  and ions of lower masses under three distinctly different sets of experimental conditions can be used to determine the parent molecules for these other ions.

When rhenium metal was heated with magnesium oxide at 2080°K, none of the ions  $\text{Re}_2\text{O}_7^+$ ,  $\text{Re}_2\text{O}_6^+$ , or  $\text{Re}_2\text{O}_5^+$ ,

which are important in the  $\text{Re}_2\text{O}_7(\text{g})$  mass spectrum, was observed at intensities as high as 0.1% that observed for  $\text{ReO}_3^+$ . The  $\text{ReO}_3^+$ ,  $\text{ReO}_2^+$ , and  $\text{ReO}^+$  ions which were observed, therefore, must have as parents a molecule no more complex than  $\text{ReO}_3$ . The apparent enthalpies of reaction of rhenium with magnesium oxide to produce the parent of the three ions were  $108.9 \pm 2.6$  kcal/mol for  $\text{ReO}_3^+$ ,  $113.9 \pm 2.9$  for  $\text{ReO}_2^+$ , and  $115.4 \pm 2.9$ , where the uncertainties are standard deviations. These similar enthalpy values constitute strong evidence that the principal parent for all three ions is  $\text{ReO}_3$ . The measured appearance potentials support this conclusion because the appearance potential found for  $\text{ReO}_3^+$  is about the same as found for  $\text{Re}_2\text{O}_7^+$ , which must be formed by simple ionization of  $\text{Re}_2\text{O}_7^+$ , while the appearance potential for  $\text{ReO}_2^+$  is 2 eV higher and that of  $\text{ReO}^+$  is some 5 eV higher than that found in the same experiment for  $\text{ReO}_3^+$ .

It should be remarked that the method of extrapolated differences that was used in obtaining appearance potentials seemed to give an apparent appearance potential for any ion which has two different parents that is a function of the relative concentrations of the two parents in the vapor. Thus the apparent appearance potentials of  $\text{ReO}_3^+$  drops from 16 eV when  $\text{Re}_2\text{O}_7$  gas is its only important parent to 15 eV when  $\text{Re}_2\text{O}_7$  and  $\text{ReO}_3$  are present in roughly equal concentrations to 12.5 eV when  $\text{ReO}_3$  is the only significant parent. The apparent appearance potentials of  $\text{ReO}_2^+$  show similar variations as the proportions of  $\text{Re}_2\text{O}_7$  and  $\text{ReO}_3$  change. The values measured over  $\text{Re}_2\text{O}_7$  are measures of the appearance potentials from fragmentation of  $\text{Re}_2\text{O}_7$  and the value for  $\text{ReO}_3^+$  measured when rhenium was heated with zinc oxide is a measure of the ionization potential of  $\text{ReO}_3(\text{g})$ . Appearance potentials measured by Battles, *et al.*, under conditions which they concluded gave  $\text{Re}_2\text{O}_7$  as the only important vapor species are similar to those found in the present study (Table I) for  $\text{Re}_2\text{O}_7$  solid vaporization: 13.0, 16.0, 17.0, ~20, and ~20 eV for  $\text{Re}_2\text{O}_7^+$ ,  $\text{Re}_2\text{O}_6^+$ ,  $\text{Re}_2\text{O}_5^+$ ,  $\text{ReO}_3^+$ , and  $\text{ReO}_2^+$ , respectively.

A most negative possible value for the heat of formation of  $\text{ReO}_2$  gas is calculated to be  $\geq -10$  kcal/mol and for  $\text{ReO} \geq 48$  kcal/mol, both at 1980°K. These limits are obtained by adding a 5 kcal/mol uncertainty to the heats of formations calculated on the assumption that the  $\text{ReO}_2^+$  and  $\text{ReO}^+$  ions have  $\text{ReO}_2$  and  $\text{ReO}$  as their respective parents.

When the heats of formation, or limits to heats of formation, which were determined for  $\text{ReO}_3$ ,  $\text{ReO}_2$ , and  $\text{ReO}$  from the rhenium metal reaction with magnesium oxide are used with entropy and heat capacity data estimated to be the same for the gaseous rhenium oxides as for corresponding tungsten oxides, the conclusion that none of

TABLE VI: Measured Heats of Formation of  $\text{Re}_2\text{O}_7(\text{s})$  and  $\text{ReO}_3(\text{s})$  and Calculated Heats of the Reaction  $\text{Re}_2\text{O}_7(\text{s}) = 2\text{ReO}_3(\text{s}) + \frac{1}{2}\text{O}_2(\text{g})$

Solid	$\Delta H_f^{298}$ , kcal	Heat of reaction, kcal	Ref
$\text{ReO}_3$	-83.0		a
$\text{Re}_2\text{O}_7$	-297.5	131.5	a
$\text{ReO}_3$	$-140.8 \pm 0.9$		20
$\text{Re}_2\text{O}_7$	$-301.9 \pm 1.8$	20.3	20
$\text{ReO}_3$	$-146.0 \pm 3.0$		b
$\text{Re}_2\text{O}_7$	$-295.0 \pm 2.0$	2.8	b
$\text{ReO}_3$	$-146.1 \pm 0.8$		11
$\text{ReO}_3$	$-140.7 \pm 2$		5

<sup>a</sup>W. A. Roth and G. Becker, *Z. Phys. Chem.*, **A159**, 27 (1932), taken from Bureau of Standards "Selected Values of Chemical Thermodynamic Properties" (1948). <sup>b</sup>G. E. Boyd, J. W. Cobble, and W. T. Smith, Jr., *J. Amer. Chem. Soc.*, **75**, 4783 (1953).

these three oxides is an important species in the vapor above a solid  $\text{ReO}_3$ -solid  $\text{Re}_2\text{O}_7$  mixture is confirmed.

Above mixtures of rhenium metal with zinc oxide, however,  $\text{ReO}_3$  gas is present in concentrations comparable to  $\text{Re}_2\text{O}_7$  gas. This conclusion is warranted both by the observed increase in  $\text{ReO}_3^+/\text{Re}_2\text{O}_7^+$  ratio and by the agreement between the enthalpy of formation of  $\text{ReO}_3$  calculated from the Re-MgO data with that calculated from the Re-ZnO data after correction for fragmentation of  $\text{Re}_2\text{O}_7^+$ .

The observed  $\text{Re}_2\text{O}_5^+$  must be essentially all produced by fragmentation of  $\text{Re}_2\text{O}_7^+$  since the intensity ratio  $\text{Re}_2\text{O}_5^+/\text{Re}_2\text{O}_7^+$  is not measurably changed by alterations in reaction conditions or temperature and since the appearance potential for  $\text{Re}_2\text{O}_5^+$  is relatively high.

The principal parent of  $\text{Re}_2\text{O}_6^+$  must be  $\text{Re}_2\text{O}_7$  gas even when the ion was produced by heating rhenium metal with zinc oxide. The increase in  $\text{Re}_2\text{O}_6^+/\text{Re}_2\text{O}_7^+$  ratios with temperature and time in the cell exhaustion experiment and the increase in the same ratio when rhenium was heated with zinc oxide over that when the solid  $\text{ReO}_3$ -solid  $\text{Re}_2\text{O}_7$  mixture was heated suggest that  $\text{Re}_2\text{O}_6^+$  has a second parent, which could only be  $\text{Re}_2\text{O}_6$  gas.

The closely similar temperature dependences measured for  $\text{Re}_2\text{O}_6^+$  and  $\text{Re}_2\text{O}_7^+$  ion intensities in the rhenium metal-zinc oxide heatings (the apparent heat of vaporization for  $\text{Re}_2\text{O}_6^+$  was  $59.5 \pm 0.9$  kcal/mol and for  $\text{Re}_2\text{O}_7^+$  was  $58.3 \pm 0.7$  kcal/mol) implies, on the other hand, a single common parent, although the result could be coincidentally obtained if  $\text{Re}_2\text{O}_6$  gas is a significant parent for  $\text{Re}_2\text{O}_6^+$ . A stronger argument against  $\text{Re}_2\text{O}_6$  gas as a parent for a significant fraction of the observed  $\text{Re}_2\text{O}_6^+$  ion intensity is the high appearance potential, 16 eV measured for  $\text{Re}_2\text{O}_6^+$  compared to about 12.5 eV for  $\text{Re}_2\text{O}_7^+$  and  $\text{ReO}_3^+$  when these ions are produced from  $\text{Re}_2\text{O}_7(\text{g})$  and  $\text{ReO}_3(\text{g})$ , respectively. In light of the conflicting data, we can only calculate a maximum stability for  $\text{Re}_2\text{O}_6$  gas.

Values calculated for the heat of formation of  $\text{ReO}_3$  from data of three different investigations are listed in Table V. All values are calculated with the assumption that the free energy functions for  $\text{ReO}_3$  gas are the same as JANAF free energy functions for  $\text{WO}_3$ . In addition to the results of Norman, *et al.*,<sup>6</sup> and of the present investigation, a value calculated by Franklin and Stickney<sup>16</sup>

from measurements by Weber, Fusy, and Cassuto<sup>17,18</sup> of the rate of reaction of  $\text{O}_2$  with rhenium metal to form  $\text{ReO}_3$  gas is included. The assumption necessary to obtain thermodynamic data by their method is equivalent to that used to calculate thermodynamic data from rates of vaporization determined by the Langmuir method<sup>19</sup> (that complete equilibrium is maintained between the bulk solid and molecules adsorbed on the solid surface). The calculated value of the heat of formation of  $\text{ReO}_3$  from the kinetic data is therefore a limiting value which (neglecting experimental error) cannot be more negative than the true heat of formation, but may be more positive by an amount that can only be determined by comparison with equilibrium data. The listed uncertainties from our measurements are those we would usually assign from experience with the apparatus without consideration of uncertainties in partition functions. For the kinetic data, the uncertainty was estimated by Franklin and Stickney.

The third-law calculations of Table V assign the value unity to the electronic partition function for  $\text{ReO}_3(\text{g})$ . This is a minimum estimated value. The actual electronic partition function may contribute the equivalent of several entropy units to the total partition function. An underestimate of the electronic partition function, for example, by the equivalent of 3 eu would make the calculated third-law heats of formation of the present study too negative by about 3.6 kcal and the limiting value calculated from the kinetic measurements at much higher temperature too negative by about 7 kcal. In light of this uncertainty in value for the partition function, we place principal reliance on the two closely agreeing second-law measurements of this study and recommend  $-68 \pm 5$  kcal as a value for the heat of formation of  $\text{ReO}_3$  gas at 298°K. The quoted uncertainty indicates our 90% confidence limit.

The partition function assumed for  $\text{Re}_2\text{O}_6$  gas may be low for the reason just discussed for  $\text{ReO}_3$ . On the other hand, the second-law heat of formation for  $\text{Re}_2\text{O}_6$  gas reported in Table V depends on corrections of observed intensities of the  $\text{Re}_2\text{O}_6^+$  for the contribution presumed to arise from fragmentation of  $\text{Re}_2\text{O}_7$ . Uncertainties in both calculations are high, and a limiting value of  $\Delta H^{298} \geq -212 \pm 20$  kcal is recommended.

The measurements of weight losses for dirhenium heptoxide make it possible to estimate the heat of the reaction  $\text{Re}_2\text{O}_7(\text{s}) = 2\text{ReO}_3(\text{s}) + \frac{1}{2}\text{O}_2(\text{g})$  (Table VI). The weight loss experiments establish the minimum oxygen content of solid dirhenium heptoxide as about  $\text{Re}_2\text{O}_{6.97}$  when in equilibrium with the  $\text{ReO}_3$  solid phase at  $\sim 400^\circ\text{K}$ . If  $\text{Re}_2\text{O}_{6.97}$  were the actual composition, the  $\text{O}_2$  dissociation pressure would have to be negligible and the heat of the invariant dissociation reaction very high. The heat is calculated to be 13 kcal when the phase boundary for the dirhenium heptoxide phase is assumed to be at the stoichiometric composition. The heats of formations measured by King, *et al.*,<sup>20</sup> are probably most nearly correct and the oxygen-deficient phase boundary for dirhenium heptoxide at 400°K probably lies at  $\text{Re}_2\text{O}_{6.98} \pm 0.02$ .

- (16) J. E. Franklin and R. E. Stickney, *High Temp. Sci.*, **3**, 401 (1971).
- (17) B. Weber, J. Fusy, and A. Cassuto, *Proc. Inter. Conf. Mass Spectrosc.*, Kyoto, 1969, (1970).
- (18) B. Weber and A. Cassuto, *J. Chem. Phys.*, **68**, 29 (1971).
- (19) A. W. Searcy in "Chemical and Mechanical Behavior of Inorganic Materials," A. W. Searcy, D. V. Ragone, and U. Colombo, Ed., Wiley-Interscience, New York, N. Y., 1970, p 66 and Chapter 6.
- (20) E. G. King, D. W. Richardson, and R. V. Mrazek, *U. S. Bur. Mines, Rep. Invest.*, No. 7323 (1969).

*Acknowledgments.* This work was supported by the Metallurgy and Materials Branch of the U. S. Atomic Energy Commission. Comments by Alfred Büchler, Karl

Gingerich, David J. Meschi, J. H. Norman, L. H. Rovner, and P. Winchell on a first draft of this paper were very helpful to us and are greatly appreciated.

## Reactions of Iodine Excited with 185-nm Radiation. III. Reactions with Hydrogen, Methane, Trifluoromethane, Fluoromethane, Chloromethane, and Oxygen. Mechanistic Tests<sup>1,2</sup>

L. C. Glasgow and J. E. Willard\*

University of Wisconsin, Madison, Wisconsin 53706 (Received January 16, 1973)

Publication costs assisted by the U.S. Atomic Energy Commission

The quantum yields of I<sub>2</sub> removal resulting from 185-nm absorption by I<sub>2</sub> in the presence of H<sub>2</sub>, CH<sub>4</sub>, CH<sub>3</sub>F, CF<sub>3</sub>H, CF<sub>4</sub>, CH<sub>3</sub>Cl, and O<sub>2</sub> at 100 Torr are 0.12, 0.30, 0.20, 0.07, 0.002, 0.4, and 0.12, respectively. As reported earlier, the energetics preclude a reaction mechanism involving I atoms. The effect of O<sub>2</sub> scavenger on CH<sub>3</sub>I formation in the reaction with CH<sub>4</sub> is consistent with a concerted one-step mechanism rather than a photosensitized decomposition followed by radical reaction with I<sub>2</sub>. Pressure effects in the CH<sub>3</sub>F and CF<sub>3</sub>H systems also support a concerted reaction for monoiodide formation. Diiodide formation observed from CH<sub>3</sub>F and CF<sub>3</sub>H appears to result from an I<sub>2</sub>\* photosensitized HF elimination followed by combination of the methylenic radical with I<sub>2</sub>. Absorption of 185-nm radiation by I<sub>2</sub> in polycrystalline C<sub>2</sub>H<sub>6</sub> at 77°K produces trapped C<sub>2</sub>H<sub>5</sub> radicals, with low quantum yield.

### Introduction

Excited I<sub>2</sub> molecules (I<sub>2</sub>\*) produced by 185-nm radiation in the presence of H<sub>2</sub> or hydrocarbons lead to iodide formation.<sup>3,4</sup> The energetics preclude reaction by an iodine atom mechanism<sup>3</sup> and it has been shown that the pressure must be great enough so that the excited molecules do not lose their energy by fluorescence before the first collision.<sup>4</sup> Possible mechanisms for these reactions are (1) a photosensitized decomposition of the reactant (I<sub>2</sub>\* + RH → R + H + I<sub>2</sub>), followed by reaction of the radicals with I<sub>2</sub> (R + I<sub>2</sub> → RI + I; H + I<sub>2</sub> → HI + I); (2) production of iodides in one step (I<sub>2</sub>\* + RH → RI + HI). We have sought to determine which mechanism predominates by (a) observing whether O<sub>2</sub> is as effective a scavenger as would be expected for the free-radical mechanism; (b) noting products which indicate HF elimination from photosensitized CH<sub>3</sub>F and CF<sub>3</sub>H molecules; (c) seeking evidence for reactions of the type H + D<sub>2</sub> → HD + D which would occur if hot H atoms were produced in the presence of D<sub>2</sub> by mechanism 1. In addition, new values for the quantum yields of the reactions of I<sub>2</sub>\* with H<sub>2</sub> and CH<sub>4</sub> have been obtained and reactions of I<sub>2</sub>\* with CH<sub>3</sub>Cl, CF<sub>4</sub>, O<sub>2</sub>, and polycrystalline C<sub>2</sub>H<sub>6</sub> are reported.

### Experimental Section

The reagents used were H<sub>2</sub> and CH<sub>4</sub>, Matheson Research grade; CD<sub>4</sub>, Merck Sharp and Dohme; all other gases, Matheson lecture bottle; I<sub>2</sub>, Baker AR resublimed

*in vacuo*, or produced on the vacuum line by oxidation of KI with K<sub>2</sub>Cr<sub>2</sub>O<sub>7</sub>.

Cylindrical Suprasil cells 10 cm long, 28 mm i.d. with flat end windows, and fitted with Delmar greaseless stopcocks through a side arm were used in conjunction with two Hanovia SC2537 lamps, one directed at each face of the cell.  $\gamma$ -Irradiated LiF crystals were positioned between the lamps and the cell when it was desired to eliminate the 254-nm line. Light intensities, determined using HBr actinometry,<sup>5,6</sup> were typically 10<sup>14</sup> photons absorbed sec<sup>-1</sup> at 185 nm, when using the LiF filters. Sometimes these cells were exposed in a helical low-pressure Hg lamp, described previously, giving an absorbed 185-nm intensity of ca. 10<sup>17</sup> photons sec<sup>-1</sup>. Some photolyses were performed in 8 mm i.d. Suprasil test tubes, with greaseless stopcocks, using the helical lamp with an ozone filter to remove 254-nm radiation.<sup>7</sup> The absorbed 185-nm intensity with this system was ca. 4 × 10<sup>16</sup> photons sec<sup>-1</sup>.

- (1) This work has been supported in part by the U. S. Atomic Energy Commission under Contract No. AT(11-1)-1715 and by the W. F. Vilas Trust of the University of Wisconsin.
- (2) Further details are given in the Ph.D. thesis of L. C. Glasgow, University of Wisconsin, 1971.
- (3) G. M. Harris and J. E. Willard, *J. Amer. Chem. Soc.*, **76**, 4678 (1954).
- (4) (a) T. A. Gover and J. E. Willard, *J. Amer. Chem. Soc.*, **82**, 3816 (1960); (b) T. A. Gover, Ph.D. Thesis, University of Wisconsin, 1960.
- (5) (a) R. A. Fass, *J. Phys. Chem.*, **74**, 984 (1970); (b) R. A. Fass, Ph.D. Thesis, University of Wisconsin, 1969.
- (6) R. M. Martin and J. E. Willard, *J. Chem. Phys.*, **40**, 2999 (1964).
- (7) L. C. Glasgow and J. E. Willard, *J. Phys. Chem.*, **74**, 4290 (1970).

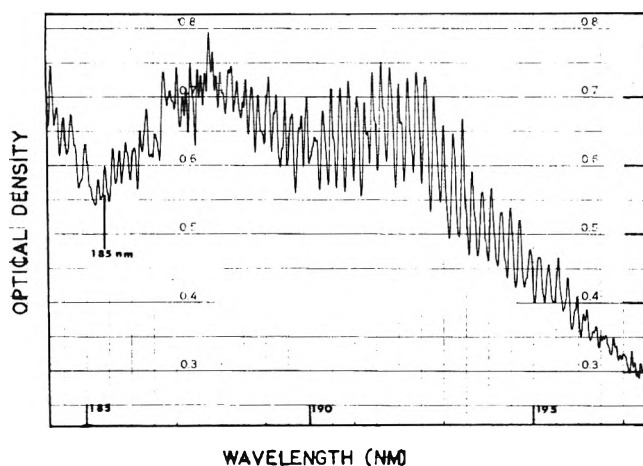


Figure 1. Absorption spectrum of 10 cm of 0.2 Torr  $I_2$  recorded with an  $N_2$ -purged Cary 15 spectrophotometer, set at a bandwidth of ca. 0.1 nm and using a hydrogen discharge source. The labeling of the abscissa is the nominal spectrophotometer scale. The exact position of the 185-nm line, indicated on the spectrum, was determined using a low-pressure Hg arc.

Reaction mixtures were prepared using standard vacuum techniques. The rate of disappearance of  $I_2$  was determined from the decrease of optical density at 500 nm [ $\epsilon(I_2) = 578 M^{-1} cm^{-1}$ ]<sup>8</sup> during photolysis and the formation of  $CH_3I$  by the increase at 201 nm [ $\epsilon(CH_3I) = 1.5 \times 10^5 M^{-1} cm^{-1}$ ].<sup>5b</sup> The extinction coefficient of HI at 201 nm is ca.  $10^3$  smaller than that of  $CH_3I$ .

The absorption spectrum of  $I_2$  in the region of 185 nm is shown in Figure 1. The extinction coefficient of  $I_2$  [ $\epsilon(I_2)$ ] at 185 nm was measured from 0.3 to 0.03 Torr using a platinum cathode phototube,<sup>3,4b</sup> which is insensitive above 230 nm, and also using an  $N_2$ -flushed Cary 15 spectrophotometer, with the concentrations determined by the absorption at 500 nm.<sup>2</sup> In each case the radiation source was a low-pressure Hg lamp.  $\epsilon(I_2)$  was  $5 \times 10^3 M^{-1} cm^{-1}$  at 0.3 Torr of  $I_2$  and increased to  $1.2 \times 10^4 M^{-1} cm^{-1}$  at 0.03 Torr. At a constant  $I_2$  pressure of 0.2 Torr, addition of 100–400 Torr of foreign gas increases  $\epsilon(I_2)$  to a maximum of ca.  $2.2 \times 10^4 M^{-1} cm^{-1}$  in reasonable agreement with previous determinations.<sup>4,9,10</sup> The cause of the increase in  $\epsilon(I_2)$  at 185 nm with decreasing pressure is not known.

## Results

**Reaction of  $I_2^*$  with  $CH_4$ .** The data of Tables I–V indicate that (1) the quantum yield for  $I_2$  consumption and  $CH_3I$  production in mixtures of 0.2 Torr of  $I_2$  and 150–200 Torr of  $CH_4$  exposed to 185-nm radiation are both  $0.32 \pm 0.03$  (Table I); (2) the quantum yield is independent of temperature from 25 to 140° (Table V) and of  $I_2$  pressure from 0.11 to 0.51 Torr (Table II); the yield decreases with increasing Ar/ $CH_4$  ratio at a constant total pressure of 700 Torr (Table III); oxygen is approximately three times more effective than Ar or  $N_2$  in reducing the yield (Table IV).

The constancy of  $\phi(CH_3I)$  in the experiments of Table II, where the initial optical density varied from 1.6 to 8.2 and the path length for 90% absorption varied from 1.2 to 6.0 cm, indicates that the steady-state concentration of reaction intermediates does not affect the yield. Consistent with this conclusion, the quantum yield was also unchanged by a fivefold variation in lamp intensity.

TABLE I: Quantum Yields of  $I_2$  Disappearance and  $CH_3I$  Formation<sup>a</sup> in the  $I_2^* - CH_4$  Reaction

$CH_4$ , Torr	$\phi(-I_2)$	$I_2$ converted, %	Filter
150	$0.29 \pm 0.03$	20	LiF
200	0.30	20	LiF
148	0.29	35	LiF
219	0.30	50	None
$\phi(CH_3I)^b$			
200	$0.32 \pm 0.05$	0.5	None
150	0.31	0.5	None
200	0.33	0.5	None

<sup>a</sup> Initial pressure of  $I_2 =$  ca. 0.2 Torr. <sup>b</sup> The high extinction coefficient of  $CH_3I$  at  $\lambda$  201 nm allowed the use of low conversions. The error limits represent uncertainty in the absolute value of the coefficient.<sup>5b</sup>

TABLE II: Effect of  $I_2$  Pressure on the  $CH_3I$  Quantum Yield in the  $CH_4 - I_2^*$  System at 40°

$I_2$ , Torr	% converted	$CH_4$ , Torr	$\phi(CH_3I)$
0.11	5	156	$0.30 \pm 0.05$
0.22	3	150	$0.31 \pm 0.05$
0.30	2	148	$0.33 \pm 0.05$
0.51	1	153	$0.35 \pm 0.05$

TABLE III: Effect of Ar/ $CH_4$  Ratio on Quantum Yield of  $I_2$  Disappearance by Reaction with  $CH_4^a$

$CH_4$ , Torr	Ar, Torr	Rate, $M min^{-1} \times 10^7$	Relative quantum yield
700	0	4.8	1
410	290	4.6	0.96
175	525	4.0	0.83
100	600	3.2	0.67

<sup>a</sup> Initial  $I_2$  pressure = 0.2 Torr.

TABLE IV: Quantum Yields of  $CH_3I$  Formation by Reaction of  $I_2^*$  with  $CH_4$  in the Presence of Foreign Gases

Gas	Additive, Torr	$CH_4$ , Torr	$I_2$ , Torr	Quantum yield
Oxygen	365	104	0.24	0.05
Argon	389	104	0.22	0.19
Nitrogen	341	112	0.26	0.14
Control	0	400	0.21	0.32

**Reaction of  $I_2^*$  with  $H_2$ .** The quantum yield of  $I_2$  disappearance at 185 nm in  $I_2 - H_2$  or  $I_2 - D_2$  mixtures, determined in this work, is 0.12 (Table VI). As with  $I_2 - CH_4$  mixtures it is independent of pressure (100–250 Torr),  $I_2$  concentration, and radiation intensity. When the 254-nm line of the low-pressure Hg arcs is allowed to enter the cell, by removal of the LiF filters, the quantum yield calculated on the basis of 185-nm radiation absorbed does not change, since HI photolyzed at 254 nm can only return to HI.

- (8) R. L. Strong, Ph.D. Thesis, University of Wisconsin, 1954.  
 (9) R. M. Martin and B. J. Huebert, *J. Phys. Chem.*, **72**, 3046 (1968).  
 (10) L. M. Julien and W. B. Person, *J. Phys. Chem.*, **72**, 3059 (1968).

**TABLE V: Effect of Temperature on the Quantum Yield of CH<sub>3</sub>I Formation by Reaction of I<sub>2</sub>\* with CH<sub>4</sub><sup>a</sup>**

T, °C	φ(CH <sub>3</sub> I)	T, °C	φ(CH <sub>3</sub> I)
25	0.30 ± 0.05	65	0.27
40	0.35	85	0.27
55	0.30	140	0.29

<sup>a</sup> 200 Torr of CH<sub>4</sub> measured at 25° was used in each experiment with a mole ratio of I<sub>2</sub>/CH<sub>4</sub> of 3.4 × 10<sup>-3</sup>. In the 25° experiment solid I<sub>2</sub> was present, leaving an I<sub>2</sub>/CH<sub>4</sub> ratio in the vapor of 1.5 × 10<sup>-3</sup>.

**TABLE VI: Quantum Yield of I<sub>2</sub> Disappearance in the I<sub>2</sub>\*-H<sub>2</sub> Reaction<sup>a</sup>**

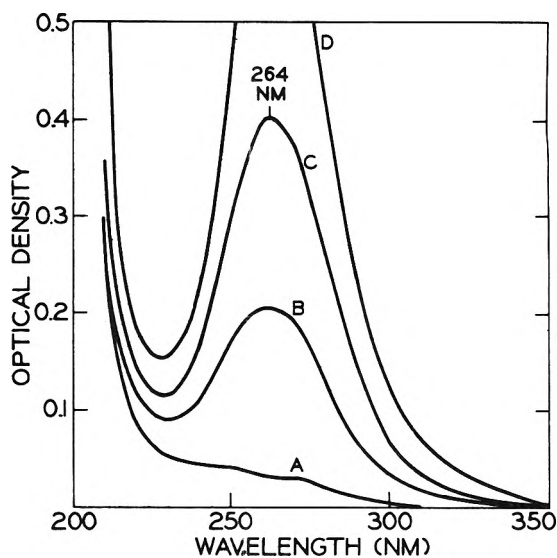
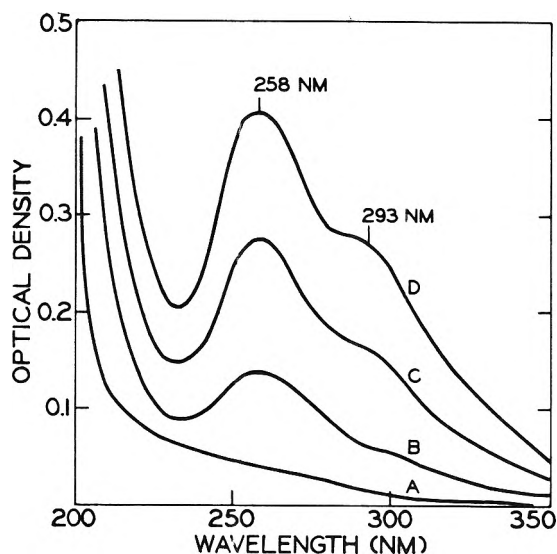
Reactant	Pressure, Torr	Quantum yield	I <sub>2</sub> converted, %	Filter
D <sub>2</sub>	100	0.113 ± 0.01	35	LiF
D <sub>2</sub>	100	0.113	25	LiF
H <sub>2</sub>	250	0.126	50	LiF
H <sub>2</sub>	100	0.127	40	LiF
H <sub>2</sub>	125	0.124	20	LiF
H <sub>2</sub>	119	0.123	40	None
H <sub>2</sub>	100	0.122	50	None

<sup>a</sup> I<sub>2</sub> initial pressure ca. 0.2 Torr.

Reaction of I<sub>2</sub>\* with CH<sub>3</sub>Cl, CH<sub>3</sub>F, CF<sub>3</sub>H, and CF<sub>4</sub>. The values found for φ(-I<sub>2</sub>) during irradiation of mixtures of 0.2 Torr of I<sub>2</sub> and 150 Torr of CH<sub>3</sub>Cl, CH<sub>3</sub>F, CF<sub>3</sub>H, or CF<sub>4</sub> at 185 nm are 0.4 ± 0.1, 0.21 ± 0.03, 0.07 ± 0.02, and 0.002 ± 0.001, respectively. With all of these compounds and also with CH<sub>4</sub>, an optical absorption peak, attributable to the monoiodide with a maximum between 258 and 273 nm grew during photolysis (Figures 2-6). With CH<sub>3</sub>F and CF<sub>3</sub>H, but not with the other compounds, an additional peak with λ<sub>max</sub> between 289 and 300 nm, attributable to the diiodide, grew concurrently. The quantum yield of the monoiodide increased by about 25% when the fluorocarbon pressure was increased from 100 to 700 Torr, but the yield of the diiodide was unaffected with both CH<sub>3</sub>F and CF<sub>3</sub>H. From the extinction coefficients<sup>3,11,12</sup> of the products of the I<sub>2</sub>\*-CH<sub>3</sub>F reaction (Table VII) and the data of Figure 3, it may be estimated that ca. 20% of the reactive events between I<sub>2</sub>\* and CH<sub>3</sub>F are of the type I<sub>2</sub>\* + CH<sub>3</sub>F → CH<sub>3</sub>F\* + I<sub>2</sub>; CH<sub>3</sub>F\* → CH<sub>2</sub> + HF.

The data of Figures 2-6 were obtained using 28 mm i.d. 10-cm long Suprasil cells exposed in the helix lamp. The pressure of the methyl halide was ca. 100 Torr in each case. That of the I<sub>2</sub> was the vapor pressure of the solid at the temperature of ca. 40° induced by the lamp, i.e., ca. 1 Torr. Continued photolysis of the CH<sub>3</sub>F and CF<sub>3</sub>H samples after all the I<sub>2</sub> was used up led to a decrease in the diiodide peak and essentially no change in the monoiodide peak.

Reaction of I<sub>2</sub>\* with O<sub>2</sub>. Pressures of 0.25 Torr of I<sub>2</sub> mixed with 100-500 Torr of O<sub>2</sub> were photolyzed in the 28 mm i.d. 10-cm long cylindrical Suprasil cell with the unfiltered light of the two low-pressure Hg arcs, one directed at each face, delivering a total intensity of 7.7 × 10<sup>14</sup> photons sec<sup>-1</sup> of 185-nm radiation, which was essentially all absorbed. A pale yellow solid with a powder-like texture was deposited in a triangular pattern on the bottom of the cell at each end with the base of the triangle toward the cell window. When the cell was heated after pumping off the gaseous O<sub>2</sub> the solid decomposed regenerating I<sub>2</sub>. The deposit dissolved readily in water yielding a solution acid to litmus.

**Figure 2.** Spectra of I<sub>2</sub>-CH<sub>3</sub>Cl mixture after photolysis in 28 mm i.d. cell with helix lamp for A, 0 sec; B, 7 sec; C, 15 sec; D, 23 sec.**Figure 3.** Spectra of I<sub>2</sub>-CH<sub>3</sub>F mixture after photolysis in 28 mm i.d. cell with helix lamp for A, 0 sec; B, 15 sec; C, 30 sec; D, 45 sec.**TABLE VII: Extinction Coefficients of Products of the I<sub>2</sub>\*-CH<sub>3</sub>F Reaction**

Product	Extinction coefficient, M <sup>-1</sup> cm <sup>-1</sup>	
	258 nm	290 nm
HI <sup>b</sup>	88	12
CH <sub>3</sub> I(CH <sub>2</sub> FI) <sup>a,c</sup>	380	22
CH <sub>2</sub> I <sub>2</sub> <sup>d</sup>	400	1320

<sup>a</sup> CH<sub>2</sub>FI, if formed, is assumed to have approximately the same extinction coefficient as CH<sub>3</sub>I, since that of CF<sub>3</sub>I (180 M<sup>-1</sup> cm<sup>-1</sup>) is not greatly different. <sup>b</sup> Reference 1. <sup>c</sup> Reference 3. <sup>d</sup> Reference 12.

The quantum yield, φ<sub>obsd</sub>, of I<sub>2</sub> disappearance in these experiments equals the sum of the quantum yields resulting from absorption of light by I<sub>2</sub> and by O<sub>2</sub> and may be expressed as φ<sub>obsd</sub> = φ<sub>I<sub>2</sub></sub> + (φ<sub>O<sub>2</sub></sub> - φ<sub>I<sub>2</sub></sub>)f<sub>O<sub>2</sub></sub> where f<sub>O<sub>2</sub></sub> is the

(11) A. A. Gordus and D. A. Caughey, Abstracts of the 150th National Meeting of the American Chemical Society, Atlantic City, N. J., Sept 1965.

(12) K. Kimura and S. Nagakura, *Spectrochim. Acta*, **17**, 166 (1961).

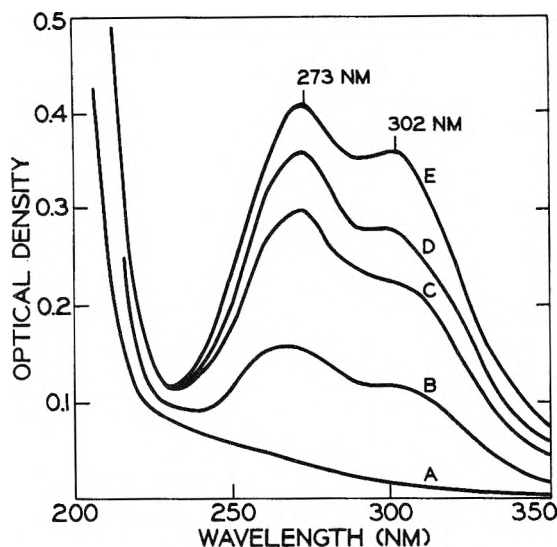


Figure 4. Spectra of  $I_2$ - $CF_3H$  mixture after photolysis in 28 mm i.d. cell with helix lamp for A, 0 min; B, 2 min; C, 4 min; D, 5 min; E, 6 min.

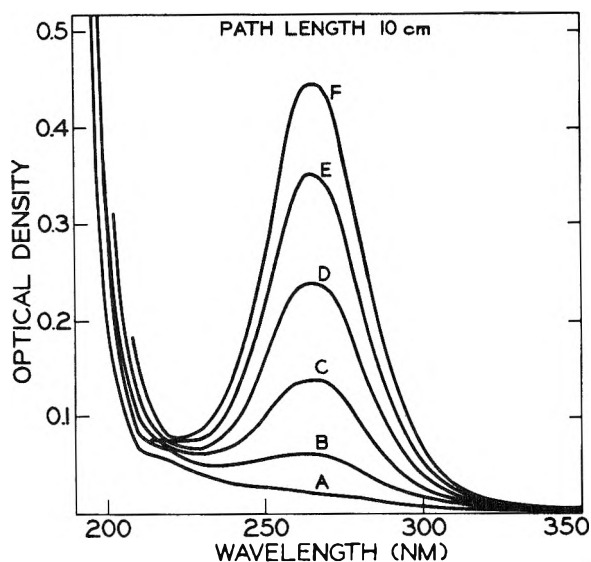


Figure 5. Spectra of  $I_2$ - $CF_4$  mixture after photolysis in 28 mm i.d. cell with helix lamp for A, 0 min; B, 5 min; C, 20 min; D, 35 min; E, 50 min; F, 66 min.

fraction of the light absorbed by  $O_2$ . The extinction coefficient of  $I_2$  for the 185-nm radiation at the total pressures used in this work is  $1 \times 10^4$ ,<sup>2,9</sup> and that of  $O_2$  is  $1.5 M^{-1} cm^{-1}$ .<sup>13</sup> A plot of quantum yield *vs.*  $f_{O_2}$  gives the line of Figure 7, where the intercept (0.12) may be interpreted as the quantum yield which would be observed if the  $O_2$  was transparent and all of the light was absorbed by  $I_2$ . This with the slope of the line of Figure 7 gives 0.5 as the quantum yield for  $I_2$  disappearance as the result of light absorbed by  $O_2$ . In these experiments the consumption of  $I_2$  was kept small so that  $f_{O_2}$  did not change more than 20%, and the average value was used.

Although  $O_3$  is formed by the photolysis of pure  $O_2$  with a quantum yield of 2,<sup>14a</sup> none was detected ( $\epsilon_{245} 3 \times 10^3 M^{-1} cm^{-1}$ )<sup>14b</sup> in the presence of  $I_2$ . The rapid reaction of  $I_2$  with  $O_3$ <sup>15</sup> was observed in this work by mixing a known amount of  $I_2$  vapor with a known amount of  $O_3$ . Approximately 3.7  $O_3$  molecules were consumed for every  $I_2$  molecule present. If  $O_3$  formation is the main process induced

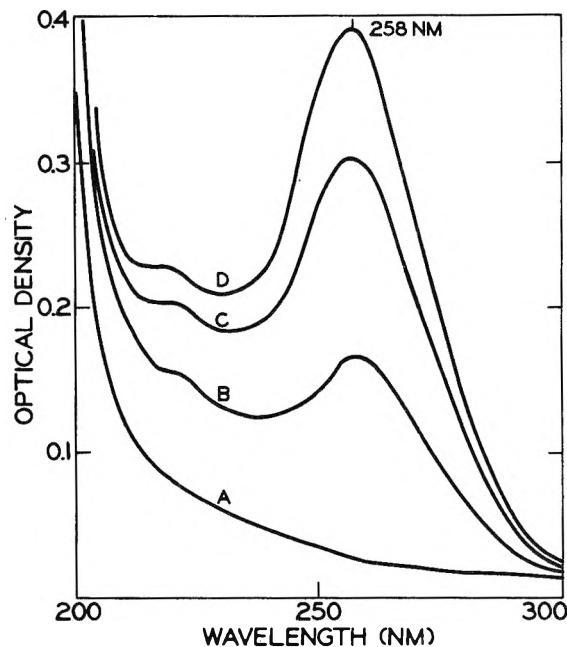


Figure 6. Spectra of  $I_2$ - $CH_4$  mixture after photolysis in 28 mm i.d. cell with helix lamp for A, 0 sec; B, 10 sec; C, 20 sec; D, 30 sec.

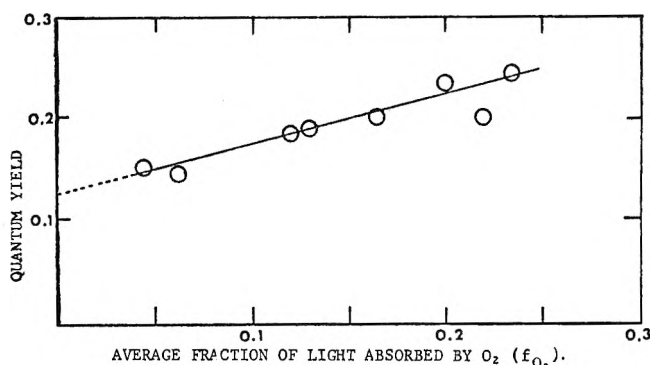


Figure 7. Quantum yields as a function of the ratio of light absorbed by  $O_2$  to the total light absorbed by  $O_2 + I_2$ .

when 185-nm radiation is absorbed by  $O_2$ ,  $\phi(-I_2)$  would be 0.5, as observed (each photon produces two  $O_3$  and each  $I_2$  consumes four  $O_3$ ).

*Reaction of  $I_2^*$  with Hydrocarbons at 77°K.* Free radicals can be produced in hydrocarbon matrices at 77°K by a variety of means including photosensitization by aromatic solutes and abstraction by hot hydrogen atoms formed by photolysis of  $HI$ .<sup>16</sup> After formation they are trapped and can be observed over periods of hours or more by electron spin resonance. To determine whether the energy of  $I_2$  excited by 185-nm radiation in such matrices is utilized in radical production, we have used  $10^{-5} M$   $I_2$  in polycrystalline  $C_2H_6$ , in glassy 3-methylpentane (3MP), and in glassy 3-ethylpentane (3EP). After 1-min photolysis of the  $C_2H_6$  with the unfiltered intensity of the helix lamp, an esr spectrum nearly identical with that report-

(13) K. Watanabe, E. C. Y. Inn, and M. Zelickoff, *J. Chem. Phys.*, **21**, 1026 (1953).

(14) (a) W. E. Vaughan and W. A. Noyes, *J. Amer. Chem. Soc.*, **52**, 559 (1930); (b) I. T. N. Jones and R. P. Wayne, *J. Chem. Phys.*, **51**, 3617 (1969).

(15) G. Brauer, Ed., "Handbuch der Präparativen Anorganischen Chemie," Vol. 1, F. Enke Verlag, Stuttgart, 1960, p 301.

(16) D. J. Henderson and J. E. Willard, *J. Amer. Chem. Soc.*, **91**, 3014 (1969).

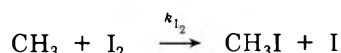
ed<sup>17a</sup> for C<sub>2</sub>H<sub>5</sub> radical produced by photolysis of C<sub>2</sub>H<sub>5</sub>I in argon at 4°K was easily observable. The quantum yield is estimated to be 10<sup>-3±1</sup>. No radicals were found after photolysis of C<sub>2</sub>H<sub>6</sub> at 77°K without I<sub>2</sub> present. Likewise no radicals were formed when the concentration of I<sub>2</sub> was 10<sup>-3</sup> M rather than 10<sup>-5</sup> M, presumably because gross aggregation of the I<sub>2</sub> occurred. Photolysis of solutions of 10<sup>-5</sup> M I<sub>2</sub> in C<sub>2</sub>H<sub>6</sub> at 77°K with a medium pressure mercury arc with a Vycor filter to remove radiation below 210 nm did not produce radicals.

By contrast with C<sub>2</sub>H<sub>6</sub>, 3MP and 3EP glasses at 77°K produce free radicals when photolyzed with the unfiltered helix lamp<sup>2</sup> in the absence of I<sub>2</sub>, the quantum yield for the 185-nm radiation absorbed being ca. 10<sup>-2</sup>. The rate of growth of the spectrum was increased about threefold by the presence of 10<sup>-5</sup> M I<sub>2</sub>, which absorbed 20-fold more light than the 3MP.

## Discussion

**Quantum Yields of Reaction with H<sub>2</sub> and CH<sub>4</sub>.** The quantum yields of I<sub>2</sub> consumption by reaction with H<sub>2</sub> and CH<sub>4</sub> following excitation at 185 nm have previously been estimated<sup>4</sup> to be 0.02 and 0.05 relative to an assumed quantum yield of unity for the I<sub>2</sub> (<sup>131</sup>I) exchange reaction with CH<sub>3</sub>I activated by 185-nm light. However, some experiments indicated an unexpectedly higher yield for the latter process.<sup>4</sup> The values of 0.12 and 0.3 for the reactions with H<sub>2</sub> and CH<sub>4</sub> (Tables VI and I) obtained in the present work, based on HBr actinometry, are in the same ratio as the old, and appear to be accurate within ca. ±10%.

**Mechanisms of Photosensitized Iodide Formation.** The results are consistent with the conclusion that the formation of the monoiodides when I<sub>2</sub> absorbs 185-nm radiation in the systems studied occurs by a concerted reaction (e.g., CH<sub>4</sub> + I<sub>2</sub>\* → CH<sub>4</sub>I<sub>2</sub>\*; CH<sub>4</sub>I<sub>2</sub>\* → CH<sub>3</sub>I + HI), rather than a free-radical reaction, but that the diiodides formed from CH<sub>3</sub>F and CF<sub>3</sub>H are formed through photosensitized decomposition to radicals which then react with I<sub>2</sub>. The finding that O<sub>2</sub> is only about three times more efficient in reducing the rate of I<sub>2</sub> consumption in the CH<sub>4</sub> system than are Ar and N<sub>2</sub> is evidence against a free-radical mechanism for the monoiodide formation (Table IV). O<sub>2</sub> decreases the rate by approximately the amount predicted for quenching on every collision with I<sub>2</sub>\* while Ar and N<sub>2</sub> decrease it by about the amount expected for quenching on one collision out of three. If I<sub>2</sub> consumption involves the I<sub>2</sub>-photosensitized formation of free radicals followed by the reaction



the I<sub>2</sub> consumption should be reduced by a factor of  $k_{\text{O}_2}(P_{\text{O}_2})^2 / (k_{12}P_{\text{I}_2} + k_{\text{O}_2}(P_{\text{O}_2})^2) = 1 / (1 + k_{12}P_{\text{I}_2} / k_{\text{O}_2}(P_{\text{O}_2})^2)$ . Taking  $k_{12}/k_{\text{O}_2}$ <sup>17b</sup> as 690 ml mol<sup>-1</sup> indicates that if I<sub>2</sub> consumption were wholly by a free-radical mechanism, a reduction by a factor of 30, below that due to deexcitation of the I<sub>2</sub>\*, would be expected. If, indeed, the reaction does not involve free radicals, it must proceed through an excited complex CH<sub>4</sub>I<sub>2</sub>\* which fragments to give the stable products CH<sub>3</sub>I and HI.

The production of CH<sub>2</sub>I<sub>2</sub> from CH<sub>3</sub>F, and of CF<sub>2</sub>I<sub>2</sub> from CF<sub>3</sub>H in about 20% of the reactive events, is strong evidence for the sequences I<sub>2</sub>\* + CH<sub>3</sub>F (CF<sub>3</sub>H) → CH<sub>3</sub>F\* (CF<sub>3</sub>H\*) + I<sub>2</sub>; CH<sub>3</sub>F\* (CF<sub>3</sub>H\*) → CH<sub>2</sub> + HF (CF<sub>2</sub> + HF).

The absence of a pressure dependence of the diiodide yields argues against formation of the methylenes by decomposition of methyl halide radicals. The monoiodide yield increases with increasing pressure, with no accompanying decrease in the diiodide yield. This implies a mechanism such as CH<sub>3</sub>FI<sub>2</sub>\* + CH<sub>3</sub>F → CH<sub>3</sub>I + IF + CH<sub>3</sub>F to account for the monoiodide yield, in competition with dissociation of the activated complex without chemical reaction.

Of the compounds used in this work, only the CH<sub>3</sub>F and CF<sub>3</sub>H give evidence of molecular elimination to form a methylenic fragment (i.e., show growth of a product with absorption in the 290-nm region). The molecular elimination of HF by CF<sub>3</sub>H is well established in shock tube studies.<sup>18,19</sup> The primary process in the photolysis of CH<sub>3</sub>F at 147 nm is also reported to be HF elimination.<sup>20</sup> Activation energies of 69<sup>18</sup> and 58 kcal mol<sup>-1</sup><sup>19</sup> have been indicated by the shock tube studies. The rate of collisional deactivation of CH<sub>3</sub>F\* at 500 Torr has been estimated as 2 × 10<sup>8</sup> sec<sup>-1</sup>.<sup>21</sup> Using the RRR method and assuming plausible constants,<sup>22a,b</sup> the lifetime with respect to decomposition of CH<sub>3</sub>F\* excited with 100 kcal mol<sup>-1</sup> or more can be estimated to be 10<sup>-12</sup>–10<sup>-13</sup> sec. Thus the excited molecules decompose within a few vibration times and are not affected by changes of pressure in the system.

**Tests with CH<sub>4</sub>-CD<sub>4</sub> and H<sub>2</sub>-D<sub>2</sub> Mixtures.** An I<sub>2</sub> molecule which has absorbed a 185-nm photon is excited by ca. 154 kcal mol<sup>-1</sup> which is ca. 50 kcal mol<sup>-1</sup> in excess of the energy required for the reaction CH<sub>4</sub> + I<sub>2</sub>\* → CH<sub>3</sub> + H + I<sub>2</sub>. If this photosensitized decomposition occurs, the H atom may have sufficient kinetic energy for the hot reaction H + CD<sub>4</sub> → CD<sub>3</sub> + HD, or the CH<sub>3</sub> radical may have sufficient vibrational energy for the CH<sub>3</sub> + CD<sub>4</sub> → CH<sub>3</sub>D + CD<sub>3</sub> reaction. Production of HD, CH<sub>3</sub>D, and CD<sub>3</sub>H in CH<sub>4</sub>-CD<sub>4</sub> mixtures would be strong evidence for the I<sub>2</sub>-photosensitized decomposition step. Similarly, production of HD in the photolysis of I<sub>2</sub> in H<sub>2</sub>-D<sub>2</sub> mixtures would indicate the reaction I<sub>2</sub>\* + H<sub>2</sub>(D<sub>2</sub>) → I<sub>2</sub> + 2H(D<sub>2</sub>). Experiments<sup>2</sup> to detect these products have been inconclusive.

**Reaction in I<sub>2</sub>-O<sub>2</sub> Mixtures.** The results indicate that φ(-I<sub>2</sub>) for 185-nm radiation absorbed by I<sub>2</sub> in an excess of O<sub>2</sub> is 0.12 and that φ(-I<sub>2</sub>) for radiation absorbed by the O<sub>2</sub> is 0.5, the latter being consistent with a mechanism involving O<sub>3</sub> formation followed by reaction of O<sub>3</sub> with I<sub>2</sub>. The mechanism for reaction of I<sub>2</sub>\* with O<sub>2</sub> may involve either a direct formation of an iodine oxide intermediate or an energy transfer yielding O atoms which form O<sub>3</sub> which reacts with I<sub>2</sub>. The mechanism of reaction of I<sub>2</sub> with O<sub>3</sub> may be similar to that postulated for the reaction of Cl<sub>2</sub> with O<sub>3</sub>.<sup>23</sup> Recent evidence suggests that the product of the reaction of I<sub>2</sub> and O<sub>3</sub> is a mixture of I<sub>2</sub>O<sub>5</sub> and I<sub>2</sub>O<sub>4</sub>.<sup>24</sup> In a flash photolysis study of I<sub>2</sub>-O<sub>2</sub> mixtures, IO was observed by its emission and it was suggested that the

- (17) (a) V. Voevodski, *Radiat. Chem., Proc. Tihany Symp.*, 1962, 118 (1964); (b) M. Christie, *Proc. Roy. Soc.*, **244**, 411 (1958).
- (18) E. Tschuikow-Roux and J. E. Marte, *J. Chem. Phys.*, **42**, 2049, 3639 (1965).
- (19) A. P. Modica and J. E. LaGriff, *J. Chem. Phys.*, **44**, 3375 (1966).
- (20) E. Tschuikow-Roux and S. Kodama, *J. Chem. Phys.*, **50**, 5297 (1969).
- (21) J. D. Allen and M. C. Flowers, *Trans. Faraday Soc.*, **64**, 3300 (1968).
- (22) (a) D. W. Placzek, B. S. Rabinowitch, G. Z. Whitten, and E. Tschuikow-Roux, *J. Chem. Phys.*, **43**, 4071 (1965); (b) B. S. Rabinowitch and D. W. Setse, *Advan. Photochem.*, **3**, 1 (1964).
- (23) G. Parties, Ed., "Mellor's Modern Inorganic Chemistry," Wiley, New York, N. Y., 1967.
- (24) K. Selti and A. Kjekshus, *Acta Chem. Scand.*, **22**, 3309 (1968).

products are the result of a concerted reaction of two  $^2P_{1/2}$  iodine atoms with  $O_2$ .<sup>25</sup> In the present work this mechanism is excluded because of the improbability of the required three-body collision involving two  $^2P_{1/2}$  atoms prior to their deexcitation.<sup>2,26</sup>

*Photolysis of  $I_2$  in Matrices.* The production of ethyl radicals by 185-nm irradiation of  $I_2$  in  $C_2H_6$  at 77°K may indicate that a photosensitized decomposition of the  $C_2H_6$  matrix is occurring. However, it is not possible to completely rule out abstraction by  $I(^2P_{1/2})$  atoms, whose im-

portance in this system is not known. In the gas phase,  $I(^2P_{1/2})$  atoms have been observed to abstract hydrogen from  $C_2H_6$  with low quantum yield.<sup>27</sup> The fact that radicals are not observed following irradiation of the  $I_2$ - $C_2H_6$  system at 77°K with visible light argues against the  $I(^2P_{1/2})$  abstraction mechanism in our case.

(25) R. A. Durie and R. A. Ramsay, *Can. J. Phys.*, **36**, 35 (1958).

(26) G. Burns and R. G. W. Norrish, *Proc. Roy. Soc., Sec. A*, **271**, 289 (1963).

(27) A. B. Callear and J. Wilson, *Trans. Faraday Soc.*, **63**, 1358, 1983 (1967).

## Substituent Parameters for Carbon-13 Chemical Shifts of 1,2-Disubstituted Ethanes<sup>1</sup>

L. Simeral and G. E. Maciel\*

Department of Chemistry, Colorado State University, Fort Collins, Colorado 80521 (Received February 5, 1973)

$^{13}C$  chemical shifts were obtained for 15 compounds of the  $XCH_2CH_2Y$  type. Together with previously reported data on substances of this type, a total of 69 compounds were considered in terms of a simple additivity model, via a linear regression analysis. Aside from the structural groups I and  $C\equiv CH$ , the predictions of the additivity model are within about 1.8 ppm of experimental data, including trimethylammonium species, such as acetylcholine.

### Introduction

Additivity relationships for  $^{13}C$  chemical shifts have played an important part in the development of  $^{13}C$  nmr.<sup>2-10</sup> They have served to help establish the general characteristics of  $^{13}C$  chemical shifts, as aids in making peak assignments and as guidelines for theoretical interpretations of  $^{13}C$  chemical shifts.

A recent paper from this laboratory<sup>10</sup> was concerned with establishing the scope of additivity of  $^{13}C$  chemical shifts in 1,2-disubstituted ethanes. In that paper,  $^{13}C$  chemical shifts that were determined on 54 compounds of the type  $XCH_2CH_2Y$  were analyzed in terms of an additivity model with characteristic  $\alpha$ - and  $\beta$ -substituent effects assigned to each group X and Y. The present note reports on an extension of that work, designed to explore the possible origins of certain cases of large deviations from simple additivity relationships and to include two additional substituents and some additional test cases of the previously reported additivity parameters.

### Experimental Section

*Measurements.* All new data reported here were obtained in the pulse-Fourier-transform mode at 22.6 MHz, using a Digilab FTS/NMR-3 data system and 400-S pulse unit interfaced with a Bruker HFX-90 spectrometer. Both coherent and pseudo-random-noise proton decoupling were employed. Unless sample volatility required probe cooling, the sample temperature was typically 38°, and the samples were neat liquids containing 10% cyclohexane as an internal standard (far less cyclohexane could have been used, but this concentration was chosen for consistency with the earlier work<sup>10</sup>).

*Materials.* All compounds except 4-methoxybutan-2-one, *N,N,N*-trimethyl-2-cyanoethylammonium iodide, and the deuterium containing compounds were obtained from commercial manufacturers, and were used as obtained, unless otherwise specified. The commercial sources were the following: Eastman 1,2-dichloroethane, *n*-propyl acetate, 2-chloroethyl acetate, 2-bromoethyl acetate, 2-phenethyl acetate, 2-methoxyethyl acetate, 2-hydroxyethyl acetate (redistilled), *N,N,N*-trimethyl-2-bromoethylammonium bromide, *N,N,N*-trimethyl-2-hydroxyethylammonium chloride, and *N,N,N*-trimethyl-2-chloroethylammonium chloride; Fisher ethyl acetate; Aldrich hex-5-en-2-one; Frinton 4-chlorobutan-2-one; J. T. Baker *N,N,N*-trimethyl-2-acetoxyethylammonium bromide (recrystallized); Chemical Samples 4-chloro-1-butene; Matheson 1,2-dibromoethane.

The *N,N,N*-trimethyl-2-cyanoethylammonium iodide was prepared by addition of methyl iodide to *N,N*-dimethyl-2-cyanoethylamine (Eastman, White Label) in chloroform. The crude product was washed with chloro-

(1) Supported by National Science Foundation Grant No. GP-33429 and by a grant from the Research Corporation.

(2) P. C. Lauterbur, *Ann. New York Acad. Sci.*, **70**, 841 (1958).

(3) G. B. Savitsky and K. Namikawa, *J. Phys. Chem.*, **67**, 2430 (1963).

(4) G. B. Savitsky, *J. Phys. Chem.*, **67**, 2723 (1963).

(5) G. B. Savitsky and K. Namikawa, *J. Phys. Chem.*, **68**, 1956 (1964).

(6) G. B. Savitsky, R. M. Pearson, and K. Namikawa, *J. Phys. Chem.*, **69**, 1425 (1965).

(7) D. M. Grant and E. G. Paul, *J. Amer. Chem. Soc.*, **86**, 2984 (1964).

(8) D. M. Grant and B. V. Cheney, *J. Amer. Chem. Soc.*, **89**, 5315, 5319 (1967).

(9) D. M. Dorman, M. Jautelat, and J. D. Roberts, *J. Org. Chem.*, **36**, 2757 (1971).

(10) G. E. Maciel, L. Simeral, R. L. Elliott, and K. Cribley, *J. Phys. Chem.*, **76**, 1466 (1972).



TABLE I: <sup>13</sup>C Chemical Shifts and Additivity Relationships for X-C<sup>x</sup>H<sub>2</sub>C<sup>y</sup>H<sub>2</sub>-Y Compounds<sup>a</sup>

X	Y	δ <sup>x</sup>	δ <sup>y</sup>	δ <sup>x</sup> <sub>calcd</sub> <sup>b</sup>	δ <sup>y</sup> <sub>calcd</sub> <sup>b</sup>	δ <sup>l</sup> <sup>d</sup>	δ <sup>j</sup>	δ <sup>k</sup>
OH	OH	63.98	63.98	66.17	66.17			
Br	Br	30.74	30.74	33.02	33.02			
Cl	Cl	44.44	44.44	46.05	46.05			
CH=CH <sub>2</sub>	CH=CH <sub>2</sub>	33.82	33.82	34.04	34.04			
OCH <sub>3</sub>	OCH <sub>3</sub>	72.53	72.53	72.07	72.07			
H	H	7.26	7.26	9.21	9.21			
CH <sub>3</sub>	CH <sub>3</sub>	25.67	25.67	25.76	25.76			
CN	CN	14.93	14.93	14.53	14.53			
C <sub>6</sub> H <sub>5</sub>	C <sub>6</sub> H <sub>5</sub>	38.23	38.23	37.87	37.87			
I	I	3.57 <sup>c</sup>	3.57 <sup>c</sup>	9.05	9.05			
COCH <sub>3</sub>	COCH <sub>3</sub>	37.34	37.34	37.42	37.42			
I	C <sub>6</sub> H <sub>5</sub>	6.52	40.71	6.80	40.12			
I	CH <sub>3</sub>	9.25	27.51	7.89	26.92			
I	OH	14.01 <sup>c</sup>	67.53 <sup>c</sup>	9.02	66.20			
I	H	-0.76	21.32	-0.13	18.39			
Br	OCH <sub>3</sub>	30.69	72.98	30.96	73.13			
Br	C <sub>6</sub> H <sub>5</sub>	33.27	39.80	32.32	38.57			
Br	CH=CH <sub>2</sub>	31.96	37.61	30.62	36.43			
Br	Cl	31.32	43.92	33.28	46.79			
Br	CN	26.75	22.63	26.91	20.64			
Br	OH	35.20	63.24	34.54	64.65			
Br	CH <sub>3</sub>	35.57	26.87	33.41	25.39			
Br	H	27.40	19.65	25.39	16.84			
Cl	CN	39.73 <sup>c</sup>	22.30 <sup>c</sup>	40.68	20.90			
Cl	H	40.54	19.16	38.16	17.10			
Cl	C <sub>6</sub> H <sub>5</sub>	44.58	39.59	45.09	38.83			
Cl	COCH <sub>3</sub>	39.27	46.31	38.00	45.47			
Cl	CH=CH <sub>2</sub>	43.96	37.54	43.40	36.69			
Cl	CH <sub>3</sub>	47.55	26.68	46.18	25.65			
Cl	OH	46.67	63.38	47.31	64.91			
CN	C <sub>6</sub> H <sub>5</sub>	19.25	31.74	19.94	32.64			
CN	OCH <sub>3</sub>	18.90	67.78	18.58	68.02			
CN	CH <sub>3</sub>	19.11	19.79	21.03	19.28			
CN	H	11.02	10.79	13.01	10.73			
CN	OH	21.79	58.03	22.16	58.54			
OH	H	57.66	18.21	57.02	18.36			
OH	CH <sub>3</sub>	64.16	26.26	65.04	26.91			
OH	CH=CH <sub>2</sub>	62.08	37.74	62.26	37.95			
OH	OCH <sub>3</sub>	61.66	74.77	62.59	75.65			
OH	C <sub>6</sub> H <sub>5</sub>	63.67	39.75	63.95	40.09			
OH	C≡CH	70.90	22.99	64.83	22.18			
OCH <sub>3</sub>	H	68.18	15.14	66.50	14.78			
OCH <sub>3</sub>	CH <sub>3</sub>	74.88	23.34	75.05	23.33			
COCH <sub>3</sub>	H	36.68	8.35	37.58	9.05			
COCH <sub>3</sub>	CH <sub>3</sub>	45.61	17.75	45.60	17.60			
COCH <sub>3</sub>	CH=CH <sub>2</sub>	42.92	28.42	42.82	28.64			
COCH <sub>3</sub>	OCH <sub>3</sub>	43.96	68.35	43.15	66.34			
C <sub>6</sub> H <sub>5</sub>	H	29.42	15.87	30.94	16.14			
C <sub>6</sub> H <sub>5</sub>	CH <sub>3</sub>	38.63	25.01	38.96	24.69			
C <sub>6</sub> H <sub>5</sub>	CH=CH <sub>2</sub>	36.10 <sup>e</sup>	35.95 <sup>e</sup>	36.18	35.73			
NO <sub>2</sub>	CH <sub>3</sub>	77.70	21.47	78.44	21.31			
NO <sub>2</sub>	H	71.16	12.18	70.42	12.56			
C≡CH	CH <sub>3</sub>	20.82	22.55	21.05	25.57			
C≡CH	H	12.42	13.94	13.03	17.02			
CH=CH <sub>2</sub>	H	27.51	13.23	28.80	14.45			
CH=CH <sub>2</sub>	CH <sub>3</sub>	36.49	22.68	36.82	23.00			
CH <sub>3</sub>	H	16.96	16.68	17.76	17.23			
C <sup>l</sup> H <sub>3</sub> C <sup>j</sup> O <sub>2</sub>	CH <sub>3</sub>	66.03	22.65	66.22	22.46	20.50	170.31	
C <sup>l</sup> H <sub>3</sub> C <sup>j</sup> O <sub>2</sub>	H	60.36	14.40	58.20	13.93	20.60	170.47	
C <sup>l</sup> H <sub>3</sub> C <sup>j</sup> O <sub>2</sub>	Br	64.41	30.10	65.83	30.11	21.04	170.58	
C <sup>l</sup> H <sub>3</sub> C <sup>j</sup> O <sub>2</sub>	C <sub>6</sub> H <sub>5</sub>	65.22	35.66	65.13	35.66	20.82	170.58	
C <sup>l</sup> H <sub>3</sub> C <sup>j</sup> O <sub>2</sub>	OCH <sub>3</sub>	63.76	70.94	63.77	71.22	20.50	170.63	
C <sup>l</sup> H <sub>3</sub> C <sup>j</sup> O <sub>2</sub>	OH	66.64 <sup>c</sup>	60.76 <sup>c</sup>	67.35	61.74	20.89 <sup>c</sup>	172.32 <sup>c</sup>	
C <sup>l</sup> H <sub>3</sub> C <sup>j</sup> O <sub>2</sub>	Cl	64.63	42.45	66.09	42.88	20.60	170.74	
N <sup>+</sup> (C <sup>l</sup> H <sub>3</sub> ) <sub>3</sub>	C <sup>j</sup> H <sub>3</sub> C <sup>k</sup> O <sub>2</sub>	65.56 <sup>c</sup>	58.49 <sup>c</sup>	64.55	56.99	54.12 <sup>c</sup>	20.35 <sup>c</sup>	171.13 <sup>c</sup>

TABLE I: (Continued)

X	Y	$\delta^x$	$\delta^y$	$\delta^x_{\text{calcd}}^b$	$\delta^y_{\text{calcd}}^b$	$\delta^i{}^d$	$\delta^j$	$\delta^k$
N <sup>+</sup> (C <sup>1</sup> H <sub>3</sub> ) <sub>3</sub>	Br	66.85 <sup>c</sup>	21.59 <sup>c</sup>	67.46	24.18	53.58 <sup>c</sup>		
N <sup>+</sup> (C <sup>1</sup> H <sub>3</sub> ) <sub>3</sub>	OH	68.55 <sup>c</sup>	56.66 <sup>c</sup>	68.92	55.8 <sup>c</sup>	54.23 <sup>c</sup>		
N <sup>+</sup> (C <sup>1</sup> H <sub>3</sub> ) <sub>3</sub>	Cl	67.18 <sup>c</sup>	36.32 <sup>c</sup>	67.72	36.95	53.85 <sup>c</sup>		
N <sup>-</sup> (C <sup>1</sup> H <sub>3</sub> ) <sub>3</sub>	CN	61.89 <sup>c</sup>	12.66 <sup>c</sup>	61.35	12.72	54.01 <sup>c</sup>		

<sup>a</sup> Chemical shifts in ppm with respect to internal TMS. Increasing  $\delta$  values correspond to decreasing shielding. <sup>b</sup> Values calculated according to eq 3. <sup>c</sup> Chemical shifts obtained with respect to internal dioxane and converted to the TMS scale using the relationship  $\delta_{\text{TMS}} = \delta_{\text{C}_4\text{H}_8\text{O}_2} + 67.40$  ppm. <sup>d</sup> Chemical shift of the C<sup>i</sup> substituent carbon, as indicated in column X or Y. <sup>e</sup> Assignments of  $\delta^x$  and  $\delta^y$  may be reversed.

form and recrystallized from methanol, mp 152° (lit.<sup>11</sup> mp 153°).

The 4-methoxybutan-2-one was prepared by addition of methanol to methyl vinyl ketone (Columbia, Red Label), using *p*-toluenesulfonic acid as a catalyst. The distilled product had bp 48–49°, 25 mm (lit.<sup>12</sup> bp 35°, 12 mm).

Deuteration of 4-chlorobutan-2-one and hex-5-en-2-one at the 3 (and 1) positions was accomplished by treating the ketones with 2% solutions of NaOD and D<sub>2</sub>O for 30 hr at 10°.

## Results and Discussion

Table I presents the <sup>13</sup>C chemical shift data obtained from this work, together with those reported earlier and not repeated. Unlike the previous report, this paper presents all <sup>13</sup>C chemical shifts with respect to tetramethylsilane (TMS), with increasing  $\delta$  values corresponding to decreasing shielding in accordance with current conventions. Except in those cases in which an alternative method is explicitly stated, the shifts were determined with respect to internal cyclohexane and converted to the TMS scale by using the relationship<sup>13</sup>

$$\delta^{\text{TMS}} = \delta^{\text{C}_6\text{H}_{12}} + 27.51 \text{ ppm} \quad (1)$$

The work reported here includes data on compounds with the CH<sub>3</sub>CO<sub>2</sub> and (CH<sub>3</sub>)<sub>3</sub>N<sup>+</sup> groups as substituents. The <sup>13</sup>C chemical shifts of the acetates were obtained on the same types of samples studied earlier.<sup>10</sup> The trimethylammonium compounds were studied as 0.5 M solutions in 90% methanol–10% dioxane (v/v);<sup>14</sup> the shifts were obtained with respect to dioxane, and converted to the TMS scale by using the relationship<sup>13</sup>

$$\delta^{\text{TMS}} = \delta^{\text{diox}} + 67.40 \text{ ppm} \quad (2)$$

Peak assignments for the acetates and trimethylammonium compounds were based on off-resonance decoupling and on the assumption of approximate additivity effects. In the trimethylammonium cases the observed effect of coupling with <sup>14</sup>N was also helpful.

Table I also presents the predictions of a simple additivity relationship for the X–C<sup>x</sup>H<sub>2</sub>–C<sup>y</sup>H<sub>2</sub>–Y system

$$\delta^x = \Delta_\alpha^x + \Delta_\beta^y + \delta_{\text{TMS}}^{\text{Et}} \quad (3)$$

$$\delta^y = \Delta_\alpha^y + \Delta_\beta^x + \delta_{\text{TMS}}^{\text{Et}} \quad (4)$$

where  $\delta^x$  is the chemical shift of the C<sup>x</sup> carbon with respect to TMS,  $\Delta_\alpha^x$  is the substituent effect exerted by X at the  $\alpha$  position and  $\delta_{\text{TMS}}^{\text{Et}}$  is the chemical shift of ethane with respect to TMS. As in the previous paper,<sup>10</sup> the <sup>13</sup>C chemical shift data were subjected to a linear regression analysis based upon eq 3 and 4; the resulting computed shifts are given in Table I.

The earlier treatment of the then-available data yielded the most serious deviations from predictions of eq 3 and

TABLE II: Additivity Constants for Substituent Effects on <sup>13</sup>C Shielding

X	$\Delta_\alpha^x$ <sup>a</sup>	$\Delta_\beta^x$	$\sigma^b$
I	–9.34	+9.18	2.92
CN	+3.80	+1.52	1.06
C≡CH	+3.82	+7.81	3.40
CH <sub>3</sub>	+8.53	+8.02	0.88
Br	+16.18	+7.63	1.71
CH=CH <sub>2</sub>	+19.59	+5.24	0.74
C <sub>6</sub> H <sub>5</sub>	+21.73	+6.93	0.66
COCH <sub>3</sub>	+28.37	–0.16	0.95
Cl	+28.95	+7.89	1.42
OH	+47.81	+9.15	1.83
CH <sub>3</sub> CO <sub>2</sub>	+48.99	+4.72	0.97
(CH <sub>3</sub> ) <sub>3</sub> N <sup>+</sup>	+50.62	–1.21	1.16
OCH <sub>3</sub>	+57.29	+5.57	0.83
NO <sub>2</sub>	+61.21	+3.35	0.65

$$\delta_{\text{TMS}}^{\text{Et}} = +9.21$$

<sup>a</sup> Values in parts per million, as defined in eq 3 and 4. <sup>b</sup> Standard deviations for the individual substituents.

4 for XCH<sub>2</sub>CH<sub>2</sub>Y systems containing the following X or Y groups: H, CH<sub>3</sub>CO, C≡CH, and I. Further consideration of the cases involving the CH<sub>3</sub>CO group raised the possibility that an improved level of agreement could be obtained if the tentative and ambiguous assignments of C<sup>x</sup> and C<sup>y</sup> in CH<sub>3</sub>COC<sup>x</sup>H<sub>2</sub>C<sup>y</sup>H<sub>2</sub>Cl and CH<sub>3</sub>COC<sup>x</sup>H<sub>2</sub>C<sup>y</sup>H<sub>2</sub>CH=CH<sub>2</sub> were reversed. In order to check this possibility, samples that were specifically deuterated at C<sup>x</sup>, and not at C<sup>y</sup>, were prepared, and it was found that reversing the earlier assignment was in order. In addition, two new compounds containing the pertinent substituents were included in the study, CH<sub>3</sub>COCH<sub>2</sub>CH<sub>2</sub>OCH<sub>3</sub> and ClCH<sub>2</sub>CH<sub>2</sub>CH=CH<sub>2</sub>; the assignments for these cases were based upon off-resonance decoupling and the predictions of eq 3 and 4. The net result of making firm assignments and of revising the regression accordingly was to remove the CH<sub>3</sub>CO group from the list of substituents associated with large deviations from additivity.

In exploring the origin of the large deviations from additivity predictions found when X and/or Y is I, it was

- (11) A. N. Kost, *Vestn. Moskov. Univ.*, **141** (1947); *Chem. Abstr.*, **42**, 3722g (1948).
- (12) A. Treibs, *Angew. Chem.*, **60**, 289 (1948).
- (13) G. C. Levy and J. D. Cargioli, *J. Magn. Resonance*, **6**, 143 (1972).
- (14) The acetates were also studied, in separate experiments, as 0.5 M solutions in the 90% methanol–10% dioxane (v/v) solvent. The maximum change in the <sup>13</sup>C chemical shifts of the ethane fragment carbons in these compounds in going from the neat liquids to dilute solutions was 0.8 ppm.
- (15) H. Spiesack and W. G. Schneider, *J. Chem. Phys.*, **25**, 722 (1961).
- (16) G. E. Maciel and J. L. Natterstad, *J. Chem. Phys.*, **42**, 2427 (1965).
- (17) M. R. Bacon and G. E. Maciel, *J. Amer. Chem. Soc.*, in press.

found, as would be expected from earlier work on organic iodides,<sup>15-17</sup> that the <sup>13</sup>C chemical shifts of ICH<sub>2</sub>CH<sub>2</sub>I is strongly dependent upon concentration and solvent. The value included in Table I was obtained on a 0.3 M solution in dioxane; a saturated solution and 0.3 and 0.12 M solutions in cyclohexane gave values of 1.58, 0.64, and 0.53 ppm, respectively, with respect to TMS. In contrast, similar experiments on BrCH<sub>2</sub>CH<sub>2</sub>Br and ClCH<sub>2</sub>CH<sub>2</sub>Cl did not reveal analogously large sensitivities to solvent and concentration.

With only two exceptions, the 24 shifts predicted by eq 3 and 4 for the acetates and the ammonium compounds are within about 1.5 ppm of the experimentally determined values. Within the list of 22 successfully predicted shifts for these two classes of compounds, and belonging to both of these classes, is the biologically important case, acetylcholine, CH<sub>3</sub>CO<sub>2</sub>CH<sub>2</sub>CH<sub>2</sub>N<sup>+</sup>(CH<sub>3</sub>)<sub>3</sub>. The fact that the <sup>13</sup>C shifts in acetylcholine are so "regular" in this case suggests that any large deviations that might be observed in biological studies could be interpreted in terms of significant alterations of structural detail, e.g., complexation or conformation effects.

Table II summarizes the substituent parameters of eq 3 and 4 for the  $\alpha$  and  $\beta$  positions which, according to the

linear least-squares regression, give the best fit to the experimental data. Also included in Table II are the individual standard deviations of the fit for the compounds corresponding to each substituent. The overall standard deviation for all of the <sup>13</sup>C chemical shifts included in this study is 1.62 ppm. The I and C $\equiv$ CH groups remain as the structural units associated with the largest deviations from simple additivity predictions. It is interesting that neither of these substituents is associated with structural characteristics such as conformational variability about the C-X bond, hydrogen bonding, or ion-dipole interactions, any of which might be expected to manifest themselves much differently from compound to compound. However, these two are probably the most polarizable substituents among the compact structural groups considered. Additivity predictions for compounds containing the other groups covered in this study are likely to be successful within about 1.8 ppm.

*Acknowledgment.* The authors are grateful to the National Science Foundation for equipment grants for purchase of the spectrometer and data system, and to Dr. Lee M. Huber of Dow Chemical, Midland Division, for pertinent suggestions.

## COMMUNICATIONS TO THE EDITOR

---

### Nuclear Magnetic Relaxation of Sodium-23 in Polyphosphate Solutions

*Publication costs assisted by The University of Leiden*

*Sir:* Nuclear magnetic relaxation of counterions in polyelectrolyte solutions should in principle yield interesting information on polyion-counterion interactions. For example, <sup>23</sup>Na relaxation, occurring by way of a quadrupolar mechanism, is determined by the electric field gradient at the site of the nucleus and the correlation time for this gradient. A study of the relaxation rate of <sup>23</sup>Na ions in the presence of negatively charged macroions should therefore contribute to our knowledge of the details of the behavior of counterions in these systems. We wish to report some results obtained on aqueous solutions of sodium polyphosphates (NaPP) with samples of different degree of polymerization (DP).

Some sodium phosphates were prepared by heating sodium dihydroorthophosphate in a platinum crucible for 40 hr at 900°. The resulting (NaPO<sub>3</sub>)<sub>n</sub> glass is very soluble in water. The polyphosphates of different degree of polymer-

ization were obtained by solubility fractionation of the aqueous solution with acetone by the method of van Wazer.<sup>1</sup> Some other polyphosphates were made by the same fractionation method of 10% aqueous solutions of commercially obtained sodium metaphosphate (E. Merck, Darmstadt).

All the fractions were freeze dried. The samples contained about 11% water. The DP was found by viscosity measurements in 0.035 N NaBr solutions with an Ostwald viscosimeter.<sup>2</sup>

The nuclear magnetic relaxation rates were measured at 26° in 15-mm diameter tubes at a frequency of 16 MHz with a Bruker B-KR 302S 16/60 MHz pulsed nmr spectrometer. All the nmr measurements were carried out within a few days after making the solutions of the sodium polyphosphates to exclude the influence of hydrolysis of the polyphosphates.<sup>3</sup> The measurements of the longitudinal relaxation time ( $T_1$ ) were performed with a 180°- $\tau$ -90° pulse sequence at different  $\tau$ 's. For a number of cases

(1) J. R. van Wazer, *J. Amer. Chem. Soc.*, **72**, 647 (1950).

(2) U. P. Strauss, E. H. Smith, and P. L. Wineman, *J. Amer. Chem. Soc.*, **75**, 3935 (1953).

(3) J. B. Gill and S. A. Riaz, *J. Chem. Soc. A*, 183 (1969).

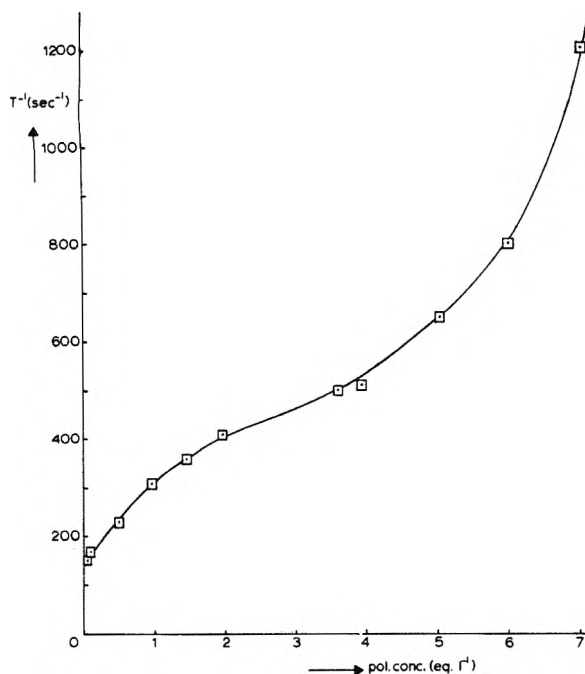


Figure 1. Concentration dependence of  $^{23}\text{Na}$  relaxation rate in aqueous NaPP solutions of NaPP sample with DP = 34.

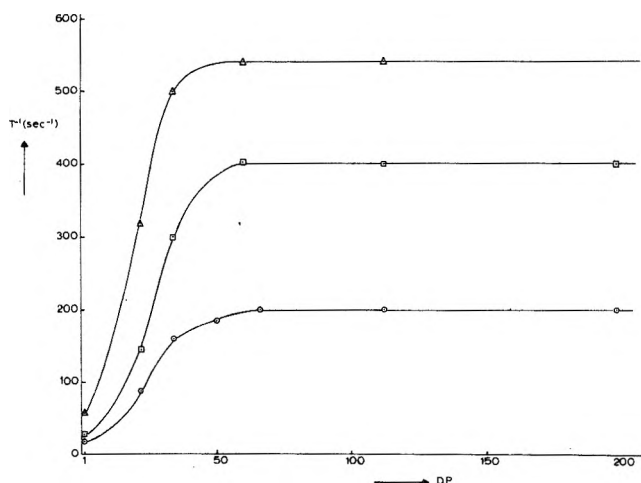


Figure 2. Variation of  $^{23}\text{Na}$  relaxation rate with DP at several polymer concentrations in aqueous solutions:  $\circ$  = 0.089 equiv  $\text{l}^{-1}$ ;  $\square$  = 0.89 equiv  $\text{l}^{-1}$ ;  $\triangle$  = 3.50 equiv  $\text{l}^{-1}$ .

TABLE I:  $^{23}\text{Na}$  Relaxation Rate in Aqueous Solutions of Sodium Dihydroorthophosphate

Concn, equiv $\text{l}^{-1}$	$T_1^{-1}$ , $\text{sec}^{-1}$	Concn, equiv $\text{l}^{-1}$	$T_1^{-1}$ , $\text{sec}^{-1}$
3.00	51	1.00	28
2.01	39	0.0	17.5
			(extrapolated) <sup>5</sup>

the transverse relaxation time ( $T_2$ ) was measured by the standard spin-echo technique, and was always found equal to  $T_1$  within experimental error. The accuracy of all  $T_1$  measurements is estimated to be 5%.

As a reference point for the investigation of the macromolecular systems, we first determined the  $^{23}\text{Na}$  relaxa-

tion rate in aqueous  $\text{NaH}_2\text{PO}_4$  solutions. The results are given in Table I and it is concluded that the longitudinal relaxation time is of the same order as has been found in other sodium salt solutions.<sup>4-6</sup>

In solutions of NaPP (degree of polymerization: 34) the relaxation rate is increased by about one order of magnitude as may be seen on comparing the results shown in Figure 1 with the experimental values for the  $\text{NaH}_2\text{PO}_4$  solutions in Table I.

Now, according to Hertz, *et al.*,<sup>7</sup> the field gradient at the nucleus contains contributions from the surrounding water molecules and all other ions. Therefore, if ion condensation<sup>8-10</sup> occurs an increase in the relaxation rate is to be expected. From the fact that  $T_1$  and  $T_2$  are equal in these solutions it is seen that the correlation time for the field gradient is very short ( $<10^{-9}$  sec) and this directly confirms to the conclusion of Schindewolf,<sup>11,12</sup> based on potentiometric and transport results, that the sodium ions do not reside for any appreciable time on given sites on the polyelectrolyte, even though ion condensation occurs.

As, in theoretical work on polyelectrolytes, the concept of infinitely long charged rods is used, it is of interest to investigate what degree of polymerization is effectively infinite from the point of view of the counterions or, in other words, at what chain length do the properties of the counterions become independent of this length.

In Figure 2 it is shown that at a degree of polymerization of about 60 a steep initial increase of  $T_1^{-1}$  as a function of the DP levels off sharply. This is observed for concentrations up to 3.50 equiv  $\text{l}^{-1}$ . For solutions of NaPP with a degree of polymerization of 338 we still found the same values for  $T_1^{-1}$  as for samples with a DP = 198. Again, these results are in surprisingly good agreement with the work of Schindewolf in view of the difference in the time scales of the methods used.

- (4) P. A. Speight and R. L. Armstrong, *Can. J. Phys.*, **45**, 2493 (1967).
- (5) M. Eisenstadt and H. L. Friedman, *J. Chem. Phys.*, **44**, 1407 (1966); **46**, 2182 (1967).
- (6) C. Hall, R. E. Richards, G. N. Shultz, and R. R. Sharp, *Mol. Phys.*, **16**, 529 (1969).
- (7) H. G. Hertz, G. Stalidis, and H. Versmold, *J. Chim. Phys. Physicochim. Biol.*, **177** (1969).
- (8) G. S. Manning, *J. Chem. Phys.*, **47**, 2010 (1967); **51**, 924 (1969).
- (9) F. Oosawa, "Polyelectrolytes," Marcel Dekker, New York, N. Y., 1970.
- (10) A. Katchalsky, *J. Pure Appl. Chem.*, **26**, 327 (1971).
- (11) U. Schindewolf and K. F. Bonhoeffer, *Z. Elektrochem.*, **57**, 216 (1953).
- (12) U. Schindewolf, *Z. Phys. Chem. (Frankfurt am Main)*, **1**, 134 (1954).

Department of Physical Chemistry III  
University of Leiden  
Leiden, The Netherlands

H. S. Kielman  
J. C. Leyte\*

Received December 27, 1972

## Effect of 2-Butanol on the Activity of Sodium Sulfate in Aqueous Solutions.

### Implications for Electrosorption Studies

Publication costs assisted by the Air Force Office of Scientific Research

Sir: In studies of the electrosorption of organic compounds on electrodes from aqueous solutions it is customary<sup>1</sup> to

use solutions with varying concentrations of the organic compound but a constant concentration of a single electrolyte. Because the thermodynamic theory of electrocapillarity<sup>2</sup> requires that the relative surface excess of the organic compound be calculated from measurements made at constant electrolyte activity, the practice of using constant electrolyte concentration is equivalent to making the implicit assumption that the activity of the electrolyte is unaffected by the presence of a neutral organic compound. During an investigation of the electrosorption of 2-butanol on mercury from aqueous sodium sulfate solutions,<sup>3</sup> we tested this assumption by measuring the activity of the sodium sulfate in the three-component mixtures at 25° by the emf method. We conclude, on the basis of this test, that for this system at least the assumption is completely untenable.

A galvanic cell without liquid junction consisting of a Corning NAS 11-18 sodium ion electrode<sup>4</sup> and a two-phase lead amalgam-lead sulfate electrode<sup>5</sup> was used. In the absence of organic compound a plot of the emf of this cell *vs.* the natural logarithm of the mean ionic activity<sup>6</sup> over a concentration range 0.05-1.4 *m* had a least-squares slope which agreed with the theoretical value of  $1.5RT/F$  to within better than one part per thousand. To prove that the cell also behaved correctly in the presence of 2-butanol we measured the emf in the presence and absence of the organic compound with solutions saturated with solid sodium sulfate. The emf in the two cases agreed to within 10  $\mu$ V.

Emf measurements were then made on a series of solutions having different concentrations of  $\text{Na}_2\text{SO}_4$  and of 2-butanol in order to determine what concentration of  $\text{Na}_2\text{SO}_4$  would be required, for a given concentration of 2-butanol, to yield the same emf (*i.e.*, salt activity) as 0.1 *M*  $\text{Na}_2\text{SO}_4$  in pure water. The results are shown in Figure 1. Had the assumption that the organic compound does not seriously affect the electrolyte activity been true, a horizontal line with ordinate 0.1 *M* would have been obtained. From Figure 1 it may be seen that this assumption is definitely false. For example, when the concentration of 2-butanol is 1.0 *M* the concentration of  $\text{Na}_2\text{SO}_4$  required to give the same emf as the solution of 0.1 *M*  $\text{Na}_2\text{SO}_4$  in pure water is only 0.0498 *M*. Moreover, a solution which was 1.0 *M* in 2-butanol and 0.1 *M* in  $\text{Na}_2\text{SO}_4$  was found to have a salt activity nearly five times larger than that of 0.1 *M*  $\text{Na}_2\text{SO}_4$  in pure water.

These results show that for this system very serious errors would result if the electrosorption data were collected from a series of solutions with constant salt concentration. Conclusions about the nature of the electrosorption isotherm reached from the analysis of such data on the assumption that the salt activity was constant would be doubtful if not meaningless. For such systems the first step must be to obtain data such as that of Figure 1 to provide the recipe for preparation of a series of solutions of varying organic concentration at constant salt activity.

The observed effect of 2-butanol on the electrolyte activity may be related to the structure-making properties of this alcohol,<sup>7</sup> and, on this assumption, the linear relation shown in Figure 1 suggests a simple correlation. If the structured water in the form of cages around the alcohol molecules is, on the average, unavailable to the ions of the salt, then the addition of the alcohol to the electrolyte solution will effectively raise the salt concentration in the remaining unstructured water. On this assumption we calculated the number of water molecules associated with

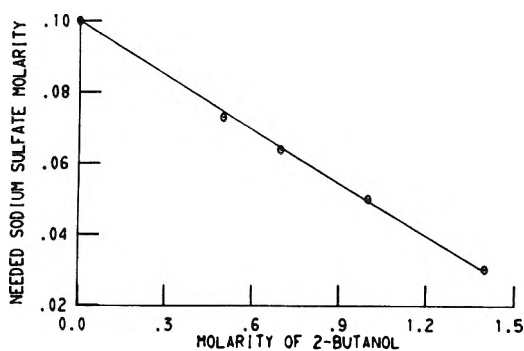


Figure 1. Plot of the molar concentration of sodium sulfate which yields the same electrolyte activity as 0.1 *M*  $\text{Na}_2\text{SO}_4$  in pure water *vs.* the corresponding molar concentration of 2-butanol in the solution at 25°.

one alcohol molecule and obtained an average number of 24.2. This number could be consistent with a cage of 24 water molecules around the alcohol molecule in the form of a tetrakaidecahedron<sup>8</sup> which has 12 pentagonal and 2 hexagonal faces. Molecular models indicate such a cage would be able to contain a molecule of 2-butanol.

*Acknowledgment.* This work was supported by the U. S. Air Force Office of Scientific Research under Grant No. AF-AFOSR-70-1887. We thank Professor T. N. Solie for helpful discussions.

- (1) For recent reviews *cf.* B. B. Damaskin, O. A. Petrii, and V. V. Batrakov, "Adsorption of Organic Compounds on Electrodes," Plenum Press, New York, N.Y., 1971; R. Payne, *J. Electroanal. Chem.*, **41**, 277 (1973).
- (2) For a review *cf.* D. M. Mohilner in "Electroanalytical Chemistry," Vol. 1, A. J. Bard, Ed., Marcel Dekker, New York, N.Y., 1966, pp 241-409.
- (3) H. Nakadomari, D. M. Mohilner, and P. R. Mohilner, to be submitted for publication.
- (4) G. Eisenman, *Advan. Anal. Chem. Instrum.*, **4**, 213 (1965).
- (5) H. S. Harned and J. C. Hecker, *J. Amer. Chem. Soc.*, **56**, 650 (1934).
- (6) H. S. Harned and B. B. Owen, "The Physical Chemistry of Electrolytic Solutions," 3rd ed, Reinhold, New York, N.Y., 1958, p 553.
- (7) G. Nemethy and H. Sheraga, *J. Chem. Phys.*, **36**, 3401 (1962); G. Wada and S. Umeda, *Bull. Chem. Soc. Jap.*, **35**, 646 (1962).
- (8) J. L. Kavanau, "Water and Solute Interactions," Holden-Day, San Francisco, Calif., 1964, p 17.

Department of Chemistry  
Colorado State University  
Fort Collins, Colorado 80521

David M. Mohilner\*  
Hisamitsu Nakadomari

Received March 19, 1973

### Substituent Effects on Excited-State Acidities of Some Substituted 8-Hydroxyquinolinium Cations<sup>1</sup>

*Sir:* Considerable interest has recently appeared concerning the acidity of organic molecules in their excited states. It has been shown that in most cases acidities of these molecules were significantly different in the ground

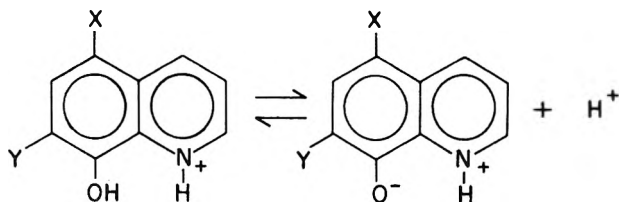
- (1) Research was carried out as a part of a study on the phosphorimetric analysis of drugs in blood and urine, supported by U. S. Public Health Service Grant No. GM-11373-08

state and the first excited singlet state,<sup>2,3</sup> which is of importance in photochemistry. Prototropic equilibria involved in the lowest singlet excited state of quinolins are especially received great attention.<sup>4-11</sup> However, significant study of substituent effects upon excited-state protolytic equilibrium constants of these heterocyclic compounds has not been reported until now. It is only in the homocyclic aromatic series that some quantitative studies based on the Hammett equation have been described.<sup>12-14</sup> For example, Wehry and Rogers<sup>13</sup> demonstrated by means of the Hammett and Taft equations that, in a series of substituted phenols, conjugative effects on acidity were more important than inductive effects, in excited states compared to the ground state. Wehry<sup>14</sup> reported also that the extent of electron-withdrawing conjugation by sulfone, sulfonium, and sulfoxide groups greatly enhanced acidities of phenols in lowest triplet, and first excited singlet states, relative to the ground state.

The purpose of the present study was to examine the influence of halogeno-, sulfo- and thiocyno-substituents upon the first singlet excited-state dissociation constants of a series of substituted derivatives of 8-hydroxyquinoline (8-HQ). We were particularly concerned by the possibility of correlation of excited-state acidities of these heterocyclic compounds with ground-state substituent constants.

First excited-state protolytic equilibrium constants ( $pK_a^*$ ) were determined *via* fluorescence titration for the equilibria between the excited singlet states of the cations and the zwitterions of 8-hydroxyquinoline substituted derivatives shown in Scheme I. We have already described in

**Scheme I:** Prototropic Equilibrium between First Excited Singlet State of Cation and Zwitterion of Substituted 8-HQ (X and Y are 5 and 7 Substituent).



detail the methods of fluorescence titration used for the determination of  $pK_a^*$ .<sup>11</sup> Data are given in Table I for 22 mono- and disubstituted 8-HQ derivatives.

The  $pK_a^*$  values are between -5.9 for 7-iodo-8-hydroxyquinoline and -9.6 for the 5,7-disulfo-8-hydroxyquinoline, which represents a large range of nearly 4 decades. For such a large acidity range, substituent effects can be considered as significant, in spite of the fact that substituents include mainly halogens. All of the groups in this study exhibit electron-withdrawing effects in the ground state.

As expected, sulfo and thiocyno derivatives are relatively strong acids; this is partly due to electron-withdrawing conjugation of sulfur  $d\pi$  orbitals probably enhanced in singlet excited states, as it has been observed in the case of sulfur-containing phenols.<sup>14</sup> In the case of the halogeno derivatives, it is of interest to notice that excited state acidities of 5- and 7-halogeno-8-hydroxyquinoline are decreasing with increasing electron-withdrawing power (or electronegativity) of the halogen atom; for example, 7-fluoro-8-hydroxyquinoline is a stronger acid than 7-iodo-8-hydroxyquinoline in the first excited singlet state. Similar sequences are observed for the dihalogeno derivatives. This acidity order is the reversal of that which would be

**TABLE I:**  $pK_a^*$  Values for 8-Hydroxyquinoline Substituted Derivatives in the Singlet Excited State<sup>a</sup>

Substituent	$pK_a^*$	Substituent	$pK_a^*$
5-Br	-8.60	5-Br-7-Cl	-8.40
5-I	-7.30	5-1-7-Cl	-7.10
5-SO <sub>3</sub> H	-9.30	5-F-7-Br	-8.60
5-SCN	-8.95	5-Cl-7-Br	-8.55
7-F	-9.40	5-Br-7-Br	-8.20
7-Cl	-9.20	5-1-7-Br	-6.95
7-Br	-8.65	5-F-7-I	-7.95
7-I	-5.90	5-Br-7-I	-7.50
7-SO <sub>3</sub> H	-9.15	5-1-7-I	-6.40
5-F-7-Cl	-8.80	5-1-7-SO <sub>3</sub> H	-6.15
5-Cl-7-Cl	-8.75	5-SO <sub>3</sub> H-7-SO <sub>3</sub> H	-9.60

<sup>a</sup> Values recorded at room temperature in sulfuric acid solvent.<sup>11</sup> All experimental values given to nearest 0.05 unit. Error  $\leq 0.15$ .

expected on the basis of the values of ground-state substituent constants, and as a result, the Hammett equation can not be applied with any success to the substituted 8-HQ.

These anomalous sequences of  $pK_a^*$  for the halogeno-8-hydroxyquinoline could not result from the enhancement in the excited state of proximity steric or polar interactions between ortho halogeno substituents (in 7 position) and the phenolate oxygen atom. Indeed, the sequence of  $pK_a^*$  values for the 5-para substituents  $I > Br > Cl > F$  is similar to the one observed for the 7-o-halogeno series and appears to be independent of the nature of the 7-halogeno substituent.

An alternative explanation would be a balance which would occur differently in the excited state, between conjugative and inductive contributions to the global electron-withdrawing effect of the halogen atoms. However, that the anomalous acidity order observed in this study is also the reverse of the one noticed by Wehry and Rogers<sup>13</sup> for 3-halogenated phenols in the first excited singlet state suggests to us that there also may be some influence of the heterocyclic part of the molecule on the acidity sequence of 8-HQ derivatives in the excited state.

In order to evaluate the respective contribution of inductive and resonance effects of the halogen substituents upon the excited state acidities of derivatives of 8-HQ,<sup>15</sup> we have used the Taft equation<sup>16</sup>

- (2) (a) C. A. Parker, "Photoluminescence of Solutions," Elsevier, Amsterdam, 1968, pp 328-341. (b) R. S. Becker, "Theory and Interpretation of Fluorescence and Phosphorescence," Wiley, New York, N. Y., 1969 pp 239-244.
- (3) E. L. Wehry and L. B. Rogers, "Fluorescence and Phosphorescence Analysis," D. M. Hercules, Ed., Wiley, New York, N. Y., 1966, Chapter 3, p 125.
- (4) C. J. Haylock, S. F. Mason, and B. E. Smith, *J. Chem. Soc.*, 4897 (1963).
- (5) R. E. Ballard and J. W. Edwards, *J. Chem. Soc.*, 4868 (1964).
- (6) S. Schulman and Q. Fernando, *J. Phys. Chem.*, **71**, 2668 (1967).
- (7) S. Schulman and Q. Fernando, *Tetrahedron*, **24**, 1777 (1968).
- (8) S. F. Mason, J. Philp, and B. E. Smith, *J. Chem. Soc. A*, 3051 (1968).
- (9) S. G. Schulman and H. Gershon, *J. Phys. Chem.*, **72**, 3693 (1968).
- (10) M. Goldman and E. L. Wehry, *Anal. Chem.*, **42**, 1178 (1970).
- (11) M. P. Bratzel, J. J. Aaron, J. D. Winefordner, S. G. Schulman, and H. Gershon, *Anal. Chem.*, **44**, 1240 (1972).
- (12) H. H. Jaffe and H. L. Jones, *J. Org. Chem.*, **30**, 964 (1965).
- (13) E. L. Wehry and L. B. Rogers, *J. Amer. Chem. Soc.*, **87**, 4234 (1965).
- (14) E. L. Wehry, *J. Amer. Chem. Soc.*, **89**, 41 (1967).
- (15) Because of the lack of available values of  $\sigma_1$  and  $\sigma_R$ , SO<sub>3</sub>H and SCN substituents were not included in the correlations.
- (16) C. D. Ritchie and N. F. Sager, "Program in Physical Organic Chemistry," Vol. 2, S. G. Cohen, A. Streitwieser, and R. W. Taft, Ed., Wiley, New York, N. Y., 1964, p 323.

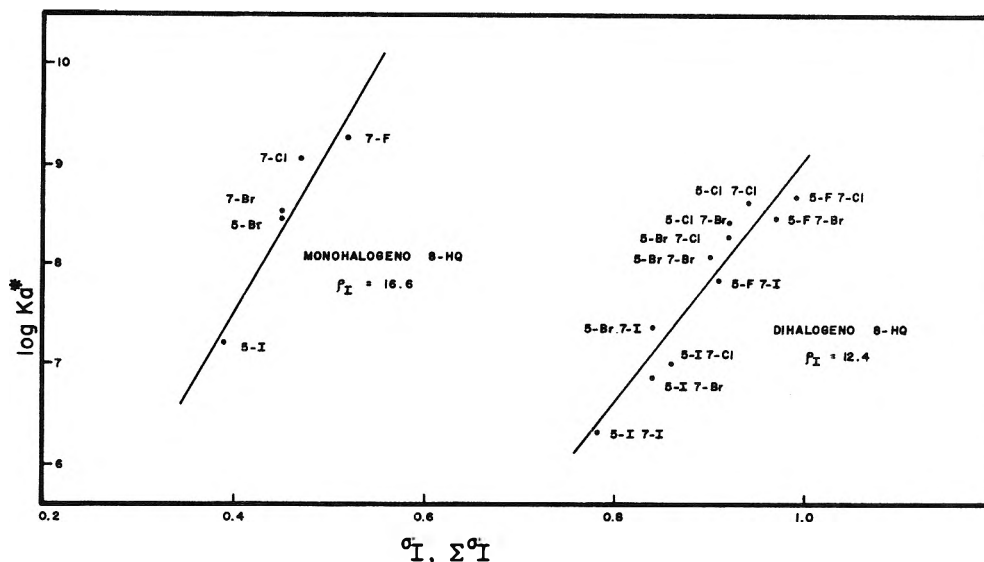


Figure 1. Correlations between excited-state dissociation constants of the monohalogeno and dihalogeno 8-hydroxyquinolines and inductive substituent constants.

$$\log K = \rho_I \sigma_I + \rho_R \sigma_R + \log K_0 \quad (1)$$

which permits a semiquantitative evaluation of inductive (I) and resonance (R) effects. Values of  $\sigma_I$  and  $\sigma_R$  proposed by Taft<sup>16</sup> were used. Therefore, the electrical effect of the halogeno substituents were assumed to be approximately equal in ortho and para positions, as suggested by several authors.<sup>17-20</sup> Mono- and disubstituted derivatives are separated according to two correlations and these correlations are described below.

The least-squares line for the five monosubstituted 8-HQ is

$$\log K_a^* = 21.1\sigma_I + 4.9\sigma_R + 0.05 \quad (2)$$

The reaction constants are  $\rho_I = 21.1$  and  $\rho_R = 4.9$ . The multiple correlation coefficient  $r = 0.89$ . For the 11 disubstituted 8-HQ's, the least-squares line is

$$\log K_a^* = 9.4\sigma_I + 0.8\sum\sigma_R - 0.05 \quad (3)$$

with  $\rho_I = 9.4$ ,  $\rho_R = 0.8$ , and  $r = 0.90$ . That satisfactory Taft correlations are found confirms that only electrical effects are involved and that there are no important steric or polar proximity interactions of 7-halogeno substituents with the ortho phenolic group. The considerably larger  $\rho_I$  values compared to  $\rho_R$  in eq 2 and 3 indicate that *inductive effects are relatively more important than the conjugative effects* in the first excited singlet states of the halogeno 8-hydroxyquinolines. The sensitivity of the prototropic equilibria in the excited singlet state to the inductive effects is also demonstrated by the satisfactory correlations found with only  $\sigma_I$  constants (see Figure 1). For the mono- and dihalogeno derivatives, the least-squares lines are, respectively

$$\log K_a^* = 16.6\sigma_I + 1.05 \quad (4)$$

$$\log K_a^* = 12.4\sigma_I - 3.25 \quad (5)$$

with  $r = 0.95$  for eq 4 and  $r = 0.96$  for eq 5.

By comparison with previous studies which indicated that enhanced conjugative interactions occurred in the excited state,<sup>12,13</sup> especially in the case of phenols, the present results may appear surprising. However, we must point out that the only substituents included in our correlations are for the halogeno species which are well known

for their ability to simultaneously use  $p\pi$  orbitals to donate  $\pi$  electrons to the ring and  $d\pi$  orbitals to accept electrons from the  $\pi$  orbitals of the aromatic ring.<sup>21</sup> As this last factor is included in the total inductive electron-withdrawing power, represented by  $\sigma_I$  constants,<sup>22</sup> it is probable that the increase of the inductive effect observed in the correlations is partly due to *enhanced interactions of the aromatic  $\pi$  electrons with the halogen  $d\pi$  orbitals* in the first singlet excited state of the 8-HQ derivatives.

Another part of the enhancement of the inductive effect would result from the influence of the heterocyclic part of the molecule on the acidity in the excited state. Most of the halogen electron-donating conjugative interactions involved in the zwitterion-cation system would be mobilized in the direction of the nitrogen of the heterocyclic ring in accordance with the enhanced basicity of the nitrogen atom observed in the lowest excited singlet state.

In the mesomeric forms A and B (Scheme II), the inductive effects of the halogeno substituents would be greatly enhanced and would consequently strengthen the acidities of the excited cations. Occurrence of the forms A and B in the first singlet excited state is supported by Hückel molecular orbital calculations,<sup>23</sup> which predict a migration of electronic charges from the homocyclic to the heterocyclic ring of the 8-hydroxyquinoline upon excitation to the first excited singlet state.

Different behavior of the monohalogeno and dihalogeno derivatives is indicated by the different slope and ordinate values found for the two series of compounds (Figure 1 and eq 4 and 5). Electrical interactions of the halogen substituents with each other in the dihalogenated derivatives may occur in the singlet excited state and partly cause the separation of the data in the two correlations. This interpretation is confirmed by the existence of a very satisfactory multiple regression of the general type de-

(17) M. T. Tribble and J. G. Traynham, *J. Amer. Chem. Soc.*, **91**, 379 (1969), and references cited therein.

(18) C. L. Liotta, *Chem. Commun.*, 338 (1968).

(19) This view has recently been disputed by Charton,<sup>20</sup> but the results of this controversy would not affect the validity of the correlations obtained in the present work.

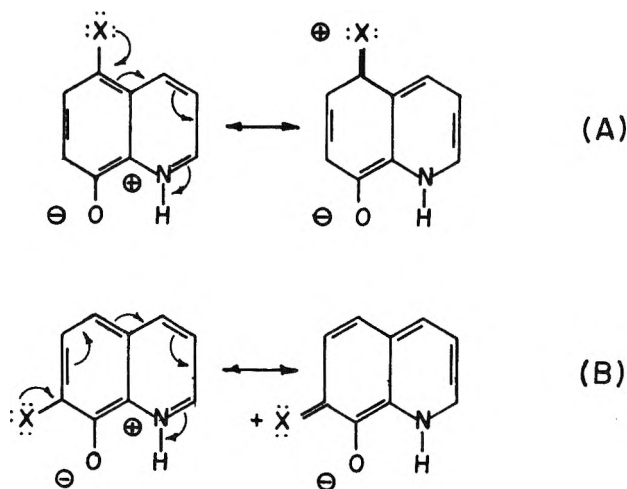
(20) M. Charton, *J. Amer. Chem. Soc.*, **91**, 6649 (1969).

(21) L. N. Fergusson, "The Modern Structural Theory of Organic Chemistry," Prentice-Hall, Englewood Cliffs, N. J., 1963, pp 393-401.

(22) R. W. Taft, Jr., *J. Chem. Phys.*, **26**, 931 (1956).

(23) R. E. Burton and W. J. Davis, *J. Chem. Soc.*, 1766 (1964).

**Scheme II:** Mesomeric Forms of the 5-Halogeno-8-hydroxyquinoline (A) and of the 7-Halogeno-8-hydroxyquinoline (B).



scribed by Leffler and Grunwald,<sup>24</sup> with an interaction term proportional to the product of the two  $\sigma_I$  values, for the dihalogeno derivatives

$$\log K_a^* = 10.6\sum\sigma_I - 1.7\sum\sigma_I^X\sigma_I^Y - 2.15 \quad (6)$$

with  $\sigma_I^X$  and  $\sigma_I^Y$  inductive constants of the halogens X and Y,  $\rho_I = 10.6$ , interaction constant  $q_I = -1.7$ , and multiple correlation coefficient  $r = 0.998$ . The significantly different  $\rho_I$  value compared with the  $\rho_I$  value of 16.6 for the monohalogeno derivatives (eq 4) indicates a greater sensitivity of these last compounds to the inductive effect.

(24) J. E. Leffler and E. Grunwald, "Rates and Equilibria of Organic Reactions," Wiley, New York, N. Y., 1963, pp 192-194.

(25) Present address, Carleton University, Ottawa, Ontario, Canada.

(26) On leave from the Laboratoire de Chimie Organique Physique, Paris, France.

Department of Chemistry  
University of Florida  
Gainesville, Florida 32601

College of Pharmacy  
University of Florida  
Gainesville, Florida 32601

Boyce Thompson Institute  
for Plant Research, Inc.,  
Yonkers, New York 10701

M. P. Bratze<sup>25</sup>  
J. J. Aaron<sup>26</sup>  
J. D. Winefordner\*

S. G. Schulman

H. Gershon

Received November 3, 1972

### Reply to the Comments of Desnoyers on the Paper, "Ionic Solvation Numbers from Compressibilities and Ionic Vibration Potentials Measurements"

Publication costs assisted by The Flinders University

Sir: We wish to discuss the points in Desnoyers' communication<sup>1</sup> in order.

(1) "It is better to use the apparent molar compressibility and apparent molal volumes to determine solvation numbers from compressibility data. In this way, one eliminates interionic effects." This could be done; we think the advantage would be nugatory. Our work is aimed at models of the solvation shell at infinite dissolution. The changes with concentration are better interpreted in terms of the interpenetration of solvation shells. (The correlations with this model are shown in our paper,<sup>2</sup> Figure 10 and Table VIII.) A similar model has been used by Ramnathan and Friedman.<sup>3</sup>

(2) "The partial molar expansivity can be related to hydration numbers and, in this case, certain assumptions give rise to a negative value for the hydration number."

We do think this relates to our paper, where we have used the relative compressibilities of solvent and solute to calculate solvation numbers. The assumption (we correct for the partial degree of its applicability in our calculation<sup>2</sup>) is that the water molecules are completely incompressible at sufficiently high field. The assumption of Dr. Desnoyers' equation relating expansivity to hydration numbers is that both the hydration number and the volume of the water molecules in the hydration sheath are independent of temperature. This assumption seems to have a different status from that which we have used. We suggest the contradiction in sign arises from the lack of applicability of the assumptions. Corresponding remarks may be applied to his comment on heat capacity data.

(3) In respect to the heat capacity data for sodium chloride solutions in H<sub>2</sub>O and D<sub>2</sub>O, we cannot agree that they are relevant to the interpretations of the compressibility data. They tell us something about how the heat capacities of solutions and salts vary in these two solvents, and it seems likely that the effects of structural changes outside the solvation sheath may be different, for heat capacities than for compressibilities.

Now let us move to the general thought behind the comments of Dr. Desnoyers, and provide a general answer. In the work of Bockris and Saluja,<sup>4</sup> the ionic vibration potentials have been combined with compressibility measurements to give individual solvation numbers, because the first measurement gives the sum and the latter measurement the difference of solvation numbers. This is the essential new thing about the experimental approach of Bockris and Saluja and the essential new thing about the theoretical approach is to distinguish quantitatively for the difference between the coordination number of the ion in aqueous solution and the number of water molecules temporarily attached to it, while it moves in the solution.<sup>5-7</sup>

Dr. Desnoyers' essential point is to suggest that the fact that we have assumed (for univalent ions) that the change of the solution compressibility can be given predominantly by the change in the layer which the solvation and coordination waters inhabit, and then one further struc-

- (1) J. E. Desnoyers, *J. Phys. Chem.*, **77**, 567 (1973).
- (2) J. O'M. Bockris and P. P. S. Saluja, *J. Phys. Chem.*, **76**, 2140 (1972).
- (3) P. S. Ramnathan and H. L. Friedman, *J. Chem. Phys.*, **54**, 1086 (1971).
- (4) J. O'M. Bockris and P. P. S. Saluja, *J. Phys. Chem.*, **76**, 2298 (1972).
- (5) J. O'M. Bockris, *Quart. Rev. Chem. Soc.*, **3**, 173 (1949).
- (6) J. O'M. Bockris and A. K. N. Reddy, "Modern Electrochemistry," Plenum Press, New York, N. Y., 1970.
- (7) O. Ya Samoilov, "Structure of Electrolyte Solutions and Hydration of Ions," Consultants Bureau, New York, N. Y., 1965; *Discuss. Faraday Soc.*, **24**, 141 (1957).



**TABLE I: Comparison of the Results of Bockris and Saluja for Ionic Solvation Values with Results of Other Authors**

	Ref 6 <sup>a</sup> (6 methods)	Ref 9 (7 methods)	Ref 2
Li <sup>+</sup>	5 ± 1	4 ± 1	4.5
Na <sup>+</sup>	5 ± 1	3 ± 0.8	4.5
K <sup>+</sup>	4 ± 2	2 ± 0.7	3.8
Rb <sup>+</sup>	3 ± 1	2 ± 0.5	3.0
F <sup>-</sup>	4 ± 1	2 ± 0.3	4.0
Cl <sup>-</sup>	1 ± 1	1 ± 0.2	2.2
Br <sup>-</sup>	1 ± 1	1 ± 1	1.8
I <sup>-</sup>	1 ± 1	1 ± 1	1.5

<sup>a</sup> Results rounded off to nearest integers for solvation numbers.

**TABLE II: Results Quoted by Desnoyers and Jolicoeur<sup>a</sup> on the Solvation Number of Some Salts Compared with Those of Bockris and Saluja<sup>b</sup>**

Salts	Ref 10	Ref 2
LiCl	4 ± 1	7 ± 1
LiI	3 ± 1	6 ± 1
NaF	4 ± 1	8 ± 1
NaCl	5 ± 1	7 ± 1
NaI	3 ± 1	6 ± 1
KF	6 ± 1	7 ± 1
KCl	4 ± 1	6 ± 1
RbCl	2 ± 1	5 ± 1

<sup>a</sup> Reference 10. Mean of three methods. <sup>b</sup> Reference 2. Results rounded off to nearest integers for solvation numbers.

ture-broken layer, might be too crude an approximation, so that the numerical results of a determination based on it would lose validity.

If there were a substantial structural change outside the first two layers of water molecules around the ion, extending, say, to the first five layers, there might be point in what he claims. The broken down water structure would be less compressible than the structured water and our results would be too high.

We do, however, have a basis for our approximation, and it has been developed in our second paper.<sup>4</sup> Here, we have gone into detail in the structure breaking and have developed a model in which we have solvational (*i.e.*, oriented) water molecules, and other water molecules, which make up the first layer around the ion, and then a second layer in which the water is regarded as broken down into freely rotating monomers. For univalent ions, we find that fits can be obtained to entropy and heat data only if we do not extend the break-down further. Thus, the model with which our attitude is consistent derives from that of Bockris,<sup>5</sup> but is modified to resemble that of Frank and Wen,<sup>8</sup> in respect to the structural assumptions, and that of Samoilov<sup>7</sup> in respect to the dynamic aspects.

Finally, the degree of damage our approximation may cause can be probed. Let us compare our results with those of other authors who used methods which did not involve our assumption.

In Table I we compare Bockris and Saluja's<sup>2</sup> results with the summary given by Bockris and Reddy (1970) of the results of five methods, and the tabulation of Case,<sup>9</sup> who quoted seven methods (mostly different from those of Bockris and Reddy). It has not been claimed that solvation numbers have the same status as thermodynamic parameters, but there can be no doubt from Table I that

Bockris and Saluja's numbers do measure the same quantity, within an overall significance of about ±1, as is being measured (if rather roughly) by many other methods.

It is also of interest to compare the values of Bockris and Saluja with those which Desnoyers and Jolicoeur quoted in 1969.<sup>10</sup> These are shown in Table II. Thus, Desnoyers and Jolicoeur<sup>10</sup> quoted values (three methods) which are distinctly less than those of the roughly consistent values of the other authors, but again (using Desnoyers' own results as a criterion) there is no doubt that the changes which are followed as one goes from ion to ion show that the results of Bockris and Saluja have not been overwhelmed by structural effects well outside the layers very near the ion. The possibility of coincidence in the agreement is negligible in the many correlations exhibited. Conversely, were we to try to take the determination of solvation numbers to, say a ±5% degree of consistency among the methods, perhaps Dr. Desnoyers' point about a more far reaching correction for the effect of the ion on compressibility of the regions would have more punch.

- (8) H. S. Frank and W. Y. Wen, *Discuss. Faraday Soc.*, **24**, 133 (1957).  
 (9) B. Case, "Molecules at Electrodes," N. Hush, Ed., New York, N. Y., 1972.  
 (10) J. E. Desnoyers and C. Jolicoeur, "Modern Aspects of Electrochemistry," B. E. Conway and J. O'M. Bockris, Ed., Vol. 5, Plenum Press, New York, N. Y., 1969.

School of Physical Sciences  
The Flinders University  
Bedford Park, South Australia

J. O'M. Bockris\*

Department of Chemistry  
Cornell University  
Ithaca, New York 14850

P. P. S. Saluja

Received February 26, 1973

## Gaseous Thallium(I) Metaborate and Thallium(I) Aluminum Fluoride

Publication costs assisted by the U. S. Atomic Energy Commission

Sir: While all the thallium(I) halides have been studied,<sup>1</sup> only two gaseous ternary compounds of monovalent thallium, thallium(I) nitrate<sup>2</sup> and thallium(I) sulfate,<sup>3</sup> have been reported so far. The purpose of this work was to extend the range of known gaseous ternary compounds of thallium(I) and to compare their mass spectrometric behavior to that of the corresponding alkali compounds. We have therefore examined the vapors above thallium(I) metaborate and an equimolar mixture of thallium(I) fluoride and aluminum fluoride.

Samples of thallium metaborate, thallium fluoride, and aluminum fluoride were obtained from Research Organic/Inorganic Chemical Corp. Mass spectra were run on an Atlas CH-4 mass spectrometer. The samples were contained

- (1) D. Cubicciotti, *J. Phys. Chem.*, **68**, 1528, 3835 (1964); **69**, 1410 (1965); F. J. Keneshea and D. Cubicciotti, *ibid.*, **69**, 4910 (1965); **71**, 1958 (1967).  
 (2) D. Cubicciotti, *High Temp. Sci.*, **2**, 131 (1970).  
 (3) D. Cubicciotti, *High Temp. Sci.*, **2**, 389 (1970).

**TABLE I: Mass Spectrum of Vapor Above Thallium(I) Metaborate at 634° (70-V Ionizing Electrons)**

Ion	Rel intensity	Ion	Rel intensity
Tl <sup>+</sup>	100	Tl <sub>2</sub> <sup>+</sup>	2.2
TlO <sup>+</sup>	0.27	Tl <sub>2</sub> O <sup>+</sup>	21.3
TlBO <sup>+</sup>	0.48	Tl <sub>2</sub> BO <sub>2</sub> <sup>+</sup>	17.5
TlBO <sub>2</sub> <sup>+</sup>	2.2		

**TABLE II: Mass Spectrum of Vapor Above an Equimolar Thallium(I) Fluoride-Aluminum Fluoride Mixture at 413° (70-V Ionizing Electrons)**

Ion	Rel intensity	Ion	Rel intensity
Tl <sup>+</sup>	100	Tl <sub>2</sub> <sup>+</sup>	0.59
TlF <sup>+</sup>	8.1	Tl <sub>2</sub> F <sup>+</sup>	3.9
TlAlF <sub>2</sub> <sup>+</sup>	0.09	Tl <sub>2</sub> F <sub>2</sub> <sup>+</sup>	1.1
TlAlF <sub>3</sub> <sup>+</sup>	2.9	Tl <sub>2</sub> AlF <sub>4</sub> <sup>+</sup>	1.3
TlAlF <sub>4</sub> <sup>+</sup>	0.13		

in platinum-lined nickel effusion cells. Mass spectra obtained are shown in Tables I and II.

The mass spectrum of thallium metaborate (Table I) is similar to that of the alkali metaborates.<sup>4</sup> Both thallium metaborate monomer, TlBO<sub>2</sub>, and dimer, Tl<sub>2</sub>(BO<sub>2</sub>)<sub>2</sub>, are present in the vapor, the latter identified by means of the fragment ion Tl<sub>2</sub>BO<sub>2</sub><sup>+</sup>. The different temperature dependence of Tl<sub>2</sub>BO<sub>2</sub><sup>+</sup> and TlBO<sub>2</sub><sup>+</sup> showed the latter to be the monomer parent ion rather than a dimer fragment. The dimer parent ion Tl<sub>2</sub>(BO<sub>2</sub>)<sub>2</sub><sup>+</sup> was not found; it was present to the extent of less than one part in 400 of the fragment ion Tl<sub>2</sub>BO<sub>2</sub><sup>+</sup>. It may be noted that for gaseous thallium nitrate dimer the fragment ion Tl<sub>2</sub>NO<sub>3</sub><sup>+</sup> was the only ion observed.<sup>2</sup> In this respect the two thallium pseudohalides resemble the alkali halides and pseudohalides, whose mass spectra only show dimer fragment ions M<sub>2</sub>X<sup>+</sup> and differ from the thallium halides, whose mass spectra contain dimer parent ions Tl<sub>2</sub>X<sub>2</sub><sup>+</sup>.<sup>2</sup> The monomer-dimer ratio in thallium metaborate vapor is difficult to establish since the thallium ion, which one would otherwise suppose to be a fragment of the monomer, had an appearance potential of 6 eV showing the presence of free thallium in the vapor.

Turning now to the mass spectrum of the vapor above the TlF-AlF<sub>3</sub> mixture (Table II) we see that the mixed thallium aluminum fluoride, TlAlF<sub>4</sub>, is indeed present. Its existence was in fact suggested by the observation of the corresponding indium compound, InAlF<sub>4</sub>, in work on the reduction of AlF<sub>3</sub> by indium.<sup>5</sup> In addition, the presence of the ion Tl<sub>2</sub>AlF<sub>4</sub><sup>+</sup> shows the existence of a higher polymer. In analogy with the assignment of the corresponding ions in

the LiF-AlF<sub>3</sub> and NaF-AlF<sub>3</sub> systems,<sup>6</sup> we are inclined to assign this ion to the double dimer Tl<sub>2</sub>(AlF<sub>4</sub>)<sub>2</sub>. The presence of the mixed trimer, Tl<sub>2</sub>AlF<sub>5</sub>, however, cannot be ruled out. In the case of TlAlF<sub>4</sub>, the parent ion, TlAlF<sub>4</sub><sup>+</sup>, is present in the mass spectrum, in contrast to LiAlF<sub>4</sub> and NaAlF<sub>4</sub>, in whose mass spectra only the fragments LiAlF<sub>3</sub><sup>+</sup> and NaAlF<sub>3</sub><sup>+</sup> are observed. The difference in behavior between the two sets of compounds may be explained by the recent work of Berkowitz.<sup>7,8</sup> In interpreting the photoelectron spectra of TlCl and TlBr he concluded that the highest lying orbital is a thallium s orbital, in agreement with the calculations of Hastie<sup>9</sup> and Cusachs.<sup>10</sup> In Berkowitz's interpretation TlCl and TlBr are essentially ionic compounds, and removal of the thallium s electron on ionization will actually strengthen the ionic bond, the ion formed being effectively Tl<sup>2+</sup>X<sup>-</sup>. Removal of a halogen p electron (the next highest orbital, but with an appearance potential below that of the thallium s orbital) removes the charge on the halogen and leads to the fragment ion Tl<sup>+</sup>.

This analysis may be extended to TlAlF<sub>4</sub> and the alkali aluminum fluorides if we assume that the mixed thallium halide has the same structure as NaAlF<sub>4</sub>, which has two bridging fluorine atoms between the sodium and aluminum atoms.<sup>11</sup> Removal of a thallium s electron leads to the parent ion TlAlF<sub>4</sub><sup>+</sup>, whereas no such process is possible in the alkali compounds. Removal of a bridging fluorine p electron, on the other hand, leads to the fragment ions MAlF<sub>3</sub><sup>+</sup> in both the thallium and the alkali compounds.

*Acknowledgments.* The authors are grateful to Professor A. W. Searcy for reading the manuscript. This work was done under the auspices of the U. S. Atomic Energy Commission.

- (4) A. Buchler and J. B. Berkowitz-Mattuck, *J. Chem. Phys.*, **39**, 286 (1963).
- (5) A. Buchler and J. L. Stauffer, unpublished work.
- (6) A. Buchler and J. B. Berkowitz-Mattuck, *Advan. High Temp. Chem.*, **1**, 95 (1967).
- (7) J. Berkowitz, *J. Chem. Phys.*, **56**, 2766 (1972).
- (8) J. Berkowitz and J. L. Dehmer, *J. Chem. Phys.*, **57**, 3194 (1972).
- (9) J. Hastie, unpublished work cited in ref 7.
- (10) L. C. Cusachs, unpublished work cited in ref 7.
- (11) V. P. Spiridonov and E. V. Erokhin, *Zh. Neorg. Khim.*, **14**, 636 (1969) (*Russ. J. Inorg. Chem.*, **14**, 332 (1969)).

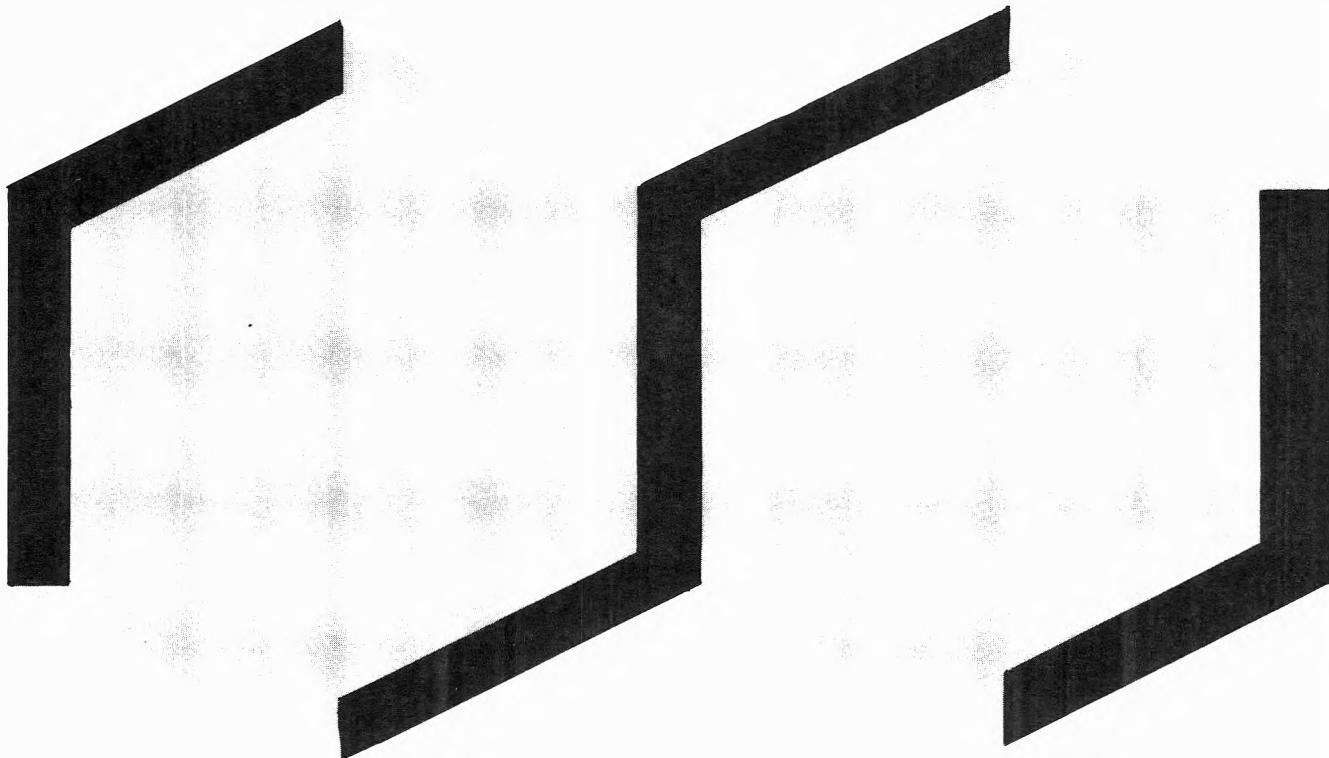
*Inorganic Materials Research Division  
Lawrence Berkeley Laboratory*

**David H. Feather  
Alfred Buchler\***

*Department of Materials Science and Engineering  
College of Engineering  
University of California  
Berkeley, California 94720*

Received March 8, 1973

# The leading American journal devoted to general organic chemistry:



## The Journal of Organic Chemistry

The career wise way to keep up with current thinking in the field. You get the *total picture* presented through forty some papers per biweekly issue. Areas of emphasis include:

- Organic reactions
- Natural products
- Studies of mechanism
- Theoretical organic chemistry
- Various aspects of spectroscopy related to organic chemistry

You get all of this, in the 1100 articles and NOTES (brief, concise accounts of studies of smaller scope) and over 4000 pages a year from your big informative issues of THE JOURNAL.

You owe it to your career to find out for yourself why The Journal of Organic Chemistry is the leader in its field.

Send your order today.



... another ACS service

### The Journal of Organic Chemistry American Chemical Society

1155 Sixteenth Street, N.W.  
Washington, D.C. 20036

Yes, I would like to receive THE JOURNAL OF ORGANIC CHEMISTRY at the one-year rate checked below:

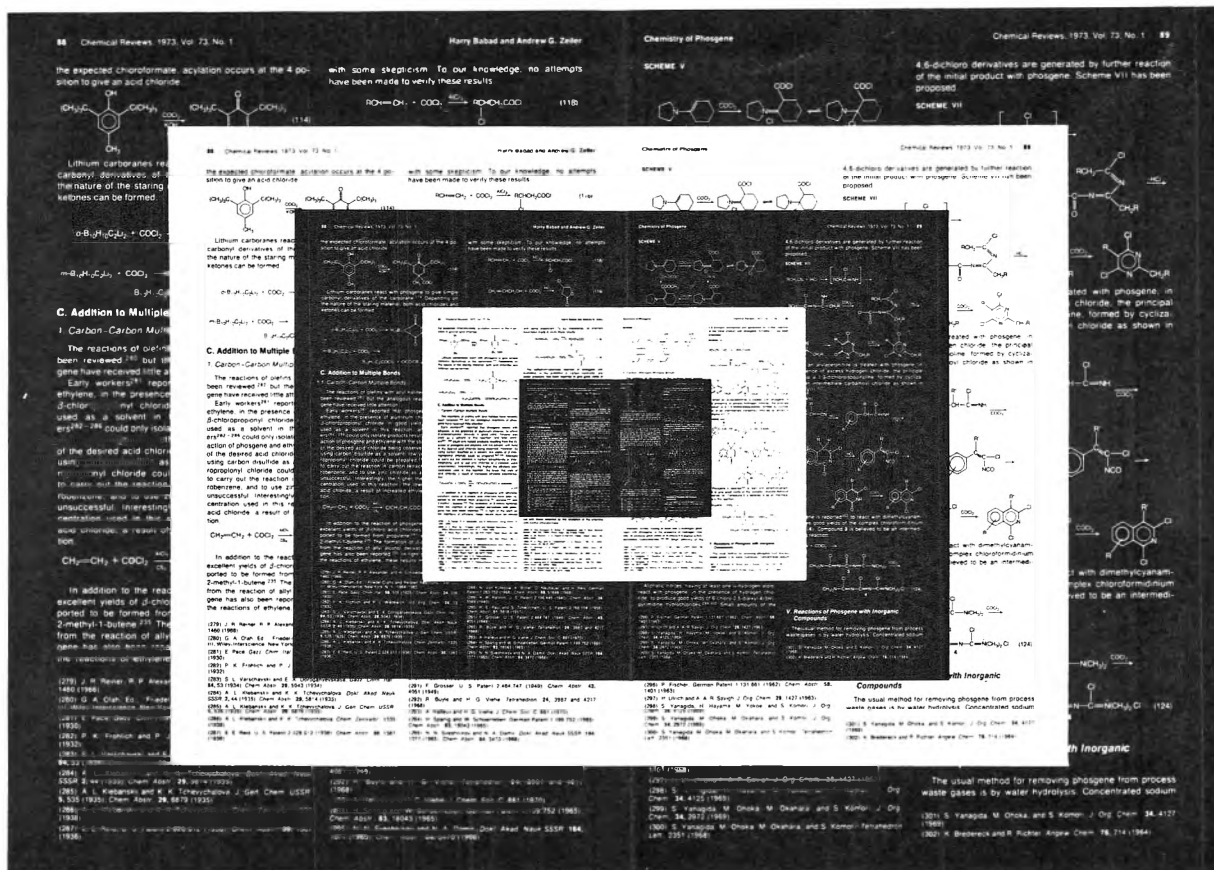
	U.S.	Canada	Latin America	Other Nations
ACS Member Personal-Use				
One-Year Rate	<input type="checkbox"/> \$20.00	<input type="checkbox"/> \$25.00	<input type="checkbox"/> \$25.00	<input type="checkbox"/> \$26.00
Nonmember	<input type="checkbox"/> \$60.00	<input type="checkbox"/> \$65.00	<input type="checkbox"/> \$65.00	<input type="checkbox"/> \$66.00
Bill me <input type="checkbox"/>	Bill company <input type="checkbox"/>	Payment enclosed <input type="checkbox"/>		

Name \_\_\_\_\_

Street \_\_\_\_\_ Home   
Business

City \_\_\_\_\_ State \_\_\_\_\_ Zip \_\_\_\_\_

G-73



# INFORMATION IMPLOSION!

## The ACS Journal Microform Program

One of the steps being taken by ACS Publications to reduce new chemical information to manageable proportions is the adoption of microform techniques for storage and publication.

We are using both microfilm and microfiche.

**MICROFILM:** Most of the ACS periodical publications are now available on microfilm, 16 mm or 35 mm, negative or positive, open reel or special cartridge. Back issues—back to Volume 1 for many journals—are available. Subscriptions to current volumes also are available; the microfilm is supplied at year's end.

Current subscriptions to microfilm editions of journals include a subscription to "hard copy" issues of the journal. Microfilm subscriptions are on a lease basis that specifically grants the subscriber a license to make unlimited numbers of photocopies for internal use.

**Microfilm** editions contain supplementary materials—such as tables, charts, computer printouts, and the like—that are not printed in the regular hard copies. They thus constitute the most complete version of each journal.

**MICROFICHE:** The supplementary materials which are included at the end of each year in the current microfilm editions of the journals are also available on 105 x 148 mm negative microfiche cards.

Journal users can obtain material supplementary to an article, on microfiche, soon after publication by following the ordering instructions given at the end of the article.

**Microfiche** cards containing supplementary material are available on a subscription basis for five journals that have a substantial, continuing volume of such material—these five are Journal of the American Chemical Society,

Journal of Organic Chemistry, Journal of Physical Chemistry, Inorganic Chemistry, and Journal of Chemical & Engineering Data. Most, but not necessarily all, issues of these journals have supplementary material. **Microfiche** subscriptions are not available on other ACS publications.

**Microfilm** edition subscribers receive all microfiche cards for the particular journal to which they subscribe and thus do not need to special-order any microfiche cards for that journal.

Note: Single issues of journals and entire articles are not available either on microfilm or on microfiche.

To: Special Issues Sales  
American Chemical Society  
1155 16th St., N.W., Washington, D.C. 20036

Please send me full information on the ACS Journal microform program.

Name

Title

Address